Position of the Triassic-Jurassic boundary in South Africa and Lesotho:

A multidisciplinary approach aimed at improving the chronostratigraphy and biostratigraphy of the Elliot Formation, Stormberg Group

Lara Sciscio

THESIS

presented in fulfilment of the requirements for the degree of

PHILOSOPHIAE DOCTOR

in

GEOLOGY

in the

FACULTY OF SCIENCE

of the

UNIVERSITY OF CAPE TOWN

IYUNIVESITHI YASEKAPA • UNIVERSITEIT VAN KAAPSTAD

Supervisor Dr. E. M. Bordy

Co-supervisor: Dr. M. O. de Kock

December 2015

DECLARATION

I declare that this thesis is my own original work, conducted under the supervision of Dr. E.M. Bordy. It is submitted for the degree of Doctor of Philosophy at the Faculty of Science at the University of Cape Town, Cape Town. No part of this research has been submitted in the past, or is being submitted, for a degree or examination at any other University.

Lara Sciscio

December 2015

"Nothing, my friends, is so sobering as an outcrop. And many a fine theory has been punctured by a drill hole."

Francis John Pettijohn (1956)

Table of Contents

ACKNOWLEDGMENTS

I would like to acknowledge the following people and organizations for their contribution to this thesis.

- Firstly, enormous gratitude and thanks to my supervisor, Dr. Emese Bordy, for her kindness not only with her resources but also with her precious time and energy. Her unfailing encouragement and guidance has always been inspirational.
- My co-supervisor, Dr Michiel de Kock, who has been not only patient but enthusiastic even through hard times with the palaeomagnetic magnometer.
- Dr. Fabien Knoll for insightful advice about palaeontology and biostratigraphy, not to mention carrying water for the drill to the top of Likhoele Mtn.
- Field work friends (Will, Tobi, Adam and Matt) who helped with the collection of samples and provided good banter and cheerful dispositions! And to Blair for happily proof-reading introductory chapters about beloved Elliot fossils.
- Basotho hospitality during field visits to beautiful Lesotho.
- The staff of the Geological Sciences Department, University of Cape Town, for logistical and technical assistance during the study; in addition to Dr. H. Wabo in the Paleomag lab at the University of Johannesburg.
- Grazie millie to my parents (Mauro and Dot) and sisters (Romie and Gia) for their encouragement and unfailing support. Their interest, sacrifices and love has always been a great motivation. I would like to thank my partner in crime, Ryan, for always understanding my quest down the geological rabbit hole.
- Lastly, I would like to acknowledge the financial assistance of the South African National Research Foundation (NRF) via the African Origins Platform (2012-2015) program, the German (DAAD) - NRF Scholarship (2013, 2014), NRF Extension Support for Doctoral Completion and the UCT award of Research Associateship (2013).

ABSTRACT

The continental red bed succession of the main Karoo Basin in South Africa and Lesotho, the Elliot Formation (Stormberg Group, Karoo Supergroup), is a significant stratigraphic unit for the regional and global understanding of the Late Triassic - Early Jurassic evolution of terrestrial vertebrate faunas, however, the temporal resolution of its biostratigraphy is inadequate for detailed regional and global correlations.

The main aim of this dissertation is to build a more comprehensive chronostratigraphic framework of the Late Triassic - Early Jurassic Elliot Formation by combining and constraining its biostratigraphy with new results obtained using magnetostratigraphic techniques. This dissertation presents magnetostratigraphic data from ten measured stratigraphic sections in the Elliot Formation across the main Karoo Basin in South Africa and Lesotho.

Palaeomagnetic analyses reveal that heating samples to between 100 mT/ 150 ^{o}C – ~300 ^{o}C removed the secondary, moderately shallowly inclined normal-polarity component of remanent magnetization. This component can overlap with the present-day field as well as being consistent with the overprint direction expected from Early Jurassic Karoo dolerite intrusions. In comparison and contrast, a likely primary, high unblocking temperature component, of duel polarity, consistently plots more steeply. This characteristic remanence passes the reversals test, except where means are based on small sample numbers.

Virtual geomagnetic poles for the entire Elliot Formation from the ten sites are comparable to the Early Jurassic pole of Gondwana. The separate poles calculated for the four sites in the lower and ten sites in the upper Elliot Formation overlap with the Late Triassic and Early to Middle Jurassic Gondwana poles, respectively. The overall Elliot Formation and upper Elliot Formation (UEF) pole positions are better constrained and therefore considered more reliable. In comparison to previously calculated poles for South Africa and South America, the Elliot Formation and UEF poles show considerable overlap with the calculated poles from a previous preliminary magnetostratigraphic study of the Elliot Formation and the lavas of the Early Jurassic (Pliensbachian) Drakensberg Group of southern Africa.

Integration of these new magnetostratigraphic sections with available biostratigraphic and geochronological data for South Africa was also undertaken. The composite magnetostratigraphic log of the Elliot Formation contains 8 polarity pairs (EF1r – 9n). When integrated with biostratigraphy, this magnetostratigraphic log can be used for global comparisons with sites of similar ages both in the

Southern (e.g., Los Colorados Formation, Argentina) and Northern Hemispheres (e.g., the Newark astrochronology and geomagnetic polarity time scale APTS, USA).

This stratigraphic integration, in conjunction with the newly calculated pole positions, has allowed the reassessment of the age of the Elliot Formation. It is now argued that the lower Elliot Formation (LEF) corresponds to either the E14r (~214 Ma) or E15r to E22 (~212 to ~202 Ma) magnetochrons of the Newark APTS. The latter Newark APTS magnetochrons correlate to the Los Colorados Formation (magnetochron LC7r), and this establishes not only a magnetostratigraphic link between the LEF and Los Colorados Formation, but also the Norian to Hettangian age of the LEF. The sedimentological break between the LEF and UEF and the lowermost UEF spans part of magnetochron EF6 and is likely Late Rhaetian in age (~202 Ma). Thus the End-Triassic mass extinction may most likely fall at this sedimentological and biostratigraphic break. The first truly Jurassic rocks of the Elliot Formation are likely those within the magnetochron EF6.2n and upwards. Therefore, the Triassic-Jurassic boundary (TJB) in the Elliot Formation is not at the sedimentological divide between the LEF and UEF but rather lies within the UEF. The current uncertainty as to whether the TJB should be placed within the EF6 or EF7 magnetochrons remains at least until new geochronological and higher resolution biostratigraphic data become available. The UEF is correlated with the Newark APTS magnetochrons E23/24 and the Moenave Formation (Glen Canyon Group) in the USA. Based on combined bio- and magnetostratigraphic considerations, the age of the uppermost UEF (magnetochrons EF8 and EF9n) is more likely to be Sinemurian (~195 – 190 Ma).

It is important to note that the stratigraphic correlation between the current study sections and other Late Triassic-Early Jurassic global continental sites remains difficult, primarily due to the dearth of absolute age indicators. Importantly, this thesis brings into question the use of single stratigraphic markers, such as the sedimentological break between the LEF and UEF, as being sufficient to enable the field recognition of the TJB and the chronostratigraphic correlation between southern African sites.

Keywords: Late Triassic, Early Jurassic, Elliot Formation, magnetostratigraphy, palaeopoles, Karoo Basin.

1 General introduction

In Southern Africa, the Karoo Basin provides a relatively continuous view of life between the Late Carboniferous/early Permian and into the Jurassic. Several interesting biological and palaeoclimatological events are recorded in these rocks, ranging from the end Permian mass extinction to the early diversification of dinosaurs. The latter point being one in which the Triassic-Jurassic Elliot Formation comes to the fore. In Southern Africa, as is the case globally, the early diversification (and even the origin) of dinosaurs has been marred by the deficits in exportable and translatable timescales.

The late Triassic - early Jurassic period transition in itself is also interesting as it marks a faunal and floral transition with evolutionary expansion and biological turnover. Colbert (1958) and Newell (1963) were some of the first to describe a terrestrial and marine mass extinction event (respectively) at the then proposed Triassic-Jurassic boundary (TJB). This has more recently been redefined as being an extinction event occurring at the end of the Triassic and predating the TJB. The misunderstandings surrounding the definitions of the TJB and the end-Triassic extinction event (ETE) have muddled earlier works. The ETE (201.566 ± 0.031; Blackburn *et al*., 2013) has now become one of the most enigmatic in the geological record due to the paucity of studies and a lack of complete (and dated) sections, globally (Raup and Sepkoski, 1982; Beerling and Berner, 2002; Hallam, 2002; Tanner *et al*., 2004; Whiteside *et al*., 2010; Wotzlaw *et al*., 2014). Temporal resolution surrounding events near and across the TJB in conjunction with the associated faunal and floral extinctions and waves of evolution are limited because of the lack of a marker(s) in the continental and/or marine realm to define the TJB itself. In recent years, this problem is being tackled incrementally with increasing success as the number of sections, relative and absolute dating methods and attention grows (e.g. Ramezani *et al*., 2014; Wotzlaw *et al*., 2014).

The placement of the TJB is largely dependent on biostratigraphic methods, ranging from conodonts, ammonoids, and palynomorphs to vertebrate fossils, conchostraca and vertebrate trackways in continental sections. Geochemical and palaeomagnetic as well as radiometric age dates acting as a complement to, and in conjunction with, the biostratigraphic records. There have been multiple eligible sections which have vied for the title as the global boundary stratotype section and point (GSSP) for the TJB (Tanner *et al*., 2004; Hesselbo *et al*., 2006). These include St. Audrie's Bay (Somerset, UK [magnetostratigraphy with palynomorphs, conodonts and ammonites]); Ferguson Hill section, New York Canyon (Nevada, USA [no palynomorphs, ammonites]), Chilingote (Utcubamba Valley, Peru [magnetostratigraphy, radiometric dates, ammonites]), Kunga Island (British Columbia, Canada) and the Karwendel Syncline

section (Kuhjoch, Eiberg Basin, northern Tyrol, Austria). More recently, a section (Kuhjoch in the Karwendel syncline) from the Eiberg Basin was accepted as the GSSP for the base of the Jurassic Hettangian Stage (Hillebrandt *et al*., 2007; Hillebrandt and Krystyn, 2009; Morton, 2012; Hillebrandt *et al*., 2013) with the first occurrence (FO) of *Psiloceras spelae tirolicum*, the earliest Jurassic ammonite. The first negative C-isotope excursion, recorded approximately 6 m below the ammonoid zone, marks the lithological transition separating the Kössen Formation (Eiberg Member) and the Kendelbach Formation (Tiefengraben Member), and is seen in other contemporaneous sections (e.g. St. Audrie's Bay).

These candidates are largely marine sections and each holds a different view as to the placement of the TJB based on the fauna or flora they preserve. For instance, the ammonoid zone at Kuhjoch is not represented in the British GSSP candidate that considers the TJB to be marked by the highest occurrence of conodonts and the lowest occurrence of the *Psiloceras planorbis* (Hounslow *et al*., 2004). In contrast, a closely related ammonoid (*Psiloceras spelae spelae*) is known from the Muller Canyon section (USA) and this is used there to mark the transition. It must be noted that the Kuhjoch section does not have a magnetostratigraphic section.

Ultimately, each GSSP candidate lack comprehensive and (to some degree) overlapping proxies for refined correlations which makes individual sections and comparative sections 'inferior' for TJB positioning. This has been changing in recent times as more studies are using multiproxy approaches (e.g. Olsen *et al*., 2011; Whiteside *et al*., 2015) over the Late Triassic and Early Jurassic transition.

1.1 Thesis rationale

The main Karoo Basin holds one of the most complete successions of Late Carboniferous to Early Jurassic terrestrial sediments (Karoo Supergroup), and may reveal important evidence as to the causes and consequences of the terrestrial end-Triassic event. The Karoo sediments not only illustrate changes in climate over geological time but are also richly fossiliferous, and aid in understanding evolution and proliferation of terrestrial flora and fauna.

The Elliot Formation encapsulates the late Triassic and early Jurassic within the Karoo Basin. Lesotho and South Africa hold multiple well exposed outcrops of terrestrial Triassic-Jurassic Elliot Formation. These provide practical sites for palaeomagnetic drilling which will contribute and augment the current

dependence on vertebrate biostratigraphy. To improve understanding of the dynamics of the ETE in Southern Africa and its impact within the terrestrial ecosystems, further study must be directed at their timing and relationship to regional and global events. Multiple drilled sections of the entire Elliot Formation as well as sections concentrating on the boundary between the Upper Elliot and Lower Elliot (biostratigraphic Triassic-Jurassic boundary) have been completed, providing a relatively high resolution geomagnetic polarity stratigraphy. This quantitative and exportable timescale will ultimately provide a reference section for all Elliot Formation palaeontological data and allow for correlation of fossil bearing outcrops within South Africa, Lesotho and more importantly, globally. This reference section can then be incorporated into a global framework which would allow for a greater impact on the assessment of ages, ranges and duration of biological events.

Calibration via geochronology (U-Pb Zircon dates) due to the presence, and very recent sampling and study, of volcanogenic sandstones (still to be chemical defined) and although showing sedimentological evidence for some reworking (e.g. Maseru, this study) will provide additional constraints to the duration of the Elliot Formation. Radiometric dates, which are novel for the Elliot Formation, should be considered with care. This powerful tool allows for discrete stratigraphic events to be dated and the potential for global cross-stratigraphic correlations. The precision of the method, within the laboratory and during interpretation, still permit for an error margin. Present studies, inclusive of the results presented here (Maseru site), have mitigated this error but previous works must be considered with thoughtfulness.

1.2 Statement of research problem

Absolute ages, within the Stormberg Group, are few and are largely dependent on the U-Pb ages derived from the overlying Drakensberg lavas. The underlying ^{40}Ar-^{39}Ar dates obtained from Hälbich *et al*. (1983) are hotly contested due to poor geochronological data sets. Hansma *et al*. (2015) have provided a revision of the timing of the Cape orogeny and a discussion of the formation of the Cape Fold Belt for use with Karoo basinal response to deformation.

The Elliot Formation contains the early evolution of dinosaurs and is richly fossiliferous. Dating of this formation is important not only for southern African studies but for global comparisons. Biostratigraphic dating of this Formation has, to date, been the sole method for deriving ages for the fossils within the

formation and the formation age itself. As always, the key to understanding cause-effect relationships within the Elliot Formation and by extension, the Stormberg Group itself, and its comparison to contemporaneous global events would be to improve the current resolution of the chronostratigraphy of the Elliot Formation and the Stormberg group.

The last formal assessment of the fossils and trace fossils within the Elliot Formation and how they contribute to understanding of the age of the Formation and the duration of certain species lies in the work of Ellenberger (1970), Kitching and Raath (1984) and Olsen and Galton (1984). Although several papers have reviewed Kitching and Raath's (1984) work, for instance Olsen and Sues (1986), Lucas and Hancox, (2001) and Knoll (2004; 2005), reassessment of the collections in consideration of taxonomic revisions as well as the increasing growth of the Elliot collections is desperately needed. This becomes especially true in light of the 31 years which have passed since the formation was formally biostratigraphically subdivided. The revision of the bio-chronology would greatly supplement and improve the work conducted here. Furthermore, limited collected rock material from the Triassic-Jurassic Elliot Formation has undergone proper assessment or laboratory preparation to provide chemostratigraphic profiles of this geological time period. This could be an additional and greatly profitable extension of the current study in terms of characterising Triassic-Jurassic climate change in southern Gondwana. Ultimately, the undertaking of both bulk rock geochemistry and biogeochemistry, specifically looking at stable carbon and oxygen isotopes of pedogenic nodules within the Formation, would allow for the qualitative and quantitative assessment of weathering and the construction of palaeoclimatic proxies (Dworkin *et al.*, 2005).

To realize a precise chronostratigraphic framework for the Elliot Formation, largely through magnetostratigraphy, detailed sedimentology of studied sections and precious radiometric date(s) would be valuable for local and global TJB section comparisons.

The main purpose and thus aim of this project is to successfully construct a composite magnetostratigraphic profile for the Elliot Formation in South Africa and Lesotho. In so doing, detailed comparisons of a composite polarity scale to those of a similar time period on a global scale would be the highlight and most profitable for regional studies in southern Africa. Ultimately, this will act as a supplementary complement to the documentation and collection of body and trace fossils for this formation in South African and Lesotho from this point forward.

1.3 Literature review (general)

1.3.1 **End Triassic extinction event (ETE)**

The ETE is the third largest of five major extinction events of the Phanerozoic (Raup and Sepkoski, 1982; McElwain *et al*,. 1999). In the marine realm, there are abrupt shifts in the size and composition of many marine families; notably, the extinction of the conodonts (with few persisting into the Hettangian); sudden changes in the brachiopod and radiolarian communities; and the disappearance of many ammoniods (Pálfy, 2008; Pálfy *et al*., 2007). In the continental realm, there is the extinction of many tetrapods (Lucas and Tanner, 2007b) and an abrupt change in the composition of floral biomes which extends into the Triassic-Jurassic transition. The latter being disputed, in terms of palynomorphs, between European (Tethyan) sections and those reported from the Newark Basin (eastern USA) based on the possibility of a Rhaetian gap in the Newark succession.

Although now considered one of the 'big five' mass extinction events, the certainty as to the significance of its magnitude has been questioned (Olsen and Glaton, 1977; Hallam, 2002; Zeigler and Geissman, 2008). This uncertainty is ultimately a feature of:

- the number of complete and dated sections,
- constraining different dating methods (vertebrate biostratigraphy, isotope stratigraphy and magnetostratigraphy) on geographically and globally separated sections,
- Accurately establishing and predicting the number of fauna/floral taxa from scarce/fragmentary remains globally,
- Linking geographically separated sections when there is no GSSP and when the LO and HO of taxa is misleading (Tanner *et al*., 2004).

Despite degrees of uncertainty relating to the event, it has been estimated that ~50 % of the global biodiversity was lost at this point (Raup and Sepkoski, 1982), and high rates of diversity loss can only be explained by a/several global natural disaster(s). Forcing mechanisms of the ETE are under dispute, and range from:

a) Sea level change and oceanic anoxia (Newell, 1967; Hallam, 1990; Hallam and Wignall, 1999; Richoz *et al*., 2012),
b) Climate change (Galli *et al*., 2005; Tanner *et al*., 2001; Beerling and Berner, 2002),

c) Bolide impact (inc. late Triassic 210 ± 4 My Manicouagan crater, Canada; Olsen *et al*., 2002a, b; Simms, 2003;Tanner *et al*., 2008 as well as the French Rochechouart impact crater ~ 201.2 ± 2.0 million years ago; Schmieder *et al*., 2010; accessory evidence includes seismites in the UK section),
d) Methane hydrate release (Lindström *et al*., 2012; Pálfy *et al*., 2001), and
e) Extensive Central Atlantic volcanism (CAMP; Marzoli *et al*., 1999, 2004; Wignall, 2001, 2005; Hesselbo *et al*., 2002; Mundil *et al*., 2010; Whiteside *et al*., 2011 & references therein).

These events are not mutually exclusive and in order to unravel the events that lead to/augmented the ETE, current research deals with its timing, causation and severity (Hallam, 2002; Beerling and Berner, 2002; Wignall, 2001, 2005; Tanner *et al*., 2004; Lucas and Tanner, 2007a, b; Whiteside *et al*., 2010; Mundil *et al*., 2010Lindström *et al*., 2012). Topical work debates the length of the extinction event, and theories of gradualistic (considering retarded timing of extinctions and gradual faunal turnover) versus catastrophic mechanisms are still polarised. The contribution of the internal dynamics of the Earth to its physical environment and its link to biotic turnover are little understood and recognising the coupling of geosphere, atmosphere and biosphere is even more complex. Unravelling the record of cause-effect motions involves the study of the fossil record to garner a deep-time perspective.

1.3.2 **Position of the Triassic-Jurassic boundary**

Studies of the ETE and the Triassic-Jurassic boundary (TJB) have been focused in the Northern Hemisphere where more complete marine and non-marine sections of this event are accessible (Table; Götz *et al*., 2009; Hesselbo *et al*., 2007; Lindstrom *et al*., 2012; Lucas & Tanner, 2007a; Pálfy *et al*., 2007; Pálfy, 2008; Whiteside *et al*., 2010).

1.3.2.1 Marine sections

The TJB is defined, largely, by the biostratigraphy, and it is here where ammonoid zones have become crucial in the positioning and correlation of the TJB in the marine realm. However, this suffers from the effects of ammonite provincialism.

The base of the Jurassic (base of Hettangian Stage) is inferred by the highest occurrence (HO) zone of the ammonite *Choristoceras marshi* (Tanner *et al*., 2004; Yin *et al*., 2007) and defined by the FO of *Psiloceras spelae tirolicum* at the GSSP Kuhjoch (western Tethys; Hillebrant & Krystyn, 2009).

The following sections use the occurrence of ammoniods to infer the base of the Jurassic:

FO of *Psiloceras planorbis*:

1. St. Audrie's Bay section, Somerset, England,
2. Waterloo Bay section, Larne, Northern Ireland, UK

FO of *Psiloceras spelae spelae*

3. Ferguson Hill section, New York Canyon, Nevada, USA
4. Pucara Group, Aramachay Formation, Utcubamba valley, northern Peru

FO of *Psiloceras spelae tirolicum*

5. Kuhjoch section, Karwendel syncline, Northern Calcareous Alps, Austria

Due to Jurassic ammonite provincialism, the LO of *P. planorbis* is frequently stratigraphically separated from the HO of *C. Marshi* (Tanner *et al*., 2004). High resolution U-Pb zircon geochronology of the Kunga Island tuff (Queen Charlotte Island, Canada) has placed a minimum age of 199.6±0.3 Ma on the TJB in the marine realm (Pálfy *et al*., 2000). Unfortunately the main biostratigraphic marker for the Kunga Island section is the evolutionary change in radiolarian populations, with the latest Triassic *Globolaxtorum tozeri* radiolarian zone LO falling five metres below and the oldest Jurassic ammonoid (*Psiloceras sp.*) occurring nine metres above the tuff layer (Pálfy *et al*., 2000). Other radiometric zircon U-Pb ages provided by Schoene *et al.* (2010) place *Psiloceras spelae* into the earliest Jurassic in Nevada and in Peru. Peruvian ammonoids and associated ash beds (Schaltegger *et al*., 2008) have been reinterpreted in light of new radiometric ages by Wotzlaw *et al*. (2014).

1.3.2.2 Continental sections

Terrestrial sections, like their marine counterparts, face a similar fate in that boundary sections are not easily correlated due to palaeobotanical and vertebrate provincialism, effects of climate gradients and climate change etc. (Tanner *et al*., 2004). There are rarities of complete continental sections that can be easily and accurately dated via biostratigraphic and chronostratigraphic means.

Palynologically defined TJB determined by floral turnover is often disputed as being indefinite due to the scarcity of adequate, complete and chronostratigraphically relevant study sections (Bonis *et al*., 2009). Studies of palynomorphs with reference to the ETE are infrequent and uncommon (Götz *et al*., 2009).

Largely, the proposed mechanism for extinction in marine and non-marine realms lies with the correlation of these events to the timing of eruptions associated with the break-up of Pangaea around the Central

Atlantic Magmatic Province (CAMP). A correlation has been drawn between CAMP volcanism and perturbations in global carbon cycling, and this likely impacted the rate of global warming, sea level stability and oceanic anoxia (Hesselbo *et al*., 2007; Pálfy *et al*., 2000; Whiteside *et al*., 2010).

1.3.2.3 Carbon isotope excursions

The T-J transition has been chemostratigraphically characterized by two negative carbon isotope excursions (CIEs). An initial 'late Triassic' CIE, of ≤7‰, is believed to have been short-lived and coincident with the ETE (Lucas and Tanner, 2008). The initial CIE precedes the longer main 'early Jurassic' isotope shift (Deenen *et al*., 2010). The second longer negative isotope shift is now considered to reflect long-term stead state values for the Early Jurassic by Ruhl *et al*. (2010). Several key marine boundary sections all bespeak of global upset in the carbon cycle:

1. Queen Charlotte Island Canada (Ward *et al*., 2001, 2004),
2. Ferguson Hill, New York Canyon, Nevada, USA (McRoberts *et al*., 2007; Ward *et al*., 2007)
3. St Audrie's Bay UK (Hesselbo *et al*., 2002),
4. Hungary (Pálfy *et al*., 2001),
5. Austria (McRoberts *et al*., 1997),
6. Northern Italy (Galli *et al*., 2005).

McElwain *et al*. (1999) carried out high resolution terrestrial carbon record and stomatal study, from fossil leaf cuticles retrieved from sites in East Greenland and southern Sweden, also point to a negative excursion on land. There are several proposals for the carbon cycle perturbation in terrestrial and marine sections. These relate to the CO_2 outgassing during end Triassic CAMP volcanism, the drop in primary productivity as well as the release of methane hydrates creating a sudden surge in isotopically light carbon over the TJB interval (McElwain *et al*., 1999; Pálfy *et al*., 2001; Beerling and Berner, 2002; Hesselbo *et al*., 2002; Hesselbo *et al*., 2007; Bonis, 2010).

1.4 The structure of the dissertation

This dissertation is structured such that it contains several results chapters that, in themselves, deal with different field sites in relation to diverse methodologies and aims. Result chapters are reflected as a

sampling transect from the thickest sections in the northern parts of the basin, to the thinnest in the southern part of the basin. These are then collated and compared to global sections in the Discussion.

Figure 1.1. Legend and facies codes used in this thesis for all lithological and magnetostratigraphic logs, geological maps and general figures.

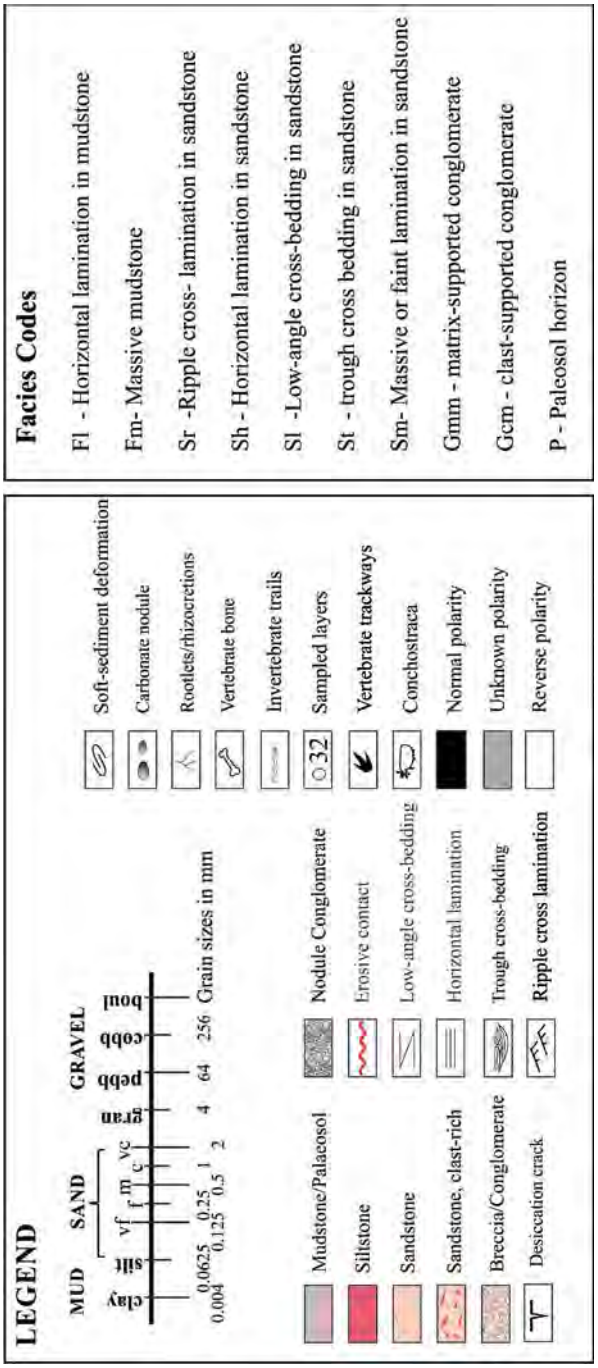

Figure 1.1. Legend and facies codes used in this thesis for all lithological and magnetostratigraphic logs, geological maps and general figures.

2 Geological background

2.1 Cape Orogeny and the main Karoo Basin

During the Carboniferous, the southern convergent margin of Gondwana was typified by a compressional regime, the northward shallow-angle subduction of the palaeo-Pacific plate and the formation of the broad Pan-Gondwanan orogen (Fig. 2.1; Johnson *et al*., 1997; Catuneanu *et al*., 1998; 2005). This orogen was fragmented during the break-up of Gondwana in the Mesozoic, and South Africa's Cape Fold Belt (CFB) is a remnant of this once extensive fold-thrust belt (Fig. 2.1; Catuneanu *et al*., 1998; 2005).

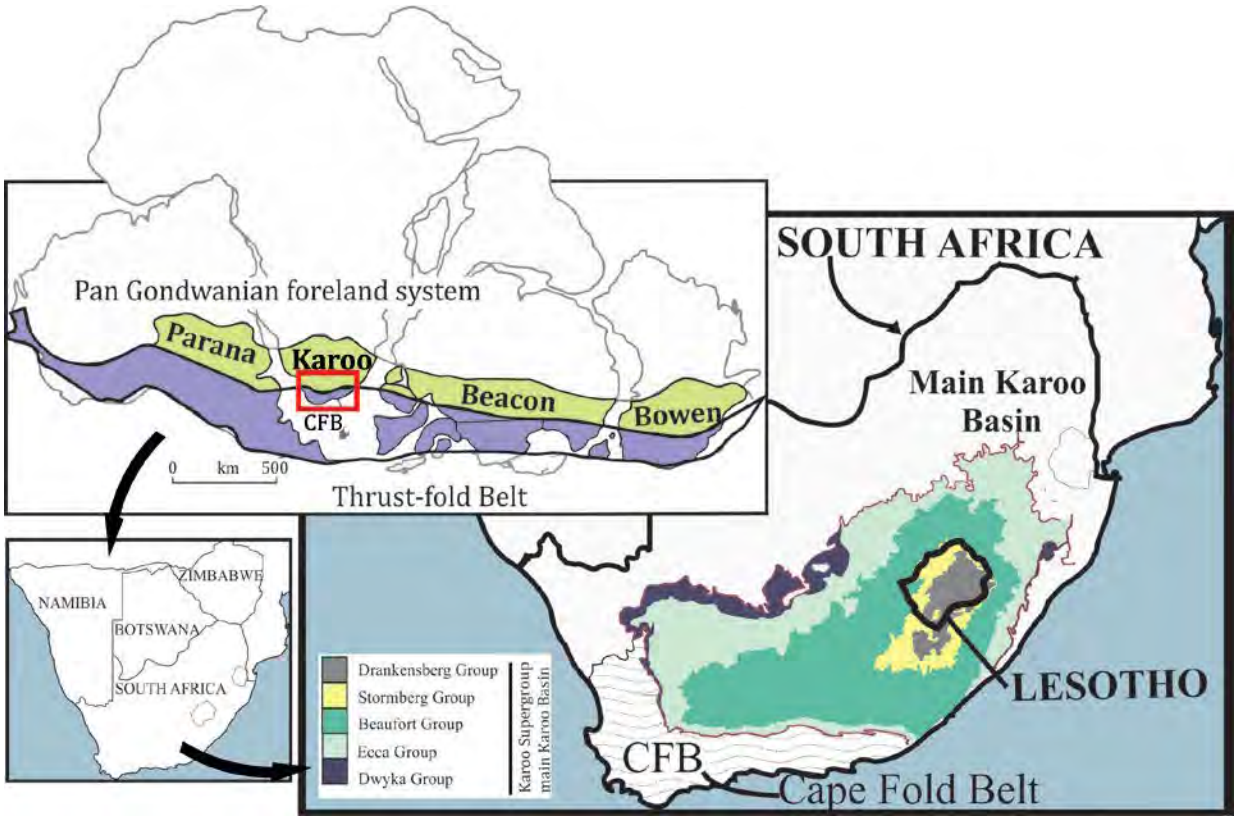

Figure 2.1. Pan-Gondwanan foreland system, illustrating the Parana, Karoo, Beacon and Bowen Basins. The insert displays the main Karoo Basin in South Africa and Lesotho. Modified after de Wit and Ransome, 1992; Johnson *et al*., 1997.

The main Karoo Basin, which today lies to the north of this fragment, is a relic of a once larger intracratonic foreland basin system within the continental interior of Gondwana (de Wit and Ransome,

1992; Johnson *et al*., 2006; Fig. 2.1). The basement rocks of the Basin are part of the Late Proterozoic Namaqua-Natal Metamorphic Belt and the Archean Kaapvaal Craton in the south and north, respectively. The sedimentary succession which fills the main Karoo Basin is known as the Karoo Supergroup which has a cumulative maximum thickness of ~5.5 – 6 km with depths reported proximal to the Cape Fold Belt of ~4 km in the south west and 5 km in the south-eastern portion of the Basin (Scheiber-Enslin *et al*., 2015). Separated from the Palaeozoic Cape Supergroup by a stratigraphic gap of at least 15 Ma (Johnson *et al*., 2006; Isbell *et al*., 2008), the Karoo Supergroup records the geological history of SW Gondwana from the Late Carboniferous (300 Ma) to the Early Jurassic (~183 Ma).

Currently, the development of the Karoo Basin is debated with several basin development models having been proposed over the last two decades. Hansma *et al*. (2015) largely consider the debate as a consequence of the poorly understood tectonic framework to account for the position and deformation of the CFB itself. Most workers consider the Karoo Basin to be a retroarc foreland basin (e.g., Johnson, 1991; Cole, 1992; Catuneanu *et al*., 1998, 2005; Isbell *et al*., 2008) that resulted primarily from flexural tectonics and the formation of the compressional retro-arc CFB which acted as a tectonic, supracrustal, orogenic load. According to Catuneanu *et al*. (1998; 2005), the evolution of the basin is characterized by three main tectonic events:

1. Late Carboniferous-Middle Triassic first-order orogenic loading (compressional) stage with sedimentation occurring mainly in the foredeep flexural province;
2. Middle Triassic-Early Jurassic first-order orogenic unloading (major quiescence) stage with erosion in the proximal (foreslope) and sedimentation in the distal (foresag) flexural provinces;
3. Early Jurassic Gondwana break-up and the formation of the Karoo Large Igneous Province around 183 Ma.

This Late Carboniferous - Early Jurassic history is punctuated by eight, small magnitude orogenic deformational compressional (tectonic paroxysms; P1 – 8) and subsequent quiescence periods (Q1 – 8; Hälbich *et al*., 1983; Catuneanu *et al*., 1998). The turnover between first-order orogenic loading (compressional) and unloading (major quiescence) stages coincides with the boundary between the lower (Dwyka, Ecca and Beaufort Groups) and upper Karoo Supergroup (Stormberg Group).

More recent hypotheses as to basin formation have been proposed by Lindeque *et al*. (2011) and Tankard *et al*. (2009; 2012). Lindeque *et al*. (2011) suggest southward subduction resulting in thin-skinned folding for the formation of the Cape Fold Belt and the main Karoo Basin as interpreted from reflection seismic data evaluation in the south-western Karoo. In contrast, Tankard *et al*. (2009; 2012) propose that the main

Karoo Basin is related to crustal uplift followed by fault controlled subsidence, lithospheric rebound and regional subsidence regulated by subduction-controlled mantle flow. To date, no one model has been unanimously accepted to account for the formation of the main Karoo Basin with each model having short falls unaccountable by present studies. These problematic areas extend from (i) seismic studies illustrating the absence of sutures needed to account for retro-arc models, (ii) lack of horizontal lineation to account for transpressional retro-arc models (Tankard *et al*., 2009), and (iii) Paton *et al*. (2006) identification of thick-skinned thrust propagation components contra Lindeque *et al*. (2011) thin-skinned tectonic model (Hansma *et al*., 2015).

2.2 The Stormberg Group (Upper Karoo Supergroup)

The Upper Triassic – Lower Jurassic Stormberg Group comprises the Molteno, Elliot and Clarens Formations and is separated from the underlying Beaufort Group by a stratigraphic gap (Cole, 1992; Catuneanu *et al*., 1998; Hancox, 2000) and capped by the lavas and other volcanogenic rocks of the Lower Jurassic Drakensberg Group.

The accumulation and preservation of the Stormberg Group are directly related to deposition during the final stages of the Karoo foreland basin development (Cole, 1992; Catuneanu *et al*., 1998). The reduced aerial extent of the Stormberg Group outcrop area relative to other groups of Karoo Supergroup was first attributed as proportional to the reduction in size of the Karoo Basin over time (Cole, 1992). Later work, however, incorporating the geodynamic nature of the basin over time by Catuneanu *et al*. (1998), revised this statement and suggested that the accumulation area of the Stormberg Group was aerially more extensive than the current outcrop area of the Stromberg Group. Support for the later hypothesis comes from the west and southwest of the current Stromberg outcrop area where the sandstone and basalt xenoliths found in kimberlite pipes were positively identified as rock fragments from the Stormberg and Drakensberg Groups. This confirms the laterally extensive nature of the accumulation area during the Late Triassic – Early Jurassic (Hanson *et al*., 2009).

The Stormberg Group has no major lateral facies changes, and contains four stratigraphic gaps linked to the final tectonic events of the Cape Fold Belt. Two of these gaps bind the base and top of the Molteno Formation and a third is found within Elliot Formation (Fig. 2.2; Hälbich *et al*., 1983; Gresse *et al*., 1992; Catuneanu *et al*., 1998; Bordy *et al*., 2005a, b). These subaerial unconformities demarcate three main

coarsening upward sequences which resulted from increased energy of the Stromberg fluvial systems due to steepening of the proximal topographic slope during final unloading of the Cape Fold Belt (Catuneanu *et al*., 1998; 2005). Based on palaeocurrent data, southern, south-eastern and minor western sources are the main areas from which Stormberg sediments were derived (Cole, 1992; Catuneanu *et al*., 1998; Bordy *et al*., 2004a). Palaeoclimatically, the deposition of the Stormberg Group took place under progressively arid conditions, reflected by the major lithological changes from the coal-bearing Molteno Formation to the aeolian-dune dominated Clarens Formation (Eriksson, 1985; Bordy *et al*., 2004a).

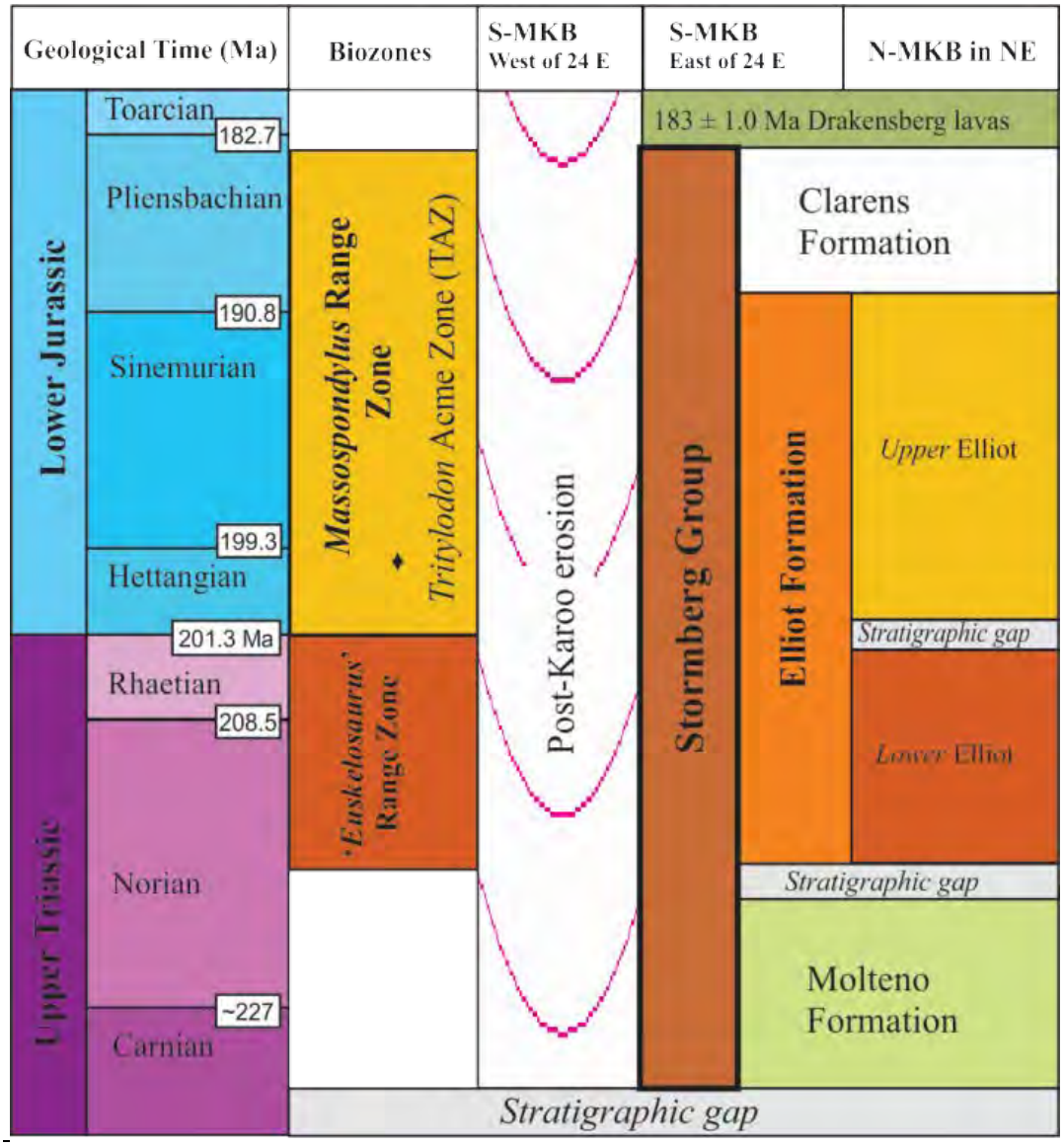

Figure 2.2. Stratigraphic chart of the Stormberg Group (comprises of the Molteno, Elliot and Clarens Formations) in relation to the radiometrically dated Drakensberg Group lavas and in conjunction to the biostratigraphically constrained depositional time period (Data from various sources, reviewed in text; geological time scale from http://www.stratigraphy.org/).

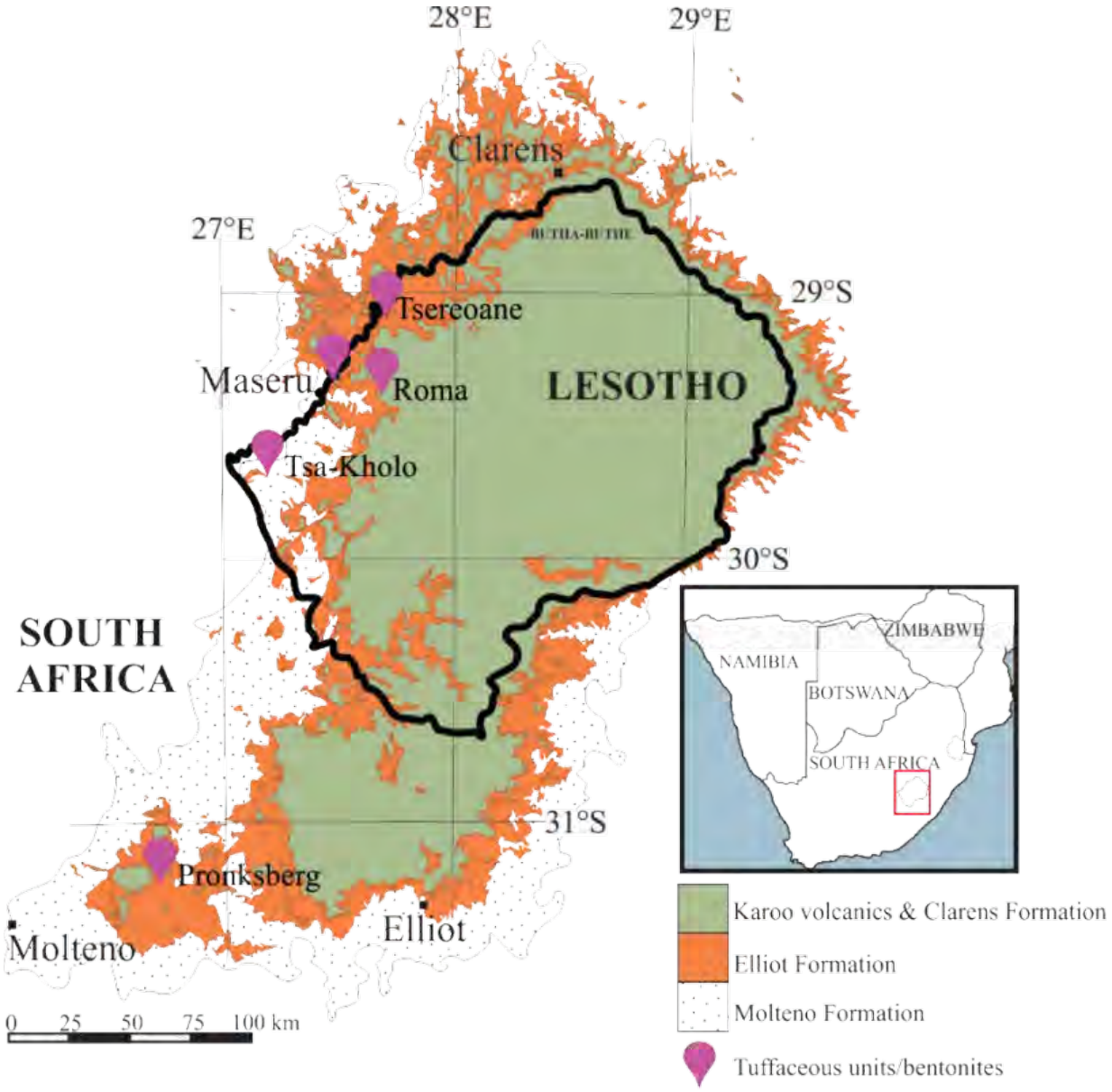

Figure 2.3. Simplified geological map of late Triassic-Early Jurassic Stormberg Group in in Lesotho and South Africa (modified after Bordy *et al*., 2004a). The location of volcanogenic deposits in the Elliot Formation, as reported by Botha and Theron (1967), Willan (1976), and Reed (1976), are also marked. The volcanogenic sandstones at Maseru were sampled in the current project and yielded detrital zircons (see p. Error! Bookmark not defined. **for more detail).**

2.3 Elliot Formation

The Late Triassic - Early Jurassic Elliot Formation is a fossiliferous sequence of mainly red, and less commonly green, mudstones and siltstones which alternate with fine- to medium-grained sandstones in a

ratio of approximately 70:30, respectively (Johnson, 1976; Bordy *et al*., 2004a, b, c; Johnson *et al*., 2006). It unconformably overlies the Molteno Formation and is conformably overlain by the Clarens Formation (Bordy *et al*., 2004a) (Fig. 2.2 &Fig. 2.3). The thickness of the Formation varies along a north-south axis (Fig. 2.3) with sections reaching a maximum of ~70 m in the north, and ~460 – 480 m in the south of the basin (Bordy *et al*., 2004a). The Formation is notable for its vertebrate and ichnofossil assemblages (Ellenberger, 1970; Kitching and Raath, 1984). Based on vertebrate biostratigraphy, the lower Elliot Formation is Norian and the upper Elliot Formation is pre-Toarcian in age (Kitching and Raath, 1984; Lucas and Hancox, 2001). The palaeontologically established age of the Formation is in agreement with Duncan *et al*. (1997) radiometric dating of the overlying Toarcian lavas of the Drakensberg Group (~183 Ma). Importantly, the position of the Triassic-Jurassic boundary within the Formation is still uncertain (Smith *et al*., 2009).

2.3.1 **Historical background**

Dunn (1898) was the first to describe the Elliot Formation as ‘red beds’ and as a discrete unit. Haughton (1924) accounted for the main depositional setting (i.e., floodplain environment) and semi-arid palaeoclimate of the Elliot Formation. Detailed qualitative work was then carried out by du Toit (1939), Stockley (1947), Botha (1968), Haughton (1969) and Johnson (1976). The formal naming of the ‘red beds’ was suggested by Botha (1968) after the town of Elliot which lies south of the unit holostratotype in the Barkly Pass in the south of the basin.

The holostratotype was comprehensively studied by Visser and Botha (1980) who propose a tripartite division of the facies associations, and interpret them, from oldest to youngest as deposits of: (1) meandering rivers and attached floodplains; (2) a “flood basin” characterised by crevasse splays; and (3) a low gradient alluvial plain prone to ephemeral sheet flooding and dotted by aeolian dunes and playa lakes.

Generally studies of the Formation have been divided between exposures in the north and north east (Eriksson, 1984; 1985) with one of the initial major detailed studies throughout the Karoo Basin presented by Le Roux (1974). Many of these early investigations were of limited spatial extent and focused heavily on the sandstones, with information gained specifically for palaeoenvironmental reconstructions. More recently, Bordy *et al*. (2004a, b, c) conducted an extensive qualitative and quantitative investigation into the fluvial style variability, provenance and basin development during deposition of the Elliot Formation. According to these authors, the contact between the lower and the upper Elliot Formations, which demarcates major facies changes within the Formation (see below), is a

regional paraconformity that represents a stratigraphic gap during which the re-structuring of the sedimentary system occurred and resulted not only in a change in the fluvial style, but also in provenance.

2.3.1.1 Economic potential

In Lesotho, uraniferous radioactive horizons were noted by Reed (1976) and have been found to occur within 30 to 50 m of the contact between the Molteno and Elliot Formations. This horizon is well within the lowermost Elliot Formation and the site is located north of Maseru at Lipeleng and Helspoort in Lesotho. It comprises uranium-rich phosphatic (?) horizons, associated with nodules and fossilised bone debris in washouts. In South Africa, uranium-enrichment in Elliot Formation has been recorded in the fluvially-deposited sandstones from an area between Clocolan and Harrismith, in the north-central part of the Karoo Basin (Le Roux, 1990; 1995). According to Cole (2008), this uranium would have been derived from granitic terranes to the south-east in the main Karoo Basin and transported and deposited due to entrainment, adsorption onto clay minerals or in solution. Furthermore Cole (2008) propose that the uranium ore, the precipitation and preservation of which would require reducing, water-logged conditions, was primarily generated in sandstone bodies because they contained negligible primary calcium carbonate allowing the generation of neutral to mildly acidic and oxidising mineralising solutions.

2.3.2 **Lithostratigraphy**

The lithostratigraphy of the Elliot Formation has been recently summarized in Bordy and Eriksson (2015). Currently, the Elliot Formation is informally subdivided into two subunits, the lower Elliot (LEF) and upper Elliot UEF) Formations, based on local and regional scale differences in sediment provenance, petrography, sedimentary structures, and geometry of sandstone bodies (Fig. 2.2; Bordy *et al*., 2004a). Based on outcrops mainly in the northern outcrop area, a lithostratigraphic subdivision of the Formation was first attempted by Kitching and Raath (1984) who identified 3 informal, time transgressive lithostratigraphic zones, namely the ‘Lower’, ‘Middle’ and ‘Upper’ Elliot Formations (Fig. 2.2). Basin-wide tracing of these informal units was unsuccessful, and Bordy *et al*. (2004a) found that the Formation could be more accurately divided into a lower part, the Lower Elliot Formation (LEF) and an upper part, the Upper Elliot Formation (UEF). The latter comprises the Middle and Upper Elliot Formations of Kitching and Raath (1984). The two current informal lithostratigraphic units correspond well to the biostratigraphic zones of Kitching and Raath (1984; Fig. 2.2), because the LEF contains the *Euskelosaurus* Range Zone, whereas the UEF comprises the *Massospondylus* Range Zone (see section on biostratigraphy below; Figs 2.2, 2.4; Bordy *et al*., 2004a).

2.3.2.1 Lower Elliot Formation (LEF)

A distinguishing regional feature of the LEF is the abundance of thick, cross-bedded, stacked channel sandstones relative to the overbank mudstones. The sandstone bodies often display incision and irregular, non-persistent erosion surfaces with lateral accretion surfaces being frequently developed. Additionally, the LEF mudstone facies are characteristically massive, rarely laminated and without major pedogenic alteration. The latter is mainly restricted to rare desiccation cracks, rare and isolated carbonate nodules as well as green and purple mottling in mudstones. For a detailed review, see Bordy *et al*. (2004c).

The up to ~20 m thick, asymmetrical, lenticular, stacked channel sandstones (sublitharenites) in the LEF are interpreted as products of a low sinuosity meandering fluvial system that originated in a source area to the south and south west in the Cape Fold Belt. These facies architectural characteristics coupled with the near absence of palaeosols/pedogenic horizons are interpreted by Bordy *et al*. (2004a) to be a result of high subsidence rates during the deposition of the LEF sediments.

2.3.2.2 Upper Elliot Formation (UEF)

In the field, the UEF is easily distinguished from the LEF based on the brick-red colouration of the mudstones, siltstones and dusty pink colouration of the fine to very fine sandstones. The sandstones are laterally continuous, thin sheet-like bodies that contain horizontal and ripple cross lamination or are internally structure-less (massive - Bordy *et al*., 2004a). Furthermore, the mudstone facies of the UEF is characterised by massive or finely laminated (Fm and Fl) units, often showing pedogenic alteration (e.g., desiccation cracks, slickenlines, discolouration/mottling), bioturbation and carbonate concretions (i.e., rhizoliths, rhizocretions and nodules). Subsidence rates during UEF deposition are considered low by Bordy *et al*. (2004a), based on the preservation of pedogenic nodules/alteration within mudstones, in addition to the tabular sandstones that suggest shallow scouring (i.e., no significant down-cutting). This, together with evidence for flashy discharge in the sandstones (e.g., frequent interbedding of desiccation cracks with upper and lower flow regime sedimentary structures) allow for the reconstruction of occasionally rapidly flowing, ephemeral, shallow and mainly unconfined sheets of water over a low-gradient regional palaeoslope (Bordy *et al*., 2004a). Provenance studies indicate that the subarkoses in the UEF were sourced from a south-westerly as well as westerly direction.

The *Tritylodon* Acme Zone (TAZ; Figure 2.4) or *Tritylodon* Assemblage Zone as it was first called, falls within the UEF. It was identified by James Kitching, mentioned with reference to the location of the Rooidraai dinosaur nest site within the UEF at Golden Gate National Park (Kitching, 1979), and later detailed in Kitching and Raath (1984) for biostratigraphic purposes. Despite the term ‘acme’, the zone is

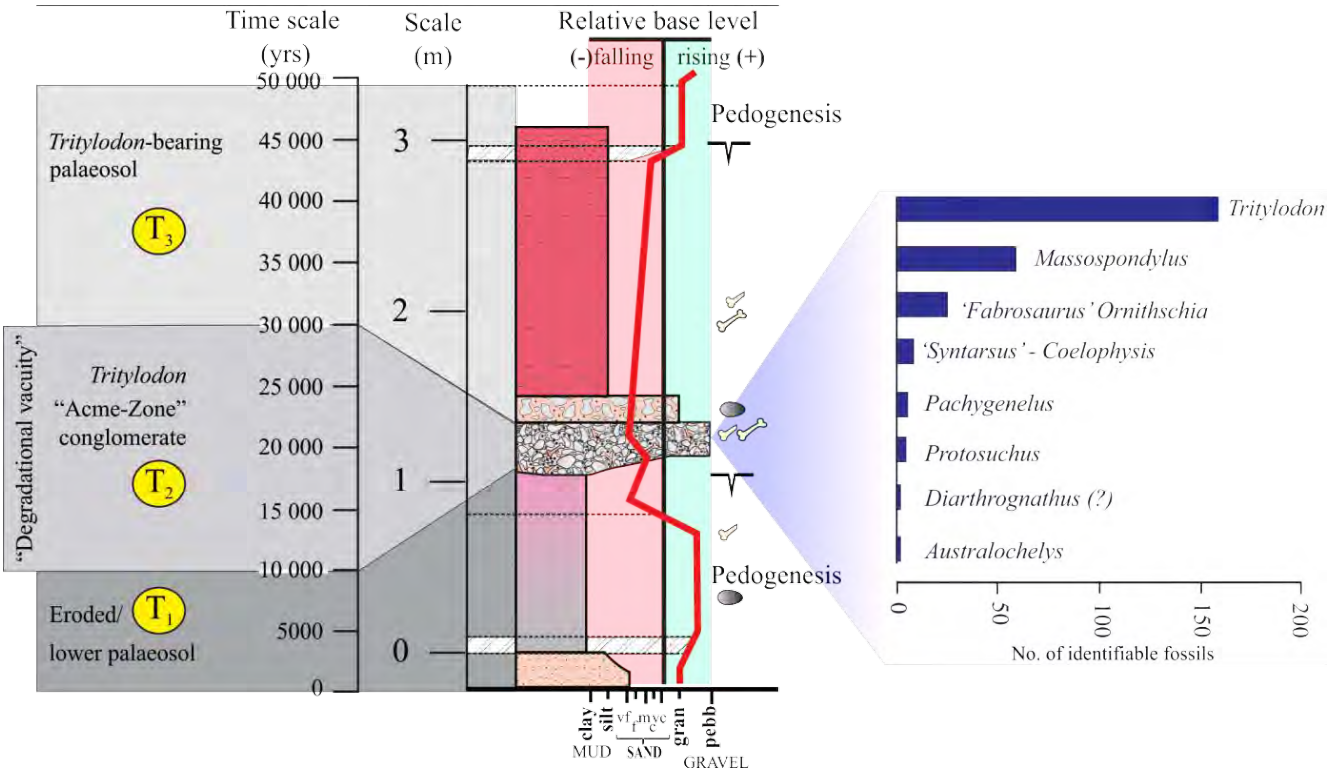

Figure 2.4. Summary of the development as well as sedimentological and palaeontological composition of the *Tritylodon* "Acme Zone" (TAZ) and associated lithofacies in the upper Elliot Formation in the north and north eastern parts of the main Karoo Basin. The illustration is based on the comprehensive account of the TAZ by Smith and Kitching (1997). Estimated rates of erosion and depositional were also taken from Smith and Kitching (1997).

assumed to represent a period of mass wasting and accumulation of reworked bone fragments, mostly of *Tritylodon sp.* remains as explained in the comprehensive account of Smith and Kitching (1997). This fossiliferous, pedogenic nodule conglomerate, with an average thickness of 1.25 m, occurs in the north and north eastern parts of the main Karoo Basin over an average area of 11 000 km^2. Due to its apparent lateral continuity, it has been considered to be a useful regional marker horizon in the northern and north-eastern part of the basin (Smith and Kitching, 1997). The TAZ lies within the *Massospondylus* Range Zone of the UEF, 1 – 3 m above a large nodule horizon which falls at the boundary between the *Euskelosaurus* and the *Massospondylus* Range Zones. The latter nodule horizon has been considered as the field guide for the position of the TJB (Smith and Kitching, 1997). The TAZ profile (Fig. 2.4) can be subdivided into 3 units which are the lower palaeosol, *Tritylodon* conglomerate and the upper palaeosol (Smith and Kitching, 1997). Time scales approximated, using estimated erosional rates of the Colorado River Basin, and constructed by Smith and Kitching (1997) for each unit range from 10 000 yr. for the lower palaeosol, 30 000 yr. for the *Tritylodon* conglomerate and 50 000 yr. for the sedimentation and

development of the upper palaeosol (Fig. 2.4). Smith *et al*. (2009) discuss semi-arid palaeosols, with typical paleopedogenic features such as those reported associated with TAZ as generally being formed within immature calcic vertisols.

More recently, the stratigraphic utility of the TAZ has been questioned, because systematic regional mapping that targeted the TAZ and associated lithofacies revealed that: (1) the TAZ is not traceable across the northern and north-eastern outcrop region; and (2) pedogenic nodule conglomerates associated with large nodule horizons can occur randomly and several times within one outcrop locality in the upper Elliot Formation (Moodley, 2015).

This is the most likely outcome when taking into consideration the formational history of TAZ. Smith and Kitching (1997) propose that the *Tritylodon* conglomerate formed as a response to rapid base level drop causing incision and gullying. This in itself would mean that the formation of the TAZ and the accumulation of the *Tritylodon* bones would be restricted to "donga" systems. These in themselves are laterally restricted. This however does not lessen the importance of the TAZ which, among others, represents a wealth of information on ecosystem dynamics during the upper Elliot Formation, including the appearance of new elements fauna (e.g. the oldest African turtle, *Australochelys africanus*).

2.3.3 **Age the Elliot Formation**

Based on the presence of globally comparable fossil material, for decades, the age of the Elliot Formations was determined to be Late Triassic (e.g., Du Toit, 1954; Romer, 1970; also see Kitching and Raath, 1984; Yates and Kitching, 2003). However, because the ages of different continental faunal assemblages mostly rest on global comparative studies, there have been numerous revisions of the relative ages of these assemblages as more numeric dates become available globally. Work in this regard is in progress, but to date, the diverse and abundant body and trace fossils assemblages of the Elliot Formation suggest an age range from upper Late Triassic (Norian/Rhaetian) to lower Early Jurassic (Toarcian) for the Formation (e.g., Kitching and Raath, 1984; Lucas and Hancox, 2001; Knoll, 2004, 2005).

No consensus has yet been reached regarding the placement of the TJB within the Elliot Formation. Smith *et al*. (2009) validate these points with their study of the Moyeni track site, an upper Elliot Formation locality (and thus considered to be Early Jurassic) but with several track-ways produced by taxa considered to be exclusively Triassic (chirotheroid-type forms). This allows debate concerning not only the age of the upper Elliot Formation (and indirectly the position of the TJB within it) but also the stratigraphic range of certain ichnotaxa.

To date, there are no published radiometric ages for the Elliot Formation; however, there are references to tuffs in Lesotho (Schmitz and Rooyani, 1987) and bentonite in South Africa (Fig. 2.3; Botha and Theron, 1967; Johnson, 1971). Several special reports, carried out by Willan (1976) and Reed (1976) in Lesotho (Figure 2.3)., identify these deposits as (1) vitric tuff interbedded with Elliot strata between Maseru and Teyateyaneng (Willan, 1976); (2) tuffaceous layers within sandstone interbeds in the Tsa-Kholo area (Reed, 1976); (3) montmorillonite clays near the Lesotho Sun Hotel in Maseru (Schmitz and Rooyani, 1987) as well as on the university campus in Roma. In the Eastern Cape Province of South Africa, the Pronksberg Mountain bentonite (Fig. 2.3) was first reported and described by Botha and Theron (1967) and revisited and sampled by Johnson (1971). It lies within the uppermost upper Elliot Formation, approximately 65 m below the contact with the overlying Clarens Formation and reaches a maximum thickness of ~2 m. Mineralogical studies reported in Horn and Strydom (1998) identify the presence on montmorillonite clays, small proportion of quartz (5%) and lesser amounts of cristobalite. As alluded to in Horn and Strydom (1998), the lack of further information on these volcanogenic layers is linked to their sub-economic potential.

The absence of radiometric dating, and the difficulty in locating the few, previously reported volcanogenic, potently *in situ* volcanic ash fall deposits within the Elliot Formation mean that there is little information to constrain its numeric age. The most proximal overlying radiometric date (183±1 Ma on the Toarcian-Pliensbachian boundary; Duncan *et al*., 1997; Hargraves *et al*., 1997) obtained from lavas interbedded with the uppermost Clarens Formation give an absolute uppermost age bracket to the Elliot Formation, meaning that the Formation cannot be younger than Toarcian (between 184 and 179 Ma; Duncan *et al*., 1997).

The uncertainty of the maximum age (lowermost constraint) of the Elliot Formation lies on the ambiguity of the age constraints of the Molteno Formation. A Carnian age has been ascribed to the Molteno Formation based on palynomorphs and palaeoflora (Anderson and Anderson, 1983, 1984; Anderson *et al.*, 1998, 1999). A stratigraphically equivalent Formation in the Karoo-aged basins of Zimbabwe (Pebbly Arkose Formation, Cabora Bassa Basin) also contain palynomorphs, palaeoflora and vertebrate fossils (*Hyperodapedon*) which also suggest a latest Carnian age (Raath *et al*., 1992; d'Engelbronner, 1996; Raath, 1996). Recently Barbolini (2014) reports on the first palynomorphs to be extracted from the Stromberg, thus providing the first insight into the palynofloras and relative age of the formation. These palynomorphs were not age diagnostic enough to give a more tightly constrained age on the formations other than Late Triassic - Early Jurassic.

3 Triassic-Jurassic fossil groups and biostratigraphic dating of the Elliot Formation

The Triassic, in addition to heralding the rise of a number of groups that retain ecological prominence to this day, is also popularly known for the group that originated within its later stages, the Dinosauria. In comparison to marine palaeo-ecosystems, the rise and diversification of this lineage is complicated by various factors, one such being the temporal resolution that vertebrate fossils can offer for the reconstruction of geological history (Barrett *et al*., 2009). Consequently, the end-Triassic extinction event was initially thought to represent a faunal turn-over of greater magnitude than that of the end-Permian or end-Cretaceous (Colbert, 1958; Olsen and Sues, 1986).

Within the Karoo Basin, the fossiliferous fluvio-lacustrine-aeolian Stromberg Group is of key importance to understanding the transition from the numerical dominance of therapsids (or non-mammalian synapsids, informally called mammal-like reptiles) at the Permo-Triassic boundary, to the global radiation of the earliest dinosaurs and mammals in the Late Triassic and Early Jurassic. Within the Elliot Formation, this radiation is often characterized as occurring in two temporally distinct phases, with Haughton (1924) being one of the first to notice the change from large bodied sauropodomorph dinosaurs at the base of the formation, to smaller, more gracile forms at the top. He attributed this to aridification of the climate with more agile, small-bodied animals able to survive under increasingly unfavourable conditions. The change from larger- to smaller-bodied dinosaurs within the Elliot Formation strata is being questioned nowadays as larger bodied forms have been recently found in the upper Elliot Formation as well (e.g., 'The Highland Giant' site on Beghensle Farm; 'Mark's quarry' on Spionkop Farm, Yates *et al*., 2010; McPhee *et al*., 2015a) or their previous position within the stratigraphy is being argued (e.g., current investigations show that an upper instead of lower Elliot provenance for the *Antetonitrus* specimen of Yates and Kitching, 2003 – Sciscio *et al*., in prep.).

The first comprehensive range chart for continental vertebrates (excluding fish) of the Late Triassic-Early Jurassic were compiled by Olsen and Galton (1977). It was from this work that Olsen *et al*. (1982) assigned a Norian-Rhaetian age for the lower Elliot Formation. These opinions were revisited by Olsen and Galton (1984) who conducted a comprehensive comparison of the vertebrate and ichnofossils of the Elliot Formation to those in the continental Triassic-Jurassic of Europe, China and North America (Chinle and Newark basins). At the time, the known vertebrate diversity within the lower Elliot Formation was low, but due to the narrow ranges of some key families and taxa (e.g., a possible rauisuchid, and

Scalenodontoides macrodontes ~Norian; Hopson, 1984), a Carnian or Norian age was assigned to the unit. Cross-correlation via radiometric dates and palynology from sections with marine invertebrates was attempted by the same authors.

In terms of trackways, the Elliot Formation presents an extensive array of sites which were brought to light and initially studied by the Ellenberger brothers for three decades from the 50's to the 70's, and then published in monograph-type works by P. Ellenberger in 1970, 1972, and 1974. The age assessment of the Stromberg Group given by Ellenberger (1970) was refined by Olsen and Galton (1984). They were able to assign a late Triassic Norian age (albeit because of no recognised Rhaetian stage) to the tracks in lower Elliot Formation and, and an early Jurassic age to those in the Upper Elliot and Clarens Formations through the comparisons of vertebrate trackways of the Newark Supergroup (USA).

3.1 Biostratigraphy of the Elliot Formation, Karoo Basin

The first comprehensive stratigraphic subdivision of the Stormberg Group is based on work by Ellenberger (1970), which was then refined by Kitching and Raath (1984) (Fig. 3.1). This subdivision was based not only on sequential changes in the composition of the faunal assemblages, but also on the differential lithostratigraphic qualities present in each of their proposed units (Fig. 3.1).

Ellenberger's (1970) work on the Molteno, Elliot and Clarens Formations in Lesotho contains a wealth of information detailing their ichnological, palaeontological and palaeobotanical interpretations. Several zones were created for the Stormberg Group in its entirety, with the lower Stormberg Group (Molteno and lower Elliot Formation) being broken into zones A1 – A7, and the upper Elliot and Clarens Formation comprising zones B1- B7. The Elliot Formation represents zones A4 – A7 and B1 – B3 for the upper and lower parts, respectively (Fig. 3.2). Typically these zonations are largely based on ichnofossils and less on tangible field evidence and therefore field-based utility of these zones is difficult.

Kitching and Raath (1984), with the introduction of their twofold biozonation, offered a simpler subdivision of the Elliot Formation into two biostratigraphic range zones. The lower one, the *Euskelosaurus* Range Zone, was confined entirely to the lower Elliot Formation (Fig. 3.1, Fig. 3.2) whereas the *Massospondylus* Range Zone captures the upper Elliot (Fig. 3.1, Fig. 3.2).

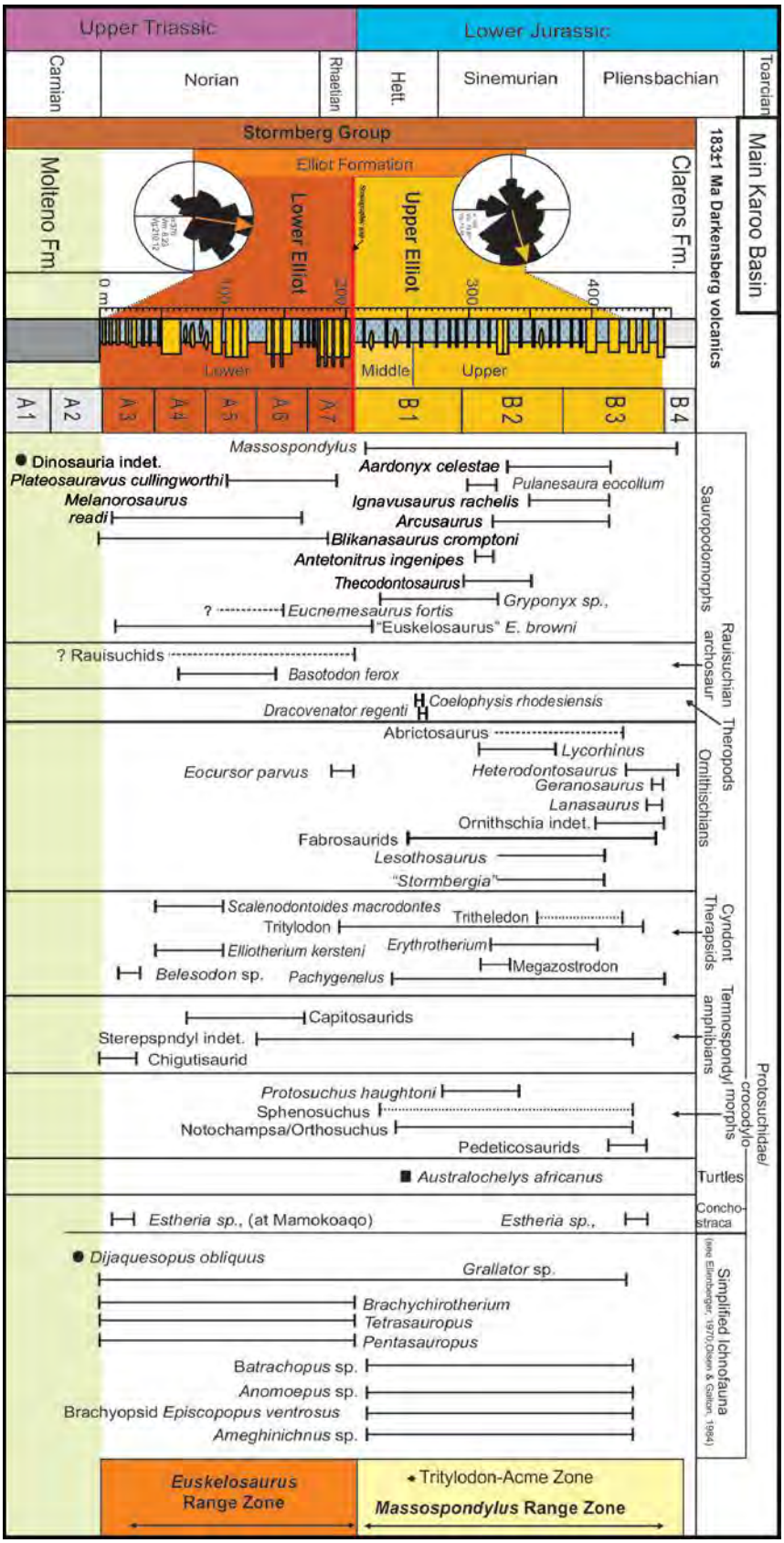

Figure 3.1. Biostratigraphy of the Elliot Formation, based on revisions of palaeontological papers with additional discoveries/new information as well as the reviews of Kitching and Raath (1984), Olsen and Galton (1984), Lucas and Hancox (2001) and Bordy *et al.* (2004a). The sedimentary log is the simplified holostratotype section of the Elliot Formation in the Barkly Pass (Eastern Cape; S31°15'23", E27°49'45"). The section was measured by Visser and Botha (1980; Figure 2) and modified by Bordy and Eriksson (2015). Range zones of Kitching and Raath (1984) and Zones A- B of Ellenberger (1970) are taken into consideration.

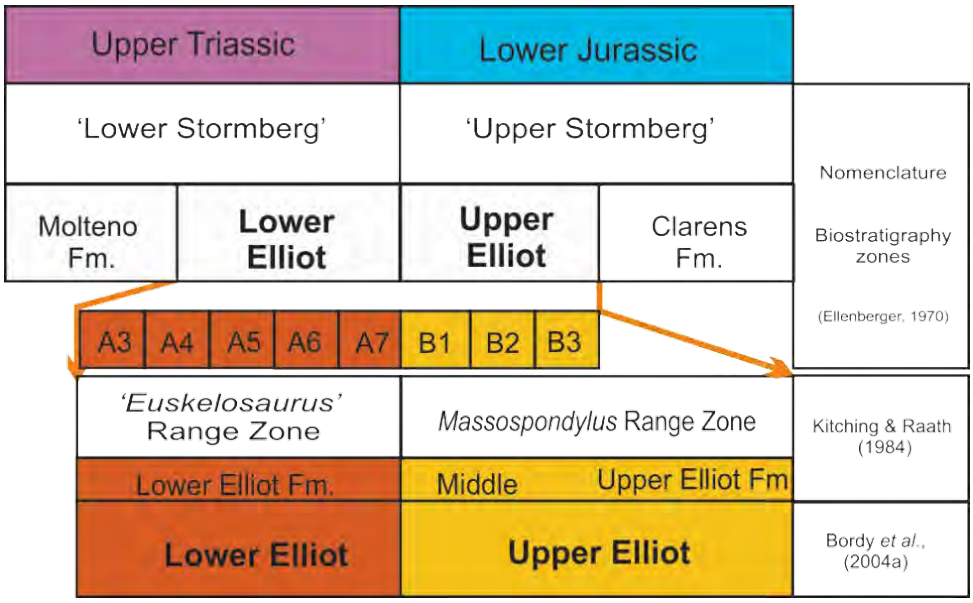

Figure 3.2. Biostratigraphic and lithostratigraphic subdivisions of the Elliot Formation. Ellenberger's (1970) zones A3 – A7 and B1 – B3 are for the upper and lower Elliot Formation respectively with the larger subdivision of the lower and upper Stormberg used by Olsen and Galton (1984). New biostratigraphic zonation of Kitching and Raath (1984) also considered the sedimentological break-down of the Elliot Formation by Visser and Botha (1980) which has been reassessed by Bordy *et al.* (2004a).

This was further refined by extensive sedimentological work of Bordy *et al.* (2004a, b, c) who established that Ellenberger's (1970) zones A4 – 6(7) and *Euskelosaurus* Range Zone of Kitching and Raath (1984) represented the lower Elliot Formation, whereas zones B1 – 3 of Ellenberger (1970) and the lower two-thirds (excluding the Clarens) of the *Massospondylus* Range Zone of Kitching and Raath (1984) belong to the upper Elliot Formation (Fig. 3.1, Fig. 3.2).

3.2 *"Euskelosaurus"* Range Zone

The lower Elliot Formation is generally characterized by the occurrence of large-bodied sauropodomorph dinosaurs and biostratigraphically separated from the upper Elliot Formation by the last occurrence of the prosauropod '*Euskelosaurus browni*' (Fig. 3.1). In addition to issues of diagnosability, '*Euskelosaurus*' was treated as something of a 'waste-basket' taxon throughout the twentieth century and is now

considered a *nomen dubium* (see Yates, 2003; Yates and Kitching, 2003). However, the name is still currently retained for the Range Zone

Fauna which typify the "*Euskelosaurus*" Range Zone are less diverse than that of the upper Elliot Formation and are listed below:

(i) Basal sauropodomorphs: *Blikanasaurus cromptoni* (Galton & van Heerden, 1985); *Melanorosaurus readi* (Haughton 1924, Yates, 2007a)*; Plateosauravus cullingworthi*, and *Eucnemesaurus fortis* (was *Aliwalia rex*) (Yates, 2007b), *Eucnemesaurus* spp. The former two are the oldest known sauropodomorphs in the Formation. NB: *Antetonitrus ingenipes* was proposed by Yates and Kitching (2003) as being from the uppermost LEF. However, recent field work has revealed that the saddle in which the holotypic assemblage was originally excavated actually lies within the upper Elliot Formation (middle to uppermost upper Elliot Formation) (Sciscio *et al*., in prep.).

(ii) Basal ornithischians: *Eocursor parvus* (Butler *et al*., 2007; Butler, 2010). Detailed stratigraphic investigation of the fossil locality, aided by the log provided by Butler *et al*. (2007, supplementary material), suggests that the fossil may have been collected from beds of the lowermost upper Elliot Formation (McPhee *et al*., in prep).

(iii) Diapsida: Rauisuchian archosaur – diagnosed largely through the number of crenulated teeth and osteoderms found in the lowermost LEF (Hopson 1984; Galton and Van Heerden 1998); *Basutodon* (Haughton, 1924; Kitching and Raath, 1984; Galton and Van Heerden, 1998; Lucas and Hancox, 2001).

(iv) Cynodonts: traversodontids *Scalenodontoides macrodontes* (Crompton and Ellenberger, 1957); and tritheledontids *Elliotherium kersteni* (Sidor and Hancox, 2006);

(v) Temnospondyl amphibians: large chigutisaurid BP/1/5252; BP/1/4750; BP/1/4935 (*Sterospondyli* indet.) (Warren and Damiani, 1999; Steyer and Damiani, 2005)

(vi) Ichnofauna: *Brachychirotherium*, *Pentasauropus*, *Tetrasauropus* and *Grallator* sp.

The two most abundant groups within the lower Elliot Formation are basal Sauropodomorpha (4 valid genera; if disregarding *Antetonitrus* as a LEF taxon) followed by the cynodonts. The only known lower Elliot Formation theraspids are the traversodontid *Scalenodontoides macrodontes* (Crompton and Ellenberger, 1957; Hopson, 1984; Gow and Hancox, 1993; Knoll, 2004), the tritheledontid *Elliotherium kersteni* (Sidor and Hancox 2006), and a diademodontid BP/1/5724 (Abdala *et al*., 2007). The

stratigraphic position of the latter as well as its identity is currently debated (Abdala personal communication, 2015 and Sciscio *et al*., in prep).

3.2.1 **Global correlatives of the lower Elliot Formation**

Detailed evaluations of the LEF body and trace fossil taxa and their comparisons to the global Upper Triassic and Lower Jurassic global record can be found in the comprehensive reviews of Olsen and Galton (1984; in conjunction with ichnofauna) and Knoll (2004, 2005). These works express a wide disparity of age determinations for the lower Elliot Formation, ranging from the Norian to the Early Jurassic.

Based primarily on a refinement of Ellenberger's (1970) initial work, ichnological studies on the lower Elliot Formation by Olsen and Galton (1984) suggests the presence of commonly occurring Late Triassic forms, which are prominent globally (i.e., Newark Supergroup, USA; Rhaeto-Liassic, France), as well as one Early Jurassic form. The former are tracks of Brachychirotheriids and *Pentasauropus* (dicynodont attributed) which closely resemble Carnian-Norian North American forms (Gettysberg Shale, Newark Supergroup; Olsen and Galton, 1984). More recently, however, *Pentasauropus jaquesi* has been referred to as *Lavinipes cheminii* from northern Italy which is credited to basal sauropods (D'Orazi Porchetti and Nicosia, 2007). In comparison, *Tetrasauropus* most closely resembles, according to Olsen and Galton (1984) and D'Orazi Porchetti and Nicosia (2007) *Navahopus* of the Lower Jurassic Navajo Sandstone Formation (Glen Canyon Group). The dating of the former is based on palynofloras, whereas the dating of the latter is relative insofar as it is based on radiometric dating of its lateral correlative, the Aztec Sandstone Formation (southern Nevada; Rowland and Mercadante, 2014). The radiometric dates, obtained from interbedded volcanic units, yielded an age between 174.1 ± 0.4 and 182.7 ± 0.5 Ma for the Aztec Sandstone Formation (Ogg and Hinnov, 2012) and thus placing it and the Navajo Sandstone Formation ichnofauna (*Navahopus* and its LEF correlative, *Tetrasauropus*) into the Early Jurassic (Toarcian). Furthermore, trackways of *Brasilichnium* and their trackmakers (likely tritylodontid cynodonts) from the Aztec and Navajo Sandstone Formations are found in other Gondwanan locations of Sinemurian-Pliensbachian age (e.g., Brazil; Rowland and Mercadante, 2014) and in southern Africa (Lockley, 1991). Finally, in conjunction with ichnofaunal interpretation and body fossils of basal sauropodomorphs, rauisuchid archosaurs and cynodonts (*Scalenodontoides*), Lucas and Hancox (2001) suggested a Norian age for the LEF.

The two most prominent LEF fauna, being Cynodontia and basal Sauropodomorpha are further reviewed below with reference to the global occurrence of similarly composed faunas. Sauropodomorphs constitute the most diverse and abundant body fossils of the Late Triassic (Irmis, 2010). The continental Argentinian Ischigualasto–Villa Union Basin is particularly famous for its early dinosaur assemblages that are generally thought to span the Carnian to lower Norian of the Late Triassic (Figure 3.3). Within this succession, the Los Colorados Formation preserves an assemblage of sauropodomorph dinosaurs that closely resembles the variation contained within the LEF. This includes the putative massospondylid *Coloradisaurus* (Apaldetti *et al*., 2013, 2014), the abundant *Riojasaurus* (Bonaparte, 1971), and the near-sauropod *Lessemsaurus* (Pol and Powell, 2007). Of these taxa, *Riojasaurus* has recently been suggested as sharing a possible sister-taxon relationship with the LEF taxon *Eucnemesaurus* (see Yates, 2007b; McPhee *et al*., 2015a), while *Antetonitrus* has consistently been recovered as the sister taxon to *Lessemsaurus* in every analysis that has included both taxa (e.g., Yates 2007b; Apaldetti, 2011; McPhee *et al*., 2014). The uppermost Los Colorados Formation, as well as the Quebrada del Barro Formation of the Marayes-El Carrizal Basin (Martínez *et al*., 2015) also contains crocodilomorphs (protosuchids and sphenosudchids) as well as fragmentary remains of rauisuchids (Arcucci *et al*., 2004), which further resemble the diversity represented in the LEF.

In the Argentinian Ischigualasto–Villa Union Basin, the base of the Ischigualasto Formation is dated at 231.4±0.3 Ma based on the geochronological age of Herr Toba bentonite in the lowermost part of the Formation (lower La Peña Member, Figure 3.3; Olsen *et al*., 2011; Martínez et *al*., 2011; Ramezani et *al*., 2014). According to Olsen *et al*. (2011), when compared to the Newark-APTS 2010, this age falls within the magnetochron E6 close to the Carnian-Norian boundary. The latter boundary has been recently moved to ~227 Ma (Figure 3.3; International Chronostratigraphic Chart 2015).

The relative age of the base of the Los Colorados Formation comes from $^{40}Ar/^{39}Ar$ dating of the underlying Valle de la Luna Member in the uppermost Ischigualasto Formation (Figure 3.3). These dates are from Shipman's (2004) unpublished dissertation cited in Ramezani *et al*. (2014), as well as Martínez *et al*. (2011), and are given as 217.0±1.7 Ma and 225.9±0.9 Ma, respectively. Although there is an age discrepancy of ~8 million years, these dates have both been obtained from beds of the upper Valle de la Luna Member, and are likely to indicate either the low-precision methods of $^{40}Ar/^{39}Ar$ dating, the complexity in underpinning a central age-date plateau, or other sedimentological complications such as a strongly diachronous Formation with many paraconformities which are difficult to detect in isolated outcrops.

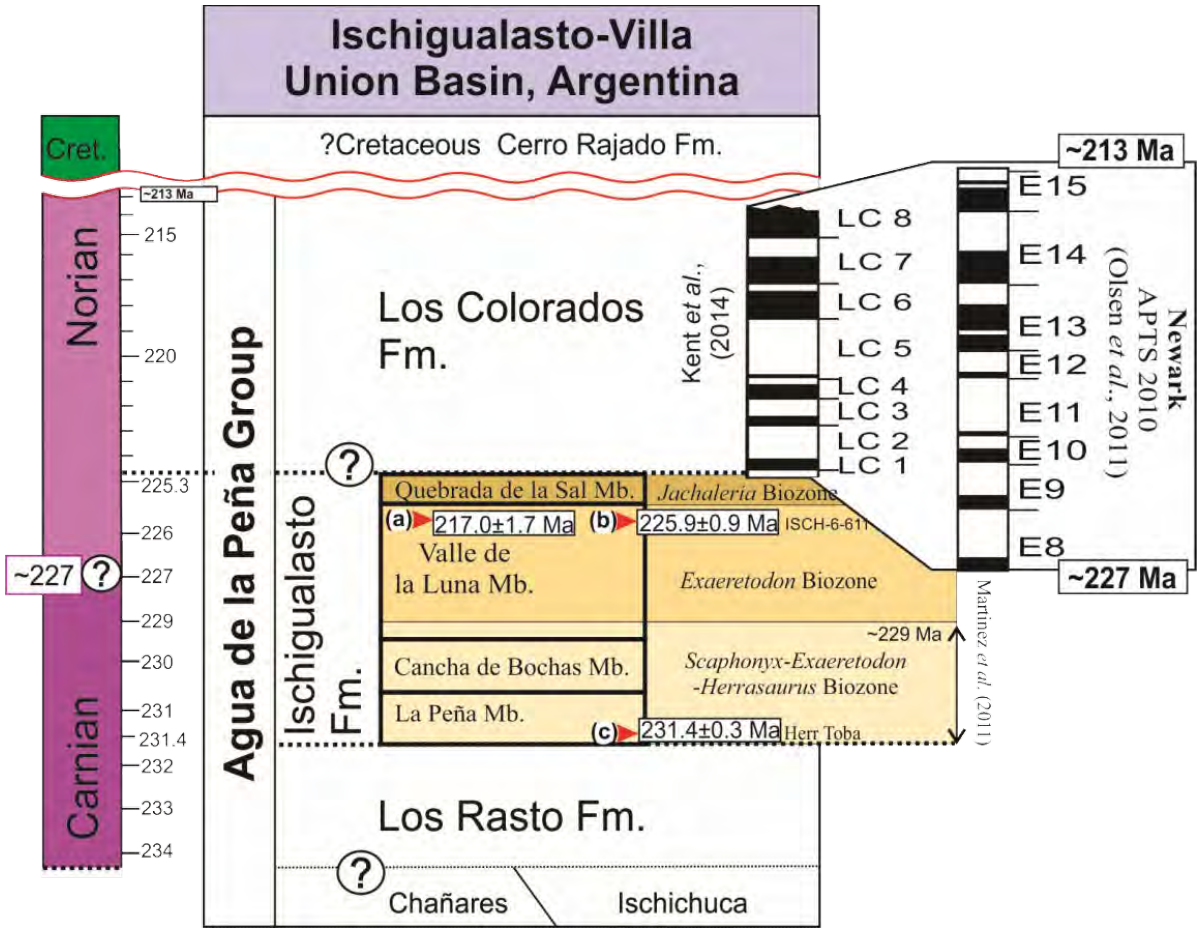

Figure 3.3. Chronostratigraphy of the Agua de la Peña Group, Ischigualasto-Villa Union Basin. Ischigualasto Formation: (a) $^{40}Ar/^{39}Ar$ date of the Valle de la Luna Member (feldspars): 217.0±1.7 Ma by Shipman (2004); (b) $^{40}Ar/^{39}Ar$ date of the Valle de la Luna Member (ISCH-6-611): 225.9±0.9 Ma by Martínez *et al.* (2011); (c) $^{40}Ar/^{39}Ar$ date of the La Peña Member (Herr Toba bentonite): 231.4±0.3 Ma (1σ total error) by Martínez *et al.* (2011). Los Colorados Formation: magnetostratigraphy of the unit and its correlation to the Newark APTS 2010 (astronomic polarity timescale) suggest that the base of the Formation is at ~227 Ma (Kent *et al.*, 2014). This implies that the upper Ischigualasto Formation and the base of the lower Los Colorados Formation overlap by at least 2 million years. Also note that the Los Colorados Formation does not extend to the base of the Jurassic, so the fauna in its upper part is not latest Triassic.

Furthermore, the $^{40}Ar/^{39}Ar$ age (225.9 ± 0.9 Ma) provided for the uppermost Valle de la Luna Member by Martínez *et al.* (2011), has several large-ranging plateau dates (226±6.46 Ma - 218.07±6.72 Ma), underscoring the uncertainties surrounding the preferred age and potentially explaining the discrepancy with the overlying magnetostratigraphy of the Los Colorados Formation (Fig. 3.4). The discrepancy between the ages within and between the underlying Ischigualasto Formation and the overlying Los Colorados Formation complicates the task of correlating between globally-separated deposits.

Recent magnetostratigraphic work in the Los Colorados Formation and its suggested correlation to the Newark APTS 2010 (Newark magnetochrons E7r and E14) by Santi Malnis *et al*. (2011) provide an age range of ~227.5 to ~215 Ma for the Formation (Fig. 3.3, Fig. 3.3). Santi Malnis' *et al*. (2011) Quebrada de la Sal section starts within the Valle de la Luna Member ash bed, dated at 225.9±0.9 Ma by Martínez *et al*. (2011), in the underlying Ischigualasto Formation.

A more recent magnetostratigraphy of the Los Colorados Formation and its correlation with the Newark APTS 2010 (Newark magnetochrons E7r and E15n) was conducted by Kent *et al*. (2014), who provided an age range of ~ 227 Ma, to ~213 Ma for the formation (Fig. 3.4). These results tie closely with that of Santi Malnis *et al*. (2011) and suggest that the Los Colorados Formation does not record the last 13 million years of the Triassic nor the Triassic-Jurassic boundary.

Consequently, its fossil assemblages are not representative of the latest Triassic contra Arcucci *et al*., (2004)/Horn *et al*. (2014). In light of the fact that the Los Colorados Formation is often argued to contain a fossil vertebrate assemblage similar to the LEF in the Karoo Basin (Arcucci *et al*., 2004; McPhee *et al*., 2014), the unexpectedly early age-determinations inferred for the formation has major implications not only for south-western Gondwanan correlation generally, but also for the highly scrutinized faunal diversification and turnover (e.g., rate, magnitude) associated with the TJB event. The supposed correlation between the fauna in the lower Elliot and that of the Argentinean section could also rest on the stratigraphic misplacement of some forms, e.g. the sauropodomorph, *Antetonitrus* (Yates and Kitching, 2003), of the Edelweiss 698 site. The recent doubts surrounding the stratigraphic provenance of *Antetonitrus* will have direct bearing on future discussions pertaining to the supposed correlation between the LEF and Los Colorados (Sciscio *et al*., 2015; McPhee *et al*., 2015a).

It is worth noting, however, the apparent discrepancy in the chosen starting-point of the Santi Malnis *et al.* (2011) section versus that of Kent *et al*. (2014). Santi Malnis *et al*. (2011) section appears to start at the radiometrically dated ash bed (225±0.9 Ma via recalculated $^{40}Ar/^{39}Ar$; Martínez *et al*., 2011; Fig. 3.4) in the underlying Valle de la Luna Member of the Ischigualasto Formation; whereas Kent *et al.* (2014) start their section at the base of the Los Colorados Formation – or at least at the change in coloration between the underlying Ischigualasto and Los Colorados Formations. This apparent inconsistency potentially problematizes the task of correlating both sections to one another and to other sections globally.

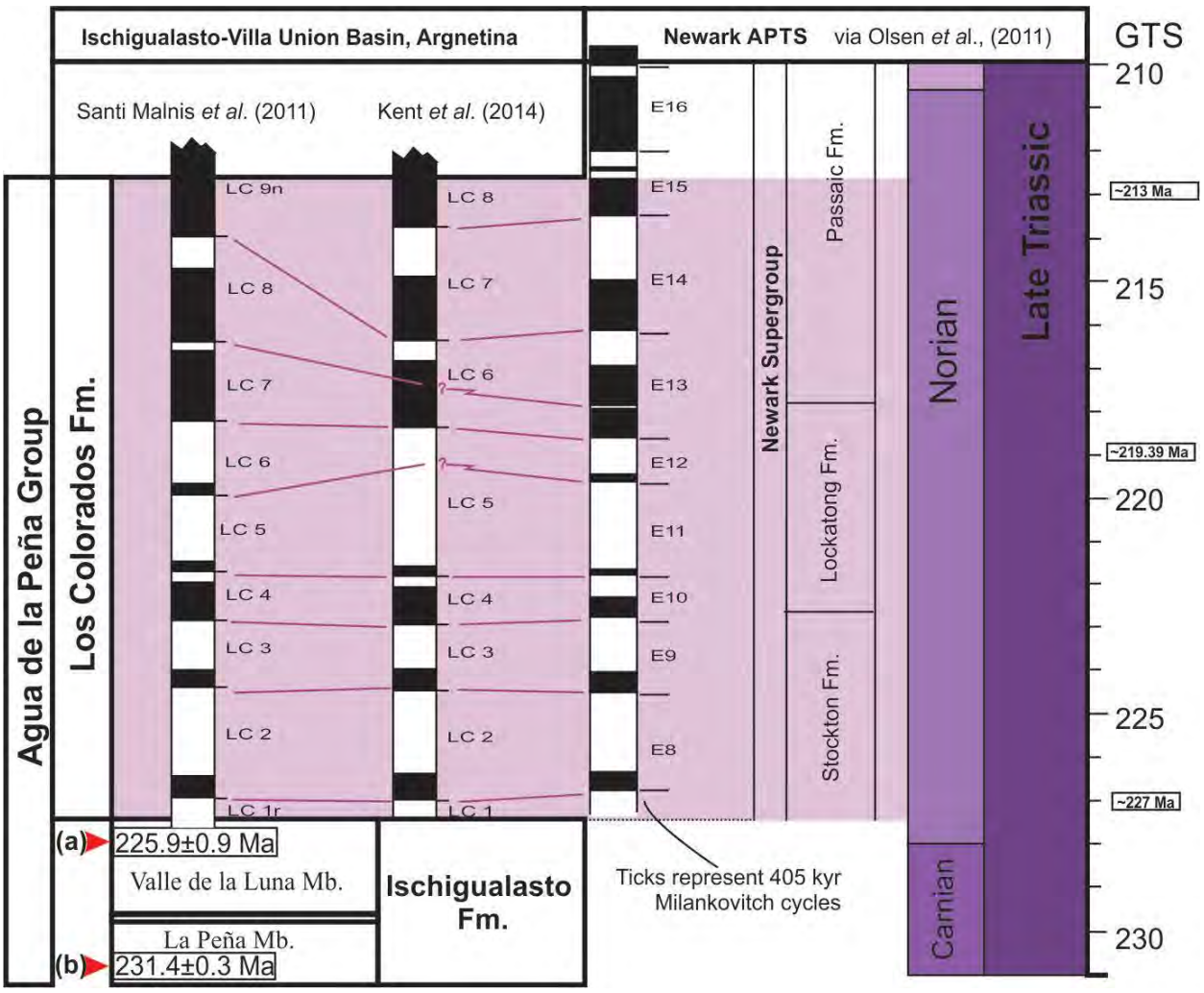

Figure 3.4. Comparison of magnetostratigraphic correlations of the Los Colorados Formation (Ischigualasto-Villa Union Basin, Argentina) of Santi Malnis *et al*. (2011) and Kent *et al.* (2014) to the Newark Basin astronomic polarity timescale APTS and the International Chronostratigraphic Chart2015 (stratigraphy.org). (a) denotes dated ash bed (225±0.9 Ma via recalculated $^{40}Ar/^{39}Ar$; Martínez *et al*., 2011) in underlying Valle de la Luna member, Ischigualasto Formation, and the stratigraphic level at which the Santi Malnis *et al*. (2011) magnetostratigraphic section starts. (b) Herr Toba bentonite age date (231.4±0.3 Ma; Martínez *et al*., 2011) encapsulates the lowermost age for the Ischigualasto Formation

Recently, Ramezani *et al*. (2014) and Kent *et al*. (2014) reviewed the position of the Los Colorados Formation relative to the Chinle Formation of southwestern USA and the Newark APTS (Fig. 3.4). Current geochronological work within the Chinle Basin (Colorado Plateau, USA) and within the Chinle Formation itself has allowed for the construction of a high resolution U-Pb zircon chronostratigraphy (Ramezani *et al*., 2011; Atchley *et al*., 2013; Ramezani *et al*., 2014) from several tuffaceous beds of this unit. As a result, the Chinle Formation is closely and independently tied to marine based Triassic correlations globally. The lowermost age constraint of the Chinle Formation (within the Mesa Redondo

Member) lies at the Carnian-Norian Boundary at ~227 Ma (see IUGS2015 Triassic time scale - stratigraphy.org). The uppermost dated bed (< 207.8 Ma) in upper Petrified Forest Member places the upper Petrified Forest, Owl Rock, Rock Point Members into the Early Rhaetian (see Fig. 2 of Ramezani *et al*., 2014). Furthermore, the U-Pb ID-TIMS age of Ramezani *et al*. (2014) for the Blue Mesa Member is 219.39±0.16 Ma helps constrain the well-known *Placerias* Quarry fauna.

These new U-Pb dates and magnetostratigraphic results have provided further evidence for a casual stratigraphic link between the LEF, the Los Colorados Formation of Argentina and the Chinle Formation in the USA. The noted similarities in fossil constituency between the Los Colorados Formation and the LEF, in association with new age determinations for the Chinle Formation, suggests an age-range for the LEF from anywhere within ~227 to ~201 Ma (Norian to Rhaetian).

This suggests that if the lower to middle LEF and the Los Colorados Formation are correlatives, having been deposited from ~227 to ~213 Ma, they may also represent potential age equivalents of the lower Chinle Formation (Mesa Redondo, Blue Mesa and lower Sonsela Members). Similarly, the upper part of the LEF may be correlated with upper Sonsela, Petrified Forest, Owl Rock and Rock Point Members of the upper Chinle as well as the overlying Moenave Formation in the USA. However, if we consider the Carnian age of the underlying Molteno Formation (Anderson, 1974; Anderson and Anderson, 1970, 1983, 1995, 1998), in conjunction with the unconformity at the base of the LEF (Bordy *et al*., 2005), and the 'floating' lowermost age of the LEF (loosely taken at *ca*. 215 Ma [Halbrich *et al*., 1983]), the base of the LEF appears as slightly younger in age. Consequently, the LEF would only correspond to (a) the uppermost part of the Los Colorados Formation of Argentina, (b) units younger than 215 Ma in the upper Chinle Formation, and (c) the overlying Moenave Formation (Fig. 3.5; and see Fig. 2 of Ramezani *et al*., 2014).

In terms of the traversodont cynodonts, Hopson (1984) suggested contemporaneous occurrence of basal Elliot Formation fauna with those of the Canadian Burntcoat fauna which occur within the Wolfville Formation, Fundy Group, Newark Supergroup. Hopson (1984) considered these fauna to be at least Early Norian in age (Fig. 3.5), an age estimate in close agreement with the new ages of Ramezani *et al*. (2014).

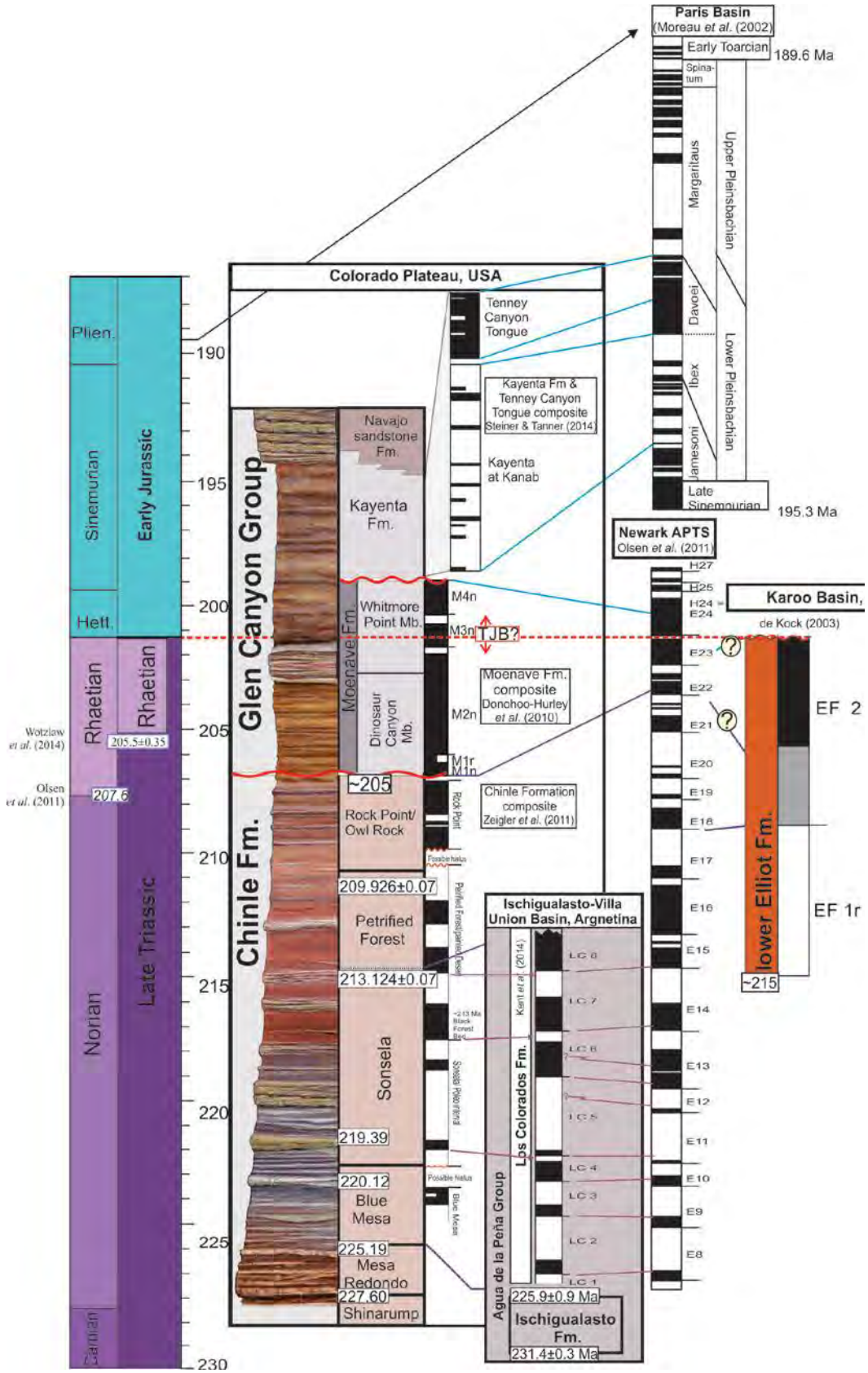

Figure 3.5. Late Triassic/ early Jurassic comparisons between the Chinle Formation, Glen Canyon Group, Los Colorados Formation and the Elliot Formation with all available radiometric and magnetostratigraphic sections. Radiometric dates from the Chinle are from Ramezani *et al.* (2011, 2013). Moenave Formation magnetostratigraphy and correlation to the Newark APTS is after Donohoo-Hurley *et al.* (2010). Los Colorados magnetostratigraphy and correlation is after Kent *et al.*, (2014). The magnetostratigraphy of lower Elliot Formation is taken from de Kock (2003). The Chinle lithological log is modified from http://www.nps.gov/pefo/learn/nature/geologicformations.htm.

With respect to the palaeobotanical record, the LEF does not provide age constrains. While Bordy *et al*. (2004b) reported on fossil wood fragments and charcoal in channel lags collected and present at several southern LEF outcrops, these were not age diagnostic (Bamford personal communication). Barbolini (2014) has conducted the first palynological study of the Elliot Formation and reports the presence of the following palynomorphs in the LEF: *Dictyophyllidites mortonii*, *Lacrimasporonites levis* and *Uvaesporites verrucosus*. These forms are present in China, New Zealand and Australia and do not provide any tight constraints of age other than spanning the Late Triassic – Early Jurassic. *Dictyophyllidites mortonii* seems, based on associations within underlying older Karoo strata (Katberg and Molteno Formation), to represent a long ranging Triassic form. The presence of *Lacrimasporonites levis* and *Uvaesporites verrucosus* are relatively short ranging taxa present in both the LEF and UEF, with the latter also occurring within the Molteno Formation. This ultimately renders use of palynology within the LEF, at this early stage, impractical.

3.3 Massospondylus Range Zone

The upper Elliot Formation (Bordy *et al*., 2004, a, b) is biostratigraphically referred to as *Massospondylus* Range Zone (Fig. 3.1, Fig. 3.2) and is distinguished from the lower Elliot Formation by the occurrence and dominance of the small-bodied prosauropod *Massospondylus carinatus* (Kitching and Raath, 1984).

Within its lower part, the *Massospondylus* Range Zone contains the *Tritylodon* Acme Zone (TAZ) (also defined in the Geological background chapter) which was named for *Tritylodon sp.*, a tritylodontid cynodont that was originally described from Wurttemberg (Germany) from “Rhaeto-Liassic” bonebeds (containing haramiyids, tritylodontids, and plateosaurs*;* Clemens, 1980; Olsen and Glaton, 1984). *Tritylodon* provides aids in the supposition of an Early Jurassic age to the lower half of the UEF (Smith and Kitching, 1997).

The *Massospondylus* Range Zone is typified by the following vertebrate fauna (Fig. 3.1):

(i) Sauropodomorphs: *Massospondylus carinatus* (Yates and Barrett, 2010), *M. kaalae* (Barrett, 2009), *Aardonyx celestae* (Yates *et al*., 2010), *Pulanesaura eocollum* (McPhee *et al*., 2015b) and potentially *Antetonitrus ingenipes* (Yates and Kitching, 2003). The latter was previously assigned to the LEF, however its exact stratigraphic position is debated and the excavation pit is considered an upper Elliot Formation site. *Ignavusaurus rachelis* (Knoll, 2010; although Yates *et al*. (2011) question as to whether it is a juvenile *Massospondylus*)

(ii) Non-plateosaurian sauropodomorph: *Arcusaurus pereirabdalorum* (Yates *et al*., 2011)

(iii) Basal ornithischians: Heterodontsaurids: *Heterodontosaurus tucki*, *Lycorhinus sp., and Abrictosaurus consors. Geranosaurus atavus and Lanasaurus scalpridens* as nomen dubium (?). 'Fabrosaurs': *Lesothosaurus diagnosticus* and *Stormbergia dangerhoeki* (the latter possibly being synonymous with *Lesothosaurus*, see Knoll *et al*. 2010).

(iv) Theropods: *Coelophysis* (= '*Megapnosaurus*') *rhodesiensis* (was *Syntarsus rhodesiensis*; Raath, 1980), *Dracovenator regenti* (Yates, 2005b)

(v) Non-mammaliaform cynodonts: tritheledontids (e.g., *Pachygenelus sp., Tritheledon riconoi, Diarthrognathus broomi*) and tritylodontids (e.g., *Tritylodon sp.;* Sidor and Hancox, 2006; Abdala *et al*., 2007).

(vi) Mammaliaformes: Morganucodontidae *Erythrotherium parringtoni* (Crompton, 1964); the Megazostrodontidae *Megazostrodon* (Crompton and Jenkins, 1968).

(vii) Temnospondyl amphibians: large Chigutisauridae BP/1/5252; BP/1/4750; BP/1/4935 (Stereospondyli indet.) (Warren and Damiani 1999) and well as giant Brachyopidae (Steyer and Damiani, 2005)

(viii) Protosuchidae: *Protosuchus haughtoni* (synonymous with holotype *Baroqueosuchus haughtoni*; Busbey and Gow, 1984; Gow, 2000); Crocodylomorphs: *Sphenosuchus*, *Protosuchus*, *Litargosuchus*, *Notochampsa* and *Orthosuchus* (Nash, 1975; Busby and Gow, 1984; Knoll, 2005).

(ix) Testudinata (Turtle)*: Australochelys africanus* (Gaffney and Kitching, 1994, 1995).

(x) Fish: *Seminotus capensis* (Ambrose, 1991; Jubb, 1973).

(xi) Spinicaudata (Conchostraca; Tasch, 1984).

(xii) Globally correlative ichnofauna: *Otozoum* (*Kalosauropus*, Ellenberger, 1970) sp., *Batrachopus* sp., *Anomoepus* sp. (*Moyenisauropus*), *Ameghinichnus* sp., *Trisauropodiscus*, *Episcopopus ventrosus* and *Grallator* sp. For a more comprehensive list of ichnofauna please see Ellenberger (1970), Olsen and Galton (1984), Rainforth (2001, 2003) and Knoll (2005).

3.3.1 **Global correlatives of the upper Elliot Formation**

Much as is the case with the LEF, age estimates for the UEF have primarily been drawn from global biostratigraphic correlations with formations displaying a similar faunal assemblage to that of the UEF. Regionally, the fauna of the UEF and lowermost parts of the Clarens Formation have been broadly correlated with deposits in Zimbabwe (Forest Sandstone and Dande Sandstone Formations).

Although a few UEF genera display close affinities with taxa from other Jurassic Pangaean successions, there are broad scale familiarities at family level (Rubidge, 2005; Smith *et al*., 2011). Correlative fauna are known from Australia (Upper Evergreen Formation), India (Upper Maleri Formation, Pranhita-Godavari Basin; Upper Dharamaram Formation, Pranhita-Godavari Valley), Namibia (Etjo Formation, Waterberg Basin), Zimbabwe (Forest Sandstone Formation), UK (British Fissure fills), Canada (McCoy Brook Formation), China (lower Lufeng Formation), Germany (Rhaeto-Liassic), Mexico (la Boca Formation, Huizachal Canyon) and the USA (Glen Canyon Group and Newark Supergroup) (Rubidge, 2005; Smith *et al*., 2011). Knoll (2005) provides a good summation of the UEF ichnotaxa, their validity and their correlation to European and American sites.

The most recent speculation about age of the upper Elliot Formation is given in Norman *et al.* (2011), who suggest that the UEF is either Pliensbachian-Toarcian or upper Sinemurian in age based on comparative work by Yates *et al*. (2004) and the personal observations of Irmis (2010). However, this age range and correlation is under constant revision, and is yet to be confirmed with respect to absolute age determinations. The generally accepted age of the UEF is earliest Jurassic, more specifically Hettangian to Sinemurian, with an age range of ~200 to <190 Ma (Fig. 3.1, Fig. 3.2; Lucas and Hancox, 2001).

The basal sauropodomorph *Massospondylus* is the most common taxon found in the UEF, and hence it typifies the UEF and lends its name to the Range zone. In recent years *Massospondylus* has been assigned a new type specimen (i.e., a neotype: BP/1/4934) in order to bolster the validity of the genus (Yates and Barrett, 2010). However, a comprehensive treatment of both the crania and post-crania of *Massospondylus* is still outstanding (although see Cooper, 1981). Attridge *et al*. (1985) recognised a prosauropod similar to *Massopsondylus* in the Kayenta Formation (early Jurassic) of the Glen Canyon Group. Recently identified as a new species (*Sarahsaurus*: Rowe *et al*., 2010), the phylogenetic affinities of this material is currently controversial. However, McPhee *et al*. (2015a) have recently reiterated that, pending further analysis, a massospondylid position for *Sarahsaurus* remains plausible. The early Jurassic record of Massospondylidae is further represented by a number of geographically widespread taxa. This includes: *Glacialisaurus* from the Hansen Formation of Antarctica (Smith and Pol, 2007), *Adeoppaposaurus* from the Cañón del Colorado Formation of Argentina (Martinez, 2009), *Leyesaurus* from the Quebrada del Barro Formation of Argentina (Apaldetti *et al*., 2011), *Lufengosaurus* from the Lufeng Formation of China, and possibly *Pradhania* from the of Upper Dharmaram Formation of India (Novas *et al*., 2010). In contrast, *Coloradisaurus brevis* from the upper Los Colorados Formation of Argentina is currently the only massospondylid known from beds dating to the Late Triassic (although see Apaldetti *et al*. (2014) for a discussion regarding the phylogenetic uncertainties of *Coloradisaurus*).

Yates *et al*. (2004) report on a sauropod dinosaur BP/1/6105 (UEF, farm Spionkop, Rosendal District) with affinities to *Vulcanodon karibaensis* (Raath, 1972; Cooper, 1984) of Zimbabwe. The latter was discovered within intercalated sandstones between two volcanic flows, and assumed to be contemporaneous with the ~183 Ma old Karoo volcanics of South Africa (Duncan *et al*., 1997). Yates *et al*. (2004) and Sidor and Hancox (2006) consider that this may indicate that there was little time between the deposition of the uppermost UEF (and Clarens Formations) and the extrusions of the basalts. Radiometric dating of the interbedded tuffs and volcanogenic rocks within the UEF of South Africa and Lesotho is therefore of paramount importance insofar as this would substantiate comparisons between biostratigraphic and magnetostratigraphic data at both the regional scale in southern Africa in addition to the global Gondwanan picture.

The oldest African turtle, *Australochelys africanus*, was discovered in the *Tritylodon* Acme Zone of the upper Elliot (Gaffney and Kitching, 1995) and is therefore considered Early Jurassic in age. Its sister taxon, *Palaeochersis talampayensis*, is considered to be Late Triassic (~Norian) in age as it was discovered in the upper section of the Argentinean Los Colorados Formation (Sterli *et al*., 2007; Santi Malnis *et al*., 2011; Kent *et al*., 2014). Sterli *et al*., (2007) propose that it forms the stem to the Testudines (see also Joyce, 2015) and that *Palaeochersis* and *Australochelys* are a monophyletic assemblage. The oldest European turtles (*Proganocheyls*) are reported from the Norian in Germany (Sterli *et al*., 2007).

With respect to the UEF ornithischian dinosaur assemblage, the heterodontosaurids have, in recent years, received much attention (Butler *et al*., 2007; Porro *et al*., 2010). The comparisons between globally occurring Ornithischians and those found within the Elliot have stemmed from what is considered the most basal ancestor, the Ischigualasto Formation's *Pisanosaurus mertii* (~Carnian in age; Butler *et al*., 2007). Báez and Marsicano (2001) reported on a *Heterodontosaurus* specimen found in the Late Triassic Laguna Colorada Formation with dental anatomy comparable to *Heterodontosaurus tucki* (Santa Luca 1980) from the UEF. In comparison, the Late Jurassic North American heterodontosaurid, *Fruitadens haagarorum*, of the Morrison Formation, is also considered closely comparable to the anatomy of *Heterodontosaurus tucki*. It appears that the temporal range of the group is, in general, relatively expansive, with reported occurrences extending from possibly the Late Triassic until as late as the Early Cretaceous. In terms of Fabrosaurid ornithischians, *Lesothosaurus diagnosticus* and *Stormbergia dangerhoeki* are reported for the UEF, with the latter considered to be synonymous with *Lesothosaurus* (Knoll *et al*., 2010). Butler (2005) considered that there was little support for *Lesothosaurus* as the basal-most Thyreophoran, with the likes of the English *Scelidosaurus harrisoni* (Norman *et al*., 2004).

The basal crocodylomorph *Protosuchus* is considered to be an index fossil for the end of the Apachean land vertebrate faunachron (Lucas, 1998), and its FAD may be coincident with the earliest Jurassic (earliest Hettangian), although the Apachean stage is considered Triassic. Occurrences of *Protosuchus* have been reported in both the lowermost Jurassic Dinosaur Canyon Member of the Moenave Formation and in the McCoy Brook Formation of the Newark Supergroup (Lucas, 1998; Donohoo-Hurley *et al*., 2010). However, Kirkland *et al*. (2014, p. 348) drew attention to the possible presence of protosuchids in rocks of a putative Triassic age and therefore their value as index fossil of the Lower Jurassic may require future revision.

Generally, the UEF has a low number/ diversity for reported carnivores with an important UEF theropod, previously termed *Syntarsus rhodesiensis*, now synonymous with *Coelophysis*. Bristowe and Raath (2004) consider the range of *Coelophysis*, within the Chinle Formation, to be Carnian – Norian, and Early Jurassic (Hettangian) with respect to the Elliot and Clarens Formations and Forest Sandstone Formation of Zimbabwe. Lehman and Chatterjee (2005), in contrast, consider that it could be used as an index fossil (at least in the USA, i.e. Dockum Group) where its range appears restricted to the Norian or Norian-assumed rocks. Although many specimens of *Coelophysis* have been found in Zimbabwe (Mana Pools area; Raath, 1969, 1977, 1990), in South Africa and Lesotho the taxon is uncommon and is invariably associated with the *Tritylodon* Acme Zone (early Jurassic; Raath, 1980; Kitching and Raath, 1984; Smith and Kitching, 1997; Munyikwa and Raath, 1999). That being said theropod ichnofossils (i.e. *Grallator* isp.) are abundant in the UEF of South Africa and Lesotho (Ellenberger, 1970; 1972; Wilson *et al*., 2009). *Dracovenator regent* (Yates, 2005b) is currently the largest theropod known from (non-dental) body fossils within the UEF (and the Elliot Formation generally). Represented primarily by fragmentary cranial material, *Dracovenator* was hypothesised to be the sister taxon of the South American *Zupaysaurus* from the Los Colorados Formation within its original description (Yates, 2005b). The presence of large (i.e., sub-allosaur in size) theropods is also alluded to by the frequent occurrence of sizeable trackways within the upper sections of the UEF and Clarens Formation, as well as the occasional discovery of large, isolated teeth (e.g., 'Predator X' from the Aardonyx quarry on Spionkop farm [although the possibility that these remains belonged to a late-lived 'rauisuchid' crurotarsian cannot be dismissed; McPhee *et al*., 2015b]).

Table 3.1. Diversity, abundance and trophic level data from the Elliot Formation (adapted and interpreted after Smith *et al*., 2011, p. 55). The pie chart suggests that the Elliot Formation fauna is largely dominated by sauropodomorphs and tritheledontids. The 'total' referred to in the table is of number of reported specimens.

	Taxa	Genus	Total	% of total population		Trophic level
Amphibia	Amphibia	Chigutisaurus	1	0.2	0.3	Carnivore
		Siderops	1	0.2		Carnivore
Parareptilia	Chelonia	Australochelys	3	0.5	0.5	Herbivore
Reptilia	Nondinosaurian archosaurs	Aetosaurus	2	0.3	3.8	Carnivore
		Basutodon	2	0.3		Carnivore
		Baroqueosuchus	2	0.3		Carnivore
		Clarensia	1	0.2		Carnivore
		Litargosuchus	1	0.2		Carnivore
		Orthosuchus	2	0.3		Carnivore
		Pedeticosaurus	1	0.2		Carnivore
		Protosuchus	5	0.8		Carnivore
		Sphenosuchus	1	0.2		Carnivore
		Notochampsa	6	1.0		Carnivore
	Dinosauria	Therapoda	11	1.8	66.1	Carnivore
		Sauropodomorpha	376	61.3		Herbivore
		Ornithischia	18	2.9		Herbivore
Therapsida	Cynodontia	Diarthrognathus	5	0.8	28.9	Carnivore
		Diademodontidae	1	0.2		Herbivore
		Elliotherium	1	0.2		Carnivore
		Pachygenelus	15	2.4		Carnivore
		Scalenodontoides	3	0.5		Herbivore
		Trithelodon	2	0.3		Carnivore
		Tritylodon	150	24.5		Herbivore
Mammaliaformes	Mammalia	Erythrotherium	1	0.2	0.5	Carnivore
		Megazostrodon	2	0.3		Carnivore
		Total	613			

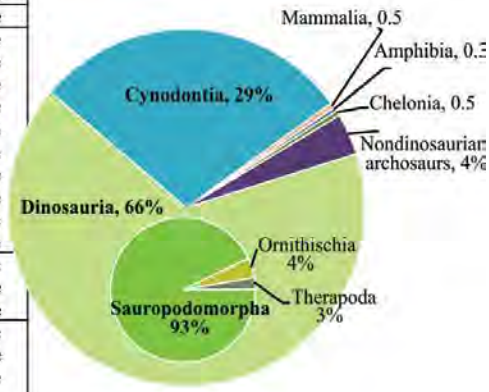

The diversity and abundance of animals within the Elliot Formation has been recently summarized by Smith *et al*. (2011) (see Table 3.1). The diversity of the known taxa within the UEF has been considered unusual given the assumed arid and therefore supposedly 'harsh' environment at the time (Barrett, 2004; Butler, 2005). Niche partitioning amongst the known herbivores/insectivorous dinosaurs of the UEF is presumed, and facultative omnivory in certain forms has been suggested (Barrett, 2000; McPhee *et al*., 2015b). The high diversity and abundance of body fossils in the upper Elliot and is paralleled by the profusion of footprints left behind by these animals. Recent re-evaluations, revisions, and summaries of the ichnological record of the upper Elliot (largely from the works of Ellenberger, 1970, 1972) are presented by Olsen and Galton (1984), Olsen and Rainforth (2003), Knoll (2005) and D'Orazi Porchetti and Nicosia (2007). Specific sites, such as the Moyeni track way in the town of Quthing (Lesotho), have been re-examined from a sedimentological and ichnological point of view by Smith *et al*. (2009), Wilson *et al*. (2009) and Marsicano *et al*. (2014). Many authors agree that there are several similarities between the upper Elliot trackways and other global Early Jurassic sites such as those within the Newark Basin, Colorado Plateau (e.g. *Navahopus* is of the Navajo Sandstone similar to *Tetrasauropus;* and *Batrachopus* of the lower Jurassic is shared).

Bamford's (2004) palaeobotanical review of the Elliot Formation reports a low diversity of both macroplants and wood taxa. The southern outcrops of UEF in Lesotho have yielded fossil wood of the conifer *Agathoxylon* (*Araucarioxylon arficanum*; BP/16/1099-1104) (Stockley, 1947; Bamford, 2004; Bordy *et al*., 2004b). To date, for the entire Elliot Formation, Bamford (2004) reports on a single find of a sphenophtye (*Equisetites*), a bennettitalean (*Otozamites*), two conifers (*Sphenolepidium* and *Pinus*) and numerous fragments of the conifer *Agathoxylon* (*Araucarioxylon arficanum)*. The genus *Araucarioxylon* is well-documented in the Late Triassic Chinle Formation (Ash and Creber, 2000; Savidge, 2007) as well as within the Late Triassic Dockum Group (Lehman and Chatterjee, 2005).

Barbolini's (2014) new palynological work has shown that the UEF (and Clarens Formation) can be distinguished from the LEF by the first occurrence of *Cyathidites minor* which is a well-known Late Triassic - Jurassic species represented in Australia and New Zealand (Barbolini, 2014). However, as noted by Barbolini (2014), there is a general accordance between all the formations of the Stormberg Group. The relative unity of the Molteno, Elliot and Clarens Formations with the synonymy of several palynomorphs between Formations is interesting. This could be a product of the broad-scale resolution of the study, but could also have wider implications for the ages of the formations themselves. The mixture of Jurassic and Triassic-age taxa throughout the Stormberg sequence, especially within the *Massospondylus* Range Zone, is curious and requires further study. This is especially pertinent in light of the low preservation potential of palynomorphs within oxidative red bed deposits (in general), and the low diversity of macroplants and woody material. Furthermore, it seems reasonable to assume that the climatic gradient between the formations and within the Elliot, should provide, albeit gradual, climate change lending to low diversity but distinguishable plant assemblages between/within formations.

4 Magnetostratigraphy: a general introduction

4.1 Late Triassic- Early Jurassic magnetostratigraphic work in South Africa

To date, the only magnetostratigraphic work of the Elliot Formation is an unpublished MSc dissertation by De Kock (2003) which collates several Elliot Formation sites from the northern and southern parts of the Karoo Basin. The results of this pioneering work are summarised in Table 4.1 below. In the southern part of the basin, samples were collected from the lowermost section of Barkly's Pass (along the R58 north of Elliot), Joubert Pass (east of Lady Grey) and Wolwehoek Pass (along the R58 north of Barkly East) (Fig. 4.1). In the northern part of the basin, three locations at Clarens Townlands, Warden's Tower (a farm between Marquard and Senekal) and Brambley's Hoek (farm northwest of Clarens) were sampled. Overprint was suspected at Joubert Pass and Wolwehoek Pass where a secondary north-north westerly, relatively steeply inclined present-field component persisted at higher levels of thermal demagnetization. Samples from these sites were not included in further analyses.

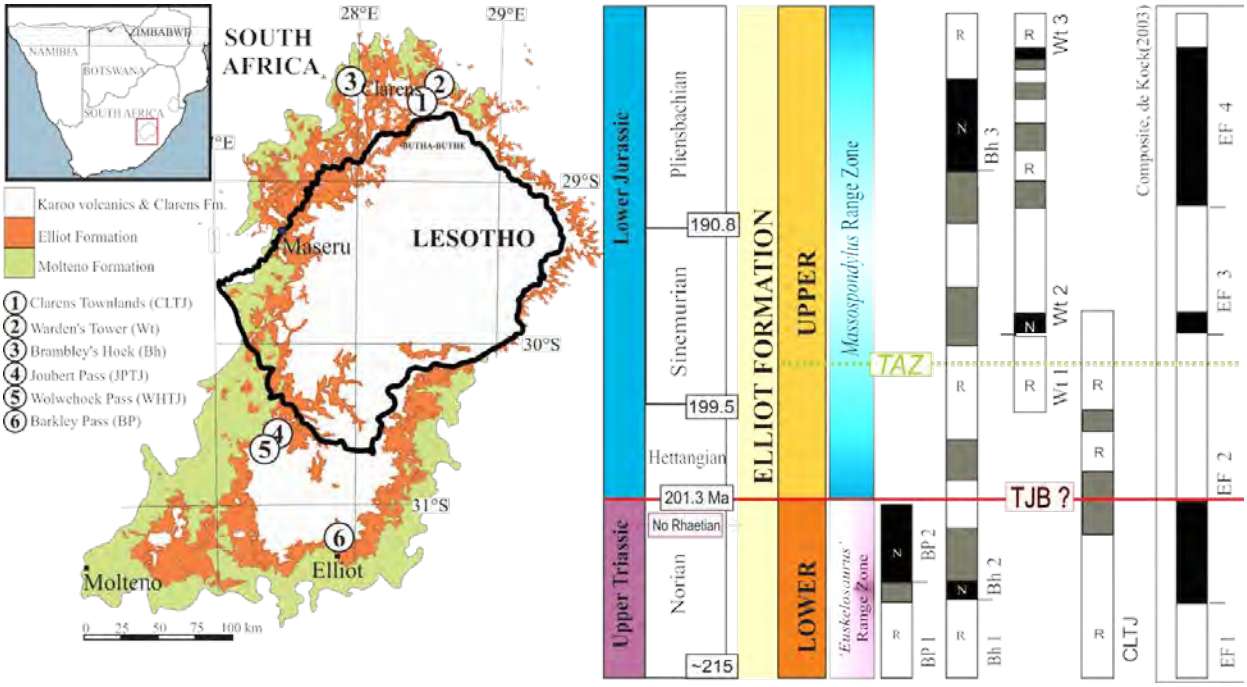

Figure 4.1. De Kock (2003) field site localities with composite magnetostratigraphic log for the Elliot Formation (EF 1 – EF 4).

Demagnetization behaviour illustrated by samples from Barkly's Pass, Clarens Townlands, Warden's Tower and Brambley's Hoek have primary components which plot either as reverse polarities following demagnetization along great circle arcs to stable relatively shallow end point positions in the south-east direction, or shorter great circle arcs to relatively shallow north western normal direction. This behaviour is similar to the results reported in the current study. These directions are considered to be characteristic of the Late Triassic-Early Jurassic as southern Africa's orientation, relative to present day, was comparable. Consequently De Kock (2003) highlights the difficulty in recognising the characteristic normal remanent magnetization direction unless, under increasing thermal demagnetization, loss of magnetization occurs along a clear great circle path.

Table 4.1. Magnetostratigraphic results of de Kock (2003) from the Elliot Formation. LEF, UEF = lower and upper Elliot Formation, respectively.

Section	Sampled stratigraphy	Directions	N (L,C)	Dec (°)	Inc (°)	k (°)	α_{95} (°)	Pole late °N	Pole long °E
Barkly Pass	lowermost LEF	Present field overprint	63 (63,0)	330.9	-58	61.3	2.3	65.1	271.3
		Normal	13 (8,5)	347.9	-57.2	17.3	11.6	78.1	259.9
		Reverse	28 (20,8)	150.4	52.6	21.3	6.6	-65	104.4
Joubert Pass	uppermost UEF	Reverse overprint (Dolerite overprint suspected)	6 (5,1)	168.2	34.4	26.8	12.5	-74.3	161.3
Wolwehoek Pass	UEF	Present field overprint	21 (21,0)	336.1	-55	57.1	4.2	69.5	227.7
Brambley's Hoek	LEF into the UEF	Present field overprint	30 (30,0)	330.3	-59.8	28.1	5	62.8	263.8
		Normal	5 (5,0)	338.9	-60.5	163.9	5.4	68.4	255.7
		Reverse	11 (1,10)	161	63.3	47.8	9.8	-67.7	66
Clarens Townlands	LEF into lowermost UEF	Present field overprint	27 (27,0)	341.6	-56.5	17	6.9	72.3	264
		Reverse	11 (0,11)	168	63.3	38.6	11.6	-70.9	55.1
Warden's Tower	entire UEF	Present field overprint	46(46,0)	349.4	-62.5	12.1	6.3	72.5	233.2
		Normal	5 (2,3)	351	-61.1	16.7	26.3	74.8	230.6
		Reverse	24 (2,22)	157.8	60.7	18.5	9.9	-67.7	75

The similarities in polarity pattern and stratigraphy among geographically separated sites of de Kock (2003) attests to the palaeomagnetic stability of samples taken from the Elliot Formation. A composite magnetic zonation pattern was then established for the Elliot Formation, splitting the unit into 4 polarity pairs (EF1, EF2, EF3 and EF4; Fig. 4.1). According to de Kock (2003), the TJB falls into a period of normal polarity period, at the biostratigraphic transition between the *Euskelosaurus* and *Massospondylus* Range Zones of Kitching and Raath (1984), where there is a lithostratigraphic transition/boundary between the lower and middle Elliot Formations (*sensu* Kitching and Raath, 1984) and between the lower and upper Elliot Formations (*sensu* Bordy *et al*. 2004a).

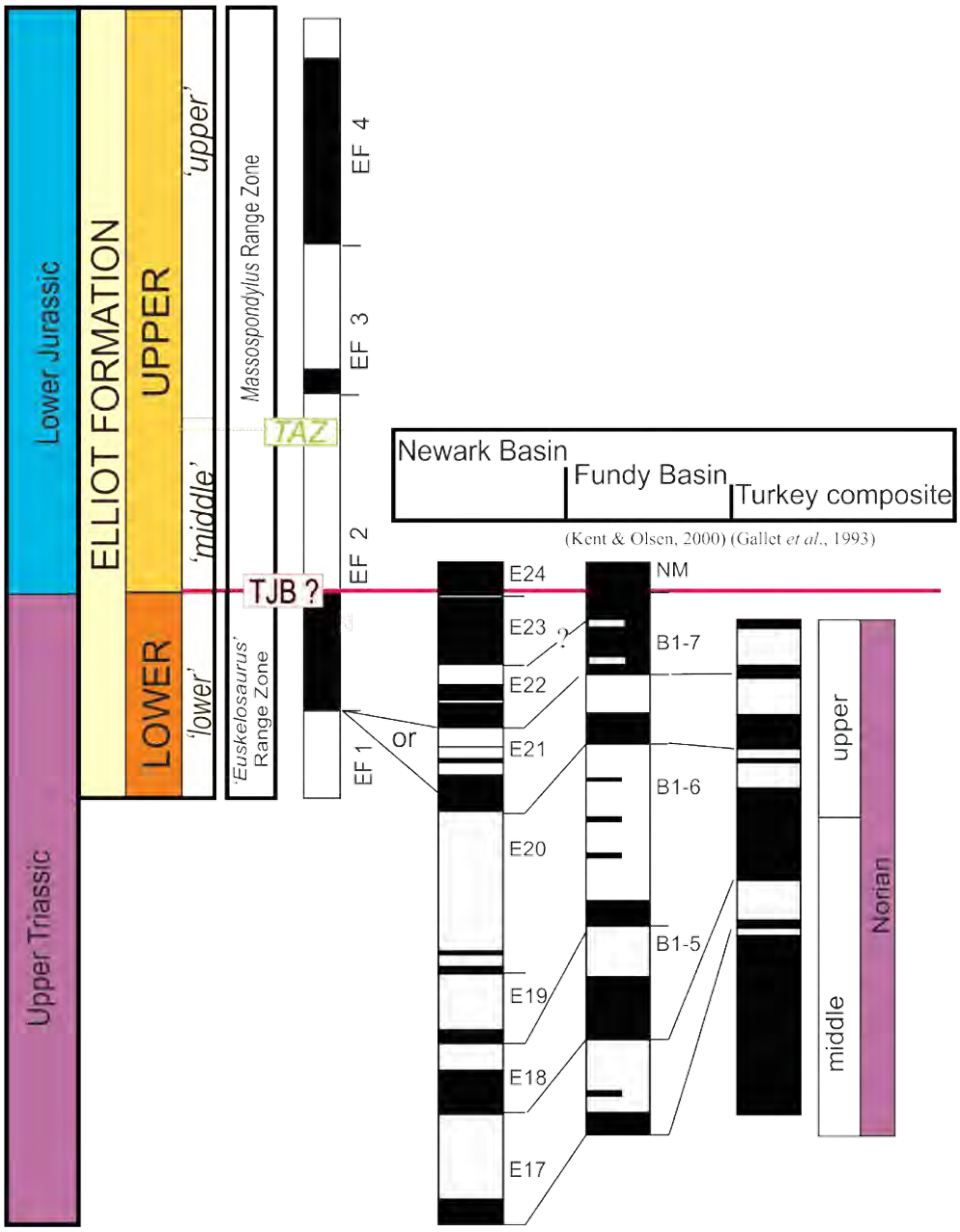

Figure 4.2. Correlations between the Elliot Formation magnetostratigraphy (magnetozones EF1 – 4) and that of the Newark and Fundy Basins and the Norian Turkish composite as per de Kock (2003).

De Kock (2003) thereby places an age of uppermost Norian, based on magnetostratigraphic correlations with other global sites (e.g., Chinle Formation, Fundy Basin; Fig. 4.2) as well as palaeontological evidence. This assigns the UEF (then the middle and upper Elliot Formations) to the Early Jurassic. Furthermore, at the time of writing of de Kock's (2003) thesis, the Rhaetian was largely considered not to

exist, and instead a long Norian Stage was present. It is important to note that the sampling of de Kock (2003) and samples which were later palaeomagnetically viable, were largely biased towards UEF sites.

De Kock (2003) found that his calculated Late Triassic-Early Jurassic Elliot Formation or Karoo paleopole (68.9^{o}N, 265.6^{o}E; de Kock, 2003) sits well with the mean Early Jurassic African palaeopole of McElhinny and McFadden (2000). Thus, he concluded that the sampled sections from the various Elliot Formation outcrops were potentially of Early Jurassic age.

Other problematic areas of de Kock (2003) sampling and correlation lie in the use of the *Tritylodon* Acme Zone of Smith and Kitching (1997) as aid of correlation. The two main reasons for this are:

1. The non-regional development of the TAZ even in northern sections, where traditionally (Smith and Kitching, 1997) it was considered to be regionally developed and traceable (see Golden Gate National Park sections GGP and GGB of current study). Simply put, the TAZ is often absent.
2. The non-diagnostic sedimentological nature of TAZ. There are often several well-developed nodular horizons and associated palaeosols/sedimentary features within the UEF that appear identical to one another and to the documented occurrences of the TAZ (see Bramley's Hoek section of Smith and Kitching, 1997). Identification of the TAZ, therefore, can be difficult if one is not well-trained in the identification of *Tritylodon* sp. fossils, because they are the only diagnostic feature of the TAZ currently. See de Kock (p. 82; 2003) "prominent nodular horizon" is questionably TAZ.

4.1.1 **The 'Van Zijl reversal' and palaeomagnetic data from the overlying Drakensberg Group**

The Karoo Igneous Province (KIP) is composed of the Drakensberg Group which is a series of volcanic (basaltic) formations of Lower Jurassic age representative of a once widespread large igneous province (LIP) which caps (and ends) sedimentation within the Karoo basin. The Drakensberg group is composed of two geochemically unique units, a lower Barkley East Formation and an upper Lesotho Formation (Marsh *et al*., 1997).

Van Zijl *et al*. (1962a, b) first undertook a palaeomagnetic study of the Drakensberg Group basaltic lavas in Lesotho. A site within the Maseru District also looked at the magnetic polarity of several samples within the Clarens Formation sandstones (3 unbaked and 6 baked) directly below the lavas. This study found that the lowermost lavas have a reverse magnetic polarity with the lavas higher up in sequence being normally magnetized. Later palaeomagnetic studies have been able to repeatedly show this single reversal (Kosterov and Perrin, 1996; Hargreaves *et al*., 1997; Prévot *et al*., 2003; Moulin *et al*., 2011,

2012) and subsequently it has been termed term the “van Zijl” Jurassic geomagnetic reversal (Moulin *et al*., 2012). The van Zijl reversal was initially utilised to express a rapid eruptive history of the basalts in the Drakensberg Group which was later radiometrically constrained (Kosterov and Perrin, 1996; Prévot *et al*., 2003; Jourdan *et al*., 2007a, b; Moulin *et al*., 2012, Moulin *et al., in press*). Rapid reversals are characteristic of the middle Jurassic globally (Gradstein *et al*., 1994) and are usually on the scale of ~0.5 Ma (Duncan *et al*., 1997). Moulin *et al*. (*in press*) state that if reversal rate of ~4 reversals/Ma is considered (as per marine sections), the long normal magnetochron (~1000 m) would not exceed ~250 kyr. Furthermore, they state that volcanism appears to have started earlier in sections at Naudes Nek, Moteng Pass and Sani Pass and persisted longer at the others e.g. Lebombo section. Ultimately, all volcanism from the Northern and Natal province (South Africa), and Antarctica (Kirwan Mountains) fall into the range 183±1.0 Ma (Duncan *et al*., 1997).

Moreover, given the inter-fingering of the uppermost Clarens Formation with the lowermost lava flows in Lesotho and Golden Gate National park areas, it is likely that, at least, the topmost section of the Clarens is contemporaneous with the lowermost (conservative) age of the KIP. Vertebrate fossil assemblages place the upper Elliot and lower Clarens Formation as Hettangian - Sinemurian, respectively, with the upper Clarens Formation Pliensbachian in age (Knoll, 2005).

4.2 Global perspectives

The most extensively studied continental Triassic-Jurassic magnetostratigraphic succession is that of the Newark Basin (USA) (Kent *et al*., 1995; Kent and Olsen, 1999; Olsen *et al*., 2011). These sections have been astrochronologically anchored while also being tied down by several radiometric dates, and form the basis for the Newark continental astronomical polarity time scale (APTS; Kent *et al*., 1995; Kent and Olsen, 1999; Olsen *et al*., 2011). The Newark magnetostratigraphic columns have long formed the comparative model for other continental Triassic and Early Jurassic magnetostratigraphic sections, such as those measured in the Colorado Plateau (USA) and Morocco (Molina-Garza *et al*., 2003; Marzoli *et al*., 2004). These studies reinforce the utility of Newark continental APTS, and highlight the mixed polarity of the Norian and the normal polarity (occasionally punctuated by short reversed intervals, Ogg *et al*., 2004; Ogg, 2012) of the Rhaetian – Hettangian transition. In comparison, the marine Tethyan realm relies more heavily on ammonoid, conodont and palynomorph biostratigraphic zonations, geochemical

correlations (C-isotope stratigraphy) and rare radiometric dates. The correlation between the marine and continental realms is therefore a source of constant revision and debate. It is here where magnetostratigraphy and radiometric dating become crucial tools in the correlation between the sedimentary records of these vastly different realms.

4.2.1 **Triassic-Jurassic magnetostratigraphy problems and perspectives**

Hounslow and Muttoni (2010) provide an excellent review, although 5 years old now, of Triassic-Jurassic magnetostratigraphy, globally, and the problems facing the evolution of the Triassic geomagnetic polarity timescale GPTS.

In contrast to the mid-Jurassic GPTS, which can be largely based on sea-floor linear magnetic anomalies, the slow progression and development of the Triassic GPTS, especially in continental settings, can be related to (a) the fragmentary nature of the continental sedimentary record; (b) the poorly constrained and incomplete nature of the continental biostratigraphy; (c) the difficulty in the correlation of the Triassic continental magnetostratigraphy with biostratigraphy; (d) the absence of preserved, pre-Jurassic oceanic crusts; (e) the scarcity of successive, definitive radiometric dates (Hounslow and Muttoni, 2010; Miall, 2014a). The resolution of which is dependent on the calibration of marine and continental biostratigraphy (Kent *et al*., 1993; Muttoni *et al*., 1996; Channell *et al*., 2003; Hounslow and Muttoni, 2010).

In forming the Triassic GPTS the meticulous correlations of Hounslow and Muttoni (2010) suggest that the Triassic lasted some ~51.5 Myr. The reversal rate decreased between that recorded for the Lower and Middle Triassic (~ 4 reversals per Ma) to that of the Upper Triassic (~2 reversals per Ma; Hounslow and Muttoni, 2010).

4.2.2 **Time resolution of magnetostratigraphic correlation**

Time resolution of magnetostratigraphic correlation is confined by the sampling interval (density), the rate of deposition and the presence of unconformities (Butler, 1992; Hounslow and Muttoni, 2010; Kadoma, 2012). Correlation using magnetostratigraphy requires the following:

1. Consistency in sedimentation rate with few and well-dated unconformities. This rests on the basis that unsteady sedimentation rates and stratigraphic gaps (created by abrupt events; Kemp and Sexton, 2014) limit temporal resolution, and thereby likely to distort magnetostratigraphy. However, this is usually not easily attainable especially in the continental realm.

Secondly,

2. Density of sampling that corresponds to the rate of sedimentation. This becomes increasingly difficult if the sedimentation rate was highly variable. In continental settings where unsteady sedimentation is prevalent a low sampling frequency is to be avoided, even if the sedimentation rate is perceived to be low, because the recovered magneto-pattern may be a poor representation of the frequency of past geomagnetic events polarity changes. In this case, and in most scenarios, dominance polarity is preferred for correlations in conjunction with other correlation tools (i.e., fossils, dated volcaniclastics). Comparison between sections with different sedimentation rates can be accounted for by vertically adjusting (stretching/shrinking) the magnetostratigraphic scale with the use of a guide such as biostratigraphy or radiometric ages (Butler, 1992; Hounslow and Muttoni, 2010; Kadoma, 2012).

For these reasons, marine sections, given their relative completeness in comparison to continental sections, and in conjunction with other tools for cross-comparison (higher resolution of marine fossils), are often used for correlation and thus the building of a consistent Triassic GPTS. Furthermore, cyclostratigraphy and astronomically-calibrated magnetostratigraphy used for marine correlations of separated sections is increasingly useful. In principle, however, correlation using magnetostratigraphic standards, will depend largely on either the patterns of changing magnetic polarity or, on a finer scale, the correlation of boundaries between magnetozones (Hounslow and Muttoni, 2010; Kadoma, 2012). The latter defines a 'barcode' for certain stratigraphic intervals because of a predictable rate of reversal. For instance, the reversal rate within the Late Triassic appears to coincide with that recorded in the Cenozoic (~30Ka magnetozones; Kent *et al*., 1995; Kent and Olsen, 2000; Hounslow and Muttoni, 2010).

4.3 Late Triassic-Early Jurassic Tethyan marine magneto- and bio-stratigraphy, in brief

4.3.1 **Norian - Rhaetian transition**

Biostratigraphically, the base of the Rhaetian is marked by the FAD of the conodont *Misikella posthernsteini*, which is typified within the stratotype Steinbergkogel section A (Austria; Fig. 4.3; Krystyn *et al*., 2005, 2007a, b; Hüsing *et al*., 2011). These are occur within the top of a long normal magnetozone which has been correlated to other European sections (on the basis of biostratigraphy) and

the E16n (~209.8 Ma) of the Newark APTS (based on magnetostratigraphic match; Hüsing *et al*., 2011). The position of the Norian-Rhaetian boundary, however, is still under considerable debate (please refer to sections below), and brings into question the methods of correlation and the completeness of the Newark Basin section.

Magnetostratigraphic correspondence of adjacent Steinbergkogel sections is also reflected in correlations with other Austrian (Scheiblkogel) and Pangean sections from Slovakia (Silická Brezová), Sicily (Pizzo Mondello; detailed latest Norian magnetostratigraphy; Hounslow and Muttoni, 2010) and Turkey (i.e., Oyuklu; Hounslow and Muttoni, 2010; Hüsing *et al*., 2011). The occurrence of several sections with both magneto- and bio-, and even chemo-stratigraphical controls makes relating and constraining the latest Norian and Rhaetian stages easier. The use of several proxies to constrain a boundary is becoming obligatory as it proves a refined outcome for cross-correlations. For example, defining the Norian-Rhaetian boundary within the Pignola-Abriola section (Italy) uses biostratigraphy, with the occurrence of the *Proparvicingula moniliformis* radiolarian zone 50 cm below the FAD of *M. posthernsteini* in conjunction with the chemostratigraphy (a prominent negative $\delta^{13}C_{org}$ spike), and magnetostratigraphy for correlation (Maron *et al*., 2015; Rigo *et al*., 2015). The use of this data in conjunction with sedimentation rates and age models allowed the placement of the Pignola-Abriola Norian-Rhaetian boundary (within the MPA 5r magnetozone) at the Newark APTS magnetozone E20r.2r, and at an approximate age of ca. 205.7 Ma (Maron *et al*., 2015). Rigo *et al*. (2015) have now recently propositioned for the Pignola-Abriola section to represent the GSSP for the NRB due to the multiple proxies available for the placement of the boundary.

While the use of magnetostratigraphic age-models, using the thickness of magnetozones, for sedimentation rate and section comparison has its use in marine sections it should be used cautiously and even more so in cross-comparisons with continental sections. This can be related to the inability to identify the presence and duration of hiatuses accurately (i.e., difficulty in quantifying how fragmentary the sedimentary record - Miall, 2013, 2015).

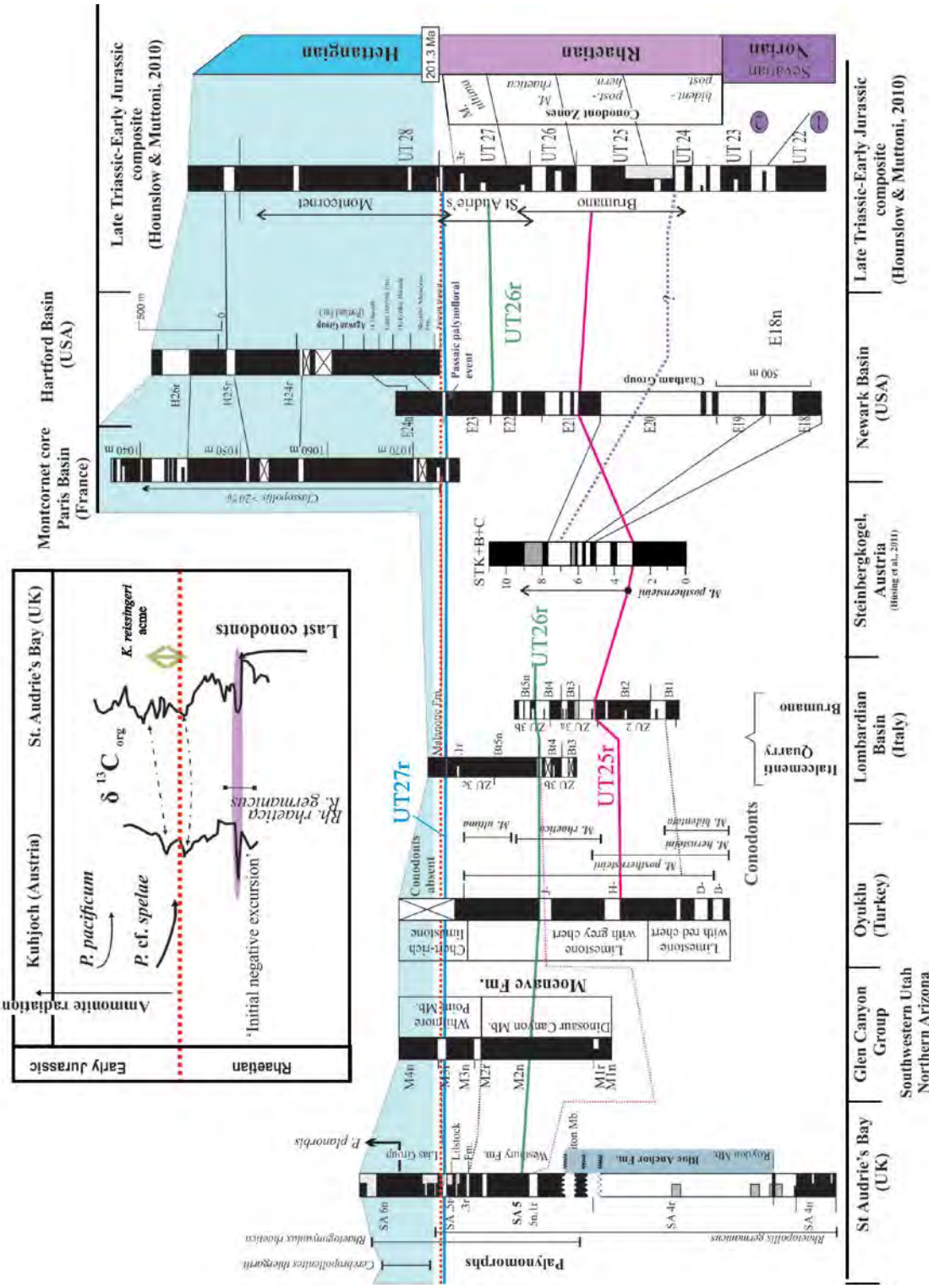

Figure 4.3. Norian-Rhaetian-Hettangian magnetostratigraphy and biostratigraphy as compiled by Hounslow and Muttoni (2010) with the composite magnetostratigraphy displayed on the right-hand side of the figure. This uses information from several northern Hemisphere localities. These are all marine sections with the exception of part of the St Audrie's Bay, and the Newark and Hartford Basins which record data from continental sediments and CAMP basalts, respectively. The inset shows the C-isotope curve indicating a decline to more negative values, with the Kuhjoch section showing *P. cf. spelae* half a metre above the peak in negative isotope values and coinciding with a small positive C-isotope excursion (adapted from Hounslow and Muttoni, 2010).

4.3.2 **Rhaetian – Hettangian transition**

The Italian sections at Brumano, Costa Imagna and Italcementi Quarry (Lombardian Basin, Southern Alps) form the most detailed magnetostratigraphic marine section for the Rhaetian (Muttoni *et al*., 2004; Muttoni *et al*., 2010). Conodonts and palynomorphs were used for the correlation between the lower Brumano and Costa Imagna sections, and the upper Brumano and Italcementi Quarry, respectively (Muttoni *et al*., 2010). The lowermost Hettangian is captured in the uppermost part of the Italcementi Quarry section at the base of the Malanotte Formation (Muttoni *et al*., 2010). This Formation records the transition from Rhaetian to Hettangian palynomorphs. This transition falls within the magnetozone BIT5n (above .1r) which can be correlated to E23r of Newark APTS (Muttoni *et al*., 2010), and additionally demarcated by negative C-isotope excursion that is correlated to the St. Audrie's Bay (UK) section (Galli *et al*., 2005).

Officially the base of the Hettangian is marked by the FO of the ammonoid Psiloceras cf. spelae (now *P. spelae tirolicum*) as it falls within the GSSP Kuhjoch section (Austria; Hillebrandt *et al*. 2007). Magnetostratigraphy on this section, its neighbours and other sections with the *Psiloceras cf. spelae* ammonoid is lacking (Hounslow and Muttoni, 2010).

Correlation and identification of the TJB and the base Hettangian in other sections with magnetostratigraphy (i.e., St Audrie's Bay U.K., or Oyuklu section, Turkey) have proven to be challenging and rely on the use other criteria, such as the changes occurring in C-isotopes and palynology across the boundary (Hounslow *et al.*, 2004; Hounslow and Muttoni, 2010). The similarity between the organic carbon isotope data at Kuhjoch and St Audrie's Bay (an initial dual-peaked negative carbon isotope excursion; Figure 4.3) both precedes the FO of *Psiloceras* and the LO of conodonts (Hounslow *et al*., 2004; Galli *et al*., 2005; Hounslow and Muttoni, 2010). This is, in turn, followed by a peak in positive $\delta^{13}C_{org}$ values which corresponds to St Audrie's magnetozone SA5r (Hounslow *et al*., 2004; Hounslow and Muttoni, 2010). Using this C-isotope data, the FO of *P. planorbis*, at St Audrie's Bay section, is coincident with the base of the Hettangian at the Kohjoch section (Galli *et al*., 2005; Hounslow and Muttoni, 2010). The second negative C-isotope excursion (M2), above the TJB, which occurs in both the Kohjoch and St Audrie's sections, is within the lower range of the *P. planoribis* of St. Audrie's Bay section (Hounslow *et al*., 2004; Hounslow and Muttoni, 2010). This is not observed in other TJB interval isotopic records (McRoberts *et al*., 1997, 2007; Hounslow and Muttoni, 2010).

Magnetostratigraphy from the St Audrie's Bay sections and the Montcornet core (Paris Basin; Yang *et al*., 1996) can be readily correlated on the basis of the detailed palynology at both sites (Moreau *et al*., 2002;

Hounslow *et al*., 2004). This palynological change is a function of the presence of acme zones with *K. ressingeri* and the dominance of *Classopollis* within otherwise low diversity miospore assemblages. On the basis of these correlations it is likely that the reverse magnetozone in the Montcornet core at 1073.8 m is equivalent to the SA5r of St Audrie's Bay section (a few metres below the likely position of the TJB at St. Audrie's Bay; Hounslow and Muttoni, 2010). This in turn complements Muttoni *et al*. (2010) palynological boundary in the Malanotte section and Italcementi Quarry correlative (magnetozone BT5n), and their correlation to the Newark E23r.

The control on correlation between the Oyuklu section (south-western Turkey) and other marine sections is based largely on the Late Triassic conodonts record and magnetostratigraphy (Gallet *et al*., 2007). The LO of conodonts appears at the initial negative C-isotope excursion (Fig. 4.3; Gallet *et al*., 2007). To date, the correlation of the SA5n.1r (St Audrie's Bay) and BT4r (Brumano section, Lombardian Basin, Italy) has been assigned to the highest reverse J-magnetozone of Oyuklu (Hounslow and Muttoni, 2010), and Gallet *et al*. (2007) consider the SA5n.1r to correlate with Newark APTS magnetochron E21 (Fig. 4.3).

4.4 Continental record

4.4.1 **Non-marine and marine TJB section comparisons**

Lucas and Tanner (2007a) state that it is important to consider that the TJB is a single datum, as defined in the marine realm (i.e., Tethyan sections); and that only through correlation of continental and marine sections can the TJB be placed within the continental sections with confidence. While the TJB should be undeniably a single datum, it is most likely that the marine-continental link will be problematic to achieve even among regionally separated sites. To date, marine-continental correlations still rely mostly on biological entities, although they are increasingly supplemented by multi-proxy datasets in addition to more recent U-Pb dates (e.g. from Peru; Wotzlaw *et al*., 2014; Nevada section; Guex *et al*., 2004) which allow higher resolution correlation. This is needed because biotic factors are often marred by provinciality or other biogeographically/ecological issues (i.e., rare reliable index fossils spanning across the two realms; spatiotemporal heterogeneity of palaeo-ecosystems). Furthermore, variations in the bio-geochemical signal of the rock record (e.g., excursions in the C-isotope curves) are controlled to a large extent by the biota and/or the dynamics of the palaeonvironment (i.e., marine vs. continental). Correlations can be augmented by radiometric age dates and magnetostratigraphy. Unfortunately, basins

that contain sedimentary records with convincingly coinciding biotic or geochemical changes or that simultaneously accommodate continuous and steady marine and continental depositional histories are rare (e.g., North-western Chinese Junggar Basin; Sha *et al*., 2015). The position moving forward for correlations would ideally rest on convincing coinciding biotic or geochemical changes barring concrete/ reliable radiometric ages.

4.4.2 **Newark and its importance**

When reviewing the continental Triassic-Jurassic successions, the most fundamental work was carried out in the Newark Basin, primary a focus of the Newark Basin Plateau Coring Project (NBCP, Kent *et al*., 1996; Kent and Olsen, 1999; Olsen *et al*., 1996, Olsen *et al*., 2002b). The Newark Supergroup (eastern North America) contains several of the most complete non-marine sections drilled, to date, and captures the continental representation of the magnetic field for the Late Triassic (Norian/Rhaetian) - Early Jurassic (Hettangian; Kent *et al*., 1993, Kent *et al*., 1995). The over ~6.5 km of Upper Triassic and lowermost Jurassic cyclical lacustrine sedimentary rocks and interbedded CAMP basalts that brought to surface provide a firm backbone for global correlation efforts within the continental realm.

The seminal work on this succession highlights the variability in magnetic field behaviour during this time, and, while it has received a large amount of scrutiny and (re)examination, it has been used for correlations between marine and non-marine sections globally, but not without difficulties. Some of the works that highlight the challenges in attempting to correlate this section to other magnetostratigraphic columns of the Late Triassic, especially with those from marine sections are by Kent and Olsen (1995); Hounslow *et al*. (2004); Gallet *et al*. (2007); Lucas and Tanner (2007a, b); Whiteside *et al*. (2007); Hounslow and Muttoni, (2010); and Muttoni *et al*. (2010). Many solutions have been considered by Gallet *et al*. (2003, 2007), Krystyn *et al*. (2002), Channell *et al*. (2003), Hounslow *et al*. (2004) and Muttoni *et al*. (2004, 2010), and the commonly found underlying problem is the inherent ambiguity of the biostratigraphic method (Hounslow and Muttoni, 2010; Lucas *et al*., 2012).

The magnetostratigraphy and climatic cyclostratigraphy of the rhythmically deposited lacustrine Newark succession form the basis for the high resolution Newark astronomically calibrated geomagnetic polarity timescale or astronomical polarity time scale (APTS), with the smallest denomination (3-6 m thick sediment packages) being the ~20 kyr precession van Houten cycles (Kent and Olsen, 1999; Olsen *et al*., 2003). These astrochronology models have been put to use to calculate the length of time for sedimentation between basalt flows. The astronomical timescale has been used to create a relative ‘floating’ timescale for the Newark, but caution is advised for the accuracy in recording and interpreting

these cycles in the rocks. The chronostratigraphic context which has been elucidated by the CPCP cores has meant that high resolution reconstructions of Triassic and Jurassic earth system process can be deduced, or at the very least, throws light onto the matter.

All in all, in spite of the uncertainties presented in the next sections, the magnetostratigraphy of the Newark Basin, refined over several years, has provided well-constrained polarity zones and palaeolatitudes for the Upper Triassic – Lower Jurassic. Together with the comparatively high resolution palynology, U-Pb dates and orbitally-forced climate cycles of the Newark lacustrine sediments, it plays a key in global stratigraphic comparisons (Fig. 4.4).

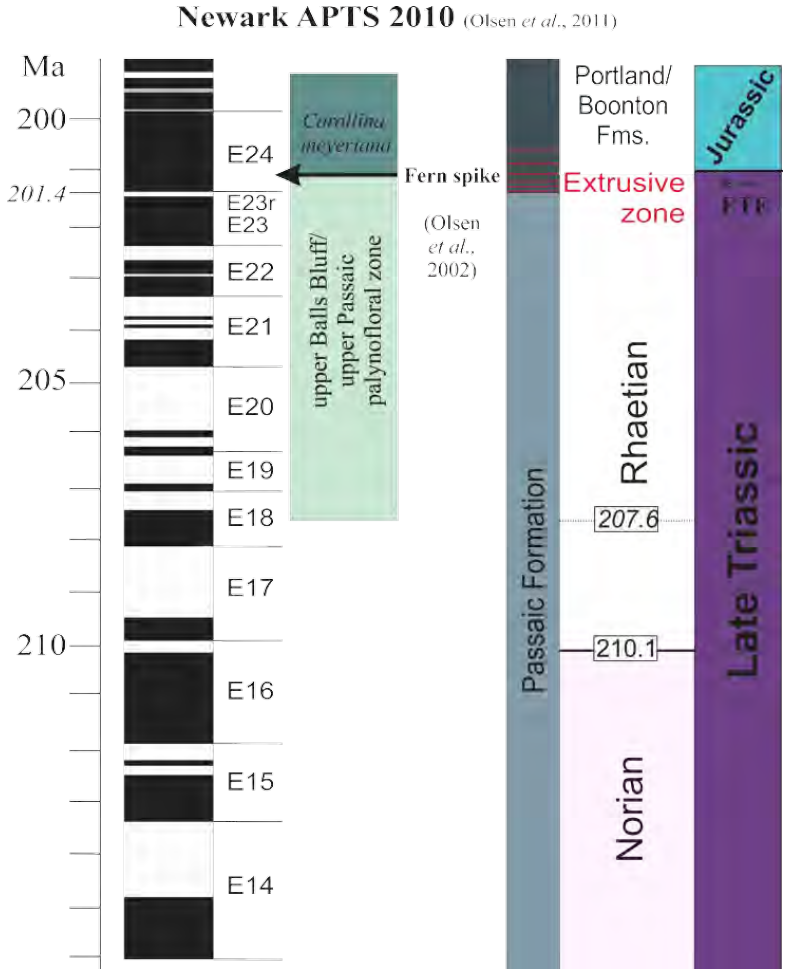

Figure 4.4. APTS 2010 taken from Olsen *et al.* (2011) and amended to fit in the Olsen *et al.* (2002) fern spike (which overlaps with the reported Ir-anomaly) and palynofloral zones. Important to note the C/N boundary currently placed at E7r was then in Olsen *et al.* (2002) at E13r2.

Kent and Olsen (1999) have revised the original magnetostratigraphy of the Newark APTS, establishing 60 polarity zones and resampling at high intervals, of 0.3 m, the polarity zones E13n-E23r. In conjunction with the astrochronology models the duration of polarity intervals was constrained to 7.9±4.5kyr (Kent and Olsen, 1999; Olsen *et al*., 2011).

Radiometric dates from the overlying CAMP basalts have given an additional framework to constrain the Newark succession (Blackburn *et al*., 2013). The latest and most accurate age is from the North Mountain Basalt (Fundy Basin, Nova Scotia, eastern Canada) with the chemical abrasion TIMS U-Pb age of 201.566±0.031 (Blackburn *et al*., 2013).The oldest CAMP lavas from the Newark, the Orange Mountain Basalts, postdate the end-Triassic continental extinction by roughly 3.2± 0.9 kyrs in eastern North America (Fig. 4.5; Kent and Olsen, 1999; Olsen *et al*., 2002a; Deenen *et al*., 2010; Blackburn *et al*., 2013). The Orange Mountain Basalts have yet to have a precise radiometric age ($^{40}Ar/^{39}Ar$ 201.0 ± 1.2 Ma; Hames *et al*., 2000; Kent and Olsen, 2008), but the geochemically identical feeder sill (Palisade sill) has been dated with U-Pb at 201.1 Ma (Dunning and Hodych, 1990). U-Pb date of 201.52 ± 0.034 Ma (Blackburn *et al*., 2013) and a $^{40}Ar/^{39}Ar$ biotite date of 202.2 ± 1.3 Ma from a recrystallized sedimentary xenolith associated with the Palisade sill are consistent with an $^{40}Ar/^{39}Ar$ age of 201.0 ± 1.2 Ma in the Orange Mountain Basalts (Hames *et al*., 2000).

Consistent ages have been returned from other CAMP lavas, such as those from Morocco (High Atlas Basin) with a CAMP $^{40}Ar/^{39}Ar$ age of 199.1 Ma for the TJB (Verati *et al*., 2007). The new zircon U/Pb ages for the CAMP basalts from North America (Newark, Fundy Basins) and Morocco (Argana Basin) as reported by Blackburn *et al*. (2013) are inter-calibrated with astrochronology to provide a time resolution between the ETE and the initiation of CAMP. Blackburn *et al*. (2013) established that the oldest CAMP basalts in the Newark Basin, the Orange Mountain Basalts (and Palisade sill) are ~3.2±0.9 kyr younger than the estimated ETE with the oldest CAMP basalts, the Tasguint Basalt (Argana Basin), being older than the OMB by 13.2±3.8 kyr (Fig. 4.5). The ETE being ~ 100± 40 kyr older than the TJB (Blackburn *et al*., 2013).

Olsen *et al*. (2002a, b) state that at Newark TJB coincides with (1) the tetrapod footprint turn over with increased size of theropods, (2) a small Ir-anomaly potentially linked to (3) the palynological spike ("fern spike") (Fig. 4.3; Fig. 4.5). Palynologically, this event is marked by the transition between *Patinasporites denus* dominated assemblages to *Classopollis*-dominated assemblages. Magnetostratigraphically, the E23r interval, a crucial short (~25 kyr) reversal, lies ~20 kyrs below these biological and geochemical events (Kent and Olsen, 1999; Olsen *et al*., 2002a, b).The palynological TJB (eastern North America)

thereby is overlain by U-Pb dated lavas (i.e., the Palisade sill at 200.9±1 Ma and Gettysburg sill 201.3 ±1 Ma; Dunning and Hodych, 1990, 1992) and the new age of the North Mountain Basalt of the Fundy Basin (201.566±0.031 Ma; Blackburn *et al*., 2013). The Rhaetian-Hettangian boundary lies above the base of the *Classopollis* palynofloral zone and at the base of the Orange Mountain Basalt within the Newark Basin (Olsen *et al*., 2011).

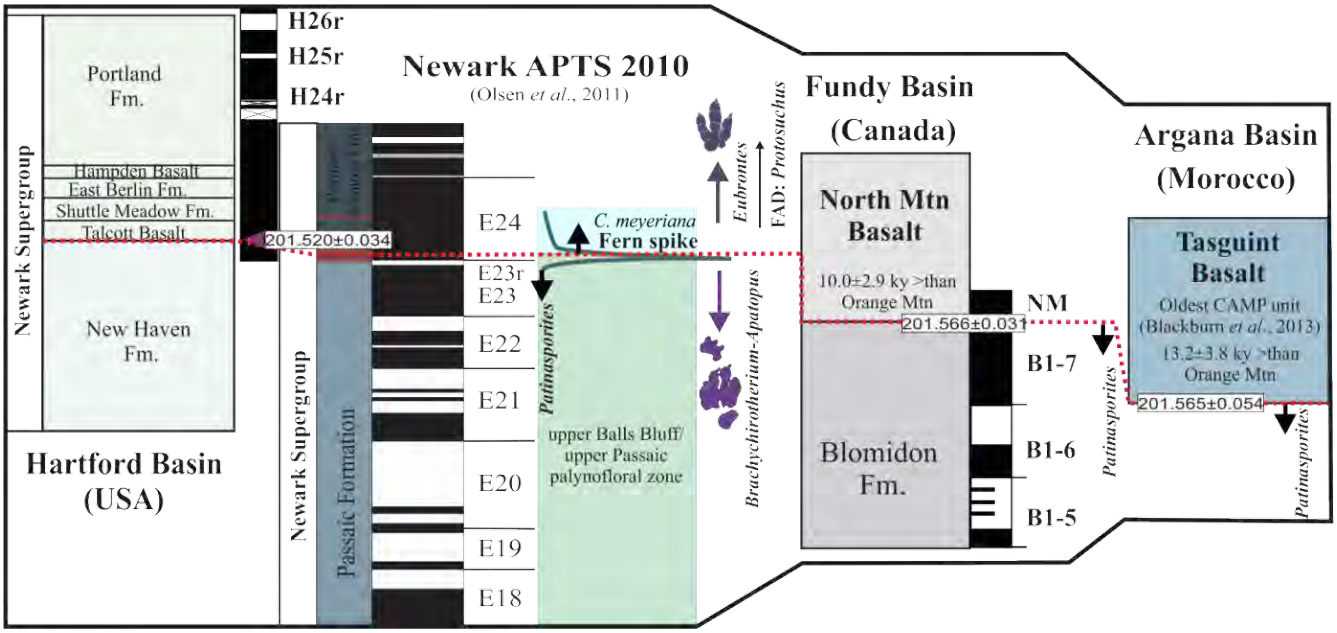

Figure 4.5. Newark APTS and correlation with the Hartford Basin with corresponding bio-events compared to and correlated with the Fundy Basin of Nova Scotia (eastern Canada) and the Argana Basin (Morocco) CAMP basalts. Radiometric ties are from Blackburn *et al.* (2013).

Correlation to Tethys marine realm has largely been dependent on the palynology in conjunction with magnetostratigraphy prior and subsequent to the radiometric dates. Palynological zones, as well as the fauna-chrons, are difficult to correlate with sections outside of the eastern USA (Hounslow and Muttoni, 2010), and appear to represent a degree of trans-Atlantic palaeoprovinciality or at least differences in environmental stress.

Lucas and Tanner (2007b) point out the problem with palynological work of the Newark Supergroup and list the various studies conducted that are divided into two camps. There are those that support Cornet (1993), Fowell and Traverse (1995), Fowell and Olsen (1995) and Fowell *et al*. (1994) in their assertion

of three palynofloral zones, the lower Passaic-Heidlersburg, the upper Balls Bluff-upper Passaic and the *Corollina meyeriana* palynozone, corresponding to the Norian, Rhaetian and Hettangian-early Sinemurian, respectively. These provide a relative date to the sediment below the CAMP basalts and within the Portland Formation overlying the basalts. In contrast, this is questioned by other palynologists and authors (i.e. Litwin *et al*. 1991; Tanner and Lucas, 2007b) that do not support these ages and correlations. For example, Litwin *et al*. (1991) consider the upper Balls Bluff-upper Passaic palynozones to be older than previously assessed and likely middle Norian in age.

Palynofloras within the upper Balls Bluff- upper Passaic palynofloral zone do not show characteristic Rhaetian palynomorphs (relative to Europe), but do show a rapid, up to ~60%, decrease in palynomorph diversity below the oldest CAMP basalt (Jacksonwald Basalt; Fowell and Olsen, 1995; Olsen *et al*., 2011).

This decline in diversity, highlighted by the *Classopollis meyeriana* fern spike, was initially linked to impact-induced extinction events around the TJB (Fig. 4.4, Fig. 4.6; Fowell and Olsen, 1995; Olsen *et al*., 2002a, b). Subsequently, Olsen *et al*. (2011) linked (albeit loosely) this event to palynofloral acme intervals from the Eiberg Basin (Austria), St. Audries Bay (Somerset, U.K.) as well as Argana Basin (Morocco) (Whiteside *et al*., 2007), which show an increase in spore abundance prior to the rise of Jurassic ammonites (Hounslow *et al*., 2004; Kürschner *et al*., 2007; Bonis *et al*., 2009).

These were in turn affirmed and correlated with tetrapod bio-chronology of Lucas (1998); although global correlations of the Apachean Land Vertebrate Faunachron (LVF) are still debated (Irmis *et al*., 2011; Parker and Martz, 2010). Lucas (1998) considers endemism and provinciality to contribute to this problem. With this in mind, Lucas and Tanner (2007b) regard the “Passaic palynofloral event” (the fern spike or “T–J palynofloral turnover” of Whiteside *et al*., 2003) to occur immediately below the TJB representing the end-Triassic biotic crisis (Fig. 4.4). They place the TJB within the succession of interbedded CAMP basalts above the late Norian/Rhaetian Passaic palynofloral event which they do not try to correlate to marine sections. They assert that the floral provinciality induced by palaeolatitude as referred to by Fowell and Olsen (1995), and later by Olsen *et al*. (2011), as not accountable for the discrepancies in Tethyan palynological correlations. Furthermore, Lucas and Tanner (2007b) suggest that the palaeogeographic reconstructions do not allow for exaggerated palaeolatitudinal differences and they cite the work of Kent and Tauxe (2005).

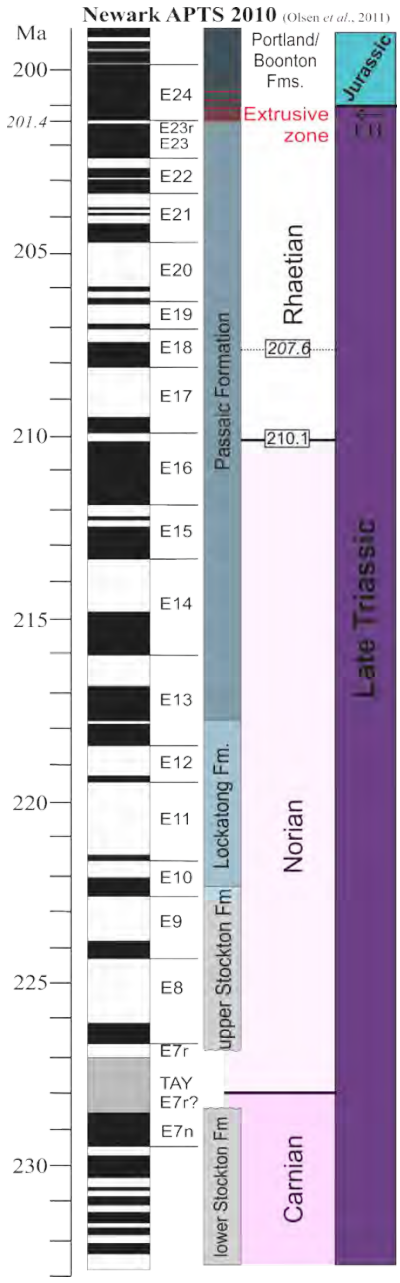

Figure 4.6. Newark APTS 2010 timescale of Olsen *et al.* (2011), extrusive zone refers to dates from the North Mountain Basalt (201.4 Ma; Blackburn *et al.*, 2013). The TJB is taken as the age reported by Schoene *et al.* (2010) of 201.31 ± 0.18 Ma. Two considerations for the base of the Rhaetian: the traditional short Rhaetian standpoint whereby it spans ~6.2 Myr and the long Rhaetian (~9.7 Myr), 207.6 or 210.1 Ma respectively.

In contrast, Hounslow *et al*. (2004) considers the upper Penarth Group palynofloras (St Audrie's Bay) to be shared with the upper Balls Bluff-upper Passaic palynofloral zone. Lucas and Tanner (2007b) disagree with this assessment and consider the Norian Mercia Mudstone Group to be the correct association of

palynofloral overlap with the Newark upper Balls Bluff-upper Passaic palynofloral zone. More recently, Deenen *et al*. (2010) effectively correlated the palaeomagnetic St. Audrie's Bay section of Hounslow *et al*. (2004) to the interval between E14r and E20r of the Newark Basin APTS with the top of the long SA3n normal representing the Norian-Rhaetian boundary (then at 210 Ma). The SA3r correlates with E17r of the Newark APTS. This places the non-marine Twyning Mudstone Formation and Blue Anchor Formation (Mercia Mudstone Group; UK) into the Rhaetian. If the new Norian-Rhaetian boundary (Wotzlaw *et al*., 2014) is taken into account this would place both into the Norian once more.

Whiteside *et al*. (2003) show that at the Passaic palynofloral event there is an associated negative C-isotope peak (similar to marine successions) which may be equivalent to SA5n.1r of the Westbury Formation at St Audrie's Bay. This re-asserts the aforementioned placement of the Newark Supergroup magnetozone E23r (considered Rhaetian) as an equivalent to the magnetozone BT5n.1r (Italcementi Quarry section; Muttoni *et al*., 2010) and UT27n.3r (composite GPST; Hounslow and Muttoni, 2010) which is considered uppermost Rhaetian in age. Although with the current redefinition of the Norian-Rhaetian boundary by Wotzlaw *et al*. (2014), this will need revision and reassessment.

In the marine GSSP at Kuhjoch (Austria) the base of the Hettangian is marked by the FA of *P. spelae* and it defines the commencement of post-extinction biotic recovery phase (Morton *et al*., 2008; Olsen *et al*., 2011; Morton, 2012). In translating this into the continental realm, for the Newark section specifically, the base of the Hettangian is likely to occur within the middle of the Feltville Formation (Olsen *et al*., 2011). This relies on indirect evidence taken from the geochemical, i.e. relatable carbon isotope excursions, and palynofloral correlations from other marine successions with comparable biozones to the Hettangian Kuhjoch GSSP (Hounslow *et al*., 2004; Whiteside *et al*., 2007; Ruhl *et al*., 2009).

The Feltville Formation lies directly above the Orange Mountain Basalt (201.520±0.034 Ma), and, using astrochronology, the middle part of the Formation was deposited 150 kyrs after the beginning of the ETE (201.564 Ma; Blackburn *et al*., 2013) placing it into the Hettangian. In the New York Canyon area (Nevada, USA), the FA of *P. spelae* is marked by the U-Pb age of an ash bed directly above it at 201.33±0.13 Ma (Schoene *et al*., 2010), and this age is considered by Olsen *et al*. (2011) to be comparable to the estimated Hettangian base within the Feltville Formation. A South American tie for continental and marine successions comes from the Pucara Basin (northern Peru) for which there is a detailed chrono- and bio-stratigraphy with U–Pb ages and biostratigraphic marine events easily relatable to the New York Canyon area and Fundy Basin (Schaltegger *et al*., 2008; Schoene *et al*., 2010; Guex *et al*., 2012).

Comparison and correlation of the Newark magnetostratigraphy with the contemporaneous non-marine Chinle Group (south-western USA; Molina-Garza *et al*., 1996, Molina-Garza *et al*., 2003) has yielded inconclusive results, largely because of the insufficient sampling density within the Chinle (Hounslow and Muttoni, 2010). Based on the similar in faunas, the upper Chinle Formation is considered to correspond to Newark composite E18 – E21 and the Wingate Formation long normal polarity to the Newark E22 and E23 (Molina-Garza *et al*., 2003). The latter intervals are further supported by data from the Fundy Basin, St Audrie's Bay and Upper Lunde Formation (Kent and Olsen, 2000; Molina-Garza *et al*., 1996; Hounslow *et al*., 2004; Müller *et al*., 2004, Hurum *et al*., 2006). Other rift basins relatable to the Newark include those in Morocco (Argana and High Atlas Basins) which have yielded palynofloral assemblages below $^{40}Ar/^{39}Ar$ dated CAMP basalts (198.1±0.4 Ma, and before the TJB at 199.1 Ma) similar to those of the Newark (Verati *et al*., 2007; Blackburn *et al*., 2013).

4.4.3 **Continental Carnian - Norian boundary**

The position of the Carnian-Norian boundary (CNB) as well as the duration of the Norian and Rhaetian Stages in the Newark Supergroup APTS is fairly contentious (Hounslow and Muttoni, 2010; Olsen *et al*., 2011; Wotzlaw *et al*., 2014). Olsen *et al*. (2011) consider that the palaeomagnetic correlations of Steiner and Lucas (2000) in conjunction with that of Channell *et al*. (2003) and Muttoni *et al*. (2004) have allowed for the proposal of negligible Carnian aged continental rocks in the western USA. They consider that the strata previously considered Carnian may indeed be early Norian in age. This interpretation would be in agreement with the new U-Pb dates (Ramezani *et al*., 2014) from detrital zircons from the lower Chinle Formation (Arizona, Petrified Forest National Park) which, when compared to Norian marine U-Pb ages of 225±3 Ma (southern Alaska), reflect dates younger than the currently defined early Norian. Atchley *et al*. (2013) and Ramezani *et al*. (2014) consider the lower Chinle Formation (uppermost Blue Mesa Member) to have a radiometric age of 220.124±0.068 Ma (Fig. 4.7) placing it well within the Norian. The duration of the Carnian in the northern USA, as proposed by Olsen *et al*. (2011), is therefore relatively short and likely lasting ~7±4 Myrs (between ~235±2 – 228±2 Ma; Brack *et al*., 2005) when the age of the base of the Carnian is that of Muttoni *et al*. (2004). The CNB is furthermore considered, through cyclostratigraphy and the Newark APTS, to fall at 228±2 Ma (E7n chron APTS 2008 from Olsen and Whiteside, 2008). Hüsing *et al*. (2011) consider the CNB to be at the top of the E7n chron based on correlations with the Pizzo Mondello and Silická Brezová magnetostratigraphic sections. This refinement of the CNB being first proposed via the correlations of Channell *et al*. (2003) at Silická Brezová were the CNB was then linked to Newark E7r zone at ~226 Ma. Conversely, recent work by Maron *et al*. (2015) correlate the Pignola-Abriola section to the Newark E13n – E20r, and suggest that the CNB should be

taken at ~227 Ma (Muttoni *et al*., 2014). Thus, the duration of the Norian in itself can range between 19 - 26.7±2 Myr, between 228±2 and 207.6/210.1 Ma (the latter incorporates Sevatian 2 into the uppermost Norian) or 205.5 Ma.

4.4.4 **Continental Norian-Rhaetian Boundary and the duration of the Rhaetian**

The Norian-Rhaetian boundary and the duration of the Rhaetian is still hotly contested (Fig. 4.7; Channell *et al*., 2003; Gallet *et al*., 2007; Hounslow and Muttoni, 2010; Hüsing *et al*., 2011; Olsen *et al*., 2011; Ogg and Hinnov 2012; Wotzlaw *et al*., 2014; Maron *et al*., 2015). Traditionally, the Rhaetian has been considered to represent very little time and this was because of the initial deficiency in biozones. More recently it has been considered to cover a longer period of time (Krystyn *et al*., 2007b; Olsen *et al*., 2011; Ogg, 2012). There are two proposed durations for the Rhaetian based on the placement of the NRB. These are either the (a) short ~4 Myr Rhaetian versus the (b) long ~9 ±2 Myr Rhaetian; with either stand point being largely dependent on biostratigraphy and magnetostratigraphic comparisons for validation (Fig. 4.7).

The exact length of the stage, however, is still uncertain as the lower and upper bounding markers change with the refinement of stratigraphic work. For example, the most recent revision of the duration of the Rhaetian and clarification of the stage boundary comes from new U/Pb ages of Wotzlaw *et al*. (2014) from ash beds occurring above the LAD of bivalve *Monotis subcircularis* within the Pucara Basin in Peru. Previously, the lower boundary of the Rhaetian Stage was placed at *ca*. 209.5 Ma, however the U/Pb age of 205.5±0.35 Ma at the base of the Peruvian Rhaetian strata (Fig. 4.7) limits the duration of the Stage to 4.14 ± 0.39 myr (Wotzlaw *et al*.2014). This is supported by the correlations of Maron *et al*. (2015) between the Newark and the Pignola-Abriola section (Fig. 4.7). The short-Rhaetian option proposed by Kozur and Weems (2005) and Gallet *et al*. (2007), and revised in the Geological Time Scale 2012 (Ogg, 2012) was later supported by Lucas *et al*. (2012), Wotzlaw *et al*. (2014) and Maron *et al*. (2015). The assertions by Lucas *et al*. (2012) of a short Newark Rhaetian Stage (~4 Myrs; Ogg and Hinnov, 2012) rest firmly with conchostracan biostratigraphy, in conjunction with tetrapod biostratigraphy, and propositions a large Rhaetian-aged gap in which the Newark hiatus is assumed to be longer than previously considered. Lucas *et al*. (2012) consider the Newark to only preserve 0.2 Ma of the Rhaetian based on an argument that uses relatively poorly constrained conchostracan biostratigraphy to correlate continental and marine successions. The conchostraca from the Germanic Basin and their

relative-age, when compared to other European sections, are the means by which the correlations rest largely.

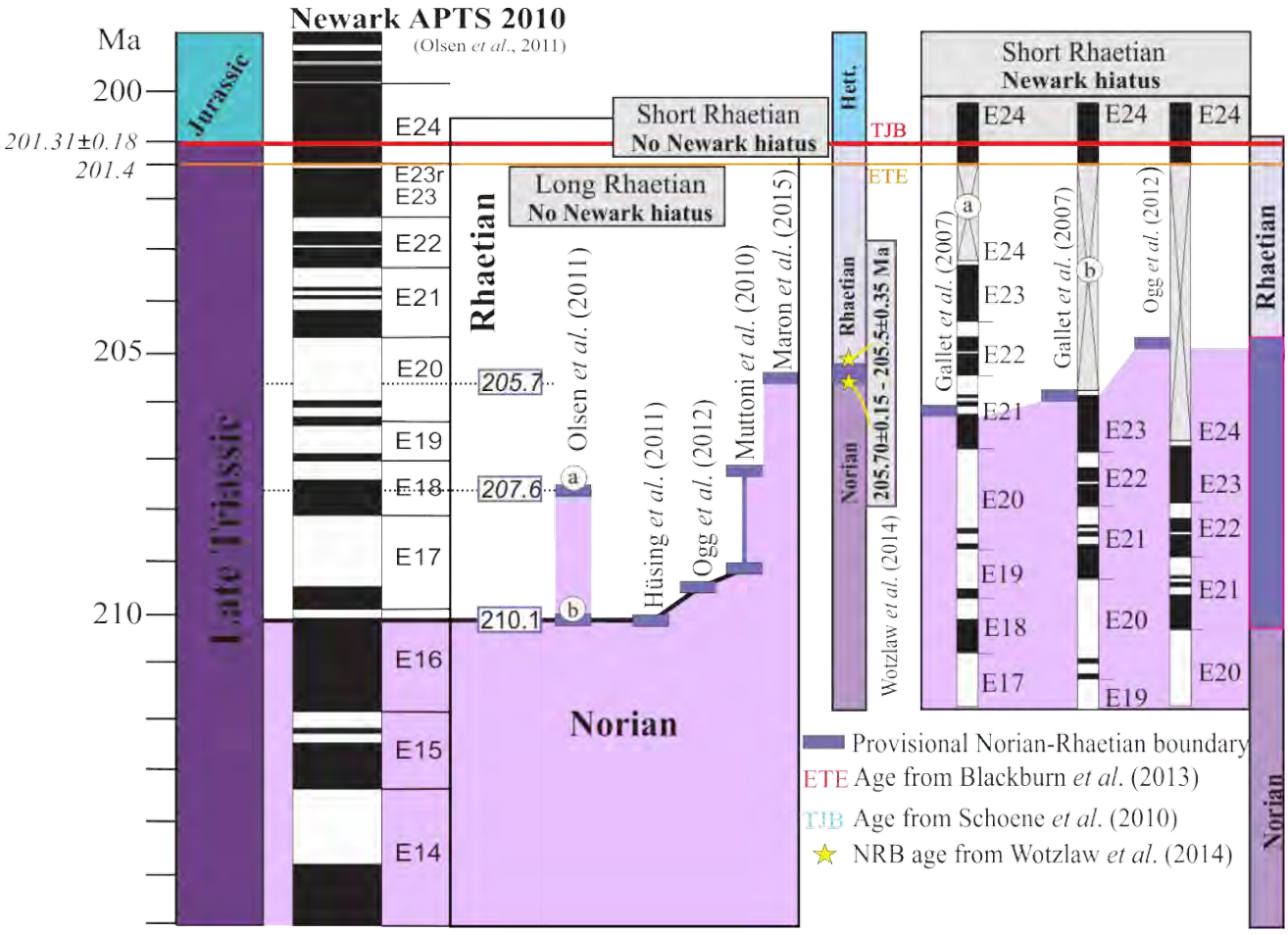

Figure 4.7. Placement of the Rhaetian-Norian boundary (NRB) and debate over the duration of the Rhaetian with inferences for a Newark hiatus as adapted from Wotzlaw *et al.* (2014) with new data from Pucara Basin, Peru. ETE = end-Triassic extinction, TJB = Triassic-Jurassic boundary.

It is important to note that the original placement of the NRB within the Newark Basin was tentatively established by palynoflora records (Cornet, 1993). It has more recently been placed at the suggested age of Maron et al. (2015) which complements the marine records of Wotzlaw et al. (2014). However, the long Rhaetian, when using the Newark APTS as a basis of basin cross-comparison, is considered by some authors (Fig. 4.7; Channell *et al.*, 2003; Muttoni *et al.*, 2010; Hüsing *et al.*, 2011) to be approximately 8 m.y. in duration (Fig. 4.7), with the NRB at ~209.5 Ma. This is on the basis of a marine-Newark

correlation and the absence of any major hiatuses. In line with this, work by Hüsing *et al.* (2011) show that correlation to the Newark APTS allows for definition of the base of the Rhaetian to fall within the E16n and E16r chrons, but only when considered in light of Sevatian 2 being part of the early Rhaetian. This is again, as pointed out by Olsen *et al*. (2011) reliant on stage definitions in the marine realm via biostratigraphy. The magnetostratigraphic correlation between the Newark APTS, in its perceived relative continuity, and marine sections is the main driver defining a long(er) Rhaetian stage.

Olsen *et al*. (2011) consider the duration of the Rhaetian, when comparing it to the Newark APTS, could be of two suppositions, the traditional short Rhaetian standpoint whereby it spans ~6.2 Myrs, or long Rhaetian (~9.7 Myr) depending on whether Sevatian 2 is considered inclusive into the Rhaetian stage. Thus the inclusivity of the Sevatian 2 into the uppermost Norian or the base of the Rhaetian would shift many palaeomagnetic scales by ~2.5 Myr. The duration and presence of the Rhaetian within the Newark is further confused by the position and identification of an unconformity. This problem largely rests on the debated palynofloral analyses. Olsen *et al.* (2011) still consider the Norian-Rhaetian boundary to coincide with the boundary between the Lower Passaic–Heidlersburg and upper Balls Bluff–upper Passaic palynofloral zones (Figs. 4.4; 4.5), which shows a dramatic increase in the number of *Classopollis* (*Corollina*) spp., as is seen in marine sections.

That said, Tethyan marine substages (i.e., Sevatian 2) are used purely, as Olsen *et al*. (2011) point out, from necessity until recognised GSSPs for stages and substages are acknowledged. The incorporation of Sevatian 2 into the uppermost Norian for the Newark APTS is largely based on the position of the palynofloral NRB which falls within E18n chron (from Olsen *et al*., 2011 Newark 2008/10 APTS; Figs. 4.6; 4.7). The Sevatian 2, although traditionally upper Norian, has been more comfortably incorporated into the Rhaetian by Krystyn *et al*. (2007a, b) and further magnetostratigraphic correlations by Hüsing *et al*. (2011) when considered principally in relation to the European marine sections (particularly the GSSP at Steinbergkogel) and primarily in terms of ammonite and conodonts occurrences. In contrast, from a continental perspective, when considered with cyclostratigraphy, magnetostratigraphy and global sections, the interpretation of Olsen *et al.* (2011) (whereby the ETE is at 201.4 Ma) would further affirm the placement of Sevatian 2 within the Norian, but largely leaning on the palynofloral NRB. Kent *et al*. (2014), in their correlations between the Newark APTS and Los Colorados Formation (Argentina), have placed the NRB at the top of the E16n chron (giving it an age of ~210.1 Ma; Figs. 4.6; 4.7). Whereas Channell *et al*. (2003) place the NRB at E17r and therefore at ~207 Ma (short Rhaetian; Fig. 4.7).

More recently, work by Wotzlaw *et al*. (2014) on the volcanic ash beds of the Aramachay Formation (Pucara Group, northern Peru) have led to interesting developments regarding the age and duration of the Rhaetian (Fig. 4.7). Within the Aramachay Formation, Schaltegger *et al*. (2008) have obtained a U-Pb age of 201.58 ± 0.28 Ma for the marine TJB in conjunction with and in relation to LO and FO of key ammonites (e.g., *Choristoceras* and *Psiloceras*, respectively) and 199.53±0.19 / 0.29 Ma for the Hettangian–Sinemurian boundary. The zircon U-Pb dates obtained are from samples near the Norian/early Rhaetian boundary and were sampled above the LO of *Monotis subcircularis* (Wotzlaw *et al*., 2014). The depositional age of these beds is between 205.70 ± 0.15 Ma and 205.30 ± 0.14 Ma (mean age of 205.5 ± 0.35 Ma) and therefore provide, when combined with Blackburn *et al*. (2013) age of the North Mountain Basalt (201.5 Ma; commonly used for the ETE/TJB) a short Rhaetian spanning ~4.14 ± 0.39 Myr (Fig. 4.7; Wotzlaw *et al*., 2014).

This shifts the Norian-Rhaetian boundary to within the E20r chron of the Newark APTS. Wotzlaw *et al*. (2014) assert that the radiometric date for the NRB means that magnetostratigraphic correlations previously used between the Newark APTS and Tethyan section are in need of revision (Fig. 4.7).

4.5 Early Jurassic magnetostratigraphy

Globally, there are few Lower Jurassic sections with detailed radiometric, bio- and magnetostratigraphy. The GTS for the Early Jurassic is, generally, not well-constrained using multiple proxies, but rather dependent on marine records (mainly biostratigraphy).

As such the GSSPs at Kuhjoch (Austria) for the Hettangian and at East Quantoxhead (UK) for the Sinemurian are dependent on ammonites which, considering that they act as GSSP ‘golden spike’ for boundaries, would require more validation. The Hartford Basin provides continental Early Jurassic magnetostratigraphy which was incorporated into the Newark APTS (Kent and Olsen, 2008). As does the Glen Canyon Group’s Moenave Formation (western USA) which has been extensively studied by Donohoo-Hurley et al. (2007, 2010), and the Kayenta Formation (Steiner, 2014; Steiner and Tanner, 2014). The Early Jurassic magnetostratigraphy from the Hartford Basin shows one long normal chron punctuated by three short reversals, and correlation with the Newark APTS (2010) placed the long normal chron with E24n (Kent and Olsen, 2008; Hounslow and Muttoni, 2010; Olsen *et al*., 2011). This

astronomically-calibrated section is in good agreement with St. Audries Bay (UK) (Hounslow *et al*., 2004).

Magnetostratigraphy, coupled with previous cyclostratigraphy from the sections at St Audries Bay and East Quantoxhead in the U.K. have allowed for better assessment of the correlation between the marine astronomical calibration framework for the early Jurassic and its correlation to the Newark APTS (Fig. 4.6; Hüsing *et al*., 2011; Hüsing *et al*., 2014). Thus, the St. Audrie's Bay/East Quantoxhead composite section (Hüsing *et al*., 2014) uses the additional and independent framework of cyclostratigraphy and astronomical calibration with magnetostratigraphy to refine for the Hettangian and Early Sinemurian Stages. Hüsing *et al*. (2014) study showed repeatability of palaeomagnetic polarity pattern (long normal punctuated by 3 short reversals) with the Hartford Basin and Paris Basin, and is likely to be used as a stratotype section for the Hettangian Stage.

5 Sampling and methodology

The Elliot Formation was sampled at ten different study localities in Lesotho and South Africa, mainly for palaeomagnetic study, however at certain sites samples were also taken for geochemistry. The strata at all localities are undeformed with a negligible dip of maximum 5°. Similar lithologies are present at all sections. Many localities provided possible field tests for palaeomagnetic stability. Simultaneously, data for sedimentological logs were also collected at the study sites, and the sedimentological break between the LEF-UEF (a rough proxy for the TJB) was marked on the logs. The stratigraphic position of body and trace fossils as well as the palaeomagnetic and geochemical samples were systematically recorded on the sedimentological log of each site.

5.1 Palaeomagnetic sampling

Sampled section localities and their descriptions are presented in detail in the subsequent result chapters.

Palaeomagnetic samples were drilled, using a hand-held portable petrol drill, at regular intervals (on av. 0.8 m) where lithology allowed. Samples, from all sites, were taken from the least weathered outcrops, and ‘cut backs’ were made where fresh outcrop was not available by using various masonry tools, brushes and a geological hammer. This rock exposing method became particularly relevant when drilling through mudstones and clay-rich siltstones the most common lithology in the Elliot Formation. Orientation of the palaeomagnetic samples was accomplished by using a magnetic compass as well as a sun compass. All cores collected were labelled in the field and later cut to ~2 by 2 cm blocks in the sample preparation laboratory at the University of Johannesburg (UJ). Clay-rich mudstone samples which cracked or slightly crumbled during drilling were carefully orientated and glued with wood-glue in the field and later further cemented in the laboratory using a mixture of sodium silicate and diatomaceous earth.

5.2 Demagnetization

Samples were measured in the Palaeomagnetic Laboratory at the University of Johannesburg in a magnetically shielded room with internal field less than 500 nT. Samples were run on a vertical 2G-Enterprises DC-4K (liquid Helium free) superconducting rock magnetometer. Samples were measured for normal remnant magnetization (NRM) prior to low field-strength alternating field (AF) demagnetization

in five 20 G steps (to 10 mT). Samples were then thermally demagnetized, in a shielded furnace, at increasing temperatures between 150 ^{o}C and 680 ^{o}C with decreasing intervals until specimen intensity was low. The thermal step intervals varied between sites from 100 ^{o}C, 50 ^{o}C, 25 ^{o}C to 15 ^{o}C, in increments, depending on the speed at which magnetization was lost.

Least squares component analysis (Kirschvink, 1980) was used to obtain the magnetic components, which were then statistically analysed using Paleomag 3 (Jones, 2002). The use of remagnetization circles for palaeomagnetic direction determination was avoided where possible.

5.3 XRD, XRF and ICP-MS analyses

To better understand palaeoenvironmental conditions and potential climatic changes during the deposition of the Elliot Formation, geochemical analysis (major, trace and rare earth elements) of a total of 126 samples drilled along three transects at Likhoele (LIK and LIKE - Lesotho) and at Damplaats (DAM – Free State, South Africa) were undertaken. The X-ray diffraction (XRD) and fluorescence (XRF) analyses of these samples were undertaken in the Department of Geological Sciences at the University of Cape Town (South Africa).

5.3.1 **XRD**

Samples were disaggregated in an agate mortar, washed with distilled water, and sonified in an ultrasonic bath for a few minutes. Powdered samples were then well-suspended for 12 hours allowing separation by settling in distilled water. Clay fraction (<2-µm) was removed via pipette and dropped onto glass slides. Evaporation of a clay–water suspension was done via drying at room temperature. The <2-µm grain-size fraction was then identified by using X-ray diffraction patterns.

The XRD instrument used is a Philips PW 1390 X-ray Diffractometer which uses a Copper K-α X-ray tube with X-ray wavelength of 1.542 Å, accelerating voltage of 40kv and current of 25mA. Bragg 2Θ angles between 20 and 50° were used for analysis. A continuous scan step size of 0.02° was applied with a scan step time of 0.75s. The resultant XRD pattern of 2Θ angles vs. intensity was used to calculate the d-spacing of the most intense peaks by applying the Bragg law.

5.3.2 **XRF & ICP-MS**

The X-ray fluorescence (XRF) analyses of these samples were undertaken in the Department of Geological Sciences at the University of Cape Town (South Africa). XRF analyses were obtained with a Panalytical Axios X-ray fluorescence spectrometer, which employs a rhodium end-window X-ray tube and a wavelength-dispersive spectrometer. Fusion disks (0.6 g rock powder to 3.6g lithium borate flux) were made using an automated Claisse M4 Fluxer instrument for major element measurements. XRF analyses were obtained with a Panalytical Axios X-ray fluorescence spectrometer, which employs a rhodium end-window X-ray tube and a wavelength-dispersive spectrometer. The total abundance of major and minor elements (Si, Al, Fe, Ca, Mg, Na, K, Mn, Ti, and Cr) is reported on the basis of 0.6 g samples.

Rare earth elements were analysed by inductively coupled plasma mass spectrometry (ICP- MS). Quantitative trace element measurements were done using a Thermo-Fisher X-Series2 quadrupole ICP-MS housed in the Geological Sciences Department at UCT. Sample preparation involved dissolving, in sealed Savilex beakers, 50 mg of a powdered sample in a 4:1 HF/HNO_3 acid mixture on a hotplate for 48 hours. This solution was then evaporated and followed by two treatments of 2 ml of concentrated HNO_3 and incipient drying. The final dried product was then re-dissolved and diluted in 5% HNO_3 solution containing 10 ppb Re, Rh, In and Bi as internal standards, and the standardisation was against artificial multi-element standards.

Result chapters for southern-most sections

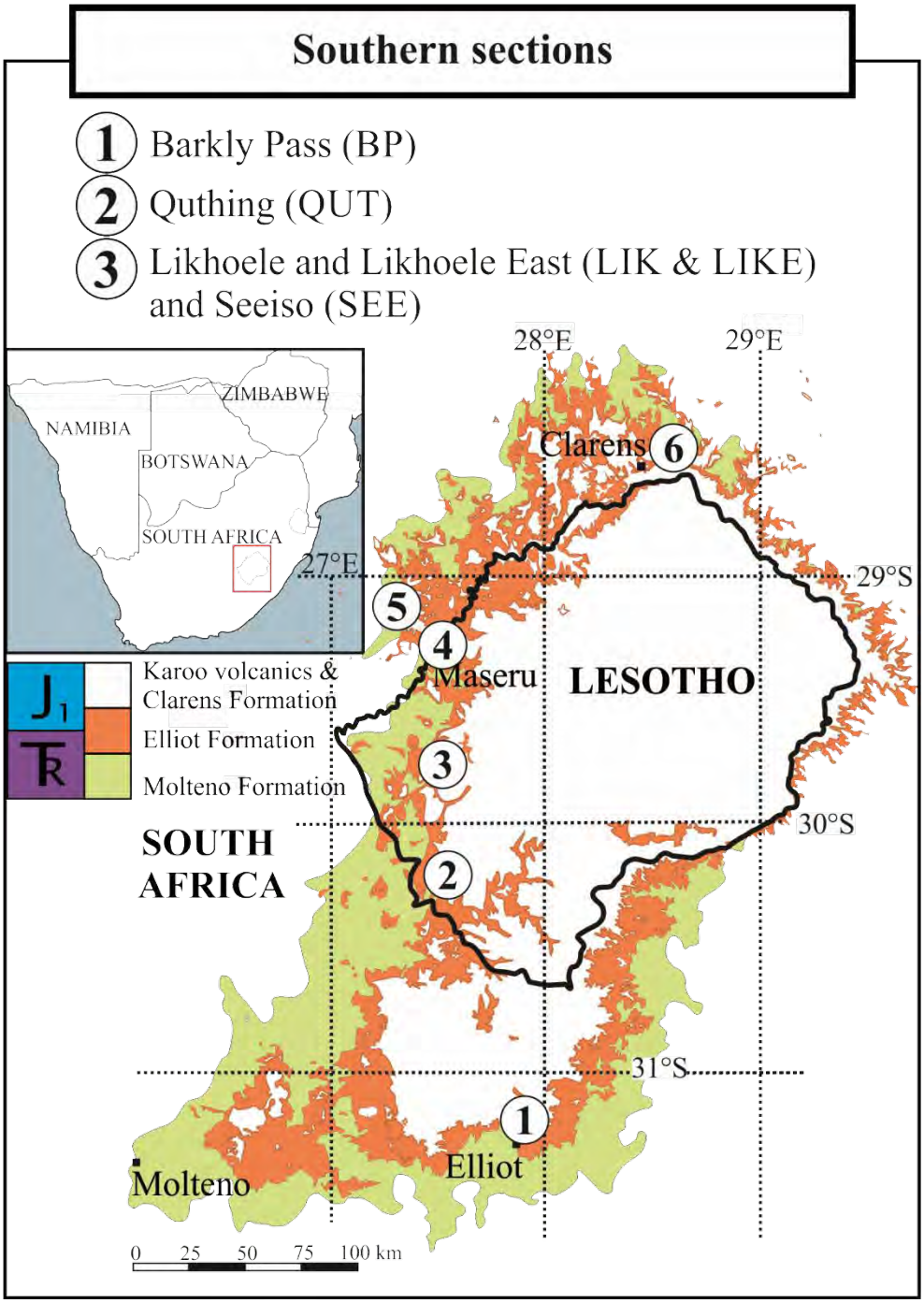

6 New palaeomagnetic constraints for the Elliot Formation at the type locality at Barkly Pass, Eastern Cape, South Africa

6.1 Introduction

In this chapter, new palaeomagnetic constraints for the lower Elliot and upper Elliot Formation are presented and combined, and therefore extend the previous work of de Kock (2003). As Barkly Pass represents the type stratotype locality for the Elliot Formation (Bordy and Eriksson 2015), the palaeomagnetic work done at this site will:

(i) Represent a baseline for section comparisons from different part of the basin, and

(ii) Show that primary magnetizations are preserved at the type locality despite the presence of several dykes, which did not significantly affect the magnetostratigraphy.

The Barkly Pass exposes natural and road cuttings along the R58 that connects the Eastern Cape towns of Elliot and Barkly East (Fig. 6.1). The road through the pass winds from Molteno Formation, within the Tsomo River valley, to the south into the lower Elliot (LEF) and upper Elliot (UEF) and through the overlying Clarens Formation as well as volcanics of the Drakensberg Group (Fig. 6.1B). Barkly Pass underwent rebuilding in the mid to late 1970s and provided clean, fresh exposure for detailed sedimentological study, which was undertaken by Visser and Botha (1980) over several years.

The Elliot Formation is between 460 – 480 m (Barkly Pass = 460 m) thick in this part of the basin and, in addition to its relatively good exposure in the Barkly Pass, has meant that the Pass was selected as the stratotype for the Elliot Formation (SACS, 1980; Bordy and Eriksson, 2015). The Elliot Formation in the Barkly Pass was first briefly described by du Toit (1904) and further detailed qualitative work was carried out by du Toit (1939), Stockley (1947), Botha (1968), Haughton (1969) Johnson (1976) and Visser, 1984 in the Eastern Cape and along the Barkly Pass. Visser and Botha (1980) provide a comprehensive sedimentological and palaeoenvironmental study of the Elliot Formation at Barkly Pass, and divide the Elliot Formation into three facies assemblages that they interpret, from base to top, as products of (i) meandering river channel-floodplain, (ii) flood-basin and (iii) flood fan and dune settings (Table 6.1). Bordy *et al*. (2004a, b) reviewed this analysis in light of the regional significance of the Elliot Formation.

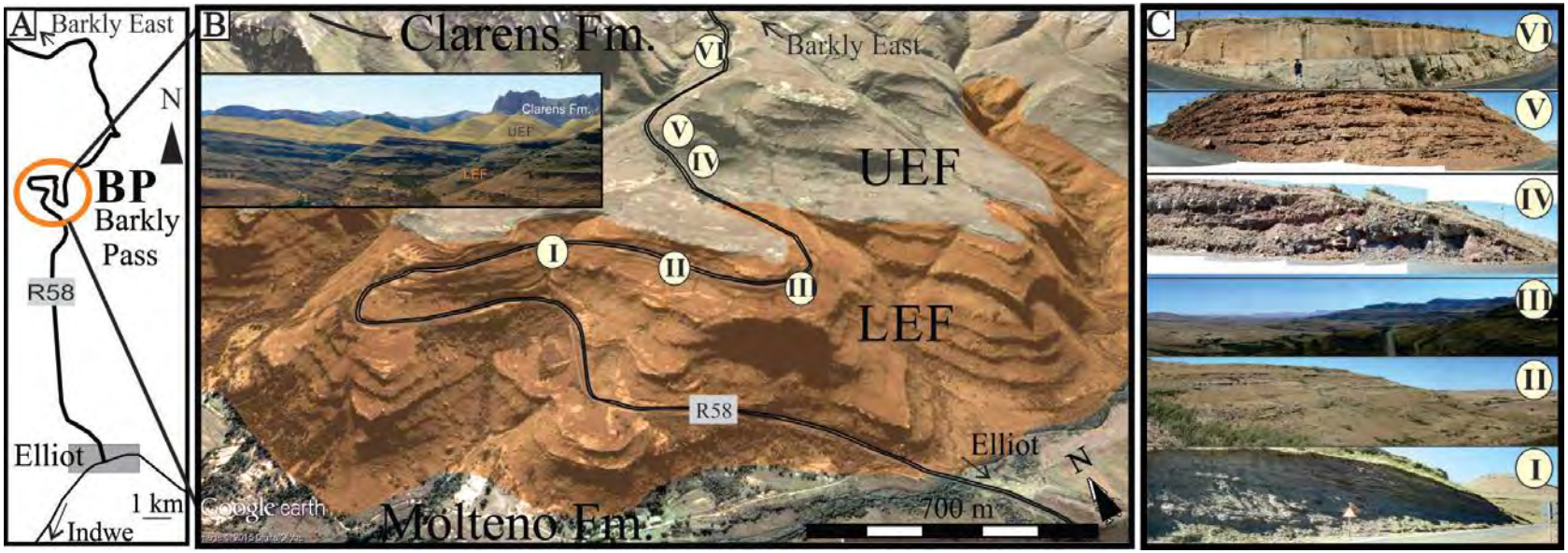

Figure 6.1. Barkly Pass (BP) site in the Eastern Cape (South Africa). (A) Locality road map, (B) annotated Google Earth image with colourised geological map overlay indicating LEF – UEF boundary and the overlying Clarens Formation, and (C) site photographs, which are shown on the Google Earth image with roman numerals (i – iii are of the LEF; iv – vi are of UEF sites). LEF = Lower Elliot Formation, UEF = Upper Elliot Formation.

6.1.1 **Previous mineralogy/geochemistry**

Johnson (1976) studied the petrography and mineral composition of 3 typical sandstone samples from Barkly Pass, and established that the sandstones are fine- to medium-grained (Mean size: 2,48 ø {0.18 mm}; Standard deviation: 0,57 ø; Maximum size: 1,11 ø {0.45 mm}) and the composition of these arenites. The composition is 59.5% quartz (incl. secondary overgrowths), 9% feldspar, 17.5% rock fragments, 1% accessory minerals, 3% cement (mainly calcite), and 10% matrix. Johnson (1976) also reported a NNE to NE directed palaeocurrent direction in the Pass, which is anomalous in comparison to other Elliot Formation sites where the dominant flow direction was from south to north (Bordy *et al.*, 2004c).

6.1.2 **Previous magnetostratigraphy**

De Kock (2003) conducted a preliminary palaeomagnetic study at the Pass, which considered only the lower 200 m of the Formation (LEF). A summary of the results of this study are presented in Figure 6.2.

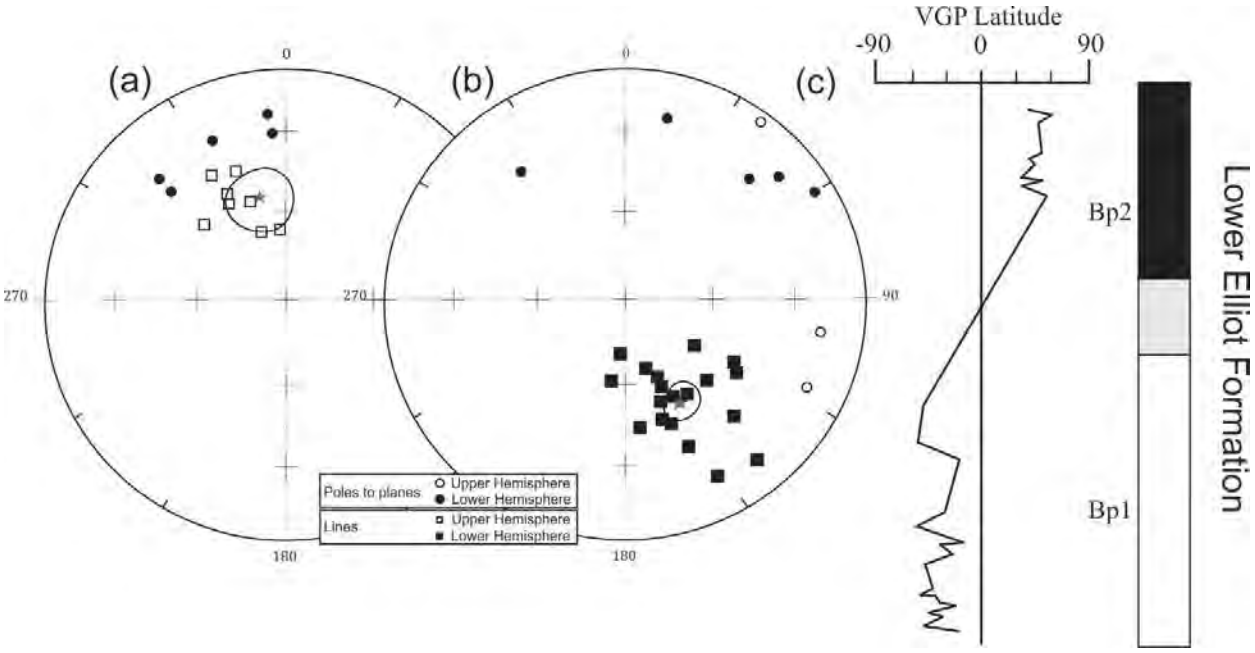

Figure 6.2. Summary of de Kock (2003) results for the lower 200 m of Barkly Pass section. Star indicates (a) mean normal directions (b) mean reverse directions. The Bp1 and Bp2 subchrons shown in (c) were established and form the basis of de Kock's (2003) EF1 chron for the lower Elliot Formation. Colour conventions hold for black = normal polarity, white = reverse polarity, grey = uncertainty in sample direction.

For this site, characteristic remnant magnetisation (NRM) directions of normal and reverse polarity were obtained, in the form of both lines as well as planes (plotted as poles to planes), using the McFadden and McElhinny (1990) method. Both the normal and reverse direction passed the palaeomagnetic reversals test (McFadden and McElhinny, 1990) on the basis that antipodal directions could not be rejected at a 95% confidence limit. De Kock (2003) placed this into a category "C" reversals test using an obtained angular separation of 3.3^{o} between directions, and a critical angular separation of 13.3^{o} at 95% confidence. At Barkly Pass, de Kock (2003) subdivided his measured succession in the LEF into a 120 m reverse polarity zone (Bp1R), for the strata that lie directly above the Molteno Formation, and into a succeeding well-defined normal polarity zone (Bp2N).

6.1.3 **Biostratigraphy: Palaeontological information from BP**

The type section for the Elliot Formation, at Barkly Pass, is considered rather depauperate in terms of fossil abundance and diversity. This makes the biostratigraphic zonation in the Pass more difficult than that of other Elliot Formation sites with a richer fossil heritage. Table 6.1 details finds at or proximal to Barkly Pass.

Table 6.1. Stratigraphic distribution of vertebrate and invertebrate taxa in the Barkly Pass and its close vicinity.

Taxonomic assignments	Age	Stratigraphic position	Catalogue no.	Notes	Source(s)
Heterodontosaurid; *Geranosaurus atavus*	Latest Triassic (but acknowledge it may be earliest Jurassic)	Clarens Fm./uppermost UEF	SAM-PK-K1871 1 SAM-PK-K1857 2	Road cutting near summit of Barkly Pass, Eastern Cape, South Africa. Partial skull Holotype Broom (1911); Hindlimb material Referred specimen Broom (1911)	Porro *et al*. (2010)
Sauropoda indet.	Latest Triassic (but acknowledge it may be earliest Jurassic)	UEF	BP/1/6105	Spioen kop Farm, Rozendal District, Free State (28°27.991'S, 27°49.476'E). Proximal caudal vertebra (showing autapomorphic character state with Vulcanodon)	Yates *et al*. (2004)
Sauropodomorpha; *Arcusaurus pereirabdalorum*, gen. et sp. nov	Latest Triassic (but acknowledge it may be earliest Jurassic)	UEF	BP/1/6235	Sauropod Quarry, Spion Kop 932, Senekal District, Free State (S28°28.002 E027°49.523)	Yates *et al*. (2011)
Conchostraca *Cyzicus* sp.	Triassic-Jurassic	uppermost UEF	-	Prominent last sandstone beds of the Elliot at Barkly Pass (see Fig. 6.5A (i - ii). Trough cross bedded, fine-grained with green mud draped surfaces. Lack of associated biota indicates short lived nature of water body and the likelihood of soft bodied protists as food resource	Tasch (1984)

6.1.4 **Sampling**

The section sampled at Barkly Pass, for the current study, was chosen for its relative degree of vertical outcrop continuity and in order to obtain a more complete palaeomagnetic zonation that is representative of the Elliot Formation (Fig. 6.3).

The extent of the sampling in the Pass was motivated by the objective (i) to sample across the sedimentological LEF-UEF transition identified in the field by using lithological features distinctive between the LEF and UEF as well as the geomorphological feature (an erosional plateau); and (ii) to reproduce a portion of the section sampled by de Kock (2003) to allow comparison with his results (Figure 6.3), and finally (iii) to obtain samples from higher in the UEF to constrain the conchostracan bearing beds at the top of the Pass in relation to other uppermost UEF conchostracan-bearing sites.

A lithological log and the stratigraphic setting of the sampling sites (BP 1 – 119) are shown in Figure 6.3.

6.2 Results

6.2.1 **Sedimentology**

6.2.1.1 Lower Elliot Formation

Several laterally continuous stacked beds of fine- to medium-grained sandstones characterize the LEF at the base of the current palaeomagnetic section (Fig. 6.4). The channels ranged in thickness from < 1m to ~3 m (Fig. 6.4A). Generally, the bases of these channels are irregular, indicate scouring and are commonly associated with mud-chip conglomerates. The uppermost contact of these sandstones is usually sharp with the overlying muddy siltstones or mudstones (Fig. 6.4).

The thick-stacked sandstone-dominated successions are regularly overlain by alternating mudstone-sandstone units, in which the sandstones form thin (≤30 cm, max. ~60 cm) lenses with horizontal lamination and ripple cross–lamination (Figure 6.4C). These sandstones lenses often display upward fining into the overlying mudstones that are either massive (Fm) or laminated (Fl). Figure 6.4A shows soft sediment deformation and slump balls within one of these fine grained sandstone units.

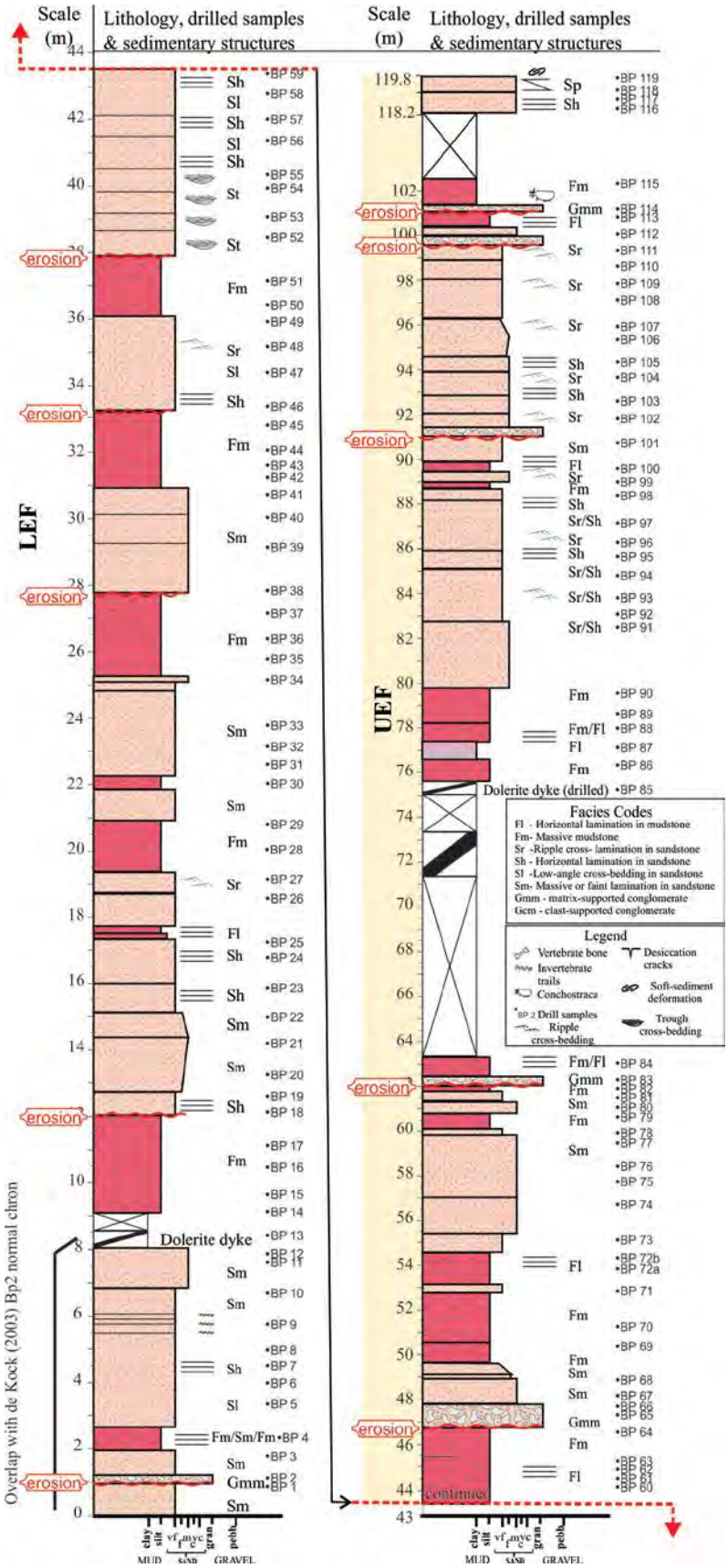

Figure 6.3. Barkly Pass lithological column showing overlap with de Kock (2003) sample sites, as well as the LEF –UEF transition based on geomorphological and sedimentological features (dashed red line). Samples were taken at a base of 1460 m and end at 1740 m (~260m drilled).

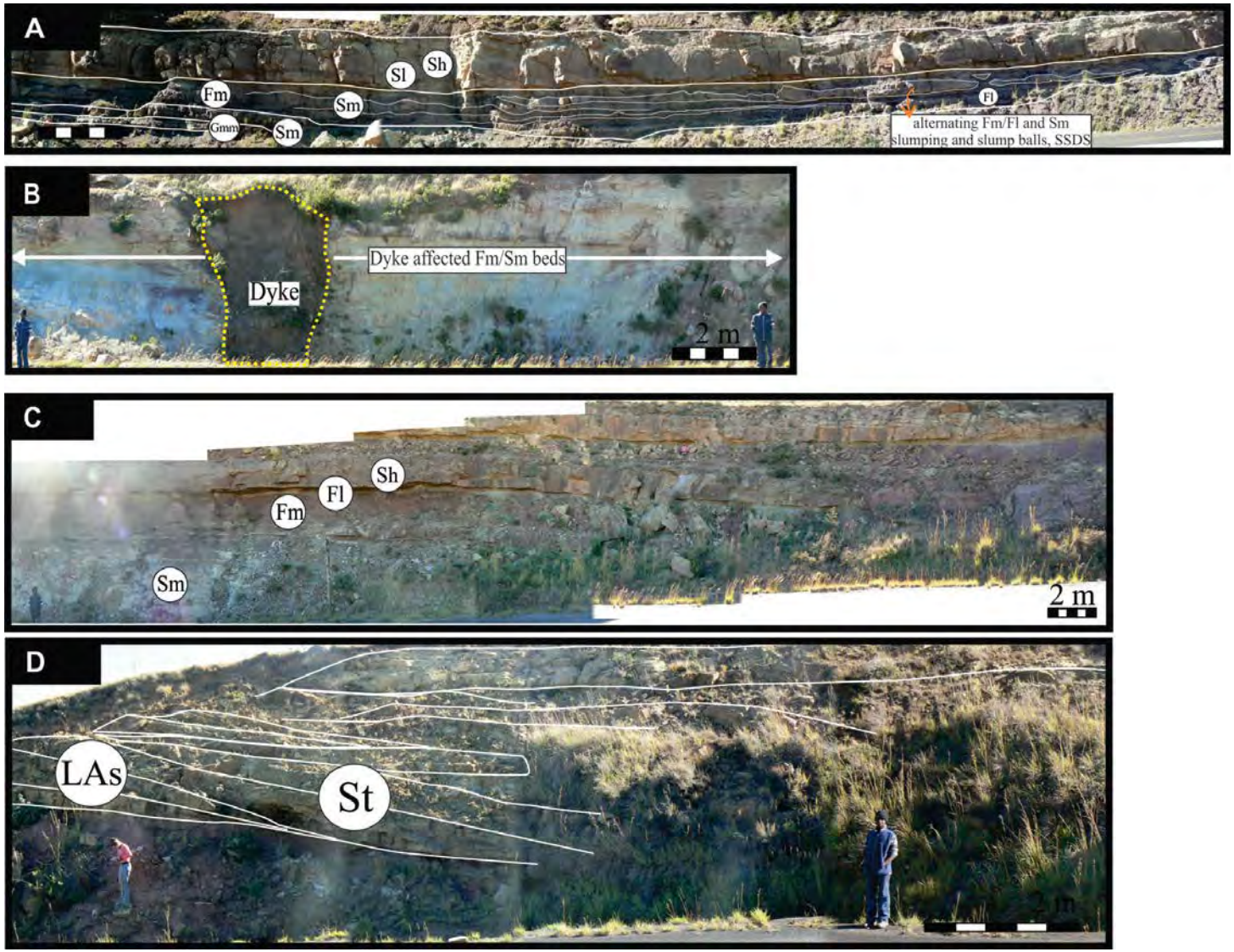

Figure 6.4. Lower Elliot Formation representing the base of the magnetostratigraphic log (A) laterally continuous horizontally laminated (Sh) to low-angle crossed bedded (Sl) fine- to medium-grained sandstones and massive (Fm) to horizontally laminated (Fl) siltstone and mudstone beds, slumping and soft sediment deformation structures (SSDS) present in mudstones and siltstones; An erosive gravel lag (Gmm) at base of sandstone bodies is also present; (B) intrusive Jurassic dolerite dyke and its pervasive alteration halo affecting a package of Fm/Fl with laterally continuous very fine- to fine grained sandstone beds; (C) typical stacked cycles of fine to medium grained sandstones and muddy siltstones and mudstones, red box indicates person for scale; (D) Laterally accreted (LA) medium-grained trough crossed bedded (St) sandstone units.

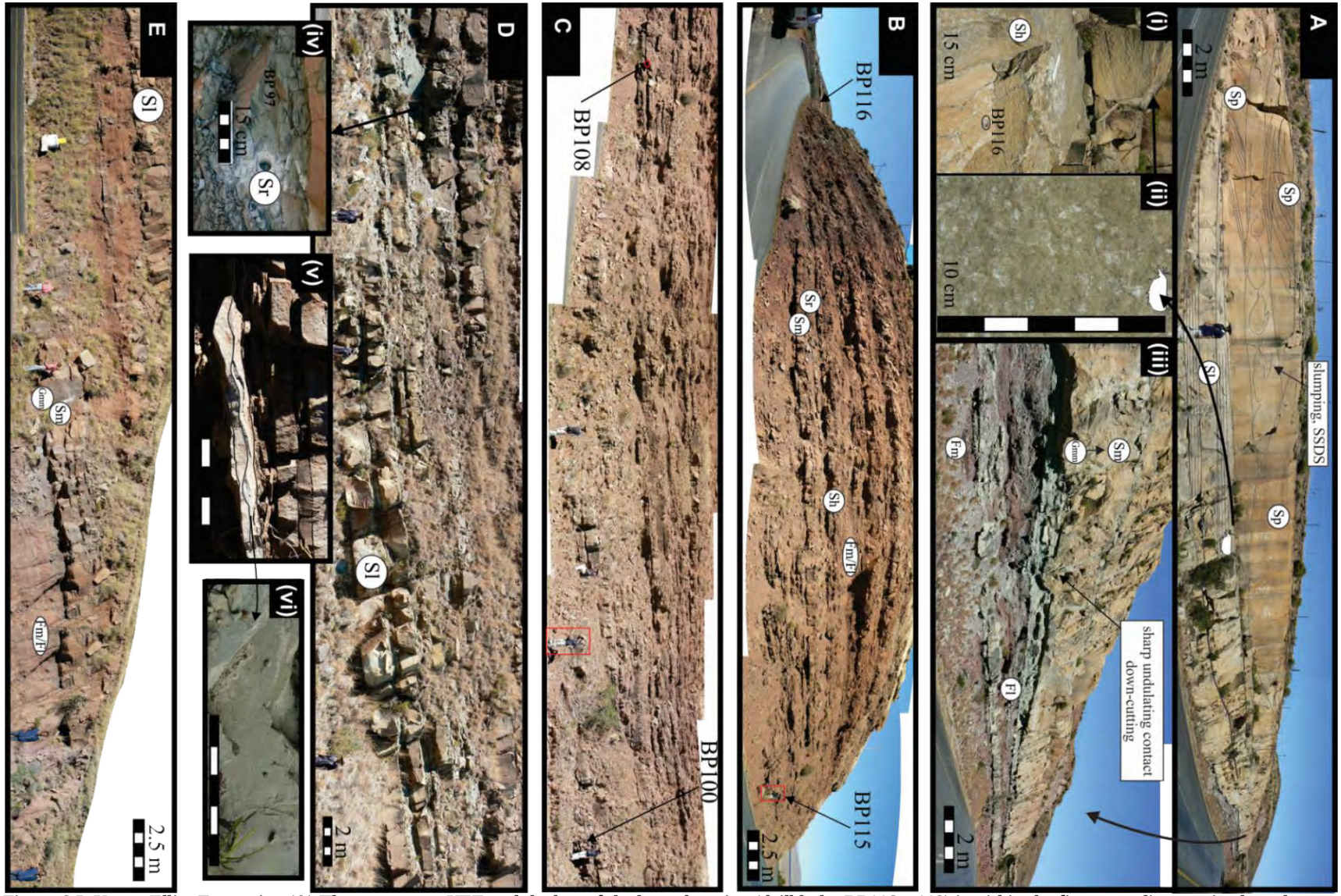

Figure 6.5. Upper Elliot Formation (A) The uppermost UEF and the last of the logged section (drill holes BP116 – 119) is within the fine to medium grained sandstone, showing planar cross-bedding (Sp), low-angle cross-bedding (Sl) and soft sediment deformation structures (SSDS) as well as the (i) horizontal laminations (Sh) that are composed of veneer of (ii) conchostraca casings visible in planar view on lamination surface, and the (iii) sharp and undulating down-cutting contact of conchostraca-bearing sandstone; (B) The alternating units of very fine grained sandstones, siltstones and mudstones with carbonate concretions in the upper part of the Pass are shown between drill holes BP 115 and BP 116; and (C) between drill holes BP 100 and 108 (D) Close up image of the very fine grained sandstones and interbedded mudstones, inserts illustrating (iv) climbing ripple cross-lamination, (v) ripple surface in transverse section and (vi) trace fossils developed on mud draped surface; (E) Section immediately overlying the paraconformity separating the lower and upper Elliot Formation illustrating the mudstone-siltstone massive/laminated alternating units (Fm/Fl), overlain by gravel lag (Gmm) of the down-cutting sandstone body which is massive (Sm). Low-angle cross beds (Sl) were also noted.

6.2.1.2 Upper Elliot Formation

In contrast to the stacked channel sandstones of the LEF, the upper part of the sampled succession at Barkly Pass shows dominance of very fine-grained, thin sandstone beds that alternate with thicker packages of siltstones and mudstones. These appear to be characteristic features of the UEF.

The mudstone and siltstone units are often bioturbated (Fig. 6.5Dvi), colour mottled, and contains carbonate concretions (rare) that collectively are indicative of pedogenesis. In the uppermost section of the Formation at Barkly Pass (Fig. 6.5A), thicker (≥ 3.5 m) medium-grained sandstones occur with lower contacts that show evidence for down cutting into underlying laminated and massive mudstones. These sandstones display horizontal lamination, low angle cross bedding, trough cross bedding and planar cross beds.

The horizontally laminated sandstones can contain conchostraca valves (partly replaced by $CaCO_3$; Fig. 6.5Aii). The conchostracan-bearing section locally shows soft sediment deformation features (e.g., slumping in a ~50 cm thick section).

6.2.2 **Demagnetization results**

Palaeomagnetic directions were determined by least-squares analysis (Kirschvink, 1980). Lines with mean angular deviation (or MAD) values ≤ 15˚, and planes with MAD values ≤ 20˚were included in analyses (exceptions to this rule are samples BP 104, 105 and 115, reverse planes with MAD values of 23.4, 26 and 22.6, respectively).

Most samples had the following two, sometimes three, well-defined components

1. Low-coercivity (soft) magnetic component (NRM – AF 100/150) (coded ‘SFT’).
2. Present local Earth field component (AF100/ 150 - 350 ^{o}C) (generally NNW and upward directed component) (PF).
3. (i) High-temperature steep (i.e., steeper than PF) NW component (between 150-350 ^{o}C to 440-660 ^{o}C) with negative inclination (normal, N).
   (ii) High-temperature steep SE component (between 150-350 ^{o}C to 440-660 ^{o}C) with positive inclination (reverse, R).

Statistical information relevant to the high-temperature components are presented in Table 6.2.

Table 6.2. Barkly Pass site-mean geographic directions and VGPs for all Elliot samples, in addition to the separation of the lower (LEF) and upper (UEF) Elliot Formation samples. Precision parameter (k) and confident limit (α_{95}) with the dm and dp = semi-axis of the confidence ellipse for poles. N = number of samples, L/P = line or poles to planes.

Barkly Pass (BP) (31.43°S, 27.31°E)						VGP			
	N(L/P)	Decl °	Incl °	k	α_{95} °	Pole Lat °N	Pole Long °E	dm	dp
Primary Directions									
EF									
All Reverse	20 (2,18)	184.1	73.3	17.5	8.0	62.3	22.8	14.4	12.9
All Normal	42 (38,4)	287.2	-64.8	26.3	4.4	33.6	259.1	7.1	5.7
Combined	62 (40,22)	303.2	-70.7	26.3	4.4	44.0	249.0	6.6	7.6
UEF									
All Reverse	18 (2,16)	182.3	72.6	15.9	8.9	63.5	24.6	15.9	14.1
All Normal	28 (25,3)	276.6	-64.2	36.7	4.6	26.3	257.7	7.3	5.8
Combined	46 (27,19)	298.8	-72.6	14.0	5.8	41.3	245.6	10.3	9.2
LEF									
All Reverse	2 (0,2)	207.2	78.3	11865.0	2.3	50.6	11.3	4.3	4.1
All Normal	14 (13,1)	308.8	-63.7	23.3	8.4	48.3	262.8	13.4	10.6
Combined	16 (13,3)	312.6	-66.7	20.3	8.4	50.5	256.4	13.9	11.4

All normal characteristic remanence directions (n = 42) have a mean inclination (I) of -64.8˚, mean declination (D) of 287.2˚ and α_{95}= 4.39˚, and the characteristic reverse directions (n = 20) have a mean declination of 184.1˚, mean inclination of 73.3˚ and α_{95} = 8.04˚. The combined mean characteristic direction for the entire Formation is I = -70.7˚, D = 303.2˚, α_{95} = 4.39˚, with site mean VGPs yielding a pole latitude of 44˚N and longitude of 249.2˚E.

The UEF has a combined I = -72.6˚, D = 298.8˚, α_{95}= 5.82˚, with site mean Virtual Geomagnetic Poles (VGPs) yielding a pole latitude of 41.3˚N and longitude of 245.6˚E (Table 6.2). In comparison, the LEF combined mean direction has an I = -66.7˚, D = 312.6˚, α_{95} = 8.4˚, with site mean VGPs yielding a pole latitude of 50.5˚N and longitude of 256.4˚E.

Randomly distributed remanence directions removed in all samples during low-field AF-treatment, and are considered to be low-coercivity components (soft) acquired either in the field through natural processes or through sample preparation. Several samples retained scattered north, north-westerly and upward magnetic component at higher levels of demagnetization. This component is identical to the present local Earth field **(**PF). Generally consistent in direction, the PF component was often removed by 150^{o}C, but infrequently, remained in some samples up to 350 ^{o}C. A few samples (e.g. BP1, BP39) were

completely overprinted by the present field, with average declination of 335.4 and inclination of -76.5 after demagnetization to 660 °C.

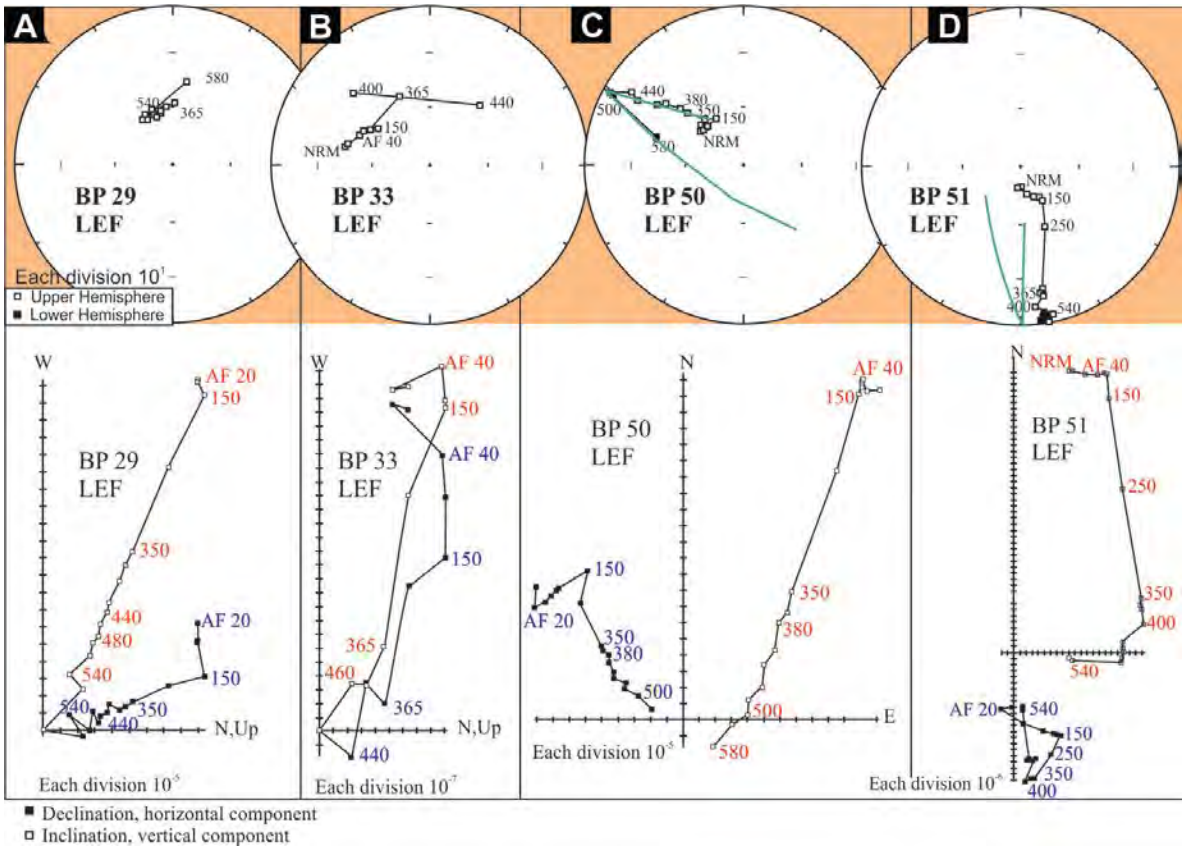

Figure 6.6. Equal area and orthogonal plots of typical sample demagnetization behaviour, BP 29, BP 33BP33, BP 50 and 51 from the lower Elliot Formation at Barkly Pass. All samples are shown in *in-situ* geographic coordinates.

Characteristic high-temperature remanence components (N or R) were stable at higher demagnetization levels, up to 580 °C, e.g. BP 29, BP51 (LEF; Fig. 6.6D); with some samples stable to ~620 °C. For example, BP 73 (UEF; Fig. 6.7A) has a soft component present until 350 °C before the unblocking of a normal direction is observed, with higher temperature components (365-620 °C) shifting westwards along a short great circle path, at steeper inclination, and having a north-westerly-directed stable end point vector direction. Forty-two samples displayed this behaviour during increasing levels of thermal demagnetization, and this is considered to represent the normal characteristic magnetization (ChRM) direction. Stable end-point vector directions to the south east were reached along great circle paths (e.g. BP 86; 250 – 440 °C; Fig. 6.7) for reverse direction samples. These ChRM N- and R-components are interpreted to be primary Late Triassic-Jurassic directions for the Elliot Formation. Typical samples for

the Barkly Pass LEF and UEF are plotted in equal area projections and orthogonal vector plots in Figure 6.6 and Figure 6.7, respectively.

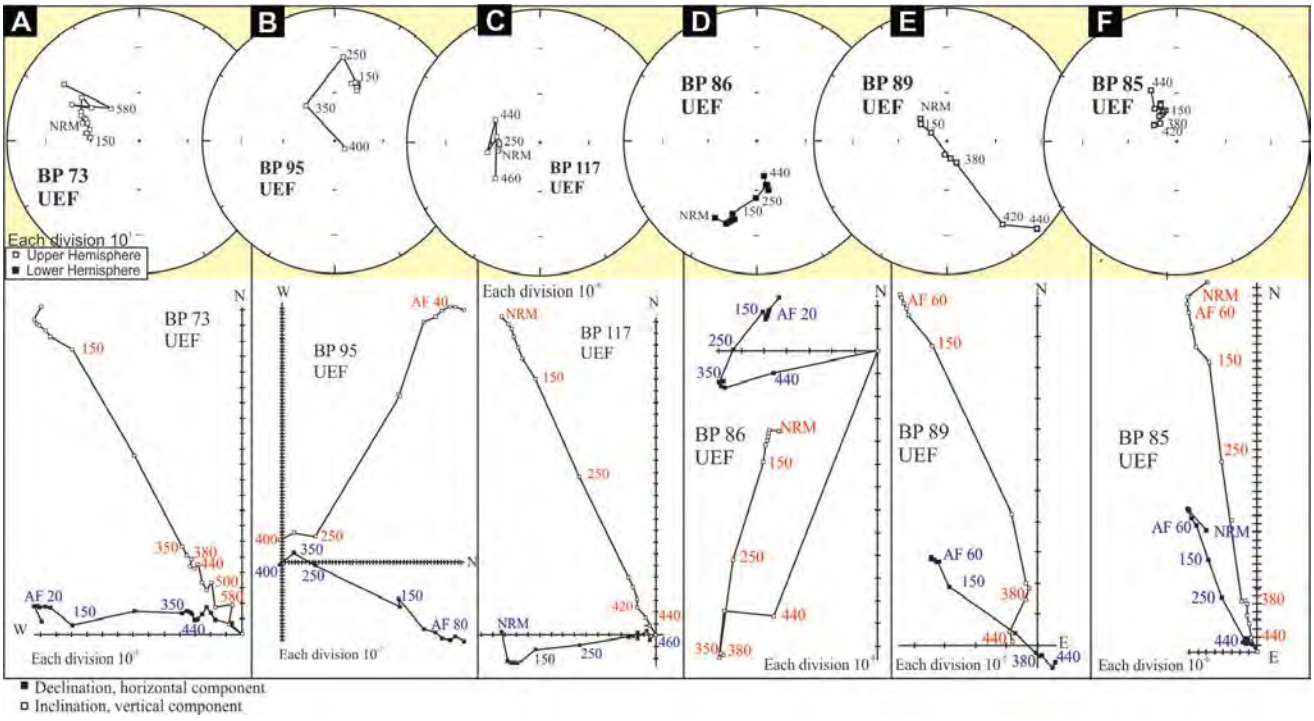

Figure 6.7. Equal area and orthogonal plots for the most typical (A-C): normal polarity samples BP 73, 95 and 117, and (D-E): reverse polarity BP86 and 89 samples from the upper Elliot at Barkly Pass relative to (F): the normal polarity dolerite dyke (BP85).

6.2.3 **Reversals test**

For palaeomagnetic stability and to establish if the LEF and UEF samples have one true mean for reversed and normal samples, the comparison of the antipode of the mean of the reversed-polarity samples is taken against the mean of the normal polarity samples, in a reversals test (McFadden and McElhinny, 1990; Butler, 1992).

The reversals test was applied to the UEF and the combined Elliot Formation at BP using the current study's results. The LEF at BP could not be tested as the dataset (n = 16) was too small with only two samples making up the reserved component (R = 2; N= 14); and as such the two modes do not share a common precision factor. Secondarily, a parametric bootstrap method could not be applied for the same

reasoning. However, a reversals test could be applied when combining the LEF results of de Kock (2003) with those presented here making a more robust dataset (n = 53, R = 23, N = 16).

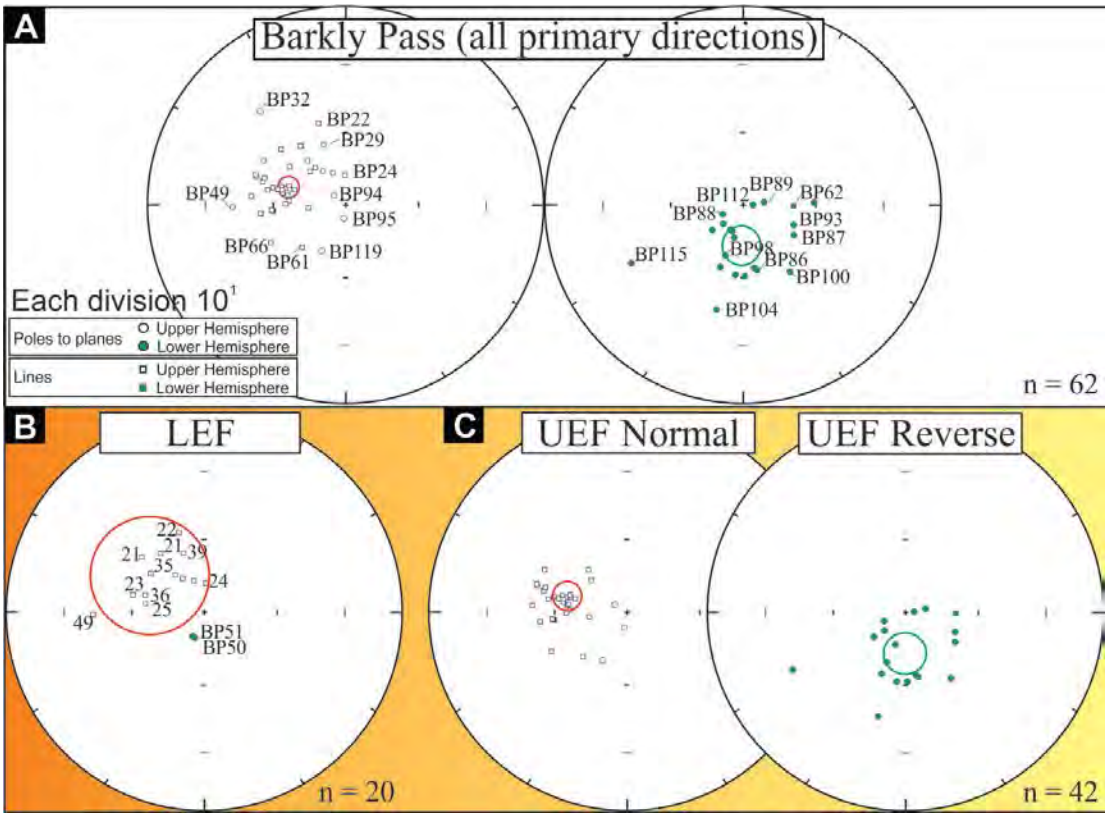

Figure 6.8. Equal area projections (lower hemisphere) of (A) all ChRM directions (normal- and reverse-polarity samples) from the Barkly Pass for this study with 95% confidence cones (N = 62). Sample numbers are indicated. (B) Lower (LEF) samples (N=20) and (C) upper Elliot (UEF, N= 42) samples with relevant cones of confidence. Normal and reverse polarity directions from the entire Elliot are not antipodal and fail the Bootstrap reversals test (Tauxe *et al*., 1991).

The combined dataset from de Kock (2003) and this study passes the McFadden and McElhinny (1990) reversals test (C class) with an angle of separation (γ_0) between the two modes of 5.4˚ being less than the critical angle (γ_c = 12.9˚). Despite the sharing a common mean (Figure 6.9) as illustrated in the Watson's V test, a bootstrap reversal test was implemented and shows that the x, y and z components of the two modes all overlap at 95% confidence. This result indicates the reliable characteristic magnetization.

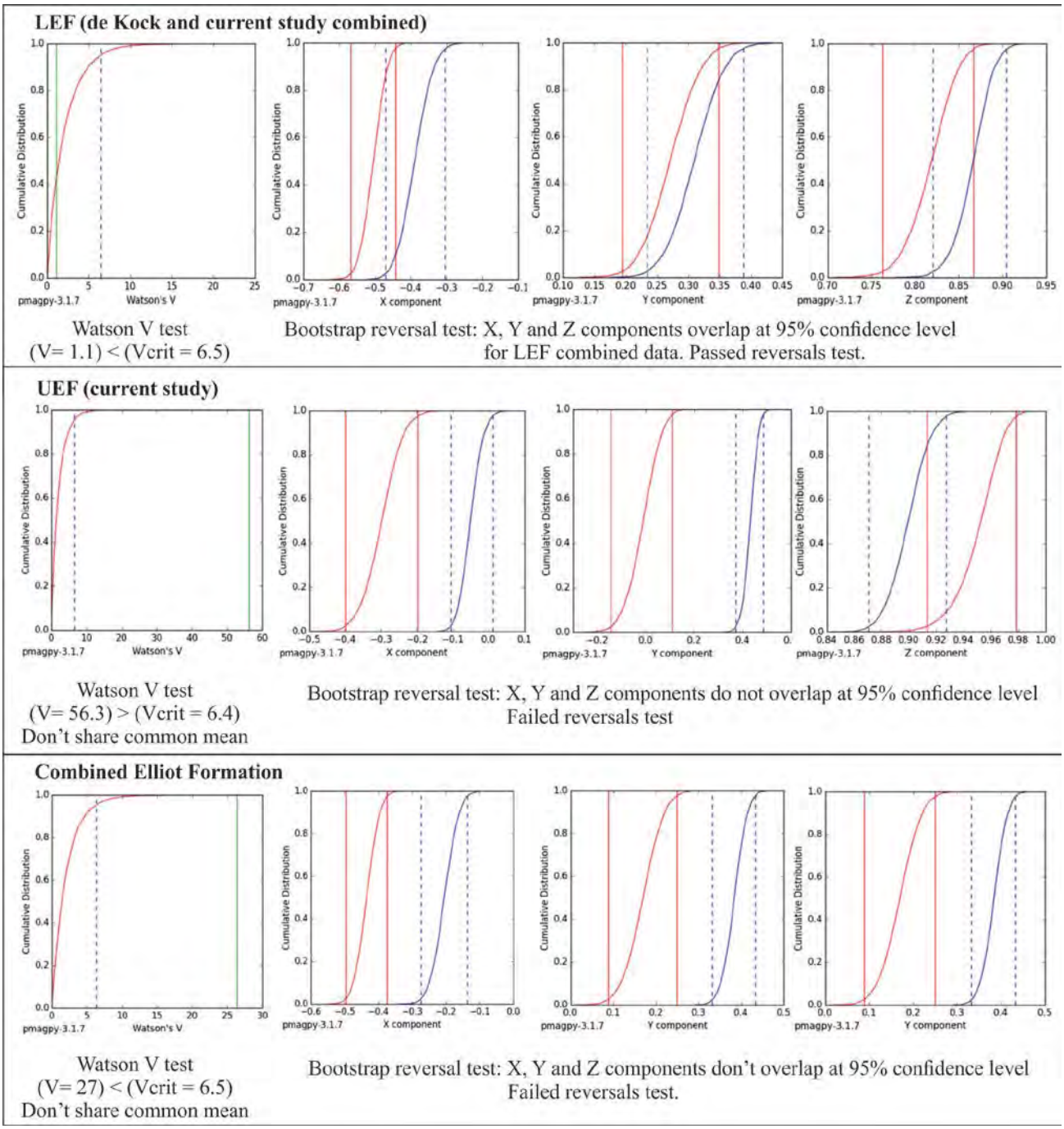

Figure 6.9. Watson's V test and the Bootstrap reversals test (Tauxe *et al*., 1991) for the LEF combined data from de Kock (2003) and this study, UEF (this study) and the combined LEF and UEF samples for Barkly Pass. The LEF combined data set passes the reversals test, whereas the UEF and combined Elliot Formation fail the reversals test.

In contrast, the UEF (n = 46, N = 28, R = 18) N- and R-modes do not share a common mean (Figure 6.9). UEF fails the McFadden and McElhinny (1990) reversals test with a γ_0 of 29.7˚ and γ_c of 9.9˚, and this is reaffirmed in the Bootstrap reversals test (Fig. 6.9).

A comparison of the combined LEF and the UEF at Barkly Pass indicates that the datasets share a common mean, but it also fails the McFadden and McElhinny (1990) reversals test with an angle of separation (γ_0) between the two modes of 18.2˚ being greater than the critical angle (γ_c = 8.9˚); and this is repeated with the failed Bootstrap reversals test presented in Figure 6.9.

The inclination and declination of stable palaeomagnetic directions (high temperature N and R) and the calculated VGPs are plotted in Figure 6.10. This current study was incorporated into the original de Kock (2003) magnetostratigraphy of the Barkly Pass section. The tie between the current lithological and magnetostratigraphic log and that by de Kock (2003) was accomplished by using the dolerite dykes that transect the exposed succession in the Pass. The resultant composite magnetostratigraphy of Barkly Pass is presented in Figure 6.10 and highlights the overlap between the current studies samples and that of de Kock's (2003) samples from the Lower Elliot. Polarity zones were considered 'real' when constituting two or more successive, same polarity samples. There are 4 normal polarity and 4 reverse polarity zones making 5 polarity pairs (EF1 – 5; Fig. 6.10).

6.3 Conclusion

Fine-grained samples (facies Fm – massive mudstones) appear to preserve the most stable NRM and ChRM in comparison to facies Sm or Gcm/Gmm (fine- to medium-grained sandstones and mud-chip conglomerates). As an example, BP32 is a fine-grained, massive, sandstone (Sm) and loses magnetization quickly at low temperatures (by 365°C). A secondary Present Field (PF) component removed with thermal demagnetisation to 350 °C and readily recognised by the shallow NW up direction. The mean directions for the entirety of the sampled Elliot Formation and the samples of the UEF fail the reversals test (Fig. 6.9), whereas the combined data of De Kock (2003) and this study for the LEF pass the reversals test (C class).

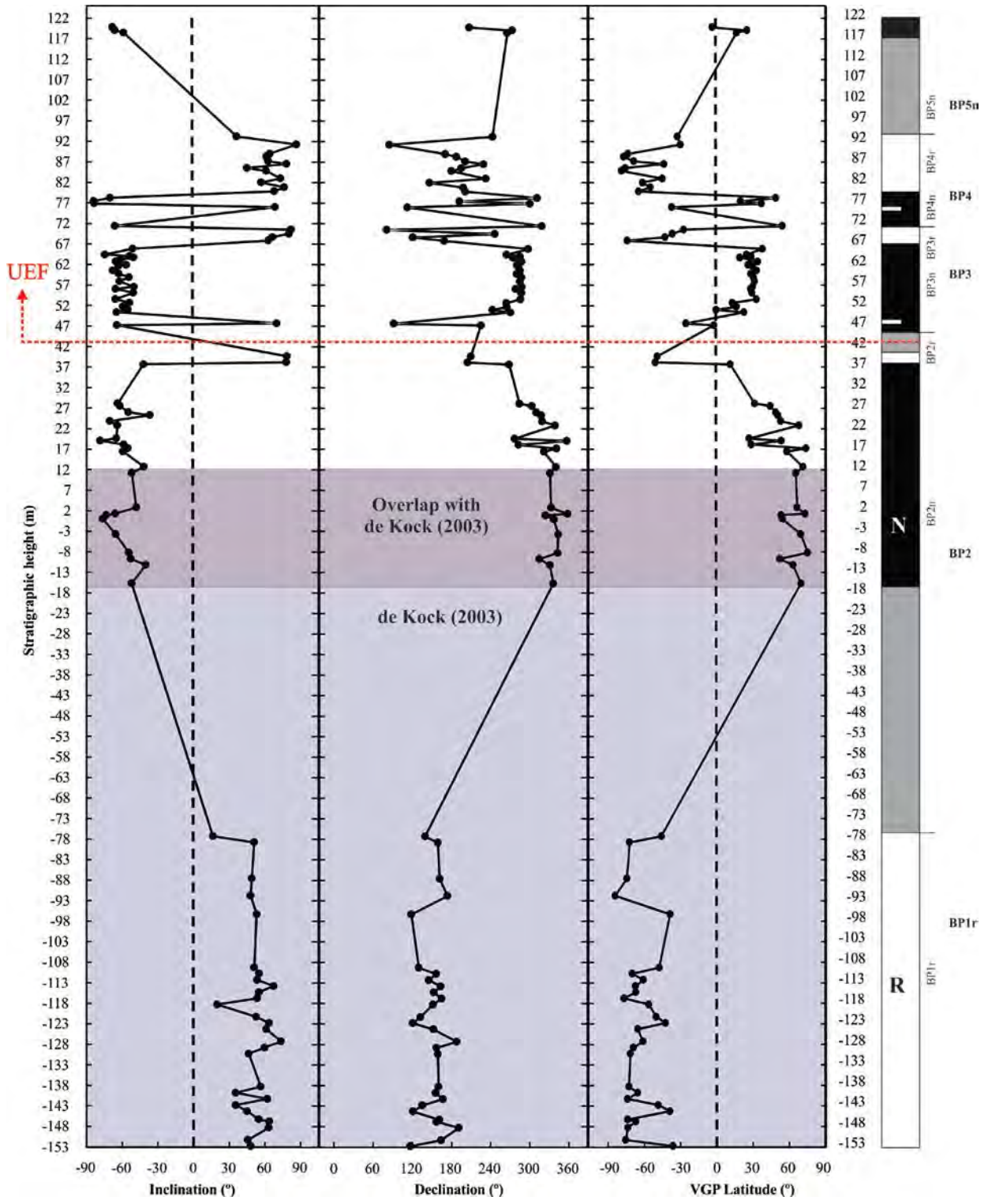

Figure 6.10. Stratigraphic height of samples versus inclination and declination (°) for the Barkly Pass site. The TJB (dashed red line) is tentatively marked onto this plot based on field observations. Polarity pairs are marked BP 1r – BP 5n.

The combined LEF result gives credence to the primary nature of the ChRM and polarity determination. However, the failure of the test for the UEF and combined Elliot Formation indicates that the normal polarity samples may be biased by a younger overprint of either the Jurassic normal polarity of the Karoo igneous event or of the present field. To factor this potential cause for bias out is not possible given the similarity of the normal Triassic-Jurassic polarity to that of the Pliensbachian KIP. Five magnetochrons are developed for the Barkly Pass, EF1 – 5 and are illustrated in Figure 6.10.

7 Newly constructed southern magnetostratigraphic section for a LEF-UEF site within the Quthing district, Lesotho

7.1 Introduction

The road cutting labelled ‘QUT’ lies on the A1 national road of Lesotho in the Quthing district, 9.1 km west of the town Quthing and 1.9 km north of Alwyns Kop (Fig. 7.1). Along the same road are classic fossil-rich Elliot Formation sites and include Masitise, Moyeni and further northeast, Fort Hartley (Table 7.1).

7.1.1 **Previous palaeontological work in the Quthing district**

In the current road cutting, there has been no published research as the cutting itself, although closely following the old road, is relatively new. It did contain little fragmentary and disarticulated vertebrate fossil bones, *in situ* as well as allochthonous, and therefore further palaeontological assessment of the site would be beneficial.

Within the Quthing district, there are various sites of palaeontological interest. There are two notable footprint sites, one at Villa Maria and the other, Moyeni, on the outskirts of the town of Quthing. Most of these palaeontological discoveries were brought to light by the Stockley (1947), the Ellenbergers in the 1950s and 60s and then later by Crompton and Jenkins (1968) (see Table 7.1 for details). Ellenberger (1970) places all of the discoveries within the Quthing area into his zones B1/B2 of the upper Stormberg Group.

One of the more spectacular discoveries in the Quthing district, which lies within the town of Quthing, is the Moyeni track site. This site sits in the lowermost UEF (Smith *et al*., 2009; personal obs.). It was initially described by Ellenberger (1970) and then later re-described by Smith *et al*. (2009) and Wilson *et al*. (2009).

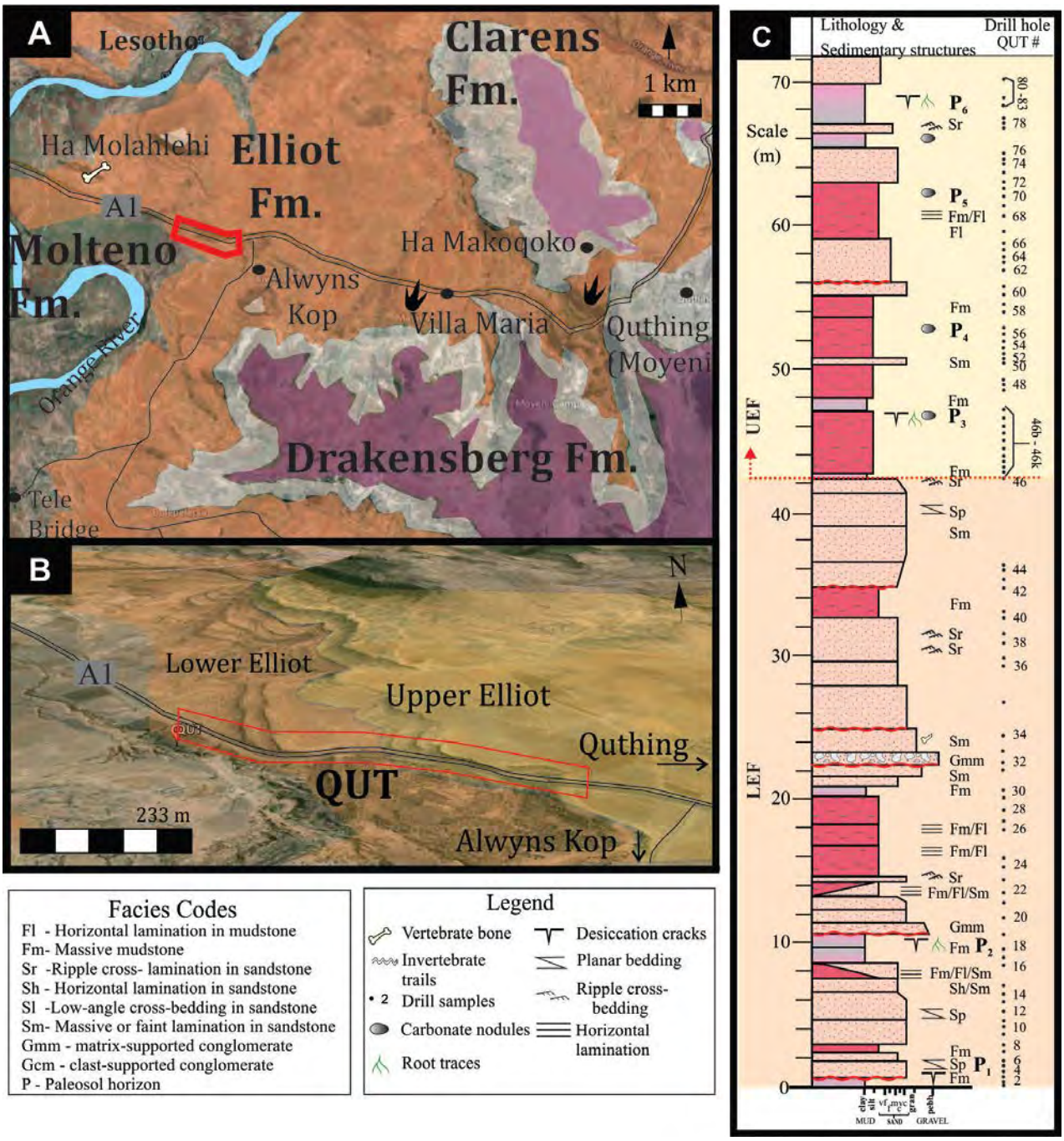

Figure 7.1. (A) Geological map of location showing the Molteno, Elliot and Clarens Formation contacts in relation to the study section at 'QUT' (red box) near Quthing, SE Lesotho and (B) Google Earth image with draped with lower Elliot (LEF) and upper Elliot Formation sedimentology over the QUT section; (C) The sedimentary log of Quthing 'QUT' site showing interval spacing of drill cores (numbers indicated on right-hand side) for palaeomagnetic analyses. The sedimentological contact between the LEF and UEF is based on sedimentological and geomorphological features and marked with dash red line.

Table 7.1. Details of fossil finds within the Quthing district proximal to Quthing road cutting drill site, Lesotho.

Taxonomic assignments	Age	Stratigraphic position	Catalogue no.	Notes	Source(s)
Heterodontosaurid, *Heterodontosaurus tucki*	• Hettangian-Sinemurian (Olsen & Galton, 1984), • Pliensbachian-Toarcian (Yates *et al*., 2004). • latest Sinemurian-Pliensbachian (Jourdan *et al*., 2005, 2007, 2008). (Norman *et al*., (2011)	Clarens Fm.	SAM-PK-K337	Found at the mountain behind Tyindini trading store, Herschel district Eastern Cape. Skull and lower jaw encrusted in thin layer of haematite". Postcranial remains also listed by Crompton & Charig (1962: 1075) but location is currently unknown.	Skull Holotype Crompton & Charig (1962); Weishampel (1990); Porro *et al*. (2010); Norman *et al*. (2011)
Heterodontosaurid	As above	UEF	SAM-PK-K1332 SAM-PK-K1334 SAM-PK-K10487	Voisana, Kromspruit 9 Farm, Herschel District, Eastern Cape Province, South Africa	Porro *et al*. (2010); Norman *et al*. (2011)
Triconodont mammaliaform; *Megazostrodon runerae*	Early Jurassic	UEF	BMNH M 26407	Thaba-ea-Litau near to Fort Hartley in Quthing District. ; Earliest mammaliaform Found in Zone B/2 (Ellenberger, 1970) – same zone as *Erythrotherium*	Crompton and Jenkins (1968)
Sauropod	Triassic-Jurassic	UEF	-	Sterkspruit; 19kms from the Quthing District boarder	Barrett (2004)
Brachyopod temnospondyl	Late Triassic – early Jurassic	LEF or UEF ?		Alwyns Kop, Quthing District, Lesotho. Found in Ellenbger's A/7 zone	Du Toit and Ginsburg (1982), Steyer and Damiani (2005)
Gryponyx taylori synonymous with *Massospondylus*	Early Jurassic	UEF		Quthing District. Zone B/1 UEF	Ellenberger (1970) Kicthing and Raath (1984)
Thecodontosaurus browni	Early Jurassic	UEF		Quthing District. Zone B/1 UEF	Stockley (1947) (Broonstra) Ellenberger (1970) Kicthing and Raath (1984) Ambrose (2007)
Pachygenelus sp.	Early Jurassic	UEF		Moyeni Zone B/2	Ellenberger (1970) Kicthing and Raath (1984)
Ornithischia; *Lesothosaurus* sp. Indet (Knoll, 2002a, b)	Lower Jurassic (Hettangian)	UEF	MNHN LES 17: articulated skull with lower jaw; MNHN LES 18: fragmentary skull with lower jaw and cervical vertebra.	Near Masitise. P. Ellenberger's field prospecting between Alwynskop and Moyeni (Quthing District),	Knoll (2002a, b)
Ornithischia; *Stormbergia drangershoeki* (Nomum dubium synonymous with *Lesothosaurus*)	Lower Jurassic: Hettangian–Sinemurian	UEF	SAM-PK-K1105 BMNH R11000 BP/1/4885	1. Dangershoek Farm, Herschel District, 2. Pokane, Lesotho by a 1966–67 British Museum/University 3. Mequatling, Clocolon District	Butler (2005)
• *Neotrisauropus*-type synonymized with *Grallator* (Olsen and Galton, 1984; Wilson et al., 2009) • *Moyenisauropus*-type synonymized with • *Anomoepus* (Olsen and Galton, 1984; Olsen and Rainforth, 2003; Wilson et al., 2009). • *Episcopopus ventrosus*	TJB (Smith *et al*., 2009; Wilson *et al*., 2009)	UEF		Quthing, Quthing District, Lesotho. 250 tetrapod footprints and trackways *Episcopopus ventrosus* studied by Marsicano *et al*. (2014) identified track makers as temnospondyl amphibian	Ellenberger (1970) Olsen and Galton (1984) Smith *et al*. (2009) Wilson *et al*. (2009) Marsicano *et al*. (2014)

The site displays several, up to 250 (Wilson *et al*., 2009) trackways, of considerable preservation and length, with the highest diversity and preservation recorded on the surface that had a biofilm/algal mat (Wilson *et al*., 2009). Identification and refinement of one particular trackmaker was carried out by Marsicano *et al*. (2014).

Smith *et al*. (2009) discuss the palaeonvironment at Moyeni, ascribing the traces to occur on one scroll bar (100 m^2) of a meandering river. The assortment of tracks of medium to large size speaks of diversity, in form and size, of the fauna.

Smith *et al*. (2009) and Wilson *et al*. (2009) highlight the presence of theropods and likely ornithischian dinosaurs (*Grallator* and *Anomoepus* ichnotaxa, respectively) as well as a short-legged basal tetrapod (*Episcopopus*), which was later identified by Marsicano *et al*. (2014) as a temnospondyl amphibian. The issue of the occurrence of basal archosaurs ('chirotheroid'-type) tracks, reported by Smith *et al*. (2009), with the above mentioned ornithischian and theropod trackways are not further substantiated with reputable evidence for their occurrence at this site.

Smith *et al*. (2009) make note that the chirotheroid-like tracks are considered to be limited to the Triassic. Their occurrence, although not formally substantiated, within an UEF site, traditionally considered Early Jurassic, would increase the complexity associated with not only the age of the Elliot Formation and the UEF, but of the consistency of track makers and their identification through time (Smith *et al*., 2009). The *Grallator* pes prints studied by Wilson *et al*. (2009) were concluded to have been produced by a theropod individual, similar in size to the South African theropod *Dracovenator regenti* (Yates, 2005b). The identification of the chirotheroid-type track *Episcopopus* by Marsicano *et al*. (2014) as being produced by a temnospondyl with semi-aquatic lifestyle speaks of the palaeonvironment at the ~Triassic-Jurassic/Early Jurassic transition.

7.1.2 **Sampling**

The road cutting (Fig. 7.1) along the A1 and west of Alwynskop and Quthing was chosen for its easy access and fresh exposures of the upper LEF and lower UEF as well as close proximity to the geomorphological plateau which marks the sedimentologically established LEF-UEF contact (Fig. 7.1B, C). It can also be correlated with the Moyeni track site which will aid in placing that famous ichnofossil site in a chronostratigraphic framework. Sampling was carried out using the standard methods discussed from page 73.

7.2 Results

7.2.1 **Sedimentology**

The transition from the LEF to the UEF at the Quthing road cutting transects the strata in the uppermost lower Elliot and lowermost upper Elliot Formation (Fig. 7.1B). The LEF section was characterised by relatively deeply incised, thicker (>1 m) and laterally accreted, fine- to medium-grained channel sandstones found between overbank floodplain mudstone/siltstones that are often massive, occasionally laminated and colour mottled (Fig. 7.1C, Fig. 7.2A, B).

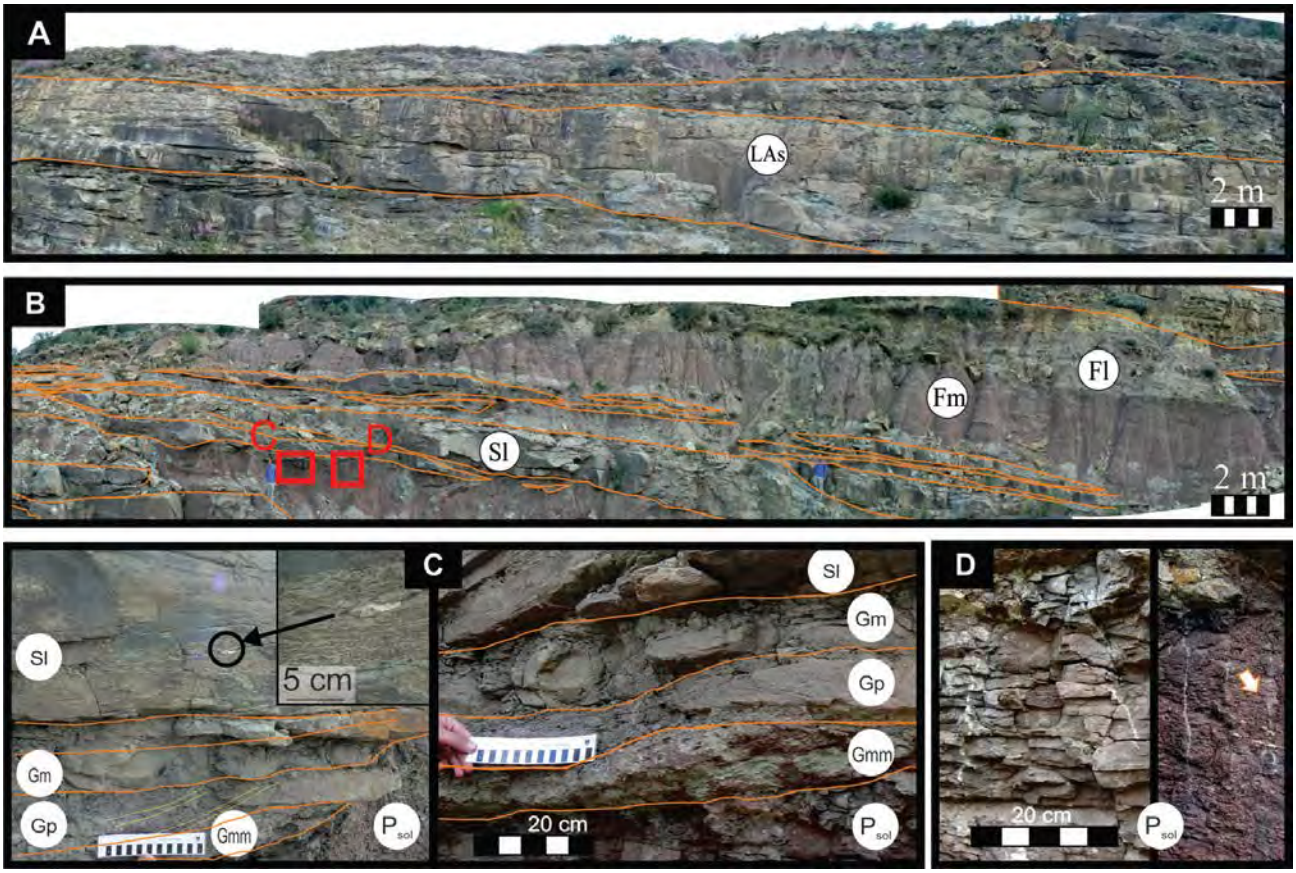

Figure 7.2. Lower Elliot section close to Alwyns Kop: (A) lateral accretion (LA) in fine-medium grained channel sandstones; (B) interbedded channel sandstone and overbak mudstone units with (C) mudchip conglomerate as basal lag which becomes planar cross bedded and grades into the overlying medium grained sandstone (inset shows a bone fragment), (D) paleosol with root haloes downcut by overlying channel body. Note root traces which are in excess of 20 cm in length and indicate an established vegetated floodplain.

Features noted in the LEF at the Quthing section are presented in Figure 7.2C, D. The overbank fines, although generally not preserving any palaeosol features in the LEF, showed a well-developed palaeosol within the first 15 m of the section, with the preservation of several bifurcating root halos, of ≥ 20 cm in length, within a ~ 2 m thick mudstone unit (shown in Fig. 7.2B and D).

In contrast to the stratigraphic architecture of LEF section, the UEF section is dominated by thick packages of mudstone-siltsone and thin, laterally extensive sheet sandstone bodies (Fig. 7.1C). The sheet sandstones are generally not thicker than 1.5 m. Figure 7.3A displays a typical, ~5 m thick UEF mudstone/siltstone-dominated section that is punctated by thin crevasse splay-type sandstone bodies (on average ~25 cm thick), which is overlain by a thin sheet of fine-grained, massive to ripple cross-laminated sandstone. Figure 7.3A displays a cross-bedded channel body that is 2.5 m in length and 1m in depth encast within the mudstone-dominated finer-grained unit.

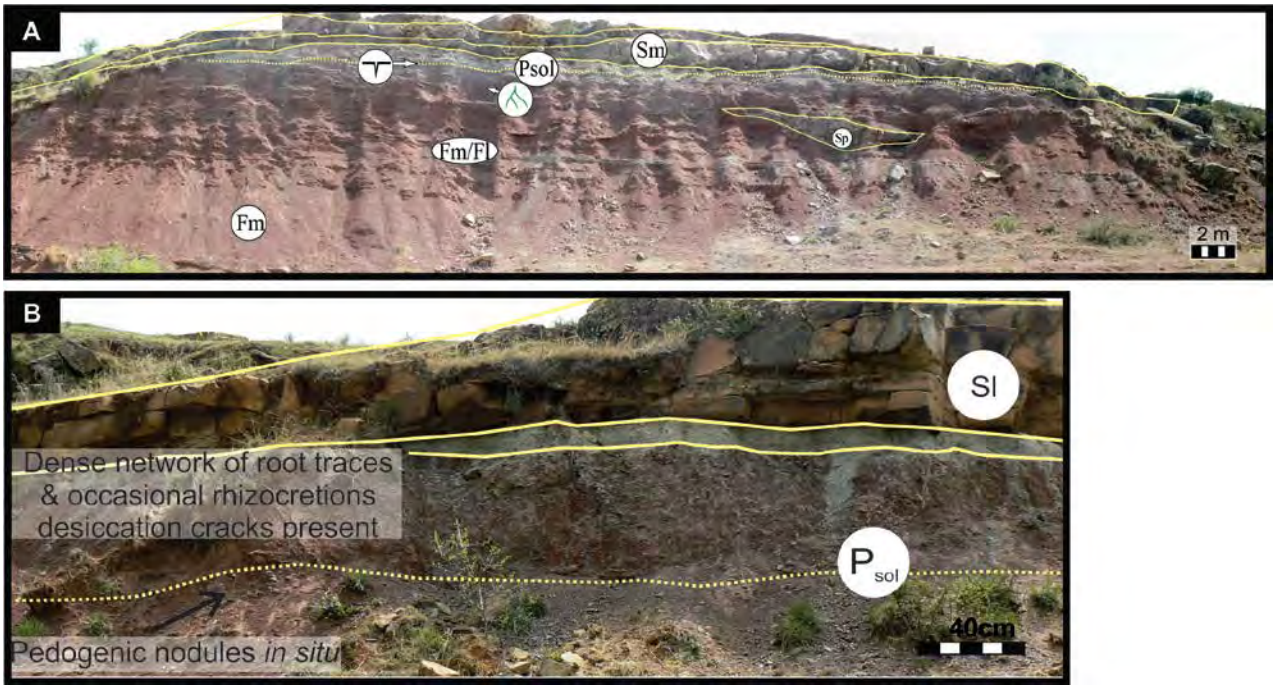

Figure 7.3. Upper Elliot Formation at Quthing comprises (A) thick fine-grained units of mudstones and silstones and occassional, less than 20 cm thick sandstones with several paleosols preserved; (B) Typical paleosol in the upper Elliot Formation with dense network of root traces, dessication cracks below which (~ 40 cm) are a layer containing, in situ pedogenic nodules. Note the discolouration (10 – 20 cm thick) directly below sandstone. This is a primary feature of the palesol, and post-depositional fluid flow along the porous contact between the mudstone and sandstone has further impacted on this rock unit.

In general, of the sites drilled and the Elliot Formation sections examined during this study, extensive development of palaeosols in the LEF are very rare to absent. If present, they are often erosionally truncated by an overlying, downcutting channel sandstone, and therfore the site at Quthing is exceptional in this regard (Fig. 7.2B, D). The UEF, however, is characterized by well-preseved palaeosols both at the present site as well as all localities visited or drilled.

7.2.2 **Magnetostratigraphy**

7.2.2.1 Demagnetization results

The palaeomagnetic data results show several components, from a low-coercivity "soft" magnetic component, occasional present local Earth-field component, to the one primary magnetic component typifying Triassic/Jurassic Normal and Reverse directions. Statistical information on all the components is provided in Table 7.2.

Table 7.2. Quthing site-mean primary geographic directions and VGPs for all samples and then the subsequently the lower (LEF) and upper (UEF) Elliot Formation. Statistical parameters are as followings: precision parameter (k) and confident limit (α_{95}) with the dm and dp = semi-axis of the confidence ellipse for poles. N = number of samples, L/P = line or poles to planes.

Quthing (QUT) (30.39°S, 27.61°E)						VGP			
	N(L/P)	Decl °	Incl °	k	α_{95} °	Pole Lat °N	Pole Long °E	dm	dp
Primary Directions									
EF									
All Reverse	19 (0,19)	171.9	49.8	12.1	10.1	83.0	113.7	13.4	8.9
All Normal	45 (44,1)	333.2	-62.0	27.4	4.1	65.2	259.0	6.4	5.0
Combined	64 (44, 20)	339.8	-58.8	17.6	4.4	70.7	260.0	6.5	4.8
UEF									
All Reverse	5 (0,5)	176.9	49.1	14.5	20.8	87.3	125.2	26.9	17.8
All Normal	23 (22,1)	336.6	-60.1	30.8	5.5	68.1	262.1	8.4	6.3
Combined	28 (23,5)	341.0	-58.4	23.7	5.7	72.2	263.2	6.5	4.8
LEF									
All Reverse	14 (0,14)	170.0	50.0	10.9	12.6	81.4	112.4	16.9	11.3
All Normal	22 (22,0)	329.1	-63.9	24.7	6.4	61.6	256.6	10.1	8.0
Combined	36 (22,14)	338.9	-59.1	14.4	6.52	70.4	263.0	9.7	7.3

Components are as follows:

1. Low-coercivity (soft) magnetic component (NRM – AF 100) (SFT);
2. Present local Earth-field component (NRM – AF100/ 250 ^{o}C) (moderately shallow, NNW directed component, generally) (PF) – can be stable to high temperatures/high field strengths;
3. a. High-temperature steep NW component (150/350 – 580-680 ^{o}C) with negative inclination. (NORMAL, N);

   b. High-temperature steep SE component (150/350 – 580-680 ^{o}C) with positive inclination. (REVERSE, R).

During AF-treatment, at demagnetization field-strength levels below 100 mT, all samples show remanence directions that are randomly distributed. This is taken to be component one, the low-coercivity (soft, 'SFT') magnetic component, which is acquired during sampling, weathering, etc., and is removed through AF treatment.

Component 2, the present local Earth-field component, was present in several samples and is moderately steeply NNW directed. The 'PF' was often unstable at higher temperatures and high-field strengths and removed from the sample. However, in some samples it is persistent and stable to very high-field strengths.

In several samples, after removal of low-coercivity components, high temperature components remained which were stable at higher demagnetization levels, e.g., QUT 16 (LEF) stable until 530 ^{o}C (Figure 7.4A). The soft component for QUT 16 is present until 375 ^{o}C before primary normal direction is observed with higher temperature components (375-530 ^{o}C) shifting westwards along short great circle paths, at steeper inclination and having a north-westerly-directed stable end point vector direction. For the entirety of the sampled Elliot Formation at the Quthing section, forty-five samples displayed this behaviour during increasing levels of thermal demagnetization (Table 7.2), and this is considered to represent the normal characteristic magnetization (ChRM) direction.

In contrast, 19 samples showed stable end-point vector directions to the south east which were obtained via great circle paths, e.g. lower Elliot Formation samples QUT 7 and 31 (Fig. 7.4) and upper Elliot Formation samples QUT 68 and 77 (Fig. 7.5) for reverse direction samples. All typical behaviour for Quthing samples from the LEF and UEF are plotted in equal area projections and orthogonal vector plots in Figure 7.4 and Figure 7.5, respectively.

Table 7.2 outlines all primary normal directions (n = 45) have a mean direction inclination (I) of -62.0˚, declination (D) of 333.2˚ and α_{95} = 4.14˚, and the reversed samples (n = 19) have a mean direction with declination of 171.9˚, inclination of 49.8˚ and α_{95} = 10.05˚. These values are comparable with the UEF normal and reverse polarity mean directions (Table 7.2). The primary mean direction for the entire Formation is Io = -58.8˚, Do = 339.8˚, α_{95} = 4.35˚, with site mean VGPs yielding a pole latitude of 71.1 (˚N) and longitude of 263.1 (˚E). The UEF has a combined Io = -58.4˚, Do = 341˚, α_{95} = 5.72˚, with site mean VGPs yielding a pole latitude of 72.2 (˚N) and longitude of 263.2 (˚E). In comparison, the LEF combined mean direction has an Io = -59.1˚, Do = 338.9˚, α_{95} = 6.5˚, with site mean VGPs yielding a pole latitude of 70.4 (˚N) and longitude of 263.0 (˚E).

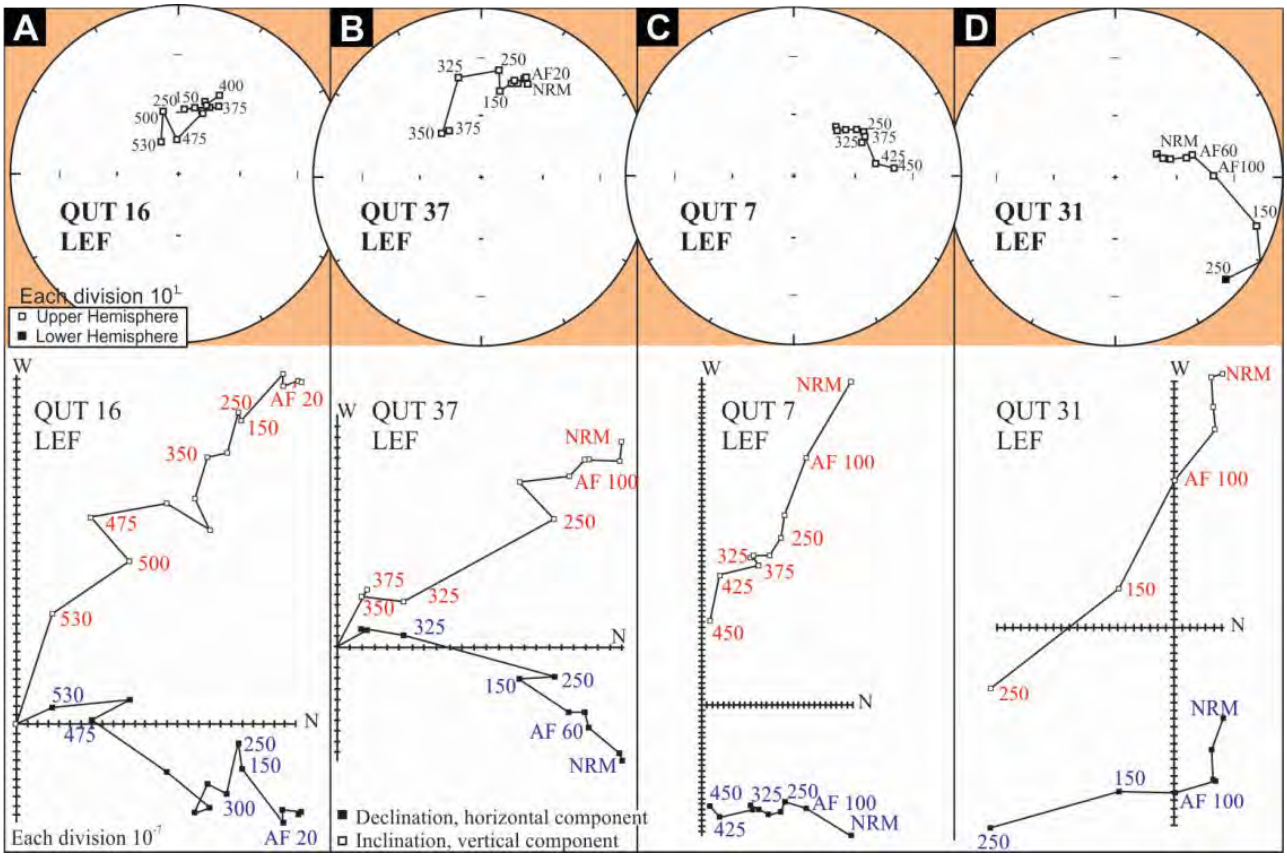

Figure 7.4. Lower Elliot Formation (LEF) samples, in equal area and orthogonal plots, displaying typical (A, B) normal (QUT 16, 37) and (C, D) reverse (QUT 7, 31) behaviour.

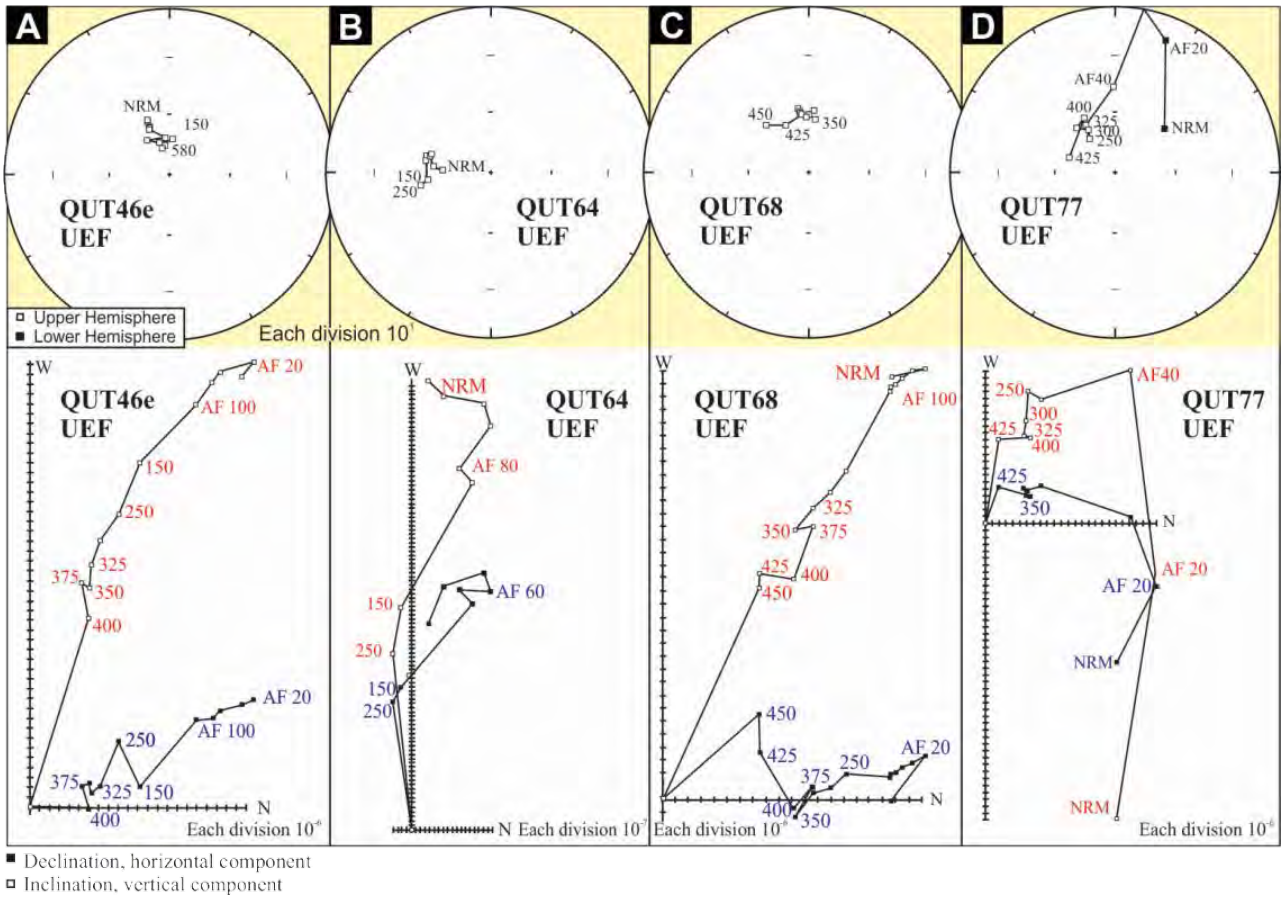

Figure 7.5. Upper Elliot Formation (UEF) samples, in equal area and orthogonal plots, displaying typical (A, B) normal (QUT 46e, 64) and (C, D) reverse (QUT 68, 77) behaviour.

7.2.2.2 Reversals test

A parametric bootstrap method was applied for the LEF at QUT and established that borderline pass of the reversals test based on the z component (Fig. 7.6). In contrast, the UEF passes the Bootstrap reversals test (Fig. 7.6) with overlap in all three components.

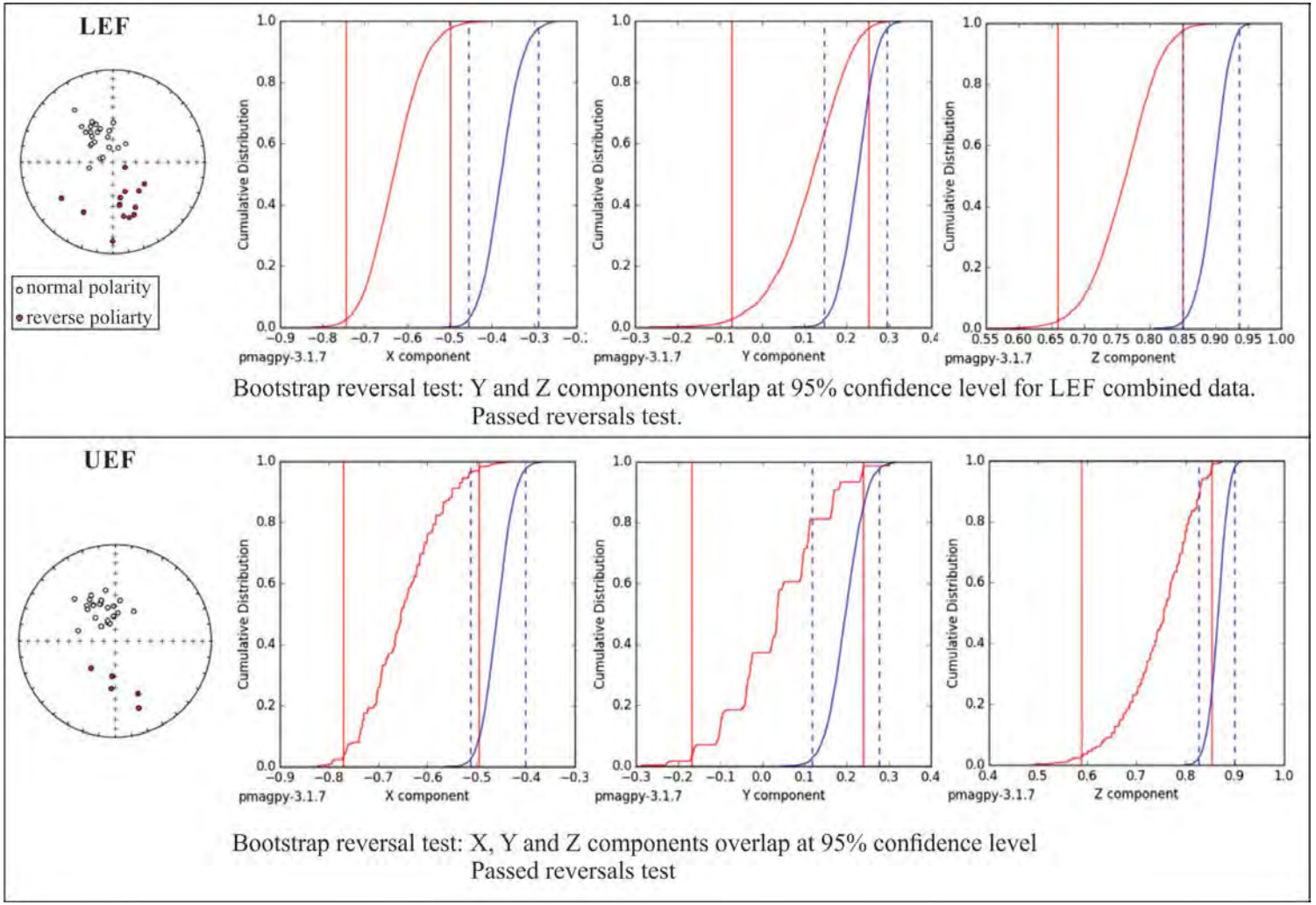

Figure 7.6. Bootstrap reversals test (Tauxe *et al.*, 1991) for the lower Elliot (LEF) and upper Elliot (UEF) Formation samples from the section at Quthing.

Figure 7.7 displays the mean Fisher directions for the entire Elliot Formation in addition to the splitting of the samples between the lower and upper Elliot Formation.

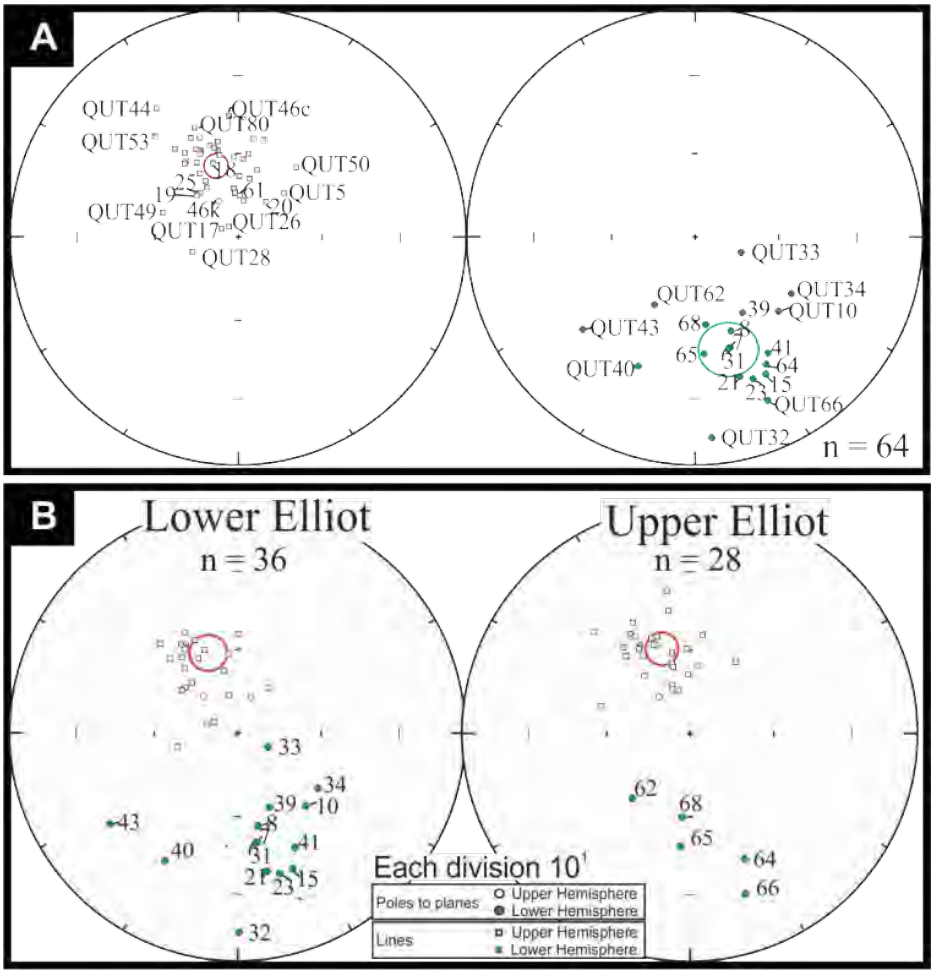

Figure 7.7. Lower hemisphere equal area projections of the geographic primary directions for the Quthing samples showing (A) all samples normal and reverse directions, (B) Lower and Upper Elliot normal and reverse directions and the 95% confidence cones. The entire EF, LEF and UEF passed the reversals test, with B- and C-classes, respectively.

The virtual geomagnetic pole (VGP Lat.) is present in Figure 7.8 with the inferred magnetostratigraphy. There are 7 normal polarity chrons and 5 reverse polarity chrons with two single samples reversals, one in the lower and one in the upper Elliot Formation. The red wavy lines on the magnetostratigraphic log indicate periods of erosion supported by the lithology (Fig. 7.8), and the paraconformity between the lower and upper Elliot Formations is indicated with a dashed line.

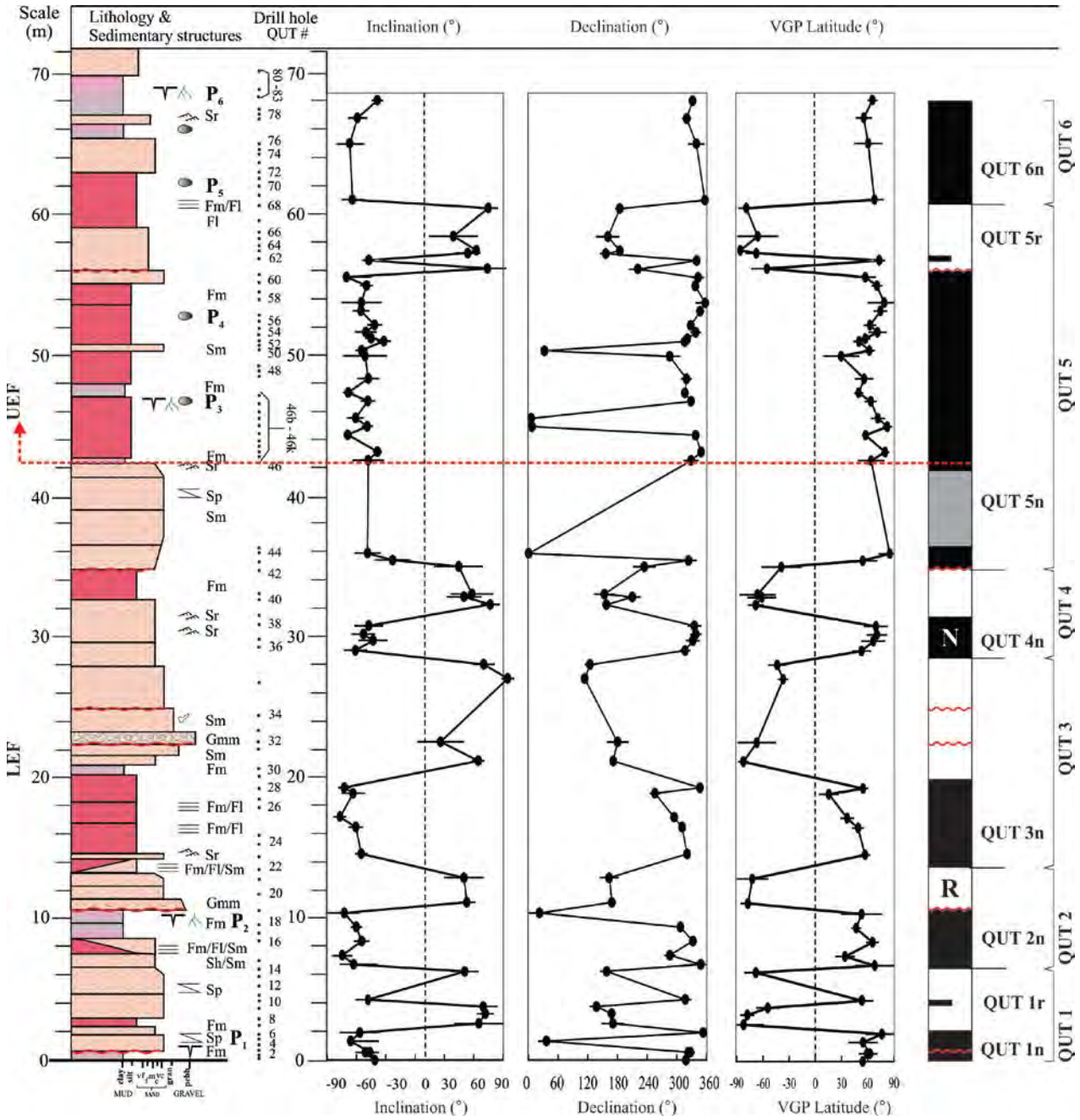

Figure 7.8. Lithological column and recorded inclination, declination and calculated VGP latitude for the Quthing section, Quthing, Lesotho. Black – normal (N/n), white – reverse (R/r). Polarity pairs are marked QUT 1 – 6.

7.3 Discussion

7.3.1 **Placing the Moyeni trackway in magnetostratigraphic context**

The Moyeni track site lies within the lowermost UEF (Smith *et al*., 2009) approximately 18 m above the LEF/UEF contact at the QUT site at 1486 m. At the Moyeni site, the Clarens Formation is at a height of 1644 m whereas at QUT the UEF-Clarens contact is at 1707 m. If the Moyeni trackway is indeed ~18 m above the LEF/UEF contact that would place it within a reversed interval (QUT5r) in the magnetostratigraphic section for QUT (Fig. 7.9).

Interestingly, the Moyeni site with its high diversity and preservation of trackways, often due to the biofilm/algal mat (Wilson *et al*., 2009) can give insight into the changes in habitat conditions during the strong seasonality, and unpredictability in rainfall, in the UEF.

The aquatic/semi-aquatic (i.e. temnospondyl amphibian; Marsicano *et al*., 2014) and non-aquatic (theropods and likely ornithischian dinosaurs Wilson *et al.*, 2009) community preserved in the trackway surface is most likely a reflectance on environmental pressures with dry season progression.

Although the trackway surface only reflectance a short interval in time it is useful, especially when compared to other trackway surfaces deposited under similar environmental conditions (e.g. Seobeng/Subeng, and Maphutseng, Lesotho). It also brings into question, with increasing environment pressure through decreasing/ lessened freely available vegetation and water, competition among the changing faunal populations who visit the water source (Gasith and Resh, 1999).

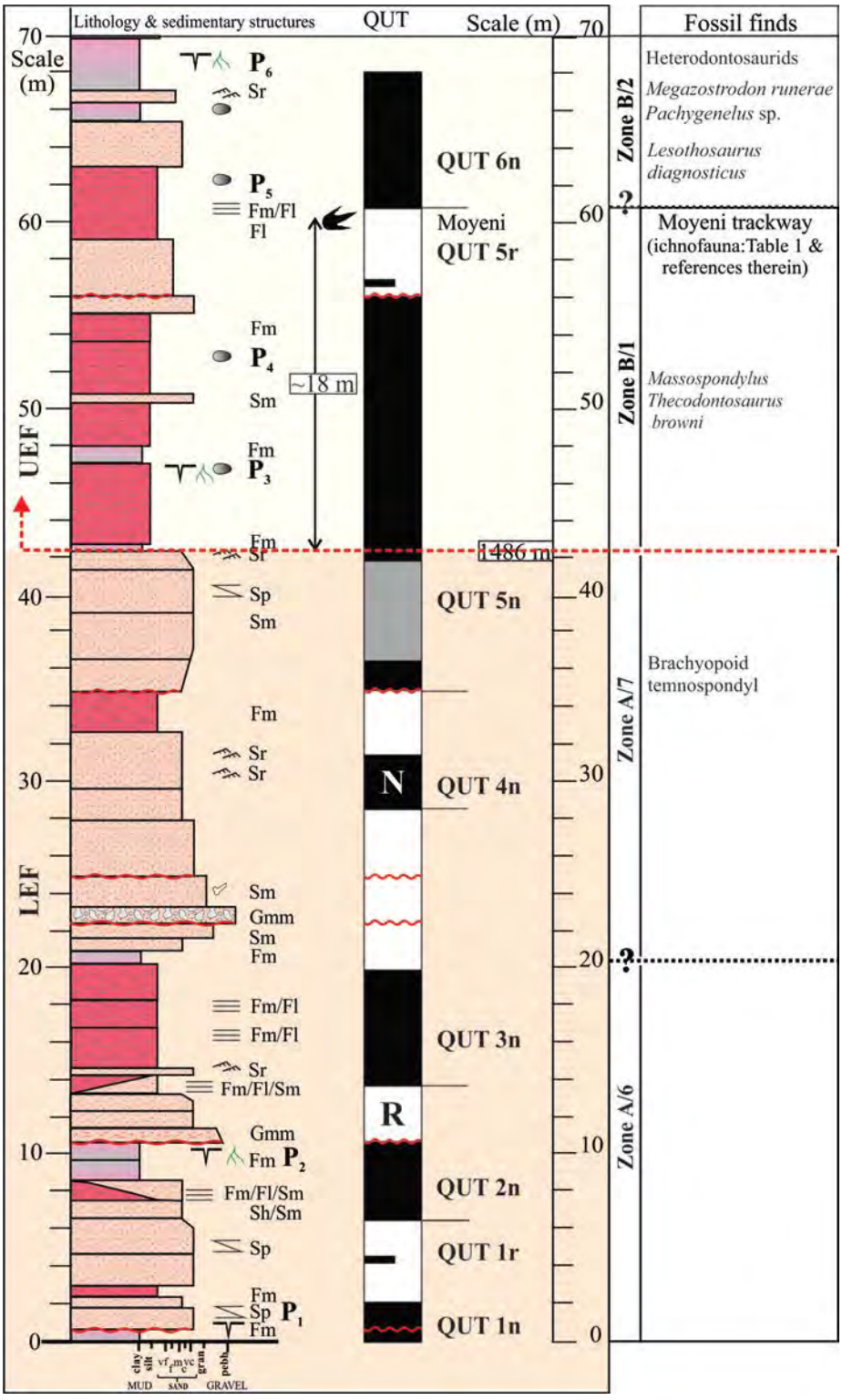

Figure 7.9. Magnetostratigraphy of the Quthing drill section with magnetochrons labels indicated (QUT 1n -6n). The Moyeni track site falls within a reversed interval in QUT 5r approximately 18 m above the sedimentological contact between the LEF and UEF (indicated with dashed red line). Other fossil finds are indicated as per Ellenberger (1970) zonation scheme.

8 Palaeomagnetic study of the transition from the lower to upper Elliot Formation at and near Likhoele Mountain, Mafeteng District, Lesotho

8.1 General introduction

Likhoele Mountain (Fig. 8.1A), one of the most productive palaeontological sites in the Elliot Formation, has been the focus of several important field expeditions in Lesotho. These started in earnest in the 1950's with several French and South African collaborations, with notable early findings such as *Scalenodontoides macrodontoides,* a traversodont cynodont from the Lower Elliot Formation (Crompton and Ellenberger, 1957). During the 1962 field season alone the South African Museum collected, from the UEF, one of the then earliest mammaliaformes, *Erythrotherium parringtoni* (Crompton, 1964).

Another notable discovery was made in 1959 when a partial right dentary (MNHN LES9) was found by Ginsburg, Ellenberger and Fabre in UEF (Table 8.1). Ginsburg (1964) later described and named this material as *Fabrosaurus australis,* a new southern hemisphere ornithischian, owing to its similarities to the ornithischian *Scelidosaurus harrisoni* from the English Lower Jurassic.

This has been revised since and is now known as a *nomen dubium* and Ornithischia indet. based on the lack of identifiable characteristics (Sereno, 1991; Butler, 2005). Subsequently, several Ornithischian remains (2 individuals and one very well preserved skull) were also collected at this site, and represent most of the ornithischian material known from the UEF (Table 8.1). Owing to the fact that the remains were numerous and inclusive of cranial material the specimens were described as a new genus and species, *Lesothosaurus diagnosticus,* and are considered to represent some of the most basal ornithischians (Thulborn, 1970, 1971 and 1972; Sereno, 1991). Detailed reviews of Ornithischian material are in Butler (2005) and Porro *et al*. (2010) (Table 8.1). A review of the history of expeditions and collections can be found in Ambrose (1991; 2005)

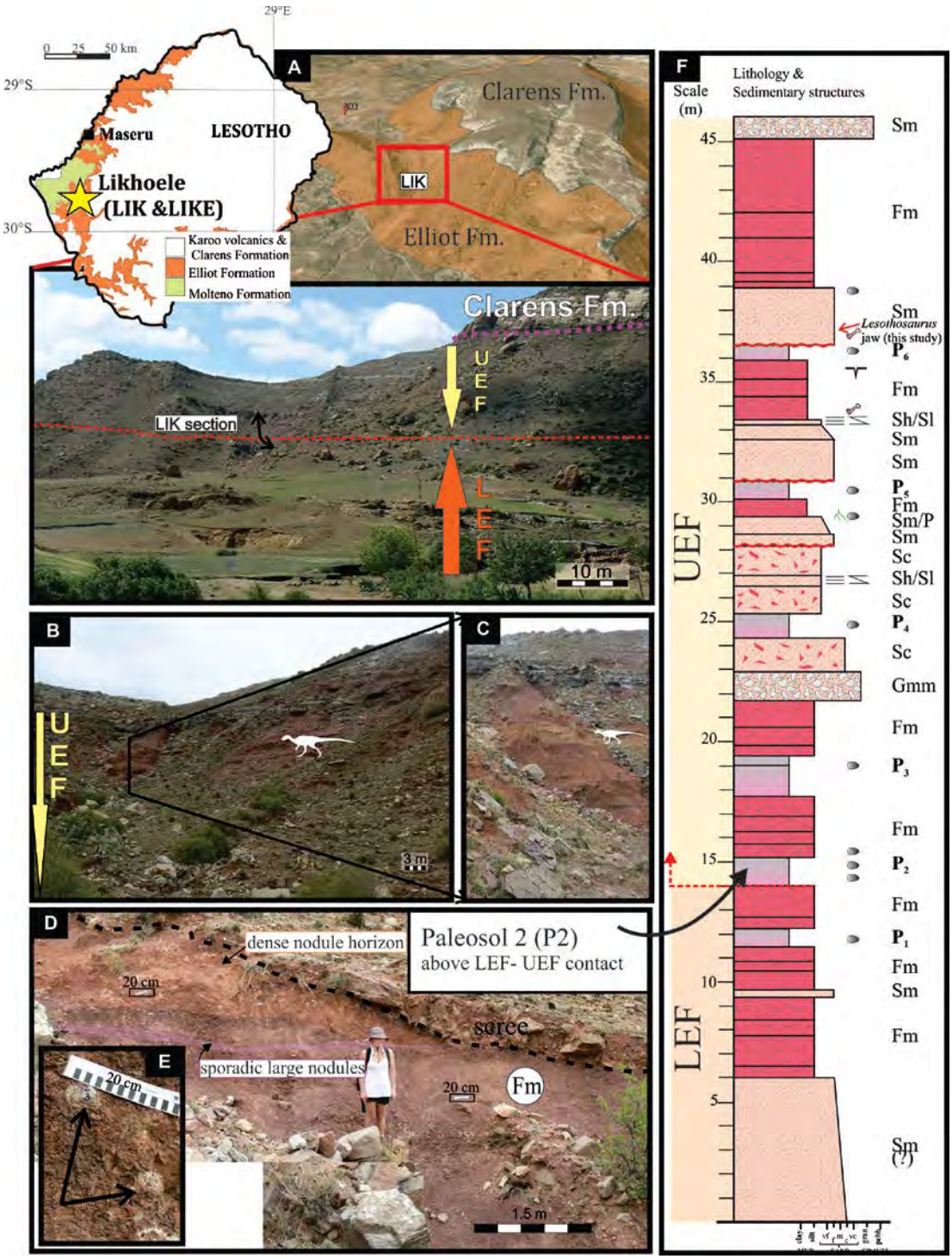

Figure 8.1. (A) Sample site at Likhoele Mountain in the Mafeteng District of Lesotho (B) view of the upper Elliot Formation with an outline of *Lesothosaurus diagnosticus* in white placed near the bed in which it was found. (C) Looking east onto bed in which lower jaw was discovered, (D) A ~2 m thick palaeosol horizon separates the lower and upper Elliot Formations in which (E) pedogenic nodules ranging from nut sized to egg sized are located. (F) Sedimentological log of the drill site indicating the sedimentological contact between the LEF and UEF with a dashed red line. The UEF is approximately 115 m thick at this site. For facies codes please see Figure 1.1, p. 9.

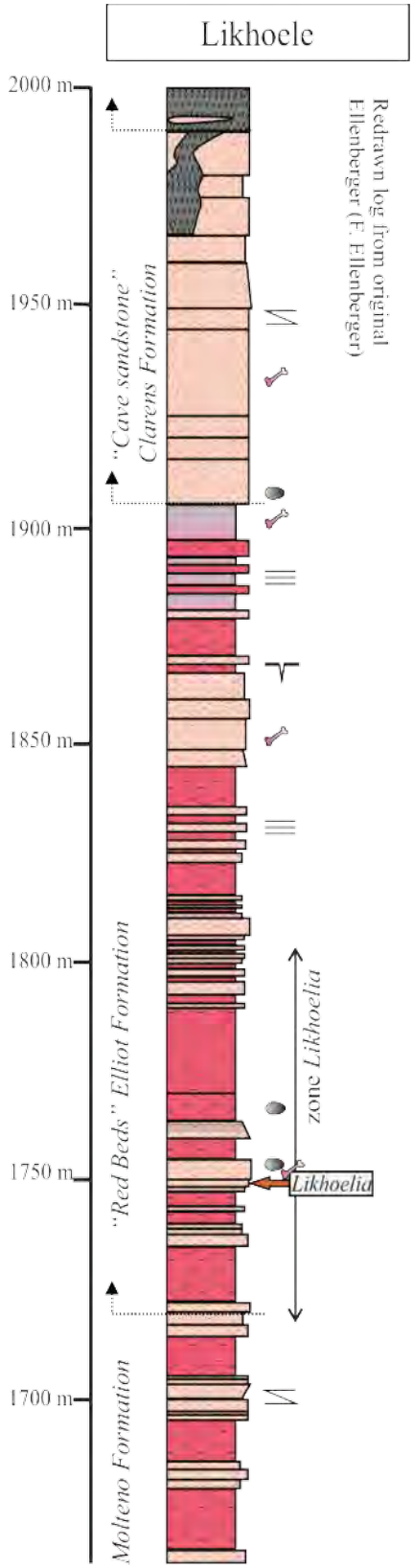

Table 8.1. Details of fossil finds in close proximity to Likhoele Mountain, Mafeteng, Lesotho with details from the original Ellenberger (F.E) log for the Likhoele locality indicating the location of Likhoelia and other fossil bone sites.

Taxonomic assignments	Age	Stratigraphic position	Catalogue no.	Notes	Source(s)
Triconodont mammialaform: *Erythrotherium parringtoni*	Jurassic	UEF (Zone B/2 as with *Megazostrodon*)	SAM K 359	Likhoele Mountain, Mapheteng, Lesotho, specifically the "'side of Likhoele mountain between Tsekong and Ha Matsepe villages". SAM K 359 juvenile (Crompton, 1974), and these small mammals = insectivorous (Kermack, Mussett & Rigney 1973; Jenkins & Parrington, 1976).	Crompton (1964); see also Crompton & Jenkins (1968); Crompton (1974)
Ornithischia indet. undescribed	Early Jurassic (Hettangian–Sinemurian; Butler, 2005)	UEF		Likhoele Mountain, Mapheteng, Lesotho. Undescribed large ornithischian, possibly phylogenetically related to *Lesothosaurus*.	Sereno (1991), Knoll (2002) Butler (2005)
Ornithischia *Lesothosaurus diagnosticus*	Upper Triassic (Ginsburg, 1964) Lower Jurassic (Sereno, 1991)	UEF	BMNH RUB 17 and RUB23 SAM-K400 and K401 UCL B.17	Syntypes- BMNH RUB 17 and RUB23 (well preserved skull); Galton, (1972): basal ornithischian SAM-K400 and K401, fragmentary dental and cranial material with postcranial remains. From the site of Ginsburg's (1959) original discovery (UCL B.17)	Ginsburg (1964) Crompton, (1968), Galton (1972), (Thulborn, 1970, 1972), Santa Luca (1984). See also: Sereno (1991) and Butler (2005) for review of Ornithischia in the UEF
?reptilian, *Pattsia likhoelensis* sp.n.	Late Triassic (Norian)	UEF (?) "Red beds from upper Stormberg series"	-	Slopes of Thaba ea Litau Mountain, Likhoele, Lesotho. Type specimen : UC C146; damaged right maxilla with canine and eight post- canine teeth (Lee & Mill, 1983). Specimen = broadly contemporaneous with *Megazostrodon* (Crompton and Jenkins,1968) and ~earlier than *Erythrotherium* (Crompton, 1964).	Lees and Mill (1983)
Trityldodon sp.,	early Jurassic	UEF	-	-	Ginsburg (1961)
Ornithischia *Ornithischia indet. (Fabrosaurus australis nomen dubium)*	Upper Triassic (Ginsburg, 1964) Lower Jurassic (Sereno, 1991)	UEF	MNHN LES9	Fragmentary dentary MNHN LES9; Ginsburg, 1964 UCL B 17. See Charig and Crompton (1974) and Sereno (1991)	Ginsburg (1964), Thulborn, (1970, 1972). See also Sereno (1991)
Lesothosaurus diagnosticus *Ornithiscian indet.*	early Jurassic	UEF		Likhoele cirque, Likhoele Mountain, Mapheteng, Lesotho. Michiel's mandible (UE) 29° 51'01.20" S 27° 16'08.45" E 1876 m	This study See Sciscio et al., *in press*
Basal sauropodomorpha *Eucnemesaurus* sp., *Likhoelesaurus ingens* (nom. nud.)	Late Triassic	LEF			Ellenberger (1970)
Traversodont cynodont: *Scalenodontoides macrodontes*	Triassic (?)	UEF	SAM K 336	Morobong Hill, SW Lesotho. Holotype appears to be an unnumbered specimen at the MNHN (Hopson, 1984)	Crompton and Ellenberger, (1957); Cooper (1981)
Cynodontes: *Belesodon* sp. (at Likhoele), *B. leribeensis* nov. sp. (at Leribe).	Late Triassic	LEF Zone A/4			Ellenberger (1970)
Sauropodomorph	Late Triassic	LEF		Distal extremity of the femur: 29° 51' 07.5" S 27° 16' 46.5" E 1818 m Two femora of a large sauropodomorph: 29° 50' 59.1" S 27°16'06.1" E 1841 m	This study

8.2 Results

8.2.1 **Sedimentology**

The sedimentological change between the lower and upper Elliot Formations at the main Likhoele site (LIK) was determined by the change in sedimentological characteristics (Fig. 8.1A). Below the sedimentological boundary, the sandstones are prominent, thicker (>2 m) and the siltstones and mudstones are interbedded with thin (<25 cm) laterally discontinuous sandstone beds. Above the boundary, prominent desiccation cracks, numerous pedogenic nodules and the predominance of siltstone/mudstone units over the sandstones is typical. Based on this, the LEF-UEF contact was defined at 1850 m above sea level (Fig. 8.1F) and placed at the base of the second main palaeosol (P2) above sample LIK10b (Fig. 8.1D, F).

More specifically, the UEF at Likhoele is characterised by several palaeosol horizons containing pedogenic nodule horizons and sporadic fragmentary bone fossils. Pedogenic nodules range in size and shape between elongate to sub-oval, egg to nut –sized, and may be associated with discolouration, desiccation cracks and root halos. Within a fine grained sandstone channel of the upper Elliot Formation, 1877 m above sea level (Fig. 8.1C, F), several fossil bones as well as the lower jaw of an ornithischian dinosaur (*Lesothosaurus diagnosticus*) were located. Given that the contact between the Elliot and Clarens Formations is at 1967 m above sea level, this new discovery is 90 m below the contact with the Clarens Formation, and 25 m above the sedimentological boundary of the LEF and UEF, in the lower part of the UEF (Fig. 8.1F).

At the Likhoele east (LIKE) section, above the sedimentological boundary of the LEF and UEF (Fig. 8.2A, B), several palaeosol horizons in addition to other typical UEF features such as the diagnostic clast-supported pedogenic nodule conglomerate were noted. These conglomerates are particularly fossiliferous at this site, and contain a multitude of small bones, bones fragments and numerous isolated teeth. In relation to the LIK main site, LIKE captures a similar succession although marginally condensed in nature (Fig. 8.2C).

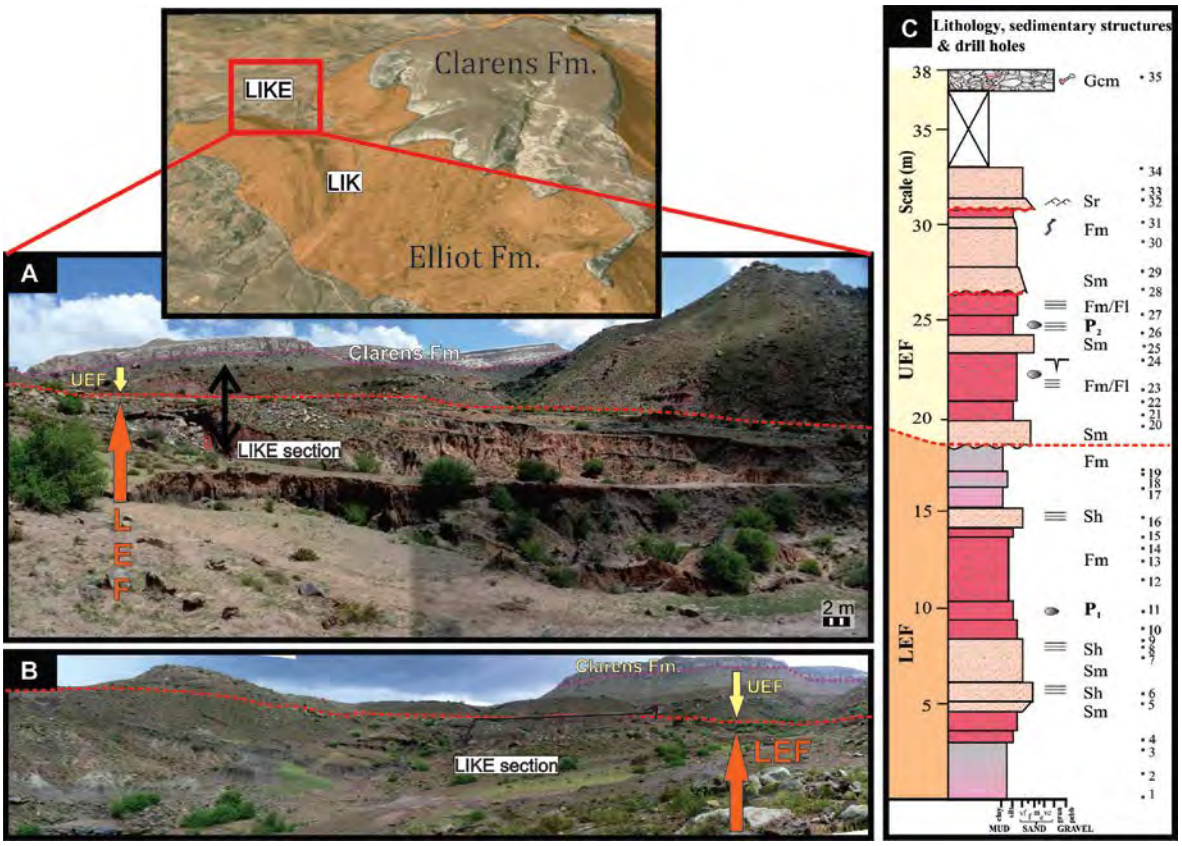

Figure 8.2. Site locality of Likhoele east (LIKE) in relation to the main site at Likhoele. (A and B) Views of the drilled section, the position of the sedimentological contact between the LEF and UEF. Note the Clarens Formation in the backgrounds. (C) Sedimentological log of the LIKE section and the position of palaeomagnetic samples within it. The sedimentological contact between the LEF and UEF is indicated with a dashed red line; wavy red lines indicate an erosive surface.

8.2.2 **Magnetostratigraphy - Main Likhoele site**

Palaeomagnetic directions were determined by least-squares analysis (Kirschvink, 1980). Lines with MAD values ≤ 15˚, and planes with MAD values ≤ 20˚were included in analyses. Most samples had two, sometimes three, well-defined components. These components being:

1. Low-coercivity (soft) magnetic component (NRM – AF 100/150) (coded ‘SFT’)
2. Present local Earth field component (AF100/ 150 - 350^{o}C; Fisher mean declination of 41.2 and inclination -55.7, generally NE upward directed component) (PF).
3. (i) High-temperature relatively steeper (than PF) NNW to NNE component (150-350 – 440-650 ^{o}C) with negative inclination (normal, N).

(ii) High-temperature steep SE component (150-350 –440-650°C) with positive inclination (reverse, R).

Statistical information relevant to high-temperature components and samples are presented in Table 8.2.

Table 8.2. Summary of Likhoele (LIK) mean Fisher palaeomagnetic directions, virtual geomagnetic pole position and related statistics. Statistical parameters are as followings: precision parameter (k) and confident limit (α_{95}) with the dm and dp = semi-axis of the confidence ellipse for poles. N = number of samples, L/P = line or poles to planes.

Likhoele (LIK) (29.31°S, 27.49°E)						VGP			
	N(L/P)	Decl °	Incl °	k	α_{95} °	Pole Lat °N	Pole Long °E	dm	dp
Primary Directions									
EF									
All Reverse	7 (0,7)	200.2	57.6	73.88	7.07	-71.0	330.2	10.4	7.6
All Normal	19 (14,5)	352.2	-71.4	11.9	10.2	62.7	216.9	17.9	15.6
Combined	26 (14,12)	5.7	-68.0	13.7	7.95	67.8	198.0	13.3	11.2
UEF									
All Reverse	7 (0,7)	200.2	57.6	73.9	7.1	(as above)		10.4	7.6
All Normal	11 (9, 3)	348.4	-64.5	13.3	13.0	70.7	232.3	20.8	16.7
Combined	18 (9,10)	4.4	-63.6	17.4	8.5	73.7	196.4	13.5	10.7
LEF									
All Reverse	0 (0,0)								
All Normal	8 (6,2)	5.7	-80.5	12.1	16.6	47.7	204.8	31.9	30.7
Combined	8 (6,2)	5.7	-80.5	10.6	16.6	47.7	204.8	31.9	30.7

During low-field AF-treatment the samples displayed randomly distributed remanence directions of low-coercivity (soft), acquired either during sampling or through natural processes. These randomly distributed low-coercivity components are often removed on completion of AF-treatment, for example LIK 11, which displays a ‘soft’ component up to AF 60, before a present field component and a Triassic/Jurassic-normal component is removed.

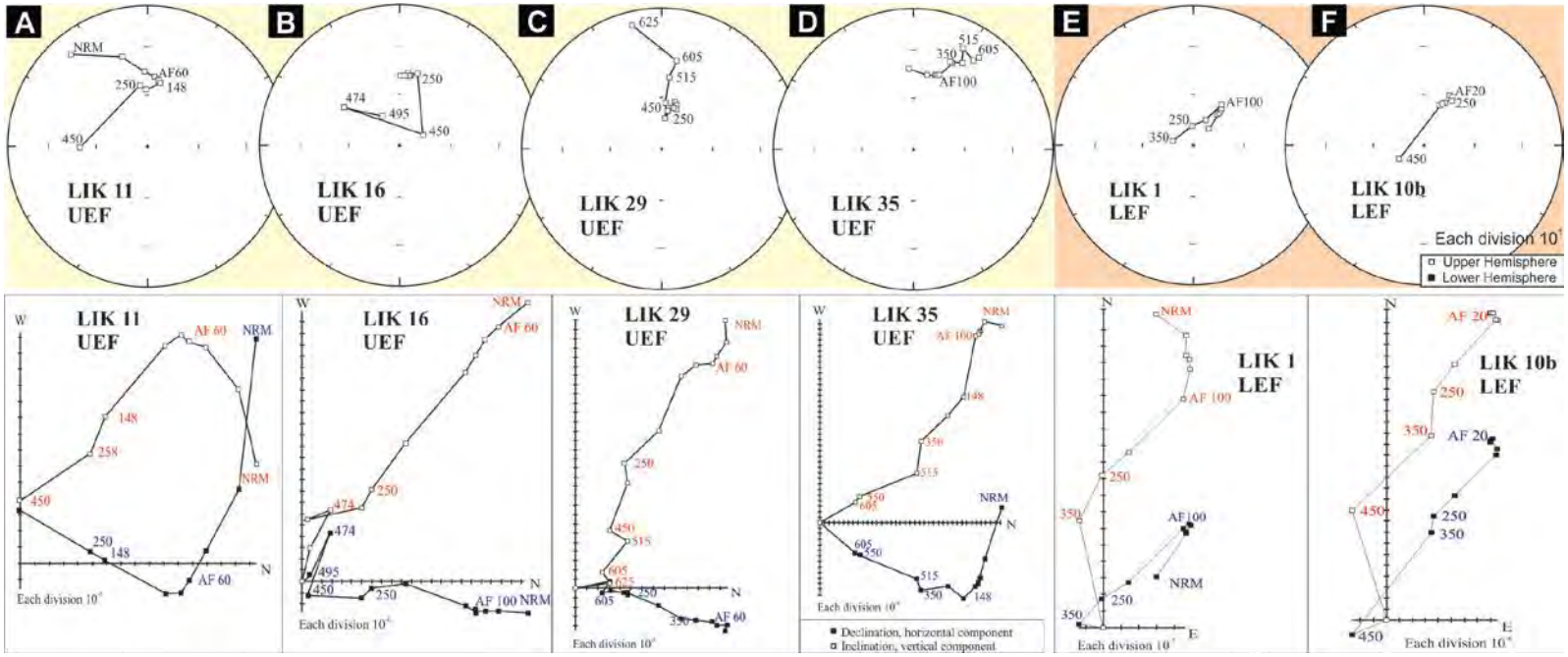

Figure 8.3. (A-D): UEF samples showing typical behaviour during thermal demagnetization along great circle paths to reverse or normal –polarities. (E-F): LEF samples displaying typical normal (LIK1) and reverse (LIKE10b) behaviour. All diagrams illustrate in situ co-ordinates.

During thermal demagnetization, a second component is identical to the present local Earth field **(**PF). The present field component is generally consistent in direction and commonly removed between 150^{o}C and 350^{o}C. Several samples, however, have been completely overprinted by the present field and are excluded from further analysis. For example, LIK 27 has a present field component that remains constant up to 650^{o}C.

As with all other sections, the present field component within the Likhoele samples appears to be constant, north-east and up-directed and overlaps strongly with the normal-polarity component. It is most likely that this PF component will bias the Triassic/Early Jurassic normal polarity data of this site, and therefore important to take this into consideration when evaluating high-temperature normal polarity samples.

High-stability characteristic remanence directions, after the removal of soft- and PF-components, were either normal or reverse components.

The normal component unblocked between temperatures of 150 – 650^{o}C and had an average mean declination of 352.2˚ and inclination of -71.4˚. If the UEF samples were isolated from the group their declination is 348.4˚ and inclination of -64.6˚ in comparison to the LEF with normal mean declination of 5.7˚ and -80.5˚. Stable end-point vector directions to the south, south-east were reached along great circle paths, for instance LIK29 shows a strong present field component (northeast and up-directed) in addition to a stable (up to 625^{o}C) R-component that demagnetizes along a great circle path (Fig. 8.3C).

Samples typical for Likhoele LEF (LIK 1 and 10b) and UEF (LIK 11, 16, 29 and 35) are plotted in *in-situ* geographic coordinates on equal area projections and orthogonal vector plots in Figure 8.3 (E and F) and (A-D), respectively.

8.2.2.1 Reversals test

The reversals test (McFadden and McElhinny, 1990) was applied to the LEF, UEF and the combined Elliot Formation at LIK.

The LEF (n = 8) at LIK could not be tested as the dataset was composed of only normal-polarity samples. In contrast, the UEF was composed of both normal (n = 11) and reverse (n = 7) polarity samples and applying Watson's V test established that the two modes do not share a common precision factor (V = 9.0, Vcrit = 6.6). Secondarily, UEF fails the McFadden and McElhinny (1990) reversals test with a γ_0 of 16.6˚ and γ_c of 14.2˚, and this is reaffirmed in the Bootstrap reversals test (Fig. 8.4).

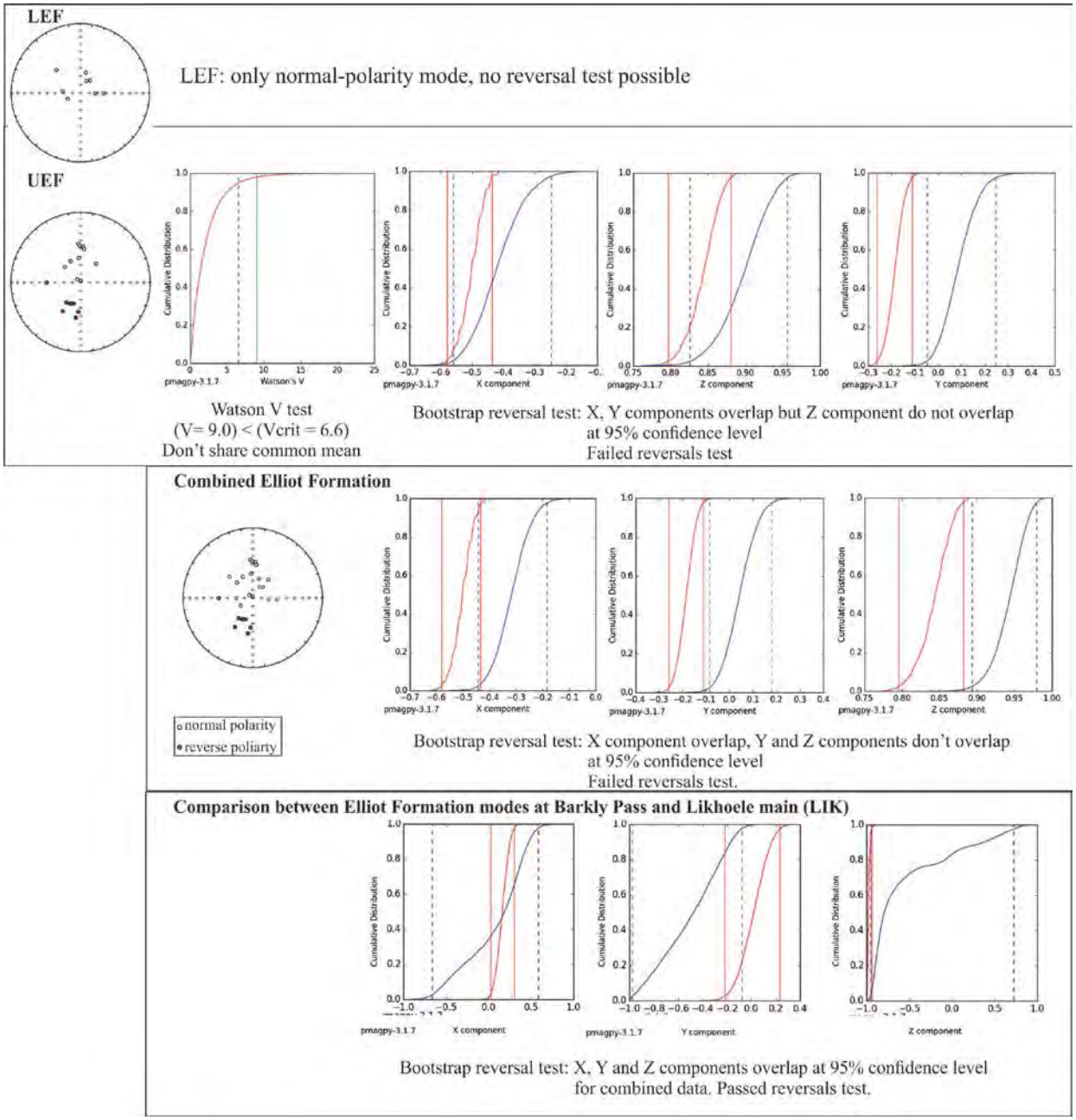

Figure 8.4. Equal area projections, Watson's V test and the Bootstrap reversals test (Tauxe *et al.*, 1991) for the LEF, UEF and the combined LEF and UEF samples for Likhoele main (LIK). The LEF samples were only normal-polarity and therefore it was not possible to conduct a reversal test. UEF and combined data for the Elliot Formation both fail the reversals test. A comparison between the Elliot Formation at Barkly Pass and LIK is presented.

The combined Elliot Formation components, however, share a common mean, but fail a Bootstrap reversals test (Fig. 8.4). A comparison of the LIK to BP, however, shows that the two sites are comparable and pass a Bootstrap reversals test (Fig. 8.4).

The latitude of the virtual geomagnetic pole (VGP Lat.), in conjunction with the inclination and declination of samples from Likhoele are plotted in Figure 8.5 to evaluate the magnetic polarity record. The resulting composite magnetostratigraphy has 3 normal polarity zones and 3 reverse polarity zones if the grey intervals of unknown polarity are considered.

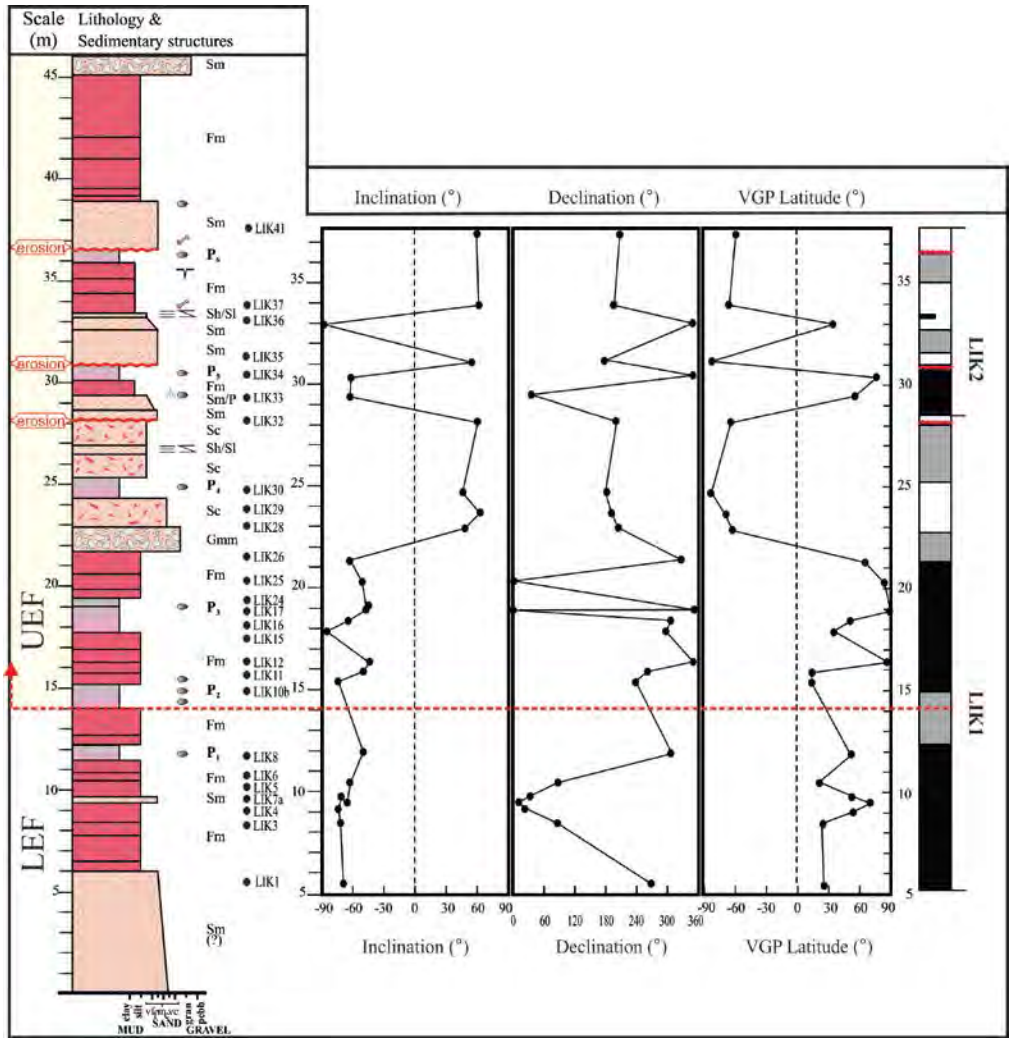

Figure 8.5. Likhoele site (LIK) sedimentology log with occurring palaeomagnetic samples, and the latitude of the virtual geomagnetic pole (VGP Lat.) used to constrain the magnetostratigraphy. The sedimentological contact between the LEF and UEF is indicated with a dashed red line. The wavy red lines marked onto the magnetostratigraphy indicate physical down-cutting/erosive contacts likely to imply the minor loss of geological record.

8.2.3 **Magnetostratigraphy - Likhoele east site**

Palaeomagnetic treatment, directions and components were analogous to those reported above for Likhoele (LIK).

Present-day field component is north-easterly directed, as was the case for the main Likhoele LIK site, with a relatively steep inclination. This component often has a steep inclination in comparison to the 'present-day field' overprint common at LIK and other sites (e.g. Barkly Pass), but the steep inclination ($\leq 70^{\circ}$) could be related to overprinting by Jurassic-aged dolerite intrusions and which would undoubtedly give an overprint direction in this favour. At the Likhoele and Likhoele east sites there were no dolerite dykes directly encountered within the sampled section, although present in the field area, and hence no sampled dolerite dykes/sills can be used as a direct comparison for the "Jurassic-day field" overprint.

The overall stable ChRM directions (N- and R-components) were plotted in equal are projections and combined data, in addition to the separation of the LEF and UEF are presented in Table 8.3.

Table 8.3. Fisher mean palaeomagnetic directions, virtual geomagnetic pole position and related statistics are presented for Likhoele east (LIKE) as a total for the entire site, as well as for the UEF and LEF. Statistical parameters are as followings: precision parameter (k) and confident limit (α_{95}) with the dm and dp = semi-axis of the confidence ellipse for poles. N = number of samples, L/P = line or poles to planes.

Likhoele 'east' (LIKE) (29.85°S, 27.28°E)						VGP			
	N(L/P)	Decl °	Incl °	k	α_{95} °	Pole Lat °N	Pole Long °E	dm	dp
Primary Directions									
EF									
All Reverse	9 (0,9)	114.0	64.6	23.34	10.65	-37.15	79.4	17.1	13.7
All Normal	6 (5,1)	326.7	-65.9	9.32	23.16	58.7	252.0	37.8	30.9
Combined	15 (5,10)	126.2	66.0	13.62	10.36	45.5	257.2	16.9	13.8
UEF									
All Reverse	9 (0,9)	114.0	64.6	23.34	10.65	(as above)		17.1	13.7
All Normal	3 (3,0)	314.7	-51.7	28.0	23.7	51.5	281.6	32.3	22.0
Combined	12 (3,9)	120.7	61.7	20.4	9.4	41.6	264.7	14.5	11.2
LEF									
All Reverse	0 (0,0)								
All Normal	3 (2,1)	6.7	-77.6	8.15	46.31	53.4	202.8	86.8	81.4
Combined	3 (2,1)	6.7	-77.6	5.44	46.31	53.4	202.8	86.8	81.4

8.2.3.1 Reversals test

The reversals test (McFadden and McElhinny, 1990) was applied to the UEF and the combined Elliot Formation at LIKE. The LEF (n = 3) at LIKE could not be tested as the dataset was composed of only three normal-polarity samples. In contrast, the UEF was composed of both normal (n = 3) and reverse (n = 10) polarity samples and applying Watson's V test established that the two modes share a common precision factor (V = 5.0, Vcrit = 8.6), and are antipodal (Fig. 8.6). However, in applying the McFadden and McElhinny (1990) reversals test, the LIKE UEF modes have a γ_0 of 16.8˚ and γ_c of 21.9˚ giving an indeterminate reversals test. This is likely attributable to the 3 normal-polarity mode samples and as such a more definite Bootstrap reversals test was applied (Fig. 8.6). There was no overlap between the modes with the x-components and therefore a failed reversals test.

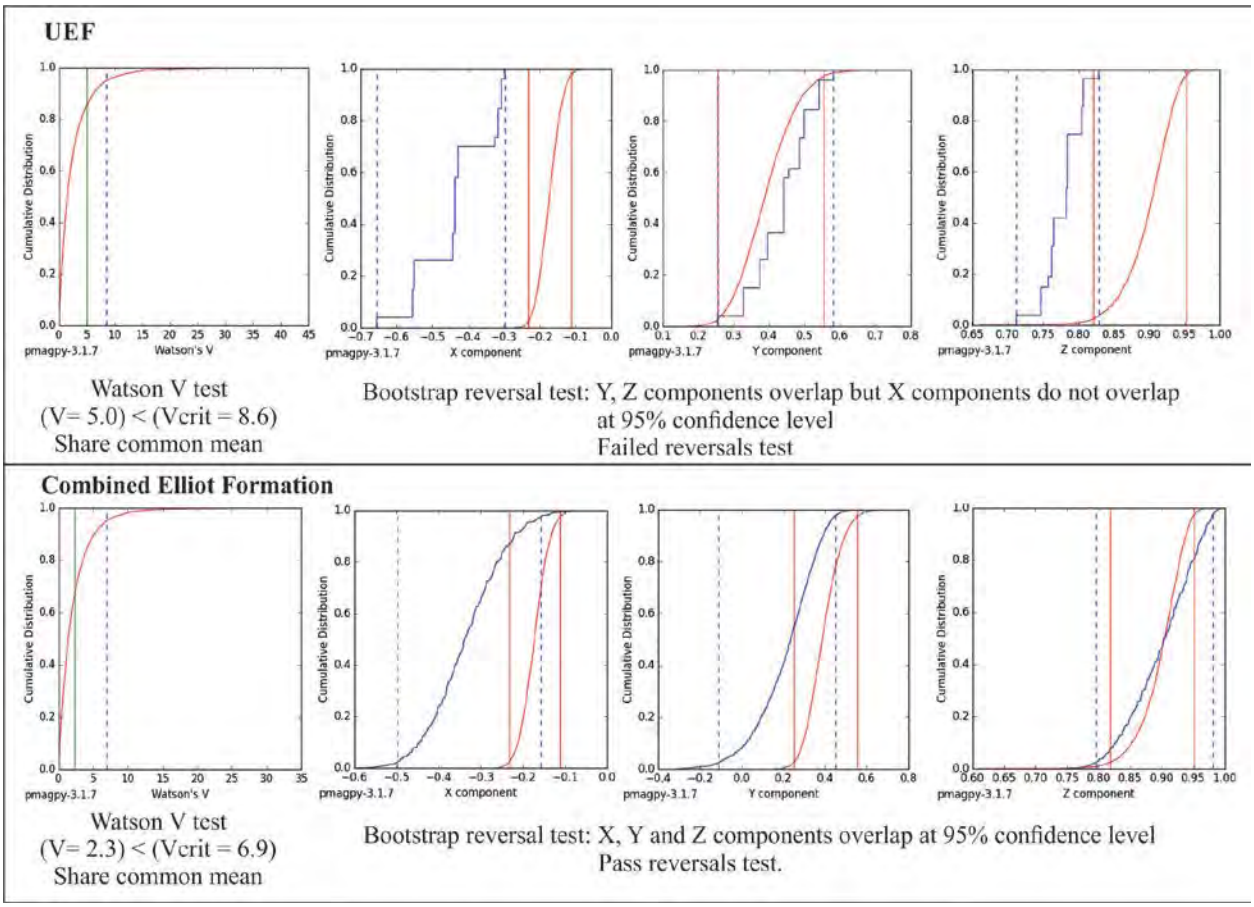

Figure 8.6. Watson's V test and the Bootstrap reversals test (Tauxe *et al*., 1991) for the UEF and the combined Elliot Formation samples for Likhoele East (LIKE) site. The LEF samples were only of normal-polarity and therefore it was not possible to conduct a reversals test. UEF fail the Bootstrap reversals test, despite sharing a common mean, and the combined data for the Elliot Formation passes the reversals test.

The combined Elliot Formation components share a common mean, and pass a Bootstrap reversals test (Fig. 8.6). In applying the McFadden and McElhinny (1990) reversals test, the LIKE Elliot Formation modes have an angle (γ_0) of 13.6˚ of and a critical angle (γ_c) of 23.7˚ giving an indeterminate reversals test (Fig. 8.6). A comparison of LIKE and LIK reveal a shared common mean, and LIKE and BP also share a common mean.

Stable palaeomagnetic components and the virtual geomagnetic pole (VGP Lat.) are plotted in Figure 8.7.

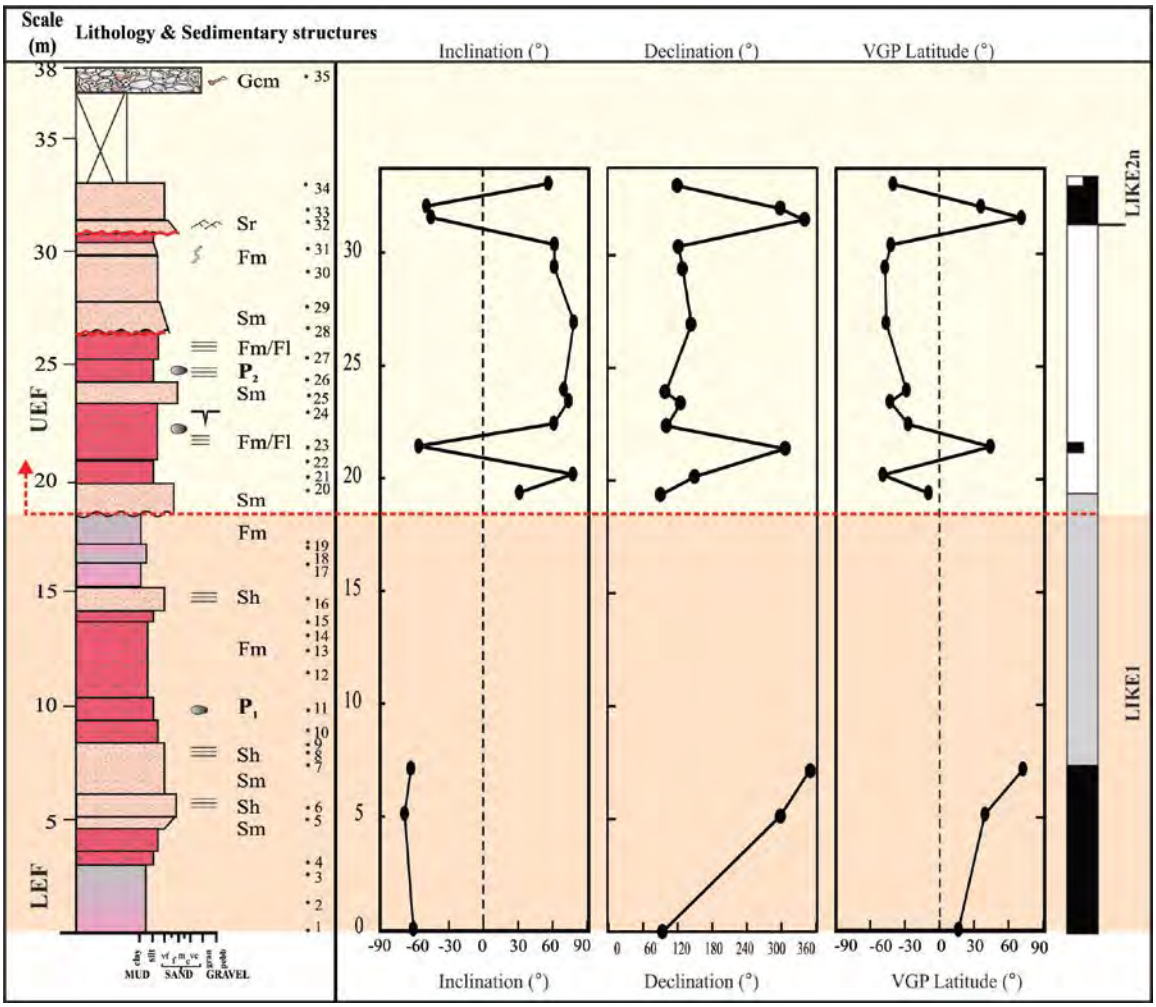

Figure 8.7. The inclination, declination and calculated virtual geomagnetic pole for the Likhoele east (LIKE) site, Mafeteng District, Lesotho. The sedimentological contact between the LEF and UEF is indicated with a dashed red line, and drill numbers are shown under the 'LIKE' abbreviation.

There are 2 normal polarity zones (LIK1n, LIKE2n) and one long reverse polarity zone (LIKE1r). Polarity zones were only identified if there two or more consecutive samples. Grey unknown polarity zones were marked onto the magnetic stratigraphy as indicative of unsampled or overprinted samples. Single sample polarity zones were used when a consistently orientated sample was present in the opposing polarity zone. This occurs in the long normal (LIKE1n) directly above the LEF-UEF contact and the uppermost samples of the LIKE2n magnetochron (Fig. 8.7).

8.3 Conclusion

Average ChRM directions of the LIK and LIKE sites are comparable, and the correlation between the magnetostratigraphy is possible with a long reversal and normal- polarity zone being apparent at both the LIK and LIKE sites (Fig. 8.8). A composite magnetostratigraphic profile was generated for the LIK and LIKE sections and is composed of two magnetochrons named LIK1 and LIK2 (Fig. 8.8). It is noteworthy that erosional bases, marked on the logs (wavy red lines), significantly influences the magnetostratigraphy at each section despite their relative close proximity.

Figure 8.8. Magnetostratigraphy of the Likhoele east (LIKE) and Likhoele (LIK) site, Mapheteng District of Lesotho, relative to their sedimentological sections, and the resultant composite Likhoele magnetostratigraphic log with magnetozones LIK1 and LIK2. Fossil occurrences are placed relative to the stratigraphy and in conjunction with proposed their zones by Ellenberger (1972). The sedimentological contact between the LEF and UEF is indicated with a dashed red line. Downcutting appears to play a crucial role in the preservation of the length of the chrons at each site.

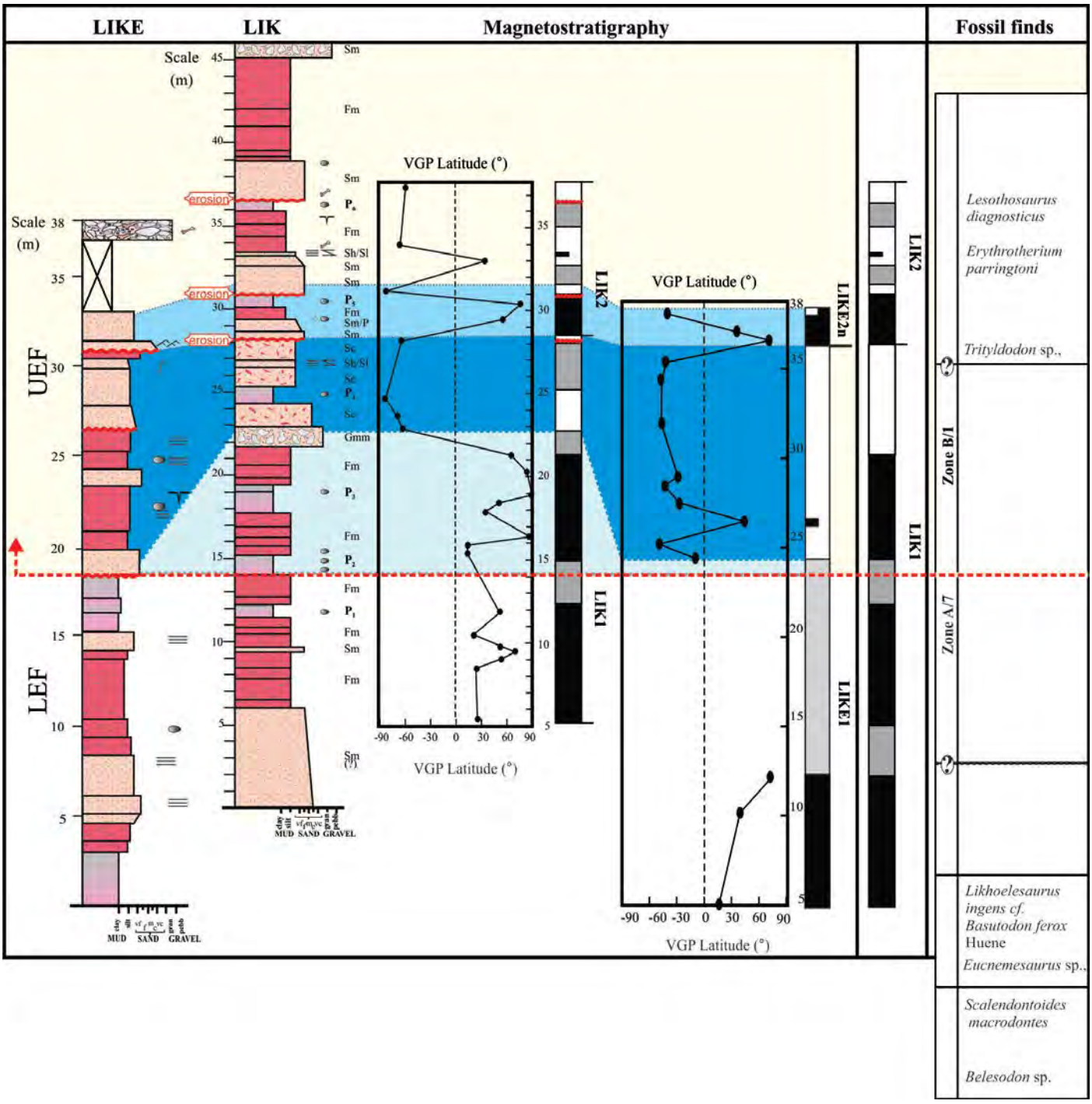
LIKE
LIK
Magnetostratigraphy
Fossil finds
Scale (m)
UEF
LEF
erosion
VGP Latitude (°)
LIK2
LIK1
LIK2n
LIK1n
Zone B/1
Zone A/7
Lesothosaurus diagnosticus
Erythrotherium parringtoni
Trityldodon sp.,
Likhoelesaurus ingens cf.
Basutodon ferox
Huene
Eucnemesaurus sp.,
Scalendontoides macrodontes
Belesodon sp.
MUD
SAND
GRAVEL

9 Conchostracans, magnetostratigraphy and the lake preserved at Seeiso, Mafeteng District, Lesotho

9.1 Introduction

'Ostracod-bearing' beds have previously been mentioned as occurring within the Clarens Formation (Cave Sandstone) by Haughton (1924), Stockley (1947), and Ellenberger *et al*., (1964) amongst others (Bordy *et al*., 2004 a). Tasch (1984) described several genera within the Clarens Formation within Lesotho. During the current study, an upper Elliot Formation (UEF) lake deposit at Seeiso Village (SEE), near Matelile in southwestern Lesotho, has yielded conchostraca (Fig. 9.1).

Previous literature on the occurrence and type of conchostracans always bears reference to the presence of the genus *Cyzicus* (*Euestheria*) (Haughton, 1924; Stockley, 1947). Locations cited in literature as containing conchostracan-bearing beds within the Clarens and upper Elliot Formation (UEF) is as follows:

South African localities:

1. Barkly Pass: At the type locality for the Elliot conchostraca have been found towards the top of the Pass in the uppermost UEF (also see p. 80). These are preserved in a fine grained sandstone, as a highly dense layer on/within a green mud-draped bedding surface. There are several of these layers preserved at the section, and Tasch (1984) referred to them as coquinas. Tasch (1984) identified large and small values preserved and that they belonged to Cyzicus but stated that further study was needed in order to identify the species. Analysis of the Barkly Pass site by Tasch (1984) suggested three possible scenarios for the presence of the conchostracan in such high densities repeatedly over four intervals. These are:
    - Sporadic rain and rapid evaporation of shallow water
    - Prolonged dry spells
    - Overpopulation placing larger demand on falling food supply
2. Siberia, South Africa
3. Nova Barletta, Lady brand, South Africa

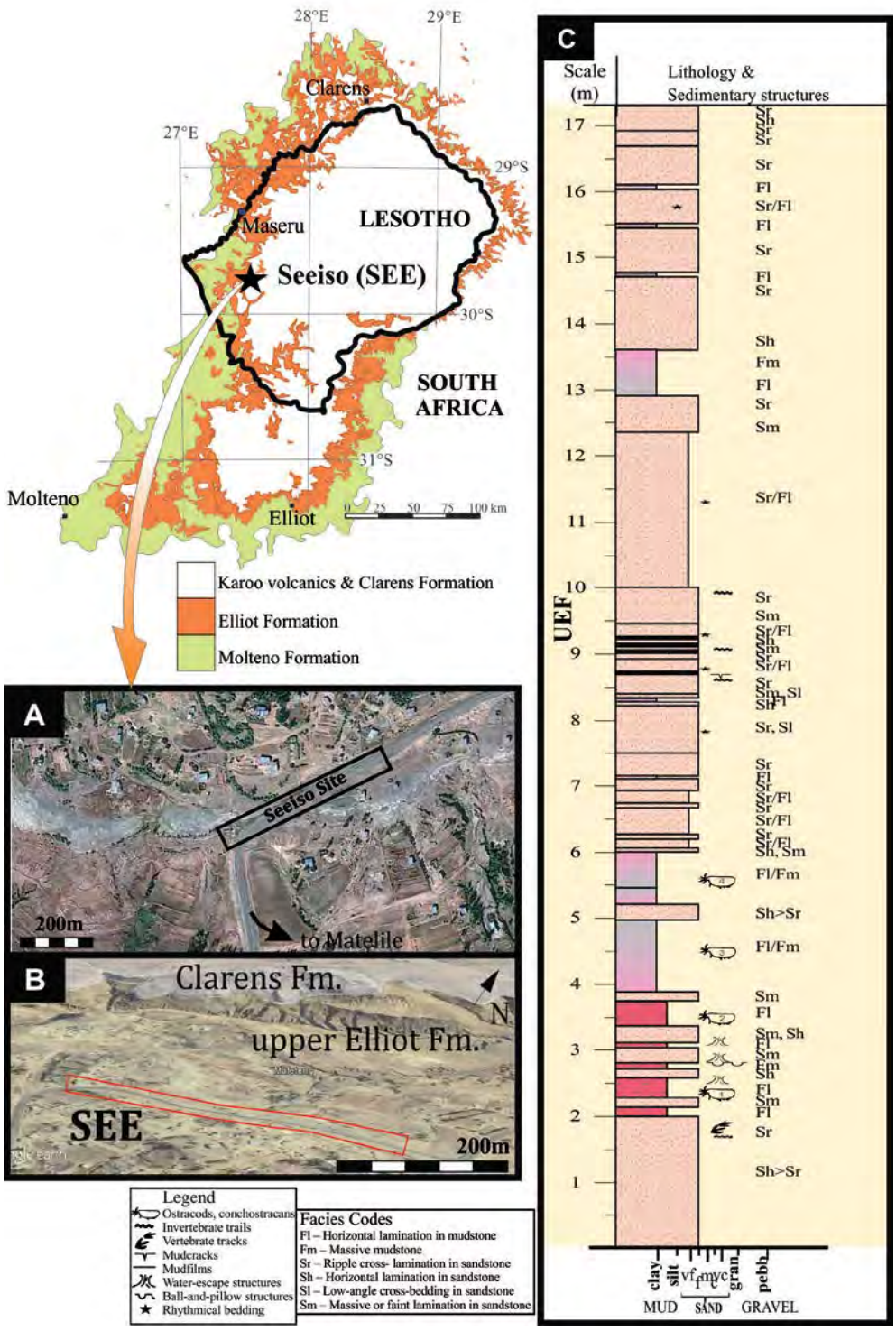

Figure 9.1. Geological map of location showing the extent of the Stormberg Group with Lesotho boundary overlay and position (star) of the field site Seeiso (SEE); (A) Google Earth bird's eye view over the section; (B) Google Earth image draped with upper Elliot and Clarens Formation contacts in relation to the study section at 'SEE' (red box) near Matelile, SW Lesotho; (C) The sedimentary log of Seeiso 'SEE' site showing intervals with conchostracans. Palaeomagnetic drilling was undertaken between 0 – 14 m of the section.

Lesotho localities

1. Thabaneng , Lesotho
2. Mofoka's Store , Lesotho (Tasch, 1984)
3. Leloaleng, Masitisi, Mohales Hoek, Brakfontein, Lesotho. Ellenberger (1970)
4. Makolaone, Mofoka's Store, and in the Setleketseng Valley proximal to Lithathone's village (p. 41, 42 and 45; Stockley, 1947)

Conchostracans (Crustacea: Branchiopoda) are small bivalve arthropods which have been shown to occur since the Devonian (Scholze and Schneider, 2015). These crustaceans predominantly occur in ephemeral freshwater lakes but are also known in alkaline ponds, floodplain pools and brackish water environments (Kozur and Mock, 1993; Scholze and Schneider, 2015). Their phosphatic and chitinous shells allow them to be found only in the environment in which they were predominant. This is because the shell material is not resistant to transportation by flowing water (Kozur and Weems, 2005, 2010). It is in these freshwater ephemeral pools that conchostracans are able to flourish for short intervals, reproducing drought and freeze-resistance eggs to be wind transport to the next viable location.

Biostratigraphically conchostracans are said to make one of the best continental markers because they are able to achieve resolutions as great as marine conodonts and ammonoids (Kozur and Weems, 2005, 2010; Lucas and Milner, 2006). This is a function of their abundance, distinct forms, wide distribution and relatively little palaeoprovinciality (Kozur and Weems, 2010), although Olsen *et al*. (2011) warn of their endemism. Furthermore, with identical species in high and low latitudes and their occurrences within a multitude of facies (inclusive of red beds) conchostracan are thought to make an excellent continental Triassic biostratigraphic marker (Kozur and Weems, 2010). This has proven true for lower and middle Triassic rocks globally but there is a separation of species during the upper Triassic as Gondwana and Pangaean forms diverge (Tasch, 1979; Kozur and Weems, 2010). South American (Chile, Argentina, Brazil) Upper Triassic conchostracans are markedly different from those of the northern hemisphere (Kozur and Weems, 2010). Only those of north-western Africa have similar species and this being solely a function of its position in Gondwana relative to south-western Europe, Canada and the eastern United States (Kozur and Weems, 2010). This contradicts their purported use as an index fossil. In Gondwana the best described conchostracans are from South America and are Middle and Late Triassic in age. Correlating these with the marine record has proven imprecise (Kozur and Weems, 2010).

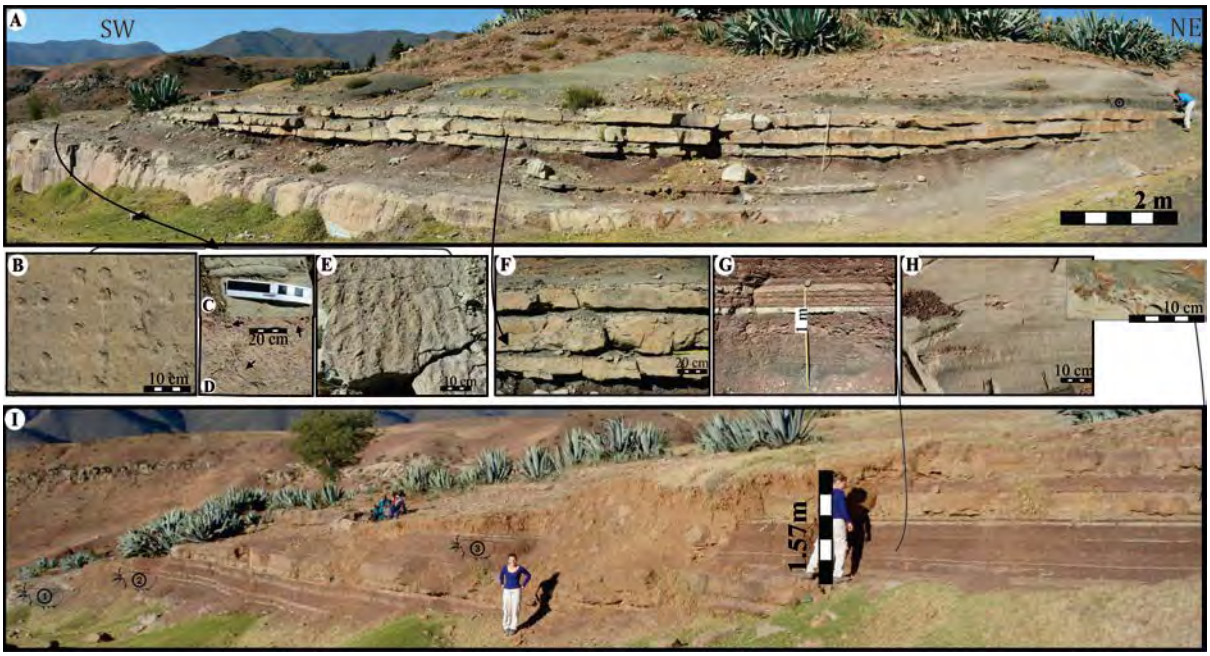

Figure 9.2. Seeiso site photographs displaying the (A) South-western most edge of outcrop showing lowermost thick sandstone channel overlying organic horizon 1, Scale bar = 1 m; (B): Track ways on palaeosurface of channel show in (A); (C) Root trace in (rhizolith ?) on channel A; (E) Rippled palaeosurface with vermiform trace fossils (potential invertebrate traces) and pits in thin mud film on surface of channel A; (F) Three successive fine grained sandstone beds overlying the first organic unit, thin mudstone layers separate each unit; (G) Organic Unit 3: repetitive finely laminated mudstone, note the blue-black coloration of lowermost layers at base; (H) Ripple cross laminated fine grained sandstone overlying organic unit 4 which is capped, characteristically for this deposit, with a thin film of bioturbated green mud (Inset); (I) Looking south-west from northern part of outcrop showing the three main organic units (i- iii).

9.2 Results

9.2.1 **Sedimentology**

The outcrop at SEE displays fossiliferous blue-black to maroon coloured organic-rich mudstones interbedded with fine grained sandstones (Fig. 9.2C). There is little variation in grain sizes (mud to very fine sand), and sandstone bodies present represent laterally persistent, tabular beds with no evidence of channeling. The mudstones show rhythmic bedding which is likely a monitor of subtle fluctuations in energy levels related to seasonal flux (Fig. 9.2C). The tabular, even, laterally extensive and overall fine-grained beds indicate an unconfined, low energy depositional setting, e.g., lake. The distinct blue-black to maroon coloured organic-rich mudstones indicates anoxic to oxic deeper lake setting. Sedimentary structures present range from climbing ripple cross lamination to soft water deformation structures and

represent times of increased depositional rates (Fig. 9.2H). There are both invertebrate and vertebrate ichnofossil assemblages present (Fig. 9.2C).

The north-eastern edge of the SEE outcrop (Fig. 9.2A) represents an ephemeral channel because of bioturbation and footprints. It is overlain by the fine grained, laminated and thinly bedded lake sediments. There are 4 dark (blue-black) coloured mudstone beds, likely organic-rich and were found to contain conchostraca. The thickest of which (110cm bed 3 from base of sequence; Fig. 9.2I) describes a long period of low energy uninterrupted deposition, and therefore also describes the deepest and most distal part of the lake system. This thick mudstone unit is overlain by several layers of fine sandstone layers and the last organic rich mudstone layer (Bed 4; Fig. 9.2I). The lowest energy unit (bed 3) is followed by several pulses of higher energy events sandstone bodies which also thicken upwards indicating in-filling of the lake. The sandstones, which become more dominant in the north-western edge of the outcrop (Fig. 9.2A), are characteristic of high (upper flow regime) and low energy (low flow regime) and are fine grained.

9.2.2 **Conchostraca**

The carapaces, carapace compound-mould and carapace moulds of various conchostraca were examined using a dissection microscope and attached camera from cubic centimeter fragments of the collected rock material (mudstone). Of the samples collected at SEE, only two main types of conchostracan were identified to date (Table 9.1). In addition to the better preserved conchostraca carapaces, several unidentified remains were photographed, classified as *incertae sedis* and are reported in Figure 9.3.

Preservation of carapaces and carapace moulds was variable, and often they exhibited concave/convex or flattened surfaces due to compaction during subsequent burial. Identified conchostracans are represented by two different morphotypes with main differences in carapace morphology and minor differences in size.

The first morphotype ‘Type 1’ (e.g. samples see_007b&007d) exhibited carapace moulds that are small to moderate in size (2 - 4 mm), and have ovate to subovate valve outlines, sub-central positioning of the umbo (Table 9.1). Generally these were all ventrally flattened parallel to bedding plane. Importantly and characteristically, better preserved specimens show rhythmic and narrow growth lines divided into sets of ~10/12 bounded by a more prominent double growth band. No ornamentation on valve or between growth lines was noted.

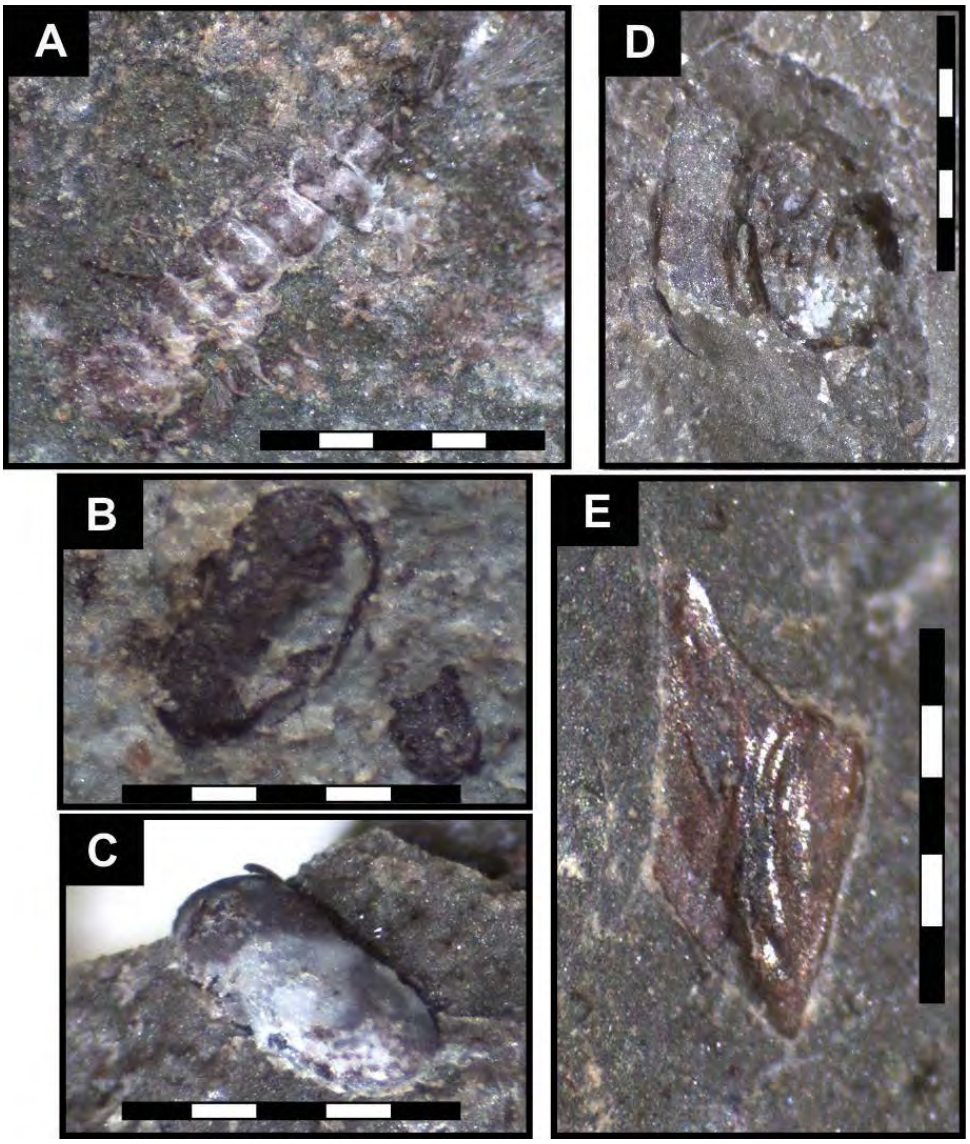

Figure 9.3. Seeiso *incertae sedis* (A) Insecta: mayfly abdomen (?); (B) and (C) coprolites (?) or fungal spore (?); D large ovate conchostracan shell, distorted and poorly preserved; (E) Actinostegii scale (pers. comm. Dr R. Gess). Scale = 2 mm

The second morphotype identified as 'Type 2' (e.g. samples: see_009 and see_010) are small in size, sub-oblong in shape, with the umbo positioned antero-subdorsally, and having a curved dorsal margin (Table 9.1). There appears to be no ornamentation but more detailed work may prove useful.

Table 9.1. Seeiso conchostracan morphotypes 1 and 2 taken from various stratigraphic intervals indicated on the sedimentological log. Illustrations of Type 1 are to show detail of the double growth bands (brown). Scale bar = 1 mm.

	morphotype 1	morphotype 2
Shape	Ovate to subovate	Sub -oblong in shape
Umbo position	Subcentral position	Antero -subdorsally
Ornamentation	No apparent ornamentation between growth lines	No ornamentation on valve or between growth lines (Lacks spines or nodes)
Growth lines	Growth lines appear smooth and paired (double banded)	Growth lines appear smooth
Dorsal margin	Smooth and straight	Curved
Length of valve, L	2 - 4 mm	1.8 - 3 mm
Height of valve, H	1.9 - 2.7 mm	1 - 2.5 mm
Genus?	?Similar to *Asmussia loockii* (Tasch, 1984)	?Similar to *Cyzicus* (*Euestheria*) *stockleyi* Tasch (1984) except in size (smaller).

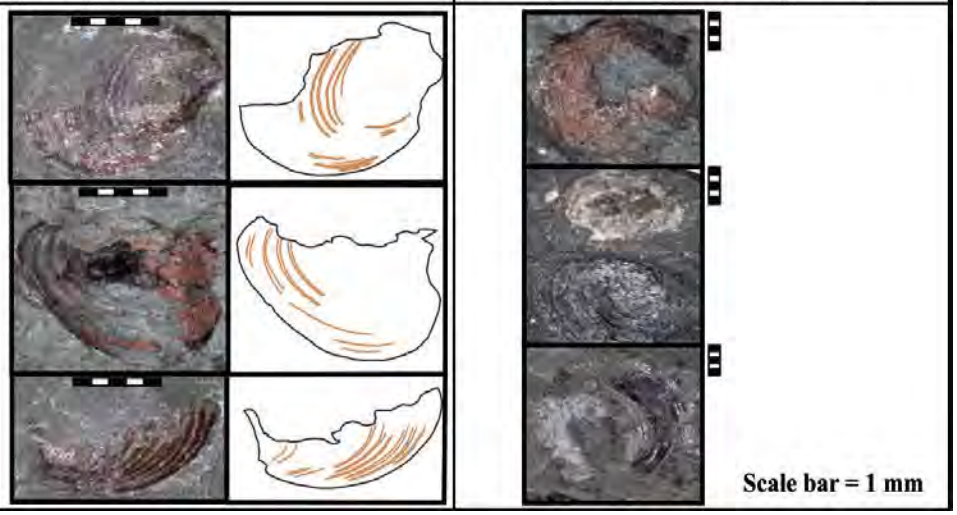

9.2.3 **Demagnetization results**

Previously noted at other sampling sites, during this study, the DAM and OLD samples had two well-defined components. Palaeomagnetic directions were determined by least-squares analysis (Kirschvink, 1980). Lines with MAD values ≤ 15°, and planes with MAD values ≤ 20° were included in analyses.

1. Present local Earth field component (NRM – AF100/ 150 - 250^{o}C; Fisher mean declination of 348^{o} and inclination -63.2^{o}, generally NNW upwards directed component) (PF).
2. High-temperature steep NW component, relative to PF, (150-350 – 580-680 ^{o}C) with negative inclination. (~NORMAL, N).
3. High-temperature steep SE component (150 - 350 – 580-680 ^{o}C) with positive inclination (~REVERSE, R).

Statistical information relevant to high-coercivity/high-temperature components and samples are presented in Table 9.2. All primary reverse directions (n = 19) have a mean direction inclination (I) of 45.1˚, declination (D) of 144.6˚ and α_{95} = 9.96˚, and the normal polarity samples (n = 4) have a mean direction with declination of 314.9˚, inclination of -54.3˚ and α_{95} = 10.77˚. The primary mean direction for the entire UEF site is Io = 46.9˚, Do = 143.1˚, α_{95} = 8.36˚, with site mean VGPs yielding a pole latitude of 57.8 (˚N) and longitude of 111.2 (˚E).

Table 9.2. Seeiso site-mean geographic directions and VGPs for upper (UEF) Elliot Formation samples. Precision parameter (k) and confident limit (α_{95}) with the dm and dp = semi-axis of the confidence ellipse for poles. N = number of samples, L/P = line or poles to planes.

Site	Fisher Stats						
Seeiso: SEE (29.81°S, 27.51°E)							
	n (L/P)	Decl. (°)	Incl. (°)	k	α_{95} (°)	Pole Lat (°N)	Pole Long. (°E)
Primary directions (UEF)							
All Reverse	19 (16,3)	144.6	45.1	12.32	9.96	-58.8	114.5
All Normal	4 (4,0)	314.9	-54.3	55.32	10.77	51.9	277.9
Combined	23 (20,3)	143.1	46.9	14.09	8.36	-57.8	111.2

The inclination and declination of stable palaeomagnetic directions (high temperature N and R) and the calculated virtual geomagnetic poles (VGP Lat.) are plotted in Figure 9.4. Notably SEE section is composed of a short (2 sample) normal polarity zone overlain by a long (~13 m) reverse polarity interval (SEE1r) which is punctuated by several small normal polarity intervals, often of only a single sample.

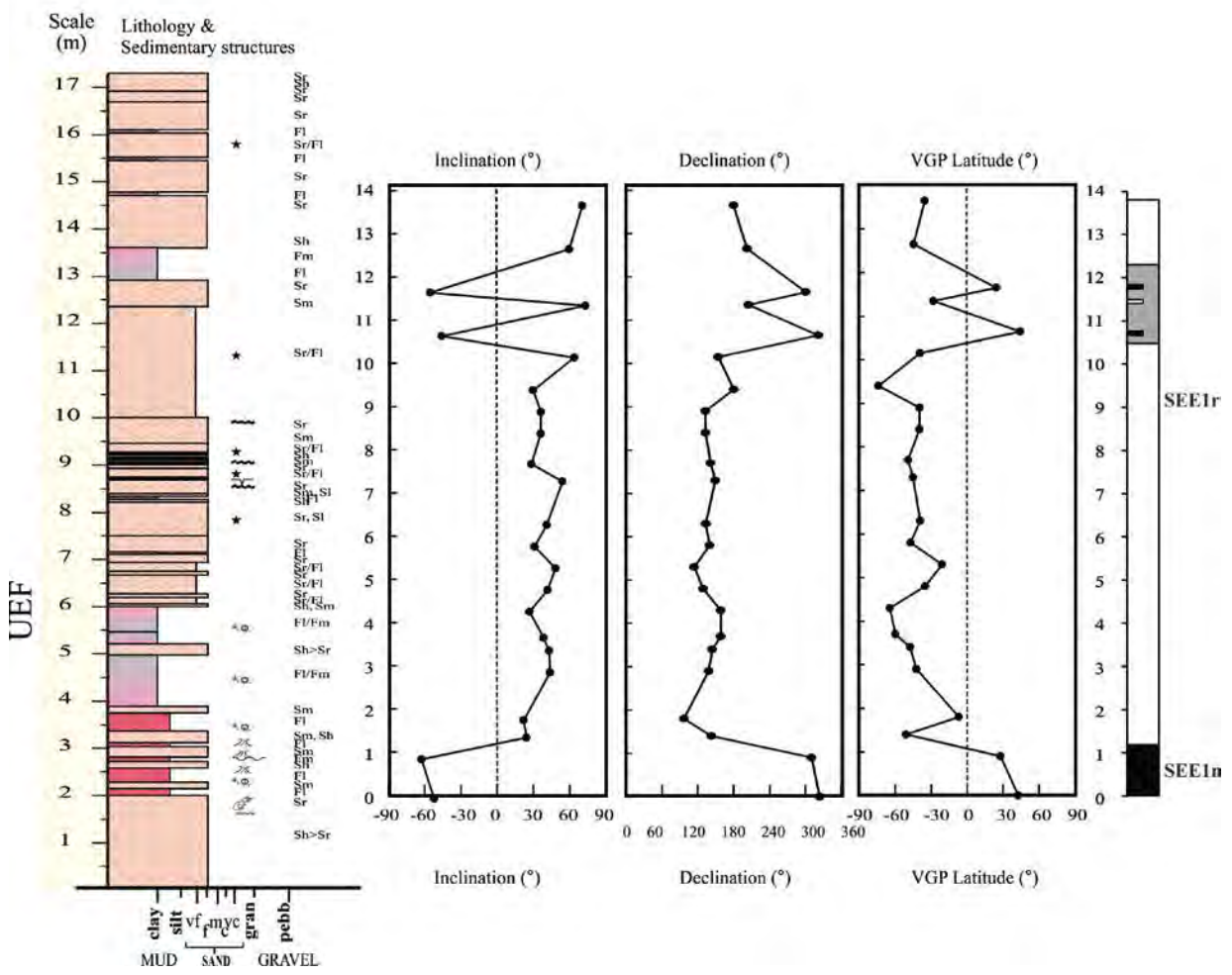

Figure 9.4. Stratigraphic height of samples versus inclination and declination (°) for the upper Elliot Formation (UEF) Seeiso site. Polarity pair marked SEE 1n – SEE1r.

9.3 Discussion

Conchostracan-bearing mudstones and siltstones at the base of the SEE sedimentary log (Fig. 9.4) appear to coincide with the transition between a normal polarity interval (SEE1n) and a long reverse interval (SEE1r). The SEE section is otherwise dominated by a long (~13m) reverse polarity interval. The majority of the samples taken at SEE indicate an extended period of slow deposition with little to no scouring or erosion. Thus, SEE likely preserves a comprehensive and detailed insight into the magnetostratigraphy of the uppermost UEF. This is often not possible at other sections (see chapter

dealing with sections at Golden Gate National Park, p. 172) where mudstones dominate the uppermost UEF creating a scree slope that does not preserve outcrop satisfactory for palaeomagnetic studies.

The proximity to the Clarens Formation of the SEE site allows for more detailed magnetostratigraphy close to the UEF –Clarens Formation contact. This will complement other sections in the Mafeteng District (e.g. Likhoele and Likhoele East sections). It is also worth noting that other reported stratigraphic positions of conchostracan-bearing lake deposits are all from the uppermost UEF and lowermost Clarens Formation. This specific occurrence could speak of palaeoenvironmental and associated preservational conditions during this timeframe.

The conchostracans found at this site need further investigation. For this thesis, as they did not present the main thrust of the investigation, they were merely studied under a dissection microscope and photographed. A further more detailed study should be conducted using standard techniques for studying these organisms, such as SEM imaging, which would provide an additional aid in accessing the more delicate intra-growth band details (Scholze and Schneider, 2015).

Furthermore, there are new studies of conchostraca and a revision of the often confusing taxonomy which has been long under debate. This has led to various forms having been classified differently, based on varying importance of different morphological features, by various authors (Scholze and Schneider, 2015). Recently classification of specimens from Johnson Farm Upper Triassic conchostraca have been recorded in the Late Triassic Chinle Formation and the Upper Jurassic Morrison Formation where they have been described as "*Lioestheria*" which may be synonymous with *Euestheria* (Tasch, 1987; Lucas & Milner, 2006). Conchostracans have been studied at Whitmore Point Member of the Moenave Formation. The Whitmore Point member is considered to contain the TJB (Donohoo-Hurley *et al*., 2010).

9.4 Conclusion

9.4.1.1 Seasonal events and palaeoecology

This UEF site represents a low diversity biota of poorly preserved conchostracans with relatively little other fragmentary remains (Actinostegii scale, Mayfly abdomen?) found to date. The presence of a likely fish scale (Actinostegii scale; Fig. 9.3E) is intriguing and Tasch (1976) report only one locality (Beardmore Glacier, Antarctica) in which fish remains (within coprolites) are within beds containing conchostracan valves. Trace fossils are found at different stratigraphic intervals throughout the section.

These vary from vertebrate trackways in the south-western most part of the section (indicate small reptile/dinosaur movement) close to the water source, to plant and invertebrate grooves, vermiform traces and small invertebrate burrows throughout the unit. Rhizoliths present in the south-westernmost part of the section indicate vegetation proximal to the waterway and lake. Four repeated units of organic-rich finely laminated mud with conchostracan remains, trace fossils, tetrapod trackways suggests repeated drying/flooding events of a shallow water lake. Growth bands, determining the length of the season (Doumani and Tasch, 1963), of better preserved specimens indicates that the pond/lake was viable for 50-60days further indicating their ephemeral nature.

Result chapters dealing with north-western and northern-most sections

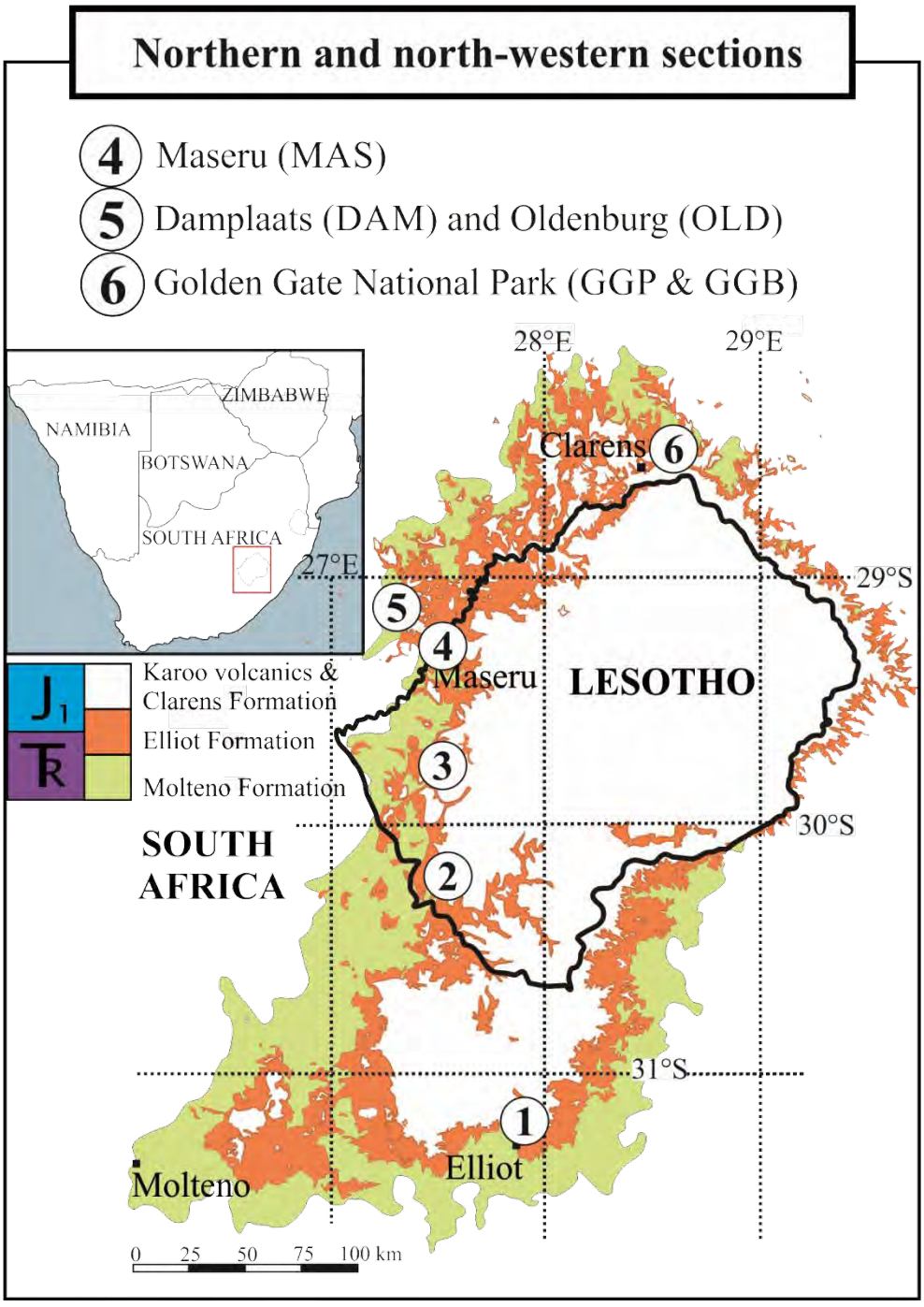

10 Stratigraphic assessment through the Triassic-Jurassic Elliot Formation, in Maseru (Lesotho), using bio-, litho- and magnetostratigraphy

10.1 Introduction

The Parliament Hill section, coded MAS, transects a hill slope (S 29˚19’08.8”, E 27˚29’31.2”; Figure 10.1) and the sedimentological contact between LEF-UEF in the city of Maseru, Lesotho. The section lies to the south of the (then) construction site of the New Parliament Buildings of Lesotho. The road towards the MAS section is called New Parliament Road (Figure 10.1).

A laterally discontinuous, detrital zircon-bearing reworked tuffaceous sandstone layer (Figure 10.2), is located within the MAS section, the lowermost UEF. U-Pb LA-ICPMS and CA TIMS age determinations of zircons that have been extracted from reworked pyroclastic rocks at this site are under investigation.

The magneto-, litho- and biostratigraphic results of this study are going to be combined with the detrital zircon ages to facilitate the more precise positioning of the TJB in Maseru. The site can be further developed to showcase the palaeontological and geological heritage of Lesotho.

10.1.1 **Previous studies at Maseru**

Maseru has a wealthy paleontological record that ranges from the Molteno to the Elliot Formation. The first reported fossils were vertebrate ichnofossils at various track sites (Table 10.1) within Maseru (Maseru Race Course, Polo Grounds, and the Mejametalan Airport) and were studied by Ellenberger (1970). Ellenberger (1970) states that these occur in A/2 - A/4 zones and are of Molteno and lower Elliot affinities, but the Molteno assertions may need further investigation. These locations have not been seen during the current study, and they may be lost due to ongoing construction/development within Maseru (Ambrose, 1983).

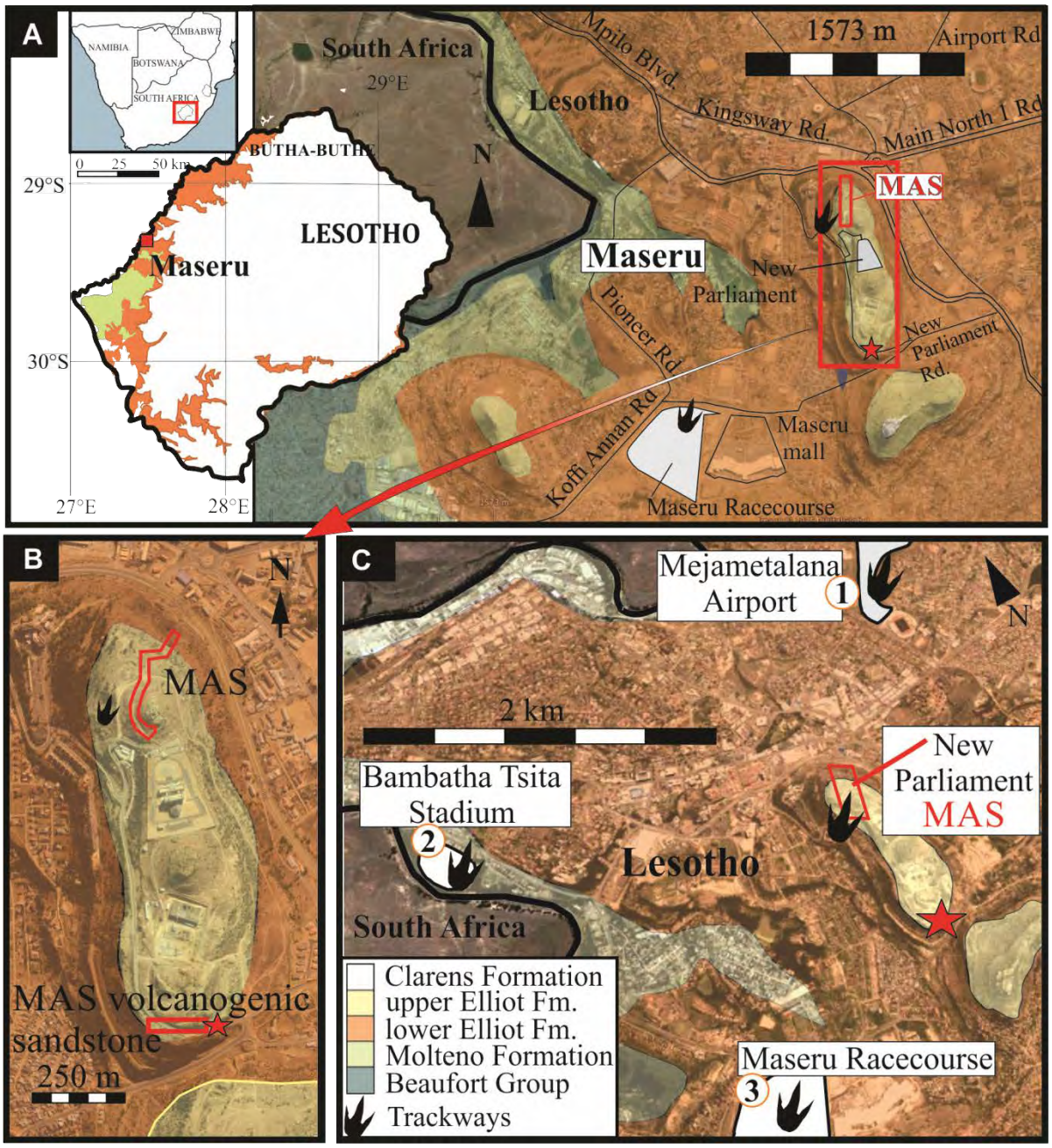

Figure 10.1. Locality map of southern Africa and Lesotho, highlighting the capital town of Maseru and the New Parliament Hill where the 'MAS' section was drilled. The red star indicated a reworked volcanogenic sandstone in a road-cutting along the New Parliament Road on the southern-side to the MAS section, within the upper Elliot Formation. Overlay of geological map onto Google Earth images.

Ellenberger and Ellenberger (1956) and Ellenberger (1970) also reported the discoveries of reptiles and amphibian bones from the capital, however, at least some of those have been assigned to units outside the Elliot Formation (Turner, 1972). An example of this discrepancy is evident in a display in the Morija Museum that shows fossil bones from Maseru which have been collected and described by Ellenberger and Ellenberger (1956) as originating from the Molteno Formation, but are in fact of the Beaufort Group (Turner, 1972).

Table 10.1. Details of fossil findings proximal or within Maseru city, Maseru District, Lesotho.

Taxonomic assignments	Age	Stratigraphic position	Catalog no.	Notes	Source(s)
Sauropodomorpha; *Gryponyx sp.*	Not specified	Elliot Formation	-	*Gryponyx africanus* is known from the holotype	Kitching and Raath (1984)
Dinosauria indet.	Not specified	Molterno Fm. And more likely Beaufort Group strata (Turner, 1972)	-	Gulley south of Maseru Race Course Information within the Morija Museum	Ellenberger (1956); Turner (1972)
1. *Paratrisauropus equester, pseudotrisauropous maserui, pentasaurpous erectus* 2. *Paratrisauropus lifofanesis*	~ Late Triassic	LEF Zone A/4 Zone A/3	-	1. Maseru Race Course (near Ratjomose Military Base) 2. Mejametala Airport	Work by Ambrose (1982) for a report on the Maseru fossil footprints prior to housing development. Previous work by Ellenberger (1962, 1970)
Dijaquesopus obliquus	~ Late Triassic	LEF/Molteno Fm. Zone A/2*s*	–	Polo Field, Bambatha Tsita Stadium	

'Tuffaceous layers' in the Maseru area were briefly mentioned by Reed (1976). In relation to these tuffaceous layers and their origin, their most likely source was explosive volcanism supplying silicic ash in subduction environments south and west of the study sites. The origin of the volcanic vent(s) is still uncertain and undetermined.

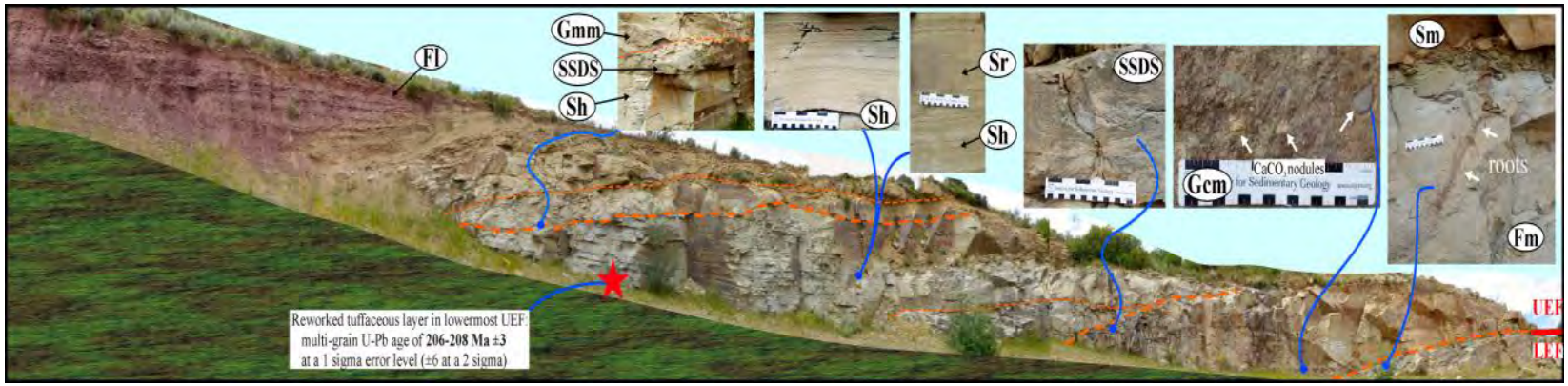

Figure 10.2. Road-cutting along the New Parliament Road exposes the reworked tuffaceous layer within the lowermost upper Elliot Formation on the southern end of Parliament Hill. Red star indicates the sampling locality for zircons.

10.1.2 **Previous palaeomagnetic work**

Van Zijl *et al*. (1962a, b) first undertook a palaeomagnetic study of the basaltic lavas in Drakensberg Group of in Lesotho, with one site being in the Maseru District (29 24 S, 27 48 E). This site also recorded the polarity of the sandstones (3 unbaked and 6 baked) in Clarens Formation directly below the lavas (Fig.10.3).

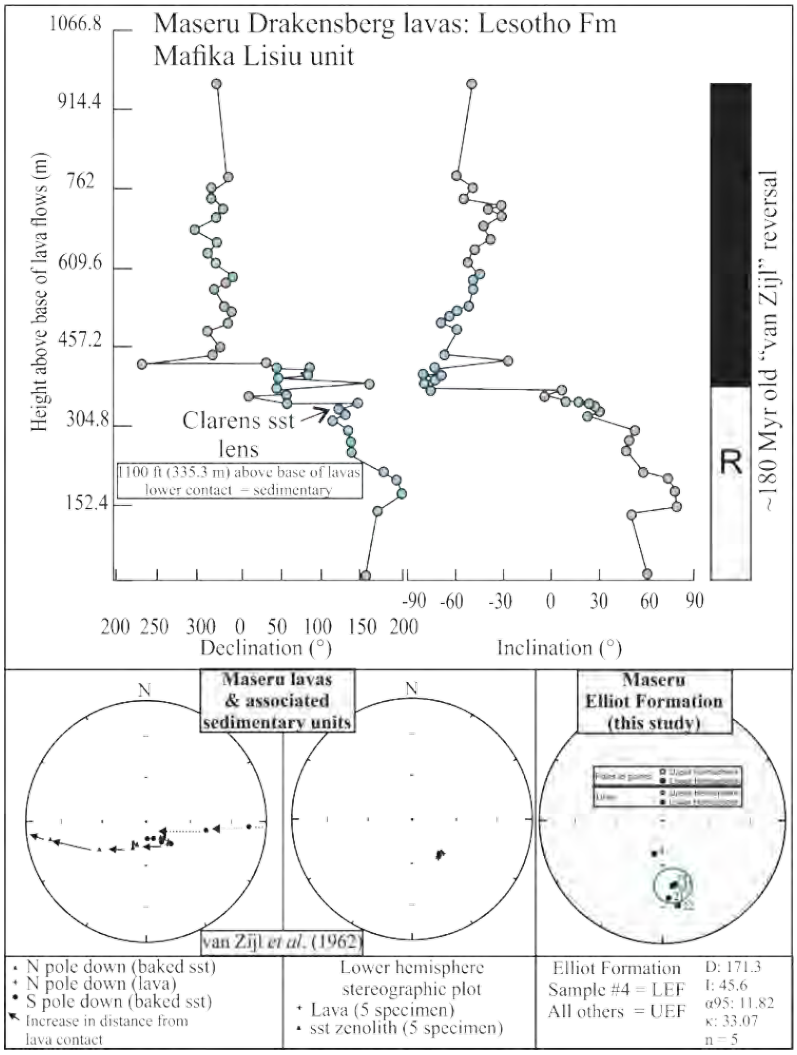

Figure 10.3. Adaptation of van Zijl *et al.* (1962a) study of the Stormberg Group outside of Maseru, Lesotho. The magnetization behaviour of lavas and several baked Clarens Formation sandstone samples are redrawn from van Zijl *et al*. (1962).

While the unbaked sandstones were unstable (due to the main magnetic carrier being maghemite) and often had magnetization directions close to that of the present field, the baked sandstone samples had the same reversed direction as the overlying lavas (Fig. 10.3). This could be due to the effect of re-magnetized via metamorphism and is not directly tested in the paper. Instead a transect from the unbaked - baked contact is sampled with the effect of unbaked samples appearing closer to present field orientations than those in the baked horizon.

Van Zijl *et al*. (1962a) also note that the sandstone samples, although showing reverse direction as the lavas, do not overlap and they hypothesise that this may be due to secular variation. The main magnetic carrier within the sandstone samples was titano-magnetite which has been altered to maghemite and hematite along grain edges. In the baked samples, hematite is the main carrier and is consider giving the stability which is lost in the unbaked maghemite containing samples. The lowermost lavas are reverse with the lavas higher up in sequence being normally magnetized (i.e., close to present field; Fig. 10.3). Moulin *et al*. (2012) term this the "van Zijl" Jurassic geomagnetic reversal, and this single reversal, which is a case for the short eruptive history of the basalts in the Drakensberg Group, has been shown to be present in other transects with radiometrically constrained ages in Lesotho (Kosterov and Perrin, 1996; Marsh *et al*., 1997; Prévot *et al*., 2003; Jourdan *et al*., 2005, 2007a; Moulin *et al*., 2011, Moulin *et al*., *in press*).

10.2 Results

10.2.1 **Sedimentology**

This site afforded access to the uppermost LEF and the overlying UEF which continues into the overlying Clarens Formation in the vicinity. The sedimentological LEF-UEF contact forms a smooth flat plateau on the hill slope (Fig. 10.4).

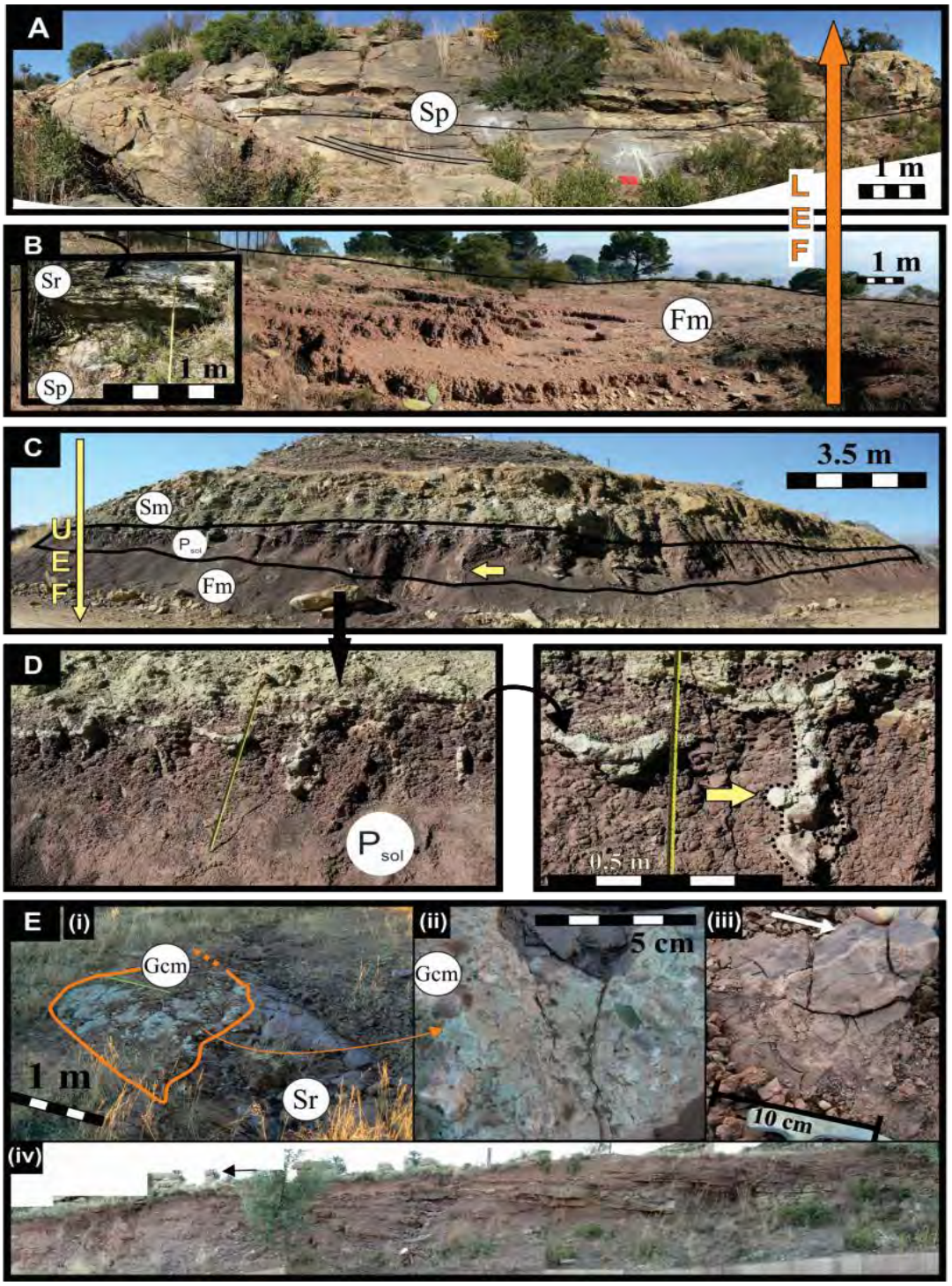

Figure 10.4. Parliament Hill, Maseru (MAS) characteristic lithology at (A, B) lower Elliot (LEF) sites, and (C) upper Elliot (UEF) palaeosol with (D) unusual concretions which appear to be calcretised in-filled burrows with branch-like structures (arrow) projecting ~90^{o} away from central, larger, vertical shaft-like structure; also present are in-filled desiccation cracks, (E) Upward fining package of (i) clast-supported conglomerate (Gcm) channel lag, overlain by ripple cross laminated sandstones (Sr) and massive sandstones interbedded with laminated siltstone and mudstones, (ii) close up of sandstone pebbles, extrabasinal clasts and pedogenic nodules clasts (not shown bone fragments and isolated tooth), (iii) with vertebrate and invertebrate footprints excavated within (iv) floodplain deposits.

The LEF, at the Parliament Hill outcrop, is characterised by thick, planar cross bedded, homogeneous and laterally restricted channel sandstones overlain overbank fines, typified by the green-to-purple and mottling colour of the mudstones (Fig. 10.4A, B). In contrast, the UEF is a much finer-grained succession, with palaeosol development over several intervals, often eroded into by the overlying fine- to medium-grained sandstone (Fig.10.4C).

The UEF fines are typified by the development of a palaeosol characterised by pedogenic nodules and rhizocretions (Fig. 10.4D). The nodules in one particular palaeosol (Fig. 10.4C) have amalgamated to make a relatively continuous layer. Several rhizocretions in this pedogenic nodule layer show preservation of primary features, such as branching and rhizome connections (Figure 10.4D and inset). The fossil trackways were found on a palaeosol of a floodplain at the top of an upward fining succession which grades laterally into fine grained sandstones and a laterally-restricted, clast-supported conglomerate (Figure 10.4E and insets). The trackways themselves were found in a silty to very fine grained sandstone interbedded with mudstones which are cut by several small crevasse splay deposits that are lenticular and laterally restricted.

10.2.2 **Palaeontological findings**

During the palaeomagnetic drilling of the MAS section, numerous *in situ* fossil bone as well as fragmentary teeth was encountered in the UEF. Numerous large (>20 cm) fragmentary bones and one large femur head were also found in excavation scree (from the parliament construction site). Furthermore, vertebrate and invertebrate footprints (Fig. 10.5) were discovered in fine to very fine grained, horizontally laminated and massive sandstones, found in association with *in situ* palaeosols and other floodplain deposits around drill hole ~ MAS 24/25.

10.2.2.1 Vertebrate and invertebrate trackways

The ichnofossil vertebrate assemblage found in the UEF of the New Parliament Hill locality in Maseru consists of several small (< 10 cm) 5 digit footprints (Figure 10.5A-B). The trackways are of at least 2 small quadruped animals although the tracks are of limited extent. In all cases the pes is larger than the manus, showing marked heteropody, and in some instances the pes displays phalangeal pads (Fig. 10.5B). The pes appears to be plantigrade with the manus imprint being disrupted by the pes occasionally. The manus is more commonly preserved semi-plantigrade to digitigrade. The digits do not splay very much and when they are spread it is at an angle of less than 10^{o}.

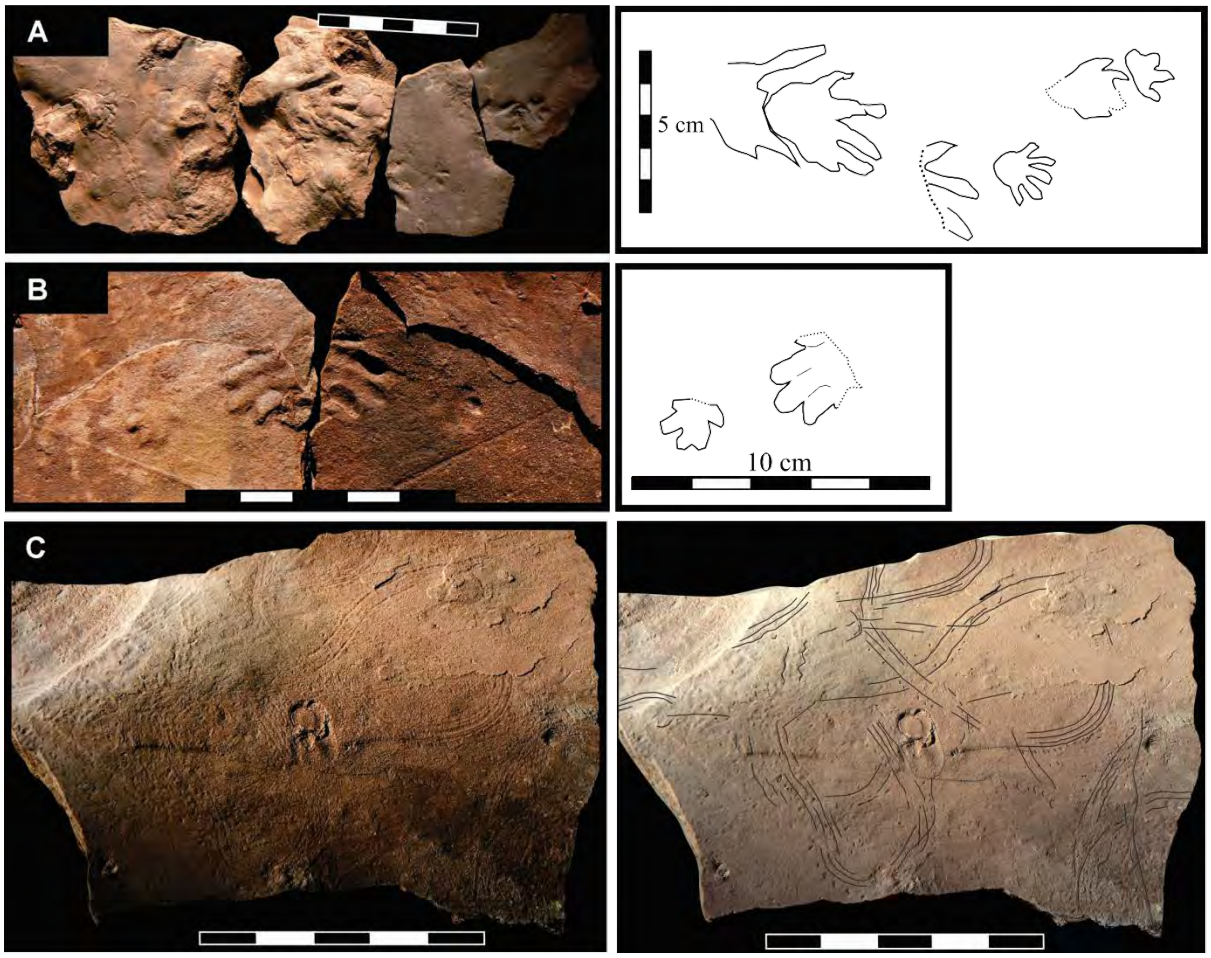

Figure 10.5. (A – B): *Batrachopus* tracks found in upper Elliot Formation (similar level to drill holes MAS 20-25) at Parliament Hill, Maseru, Lesotho. Tracks which are typically produced by Early Jurassic tetrapod archosaurs, (C): invertebrate trackways from the same site as vertebrate tracks shown in A and B, but of unknown track maker potentially a crustacean, such as a crayfish. Scale bar unless otherwise indicated = 10 cm.

The invertebrate tracks (Figure 10.5C) consist of several curving trails with three distinct, parallel grooves and tiny foot (pereiopod) impressions, running parallel, on either side. There are several sinuously curving trackways that traverse one another on the undulating slab surface.

The width of the tracks remains relatively consistent, but the state of preservation of an individual trackway as it winds along the palaeosurface changes. Due to the undulation of the palaeosurface, and inferred differences in water saturation of the substrate, less detailed tracks are composed of two parallel grooves with faint, millimetre-scale circular to elliptical to horizontal impressions running parallel and external to the main groove. Detailed trackways are composed of two parallel ridges, of heaped sediment, external to a central midline, which lies in a depression, separating the second ridge. Running parallel to

these ridges are several semi-elliptical millimetre scale imprints, which are not always consistent in their spacing, sizing, shape, depression and preservation.

10.2.3 **Palaeomagnetism**

The section sampled on Parliament Hill in Maseru was selected as a study site because of its excellent exposure, the numerous fossils which could allow biostratigraphic considerations in addition to the reworked tuffaceous sandstones in the lowermost UEF which was sampled for radiometric analyses. A lithological log and the stratigraphic setting of the sampling sites (MAS 1 – 45) are shown in Figure 10.9.

10.2.4 **Demagnetization results**

Most samples had two, sometimes three, well-defined components:

1. Low-coercivity (soft) magnetic component (NRM – AF 100) (coded 'SFT'),
2. Low-coercivity magnetic component (100 – 250 ^{o}C?) coded 'A+/-',
3. Present local Earth field component (NRM – AF100/ 150 - 250 ^{o}C) (relatively shallow, generally NNW upward directed component) (PF),
4. High -temperature steep NW component (150-350 – 580-680 ^{o}C) with negative inclination. (~NORMAL, N),
5. High-temperature steep SE component (150 - 350 – 580-680 ^{o}C) with positive inclination (~REVERSE, R).

Statistical information relevant to all components and samples are presented in Table 10.2.

For the entirety of the sampled Elliot Formation, at Maseru, all characteristic normal remanence directions (n = 18) have a mean direction inclination (I) of -54.3˚, declination (D) of 319.8˚ and α_{95} = 13.66˚, and the reversed samples (n = 6) have a mean direction with D = 171.3˚, I = 45.6˚ and α_{95} = 11.82˚.

These values are comparable with the UEF normal and reverse polarity mean directions (Table 10.2). The primary mean direction for the entire Formation has I = -51.8°, D = 332.5°, and a_{95} = 9.51°.

The site mean VGP is located at 66.3°N and 282.9°E. The UEF has a combined I = -46.4˚, D = 328˚, and α_{95} = 8.74˚, with site mean VGP at 61.9˚N and longitude of 292.9˚E. In comparison, the LEF combined

mean direction has an I = -71.8˚, D = 30.7˚, and α_{95} = 11.3˚, and with site mean VGP latitude at 55.2 ˚N and longitude of 178.1˚E.

Samples experiencing AF-treatment, essentially low demagnetization field strength, displayed randomly distributed remanence directions. These directions have been interpreted as being low-coercivity components (soft or present Earth field) acquired either in the field through natural processes, such as lighting strikes or through physical/chemical weathering or via the drilling process itself.

Table 10.2. Site-mean primary geographic directions and VGPs for the entire (EF), the lower (LEF) and the upper (UEF) Elliot Formation at Parliament Hill, Maseru, Lesotho. Statistical parameters: parameter (k) and confident limit (α_{95}), in conjunction with the dm and dp = semi-axis of the confidence ellipse for poles. N = number of samples, L/P = line or poles to planes.

Maseru (MAS) (-29.32° S, 27. 492° E)						VGP			
	N(L/P)	Decl °	Incl °	k	α_{95} °	Pole Lat °N	Pole Long °E	dm	dp
Primary Directions									
EF									
All Reverse	6 (1,5)	171.3	45.6	33.1	11.8	82.0	131.9	15	9.6
All Normal	18 (16,2)	319.8	-54.3	7.4	13.7	55.7	277.7	19.3	13.6
Combined	24 (17,7)	332.5	-51.8	10.7	9.5	66.3	282.9	13	8.8
UEF									
All Reverse	5 (0,5)	165.9	44.1	39.9	12.3	77.0	129.6	15.4	9.7
All Normal	15 (13,2)	314.7	-48.1	9.4	13.1	50.7	286.2	17.1	11.2
Combined	20 (13,7)	328.0	-46.4	14.91	8.7	61.9	292.9	11.2	7.2
LEF									
All Reverse	1 (0,1)	194.7	67.4	-	-				
All Normal	3 (3,0)	38.0	-72.9	7.1	39.9	50.9	176.7	71.1	63.4
Combined	4 (3,1)	30.7	-71.8	11.3	24.4	55.2	178.1	70.2	61.7

These randomly distributed low-coercivity components are often removed on completion of AF-treatment, however, many samples retained scattered north, north-westerly and upward magnetic component at higher levels of demagnetization (Fig. 10.6B). This component is identical to the present local Earth field **(**PF). After removal of low-coercivity components, high temperature components remained which were stable at higher demagnetization levels (stable up to ~620 ^{o}C; Fig. 10.6).

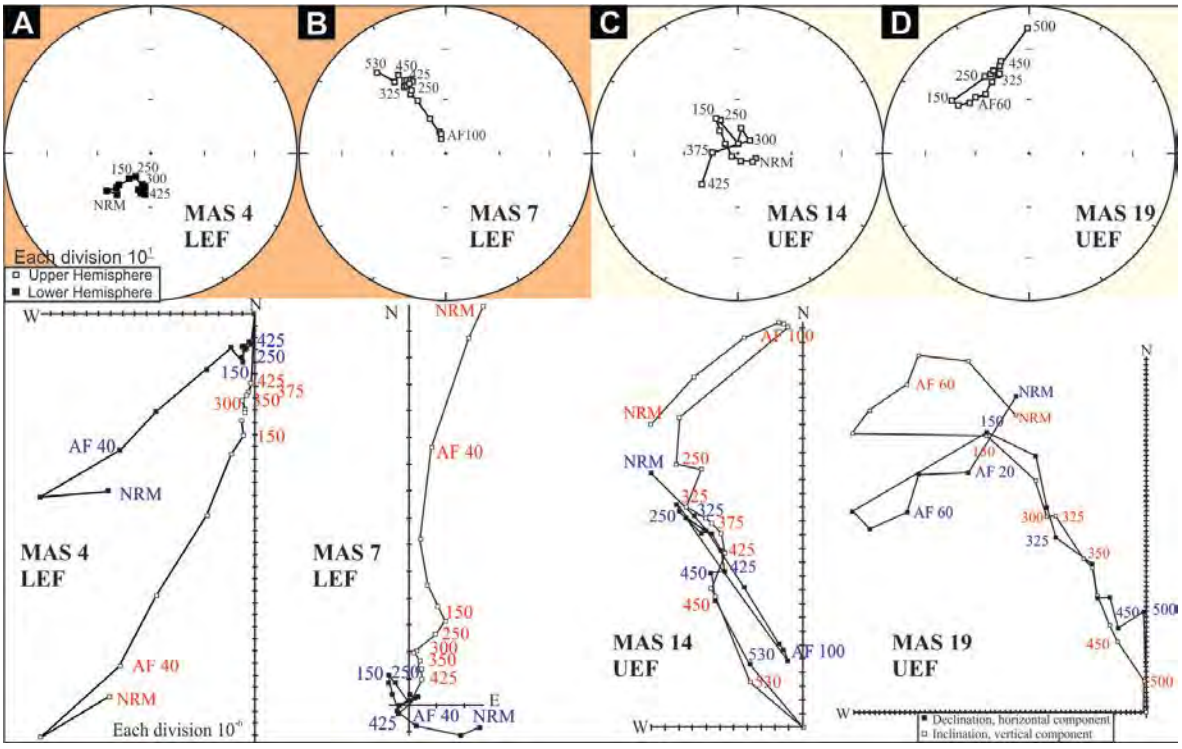

Figure 10.6. Equal area stereoplots and orthogonal vector plots of representative samples of demagnetization behaviour for two lower Elliot (A) MAS 4r, (B) MAS 7n and two upper Elliot (C) MAS 14n, (D) MAS 19r samples. MAS 19 making a great circle path and projecting into the lower south eastern quadrant. All samples are indicated in *in situ* geographic coordinates.

The MAS sample site seemed to be affected by the strong present field component which meant it was difficult to separate the "PF" component from the Late Triassic-Early Jurassic component (N/R). Therefore, several samples were best reduced to their stable end-points of demagnetization and identified as great circle arcs e.g. MAS 19, MAS 32 (Fig. 10.6D).

LEF normal polarity samples, despite lower number of samples in comparison to the UEF, have a high degree of scatter and plot more easterly in comparison to the combined or the separated UEF samples which are more north-westerly (Fig. 10.7). Additionally, if any normal lines are significantly biased by present field component which could drag them more easterly than is actually reflected by the true polarity it could bias the group dataset.

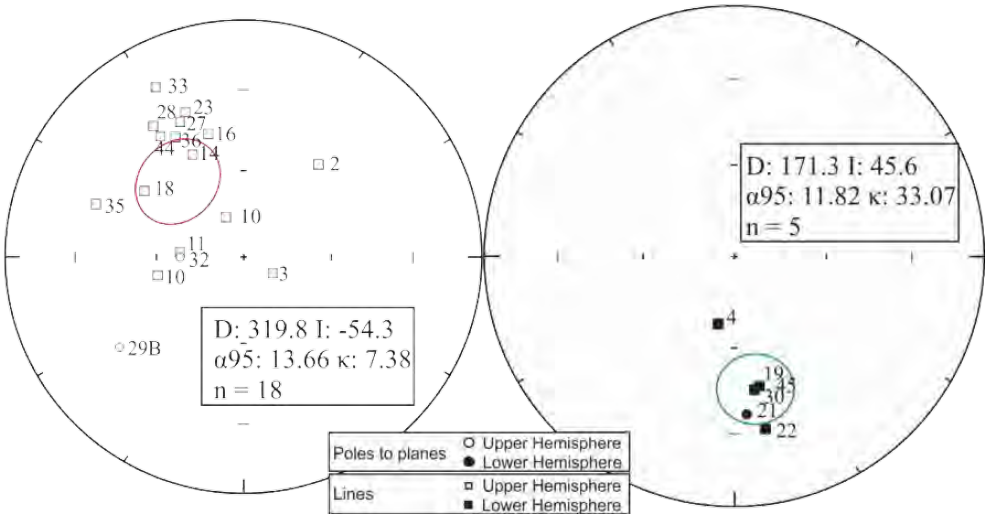

Figure 10.7. Equal area stereoplot for MAS reverse and normal Elliot Formation samples with cone of confidence illustrated.

10.2.5 **Reversals test**

For palaeomagnetic stability and to establish if the LEF and UEF samples have one true mean for reversed and normal samples, the comparison of the antipode of the mean of the reversed-polarity samples is taken against the mean of the normal polarity samples, in a reversals test (McFadden and McElhinny, 1990; Butler, 1992).

The reversals test could not be applied to the LEF at MAS due to the sample number and proportions (n = 4; N = 3, R = 1). The UEF (n = 20; N = 15, R = 5) at MAS failed the McFadden and McElhinny (1990) reversals test with an angle of separation (γ_0) between the two modes, of 21.8˚, being greater than the critical angle (γ_c = 16.8˚), as is also represented in the Watson's V test where the Watson's V value of 11.1˚ is greater that the Vcrit value of 6.6˚.

The Bootstrap reversals test was implemented and shows that the x and z components overlap, but there is no overlap with y-components and therefore, again, a failed test (Figure 10.8). The LEF and UEF at MAS do not share a common mean, and this is likely a factor of the limited sample size of the LEF (n = 4). Application of the Bootstrap reversal test, however, shows that the combined Elliot Formation passes this test (Fig. 10.8, Fig. 6.9).

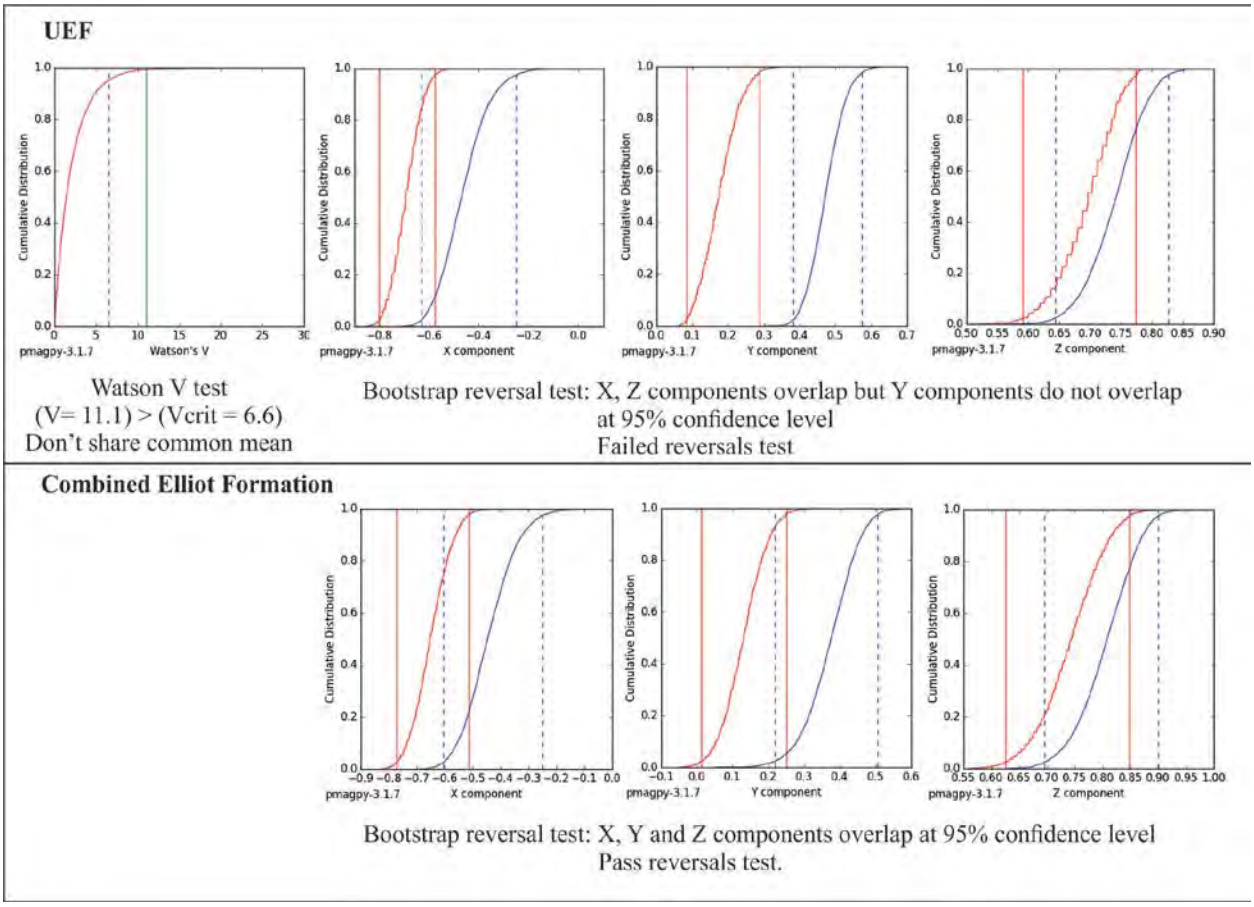

Figure 10.8. Watson's V test and the Bootstrap reversals test (Tauxe *et al.*, 1991) for the UEF and the combined Elliot Formation samples for Maseru (MAS) site. A reversals test was not possible for the LEF as there were only 4 samples (N=3, R = 1). MAS UEF failed the Bootstrap reversals test, despite sharing a common mean, and the combined data for the Elliot Formation passes the reversals test.

The virtual geomagnetic latitude (VGP Lat.) is calculated and presented in Figure 10.9 with the magnetostratigraphy of the Maseru site. The Maseru site was subdivided into 4 polarity pair MAS1 – 4. MAS 1r and MAS4 r are not samples/missing from the section.

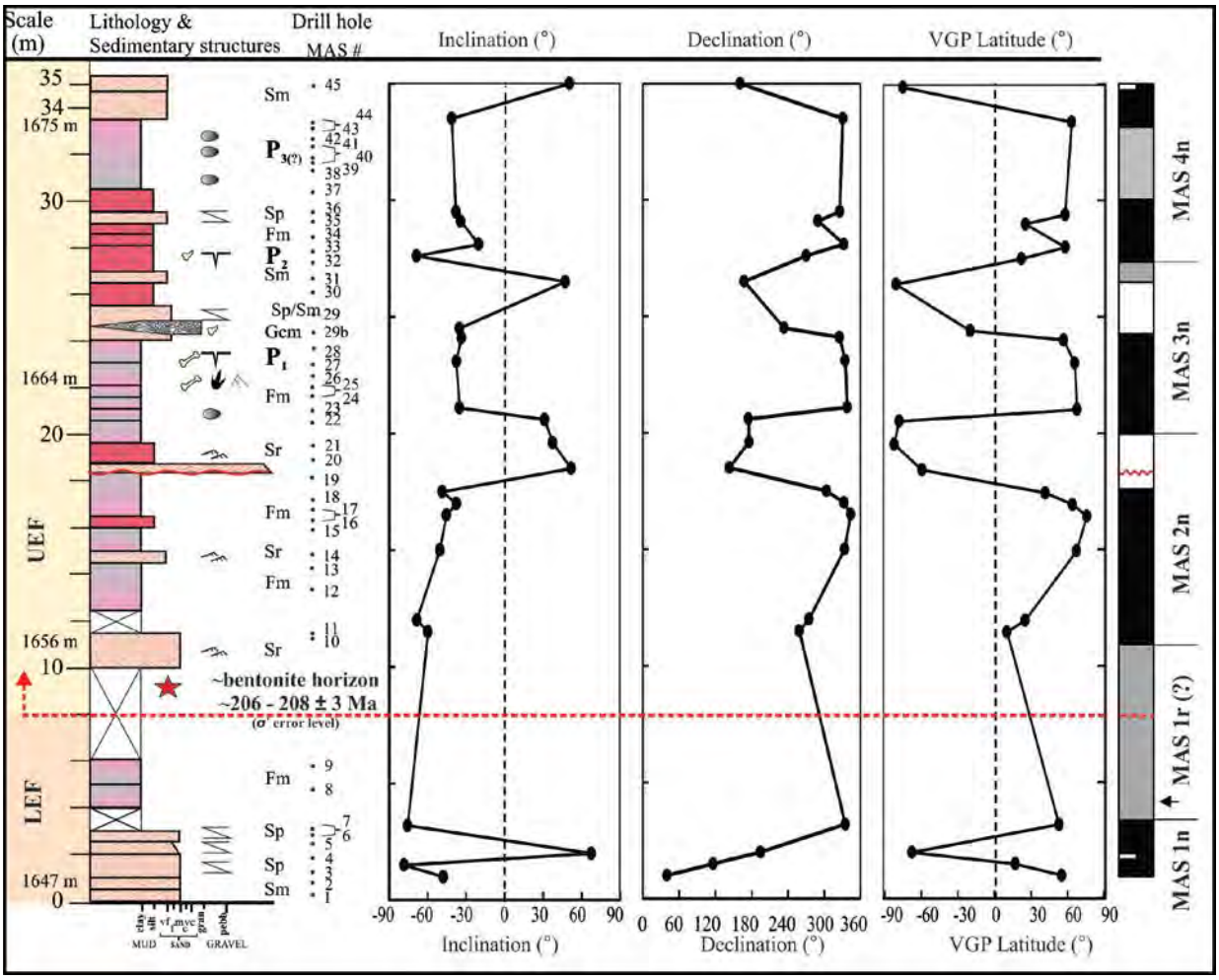

Figure 10.9. Magnetostratigraphy of the Maseru (MASn1 – 4n) site with inclination, declination and calculated virtual geomagnetic latitude (VGP Lat.) calculated against the Maseru site lithology. The sedimentological contact between the LEF and UEF is indicated with dashed red line as is the position (star) of the sampled and dated tuffaceous sandstone. The U-Pb date falls into a grey unsampled lithological zone.

10.3 Discussion

10.3.1 **Identity of the Trackmakers**

The morphology of the vertebrate trackways are similar to those described by Arcucci *et al*. (2004), from the Los Colorados Formation, as being "Chirotheroid" tracks. These are typically produced by tetrapod archosaurs and are typically unknown from strata younger than Triassic-Jurassic (but also see Kirkland *et al*., 2014), and are more characteristic of Late Triassic assemblages (Arcucci *et al*., 2004; Klein and Lucas, 2010). However, in the pes prints the digits appear to be parallel and these traits, in conjunction

with the others described, are identified as belonging to *Batrachopus* (Hitchcock 1845; Figure 10.5B; Klein *pers*. *comm*., ICCI 2015). The ichnogenus *Batrachopus* is attributed to a crocodylomorph (Olsen and Padian, 1986), and several tracks identified by Ellenberger (1970, 1972) from the upper Elliot and Clarens Formation can be attributed to this ichnotaxon (e.g. *Embrithopentapodiscus*, *Plateotetrapodiscus rugosus*, *Suchopus bakoenaorum*, *Synaptichnium motutongense*, *Molapopentapodiscus pilosus* and *Malutitetatrapodiscus*; Ellenberger 1970, 1974; Olsen and Padian, 1986; Rainforth, 2001).

Furthermore, *Batrachopus* is widely distributed in localities of Early Jurassic age, such as the East Berlin Formation (Hartford Basin), Moenave Formation of the Glen Canyon Group and the 'lower Lias' of Veillon point (south-western France) in addition to the Stormberg Group occurrences (Lapparent and Montenant, 1967; Ellenberger, 1972; Olsen and Padian, 1986; Lockley *et al*., 2004), and thereby considered a zone fossil (Olsen and Padian, 1986; Lockley *et al*., 2004).

The occurrences of this ichnotaxa in the uppermost Passaic Formation in several sections within the Newark Basin, in conjunction with Jurassic palynomorphs, have meant that Olsen and Padian (1986) propose that this ichnotaxon may have a larger range. This may be especially true if body fossils are to be incorporated and extend back into the Norian and through into the early Jurassic (i.e. crocodylomorphs of the Los Colorados Formation; see also Lockley *et al*., 2010). Rainforth (2005) emphasises the need for a revision of the ichnogenus globally.

10.3.1.1 Invertebrate track ways – crayfish-like tracks in Gondwana?

Invertebrate trackways from the Elliot Formation, in general, are poorly cited and researched. There are few reports in Elliot Formation literature (Ellenberger, 1972; Smith *et al*., 2009; Wilson *et al*., 2009, p. 2. "Moyeni tracksite records more than 250 tetrapod footprints and associated invertebrate traces on a 100 m^2 sandstone surface").

The invertebrate trackway slab (Figure 10.10) found at the Maseru site, although small (~10 cm by 15 cm), is curious and not analogous with other invertebrate tracks reported in literature (Fig. 10.11; Rainforth and Lockley, 1996; Ellenberger, 1972). The inconsistency of preservation of these imprints, over the small surface area, is likely a function of (i) imperfect preservation of the imprints (ii) partially removal/obscuring by the part of the animal creating the central furrow, i.e. the tail (iii) post-track making removal through the action of other organisms/trackmaker itself or inorganic means, i.e. through the process of creating turbulence in the water column above the sediment surface upsetting grains which were disrupted from their position by the original trackmaker.

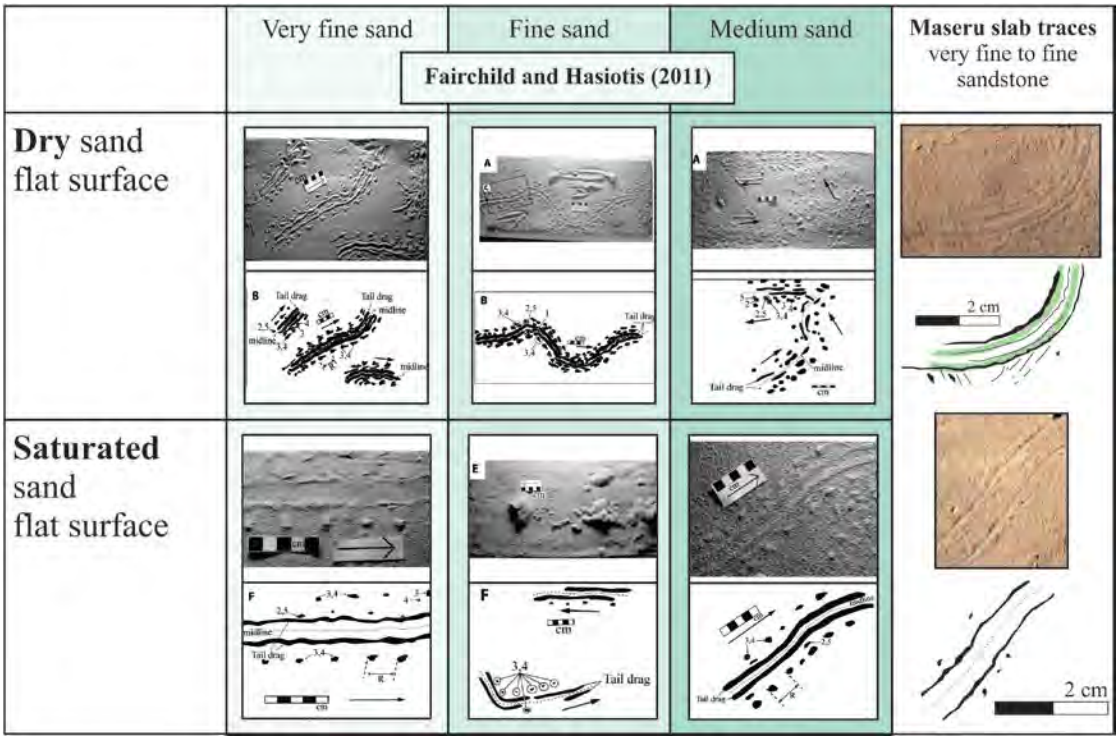

Figure 10.10 Comparison between the neoichnological study of Fairchild and Hasiotis (2011) under two conditions (i) dry sands on flat surface and (ii) saturated sand on flat surface, with representations of such conditions from the Maseru invertebrate slab on the right hand side.

Fairchild and Hasiotis (2011) describe neoichnological tracks of crayfish under laboratory conditions. The Maseru invertebrate tracks appear to be a fair natural replication as they show several similarities to the casts of crayfish tracks produced by Fairchild and Hasiotis (2011), in particular, to the trackways formed on a flat surface in saturated, very fine sand (Fig. 10.10).

The trackmakers of the invertebrate footprints are most likely freshwater arthropods, possibly freshwater crayfish. Crayfish are currently not indigenous to the African continent, however; their fossil burrows have been found to have a global distribution since the Upper Triassic (Hasiotis, 1999). In Gondwana, Hasiotis (2002) was one of the first to point out the deficiency in fossil evidence (body, burrow or track-way) for crayfish. This is in light of the high diversity and abundance of modern crayfish (the parastacids) in Australia. To date, the oldest described parastacid crayfish body fossils (*Palaeoechinastacus australianus*), from Gondwana, are reported from the Otway Group (Victoria, Australia; Martin *et al*., 2008). These Albian-aged body fossils are complemented with Aptian-aged burrows of parastacoidean

origin from the Otway and Strzelecki Groups, and show close similarities to modern crayfish burrows (Martin *et al*., 2008).

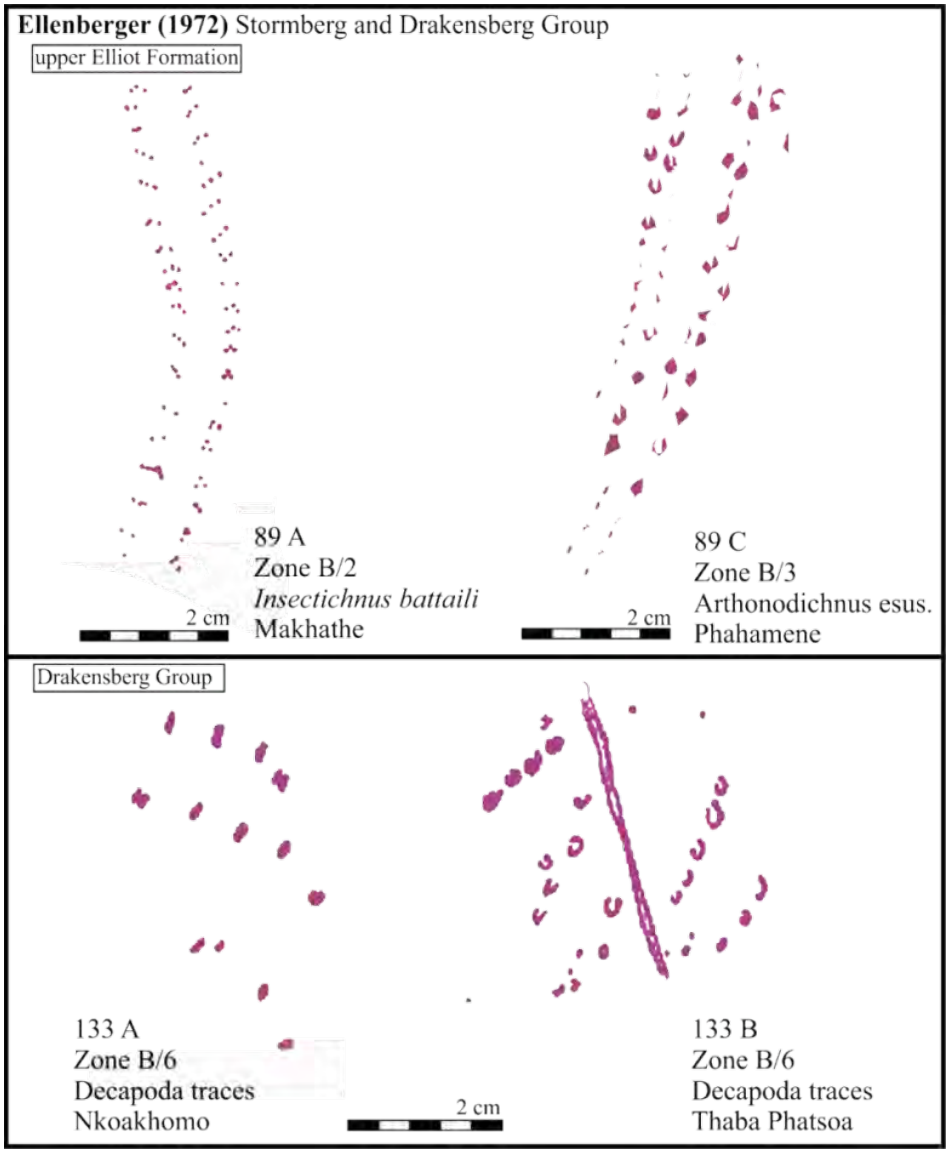

Figure 10.11. Reported invertebrate trackways in southern Africa from the upper Elliot Formation in zones B/2, B/3 and Drakensberg B/6 of Ellenberger (1972).

Fossil crayfish burrows and suspected trackways have been reported in North America, Australia, China and Europe. Invertebrate trackways are slightly contentious because of the ability for the tracks to

resemble a variety of invertebrate makers, and therefore the neoichnological study of Fairchild and Hasiotis (2011) sheds light onto the traces made by modern crayfish for comparison purposes. There has yet been an ichnotaxa assigned to crayfish movement although several authors have referred to crayfish-like traces, such as the illustration in Rainforth and Lockley (1996) from the Navajo Sandstone.

10.4 Conclusion

The fossils assemblage found at the site, including the distinctive ichnofossils (*Batrachopus* tracks and a potential crayfish trackway; Fig. 10.5A) are of great use in conjunction with the magnetostratigraphy and the reworked radiometric ages. All the tracks reported here are likely to fall within the zone B/1 of Ellenberger (1970), which was previously termed “transition beds” and which correlate with the upper part of the UEF. This falls within the MAS3n magnetochron of the current magnetostratigraphic log (Fig. 10.9).

Batrochopus is known to occur in Early Jurassic aged rocks, globally (Lockley *et al*., 2010). There are no reported putative crayfish tracks for comparison purposes, but their fossil burrow casings range from the upper Triassic (Hasiotis, pers. com.). It is possible that there is a paraconformity between the deposition of the reworked tuffaceous material and the time that the footprint impressions where made if the *Batrachopus* tracks are relied upon as an indicator of age. An erosive surface which appears in the MAS2r magnetochron is a likely culprit for a break in deposition (Fig. 10.9). The length of this break, the amount of material removed etc. is unknown, and may in fact represent very little geological time (Fig. 10.9). This is the erosive base of a mud-chip conglomerate is marked on the log in Figure 10.9.

In general, other trackway sites (e.g. Hartford, Fundy and Newark Basins) have several ichnotaxa which appear in the early Jurassic and are shared with the upper Elliot (e.g. *Anomoepus*, *Otozoum*; Rainforth, 2001; Wilson *et al*., 2009; Marsicano *et al*., 2014).

11 Magnetostratigraphic zonation for the Farm Damplaats (DAM) and the Tritylodon Acme Zone (TAZ) in the Ladybrand District, Free State, South Africa

11.1 Introduction

This chapter seeks to: (1) establish a magnetostratigraphic framework for the well-known fossil locality at Damplaats Farm (Ladybrand District, Free State, South Africa; Fig. 11.1), and (2) correlate the UEF section that comprise a distinctive and excellently exposed *Tritylodon* Acme Zone (TAZ) at Oldenburg Farm (Fig. 11.1; Smith and Kitching, 1997) with the Damplaats section. In order to achieve these aims, detailed sedimentological logs were measured and palaeomagnetic sampling was undertaken on the Farm Damplaats (DAM; Fig. 11.1) and at the TAZ locality on Farm Oldenburg (OLD; Fig. 1A, B;).

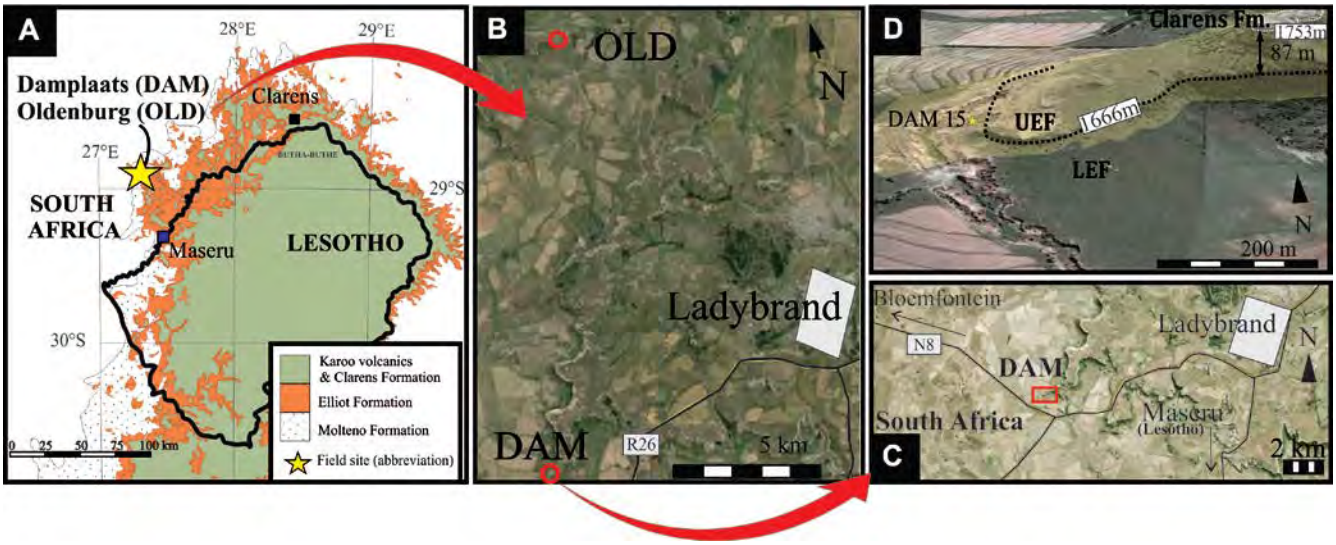

Figure 11.1. (A) Regional context of the Damplaats (DAM - S 29°13'20.7", E 27°20'14.1") and Oldenburg (OLD - S 29°05'37.5", E 27°23'28.2") Farm sites. (B) Google Earth image of the proximity of the Damplaats and Oldenburg sites (C) Locality information for the DAM site relative to the N8 national road. (D) Google earth image of the section drilled at DAM showing the location of the sedimentological contact between the LEF and UEF. The dashed line at 1666 m represents the first major fine-grained sandstone body in the UEF, which is directly above a palaeosol and ~87 m below the contact with the Clarens Formation.

Damplaats Farm is 19 km southwest of the town of Ladybrand on the R26 (Fig. 11.1A, B), however, the current site (DAM; Fig. 11.1C, D) lies between the boundaries of several properties termed De Hart 127,

Marseilles, and Fort Savage 69. The drill site on the Oldenburg Farm is on a small hill (OLD 1 at elevation 1739 m) overlooking the farmhouse and is only ~15 km from the Damplaats Farm (DAM).

11.1.1 **Previous paleontological work in the Ladybrand District**

The first paleontological collections at Damplaats were made in the 1980s when the protosuchian *Baroqueosuchus haughtoni* (BP-1-4946) was discovered by Busby and Gow (1984). It was described as occurring in the UEF in conjunction with rolled post-cranial material and a fabrosaurid skeleton (Table 11.1).

Table 11.1. Details of fossil finds proximal/at Damplaats and Oldenburg Farms, Ladybrand District, Free State, South Africa

Taxonomic assignments	Age	Stratigraphic position	Catalogue no.	Notes	Source(s)
Protosuchian: *Baroqueosuchus haughtoni*	Latest Triassic (but acknowledge it may be earliest Jurassic)	UEF	Paratype. BP-1-4946	29°13'12"S; 27°20'30"E Partial braincase with disarticulated squamosals. Most primitive protosuchian crocodilian. Found associated with rolled postcranial bones & remains of a fabrosaurid.	Busbey and Gow (1984)
Cynodontid; *Tritylodon*	Latest Triassic (but acknowledge it may be earliest Jurassic)	lower UEF	-	Co-ordinates as above. Tritylodon conglomerate = *Tritylodon* Acme Zone (TAZ)	Busbey and Gow (1984); Smith and Kitching (1997)
Sauropodomorph; *Massospondylus*	as above	lower UEF	-	Also reported within the *Tritylodon* Acme zone	Busbey and Gow (1984); Smith and Kitching (1997)
Ornithschian; *Eocursor parvus*	as above	lower UEF	SAM-PK-K8025	SAM-PK-K8025 holotype stratigraphically10.5 m above *Melanosaurus readi* (Yates, 2005), and 5.5 m below reworked paleosol.	Butler et al. (2007)
Sauropodomorpha; *Melanosaurus readi*	Upper Triassic	LEF	NMQR3314	Articulated skull and skeleton lies 16.5 metres below a reworked paleosol (&TAZ). Original identification by Welman (1999) as *Euskelosaurus* sp.	Yates (2005)
Basal sauropodomorpha; *Antetonitrus ingenipes gen. et sp. nov.*	Current consensus places it in the Norian (Battail 1993; Lucas & Hancox 2001).	LEF	BP/1/4952	Saddle between the farms Welbedacht 611 and Edelweiss 698, Ladybrand District. A photograph of the excavation and the partial disarticulated skeleton can be seen in Kitching & Raath (1984).	Yates and Kitching (2003)

Later field expeditions in 1993 lead to the recovery of SAM-PK-K8025, which now is known as one of the earliest ornithischian, *Eocursor parvus* (Butler *et al*., 2007, Butler, 2010), as well as the skull and post-cranial material of *Melanosaurus readi*, some 10.5 m below the *Eocursor* material (Welman, 1998, 2000; Yates 2005a, 2007a; Butler *et al*., 2007). Other important fossil finds in the immediate vicinity are listed in Table 11.1.

Eocursor parvus was found 5.5 m below a semi-continuous large nodule horizon, marked by desiccation cracks, rhizocretions and a change in mudrock colour, which Butler *et al*. (2007) consider to mark the contact between the LEF and UEF (as per Smith and Kitching, 1997), and thus place the *Eocursor* specimen within the LEF. From current investigation of the site, it appears the semi-continuous large nodule horizon mentioned in the supplementary material of Butler *et al*. (2007) is the transition zone between drill samples DAM 22 – 25 (Fig.11.2).

In this current work, however, this pedogenically altered zone is considered to be diagnostic of the UEF (Fig. 11.2) and was confirmed to be above the sedimentologically and geomorphologically defined contact between the LEF and UEF. Consequently, the *Eocursor* specimen would be comfortably within the lowermost UEF. Given this uncertainly which stems from the subjective and qualitative placement of the contact between the LEF and UEF, the magnetostratigraphic survey of the DAM site was deemed important as it could potentially assist in the placement of the TJB at this palaeontologically important site.

11.2 Results

11.2.1 **Sedimentology at Damplaats (DAM)**

The DAM site afforded access to the entire Elliot Formation and is considered representative of the Formation, which is usually condensed in the northern main Karoo Basin. Sampling of this site commenced at the first exposed and relatively unweathered interval of the LEF within the donga-system (i.e., erosional gulley; Fig. 11.2I).

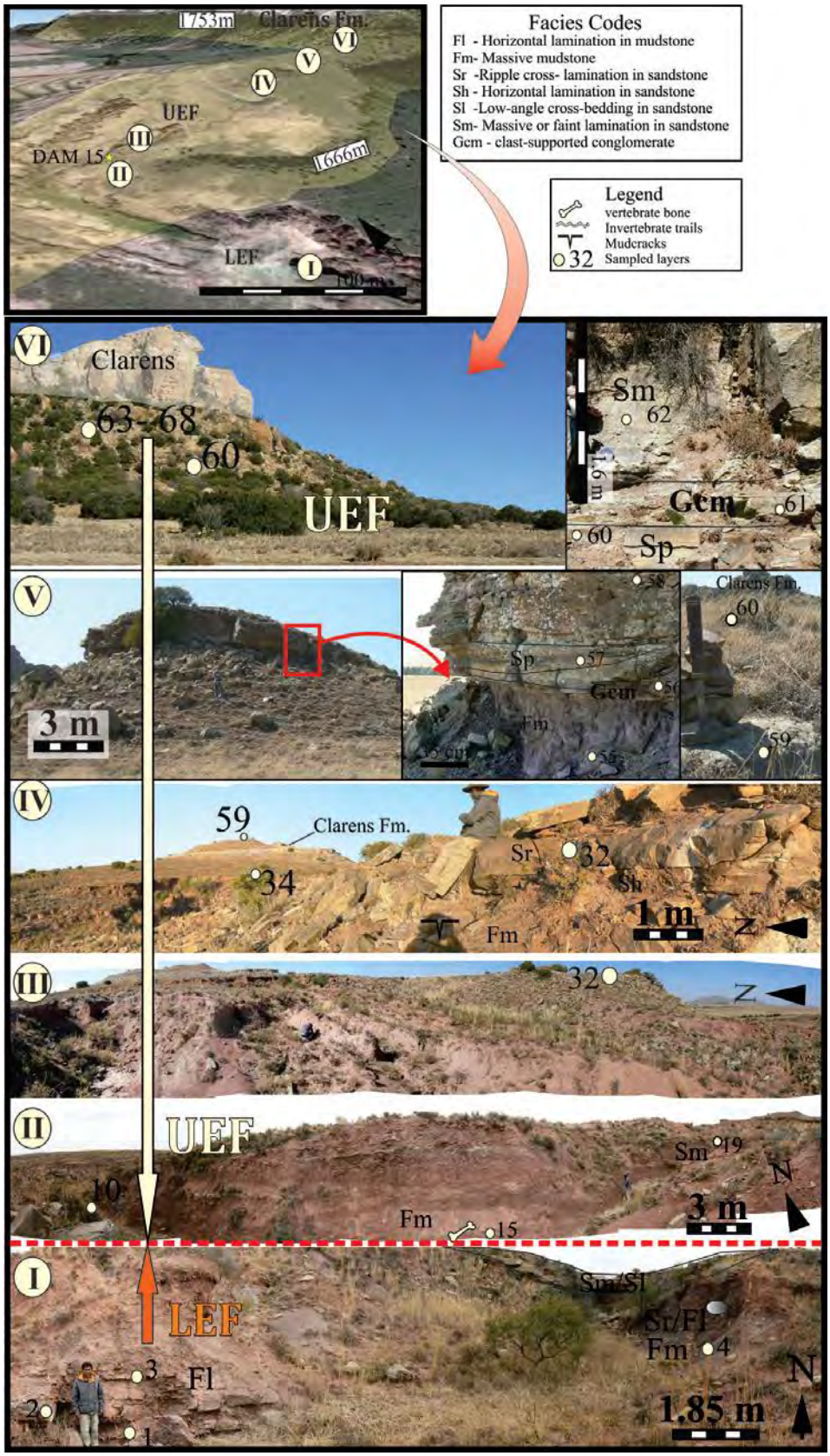

Figure 11.2. Damplaats (DAM) site locality maps and transect with photographs (I-VI) of lower Elliot (LEF) and upper Elliot (UEF) drill sites and points (labelled with drill hole number). Facies codes: Fm = massive mudstone/siltstone, Fl = laminated mudstones/siltstone, Sm = massive sandstone, Sl = low-angle cross bedded sandstone, Sp = planar cross bedded sandstone, Sr = ripple cross laminated sandstone, Gcm = clast-supported conglomerates.

Further characteristics of the LEF section drilled at Damplaats (Fig. 11.2) are the heterolitic unit of laminated mudstones (facies Fl) overlain by thin beds (≤50 cm) of climbing ripple cross-laminated silty- very fine-grained sandstone (facies Sr; Fig. 11.2I). These contain mud-draped surfaces and are interbedded with, on average, 10 cm thick, laminated mudstones (facies Fl). The unit grades upwards into silty- to very fine-grained sandstones (facies Sm/Sl). This is overlain by a ~3.6 m thick silt- to clay-rich silty-mudstone (facies Fm). An altered pedogenic horizon occurs ~1 m below the overlying, >2 m thick, massive (facies Sm) channel sandstone with a mud-chip conglomerate lag at its base. This sandstone, which can be traced over several tens of meters to the east and west, has incised into the underlying mudstone (facies Fm - Figure 11.2I; nodule symbol shown). The pedogenic horizon below the sandstone channel contains sporadic and randomly distributed, large, elongated (>7 cm in length) pedogenic nodules that do not define a consistent palaeosurface. Above the massive, >2 m thick channel sandstone body, several metres of massive mudstone show incipient pedogenic alternation which is limited to colour mottling.

The relative vertical removal of the LEF exposure to the contact of the Molteno and Elliot Formations is unknown because bedrock exposures to the south, within the donga that is deeply incised and extends to main road (N8), are lacking. While the LEF-UEF contact is also less obvious here than in the southern main Karoo Basin due to the condensed nature of the Elliot Formation in the north, the sedimentological contact between LEF and UEF is made clear by: (1) the difference in the sedimentary facies attributes below and above the contact, namely the limited pedogenic overprinting of the mudstones as well as the presence of channel sandstone with some mud-chip conglomerates in the LEF vs. the palaeosol-rich units of the UEF; (2) the presence of a subdued geomorphological plateau at the contact (which currently, is also marked by the termination in branching in the donga system) (Fig. 11.1D and overview in Fig. 11.2). Drill samples above this level (from DAM10) were taken from rocks with characteristic UEF sedimentological features, which include multiple thin channel sandstones, alternating massive and laminated mudstone and siltstone (Fm/Fl) layers, with strongly developed pedogenic alteration features, desiccation cracks, rhizocretions, carbonate nodule horizons and most importantly the clast-supported carbonate conglomerates often containing bone and teeth fragments.

Above drill hole DAM 20, the sedimentological characteristics of the UEF are even more strongly and repetitively developed (Fig. 11.2II) and comprise several thick, brick-red mudstones and siltstones that are pedogenically altered and contain relatively thick and repetitive nodule horizons with rhizocretions and root halos, desiccation cracks, invertebrate traces (*Planolites* ichnosp., *Skolithos* ichnosp.) and slickenslides (Fig. 11.2II). Characteristic carbonate nodule conglomerates (facies Gcm) became abundant

above the first thick palaeosol horizon towards the middle and uppermost UEF (Fig. 11.2V, VI). This conglomerate, at this site, commonly contains abraded bone and teeth fragments.

Within the current drilled section, although collecting of vertebrate fossils were not the focus of the study, fragmentary bones were found in the field, of which the most notable is a fossil long bone, possibly a rib (?; 50 cm length, girth 10 cm at midsection; S29° 13’ 20.5’’, E27° 20’ 16.3’’, 1657 m) at drill hole 15 (Fig. 11.3).

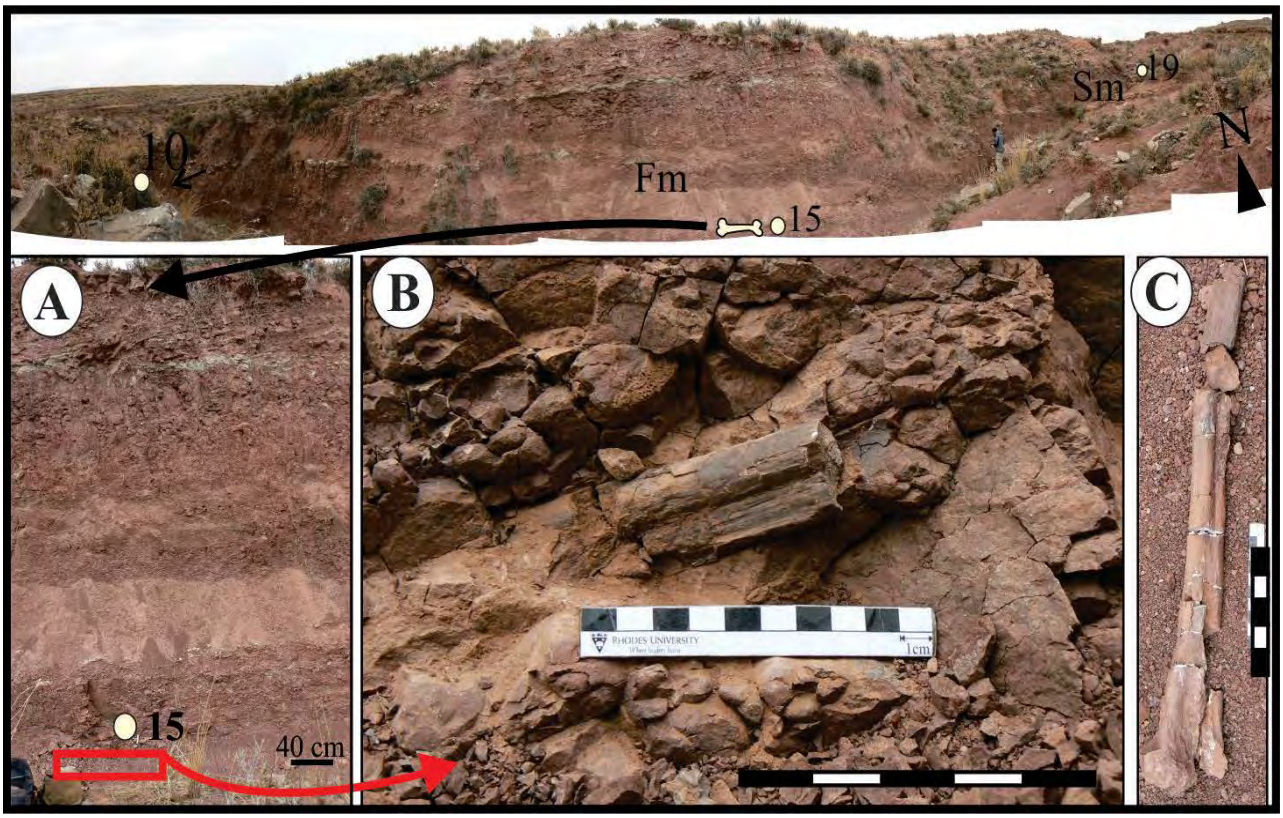

Figure 11.3. Geological context of the long bone found at (A) drill hole 15 in the lowermost part of the UEF at Damplaats. It occurs in a thick package (>2 m) of mudstone – siltstone and crevasse splay sandstones. (B) Shows *in situ* exposure of the bone and (C) and after gluing.

11.2.2 **Sedimentology at Oldenburg (OLD)**

The *Tritylodon* “Acme” Zone (TAZ) in the UEF was targeted for magnetostratigraphic sampling near the Oldenburg Farmhouse (Fig. 11.4A, B, D) in order to allow its correlation with the DAM magnetostratigraphic section, in hope to place the TAZ into a more refined stratigraphic framework (Fig.

11.4C). The components of the TAZ in the UEF (as per Smith and Kitching, 1997) were easily identified at Oldenburg and the uppermost palaeosol that was drilled is ~28 m below the contact of the UEF with the Clarens Formation (Fig. 11.4B, C, D).

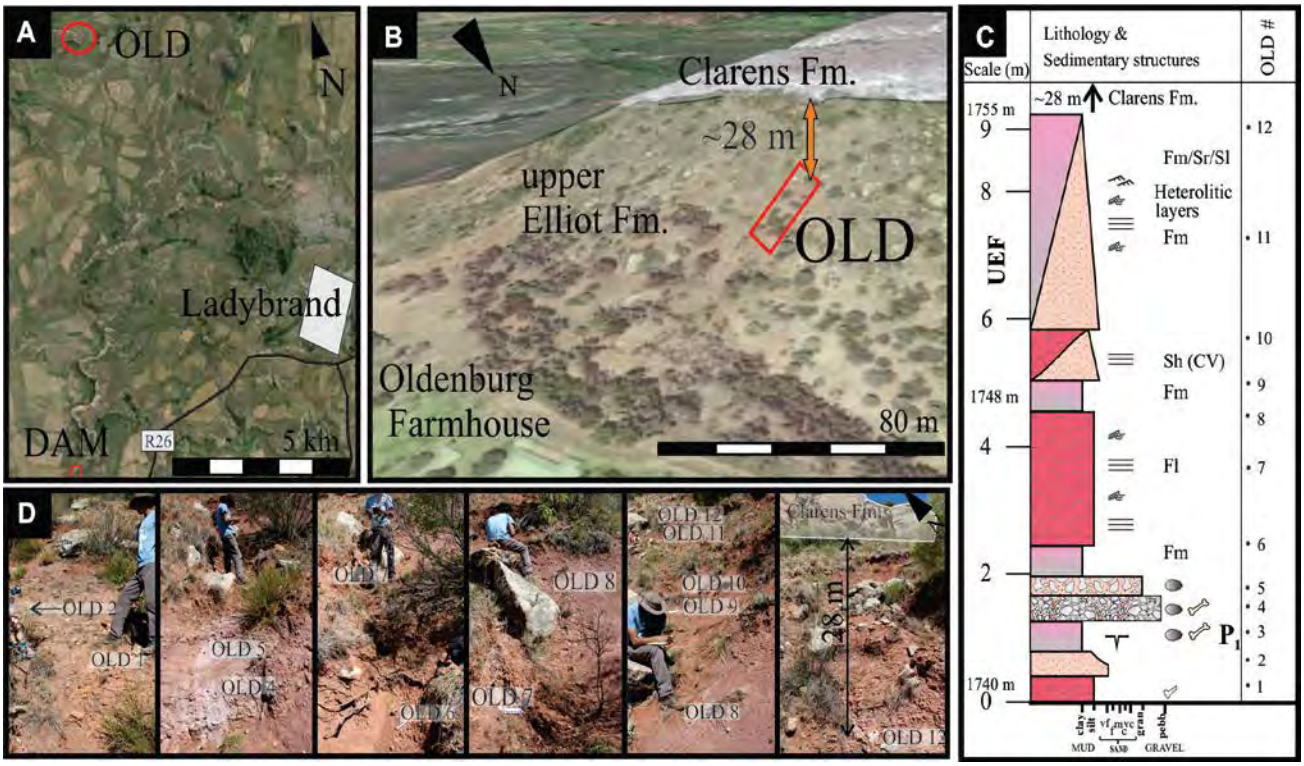

Figure 11.4. (A) Locality information of the UEF drill site at Farm Oldenburg (45) 'OLD' which is ~14.8 km north of Damplaats (DAM); (B) Google Earth image of hill slope exposure and relative distance to the Clarens Formation; (C) sedimentary log of the drilled section; (D) Sedimentological context of drill sites 1 – 12.

The sampled section starts in massive mudstone (facies Fm) at 1740 m above sea level (Fig. 11.4B, D). This is overlain by a laterally discontinuous, fine- to very fine-grained sandstone that fines upwards into the overlying red, clay-rich mudstone with incipient pedogenic alteration, sporadic, small (< 5cm) nodules and few bone fragments. The boundary between the mudstone and the overlying pedogenic nodule conglomerate is erosional and irregular.

The pedogenic conglomerate is an elongated, shallow trough-shaped body of 4 m in length and ~80 cm in maximum width that is also laterally restricted and discontinuous (Fig. 11.4C). It is characterised by the abundance of poorly sorted, carbonate nodules (pebble-sized 0.5 – 7 cm in diameter), which are set in a

massive red (calcareous) to slightly mottled green-grey siltstone matrix. This nodule-supported conglomerate is massive and contains numerous, fractured, disarticulated bone fragments. The nodules themselves are irregular in shape, ranging from irregularly spherical to oblong, and often several nodules form a coalesced unit within the conglomerate. Bone fragments are small, ranging from 5 mm to 5 cm, and coated in a thin skin of red-purple iron-oxide (?hematite). No bone fragments where anatomically identifiable. The conglomerate grades upwards into a maximum ~ 1 m thick matrix-supported conglomerate with a massive, silty very fine-grained sandstone matrix. This in turn is overlain by massive (facies Fm) and then horizontally laminated mudstones and siltstones (facies Fl) often with soft sediment deformation structures convoluting the primary bedding. The next unit is >2 m thick and comprise inter-beds of siltstone and fine-grained sandstones (? crevasse splays; Fig. 11.4C).

Comparison of the Oldenburg palaeosols and pedogenic nodule conglomerate to that of the representative section of Smith and Kitching (1997) is illustrated in Figure 11.5. The time sequences conceptualised for the idealised lower palaeosol, *Tritylodon* Acme Zone and *Tritylodon*-bearing palaeosol of Smith and Kitching (1997) have been attempted to be linked to the Oldenburg section. However, it must be stressed that the incomplete nature of the stratigraphic record, as discussed by Miall (2014a, b), and the sedimentation rate scales, over 11 orders of magnitude, make approximating depositional and non-depositional events extremely difficult without radiometric or astrochronological controls. This further emphases the fractal nature of sedimentation rates and hiatuses and questions the simplistic view of the TAZ timescale taken by Smith and Kitching (1997).

11.3 Results

11.3.1 **Demagnetization results**

Previously noted at other sampling sites, during this study, the DAM and OLD samples had two well-defined components. Palaeomagnetic directions were determined by least-squares analysis (Kirschvink, 1980). Lines with MAD values ≤ 15°, and planes with MAD values ≤ 20° were included in analyses.

1. Present local Earth field component (NRM – AF100/ 150 – 250 ^{o}C; Fisher mean declination of 348^{o} and inclination -63.2^{o}, generally NNW upwards directed component) (PF).
2. (i) High-temperature steep NW component, relative to PF, (150-350 – 580-680 ^{o}C) with negative inclination. (~NORMAL, N).

(ii) High-temperature steep SE component (150 - 350 – 580-680 ^{o}C) with positive inclination (~REVERSE, R).

Statistical information relevant to high-coercivity/high-temperature components and samples are presented in Table 11.2.

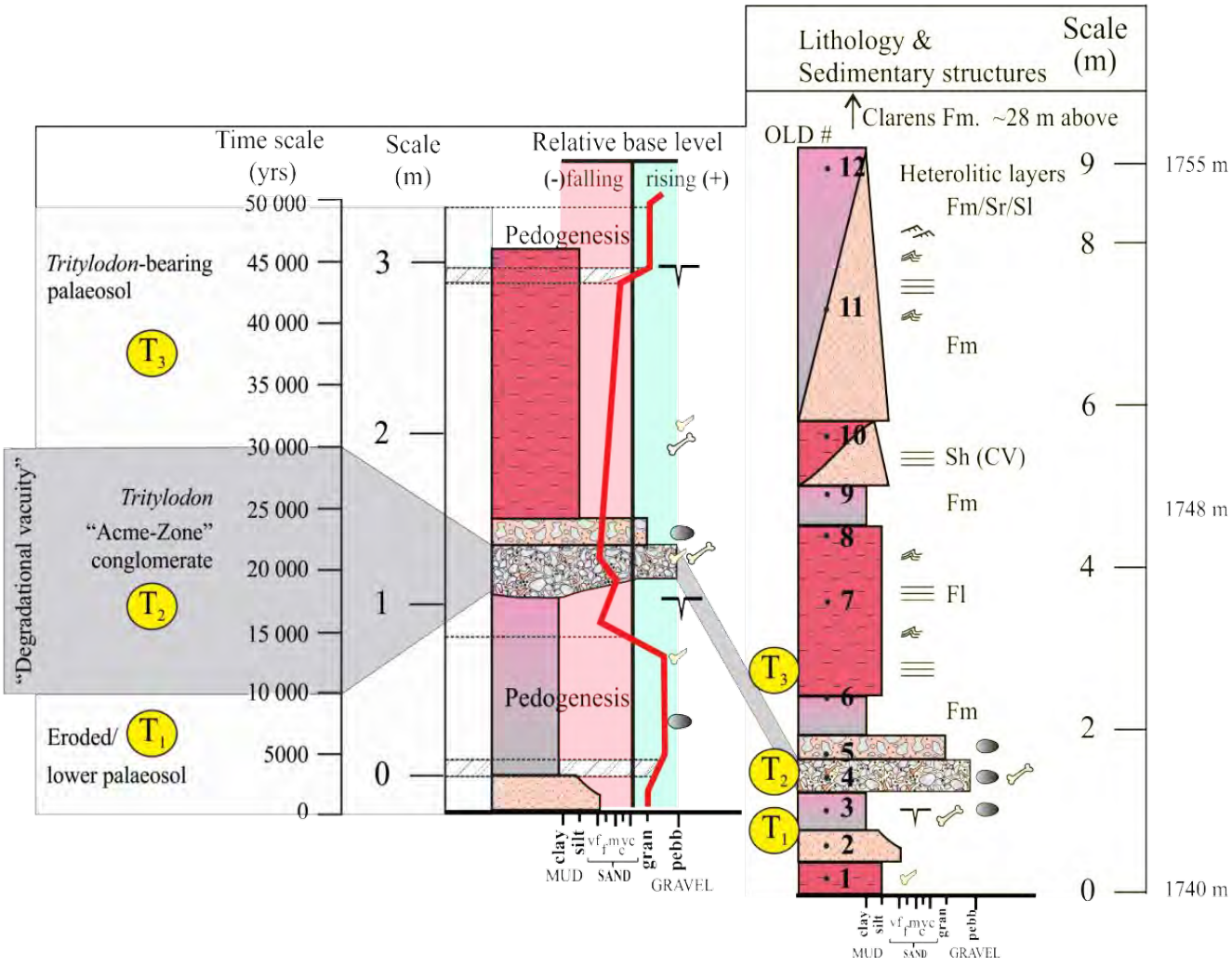

Figure 11.5. Comparison and correlation of the idealized *Tritylodon* Acme Zone (TAZ) of Smith and Kitching (1997) to the Oldenburg 'OLD' – TAZ section of this study. 'T_1' – 'T_3' are time zones of relative accumulation rates for each particular palaeosol and conglomerate horizon as per Smith and Kitching (1997). Numbers indicated on the OLD log are the location of the palaeomagnetic samples.

All characteristic normal remanent directions (Elliot Formation; n = 25) have a mean direction inclination (I) of -61.2°, declination (D) of 312.1° and α_{95} = 8.39°, and the reversed samples (n = 20) have a mean direction with D = 137.4°, I = 60.8° and α_{95} = 7.23° (Table 11.2).

The mean direction for the Elliot Formation has inclination, I, = -61.1°, declination, D = 314.5°, and α_{95} = 5.5°. The site mean VGPs yield a pole latitude of 51.4° N and longitude of 265.2° E. The UEF has a combined I = -60.2°, D = 316.7°, α_{95} = 6.11°, which translates to a site mean VGP at 53.1 °N and 266° E.

In comparison, the LEF combined mean direction has an I = 66.3°, D = 123.8°, and α_{95} = 13.64°, and a VGP at -43.4° N and 076.3 °E. The samples from Oldenburg (OLD) have a characteristic mean remanence direction for the upper Elliot with an inclination, I, = -61.2°, declination, D = 317.7°, and α_{95} = 12.35°. The site mean VGP is located at 53.6°N and 264.5°E.

Table 11.2. Damplaats (DAM) and Oldenburg (OLD) site-mean directions for primary directions, broken into three groups, the entire Elliot Formation (EF), the upper (UEF) and lower (LEF) Elliot Formation. Pole location and the paleopole are indicated. Abbreviations used: N = number of samples, L/P = line or poles to planes; Decl. = declination in degrees; Incl. = inclination in degrees; k = precision parameter and confident limit (α_{95}).

Damplaats (DAM) (29.22°S, 27.34°E)						VGP			
	N(L/P)	Decl °	Incl °	k	α_{95} °	Pole Lat °N	Pole Long °E	dm	dp
Primary Directions									
EF									
All Reverse	20 (12,8)	137.4	60.8	21.36	7.23	53.5	265.4	2.6	2
All Normal	25 (25,0)	312.1	-61.2	12.9	8.39	49.6	265.2	12.9	9.9
Combined	45 (37,8)	314.5	-61.1	15.92	5.5	51.4	265.1	8.4	6.5
UEF									
All Reverse	15 (7,9)	136.0	61.9	14.4	10.43	52.4	83.5	16.2	12.5
All Normal	23 (19,0)	312.8	-59.2	14.0	8.4	50.2	268.7	12.6	9.4
Combined	38 (29,9)	316.7	-60.2	15.5	6.1	53.1	266.6	9.2	7
LEF									
All Reverse	5 (5,0)	126.4	59.3	92.26	8.01	45.3	268.4	12.0	9.0
All Normal	2 (2,0)	270.8	-83.6	8.9	97.44	28.6	221.8	15.7	15.4
Combined	7 (7,0)	123.8	66.3	17.6	13.64	43.4	256.3	22.4	18.4

Oldenburg (OLD) (-29.09° S, 27. 39° E)						VGP			
	N(L/P)	Decl °	Incl °	k	α_{95} °	Pole Lat °N	Pole Long °E	dm	dp
Primary Directions									
UEF									
All Reverse	0 (0,0)								
All Normal	12 (11,1)	317.7	-61.2	12.2	12.4	50.2	264.5	19.0	14.6
Combined	12 (11,1)	317.7	-61.2	12.2	12.4	43.4	256.3	19.0	14.6

For both the Damplaats and Oldenburg sites, low-coercivity components with randomly distributed remanence directions were removed during low-field AF-treatment. These directions have been interpreted as being (soft or present local Earth field) acquired either in the field or through natural processes. Low-coercivity components are often removed on completion of AF-treatment. However, many samples retained scattered NNW and upward directed magnetic components at higher levels of demagnetization, which is comparable to the present local Earth field **(**PF).

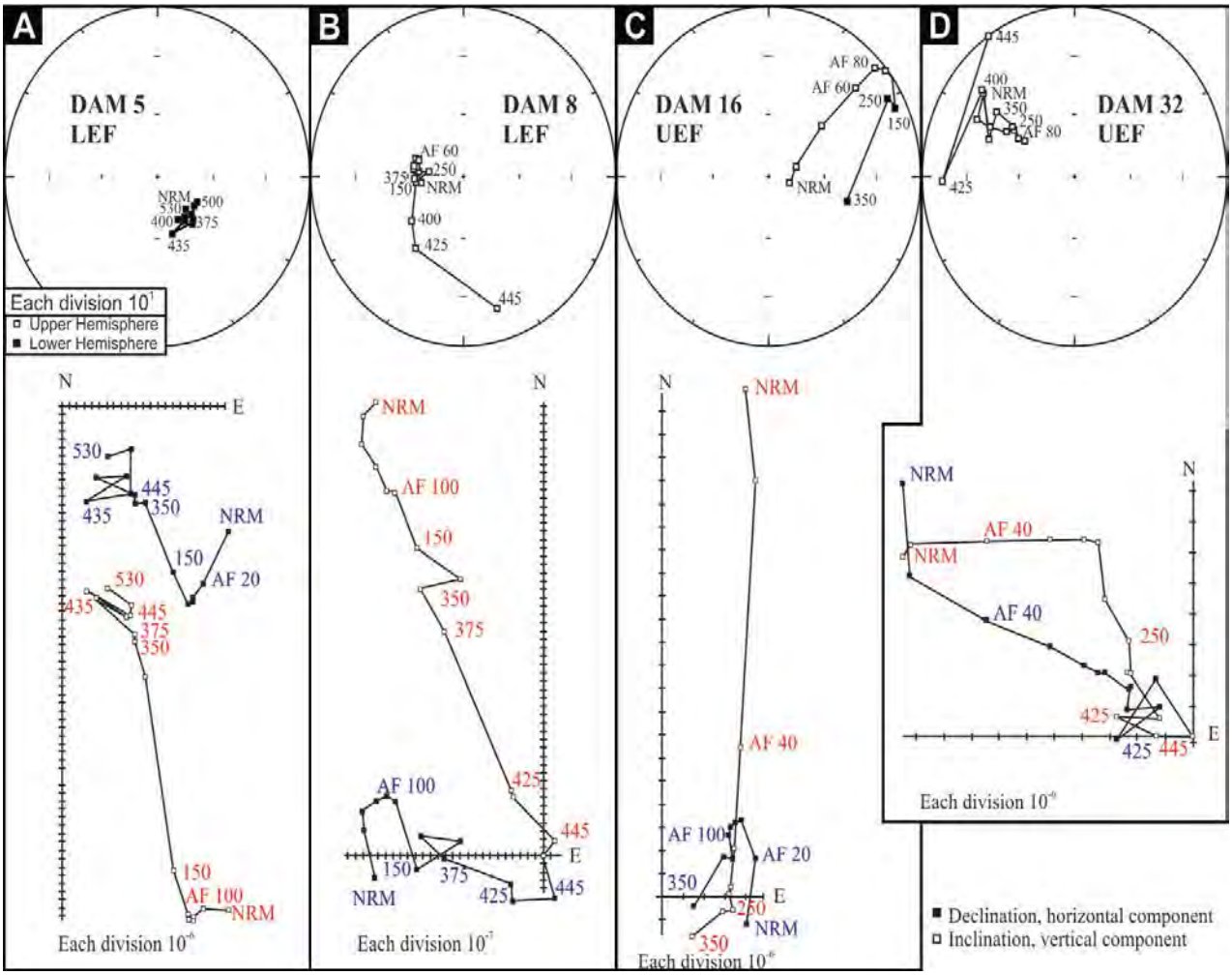

Figure 11.6. Equal area stereoplots and orthogonal vector plots of representative samples of demagnetization behaviour for two lower Elliot samples: (A) DAM 5, (B) DAM 8, and two upper Elliot samples: (C) DAM 16, (D) DAM 32 samples. DAM 16 making a great circle path and projecting into the lower south eastern quadrant. . Demagnetization behaviour of all samples is illustrated in *in-situ* geographic coordinates.

The latter is generally consistent in direction and commonly removed between 150°C and 350°C. Several samples (i.e., DAM 1, 9, 11) retained only the PF component, and then rapidly lost demagnetisation at

low temperature demagnetization. After removal of low-coercivity components and during progressive thermal demagnetization, stable high-temperature characteristic remanent components remained (stable up to ~540 ^{o}C; Fig. 11.6, Fig. 11.7). The PF component often overlaps with the characteristic normal–polarity remanence components. It is important to keep this in mind when assessing and line fitting this particular component, and care was taken in the evaluation of all high-temperature normal polarity line fits.

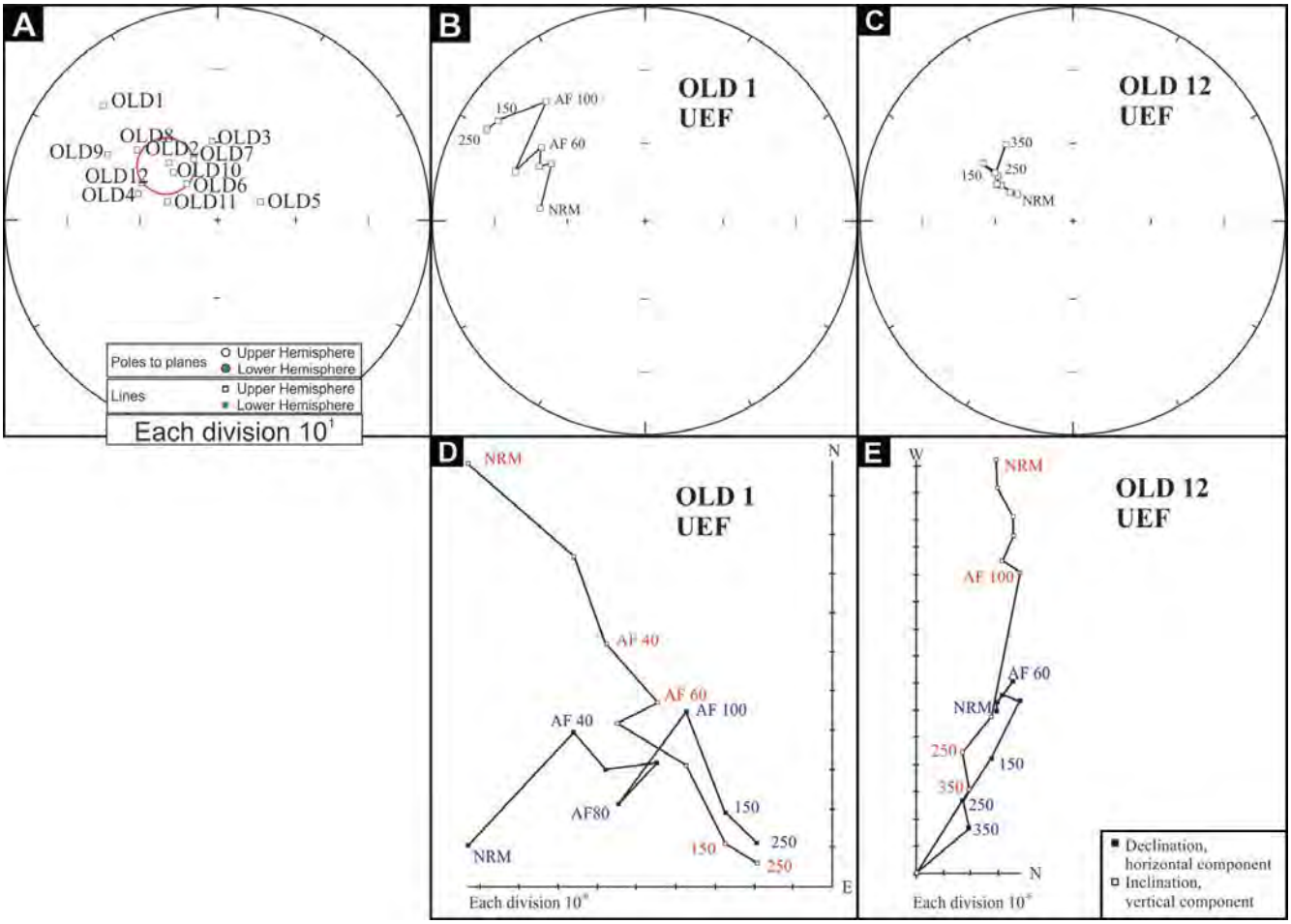

Figure 11.7. Oldenburg (A – C) equal area projections for (A) combined site distribution, (B) OLD 1 sample and (C) OLD 12 sample showing characteristic behaviour, (C- D) respective orthogonal projections.

The behaviour of Oldenburg samples is illustrated in Figure 11.7A-E. In comparison to the DAM samples, the OLD samples had a present-day overprint/low-coercivity component that was often removed before AF100 mT/150 ^{o}C (Fig. 11.7B). Fourteen samples were taken across the OLD section, and all

these yielded characteristic normal-polarity components during step-wise heating between 150 ^{o}C and 350 ^{o}C (Fig. 11.7B-E). These samples form a well-defined normal-polarity grouping with Fisher mean direction declination of 317.7^{o} and inclination of -61.2^{o} (α_{95} = 12.4^{o}).

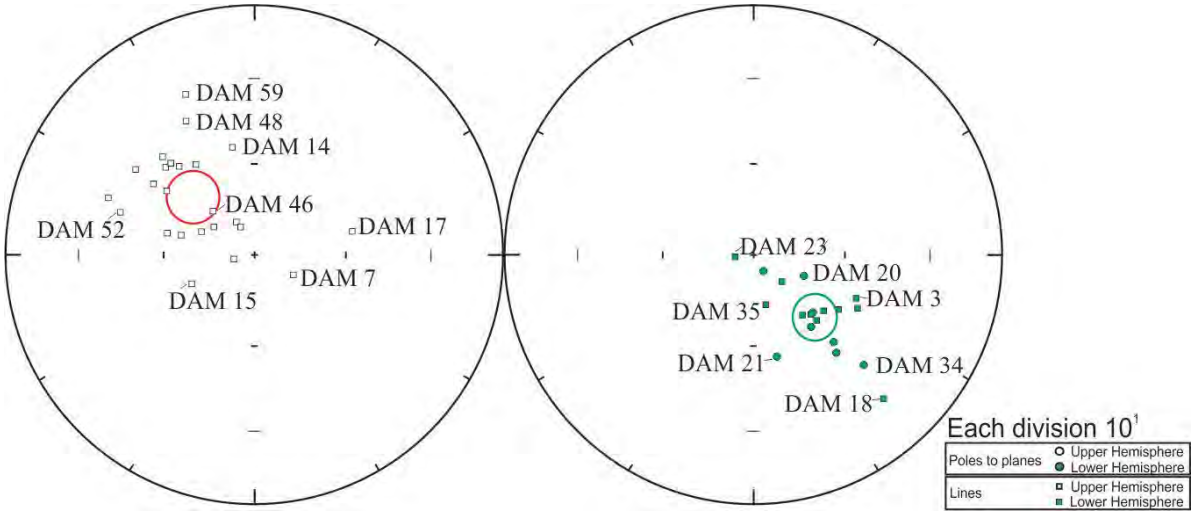

Figure 11.8. Equal area stereoplot for DAM reverse and normal Elliot samples with cone of confidence illustrated.

11.3.2 **Reversals test**

Samples from Damplaats pass the reversals test in the C-class (McFadden and McElhinny, 1990; Butler, 1992).

- Entire Elliot Formation passes the reversals test, class C, γ_c = 11.18° (γ_c<20°).
- LEF and UEF pass the reversals test, class C, with γ_c = 14.3° and 13.09°, respectively.

The class C reversal test for the Elliot Formation, LEF and UEF is most likely explained by the small number of reversed samples dependent on planes rather than anchored with lines providing a less tightly constrained 95% confidence interval. The two directions from the combined Elliot Formation (Figure 11.8), although having a large 95% confidence interval and a C-class reversals test, sit only 0.4° apart.

This demonstrates that the characteristic directions measured at Damplaats are a credible representation of the paleofield.

The virtual geomagnetic latitude (VGP Lat) is calculated and presented in Figure 11.9 and Figure 11.10 for Damplaats and Oldenburg sites, respectively. The Damplaats site was divided into 3 polarity chrons DAM1 – 3 (Fig. 11.9), whereas Oldenburg represents a single normal polarity subchron (OLD1n).

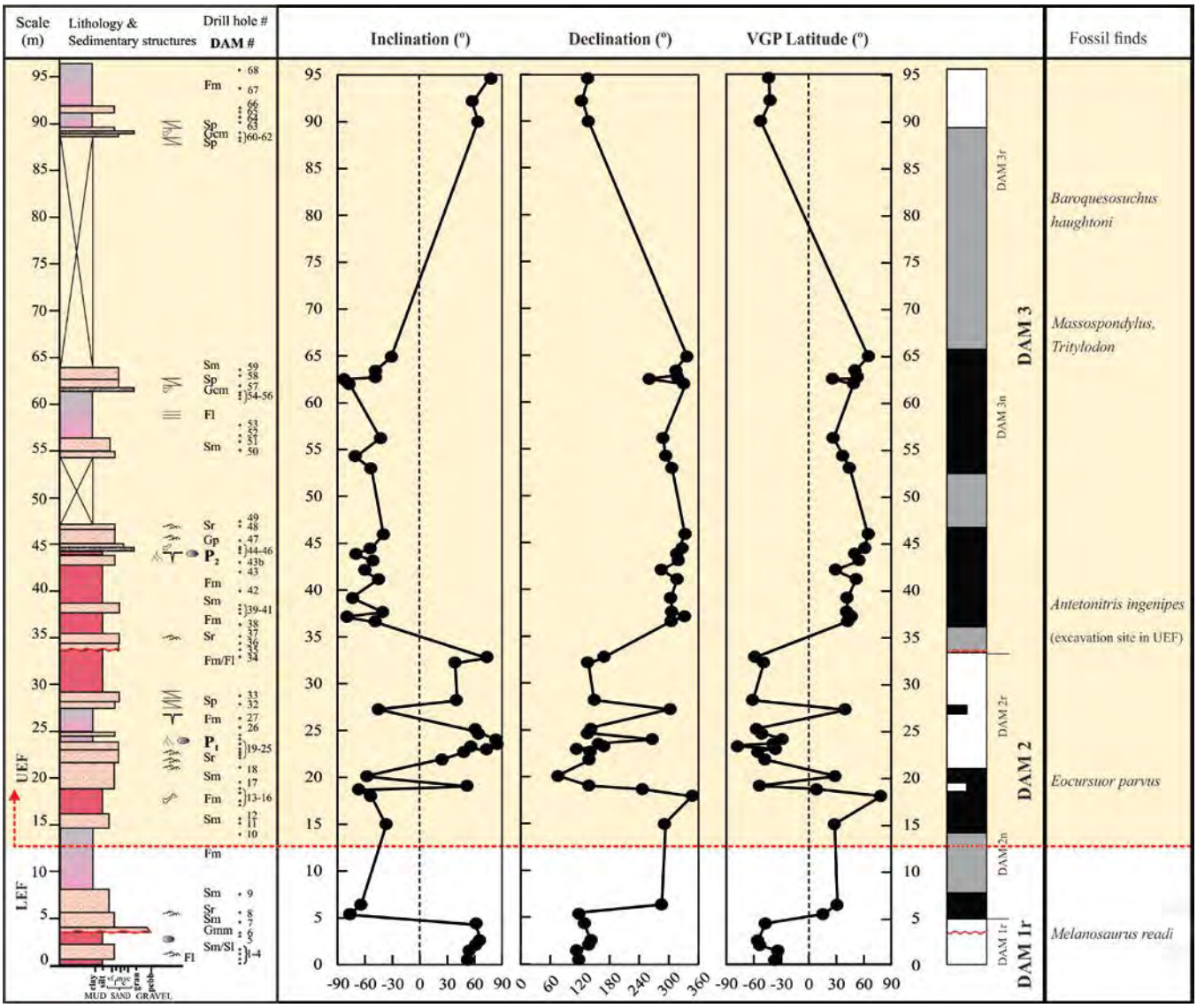

Figure 11.9. Magnetostratigraphy of the Damplaats, DAM 1r – 3, site with inclination, declination and calculated virtual geomagnetic latitude (VGP Lat) calculated against the Damplaats site lithology. The LEF/UEF contact unconformity is indicated wit dashed red line.

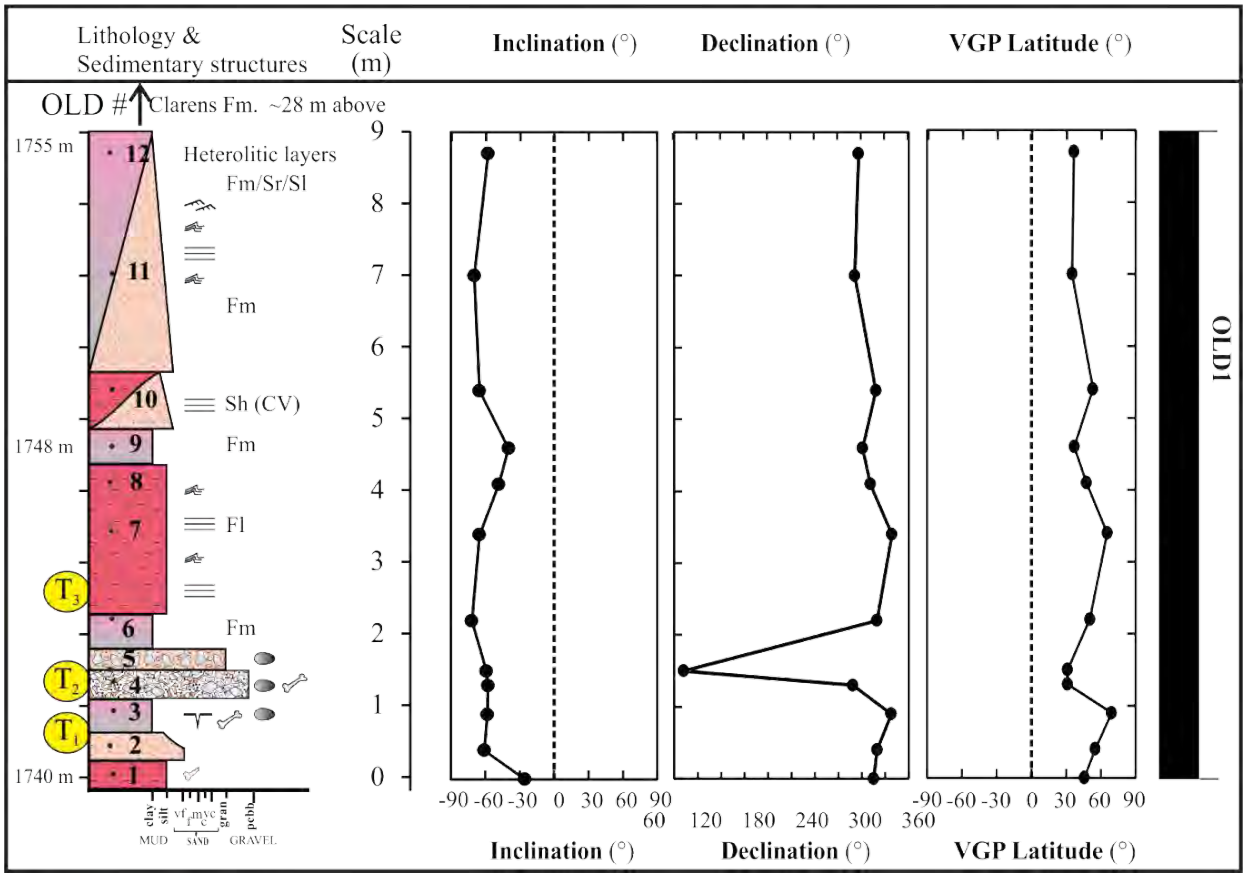

Figure 11.10. Upper Elliot Formation Oldenburg 'OLD' site magnetostratigraphy with site inclination, declination and calculated virtual geomagnetic latitude (VGP Lat) shown against the site lithology. T_1 – T_3 are indicated as compared to the *Tritylodon* Acme Zone of Smith and Kitching (1997). The Clarens Formation is approximately 28 m above the last drill hole (OLD12).

11.4 Conclusion

This chapter has provided a magnetostratigraphic framework for the well-known fossil locality at Damplaats Farm (Ladybrand District, Free State, South Africa; Fig. 11.1). Furthermore, an attempt has been made to place the TAZ (located at OLD) into a composite magnetostratigraphic section for the Elliot Formation (Fig. 11.11; Smith and Kitching, 1997). This was done because no exposure of the TAZ was

identified with any confidence while detailed logging of the DAM section was underway. However, a section with convincing TAZ sedimentological characteristics was located at OLD (as has been previously identified by Smith and Kitching, 1997). Importantly, the OLD section was sampled for palaeomagnetic study as the TAZ is often used as a datum for correlations in the northern part of the Karoo basin.

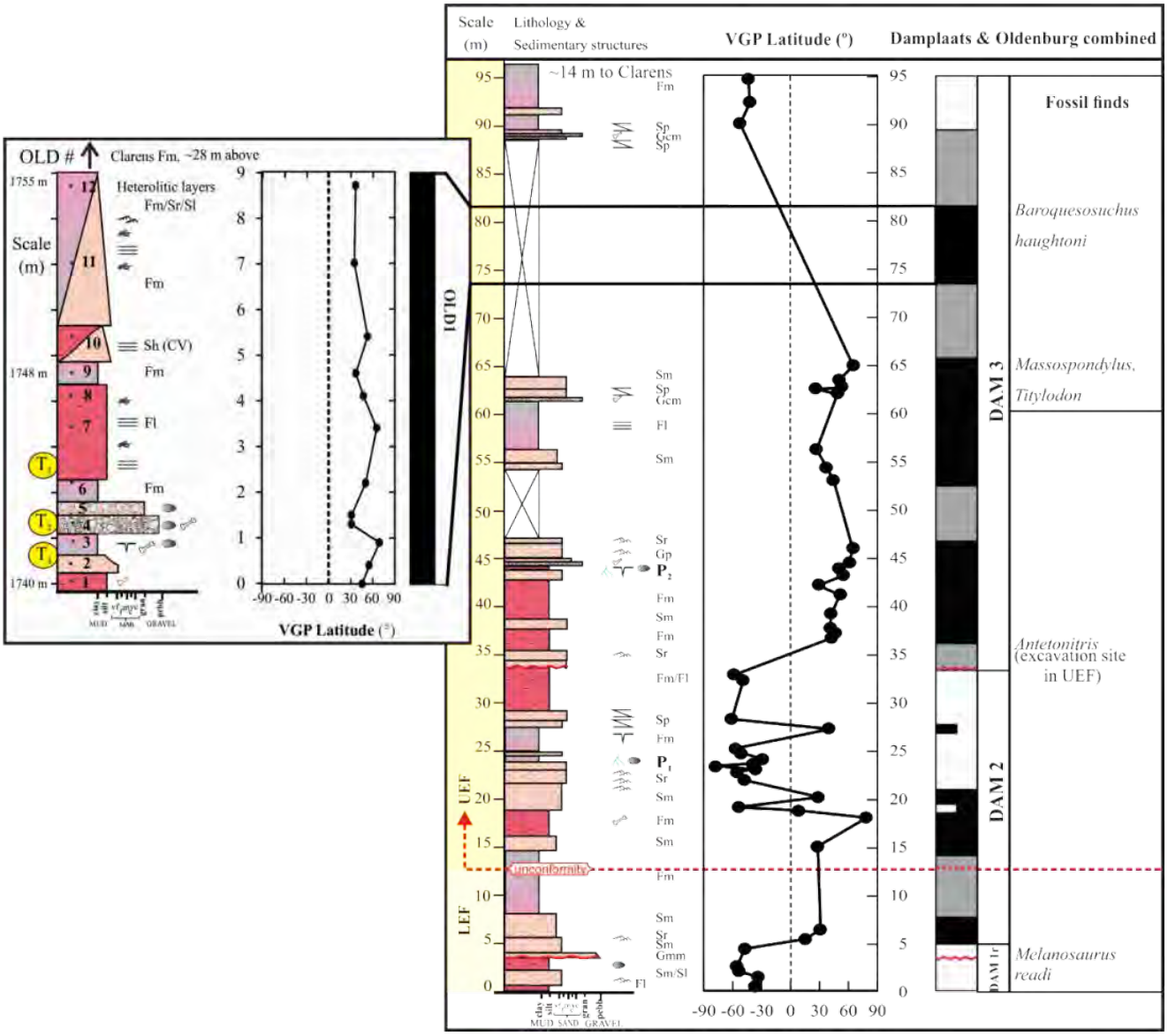

Figure 11.11. Composite of the Damplaats and Oldenburg magnetostratigraphic logs with the known fossil occurrence in approximate location given their upper or lower Elliot assignment. Dashed red line labelled unconformity divides the Formation into the lower (LEF) and upper (UEF) Elliot Formation.

Additionally, given this uncertainly which stems from the subjective and qualitative placement of the contact between the LEF and UEF, the magnetostratigraphic survey of the DAM site was deemed important as it could potentially assist in the placement of the TJB at this palaeontologically important site.

In comparing the DAM and OLD sections, it is most likely that the OLD normal polarity subchron falls immediately below the uppermost DAM reversal (DAM3r) as it is, sedimentologically, an upper to uppermost Elliot Formation site (Fig. 11.11). The distance between last palaeomagnetic sample and the Clarens Formation at these two sites was used in conjunction with the sedimentology largely because the sections are only ~15 km apart from each other. However, it is worth noting that the contact of the UEF and Clarens Formation is an irregular surface which can be stratigraphically variable from place to place by several meters. Caution should be used when considering it, the UEF-Clarens contact, for correlations as it should not to be considered as a synchronous datum.

The DAM3n normal magnetochron is likely to carry the fossil protosuchian, *Baroqueosuchus haughtoni* which is also considered a junior synonym of the Early Jurassic crocodylomorph *Protosuchus* (Fig. 11.9, Fig. 11.11). The taxon is known from the Navajo Sandstone (north eastern Arizona, USA) along with prosauropod dinosaurs, a single specimen of a tritylodont and several trackways similar to those of the UEF i.e. *Batrachopus*, *Anomoepus* and *Grallator* (Galton, 1971; Irmis, 2005a, b). Recent magnetostratigraphic correlations of Steiner and Tanner (2014) place the Navajo Sandstone and the underlying Kayenta Formation into the Lower Pliensbachian (i.e., approximate age: <189 Ma but >186 Ma).

12 Magnetostratigraphic section through the condensed Elliot Formation at Golden Gate National Park.

12.1 Introduction

Golden Gate Highlands National Park (GGHNP) is a geo-heritage site that covers a 120 km^2 area (Fig. 12.1A) in the eastern Free State, and falls within the Drakensberg-Maluti Mountain range in the northern part of the main Karoo Basin (Groenevold, 1986).

12.1.1 **Golden Gate Highlands National Park – sample localities**

With permission from the South African National Parks Authorities (Report reference SCICL1146), two sections were drilled through the Elliot Formation at this locality.

The first and main section (coded GGP; S28˚ 30’ 54’’ E28 ˚ 40’ 44.3’’) encompasses the entirety of the Elliot Formation and contains sections from the underlying Molteno and overlying Clarens Formations (Fig. 12.1C). The main drill locality is adjacent to the R712 (Fig. 12.1B, C) and traverses a ridge leading up to the cream to buff coloured sandstone cliffs of the Clarens Formation. This main locality provided a typical exposure of the Elliot Formation in the northern main Karoo Basin in terms of its overall thickness and main sedimentary features. Notable exceptions, lithologically, are the absence of the TAZ and carbonate nodule conglomerates which often typify the upper Elliot Formation in other northern sites of the main Karoo Basin.

The second locality, GGB (S28˚ 30’ 38.4’’ E28 ˚ 37’44’ 31.2’’), is off of the main road (R712) and lies adjacent to a subsidiary park road (Blesbok Loop; Figure 12.2). The site only encompasses the uppermost, most continuous part of the upper Elliot Formation and was sampled because it overlaps, in lithology and height, with the Rooidraai nest site, and contains *in situ* pedogenic nodules, carbonate nodule conglomerates and fossils, diagnostic of the UEF.

12.1.2 **Previous work**

In recent years much attention (see Reisz *et al*., 2012 and refs therein) has been drawn to the famous Rooidraai dinosaur nest site in the GGHNP. This site first yielded a fallen block of siltstone containing several well-preserved dinosaur eggs and embryos (BP/1/5347) which were examined by Kitching in the

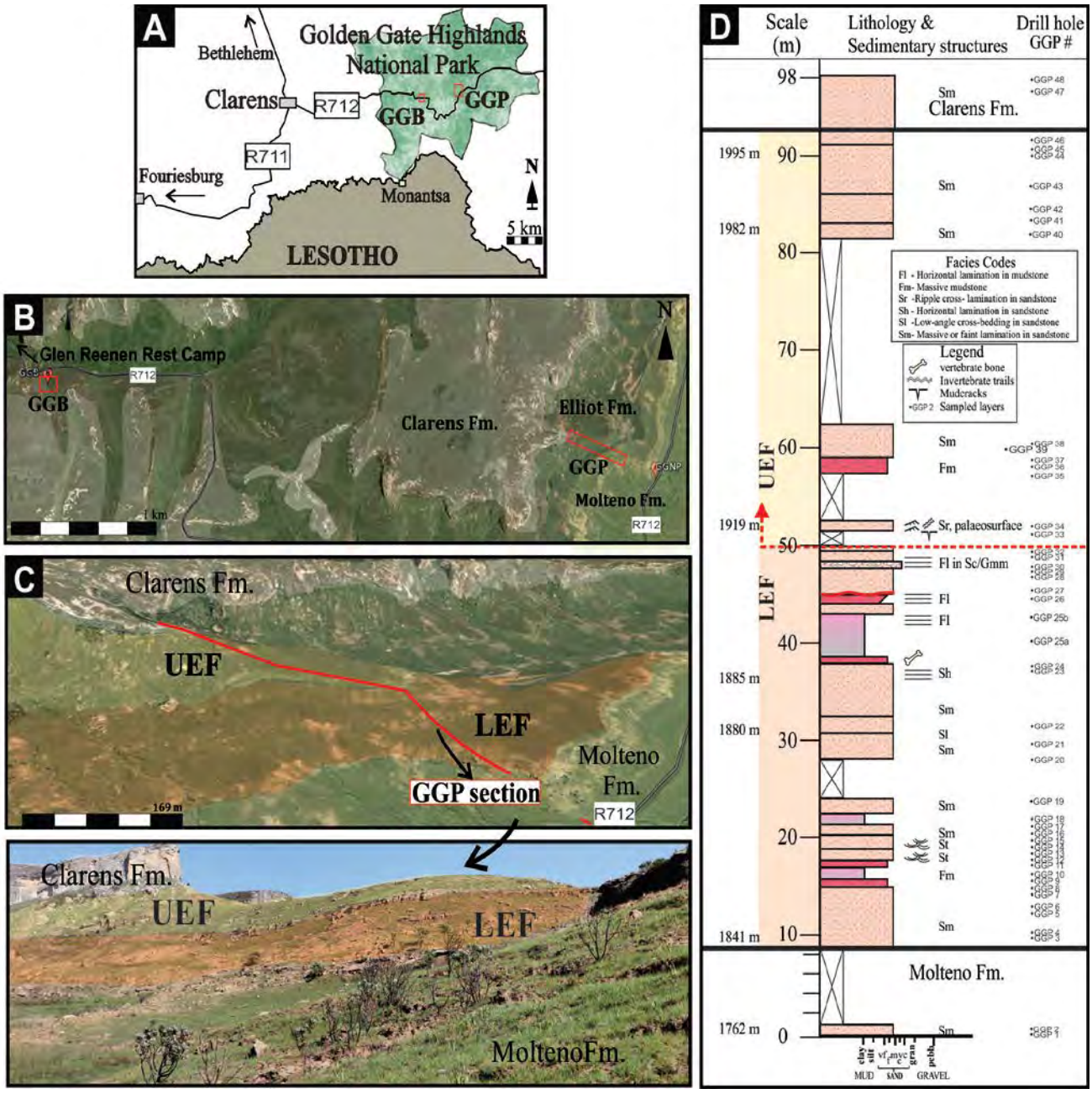

Figure 12.1. (A) Simplified regional map of Golden Gate Highlands National Park (GGHNP) in South Africa; (B) Google Earth image showing the relative position of the two drill sites: (i) GGB in the western part of the GGHNP and (ii) GGP in the eastern part of the GGHNP; (C and insert) the GGP section in relation to the Clarens and Molteno Formations; (D) lithological log of the GGP section.

late 1970s (Fig. 12.3). Kitching (1979, 1981) later published the initial findings on the egg clutch, the exposed partial *Massospondylus* skeleton and the stratigraphic position of the site which was determined to be above Kitching's, then unpublished, *Tritylodon* Acme Zone. Kitching (1979) tentatively identified

the embryos as belonging to prosauropods, and Reisz *et al*. (2005) attributed them to *Massospondylus carinatus*. Other important palaeontological remains collected at and in the vicinity of the Rooidraai dinosaur nest site are listed in Table 12.1.

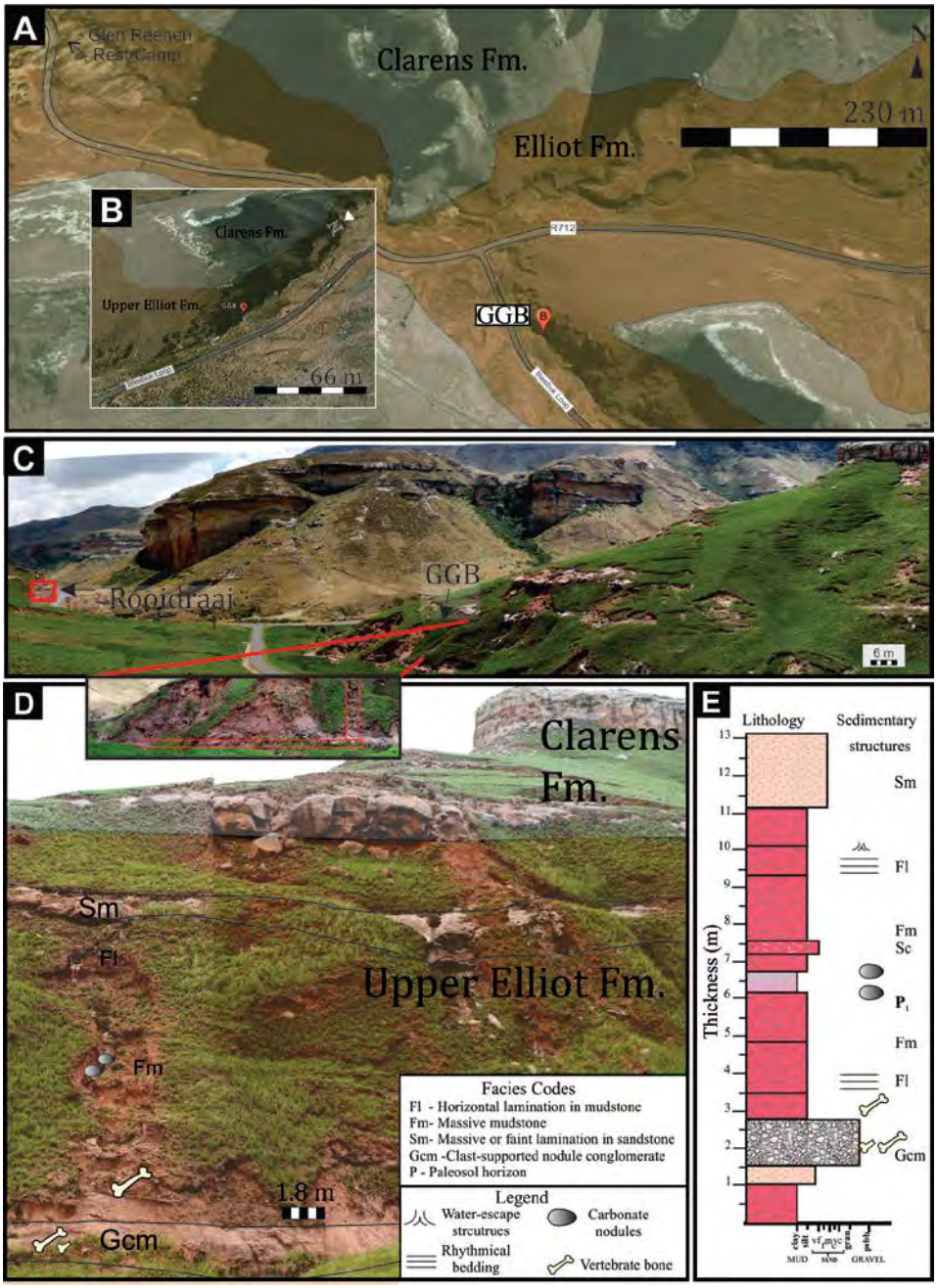

Figure 12.2. (A, inset B) Location map of GGB drill site, which runs parallel to the 'Blesbok Loop' park road, (C) GGB location relative to the Rooidraai dinosaur nest site (D, E) outcrop at the GGB site and its sedimentary log, respectively.

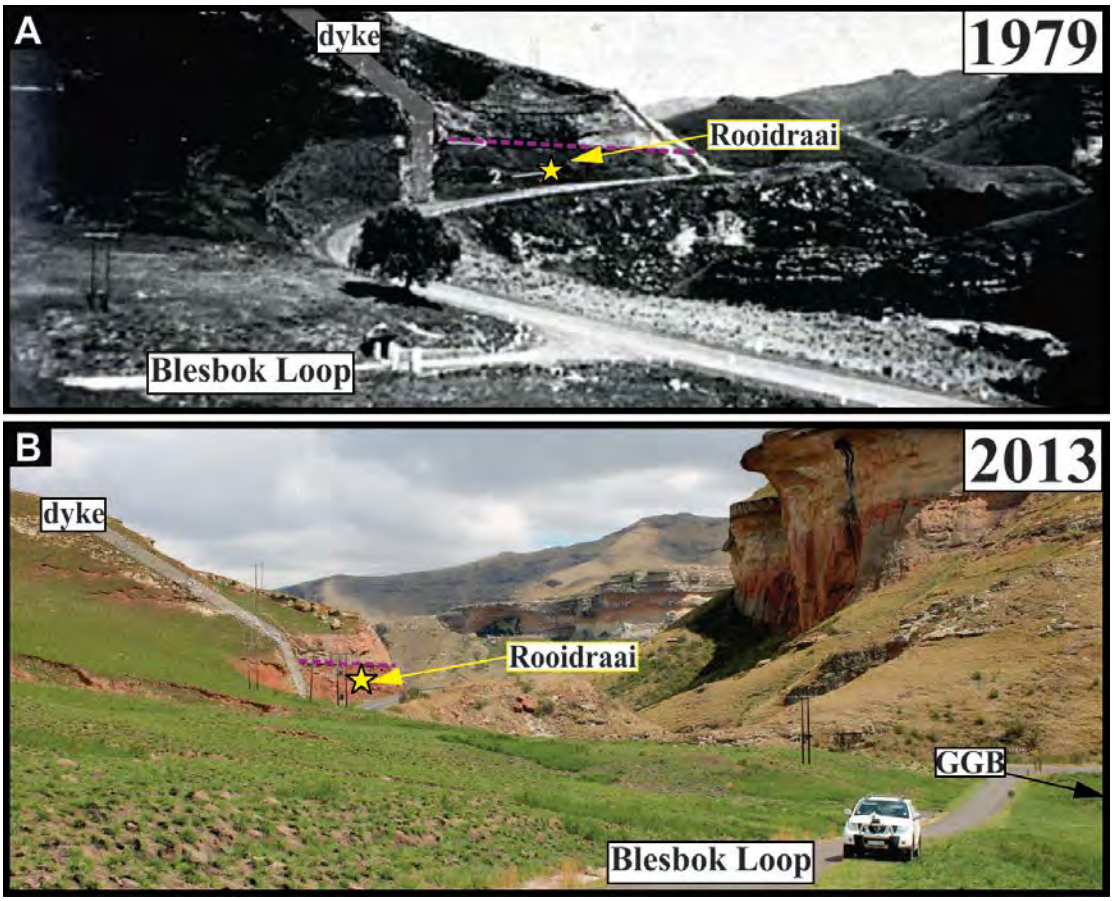

Figure 12.3. Marked up photographs of the Rooidraai outcrop in the GGHNP. (A) Adopted from Kitching (1979); (B) taken during this study from the hill side near the Blesbok Loop, adjacent to GGB drill site. The purple dash line in both photos is the original designation of the UEF-Clarens contact by Kitching (1979); the star indicates the approximate locality of the clutch of eggs in the dinosaur nest found by Kitching (1979). This site is still considered to be in the uppermost UEF (see also Reisz *et al*., 2012).

Other finds at this site, within the UEF, were by Brink (1959) with the discovery of the thecodont *Clarencea gracilis*, as well as *Massospondylus* sp., *Pachygenelus* sp., *Notochampsa* sp., etc (Kitching and Raath, 1984; Busbey and Gow, 1984; Groenevold, 1986). More recently Porro *et al*., (2010) reviewed heterodontosaurids remains and reported on finds in the UEF near Buck camp: specimen BP/1/4244 11 *Lanasaurus scalpridens* Holotype Gow (1975, 1990).

Table 12.1. Details of fossil finds proximal/at the GGHNP, Free State, South Africa.

Taxonomic assignments	Age	Stratigraphic position	Catalogue no.	Notes	Source(s)
Sphenosuchus, *Clarencia gracilis*	Early Jurassic	Clarens Fm./uppermost	-	-	Brink (1959)
Tritheledontid *Pachygenelus* sp.	Early Jurassic	uppermost UEF	BP/1/4982 BP/1/5110 BP/1/5292 BP/1/5691	BP/1/4982, 5110, 5292, and 5691 are all recorded as being from within 3 m of the Elliot–Clarens contact.	Kitching and Raath (1984); Hopson and Kitching, (2001); Sidor and Hancox, (2006)
Prosauropod *Massospondylus carinatus*	Early Jurassic	uppermost UEF	BP/1/5347	Rooidraai, along the R712, near Glen Reenen camp. Rooidraai clutch – earliest dinosaur eggs+embryos	Reisz *et al.* (2012) and refrences therein
Heterodontosaurids *Lanasaurus scalpridens*	Early Jurassic	UEF	BP/1/4244 11	Near Buck camp, Golden gate National Park. Maxilla Holotype Gow (1975, 1990).	Gow (1990) Porro *et al.* (2010)
Protosuchidae *Baroqueosuchus haughtoni*.	Upper Triassic	lower UEF	BP-1-4746	Farm Sunnyside, outside Clarens on the R712. 28°31' 40"S; 28°30'06"E Partial braincase of a Protosuchin crocodilian.	Busbey and Gow (1984)
Tritheledontid: *Elliotherium kersteni*	Upper Triassic	LEF	BP/1/6106	Farm Beatrix, Rosendal District, Free State Province, South Africa. Partial skull lacking tip of snout, occiput, and mandible. First record of a tritheledontid from LEF.	Sidor and Hancox (2006)
Tridactyl prints: *Grallator* sp. Planolites	Upper Triassic	Lowermost LEF	-	Tweedegeluk, Qwa Qwa District, NE Free State (Golden Gate National Park). Proposed *Coelophysis* as likely track maker (and/or Ornithopods) and predict a lower extension to the stratigraphic range of this theropod.	Gow and Latimer (1999)

12.2 Results

12.2.1 **Sedimentology**

Overlying the medium-grained, 'sparkly' sandstones of the Molteno Formation, the LEF in the GGHNP is noted by the appearance of fine-grained green and purple, massive mudstones and finer grained sandstones (see sedimentological log in Fig. 12.1D).

The main sedimentary characteristics of the UEF in the GGHNP are typified by the GGB section (Fig. 12.2E). The GGB site exposes a ~12 m thick unit of the UEF, with the lower portion comprising a massive siltstone to silty sandstone which is overlain by horizontally bedded, massive sandstones (Sm - samples GGB 1-4). At drill core GGB 5, there is a laterally discontinuous carbonate nodule (≤1 cm) and bone fragment-bearing conglomerate (Gmm). The base of this bed is irregular and appears to scour into the underlying layers. The conglomerate is overlain by a 7 m thick succession of fine muddy siltstone and finer mudstone beds (Fm/Fl) which are irregularly interbedded with thin (<40 cm), fine-grained sandstones (CV). Two nodule horizons occur ~3 m above the conglomerate and 70 cm apart from one another. The lower nodule horizon contains *in situ* egg-sized nodules and the upper nodule horizon is in siltstone that contains rip-up mudstone clasts. This drilled succession is overlain by a 2 m wide, deeply down-cutting cream sandstone channel, which was not sampled, and appears to represent one of the last major channels of the UEF. Sedimentary structures within the 7 m muddy siltstone unit range from horizontal lamination ripple cross-lamination, water escape structures and small desiccation cracks on mud draped surfaces (Fig. 12.2E).

12.2.2 **Magnetostratigraphy**

Least-squares analysis (Kirschvink, 1980) was used to determine palaeomagnetic components of GGP and GGB samples. Lines with MAD values ≤ 15˚, and planes with MAD values ≤ 20˚were included in analyses. Most samples have two, sometimes three, well-defined components which are:

1. Low-coercivity (soft) magnetic component (NRM – AF 100/150) (coded 'SFT').
2. High-temperature relatively steeper (than PF) NNW to NNE component (150-350 – 440-650 ^{o}C) with negative inclination (normal, N).
3. High-temperature steep SE component (150-350 – 440-650 ^{o}C) with positive inclination (reverse, R).

Statistical information relevant to high-coercivity components are presented in Table 12.2.

During low-field AF-treatment, samples displayed randomly distributed remanence directions of low-coercivity (soft) which are often removed on completion of AF-treatment. Several samples are weakly magnetized, and lose remanent magnetization at low levels of thermal demagnetization (below 250-350 ˚C). For example, sample GGP 5 shows a weak and unstable, west-south-west component below 350 ˚C.

Table 12.2. Summary of the GGP and GGB sites in the GGHNP. Mean Fisher palaeomagnetic directions and subsequently calculated pole latitude and longitude are also shown.

Site	Fisher Stats						
Golden Gate National Park (GGP) (-28.52° S, 28. 68° E)							
	n (L/P)	Decl. (°)	Incl. (°)	k	α_{95} (°)	Pole Lat (°N)	Pole Long. (°E)
Primary Directions (EF)							
All Reverse	6 (1,5)	164.1	72.3	11.06	21.08	-59.0	045.3
All Normal	31 (29,2)	317.4	-54.1	15.80	6.21	53.5	278.0
Combined	36 (30,6)	319.1	-56.2	15.80	6.21	54.6	274.4
LEF							
All Reverse	2 (1,1)	270.9	84.3	38.21	41.57	-27.7	015.9
All Normal	18 (16,2)	321.4	-51.7	18.76	8.20	56.7	282.3
Combined	20 (3,1)	322.2	-55.8	13.62	9.18	57.4	275.0
UEF							
All Reverse	4 (0,4)	157.9	62.1	12.30	27.30	-66.9	072.8
All Normal	12 (12,0)	314.7	-54.3	28.59	8.26	51.3	277.5
Combined	16 (12,4)	319.4	-56.5	20.87	8.27	55.1	273.8
Site	Fisher Stats						
Golden Gate National Park Blesbok Loop (GGB) (-28.52° S, 28. 68° E)							
	n (L/P)	Decl. (°)	Incl. (°)	k	α_{95} (°)	Pole Lat (°N)	Pole Long. (°E)
Primary Directions (UEF)							
All Reverse	2 (0,2)	269.9	38.0	152.27	20.38	-10.1	317.6
All Normal	12 (12,0)	334.1	-50.2	28.54	8.27	67.4	286.1
Combined	14 (12,2)	345.9	-55.8	6.89	15.53	75.8	261.7

High-stability characteristic remanence directions, after the removal of soft components, were either normal or reverse components. These were distinguished during stepwise heating during thermal demagnetization. The normal component was unblocked between temperatures of 150 – 650 ^{o}C and had an average declination of 317.4˚ and inclination of -54.1˚ (entire Elliot Formation {Fig. 12.4}, including the lowermost two Molteno Formation and uppermost two Clarens Formation samples). When the UEF

samples were isolated from the group, their mean declination is 319.4˚ and inclination of -56.5˚ in comparison to the LEF samples with a mean declination of 322.2˚ and inclination of -55.8˚ (Fig. 12.4). Equal area and orthogonal projections for the samples from the uppermost Molteno (Fig. 12.5A) and lowermost Clarens (Fig. 12.5B) Formations are illustrated in *in-situ* geographic coordinates. The behaviour was similar to that shown by typical LEF and UEF samples elsewhere. The GGB site recorded only UEF samples with a mean declination of 345.9˚ and inclination of -55.8˚. The normal components at the GGB site are more north-north-westerly orientated than those of the UEF from the main site at GGP, which group more towards the north-west.

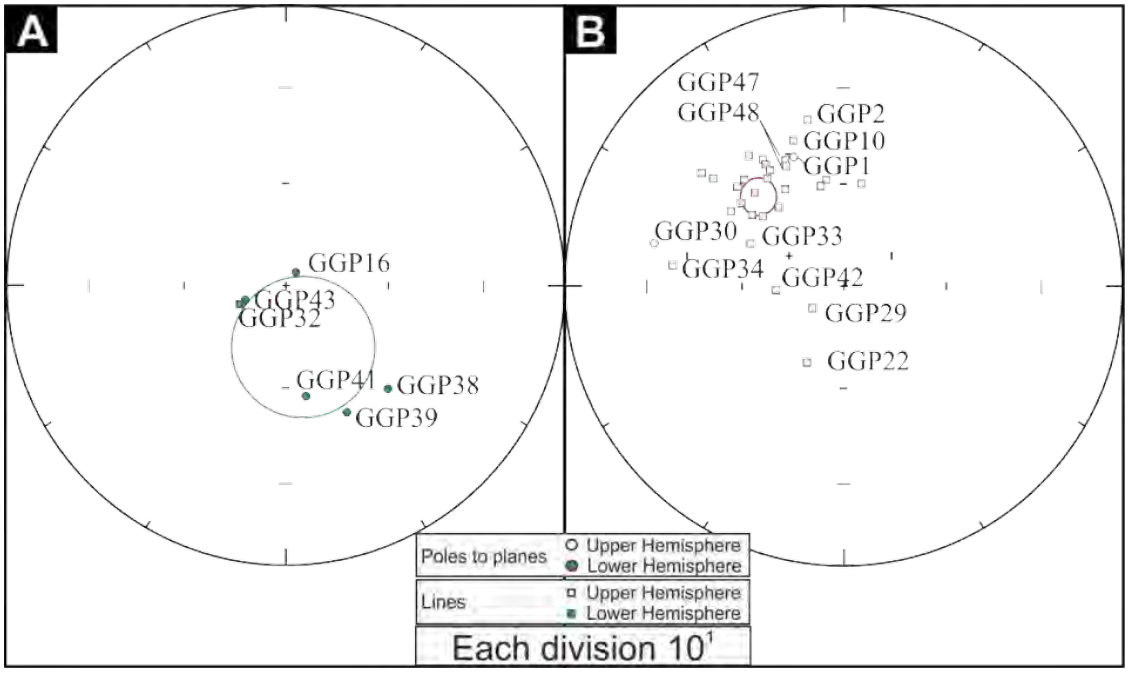

Figure 12.4. Equal area projection of geographic site mean directions for the GGP site in the GGHNP.

Reverse magnetized samples have stable end-point vector directions to the south or, south-east that were reached along great circle paths, with a mean declination of 164.1˚ and inclination of 72.3˚. Sample GGP 16 (Fig. 12.6A) shows a reverse component, which demagnetizes along a great circle path. Samples typical for Golden Gate GGP lower Elliot Formation (GGP 7, 10 and 16) and upper Elliot Formation (GGP 35, 39 and 43) are plotted in equal area projections and orthogonal vector plots in Figure 12.6(A and B).

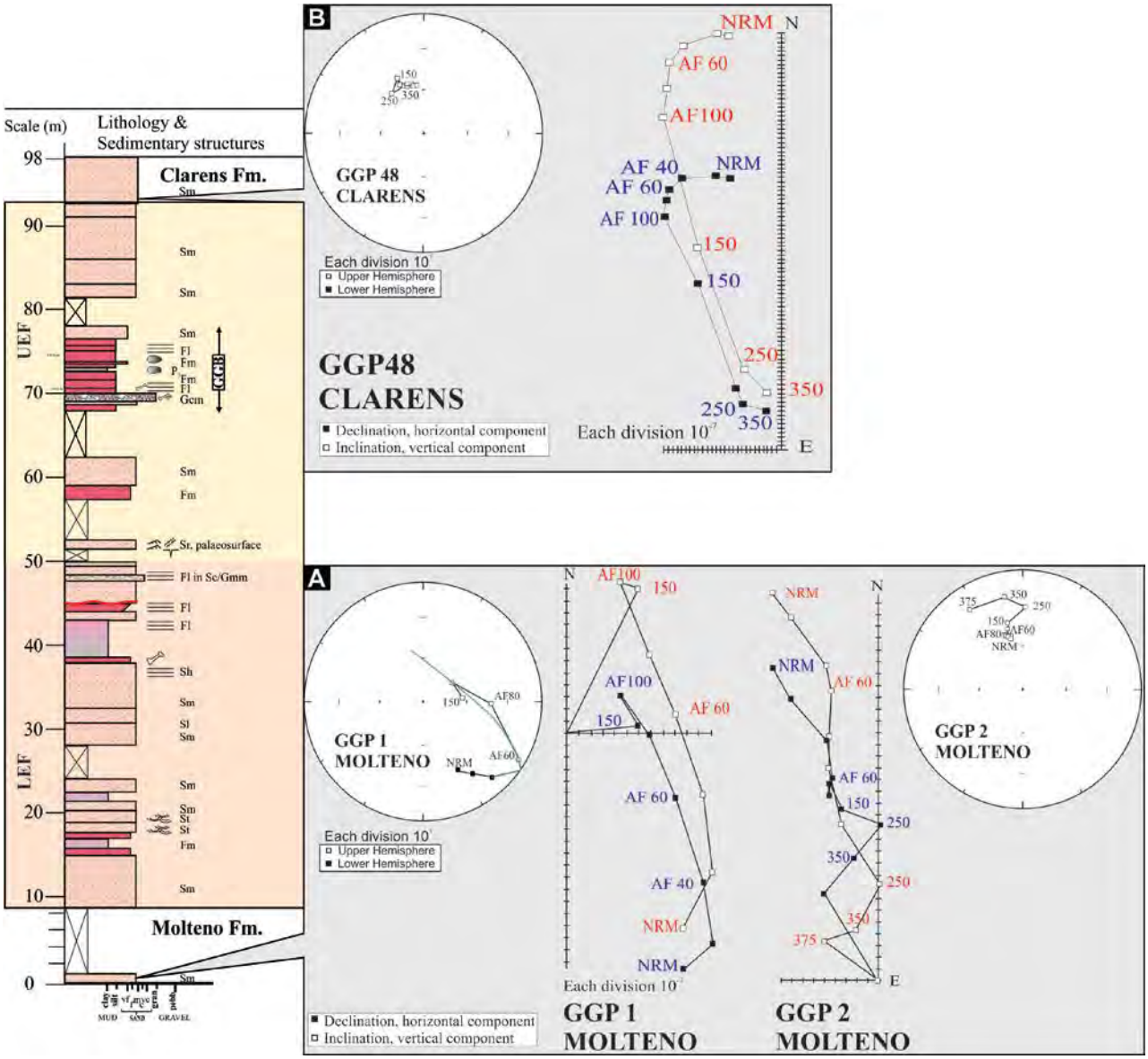

Figure 12.5. Samples from the (A) Molteno, (B) Clarens Formations at the GGP site in the GGHNP, showing typical behaviour during thermal demagnetization in equal area plots along great circle paths and orthogonal projections to reverse or normal polarities. All diagrams illustrate *in situ* co-ordinates.

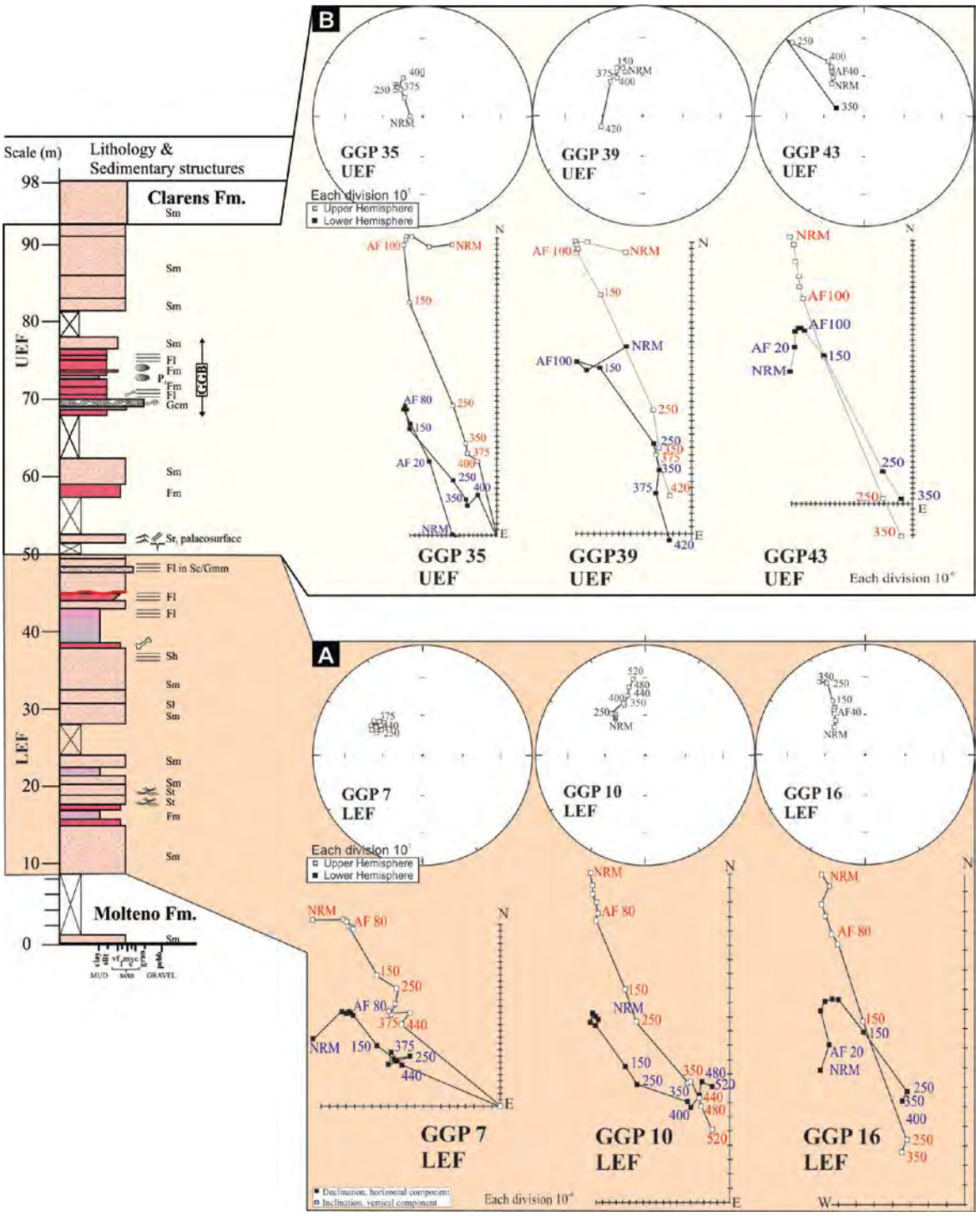

Figure 12.6. Representative samples showing typical demagnetization behaviour in equal area and orthogonal projections of the samples from the (A) LEF and (B) UEF, in the GGHNP. UEF and (D) Clarens Formations at the GGP site in the GGHNP, showing typical behaviour during thermal demagnetization along great circle paths to reverse or normal polarities. All diagrams illustrate *in situ* co-ordinates.

12.2.2.1 Reversals test

To establish palaeomagnetic stability in the LEF and UEF a comparison of the antipode of the mean of the reversed-polarity samples is taken against the mean of the normal-polarity samples, in a reversals test (McFadden and McElhinny, 1990; Butler, 1992). The test results show that:

1. The entire Elliot Formation passes the reversal test with an y_0 of 158.59 (y_c = 17.3) as a "C" quality reversal test with a common shared precision.
2. LEF gives an indeterminate reversals test with γ_c >20˚, γ_0 of 137.88˚ (γ_c = 24.72˚), with the two groups not sharing a common precision.
3. UEF (and two Clarens samples) passes the reversal test with a γ_0 of 165.62˚, γ_c = 18.71˚ (<20˚), as a "C" reversals test.

The latitude of the virtual geomagnetic pole (VGP Lat.), in conjunction with the inclination and declination of samples from the GGP and GGB sites in the GGHNP are plotted in Figure 12.7 to evaluate the magnetic polarity record. The resulting composite magnetostratigraphy has 2 normal polarity zones and 1 reverse polarity zone, labelled GGP1 and GGP 2. All grey intervals are of unknown polarity.

12.3 Conclusion

The UEF in the GGHNP, from the sedimentological features discussed above, appears to indicate periods of scouring (pedogenic nodule conglomerate formation) followed by rapid and then very slow deposition due to the incipient development of pedogenic features in massive siltstones. Periods of rapid deposition and followed by erosion or non-deposition are indicated by the Fm/Fl sections, with soft sediment deformation structures, interbedded with thin, laterally discontinuous, fine-grained crevasse splay sandstones interspersed with several palaeosol horizons that are marked by desiccation cracks and pedogenic nodules.

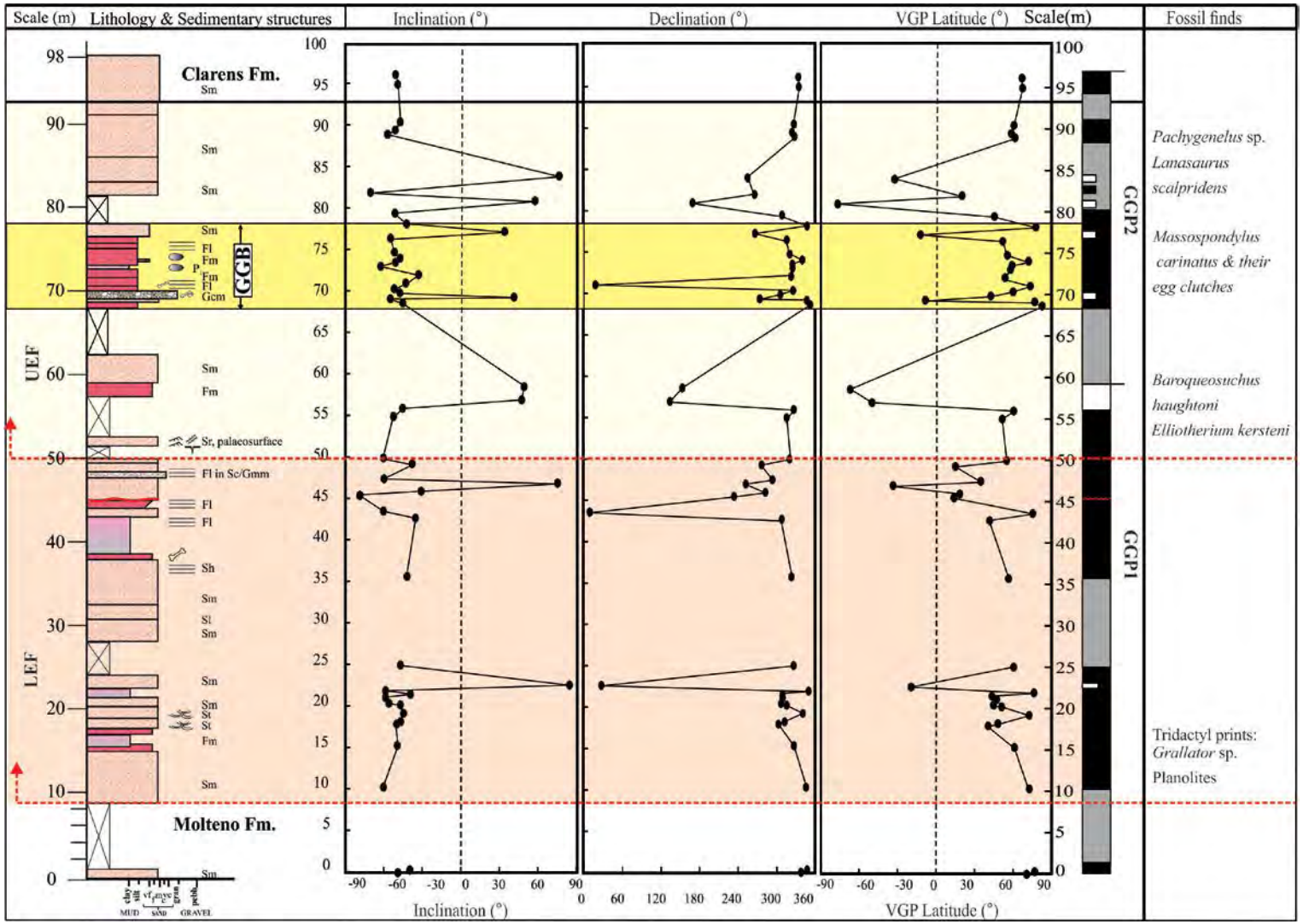

Figure 12.7. Inclination, declination, VGP latitude values and the reconstructed magnetostratigraphic log for the combined GGP and GGB sites in the GGHNP shown against the sedimentological log at site GGP. Paraconformities between the Molteno and the Elliot Formations and within the Elliot Formation are indicated with dashed red lines. The approximate stratigraphic position of the GGB section is marked into the GGP log. Two polarity intervals (GGP1 and GGP2) are marked for the GGHNP.

Furthermore, the *Massospondylus* nest site also attests to the variable and unpredictable nature of the rate of deposition within the upper Elliot Formation during the Early Jurassic. The eggs site occurs in several metre thick package of fine-grained mudstones and silty-sandstones. It is likely that the nesting site was chosen by *Massospondylus* because it represented a 'safe', undisturbed place ideal nesting and raising of hatchlings. The periods of sedimentation quiescence is revealed by several egg clutches in close proximity to one another, on what would be assumed to have been a flat ground surface trampled by juveniles and now forming isolated trackways (Reisz *et al*., 2012). Sedimentary structures of the overlying sediments (e.g., soft sediment deformation, rünzel marks, massive siltstones with rip up mudstone clasts, massive to laminated fine-grained sandstones) however indicate rare, high magnitude flashy-flood conditions that caused the rapid deposition of sediments and instant, 'Pompeiian' entombing of the nest sites with many hatchlings buried alive *in situ*.

Figure 12.7 illustrates the composite GGHNP magnetostratigraphic log with the placement of the GGB section in context of the main site at GGP. Thus, the long normal polarity period represented by the GGB section and the *Massospondylus* nest site.

13 Geochemistry of the Elliot Formation

13.1 Introduction

To better understand the palaeoenvironmental changes within the Elliot Formation geochemical analysis of samples drilled along three magnetostratigraphic transects at Likhoele (LIK and LIKE) and at Damplaats (DAM) were undertaken. Typically, the Elliot Formation is known to have been deposited in a semi-arid setting, but to date, no quantitative study was conducted on the unit with a view to determine the degree of aridity and potential fluctuations of the palaeoclimate. Except for a preliminary study by Eriksson (1983), which only focused on the sandstone composition of the Formation in the NE part of the Basin, the geochemical composition of the Elliot Formation is unknown.

This current assessment is based on the premise that the chemical composition of the samples is dependent on the prevailing palaeoenvironmental conditions as well as the mineralogy of the sediment which in turn is a function of the composition of the source rocks as well as weathering, erosional, transportational, depositional and diagenetic processes that act upon the sediment from source to sink (Weltje and von Eynatten, 2004, Zhang *et al*., 2014). This approach relies on the solubility and mobility of several elements during the weathering process after sediment was deposited on a substrate. It also works on the premise that the degree of weathering decreases, in a sediment profile, with increasing depth below surface (Sheldon and Tabor, 2009; Depetris *et al*., 2014). In addition, minerals which are broken down close to the surface release more soluble and mobile elements more readily (e.g., Ca, Na, U, Rb) than less soluble/immobile ones. Highly mobile elements may be leached away from the soil profile or may combine to form new minerals. An example is the breakdown of feldspar into clay minerals, which under humid, warm climate tends to generate illite (Depetris *et al*., 2014).

The objectives of this geochemical study were to determine the chemical changes of a typical Elliot Formation sedimentary rock profile to examine the weathering history shortly after the sediments were deposited (e.g., early diagenetic and pedogenic stages). To this effect, the use of the chemical index of alteration (CIA) and the index of compositional variability (ICV) were employed. The CIA is a method defined by Nesbitt and Young (1982) for lutites, and was designed to quantify the degree of chemical weathering experienced by fine grained sedimentary rocks. Secondarily, it allows for climatic controls and palaeoenvironment to be deciphered. The CIA index used here is shown in Equation 1 and all values

are in molar proportions. In calculating this index, the assumption is fact that Al_2O_3 is relatively immobile compared to CaO, K_2O and Na_2O which are mobile during weathering processes, and form soluble cations in aqueous solutions (Scheffler *et al*., 2006). The CIA (molar) index (see Equation 2; Goldberg and Humayun, 2010) was later developed to aid in managing the CaO values present from carbonates. The CIA (molar) also allows for easy calculation of degree of chemical weathering when compared to molar proportions of minerals. For example: in case of fresh feldspars, the CIA (molar) is 1 because of the ratio K/Na: Al is 1:1. The illite CIA (molar) value is 4 as the ratio of K: Al is 1:4 (Goldberg and Humayun, 2010). Accordingly, the CIA (molar) value will increase with increasing degrees of chemical weathering.

$$CIA = \frac{Al_2O_3}{Al_2O_3 + CaO^* + Na_2O + K_2O} \times 100 \quad (1)$$

CaO* non-silicate CaO must be subtracted as CaO here is only attributable to silicates (i.e., plagioclase) and not carbonate minerals.

$$CIAmolar = \left[\frac{Al_2O_3 molar}{CaO^* molar + Na_2O molar + K_2O molar}\right] \quad (2)$$

Cox *et al*. (1995) introduced the index of compositional variability (ICV; Equation 3) which uses the weight percent of oxides in the following equation:

$$ICV = (CaO + Na_2O + K_2O + Fe_2O_3 + MgO + MnO + TiO_2)/Al_2O_3) \quad (3)$$

In comparison to the CIA, the ICV index is less affected by diagenesis and takes into account all sources of CaO as well as the total iron content (Potter *et al.*, 2005). The ICV values decrease with increasing degrees of weathering. A CIA versus ICV plot can aid in differentiating source area of samples with the same degree of weathering (Potter *et al.*, 2005).

In view of these ratios and the methods employed to calculate the proxies, it is important for CIA, ICV and CIA (molar) calculations to be carried out on samples that are preferably (i) not undergoing present day chemical or physical weathering processes or any other secondary alteration, (ii) clay- to silt-sized to minimise the effect of transportation and segregation of components and (iii) rocks with low carbonate content (< 30%). In the latter case, post-sampling removal of secondary carbonates is needed to ensure

that the CaO in the samples is primarily contained within silicate minerals (Goldberg and Humayun, 2010).

13.2 Methods

Please refer to Sampling and methodology chapter, p. 73. Samples presented here are grouped according to their distribution in the stratigraphy (LEF vs. UEF) in addition to their grain size. The latter has been broken into fine-grained sedimentary rocks ("Fines" under the facies code 'Fm') which constitute all mud rocks and siltstones, and the coarse-grained sedimentary clastics (under facies code 'Sm – Gcm') which includes all sandstone and conglomerates samples.

13.3 Results

13.3.1 **Clay mineralogy at Likhoele**

The XRD analysis of the clay fraction of the Likhoele samples show that the clay minerals are illite, montmorillonite, smectite group mixed layer clays (i.e., tosudite {chlorite-montmorillonite group}, rectorite {illite-montmorillonite group}) and mica (muscovite) (see Appendices Fig. A1). Illite was identified by its basal reflections at d-spacing of 10.04 and 4.95 Å. Strong quartz peaks were noted in all samples, including those of the clay separates. Goethite and hematite are also present in several specimens.

13.3.2 **1. Likhoele site (LIK)**

13.3.2.1 Major element geochemistry

Bulk geochemistry of major elements of 35 LIK samples from the Elliot Formation at Likhoele are provided in Table 13.1. These are presented as weight percentages, with mean and standard deviation values for the Elliot Formation, LEF and UEF and the fine- and coarse-grained samples therein (Table 13.1).

Table 13.1. Average weight percents (wt %) of major elements compositions and respective ratios of the Elliot Formation, the LEF and UEF and the fine- and coarse-grained rocks therein. Av. = average, Std. dev. = standard deviation, n = number of samples. Facies codes as per text (also see Figure 1.1).

	Elliot Formation (n = 35)		LEF (n = 10)		UEF (n = 25)		Coarse-grained (Sm-Gcm) (n = 12)		Fine-grained (Fm) (n = 23)	
	Av. (wt %)	Std. dev.	Av.	Std. dev.	Av.	Std. dev.	Av.	Std. dev.	Av.	Std. dev.
SiO_2	72.81	3.74	71.42	3.92	73.36	3.59	74.82	3.34	71.76	3.56
TiO_2	0.51	0.08	0.56	0.07	0.49	0.07	0.46	0.08	0.54	0.06
Al_2O_3	10.11	1.37	10.77	1.33	9.85	1.32	8.91	0.91	10.74	1.13
Fe_2O_3	2.40	0.66	2.65	0.58	2.30	0.67	1.76	0.37	2.73	0.51
MnO	0.08	0.06	0.07	0.05	0.09	0.07	0.11	0.09	0.07	0.04
MgO	1.17	0.20	1.21	0.19	1.16	0.20	0.99	0.11	1.27	0.16
CaO	2.53	2.22	2.56	3.20	2.52	1.77	3.30	2.76	2.13	1.81
Na_2O	2.24	0.30	2.15	0.32	2.27	0.29	2.15	0.30	2.28	0.29
K_2O	2.52	0.41	2.66	0.50	2.47	0.36	2.16	0.25	2.71	0.34
P_2O_5	0.04	0.02	0.04	0.02	0.03	0.02	0.03	0.02	0.04	0.02
SO_3	0.02	0.01	0.01	0.01	0.02	0.01	0.02	0.01	0.01	0.01
Cr_2O_3	0.01	0.00	0.01	0.00	0.01	0.00	0.01	0.00	0.01	0.00
NiO	0.00	0.00	0.01	0.00	0.00	0.00	0.00	0.00	0.01	0.00
LOI	3.93	1.44	4.15	2.05	3.85	1.16	3.97	1.74	3.91	1.30
Total	99.56	0.31	99.58	0.27	99.55	0.33	99.59	0.31	99.54	0.31
CIA	49.01	9.26	51.48	12.40	48.02	7.77	44.72	10.91	51.24	7.61
CIA(molar)	1.02	0.34	1.17	0.46	0.96	0.27	0.88	0.37	1.10	0.31
ICV	1.15	0.27	1.13	0.37	1.16	0.22	1.25	0.36	1.10	0.19
SiO_2/Al_2O_3	7.36	1.24	6.72	0.88	7.61	1.28	8.46	0.78	6.78	1.03
Fe_2O_3/Al_2O_3	0.23	0.04	0.24	0.03	0.23	0.04	0.20	0.03	0.25	0.03
$K2O/Al_2O_3$	0.25	0.02	0.25	0.02	0.25	0.02	0.24	0.02	0.25	0.02
$Al_2O_3/TiO2$	20.00	2.29	19.34	1.85	20.27	2.43	19.77	2.82	20.13	2.02
MgO/Al_2O_3	0.12	0.01	0.11	0.01	0.12	0.01	0.11	0.01	0.12	0.01
CaO/Al_2O_3	0.27	0.27	0.27	0.37	0.27	0.22	0.40	0.36	0.21	0.18
Na_2O/Al_2O_3	0.22	0.03	0.20	0.03	0.23	0.03	0.24	0.03	0.21	0.03
K_2O/Na_2O	1.14	0.23	1.25	0.28	1.10	0.19	1.02	0.17	1.21	0.23
Sc	4.08	1.40	5.30	1.28	3.53	1.08	3.07	1.08	4.69	1.22
V	40.03	10.86	47.23	13.42	36.76	7.83	35.63	11.22	42.68	10.00
Cr	27.20	6.66	33.11	7.58	24.52	4.09	24.08	7.01	29.08	5.83
Co	4.52	2.10	6.02	2.60	3.87	1.49	3.71	2.32	4.92	1.91
Ni	10.84	6.02	13.63	4.51	9.78	6.27	11.49	8.44	10.50	4.52
Cu	14.39	2.96	15.47	1.96	13.90	3.23	13.32	2.99	15.03	2.81
Zn	39.91	15.68	49.64	14.59	35.48	14.35	32.63	15.37	44.28	14.51
Ga	25.75	6.94	24.28	3.33	26.41	8.06	24.05	4.43	26.76	8.03
Rb	87.49	16.81	98.06	19.37	82.68	13.37	74.69	9.68	95.17	15.53
Sr	153.38	40.23	147.13	47.09	156.23	37.56	161.75	49.41	148.36	34.00
Y	19.66	4.56	25.22	2.11	17.13	2.72	17.55	4.09	20.93	4.44
Zr	182.55	33.37	202.97	12.27	173.27	35.92	179.39	45.27	184.45	24.90
Nb	9.68	1.54	10.99	1.51	9.09	1.16	8.56	1.28	10.36	1.28
Cs	5.16	1.79	6.62	1.94	4.50	1.28	3.71	0.74	6.04	1.66
Ba	536.87	273.71	459.83	104.90	571.88	319.00	517.16	142.13	548.69	331.88
La	28.96	4.49	32.94	3.32	27.15	3.75	27.88	5.36	29.60	3.89
Ce	57.29	12.64	69.57	8.73	51.70	9.94	52.66	14.36	60.06	10.95
Nd	26.54	4.36	30.77	2.96	24.62	3.46	25.44	5.26	27.21	3.71
Sm	5.05	0.91	5.97	0.58	4.64	0.69	4.79	1.07	5.21	0.78
Eu	0.88	0.14	1.03	0.10	0.82	0.10	0.85	0.17	0.91	0.12
Gd	4.15	0.88	5.14	0.53	3.71	0.59	3.87	0.99	4.32	0.79
Yb	2.09	0.42	2.56	0.19	1.87	0.29	1.88	0.38	2.21	0.40
Lu	0.31	0.06	0.37	0.03	0.28	0.04	0.28	0.05	0.32	0.06
Hf	5.11	0.98	5.63	0.40	4.87	1.07	5.00	1.39	5.17	0.65
Ta	0.74	0.12	0.83	0.16	0.70	0.07	0.67	0.10	0.78	0.12
Pb	15.86	2.53	18.02	2.51	14.88	1.87	14.90	2.97	16.44	2.09
Th	9.70	2.38	11.92	1.33	8.68	2.05	8.70	2.57	10.29	2.11
U	1.76	0.40	2.14	0.31	1.59	0.30	1.65	0.50	1.83	0.32
La/Sc	7.86	3.13	6.46	1.16	8.50	3.54	9.98	4.08	6.60	1.36
Sc/Th	0.42	0.11	0.44	0.07	0.42	0.12	0.37	0.12	0.46	0.08
Co/Th	0.45	0.16	0.48	0.19	0.43	0.14	0.39	0.15	0.48	0.16
Cr/Th	2.89	0.60	2.76	0.46	2.94	0.66	2.88	0.66	2.89	0.58
Th/U	5.55	1.03	5.63	0.72	5.51	1.16	5.36	1.24	5.66	0.90
La/Y	1.51	0.26	1.31	0.08	1.61	0.26	1.62	0.30	1.45	0.22
U/Th	0.19	0.03	0.18	0.02	0.19	0.04	0.20	0.04	0.18	0.03
V/Cr	1.48	0.25	1.42	0.19	1.51	0.27	1.50	0.34	1.47	0.18

At LIK, the concentration of the major oxides is very similar between samples from the LEF and UEF with only minor elevations of Al, Fe_2O_3 and K_2O (Table 13.1). The Elliot Formation has a mean SiO_2 of 72.8 wt %, with the average SiO_2 composition of the LEF relative to the UEF at 71.4 to 73.4 wt %, respectively. The variances of the two populations being equal as indicated by the F-test (F<Fcrit, 1.2<2.3; see Appendices Table A1).

Massive sandstones and mud-chip conglomerates of the coarse-grained fraction (Sm and Gmm facies) do not have meaningfully higher SiO_2 compositional values than the fine-grained samples (Fm) or the samples from the pedogenic horizons, but do show lower Al_2O_3 contents. For example, LIK 17, which is a mud-chip conglomerate, has 73 wt % SiO_2 and 8.3 wt % of Al_2O_3 versus LIK 2, a mudstone, that has 74 wt % SiO_2 and 11.3 wt % Al_2O_3 (Appendices Table A1). F-test suggests that the variances are not equal. The content of CaO is also enriched in the coarser fraction relative to the fines, variance being equal ($F \geq F_{crit}$). The Fe_2O_3 concentration is marginally higher in the fine grained (Fm) samples (2.7 wt %) relative to the coarse grained samples (Sm – Gcm) at 1.8 wt %. The same is true for the MgO, Na_2O and P_2O_5 are elevated in the fine grained samples over the coarse-grained samples (Table 13.1).

Co-variance of Al_2O_3 against major oxides is illustrated in Figure 13.1 for both the fine grained (Fm) and coarse grained (Sm- Gcm) samples for the entirety of the Elliot Formation sampled at LIK. Positive linear co-variance is established with Fe_2O_3, MgO, Na_2O and K_2O (Fig. 3 B, C, E and F) and Al_2O_3. There is a strong positive correlation between Al_2O_3 and Fe_2O_3, MgO and K_2O with correlation coefficients of 0.9. Al_2O_3 and Na_2O are only weakly correlated with a correlation coefficient of 0.3 (Fig. 13.1E).The major oxides SiO_2 and CaO show negative linear correlations of R^2 values of 0.19 and 0.24, respectively.

Figure 13.2 (A) shows major element abundances for the Elliot Formation compared with the upper continental crust (UCC) values reported by Rudnick and Gao (2003). For the average LEF and UEF, all major elements are depleted relative to the average UCC with the exception of SiO_2. The mean UCC-normalised values for coarse-grained samples show more substantial deficit in Fe_2O_3 and MgO relative to the UCC and fine-grained samples. The latter shows lower abundances of CaO and marginally increased abundances of TiO and Al_2O_3 relative to the averages for the LEF and UEF and the UCC. There is a moderate positive correlation between Al_2O_3 and TiO_2 (correlation coefficient 0.7). TiO_2 values for samples were low with an average of 0.51±0.08 in comparison to Post-Achaean average Australian shale (PAAS) values of 0.99. Weathering sensitive cations (K+ and Na+) are enriched with mean values of Na_2O in both the fine- (Fm) and coarse-grained (Sm- Gcm) samples of 2.25±0.3 wt % and slightly depleted in K_2O with average of 2.5 wt %, in comparison to the average value of PAAS 1.2 wt % and 3.7

wt %, respectively (Taylor and McLennan, 1985). In comparison to the PAAS, the coarser-grained sandstones and finer-grained samples are depleted in all major elements except SiO_2, CaO and Na_2O (Appendices Table A2).

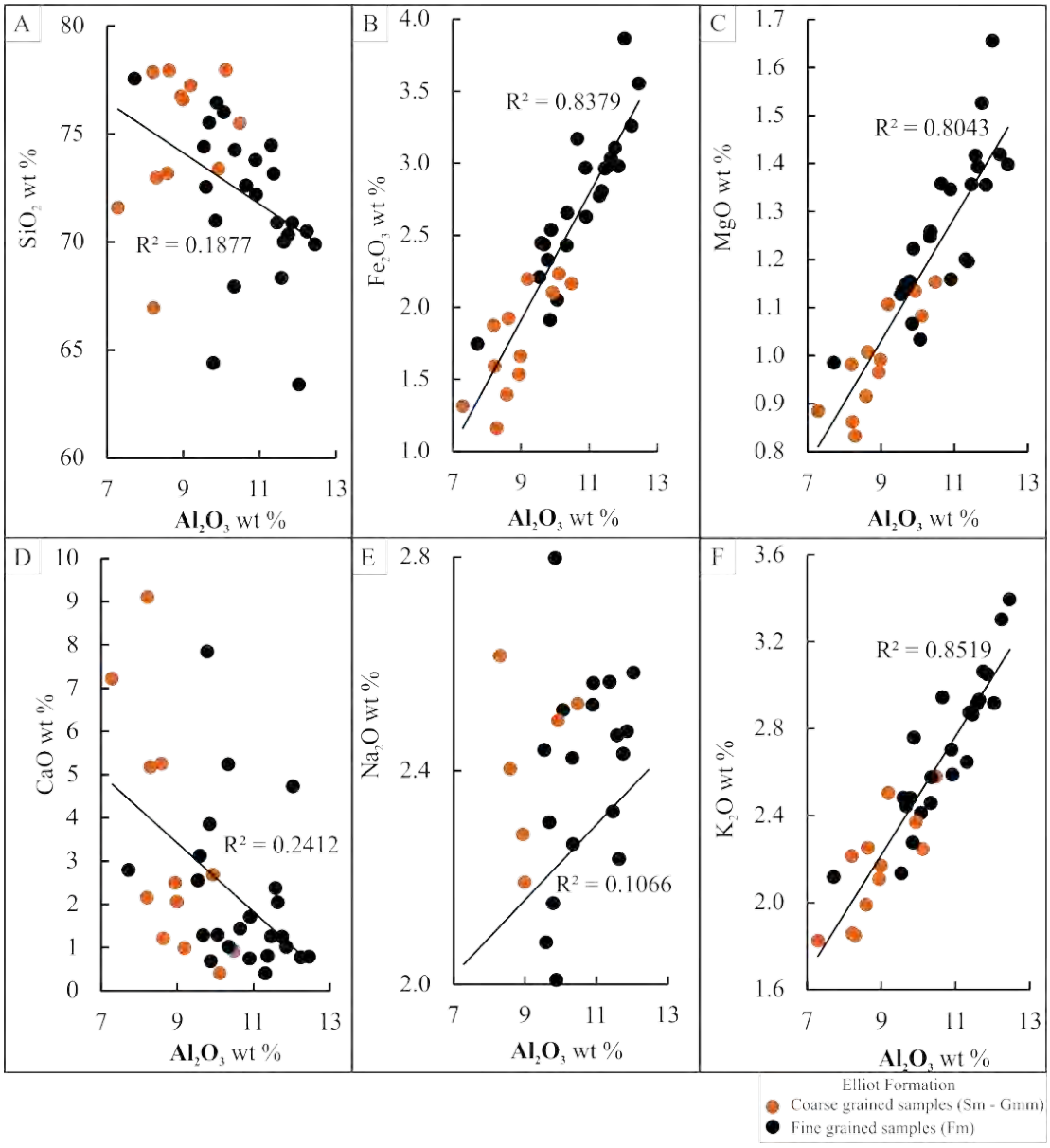

Figure 13.1. Major element distributions in the Elliot Formation at Likhoele. (A) SiO_2 (B) Fe_2O_3 (C) MgO (D) CaO (E) Na_2O and (F) K_2O plotted against Al_2O_3 in order to analyse co-variation. Orange circles indicate coarse clastics, black circles are fine clastics. Negative correlations between (A) SiO_2 and (D) CaO with Al_2O_3.

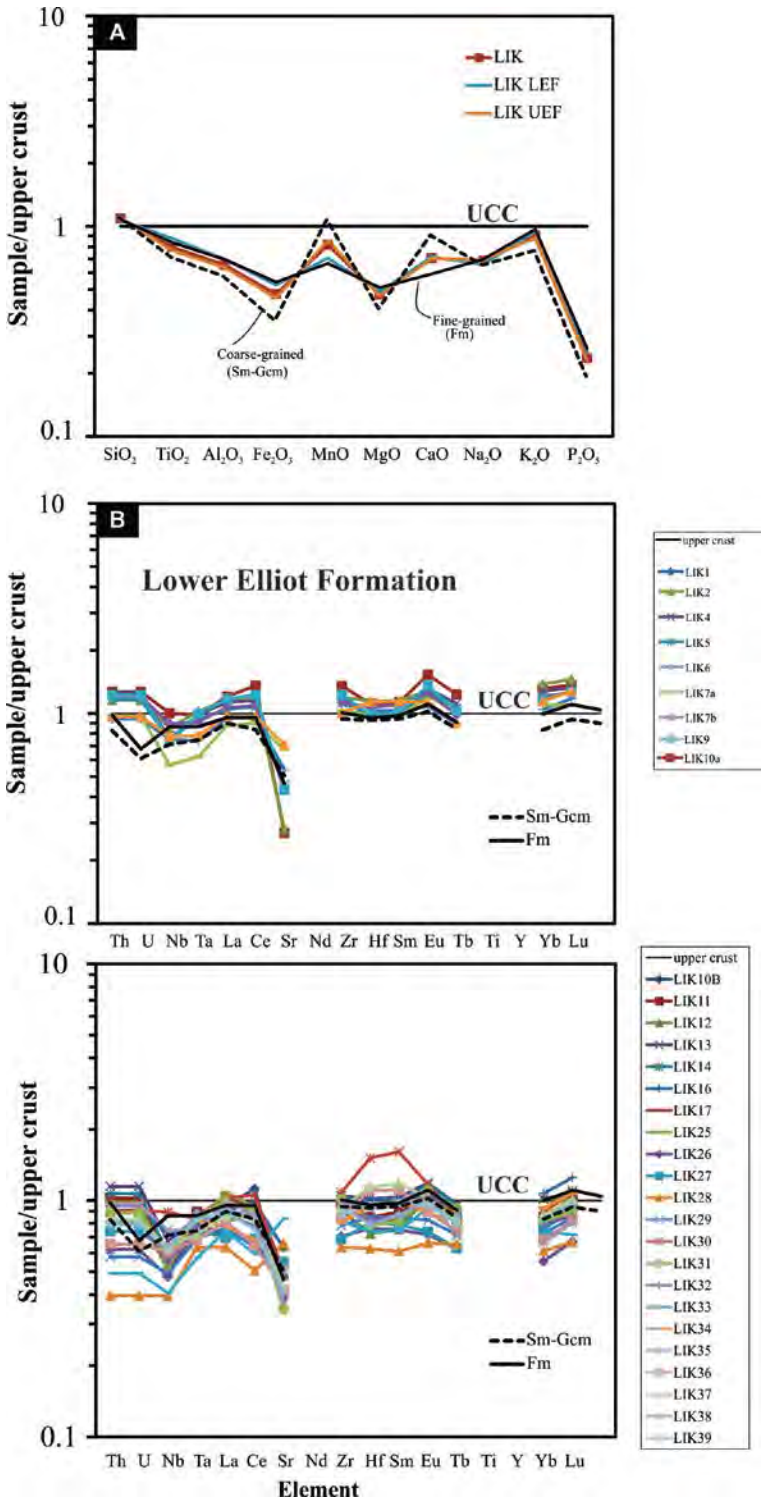

Figure 13.2. Upper crust-normalized (A) major and (B, C) trace element diagrams for LEF and UEF samples at Likhoele (LIK) main site. Data presented in Table 1 and appendices.

13.3.2.2 Trace and rare earth elements

Trace and rare earth element contents were analysed for 32 samples from the Likhoele section and are presented in Table 13.1 and normalised to the UCC as presented in Figure 13.2 B and C. Most trace and rare earth element concentrations fell below 100 ppm with the exceptions of Sr (86.4 – 268), Zr (143 – 215), and Ba (335 - 1884). Coarse-grained samples (sandstones, mud-chip conglomerates etc.) are depleted in trace elements in comparison to fine-grained samples (Fig. 13.2 B, C).

UCC-normalised trace and rare earth element diagrams (Fig. 13.2B, C) shows depletions in most elements, with several samples showing more significant depletions than others, e.g. UEF sample LIK28. High-field strength elements La, Ce, Nd, and Hf are enriched in several LEF and UEF samples (e.g., LIK 1, LIK2, LIK 30) with LEF samples showing higher abundances of Zr, Hf, Sm and Eu in comparison to the UCC and the UEF. Relative to the PAAS, the Elliot Formation samples showed significantly lower concentration of all trace elements with the exceptions of Sr (153 ppm relative to PAAS 200 ppm), Zr (183 ppm relative to PAAS 210 ppm), and Nb (9.7 ppm relative to PAAS 1.9 ppm).

Mean ratios of La/Sc, Sc/Th, Cr/Th and Co/Th in the coarse-grained samples are 9.98, 0.37, 2.76 and 0.39, respectively (Table 13.1). In contrast, fine-grained ratios of La/Sc, Sc/Th, Cr/Th and Th/Co are 6.59, 0.52, 2.88, and 0.477, respectively (Table 13.1). Lower La/Sc ratios are shown in UCC (2.21) and PAAS (2.81), with higher values for UCC Sc/Th (1.33), Cr/Th (8.76) and Co/Th (1.64) in comparison to the coarse- and fine-grained samples. Fine-grained samples have higher Sc/Th, Cr/Th and Co/Th but lower La/Sc ratios when compared to coarse-grained samples.

13.3.2.3 Major element ratios

Figure 13.3 shows stratigraphic variations of LIK major element ratios and the CIA and CIA (molar) values.

The entire Elliot Formation has a SiO_2/Al_2O_3 average of 7.4 with less variability in ratio for the samples LIK1 – 30 (samples below 27 m) versus LIK31 – 42. This sample grouping is illustrated in other ratio values (Fig. 13.3) for the degree of variability and compositional changes up profile. The average SiO_2/Al_2O_3 value for the LEF is 6.7 (variance $\sigma = 0.78$), and the average for the UEF of 7.6 (variance $\sigma = 1.65$).

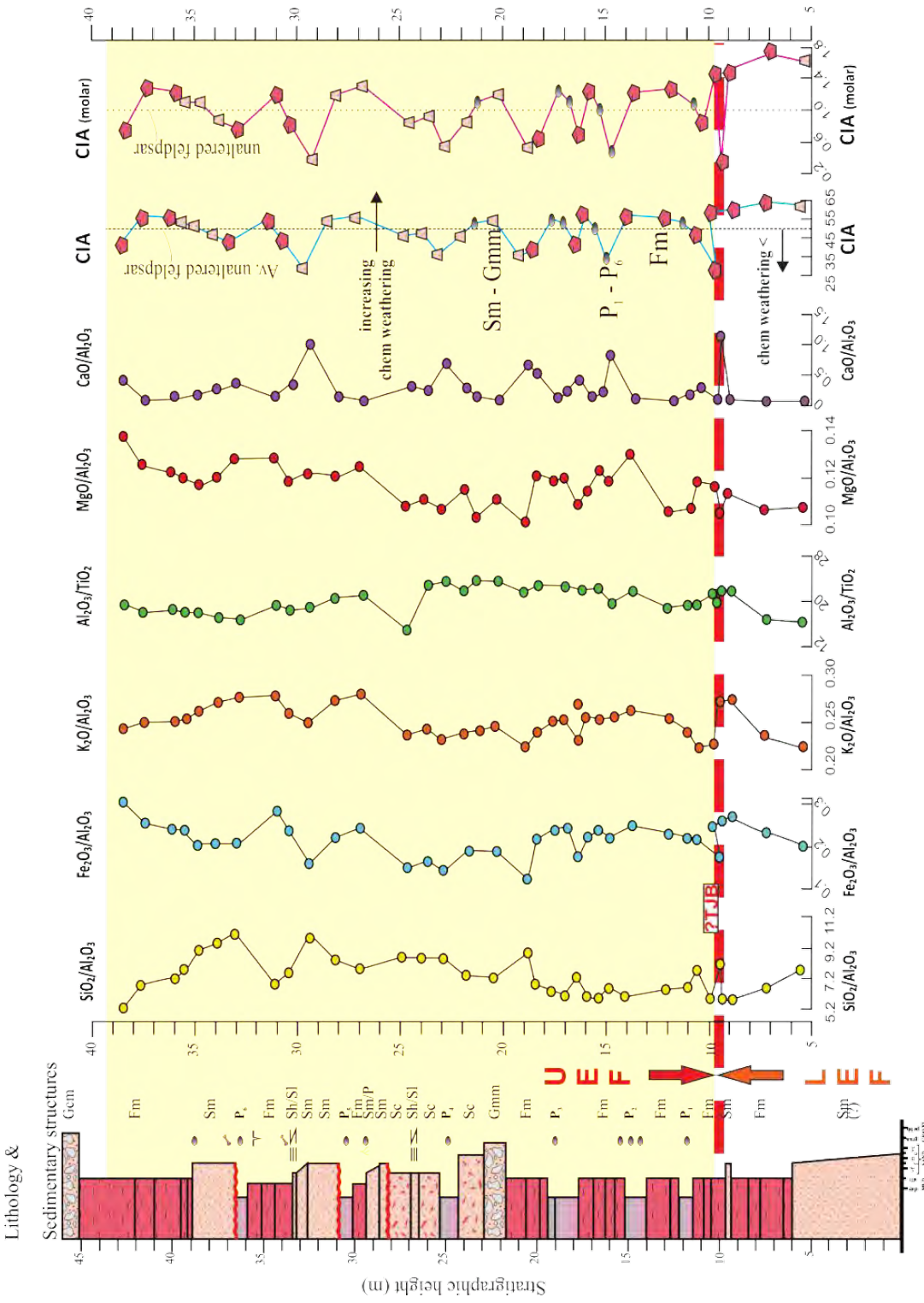

Figure 13.3. Likhoele major element ratios, CIA and CIA (molar) indices of chemical alteration. Red dashed line indicates the sedimentological contact between the LEF and UEF. Fm is used for mudstones and siltstones, Sm – Gm for coarse clastics (sandstones, mud-chip and pedogenic nodule conglomerates) and P1-P6 for palaeosol horizons, respectively. In the latter, pedogenic nodules and other palaeosol features (desiccation cracks, rhizocretions, etc.) were common.

Variation in the grouping of the LIK1 – 30 samples versus LIK31 – 42 for the ratio Al_2O_3/TiO_2 has a probability of p= 8.1 (T<=t; one tail; t-Test with equal variances). This is coincident with increasing Th values with decreasing stratigraphic height. The same is true for Ni which shows a linear decrease up profile (Appendices Table A1 - 3). The K_2O/Al_2O_3 ratio did not show a distinct grouping above or below 27 m and instead fell within the interval of 0.0 – 0.3 (0.25±0.013, n = 35). The CaO/ Al_2O_3 ratio fluctuates along the profile with several small excursions to higher Al values over CaO (Fig. 13.3).

Low compositional variability, and therefore geochemical grouping below and above 27 m, between the LIK1 – 30 and LIK31 – 42, does not occur over the sedimentological divide between the LEF and UEF. At the sedimentological break, there is a sudden increase in the ratio values of SiO_2/Al_2O_3, K_2O/Al_2O_3 CaO/Al_2O_3 and decrease in ratio values for Fe_2O_3/Al_2O_3 and MgO/Al_2O_3 as well as the CIA and CIA (molar) values (Fig. 13.3).

13.3.2.4 Weathering indices

Calculated CIA, CIA (molar) and ICV values are presented in Table 13.1 and Figures 13.4 and 13.5 for the Elliot Formation, LEF, UEF and fine- and coarse-grained samples.

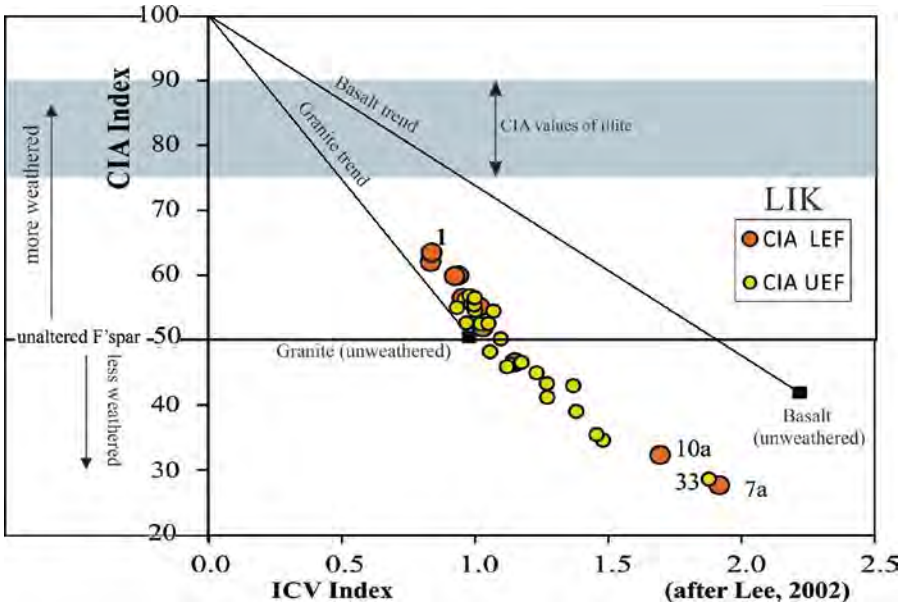

Figure 13.4. Plot of the ICV versus the CIA indices (after Lee, 2002) of the Likhoele (LIK) main site showing a fairly high degree of weathering parallel to the granite trend. UEF samples are presented in yellow, LEF samples are orange. Samples follow the unaltered granite trend. All LEF samples plot above the unaltered feldspar (F'spar) line with the exception of LIK 7a and 10a..

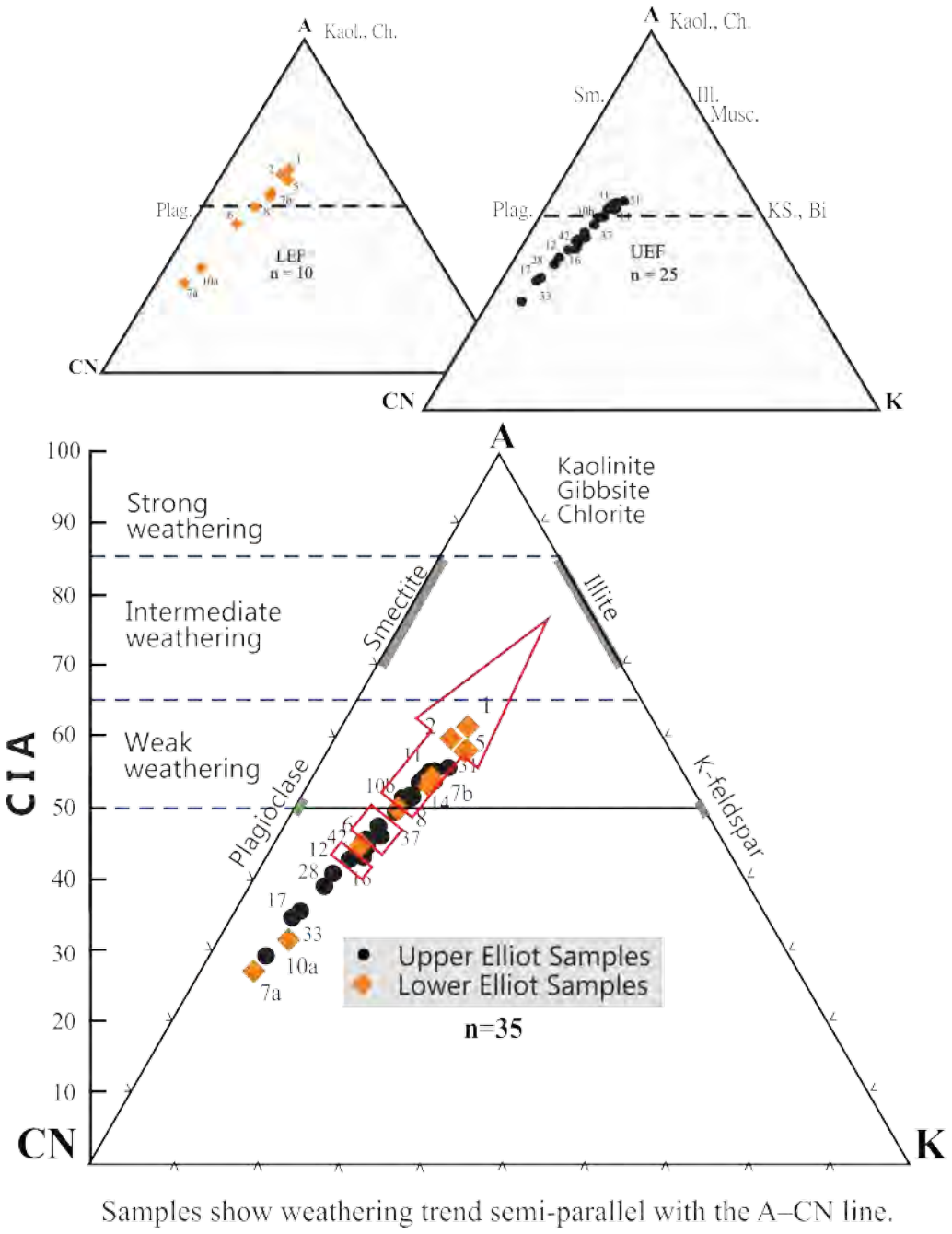

Figure 13.5. LIK A-CN-K ternary diagram indicate a weathering trend towards illite with the loss of Ca and Na elements. Samples from the LEF (orange circles) and UEF (black circles) are indicated with all samples grouping towards higher CIA values.

CIA values ranged between 28 (LIK7a) and 63 (LIK2), with mean of 49±9.3 falling below the line for unaltered feldspars (CIA = 50). CIA (molar) values ranged between 0.4 (LIK7a) and 1.7 (LIK2) with an

average value of 1.02±0.34 (Table 13.1). Fine-grained (Fm) samples have a higher CIA value (51.24) and CIA (molar) value (1.10) than the coarse-grained (Sm-Gcm) samples with values of 44.72 and 0.88, respectively.

ICV values have a range between 0.8 (very weathered) and 1.9 (least weathered) with a mean value 1.15±0.3 and with LEF samples having a low mean value (1.13) than UEF samples (1.16) (Table 13.1). Coarse-grained samples have a higher mean ICV value (1.25) than fine-grained samples (1.10). A linear trend is noted when plotting the ICV against the CIA for the LEF and UEF (Fig. 13.4) which is parallel to the granite trend. Two LEF and one UEF sample (LIK 7a, 10a and 33 respectively) have both high ICV but low CIA values.

CIA values presented in the Al_2O_3-($CaO+Na_2O$)-K_2O (A-CN-K) ternary plot illustrates a weathering trend almost parallel to the A-CN line, but trending towards illite/muscovite (Fig. 13.5). The samples plot away from plagioclase and K-feldspar tie and trend towards the apex (illite direction) reflecting higher proportion of clay minerals relative to fresh feldspar (Fig. 13.5).

13.4 Likhoele East site (LIKE)

13.4.1 **Major element geochemistry**

Major elements compositions from 33 Elliot Formation samples taken from Likhoele East (LIKE) are provided in Table 13.2 and are presented as weight percentages, with mean and standard deviation values.

At LIKE, the mean concentrations of LEF and UEF major oxides show only marginal differences between samples (Table 13.2). There appears to be a compositional change up profile with two geochemical groups. The first is samples LIKE 1 – 20 (below 19.4 m), which crosses the LEF-UEF sedimentology contact, and the second is between LIKE21 – 33 (Appendices Table A6).

SiO_2 compositional range within the LIKE samples is between 67.3 wt % and 83.7 wt % with an average of 74 wt %. This is higher than the Likhoele main site (LIK) were the range was narrower, between 63.4 wt % and 77.9 wt %. Massive sandstones (Sm - Gcm) have marginally higher mean SiO_2 compositional values than the massive mudstones (Fm) and pedogenic horizons (76.6 wt % to 72.8 wt %, respectively; Table 13.2). For example, LIKE 3, a LEF mudstone, has 72 wt % SiO_2 and 14 wt % Al_2O_3 versus LIKE 8,

a LEF horizontally laminated sandstone, that has 78 wt % SiO_2 and 10.3 wt % Al_2O_3 (Appendices Table A6).

Table 13.2. Average weight percent (wt %) of major elements compositions and respective ratios of the Elliot Formation, the LEF and UEF and the fine- and coarse-grained rocks therein at the Likhoele East site.

	Elliot Formation (n = 33)		LEF (n = 19)		UEF (n = 14)		Coarse-grained (Sm-Gcm) (n = 13)		Fine-grained (Fm) (n = 20)	
	Av. (wt %)	Std. dev.	Av.	Std. dev.	Av.	Std. dev.	Av.	Std. dev.	Av.	Std. dev.
SiO_2	74.17	4.26	72.38	2.16	76.60	5.21	76.15	5.50	72.88	2.64
TiO_2	0.60	0.09	0.65	0.04	0.53	0.08	0.56	0.10	0.62	0.06
Al_2O_3	12.10	2.20	13.29	0.96	10.48	2.40	11.32	2.74	12.61	1.65
Fe_2O_3	3.19	0.83	3.57	0.38	2.68	1.00	2.99	1.02	3.32	0.67
MnO	0.05	0.05	0.04	0.02	0.07	0.07	0.06	0.04	0.05	0.06
MgO	0.83	0.21	0.94	0.15	0.67	0.18	0.81	0.26	0.84	0.18
CaO	1.19	1.78	0.86	0.61	1.63	2.63	0.92	0.56	1.37	2.25
Na_2O	1.41	0.19	1.48	0.11	1.31	0.24	1.32	0.26	1.47	0.11
K_2O	2.63	0.55	2.92	0.25	2.24	0.60	2.46	0.70	2.74	0.41
P_2O_5	0.04	0.01	0.04	0.01	0.04	0.01	0.04	0.01	0.04	0.01
SO_3	0.02	0.04	0.01	0.02	0.03	0.06	0.02	0.02	0.02	0.05
Cr_2O_3	0.01	0.01	0.00	0.00	0.01	0.01	0.01	0.00	0.01	0.01
NiO	0.01	0.02	0.01	0.00	0.02	0.02	0.01	0.01	0.01	0.02
LOI	3.31	1.27	3.39	0.55	3.20	1.87	2.93	0.77	3.55	1.47
Total	99.56	0.26	99.60	0.25	99.51	0.28	99.59	0.23	99.54	0.29
CIA	62.89	8.23	65.08	3.54	59.92	11.52	63.26	4.43	62.65	10.07
CIA(molar)	1.78	0.40	1.89	0.25	1.63	0.52	1.76	0.32	1.79	0.45
ICV	0.77	0.24	0.72	0.05	0.84	0.35	0.74	0.06	0.79	0.30
SiO_2/Al_2O_3	6.45	1.72	5.48	0.62	7.76	1.88	7.24	2.05	5.94	1.28
Fe_2O_3/Al_2O_3	0.26	0.03	0.27	0.02	0.25	0.05	0.26	0.04	0.26	0.03
K_2O/Al_2O_3	0.22	0.01	0.22	0.01	0.21	0.01	0.22	0.01	0.22	0.01
Al_2O_3/TiO_2	20.12	2.12	20.39	0.91	19.76	3.10	20.10	3.00	20.14	1.37
MgO/Al_2O_3	0.07	0.01	0.07	0.01	0.06	0.01	0.07	0.01	0.07	0.01
CaO/Al_2O_3	0.12	0.23	0.07	0.05	0.19	0.35	0.09	0.05	0.14	0.30
Na_2O/Al_2O_3	0.12	0.02	0.11	0.01	0.13	0.03	0.12	0.03	0.12	0.02

The mean abundance of CaO is also enriched in the fine-grained (Fm) samples relative to the coarse-grained (Sm-Gcm) samples, variance being equal ($F \geq F_{crit}$). The Fe_2O_3 concentration is marginally higher in the fine grained (Fm) samples (3.3 wt %) relative to the coarse grained samples (Sm – Gcm) at 3.0 wt %. The same is true for the Na_2O, K_2O and P_2O_5 are elevated in the fine grained samples over the coarse-grained samples (Table 13.2).

Major element abundances are compared with the upper continental crust (UCC) values reported by Rudnick and Gao (2003) in Figure 13.6. All major element averages are depleted for the LEF and UEF relative to the average UCC with the exception of SiO_2 and marginally K_2O for the LEF. UEF samples are enriched in MnO and CaO relative to the LEF. LEF samples have higher mean TiO_2, Al_2O_3, Fe_2O_3, MgO and K_2O abundances compared to UEF samples (Fig. 13.6). The mean UCC-normalised values for coarse-grained samples show more substantial deficits in TiO_2, Al_2O_3, Fe_2O_3, CaO, Na_2O and K_2O relative to fine-grained samples (Fig. 13.6).

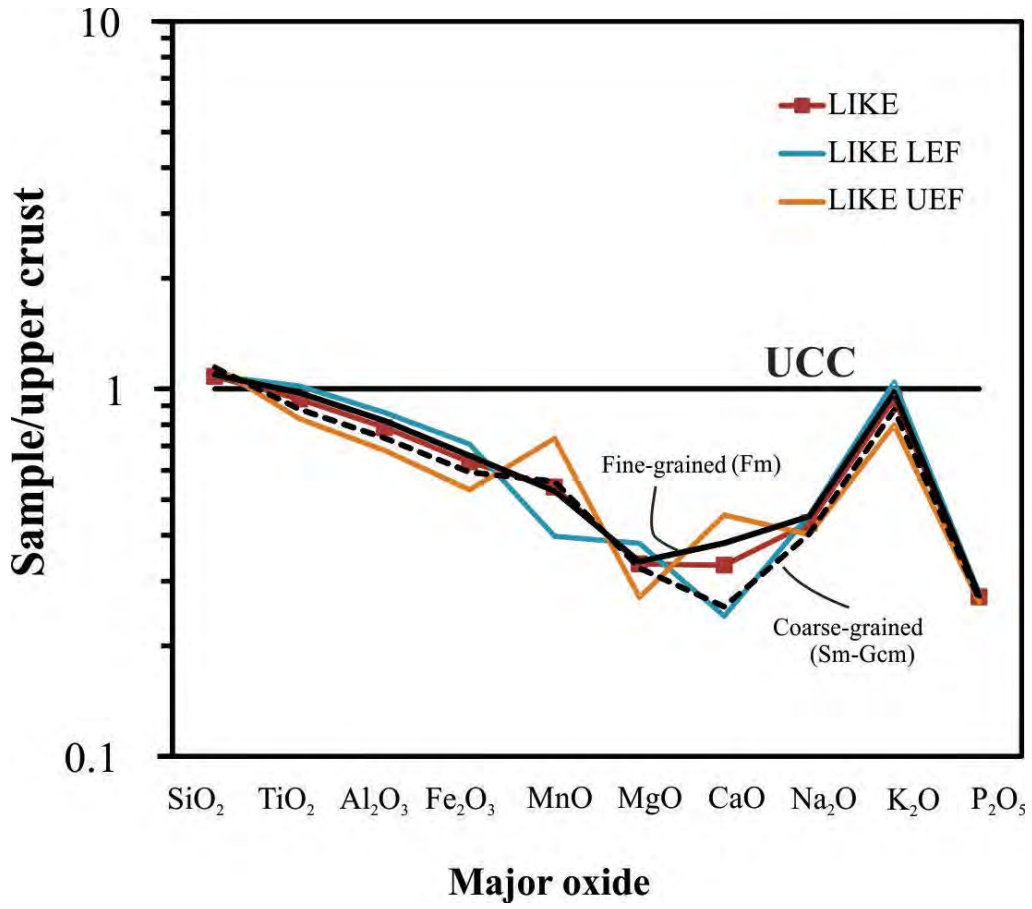

Figure 13.6. Upper crust-normalized major element diagram of the fine- and coarse-grained samples in the LEF, UEF and overall (combined: LIKE) samples at Likhoele East (LIKE) site. Data presented in Table 2 and appendices.

13.4.2 **Major element ratios**

Stratigraphic variation of LIKE major element ratios and the CIA and CIA (molar) values are presented in Figure 13.7. SiO_2/Al_2O_3 ratio shows little variation for the first 19 m up profile (LIKE1 – 20), with samples having an average value of 5.6±0.9. In contrast, LIKE 21 –33 (19.4 – 32.1 m) have an average SiO_2/Al_2O_3 ratio of 7.7±1.9 indicating a higher proportion of Si to Al with greater variability about the mean within this group. The average SiO_2/Al_2O_3 value for the LEF is 6.7 (variance $\sigma = 0.78$), and the average for the UEF of 7.6 (variance $\sigma = 1.65$).

The Fe_2O_3/Al_2O_3 ratio value decreases up profile with the highest values falling within the first 20 samples (LIKE1 – 20; av. 0.3); whereas the MgO/Al_2O_3 ratio remains constant up profile with little variation between previously grouped samples (Fig. 13.7). The same trend is repeated in the Al_2O_3:TiO_2 ratio as the first 20 samples, above 19.4 m, a higher proportion of Al to Ti (av. 20.4± 0.9) than the LIKE samples falling between 21 – 33 (av. 19.8± 3.1; Fig. 13.7).

The K_2O/Al_2O_3 ratio shows a greater degree of variability above 19.4 m. The CaO/Al_2O_3 is relatively consistent up profile with minor excursions being related to the presence of palaeosols (i.e., P2; Fig. 13.7) where LIKE 27 shows a marked increase in CaO relative to Al_2O_3 with CaO abundance at 10.3 wt % relative to the mean 1.2 wt %. The sample grouping above and below 19.4 m highlights compositional changes up profile which are broadly coincident with the sedimentological break between the LEF and UEF (Fig. 13.7).

13.4.2.1 Weathering indices

Calculated CIA, CIA (molar) and ICV values are presented in Table 13.2 for the fine- and coarse-grained samples of the Elliot Formation as well as LEF and UEF. CIA values ranged between 25 (LIKE27 {Fl} and due to proportion of secondary carbonate) and 69 (LIKE9 {Sm}), with mean of 62.8±8.2 falling above the line for unaltered feldspars (CIA = 50; Fig. 13.8). Calculated CIA (molar) values ranged from 2.2 (LIKE9) to 0.3 (LIKE27) with an average value of 1.8±0.4 (Table 13.2; Fig. 13.7). Coarse-grained (Sm-Gcm) samples have a higher CIA (63.26) and lower CIA (molar; 1.76) than the fine-grained (Fm) samples with a CIA of 62.65 and CIA (molar) value of 1.79.

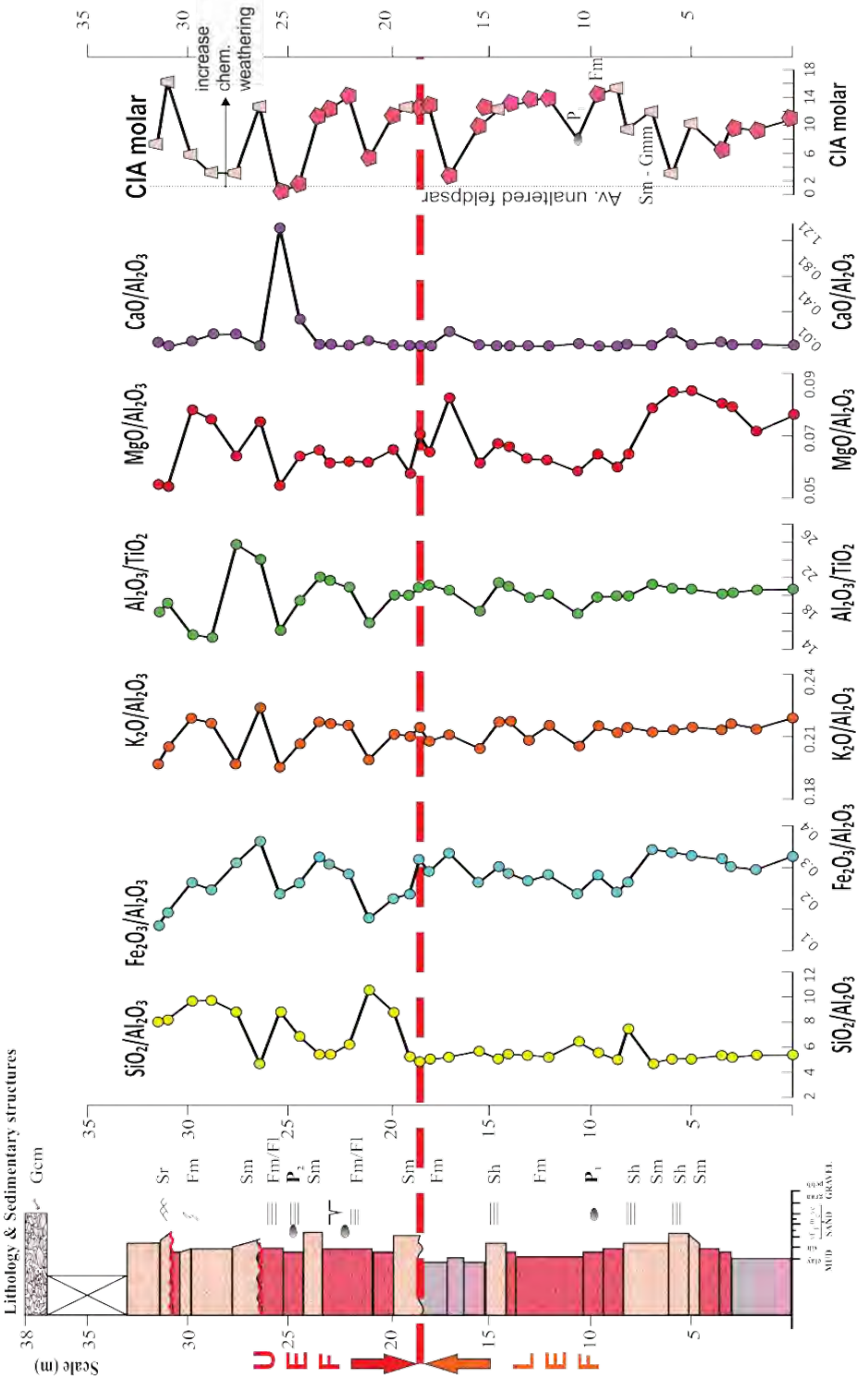

Figure 13.7. Likhoele East (LIKE) major element ratios, CIA and CIA (molar) indices of chemical alteration. Red dashed line indicates the sedimentological contact between the LEF and UEF. Fm is used for mudstones and siltstones, Sm – Gm for coarse clastics (sandstones, mud-chip and pedogenic nodule conglomerates) and P for palaeosol horizons, respectively. In the latter category, pedogenic nodules and other palaeosol features (desiccation cracks, rhizocretions, etc.) were common.

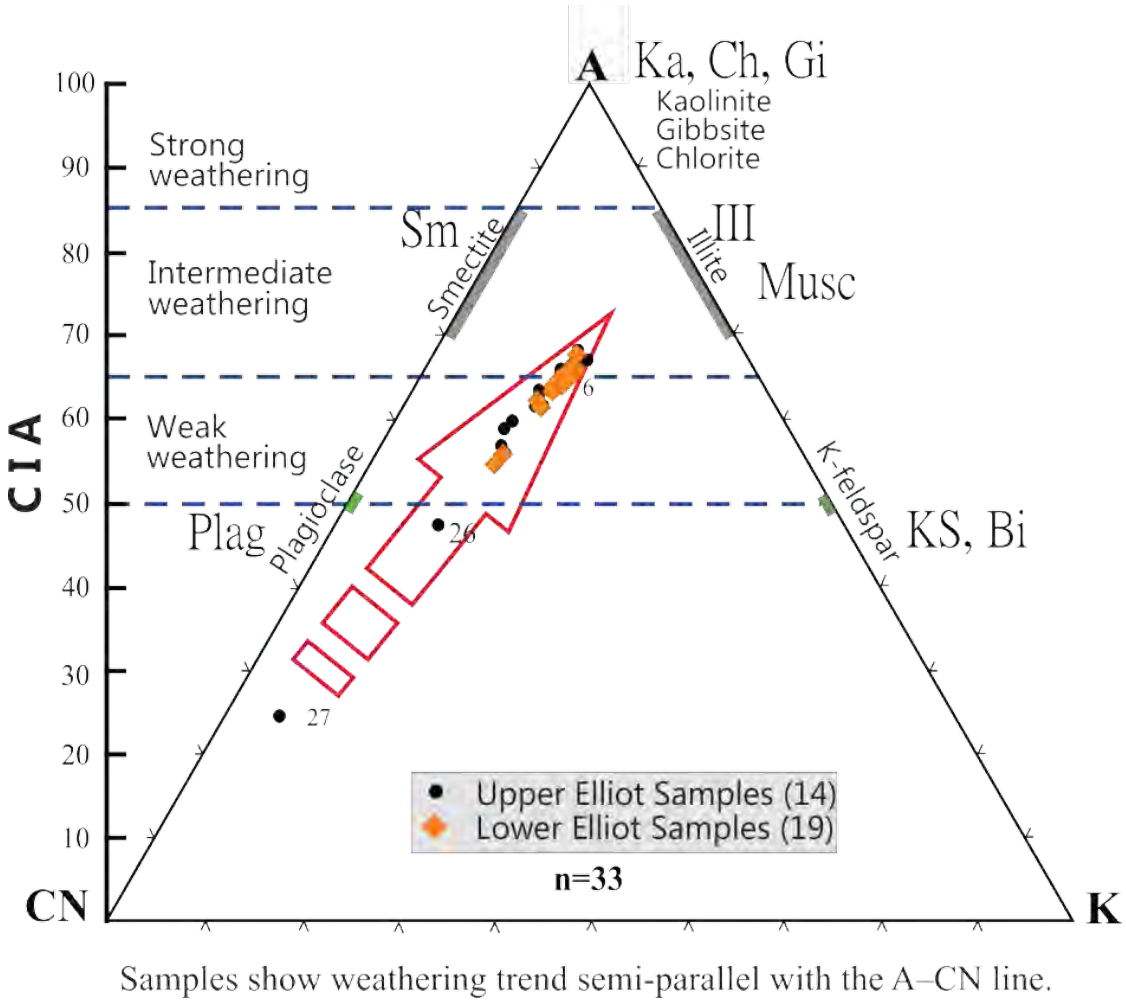

Figure 13.8. LIKE A-CN-K ternary diagram indicate a weathering trend towards illite with the loss of Ca and Na elements. Samples from the LEF (orange circles) and UEF (black circles) are indicated with all samples grouping towards higher CIA values.

CIA and CIA (molar) indices do not show any vertical trends up profile other than indicating less variability between samples below LIKE 19 (below 18 m) and increased variability between samples above 18 m (Fig. 13.7).

ICV values have a range between 0.7 (very weathered) and 2.0 (least weathered) with a mean value 0.77± 0.2 and with LEF samples having a low mean value (0.72) relative to UEF samples (0.84) (Table 13.2). Fine-grained samples have a higher mean ICV value (0.79) than coarse-grained samples (0.74). A linear trend is noted when plotting the ICV against the CIA values for the LEF and UEF (Fig. 13.9) which is

parallel to the granite trend. Two UEF sample (LIKE 27 and 26) have both high ICV but low CIA values (Fig. 13.8, Fig. 13.9).

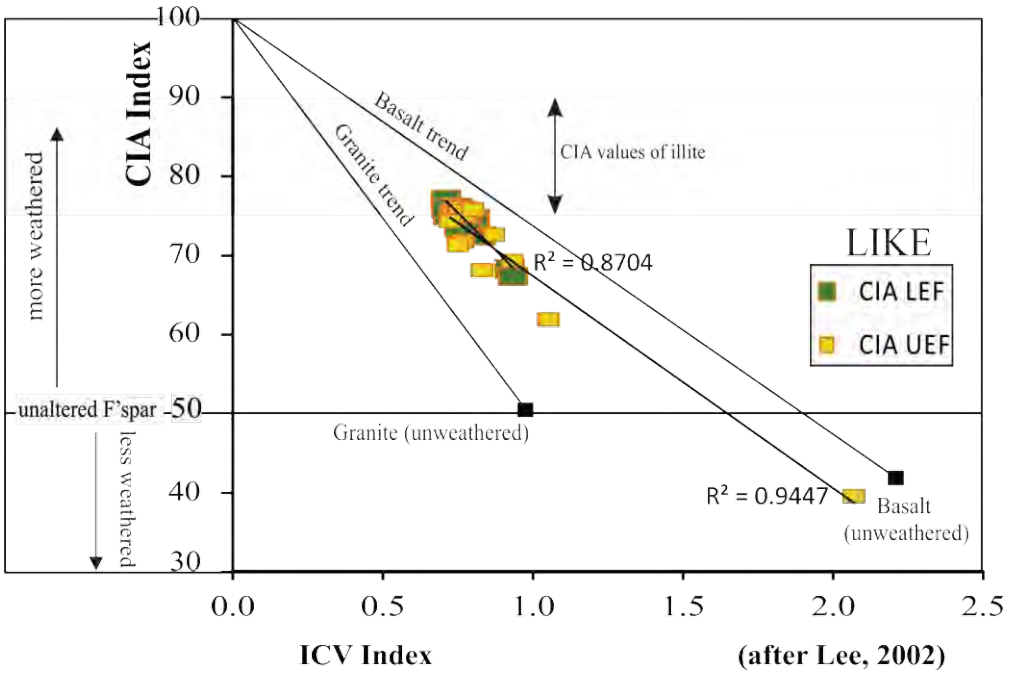

Figure 13.9. Plot of the ICV versus the CIA indices (after Lee, 2002) of the Likhoele East (LIKE) site showing a fairly high degree of weathering parallel to the granite trend (for LEF) and basalt trends (for UEF) A single outlier (LIKE 27) with low CIA value (36) illustrates the higher than average CaO content for that sample. LEF and UEF r^2 values are at 0.87 and 0.94, respectively. All other LEF and UEF samples plot above the unaltered F'spar (feldspar) line indicating weathering.

13.4.2.2 Summary of the geochemical results from the Likhoele sections

Elliot Formation major element compositions and derived ratios suggest that the fine- and coarse-grained rocks from the LEF and UEF at Likhoele (LIK) and Likhoele East (LIKE) are comparable (Fig. 13.10). Exceptions to this generally good correspondence are for the major elements MnO, MgO, CaO and Na2O which show a marked decrease in mean abundances in the LIKE section (Fig. 13.10). At both sections, there are two geochemical groupings based on increased variance of elements up section (Fig. 13.7). This compositional change is marginal and does not coincide with the sedimentological boundary between the LEF and UEF at either section. This compositional variability is ~11.5 m within the UEF at LIK and just above the sedimentological boundary between the LEF and UEF at LIKE (Fig. 13.7).

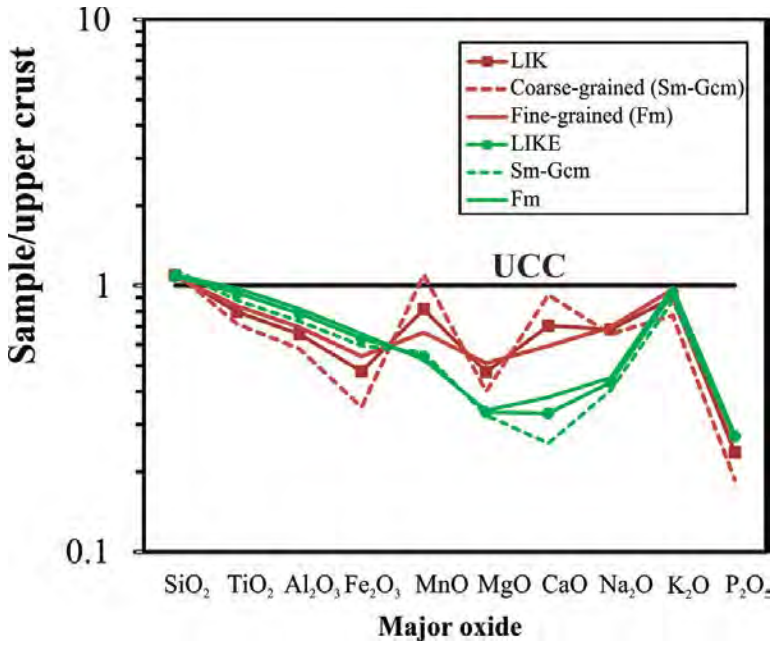

Figure 13.10. Upper crust-normalized major element diagram for Elliot Formation samples at Likhoele (LIK) and Likhoele East (LIKE). Data presented in Table 1, 2 and appendices.

Comparisons of weathering sensitive cations (Na^+ and K^+) at LIK and LIKE to the mean values of the PAAS and UCC show enrichment relative to PAAS, and depletion relative to UCC. For example, the mean LIK value for Na_2O in fine- and coarse-grained rocks (2.3 wt % and 2.15 wt %, respectively) is below the mean of the Formation (2.25 ± 0.3) with marginal depletion in K_2O (average of 2.5 wt %), in comparison to PAAS values of 1.2 wt % and 3.7 wt %, respectively (Taylor and McLennan, 1985). Considering the mean UCC values of 3.27 wt % and 2.8 wt % for Na_2O and K_2O, these values are depleted (Table 13.1). Ca, Na and K cations are most likely controlled by feldspars and their abundances relates to the degree of weathering. In general, higher abundances of the feldspars plagioclase and microcline are recorded in the UEF in the northern part of the basin (Bordy *et al*., 2004c). The differential weathering of these feldspars could be illustrated by the increased variability of CaO, Na_2O and K_2O values up section in addition to contributing to the broad geochemical groups reflected within the Elliot Formation at both LIK and LIKE.

At both sections, the fine-grained samples, in general, have higher Al_2O_3 contents in conjunction with Fe_2O_3, TiO_2, MgO, Na_2O and K_2O, in comparison to the coarser grained counterparts, and this is a function of mineralogy of the samples (Fig. 13.10). The presence of clay minerals (illite, montmorillonite, and smectite group clays) and the elements which make up these clays are likely to be reflected in higher

abundances in mudstones and siltstones as opposed to the sandstones. Contrastingly, increased abundances of CaO in the coarser fraction relative to the fines is more likely to be related to secondary calcite cement in the sandstones and conglomerates than related to primary mineralogy. Additionally, Fig. 13.1D shows that the CaO within the samples is negatively correlated to the presences of Al_2O_3 indicating that CaO is dissociated with silicates. The generally low concentrations of Fe_2O_3 and TiO_2 at both sections are a reflection on the low abundances of Ti-bearing minerals (biotite, ilmenite, and rutile) (Armstrong-Altrin *et al.*, 2004).

13.4.2.3 Weathering indices

The CIA and CIA (molar) values conform to an environmental warm-dry weathering regime with CIA (molar) between 0.4 and 2.2 (for both sites) and plot close to the feldspar line (average value of 1), and well below the illite line of 4 (Figs. 13.5, 13.8). Therefore, the CIA and CIA (molar) values for both sections indicate erosion from a relatively unweathered source under sub-humid and sub-arid climatic conditions. Similarly, ICV values reported for the LIK and LIKE sites show a large range and generally high values indicating little evidence for weathering. The presence of labile plagioclase and microcline, common in the sandstone thin sections of the Elliot Formation, further indicates that the sediment were accumulated under semi-arid, rather than humid conditions.

Samples analysed from LIK and LIKE illustrate that the fine-grained rocks, in general, have lower CIA values than coarse-grained samples with the exception of pedogenically altered samples where secondary CaO enrichment occurred. The CaO value, in the CIA index, was assumed to be CaO in the silicates and this is largely justified by the low CaO content (e.g., LIK av. 2.5±2.2 wt %; LIKE av. 1.2±1.8 wt %). Exception are three samples from the LIK section that fall above 5 wt %, namely fine-grained sandstone LIK07a (9.1 wt %), palaeosol siltstone LIK10a (7.8 wt %) and mudstone LIK16 (5.2 wt %), and sample #27 from LIKE (Fm). These samples are a likely reflection on interstitial carbonate cement, because carbonate was not present when tested with diluted HCl. Hence, the more reliable CIA (molar) index was then adopted to account for the presence of CaO which uses results more proportionally between alkalis and CaO and the Al_2O_3 (Goldberg and Humayun, 2010).

Furthermore, the subdivision of the Elliot Formation into two geochemical units, shown at both LIK and LIKE sites, based on the following ratios: K_2O vs. Al_2O_3, Al_2O_3/TiO_2, MgO/Al_2O_3 and Th/U is likely linked to the unroofing of some felsic igneous source rocks during the deposition of the UEF as explained in Bordy *et al.* (2004a, c). This shift in ratios is noted above 27 m and 19.4 m in the LIK and LIKE profiles, respectively, and occurs within the UEF (Figs. 13.3, 13.7).

Changes to the dominant source rock composition can be monitored by the Al_20_3/TiO_2 ratio (Nesbitt *et al*., 1997). LIK and LIKE profiles demonstrates a slight change in the dominant geochemistry above 27 m (LIK 31) and 19.4 m (LIKE20), respectively in most ratios with the variability in the Al_20_3/TiO_2 ratio more pronounced at the LIKE site above 19.4 m (Figure 13.7). The increased variability monitored by the major element ratios at LIK and LIKE is well within the UEF and just above the LEF-UEF, respectively (Figs. 13.3, 13.7).

The K2O/Al2O3 (Figs. 13.3, 13.7) is used to determine source rock composition with a clay minerals average of 0.0–0.3, and feldspars 0.3–0.9 (Cox *et al*., 1995). The LIK and LIKE K2O/Al2O3 ratio did not show a distinct grouping between samples above or below the 27 m and 19.4 m stratigraphic height markers, instead they all fell within the interval of 0.0–0.3 (LIK: 0.25±0.013, n = 35; LIKE:0.22±0.01, n = 33) for clay minerals. At both LIK and LIKE, the K2O/Al2O3 ratios are at the upper range of the clay mineral group suggesting that illite is a dominant mineral present. These results are further reflected in the A-CN-K diagrams (Figure 13.5, Figure **13.8**) and XRD analyses, and provide additional support for the inference that the climatic conditions during the deposition of the LEF and UEF were semi-arid.

13.5 Damplaats site (DAM)

13.5.1.1 Major element geochemistry

Bulk geochemistry of major elements, presented as weight percentages, with mean and standard deviation values, for 58 samples for the Elliot Formation at Damplaats (DAM) Farm is provided in Table 13.3 (see Table A9, A10).

At DAM, average SiO_2 composition of the LEF samples relative to the UEF is 77.4 ± 11.3 to 71.3 ± 11.5 wt %, respectively (F<Fcrit, 1.01<2.1; Table 13.3). The coarse-grained samples (Sm; sandstones) have slightly higher SiO_2 compositional values (78.9 wt %) than fine-grained samples (Fm; 72.3 wt %), and show lower Al_2O_3 contents (av. 8.5 wt % to 9.9 wt %, respectively). For instance, DAM 12 is a massive lower UEF sandstone with a SiO_2 content of 80 wt %, and Al_2O_3 content of 8.4 wt % whereas DAM 13, a lower UEF mudstone, has a lower SiO_2 content (74 wt %) but, in comparison to DAM 12, has a marginally higher Al_2O_3 content of 11.3 wt %.

The pedogenic carbonate nodule conglomerates (DAM46, 56 and 61) are a facies specific to the middle to upper UEF. Pedogenic nodule conglomerates (Gcm) have not been included with the coarse-grained

samples on account of their significantly lower SiO2 (36.5 wt %) and Al_2O_3 (5.5 wt %) and elevated CaO (28.9 wt %) values (Table 13.3). The Al_2O_3 content within these samples is also lower than the average for the Elliot Formation, and within the UEF, with a range of 5.3 – 5.9 wt % (Table 13.3). If the nodules are included in the coarse-grained population, the SiO_2 abundance drops to 69 wt %. The CaO content is marginally lower in the coarse-grained samples (av. 2.5 wt %) relative to the fine-grained samples (av. 4 wt %), variance being equal ($F \geq F_{crit}$).

Table 13.3. Average weight percent (wt %) of major elements compositions and respective ratios of the Elliot Formation, the LEF and UEF and the fine- and coarse-grained rocks therein at the Damplaats site.

	Elliot Formation (n = 58)		LEF (n = 9)		UEF (n = 49)		Coarse-grained (Sm) (n = 28)		Pedogenic nodule conglomerates (Gcm) (n = 3)		Fine-grained (Fm) (n = 27)	
	Av. (wt %)	Std. dev.	Av.	Std. dev.	Av.	Std. dev.	Av.	Std. dev.	Av.	Std. dev.	Av.	Std. dev.
SiO_2	72.26	11.49	77.42	10.62	71.31	11.39	78.91	6.61	36.48	1.72	72.26	11.49
TiO_2	0.48	0.13	0.53	0.13	0.47	0.13	0.45	0.12	0.33	0.02	0.48	0.13
Al_2O_3	9.88	3.05	9.15	1.73	10.01	3.21	8.54	1.96	5.49	0.33	9.88	3.05
Fe_2O_3	2.28	1.31	2.00	0.87	2.33	1.37	1.61	0.72	1.30	0.36	2.28	1.31
MnO	0.08	0.04	0.07	0.04	0.08	0.04	0.08	0.04	0.17	0.04	0.08	0.04
MgO	0.73	0.38	0.48	0.17	0.78	0.39	0.51	0.19	0.73	0.18	0.73	0.38
CaO	4.42	6.61	2.64	5.82	4.75	6.70	2.45	2.52	28.85	0.49	4.42	6.61
Na_2O	1.64	0.35	1.68	0.39	1.64	0.35	1.69	0.35	0.88	0.04	1.64	0.35
K_2O	2.14	0.78	1.75	0.49	2.22	0.80	1.70	0.50	1.23	0.03	2.14	0.78
P_2O_5	0.10	0.14	0.05	0.05	0.11	0.15	0.05	0.03	0.38	0.29	0.10	0.14
SO_3	0.01	0.01	0.01	0.01	0.01	0.02	0.01	0.02	0.04	0.00	0.01	0.01
Cr_2O_3	0.00	0.00	0.00	0.00	0.00	0.01	0.00	0.01	0.00	0.00	0.00	0.00
NiO	0.01	0.01	0.01	0.01	0.01	0.01	0.01	0.01	0.01	0.00	0.01	0.01
LOI	5.51	4.97	3.79	4.72	5.83	4.95	3.51	2.07	23.50	0.17	5.51	4.97
Total	99.55	0.30	99.58	0.27	99.55	0.31	99.53	0.29	99.39	0.36	99.55	0.30
CIA	48.84	15.24	56.49	14.00	47.44	15.04	51.35	10.89	9.03	0.38	48.84	15.24
CIA(molar)	1.10	0.51	1.44	0.46	1.04	0.50	1.15	0.44	0.10	0.00	1.10	0.51
ICV	1.27	1.19	0.97	0.73	1.32	1.25	0.93	0.34	5.98	0.22	1.27	1.19
SiO_2/Al_2O_3	8.07	3.12	8.73	1.95	7.95	3.28	9.90	3.27	6.68	0.69	8.07	3.12
Fe_2O_3/Al_2O_3	0.22	0.06	0.22	0.06	0.22	0.06	0.21	0.05	0.23	0.03	0.22	0.06
K_2O/Al_2O_3	0.21	0.02	0.19	0.02	0.22	0.02	0.20	0.02	0.23	0.02	0.21	0.02
Al_2O_3/TiO_2	20.86	3.86	17.83	2.62	21.42	3.79	19.45	4.06	16.49	2.02	20.86	3.86
MgO/Al_2O_3	0.07	0.02	0.05	0.01	0.08	0.02	0.06	0.01	0.13	0.02	0.07	0.02
CaO/Al_2O_3	0.60	1.17	0.32	0.73	0.65	1.23	0.28	0.32	5.27	0.23	0.60	1.17
Na_2O/Al_2O_3	0.18	0.05	0.19	0.05	0.17	0.05	0.20	0.04	0.16	0.02	0.18	0.05

Coarser-grained facies (with or without the pedogenic nodules samples) have lower Al_2O_3, Fe_2O_3, and CaO in comparison to finer grained samples. This is a reflection on (i) the mineralogy with these samples likely bearing lower concentrations/absence of Ti-bearing clay mineral phases such as ilmenite and (ii) the abundance of clay phases being lower in less mature rock units (cf. Armstrong-Altrin *et al*., 2004).

Co-variance of Al_2O_3 against major oxides is illustrated in Figure 13.11 for fine-, coarse-grained samples and the pedogenic nodule conglomerates.

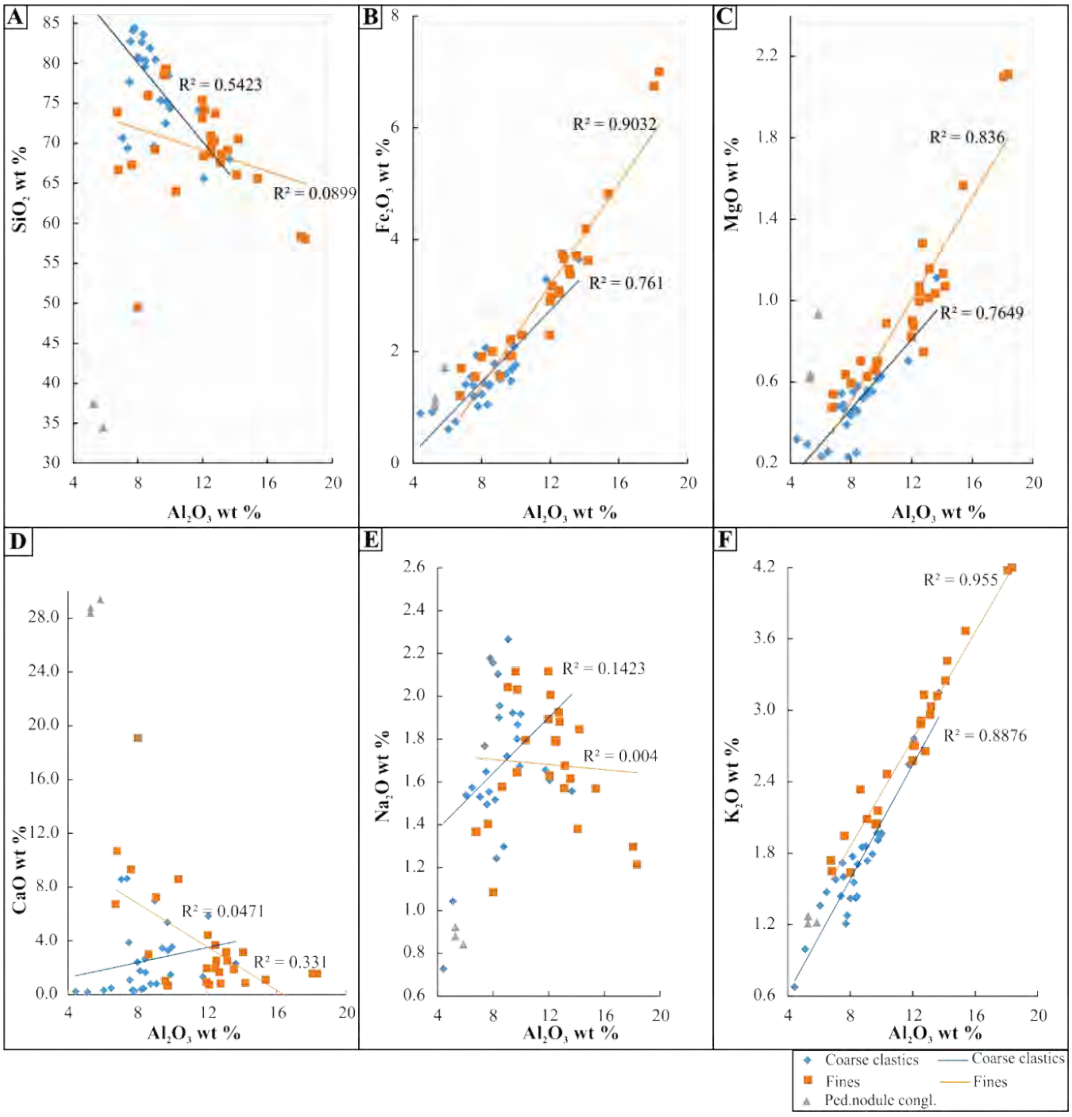

Figure 13.11. Major element distributions in the Elliot Formation at Damplaats (A) SiO_2 (B) Fe_2O_3 (C) MgO (D) CaO (E) Na_2O and (F) K_2O co-variation with Al_2O_3. Orange squares indicate fine clastics, blue circles are coarse clastics, and grey diamonds are the UEF pedogenic nodule conglomerates. Negative correlations of (A) SiO_2 (D) CaO and (E) Na_2O with Al_2O_3.

Positive linear co-variance is established with Fe_2O_3, MgO and K_2O (Fig. 12 B, C and F) and Al_2O_3 (with $R^2 \geq 0.75$). The SiO_2, CaO and Na_2O co-variance with Al_2O_3 displays negative linear relationships with low R^2 values less than 0.2. There is a strong positive correlation between Al_2O_3 and Fe_2O_3 for fine-

grained (Fm) clastics (R^2 = 0.91), and less so for coarse-grained clastics (R^2 = 0.75). This is also expressed in the relationship between MgO and K_2O with fine-grained samples having a stronger correlation to Al_2O_3 than the coarse-grained clastics (Fig. 13.11). There is a moderate positive correlation between Al_2O_3 and TiO_2 (correlation coefficient 0.7). TiO_2 values for samples were low with an average of 0.51 in comparison to PAAS values of 0.99 (Taylor and McLennan, 1985). In comparison to PAAS, the DAM samples are enriched in SiO_2, CaO and marginally in Na_2O, and depleted in Al_2O_3.

Figure 13.12 shows major element abundances compared with the upper continental crust (UCC) values reported by Rudnick and Gao (2003) for the Elliot Formation. For the average LEF and UEF all major elements are depleted relative to the average UCC with the exception of SiO_2 (Fig. 13.12). The mean UCC-normalised values for coarse-grained samples show more substantial deficit in TiO_2, Al_2O_3, Fe_2O_3, MgO, CaO and K_2O relative to the UCC and fine-grained samples. The latter shows elevated abundances of CaO in comparison to the UCC, and marginally increased abundances of TiO_2, Al_2O_3, and Fe_2O_3, relative to the averages of the LEF with values still comparable to UEF (Fig. 13.12). Pedogenic nodule conglomerates show elevated abundances of MnO, CaO and P_2O_5 relative to UCC and the other UEF and LEF samples (Fig. 13.12). These samples also show depletions in SiO_2, TiO_2, Al_2O_3, Fe_2O_3, Na_2O and K_2O in comparison to all other samples.

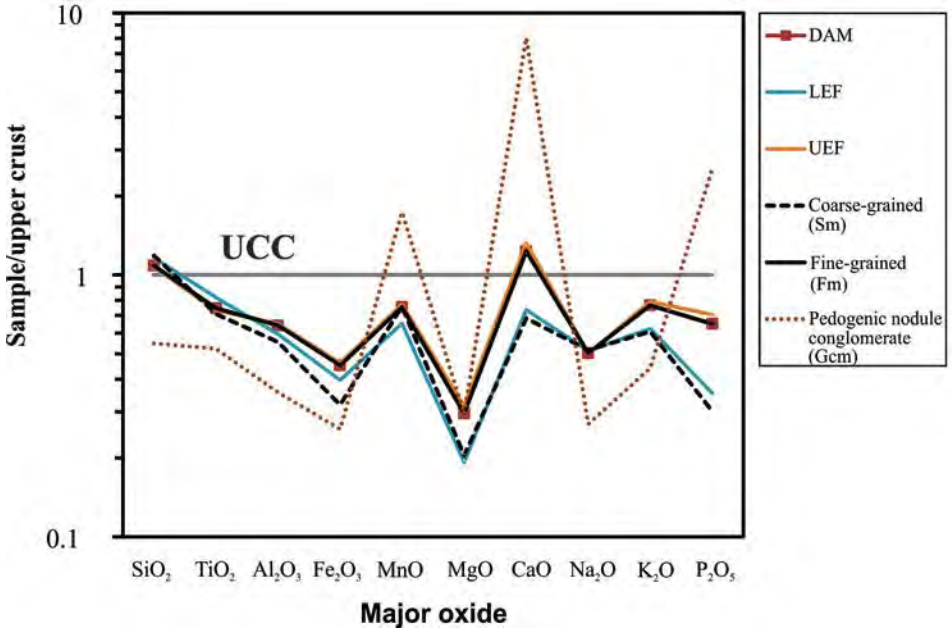

Figure 13.12. Upper continental crust-normalized major element diagram for Elliot samples at Damplaats (DAM) site. Data presented in Table 3 and appendices.

13.5.1.2 Major element ratios

The major element ratios plotted in Figure 13.13, $SiO_2/Al2O_3$, K_2O /Al_2O_3, Al_2O_3/TiO_2, MgO/Al_2O_3 and CaO_2/Al_2O_3, illustrate compositional variability with increasing stratigraphic height. Compositional variability is higher in the UEF in comparison to the LEF, largely as a function of a larger sampling interval. Akarish and El-Gohary (2011) have illustrated that the use of the SiO_2/Al_2O_3 ratio can express the degree of sedimentary maturation (transport and recycling), with higher values a function of increased quartz relative to less resistant lithic fragments and feldspar. At Damplaats, the Elliot Formation ratio of SiO_2 to Al_2O_3 has an average of 8.1±3.1, with the average for the LEF (DAM1-9) at 8.7 being nominally higher than the average of the UEF (7.8; Fig. 13.13).

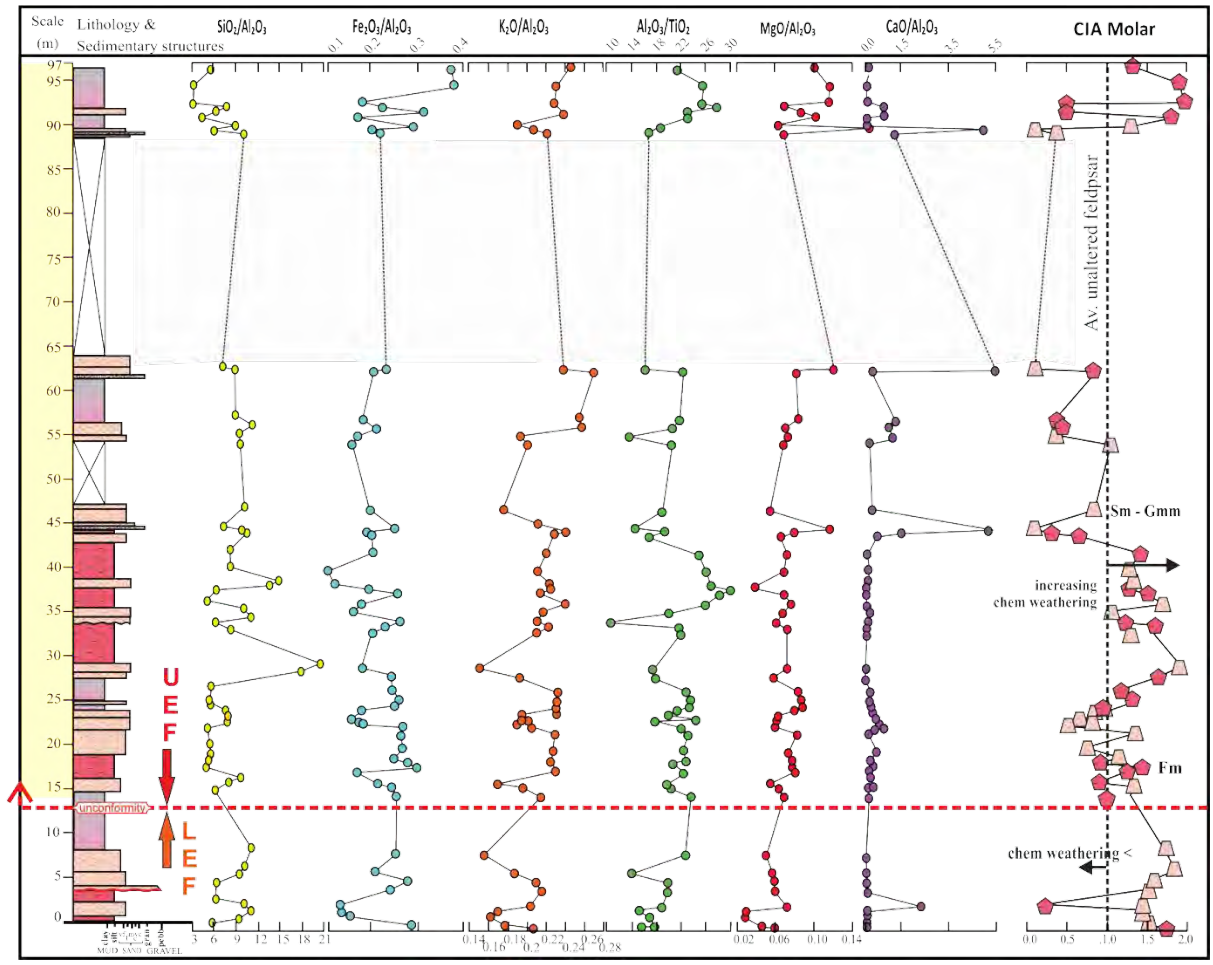

Figure 13.13. Damplaats major element ratios and CIA (molar) index. Red dashed line indicates the sedimentological contact between the LEF and UEF. Fm is used for mudstones and siltstones, Sm – Gm for coarse clastics (sandstones, mud-chip and pedogenic nodule conglomerates).

The maturity of samples in the LEF is comparable to that of the UEF samples. High variability is noted in the K_2O vs. Al_2O_3 and Al_2O_3 vs. TiO_2 ratios, with no strict group by grain size, and with the marginal increase in the Al_2O_3 vs. TiO_2 values over the fine-grained (Fm) intervals (e.g. between ~30 – 40 m). The DAM K_2O/Al_2O_3 ratio did not show a distinct grouping between samples and had an average value of 0.2±0.02. The otherwise low and consistent values for the MgO/Al_2O_3 and CaO/Al_2O_3 ratios is punctuated by the exceptionally high CaO and elevated MgO content of carbonate nodule conglomerate samples. The Elliot Formation at Damplaats could not be subdivided into geochemical units because there was no apparent subdivision in the geochemical indices up profile.

13.5.1.3 Weathering indices

Calculated CIA, CIA (molar) and ICV values are presented in Table 13.3 for the fine- and coarse-grained samples of Elliot Formation, LEF, UEF at the DAM site. CIA values of the Elliot Formation ranged between 8.8 (DAM56; carbonate nodule conglomerate) to 17.3 (DAM5; mudstone), 65.1 (DAM8; ripple cross-laminated sandstone) and 66.2 (DAM66; mudstone), with the average value being 48.8. CIA molar values were also calculated and ranged between 0.1 (DAM 61) and 2.0 (DAM 66) with an average value of 1.1 ± 0.5.

DAM samples show low but variable ICV values with a range from 0.7 to 6.2 (av. 1.3± 1.2). Lower ICV values correspond with increasing weathering with the least weathered samples showing a larger value. Samples DAM 56 (6.2), DAM 46 (6.1), DAM 61 (5.7), DAM 5 (3) and DAM 45 (2.3) show the highest ICV values (least degree of weathering).

Weathering sensitive cations (K^+ and Na^+) are enriched with average values of Na_2O in fine- and coarse-grained samples are 1.7, 1.6 and 0.9 wt %, respectively and in comparison to the 1.2 wt % value of the Post-Achaean average Australian shale (PAAS). Reductions in K_2O is noticeable in the coarse clastics grouping (1.7 wt %) and carbonate nodule conglomerates (1.2 wt %) when compared to the fine-grained samples (2.6 wt %), and both relative to the average value of PAAS at 3.7 wt % (Taylor and McLennan, 1985).

A-CN-K ternary plot (Fig. 13.14) illustrates little to no chemical weathering, with a weathering trend running closely to the A-CN line, and trending towards illite/muscovite. The DAM samples plot away from plagioclase and K-feldspar tie line and trend towards the apex (illite direction) reflecting higher proportion of clay minerals relative to fresh feldspar (Fig. 13.14).

13.5.1.4 Summary of the geochemical results from the Damplaats section

The CIA values in the samples collected at Damplaats range from 8.8 to 66.2, with an average of 48.8 corresponding to warm-dry conditions typical of unweathered to slightly weathered detritus (Bahlburg & Dobrzinski, 2011). In comparison, the CIA (molar) values, which take into account CaO, range between 0.1 and 2.0, and an average of 1.1. These values plot close to the feldspar line (average value of 1) and well below the illite line.

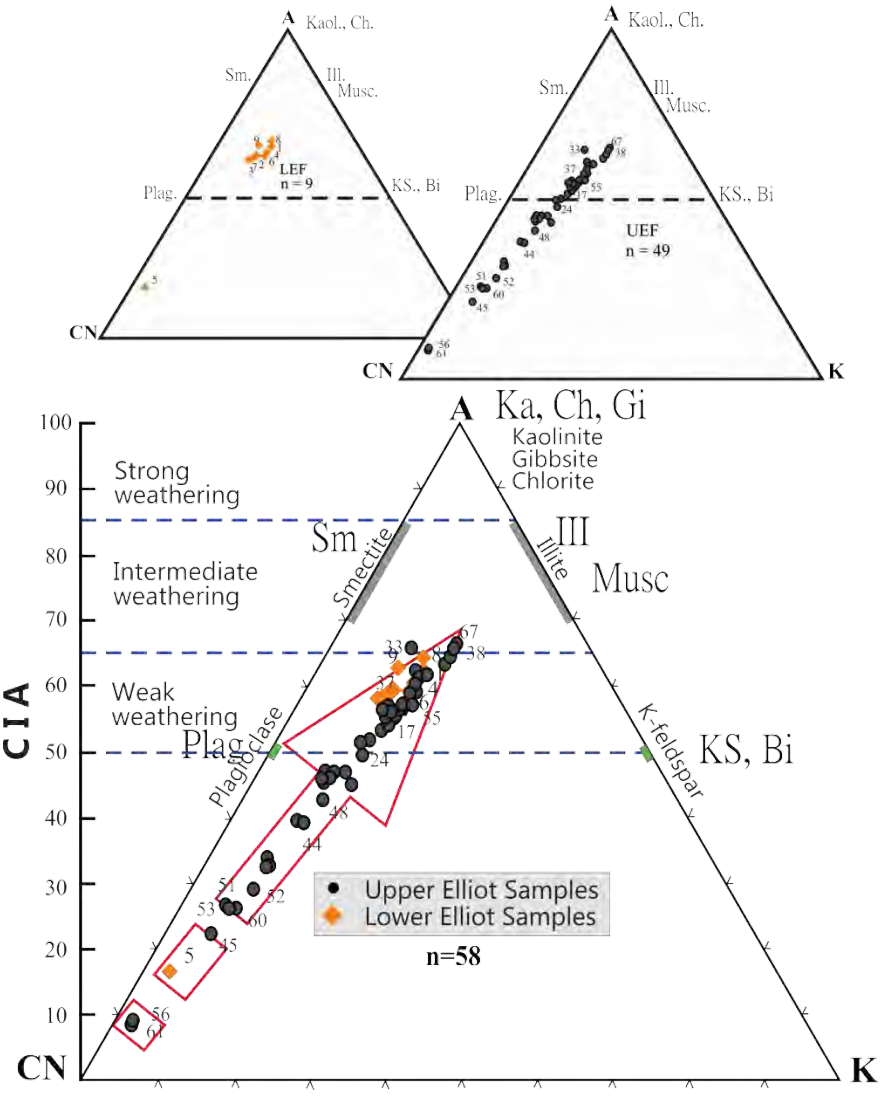

Figure 13.14. DAM A-CN-K ternary diagram indicate a weathering trend towards illite with the loss of Ca and Na elements. Samples from the LEF (orange circles) and UEF (black circles) are indicated with all samples grouping towards higher CIA values.

As with the Likhoele sites, CaO values in the samples from Damplaats, used in the CIA index, were assumed to be contained within silicates (feldspars), and not carbonate hosted. This assumption was reasonable because the CaO content was low (range < 10 wt %, with an average 4.8 wt %). Exceptions were noted where samples CaO values were significantly higher than the average value, i.e. DAM61 (29.3 wt %), 56 (28.7 wt %), 46 (28.4 wt %), 5 (19 wt %), 45 (10.7 wt %). DAM 61, 56 and 46 are carbonate nodule conglomerate, where the main clast is a reworked carbonate nodule (of pedogenic origin) and hence add significantly to the CaO value of the rock. In comparison DAM 5 and 45 are both fine-grained samples (mudstones/siltstones; Fm) in close proximity to a palaeosol horizon bearing pedogenic nodules. It is probable that the section where these samples were taken contain pervasive carbonate cement related to pedogenic overprinting. The negative correlation between CaO and Al2O3 (Fig. 13.11D) in the mudstones indicates that the CaO is relatable to either (i) clay fraction or (ii) carbonate cement and not silicates. Lower CIA values are otherwise shown to be within the coarse-grained sandstone samples. Higher CIA and CIA (molar) values were seen in the clay- and silt-dominated rocks. The generally low and variable values of the CIA, CIA (molar) and ICV indicate an arid climate where physical weathering is expected to dominate over chemical weathering.

13.6 Discussion

13.6.1.1 Clay minerals

The XRD results illustrate that the production of illite-smectite mixed layer clays, relatively immature weathering by-products, and are considered to be the likeliest weathering products formed under arid conditions (cf. McKinley *et al*., 2003). Smectite clays, specifically montmorillonite, result from the weathering of plagioclase and alkali feldspars (McKinley *et al*., 2003). During prolonged chemical and physical weathering, the process of smectite converting to illite can be effected (Nadeau *et al*., 1985).

13.6.1.2 Major and trace element geochemistry

The composition of the sedimentary rocks of the Elliot Formation is largely controlled by their provenance (basement rock in source area) and the *in situ* and intensity of weathering of sediments during deposition. This in turn can be altered by the downstream sorting and diagenesis (McLennan, 1989, 2001).

Elliot Formation major element compositions and derived ratios suggest that the fine- and coarse-grained rocks from the LEF and UEF at Likhoele, Likhoele East and Damplaats are comparable, and suggest similar (i) protolith and (ii) prevalent palaeoclimate resulting in moderate weathering conditions. The former point (i.e., provenance of the Formation) is already discussed in some detailed in Bordy *et al.* (2004c) where two sets of palaeocurrent directions indicate that the LEF is sourced from the north, with a shift during UEF times to a source in an east-north-easterly direction.

For all three sites, high SiO_2 abundance (LIK: 72.8 wt %, LIKE: 74 wt %, DAM: 72.3 wt %) are higher than the values reported for PAAS (62.4 wt %) and UCC (66.6 wt %; Figure 13.15A). Quartz dilution (i.e., masking effect by high quartz content) is therefore a likely problem in recognising the true abundances of other elements (McLennan, 1989; Kasanzu *et al*., 2008). Furthermore, a measure sandstone immaturity is through the percentage of SiO_2 within a sample. For example, at DAM the LEF is relatively more immature than the UEF (Table 13.3; Appendices Table A9, A10). This is in line with previous petrological work on the mineralogy of the sandstones in the Elliot Formation that shows that the LEF is dominated by sublitharenites, whereas the UEF contains more subarkoses (Bordy *et al*., 2004c).

For the three sites, there is a positive linear co-variance of Al_2O_3 with several major oxides (Fe_2O_3, MgO, Na_2O and K_2O) which indicate that these are likely associated with clay minerals or aluminosilicates and are derived from silicates (Jin *et al*., 2006). This also reflects on the little chemical weathering affecting the LEF and UEF.

In general, the mudstones and siltstones have lower SiO_2 with higher Al_2O_3, Fe_2O_3, CaO and K_2O contents in comparison to the coarser grained counterparts. A probable explanation for this rests on the function of mineralogy with Al_2O_3, Fe_2O_3, and K_2O being sequestered into clay mineral fraction. XRD analyses (e.g., Likhoele site) shows that the presence of the clay minerals illite, montmorrillonite, and smectite group clays. Elements important in the building of these mixed layer clays are more likely to be found in the fine-grained rocks, as a function of weathering and transportation and their subsequent (moderately) higher degree of maturity. However, at DAM SiO_2, CaO and Na2O co-variance with Al2O3 displays negative linear relationships with low R^2 values less than 0.2 (Fig. 13.11). According to Jin *et al.* (2006), this could indicate that the aluminosilicates and clay minerals are not the sole residence of these oxides. These may be retained in micaceous minerals and/or secondary carbonates,

To indicate the sedimentary processes that have affected mineral abundances a plot of Zr/Sc versus Th/Sc (Fig. 13.15C) illustrates the heavy mineral accumulation (by Zr enrichment) relative to Th (McLennan *et al*., 1993). Sources that are mature/recycled have Th/Sc ratios > 0.8 and higher Zr/Sc (Fig. 13.15C). This

confirms sediment recycling in the source region (McLennan *et al*., 1993) for Likhoele samples and complements the previous assertion of recycled-orogen and transitional continental sources (Bordy *et al*., 2004c). Ratios between the low Cr/V and low and variable Y/Ni for Likhoele indicate that the source area was predominately felsic although several samples (i.e. mudstones LIK12, LIK35 and sandstone LIK33; appendices Table A) indicate a more mafic provenance. Furthermore, the ratios of La/Sc, Th/Sc, Cr/Th, Th/Co (Table 13.1) indicate a felsic source.

13.6.1.3 Major element ratios

SiO_2/Al_2O_3 ratio is used as an index of sedimentary maturation (transport and recycling), with higher values being a function of increased quartz relative to less resistant lithic fragments and feldspar (Akarish and El-Gohary, 2011). LIK Elliot Formation has a SiO_2/Al_2O_3 average of 7.4 (av. LEF: 6.7, variance σ = 0.8; av. UEF: 7.6, variance σ = 1.65) which is higher than the mean value for LIKE (av. 6.5) and lower than the mean of DAM (av.8.1). Roser *et al*. (1996) report any ratio value greater than and within the range of between 5 and 6 as evidence for sedimentary maturation. The CaO/Al_2O_3 is a measure of the relative proportions of carbonate and CaO/Al_2O_3 in conjunction with K2O/Al2O3 can be a good measure of changes in clay mineral contents. These are all low at the three sites with exceptions pertaining to individual samples that are facies specific, e.g. the carbonate nodule conglomerates.

13.6.1.4 Weathering indices

The degree of chemical weathering can be predicted by the CIA and CIA (molar) index, under the provision that the dominant process occurring is the breakdown of feldspars to clay minerals (Nesbitt and Young, 1982; Goldberg and Humayun, 2010). Higher CIA values are a reflection of a greater degree of chemical weathering producing a larger proportion of aluminous clays, e.g. kaolinite-dominated muds formed under tropical environmental conditions (hot-humid; Nesbitt and Young, 1982; Goldberg and Humayun, 2010). In contrast, fresh unweathered rock has CIA values between 0 – 55 depending on composition (Bahlburg & Dobrzinski, 2011). The influence of post-depositional processes, such as diagenetic illitization, provenance, physical weathering and sorting of the sediment is not accounted for under the index (Goldberg and Humayun, 2010). Differences in provenance and the contribution of different source rocks are examined using the A-CN-K plot and the ICV values (Fig. 13.15B; Nesbitt and Young, 1984, 1989; Akarish and El-Gohary, 2011).

The CIA values reported here, for all sites (LIK, LIKE and DAM), are typical of unweathered to slightly weathered detritus (Bahlburg & Dobrzinski, 2011). In weathering profiles, Al, Mg, K, Cs and Rb are generally retained while Na, Ca and Sr are lost due to dissolution (Nesbitt and Young, 1982; Condie *et*

al., 1992). Figure 13.15(B) establishes that the sediments sampled all three sites were deposited in the early stages of chemical weathering, the minimal loss of Na^{2+} and Ca^{2+} driving the trend towards the A-apex. The primary mineral produced during this process is illite (Fedo *et al*., 1995) which is illustrated in the XRD composition of the Likhoele rocks. The LIK, LIKE and DAM samples do not reach the completion of this weathering trend. This, coupled with the low CIA (CIA molar) and high ICV values, reinforces the minor effect of chemical weathering on their geochemistry and reiterates the more probable dominance of physical weathering in a semi-arid to arid setting (Fig. 13.15B).

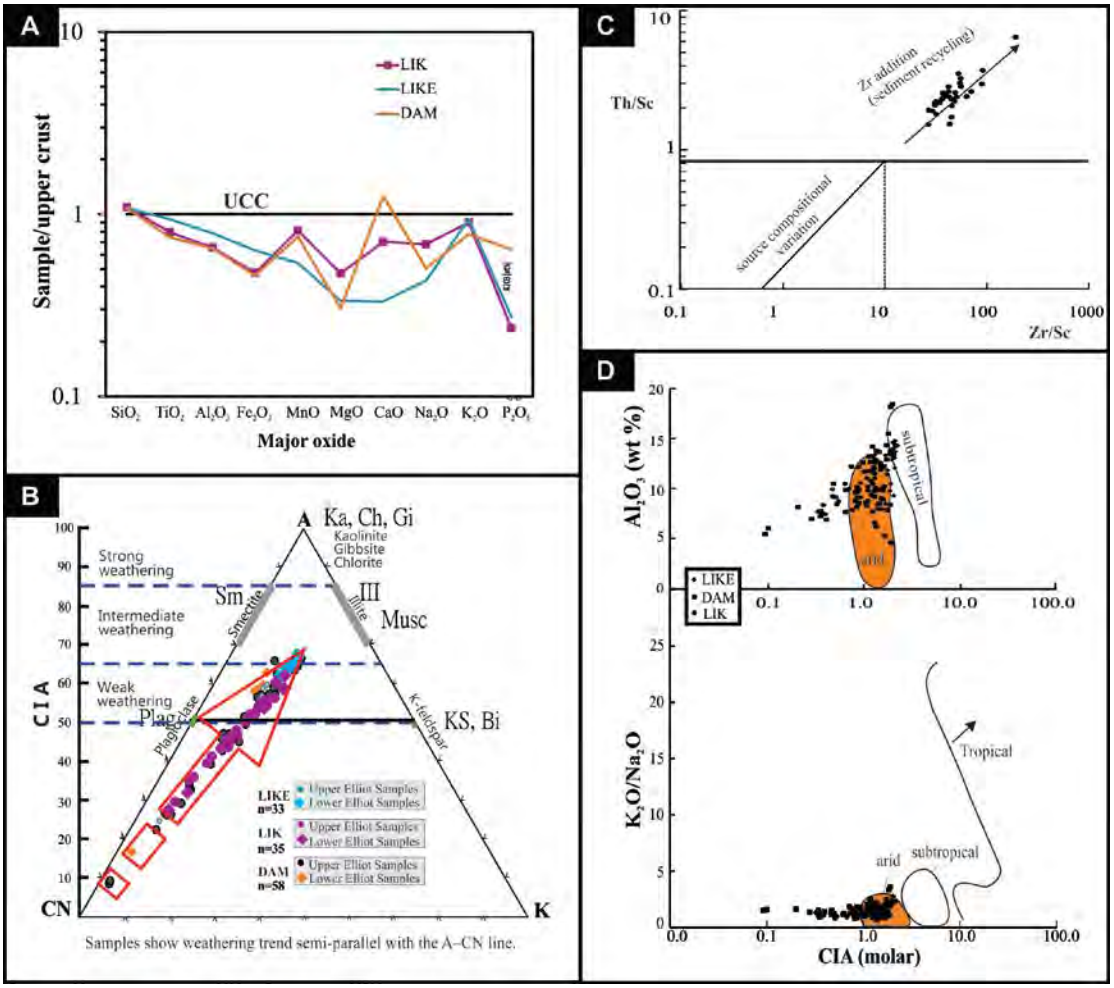

Figure 13.15. The upper crust-normalized major element diagram (A) and A-CN-K ternary diagram (B) for the LIK, LIKE and DAM samples indicate a weathering trend towards illite with the loss of Ca and Na elements. Furthermore Th/Sc versus Zr/Sc plot in C (adapted after McLennan *et al*., 1993) indicates zircon addition due to sediment recycling at LIK Plot of (D) arid setting indicator (D) for CIA (molar) index versus the ratio K2O/Na_2O and Al_2O_3 (as per Goldberg and Humayun, 2010).

Fine grained clay and silt-dominated rocks are expected to have CIA values narrowly ranging between ~70 – 75. LIK, LIKE and DAM fine-grained samples (Fm) have average values of 51.2, 62.7 and 48.8, respectively. These values are relatively low, plotting close to the feldspar-line, indicating limited chemical weathering with the LIKE site showing slightly elevated mean values relative to LIK and DAM. Considering the climate at the time was most likely semi-arid (Bordy and Eriksson, 2015) these values are acceptable, but taking into account that the sediments may largely reflect floodplain mudstones this value is then quite low and may indicate negligible reworking, because sorting has been shown to increase the proportion of clay minerals downstream in a fluvial setting and consequently results in higher CIA values (cf. Nesbitt *et al*., 1997). This approximation did not always hold for the LIKE site where there is more variability in the index. Here finer grained sediments held lower CIA values (e.g. LIKE 26 = 48; LIKE 27 = 45), but with comparable mean values for the coarse-grained rocks (Sm Gmm facies; av. 63.3) in comparison to the finer grained (Fm facies; av. 62.6) counterparts.

Samples with high ICV values coupled with relatively low CIA values (e.g. LIK 7a, 10a and 33, LIKE27) are most likely to indicate a juvenile (i) igneous or (ii) sedimentary source rock (Fig. 13.4; 13.9; Potter *et al.*, 2005). Low ICV values coupled with high CIA values may suggest recycling of source material (Potter *et al.*, 2005) which is confirmed by the geochemical ratios (Fig. 13.15C). The highest ICV values (least degree of weathering) were reported for the DAM site, e.g. samples DAM 5 (3), DAM 45 (2.3), DAM 46 (6.1), DAM 56 (6.2), and DAM 61 (5.7). DAM 46, 56 and 61 are carbonate nodule conglomerates and although possibly composed of clasts of materials which have experienced weathering have high values due to the abundance of CaO within the carbonate nodules which make up this rock. In contrast, DAM 5 and 45 are massive mudstones and as such as more likely to represent a significant period of sorting and complex weathering history.

The UEF, regardless of grain size, from all sites, often shows the lowest degree of chemical weathering illustrated by low CIA, CIA (molar) and high ICV values as would be expected from palaeoclimatic inferences based on sedimentological observations. These indices complement SiO_2/Al_2O_3 values which indicate a higher degree of immaturity of the sediments (less weathering and transportation). The exceptions to this generalisation being with the carbonate nodule conglomerates which show the high ICV values (least degree of weathering) and high CIA values within the UEF. The grain size and facies plays a key role in the CIA values of the samples, somewhat regardless of the climatic control. The CIA (molar) values showed less variability than the CIA values and had more predictable/expect outcomes in terms of comparisons between the LEF and UEF samples with the suggested increasing aridity. This could be a

function of better sorting and finer-grain size for the UEF than the LEF (Bordy *et al.*, 2004c) in conjunction with the increased aridity.

13.7 Conclusion

The results presented here stem from the first quantitative evaluation and detailed geochemical assessment of Elliot Formation samples collected from three sites (LIK, LIKE, DAM) in South Africa and Lesotho. The major and trace elements and their ratios show that there is no formal distinction between the geochemistry of the LEF and UEF. The geochemical subsets identified at LIK and LIKE sites only very broadly coincide with the sedimentological boundary between the LEF and UEF. At face value, if the unit was subdivided by these very marginal geochemical groupings, the LEF-UEF boundary would fall within the UEF. The different geochemical patterns of the fine-grained vs. coarse-grained samples can be accounted for by grain size, sediment sorting and the variable depositional energy levels and subenvironments of the sediments (low energy floodplain vs. high energy channel). Ultimately, the study reaffirms the semi-arid nature of the Elliot Formation consistent with low degrees of chemical weathering. Finally, it is assumed that the outcome of this quantitative geochemical study would be applicable for the Elliot Formation elsewhere in the main Karoo Basin, given the regional similarities in the sedimentary facies and the outcomes of previous, more qualitative studies on the semi-arid to arid palaeonvironment of this unit (e.g., Bordy and Eriksson, 2015).

14 Discussion

Vertebrate fossils and ichnological records from the Elliot Formation have been used as early as the 1950s as a standard for relative age dating and correlating the Triassic-Jurassic assemblages of the main Karoo Basin to other sections globally. The end-Triassic extinction (ETE) records one of the largest ecological disasters of the Phanerozoic and is well-documented in the marine realm but its occurrence in the continental record is somewhat less certain. That being said, faunal transitions and turn over have been noted in several continental deposits (e.g., Newark Basin). Along the same lines, the ETE within the Elliot Formation has not received as much attention as the Permo-Triassic extinction event in the main Karoo Basin. This is because the faunal turnover is not nearly as well-documented and the appearance of new taxa not strictly related to the end-Triassic event and/or its recovery period in the Early Jurassic. Principally, this is influenced by several factors, such as the indefinite stratigraphic position of the end-Triassic event beds and the TJB within the Elliot Formation as well as the unsystematic turnover of fauna within/between the assemblage zones. The latter being an expression of the documentation with relation to a fossils position within the stratigraphy, taxonomic revision and new discoveries of fauna from the Elliot Formation. The current reference to the TJB rests on two main sedimentological properties:

(i) the sedimentological break between the lower and upper Elliot formation (Bordy *et al*., 2004a);

(ii) the traditional use of a large nodule horizon in the middle of the Formation (Kitching and Raath, 1984; Smith and Kitching, 1997),

with the former being utilised in this study.

The TJB and the sedimentological divide are also thought to be reflected in the biostratigraphic break in the formation which was noted and reported as early as 1947 by Stockley. This break - which then was solely used as an indicator of increasing aridity of the palaeoclimate - occurs between the '*Euskelosaurus*' Range Zone and the *Massospondylus* Range zone defined by Kitching and Raath (1984), who also speculated that the TJB falls at the break between the two range zones. It is noteworthy that no taxa were identified as representative of last/first appearance datums (LADs or FADs) for the terrestrial ecosystem response to rapid climatic change; nor is there an ichnologically defined boundary (e.g., change in the type, abundance and diversity of trackways) given for the formation. This brings to light the question of whether the Elliot Formation records the end-Triassic extinction and recovery events or merely represents changing palaeoclimate over time causing gradualistic change in fauna; or conversely, that the TJB

coincides with an unconformity and the ETE is not recorded. The increasing aridity of the palaeoclimate has been so far demonstrated on sedimentological grounds suggesting that arid climate indicators, albeit indirect, become increasingly more common in the upper Elliot Formation (calcareous palaeosols; loess interbeds, etc.,) with this evidence suggesting seasonally wet and then dry conditions, prior to the development of the extensive sand sea in the later part of the Early Jurassic (Clarens Formation – Eriksson, 1985; Bordy *et al*., 2004b).

This question could be answered by effectively linking the stratigraphic record to the current biochronological one which, to date, has often been neglected. Many of the palaeontological papers solely provide information on the fossil locality as being in the lower or upper Elliot Formation, at best, and very few authors provide a sedimentological log of the site locality or more detailed information as to the stratigraphic position of the fossil discoveries. In recent times this means of documenting fossils has been undergoing change; e.g. Butler *et al*. (2007) provide detailed log and geological information in the supplementary material; and it is becoming increasingly common to give sedimentological and stratigraphic evidence as to the occurrence of a fossil. A pertinent example of where this has failed, in South Africa, is the poor documentation of the articulated skull and skeleton of *Melanorosaurus readi* (‘*Euskelosaurus* sp.; Welman 2000; Yates, 2005a). The rarity of a skull associated with post-cranial material for sauropodomorphs in South Africa is infamous. The lack of published detailed information pertaining to the locality (barring the referral in Butler *et al*. 2007 supplementary material), in terms of it sedimentological and stratigraphic locality, makes the use of this fossil less hard-hitting. Secondarily connecting the two methodologies, via publication and literature review analyses, and even revisiting sites, proves difficult and inaccurate. Thus, the aim of this thesis was to achieve a composite magnetostratigraphic log for the Elliot Formation in which the stratigraphic position of the sedimentological LEF-UEF divide relative to global TJB would be resolved through the use of relatively high resolution of magnetostratigraphy at key sections throughout the basin.

All palaeomagnetic samples were collected by drilling orientated cores using a portable drill and a sun compass. Sections drilled were chosen for the relative ease of access, the fossil content/previous work and the absence of conspicuous Early Jurassic Karoo dolerite intrusions which are likely to give a secondary early Jurassic partial (or complete) overprint to samples. Completely avoiding intrusions is difficult, because in some areas the intrusions are very pervasive, and the country rock alteration is prominent (for sampling methodology, refer to the Barkly Pass chapter). At sites close to the contact of the Elliot-Clarens Formations, the Karoo lavas are another source of bias, especially considering that Moulin *et al*. (in press) reports new radiometric age and magnetostratigraphic data suggesting an early, but volumetrically

negligible igneous event at ~189 Ma. All in all, due care has been taken to understand and manage any partial overprint by Karoo lavas and intrusions.

All lithologies were sampled, from mud-chip and pedogenic nodule conglomerates to sandstones, siltstones, mudstones and palaeosol horizons. Where lithologies allowed, sampling resolution was relatively high in order to increase the resolution of the study, to obtain the true representation of the change in the magnetic field during the deposition of the Elliot Formation, as well as to monitor any homogeneity in the magnetization between and within sites.

14.1 Late Triassic- Early Jurassic palaeopole of the Elliot Formation

Palaeomagnetic data from Barkly Pass (BP), Quthing (QUT), Likhoele and Likhoele east (LIK, LIKE), Maseru (MAS), Damplaats (DAM), Golden Gate National Park and Blesbok Loop (GGP, GGB) were used to calculated a Late Triassic-Early Jurassic palaeopole for the Elliot Formation (Table 14.1).

The palaeomagnetic data from the 10 sections (with $\alpha95 < 16$) covering the LEF-UEF transition results in a mean direction for normal- and reverse-polarity samples for the LEF of Dec = 320.8˚ and Inc = -62.6˚ ($\alpha95 = 10.0$, k =85.09, n = 4), the UEF of Dec. = 327.7˚ and Inc. = -62.7 ˚ ($\alpha95 = 26.9$, k = 4.3, n = 10) and Elliot Formation combined with Dec. = 328.6˚and Inc. = -64.3˚ ($\alpha95 = 26.5$, k =4.3, n = 10; Table 14.1). The UEF sites (OLD, SEE and GGB) are included in the EF calculations (Table 14.1). The mean magnetic directions for normal and reverse directions, used for virtual geomagnetic pole (VGPs) calculations, for the LEF, UEF and combined (lower + upper) Elliot Formation were used for the palaeopole calculation. Sites with large $\alpha95$ values greater than 16° were discarded from the final calculation.

Table 14.1. Elliot Formation sites and their site means in conjunction with the co-ordinates of the current site location, the calculated pole location and the palaeopole. Mean virtual geomagnetic pole is given for the combined Elliot Formation (EF), lower Elliot Formation (LEF) and upper Elliot Formation (UEF). α95 = 95% confidence interval, pole; A95 95% confidence interval; n = samples per site, N = number of sites

Elliot Formation combined (LEF+UEF)					Site location		Pole location				VGP	
Site #	n	Decl °	Incl °	α_{95} °	Lat °N	Long °E	Pole Lat °N	Pole Long °E	dm	dp	Lat °N	Long °E
BP EF	62	303.2	-70.7	4.4	-31.4	27.3	44	249	7.6	6.6	-44.0	69.2
QUT EF	64	339.8	-59.8	4.4	-30.4	27.6	70.7	260.0	6.6	5.0	-70.7	80.0
MAS EF	24	332.5	-51.8	9.5	-29.3	27.5	66.3	282.9	13.0	8.8	-66.3	102.9
DAM EF	45	314.5	-61.1	5.5	-29.2	27.3	51.4	265.1	8.4	6.5	-51.4	85.1
GGP EF	36	319.1	-56.8	6.2	-28.5	28.7	54.8	273.3	9.0	6.5	-54.8	93.2
GGB UEF	14	345.9	-55.8	15.5	-28.5	28.7	75.8	261.7	22.2	15.9	-75.8	81.7
LIK EF	26	5.7	-68	8	-29.3	27.5	67.8	198.0	13.4	11.3	-67.8	18.0
LIKE EF	15	306.2	-66	10.4	-29.9	27.3	45.5	257.2	17.0	13.9	-45.5	77.2
OLD UEF	12	317.7	-61.2	12.4	-29.1	27.4	53.6	264.5	19.0	14.6	-53.6	84.5
SEE UEF	23	143.1	46.9	8.4	-29.8	27.5	-57.8	111.2	10.8	7.0	-57.8	111.2

EF	**Decl °**	**Incl °**	**α_{95} °**	**k**
site mean	328.6	-64.3	26.5	4.3
	Lat °N	**Long °E**	**A_{95} °**	**K**
Mean Pole	-60.47	082.06	9.5	27.04

N =	10

lower Elliot (LEF)

Site #	n	Decl °	Incl °	α_{95} °	Lat °N	Long °E	Pole Lat °N	Pole Long °E	dm	dp	Lat °N	Long °E
BP LEF	16	312.6	-66.7	8.4	-31.4	27.3	50.5	256.4	13.9	11.4	-50.5	76.4
QUT LEF	36	338.9	-59.1	6.5	-30.4	27.6	70.4	263.0	9.7	7.3	-70.4	83.0
DAM LEF	38	303.8	-66.3	13.6	-29.2	27.3	43.4	256.3	22.3	18.3	-43.4	76.3
GGP LEF	20	322.2	-55.8	9.2	-28.5	28.7	57.4	275	13.2	9.4	-57.4	95.0

LEF	**Decl °**	**Incl °**	**α_{95} °**	**k**
site mean	320.8	-62.6	10.0	85.08594
	Lat °N	**Long °E**	**A_{95} °**	**K**
Mean Pole	-55.7	081.8	14.4	41.8

N =	4

upper Elliot (UEF)

Site #	n	Decl °	Incl °	α_{95} °	Lat °N	Long °E	Pole Lat °N	Pole Long °E	dm	dp	Lat °N	Long °E
BP UEF	46	298.8	-72.6	5.8	-31.4	27.3	41.3	245.6	10.3	9.1	-41.3	65.6
QUT UEF	28	341	-58.4	5.7	-30.4	27.6	72.2	263.2	8.4	6.3	-72.2	83.2
MAS UEF	20	328	-46.4	8.7	-29.3	27.5	61.9	292.9	11.2	7.2	-61.9	112.9
DAM UEF	38	316.7	-60.2	6.1	-29.2	27.3	53.1	266.6	9.2	7.0	-53.1	86.6
GGP UEF	16	319.4	-56.5	8.3	-28.5	28.7	55.1	273.8	12.0	8.7	-55.1	93.8
GGB UEF	14	345.9	-55.8	15.5	-28.5	28.7	75.8	261.7	22.2	15.9	-75.8	81.7
LIK UEF	18	4.4	-63.6	8.5	-29.3	27.5	73.7	196.4	13.5	10.7	-73.7	16.4
LIKE UEF	12	300.7	-61.7	9.4	-29.9	27.3	41.6	264.7	14.5	11.2	-41.6	84.7
OLD UEF	12	317.7	-61.2	12.4	-29.1	27.4	53.6	264.5	19.0	14.6	-53.6	84.5
SEE UEF	23	143.1	46.9	8.4	-29.8	27.5	-57.8	111.2	10.8	7.0	-57.8	111.2

UEF	**Decl °**	**Incl °**	**α_{95} °**	**k**
site mean	327.7	-62.7	26.9	4.16
	Lat °N	**Long °E**	**A_{95} °**	**K**
Mean Pole	-60.3	085.2	10.1	23.7

N =	10

.

The site average D, I and α_{95} for LEF (N+R), UEF (N+R) and combined Elliot Formation (EF, N+R) in conjunction with the site location (Lat. N, Long E) were used to calculate the virtual geomagnetic pole, VGP, co-ordinates and the calculated palaeopole (Table 14.1). Twenty-four new VGPs, of various qualities, were calculated for the LEF, UEF and the Elliot Formation. Age constraints for these poles are taken from the biostratigraphic evidence which considers the LEF to be Late Triassic (~213 – ~201 Ma), and the UEF to be Early Jurassic (~201 – ~195 Ma), with an approximate age of the Elliot Formation to ranging from ~213 Ma to ~195 Ma (Lucas and Hancox, 2001; Knoll, 2005). The mean palaeopole position is indicated at palaeolatitude 55.7 ˚S during the LEF in comparison to the 60.3˚ S during the UEF. The overall Elliot Formation palaeopole position is indicated at palaeolatitude 60.5 ˚S. The paleopole calculated here for the EF is moderately comparable to that of McElhinny and McFadden (2000) for the Early Jurassic of Africa, i.e. EF (this study): 60.5˚S, 082.6˚E vs. African Early Jurassic: 68 ˚S, 247 ˚E. Late Triassic African paleopole sits at 65.8 ˚S and 259.7 ˚E (McElhinny and McFadden, 2000).

Figure 14.1 illustrates the geographical setting of the mean palaeomagnetic pole calculated in this study for the combined Elliot Formation, LEF and UEF. Comparable, previously published palaeopoles for South America and South Africa, in addition to the Gondwana apparent polar wander path are listed in Table 14.2 and illustrated in Figure 14.2. Southern African co-ordinates rotated -7.8˚, to West African co-ordinates, about an Euler pole that is situated at 9.3˚N and 5.7˚E.

The position of a previously obtained palaeopole for the Elliot Formation (de Kock 2003) overlaps with the mean EF and UEF of this study (Figure 14.2). De Kock (2003) pole shows good correspondence with new poles obtained from the Drakensberg Group (shared 95% confidence circle), specifically with the combined Naudes' Nek-Oxbow Moteng Pass data by Moulin *et al. in press* (Figure 14.1). This argues for either (i) Elliot Formation bias to UEF as there is overlap between the 95% confidence circles of the current study UEF and combined EF with the de Kock (2003) Elliot pole, or (ii) secondary late Early Jurassic (~Toarcian) overprint for these samples being indistinguishable from the primary remanent magnetisation. The former is true based on the number of samples which were viable in the UEF versus the LEF at all sites.

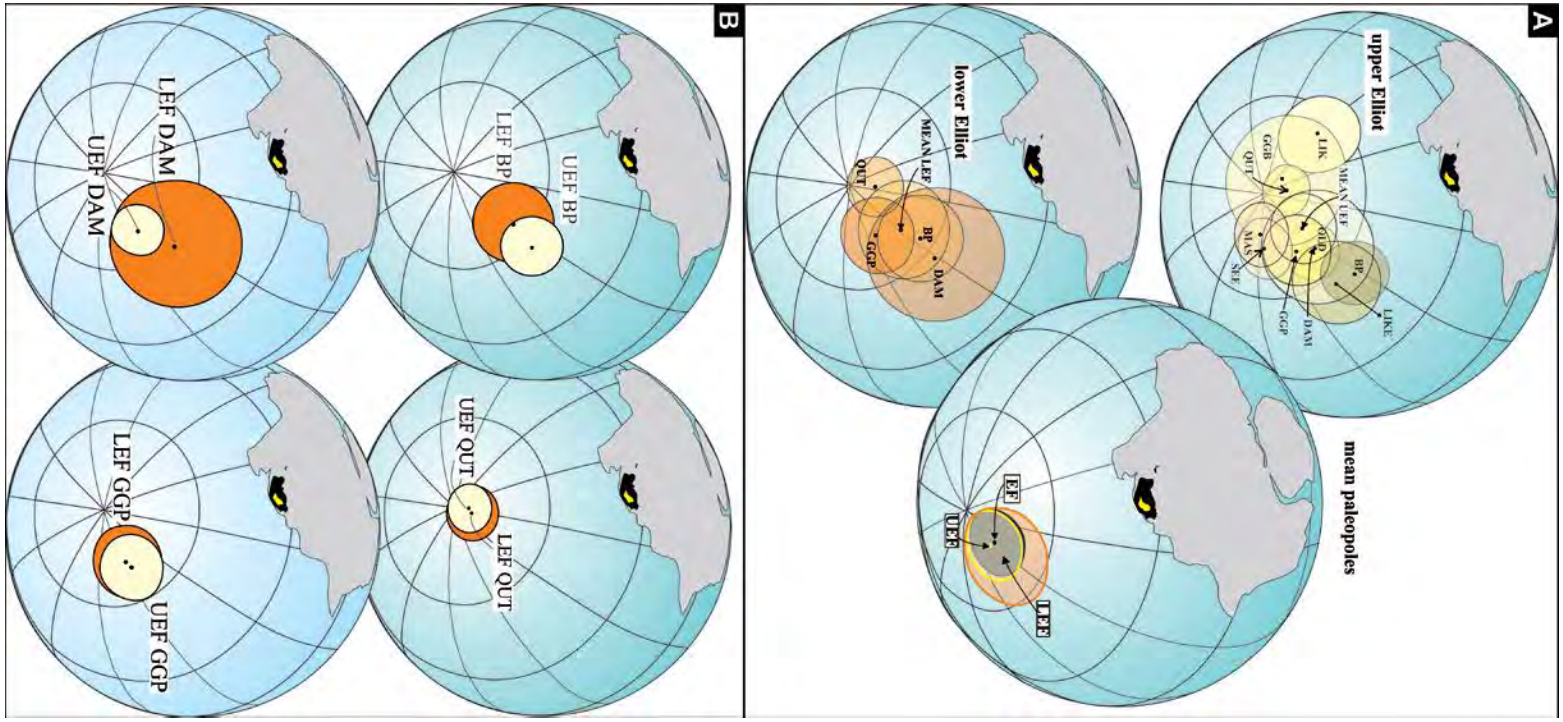

Figure 14.1. (A) Mean LEF, UEF and Elliot Formation (EF) palaeopoles. Section abbreviations: BP: Barkly Pass, QUT: Quthing, LIK & LIKE: Likhoele Mountain; SEE: Seeiso; MAS: Maseru; DAM: Damplaats, OLD: Oldenburg, GGP &GGB: Golden Gate Highlands National Park; (B) LEF (orange) and UEF (cream) confidence intervals for Barkly Pass (BP), Quthing (QUT), Damplaats (DAM) and Golden Gate National Park (GGP). The outline of the main Karoo Basin within Gondwana is in black and Stormberg Group is in yellow. Southern African co-ordinates rotated to West African co-ordinates about an Euler pole that is situtated at 9.3˚N and 5.7˚E and rotates through an angle of -7.8˚ to restore East Gondwana.

Table 14.2. Selected Late Triassic - Early Jurassic palaeomagnetic poles from South America and Africa. Lat S, Long E, A95= latitude, longitude and semi angle of 95% confidence. (Taken from Iglesia Llanos and Prezzi, 2012 with new results from the Karoo basalts from Moulin *et al*. *in press*).

Africa	Mean Age (Ma)	Lat S	Long E	A95	References		Ref #
Upper Triassic Sed.	221.5	54.9	43.3	11.5?	Ghorabi and Henry	-1991	3020
Foum-Zguid	200	67.9	67.9	3.9?	Palencia-Ortas *et al*.	-2011	–
Zarzaitine Fm.	206.5	70.9	55.1	2.6?	Kies *et al*.	-1995	2932
Karroo Comb.	198	65.4	75.1	9.5?	McElhinny and Jones	-1965	317
Karroo Ign.	186	62.9	98.3	3.0?	Hargraves *et al*.	-1997	3430
Marangudzi Cplx.a	186	70.7	106.7	8.7?	Brock	-1968	470
Naudes Nek-Oxbow Moteng Pass	180.3 -182.8	68.9	268.1	4.3	Moulin *et al*.	*in press*	
Oxbow-Moteng Pass	180.3 -182.8	65.3	267.9	5.2	Moulin *et al*.	*in press*	
Stormberg Lavas	185	71.6	93.5	3.2?	Kosterov and Perrin	-1996	3090
South America							
Los Colorados Fm.	210	76	280	8.0?	Vizañ *et al*.	-2004	–
Anari-Tapirapua Fm.	196.6 ± 0.4	65.5	250	3.5?	Montes-Lauar *et al*.	-1994	3316
Neuque ´n basin	197	51	223	6.0?	Iglesia Llanos *et al*.	-2006	–
Lepa´-Osta Arena Fm.	180 –186	75.5	129.5	6.0?	Vizañ	-1998	3314
Neuque ´n basin	185	74	67	5.0?	Iglesia Llanos *et al*.	-2006	-

For comparison with global palaeopoles of similar time periods, Africa was used as the reference plate to which other continental plates (in this case in particular, South America) were restored. South American co-ordinates were rotated to West African co-ordinates about an Euler pole situated at 53˚N and 325˚E. Figure 14.2 expresses LEF pole positions with those of similar assumed age of Late Triassic from Africa and South America in addition to the true polar wander path for ~215Ma of Iglesia llanos and Prezzi (2012). The mean LEF palaeopole and confidence interval shows overlaps most significantly with the Los Colorados Formation at ~210 Ma and the Foum-Zguid dykes of Morocco (200 Ma) as well as the African Late Triassic sediments (~221 Ma) and Suriname dolerite dykes (~227 0 237 Ma; Figure 14.2). Two Los Colorados Formation palaeopoles are plotted in Figure 14.2, #2 is by Iglesia llanos and Prezzi (2012) whereas #4 is a more recent study of Kent *et al*. (2014). The overlap with the original ~210 Ma pole (#2; Figure 14.2) shows considerable overlap LEF palaeopoles of BP and DAM.

Lower Elliot Formation comparisons

No.	Unit	Age (Ma)	References
1	African Upper Triassic Sediments	221	Iglesia Llanos &Prezzi (2012)
2	Los Colorados Fm. (Argentina)	210	Iglesia Llanos &Prezzi (2012)
3	Dolerite Dykes (Suriname)	237-227	Database
4	Los Colorados Fm	213-227	Kent et al (2014)
5	Triassic - Jurassic TPW	227-213	Iglesia Llanos &Prezzi (2012)
6	Triassic - Jurassic TPW	215	Iglesia Llanos &Prezzi (2012)
7	Zarzaitine Fm. (SE Algeria)	206	Iglesia Llanos &Prezzi (2012)
8	CAMP lavas (Morocco)	200	Iglesia Llanos &Prezzi (2012)
9	Foum-Zguid dyke (Morocco)	200	Iglesia Llanos &Prezzi (2012)

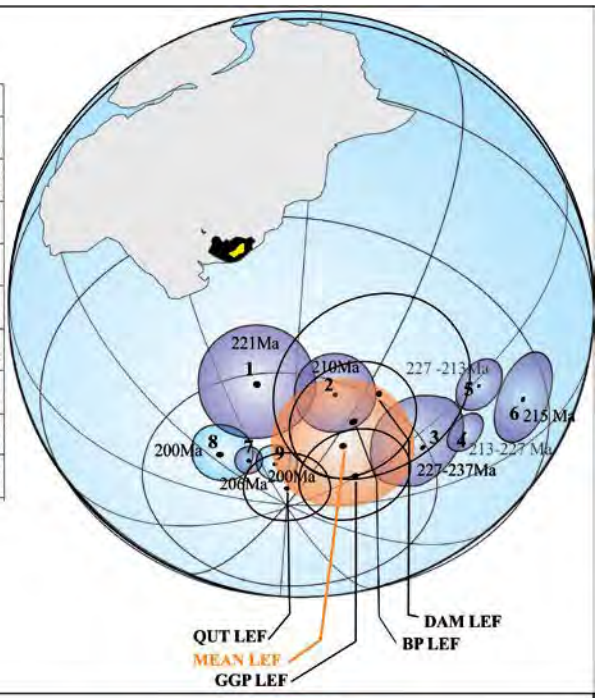

Upper Elliot Formation comparisons

No.	Unit	Age (Ma)	References
1	Los Colorados Fm. (Argentina)	210	Iglesia Llanos &Prezzi (2012)
2	Neuquén Basin	~197	Iglesia Llanos &Prezzi (2012)
3	Anari-Tapirapua Fm	196.6±0.4	Database
4	Oxbow-Moteng Pass basalts	~180-182	Drakenberg Group poles (Moulin et al., *in press*)
5	Naudes' Nek-Oxbow Moteng Pass basalts		
6	Elliot Formation	Early Jurassic	de Kock (2003)

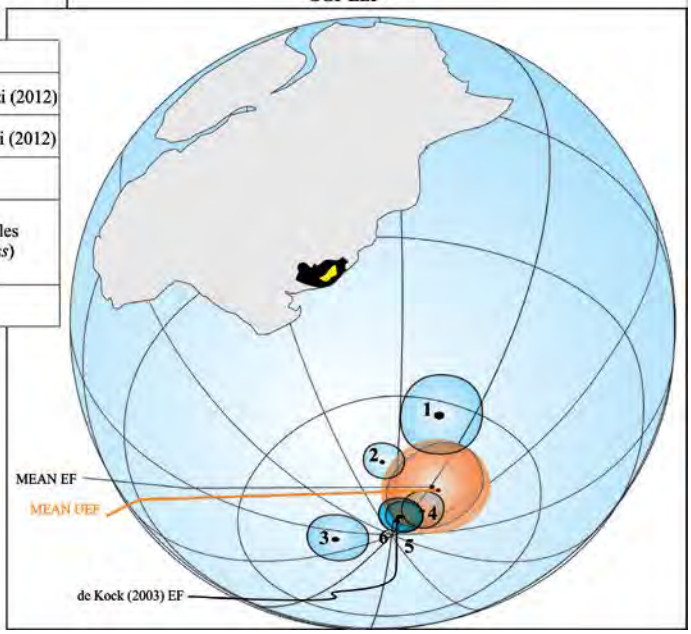

Figure 14.2. Palaeomagnetic poles with 95% confidence circles for mean Elliot Formation (EF; orange), LEF and UEF (this study), Elliot Formation (de Kock, 2003) and previously published Late Triassic-Early Jurassic palaeopoles with their confidence limits (purple = Late Triassic; blue = Early Jurassic). The outline of the main Karoo Basin within Gondwana is in black and Stormberg Group is in yellow. Southern African co-ordinates rotated to West African co-ordinates about an Euler pole that is situated at 9.3˚N and 5.7˚E. South American co-ordinates rotated to West African co-ordinates about an Euler pole that is situated at 53˚N and 325˚E.

The overall Elliot Formation and UEF poles (Fig. 14.2) are consistent with and close to previous Early Jurassic palaeopoles determinations from the Anari-Tapirapua Formation (~196.6 Ma), Neuquén Basin (~197 Ma) by Iglesia llanos and Prezzi (2012); in addition to showing significant overlap with poles calculated for the Drakensberg Group lavas and previous Elliot Formation study. The uppermost UEF site of SEE has a palaeopole position which falls onto the Iglesia llanos and Prezzi (2012) ~197 Ma Triassic-Jurassic TPW. Iglesia llanos and Prezzi (2012) established that Pangea was at its southernmost position during the Late Triassic from ~215 Ma, and from its counter-clockwise rotation into the Sinemurian (although given at ~200 Ma which is well within the Hettangian); it progressed northward, until at ~197 Ma. At this time, the supercontinent commenced a clockwise rotation, and by the Pliensbachian (~185 Ma), Pangea had reached its most northerly position (Iglesia llanos and Prezzi, 2012).

Palaeopoles from North American taken from Donohoo-Hurley *et al*. (2010) for the Moenave Formation (~197 Ma), and reported and rotated to southern Africa in Torsvik *et al*. (2012), have a palaeopole at lat.-73.2˚, long. 55.4˚ (α_{95} = 2.8). The geographic location of this paleopole is comparable to that reported for the Hartford Newark basin volcanics (-65.4˚, 69.2˚, α_{95} = 4; Torsvik *et al*., 2012). The latter palaeopole is more closely comparable to the mean EF and UEF paleopole (Table 14.1). The earliest radiometrically dated CAMP volcanism (i.e., the North Mountain basalts, ~201.6 Ma) has a palaeopole of -71.9˚S, 68.2˚E (α_{95} = 10.7; Torsvik *et al*., 2012).

14.2 Stratigraphic correlation and magnetostratigraphy

14.2.1 **Magnetostratigraphic constraints**

Correlation of strata/individual beds between the isolated Elliot Formation sites was not attempted or conceived for this project because:

i. Depositional conditions, including sedimentation rates, are highly variable laterally on localised and regional scale both within and between sedimentary environments, despite the “continental red bed” facies of the Elliot Formation being a unifying feature of the entire unit;
ii. No section represents continuous sedimentation rate through time, although hypothetically assumed;
iii. Isopach changes along the N-S axis of the basin;

iv. Variability and unpredictable nature of the erosional events in terms of their occurrence as well as magnitude/ leading to, currently, unquantified gaps in the sedimentation that can have a non-uniform spatiotemporal distribution within the Basin (i.e., the 'missing slices of time' or hiatuses may have resulted in diastems but could have also led to unconformities);

v. The biostratigraphy of the Elliot Formations, although in need of revision and increased resolution, shows some degree of disparity in the ages of specimens and in evolutionary paths, which indicates numerous long term hiatuses.

As there are no recognisable event markers, to date, within the Elliot Formation, the sedimentological change that defines the boundary between LEF and UEF was used as a first order datum for correlations (Fig. 14.3). Using the sedimentological break, often expressed as a geomorphological plateau along hill slopes that expose most of the formation, as a tool of correlation is practical, aids visual, large-scale subdivision of the formation in the field (Fig. 14.3) and most importantly is not reliant on other methodologies like palaeomagnetism, radiometric dates or biostratigraphy, none of which are readily applicable during field work.

In conjunction with the sedimentological change, interpreted as an unconformity by Bordy *et al*. (2004b) and always indicated with a dashed red line in the figures of this project, the fossil content, radiometric ages (where available) and similarity in the polarity pattern represented by magnetozones were also used as aids for correlations. Well-defined groups of normal and reverse primary magnetization directions from all sites (Fig. 14.3) were used to construct magnetic polarity zonation patterns for the Elliot Formation. The magnetic polarity patterns are grouped into numbered normal-reverse polarity pairs.

14.2.2 **Lower Eliot Formation (LEF)**

One, up to ~75 m long reverse magnetic chron (EF1r) and four polarity pairs (EF2 – 5) were identified in the lower Elliot Formation. This complements and supplements the two chrons (EF1r – EF2n) described by de Kock (2003) (Figs. 14.4, 14.5, 14.6). The Barkly Pass (BP), Quthing (QUT) and Golden Gate National Park (GGP) sites represent the longest LEF sections and aided in detailing the LEF magnetic polarity zonation patterns across the basin (Fig. 14.4).

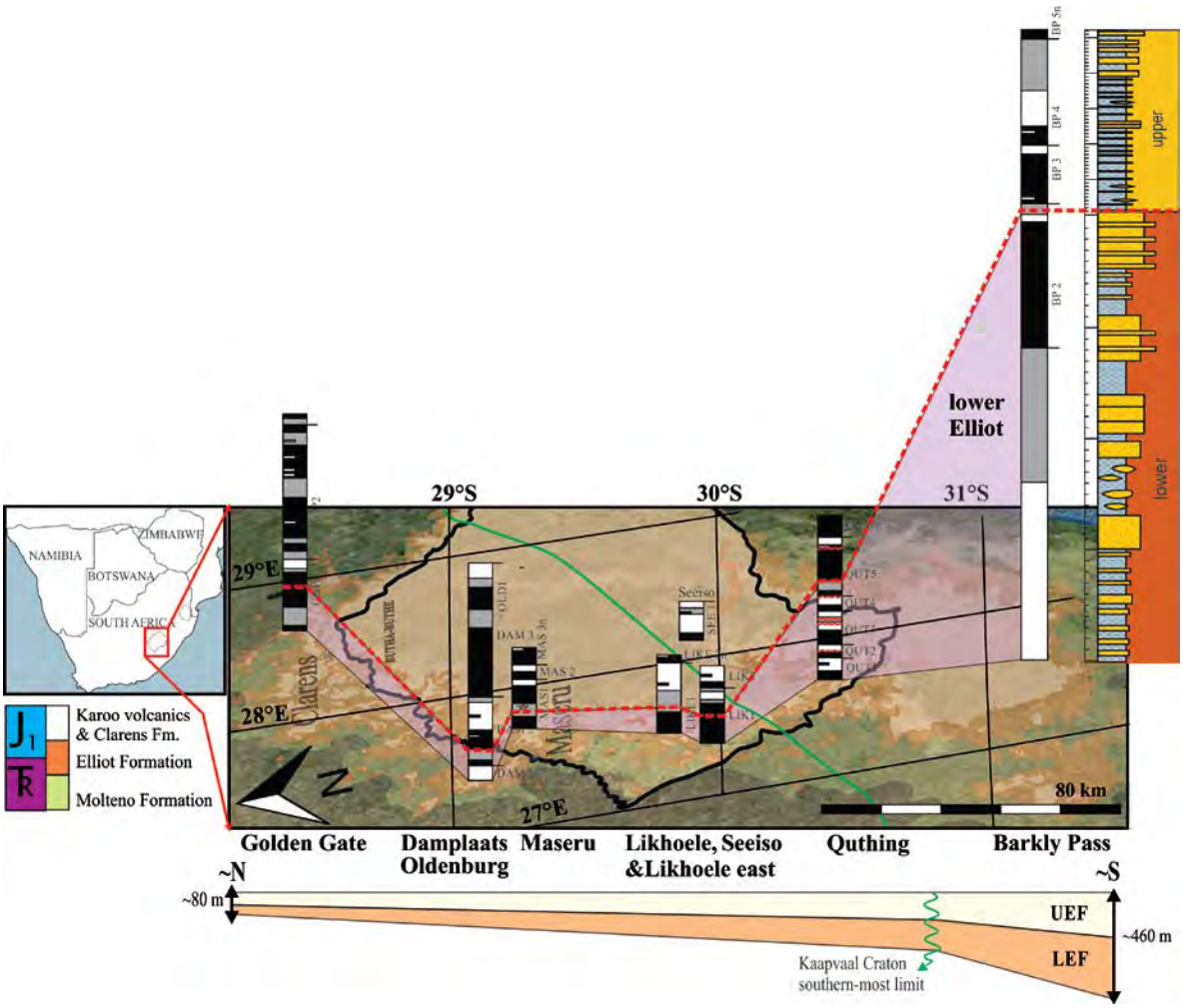

Figure 14.3. Geological map indicating the geographical and spatial distribution of the main sampling sites, represented by their respective magnetostratigraphic logs, across Lesotho and South Africa. The LEF is correlated (purple) between sites, and the sedimentological contact between the LEF and UEF is indicated with dashed red line. Lateral thickness variation along the north-south gradient, in the main Karoo Basin, is indicated and modified after Bordy *et al*. (2004b).

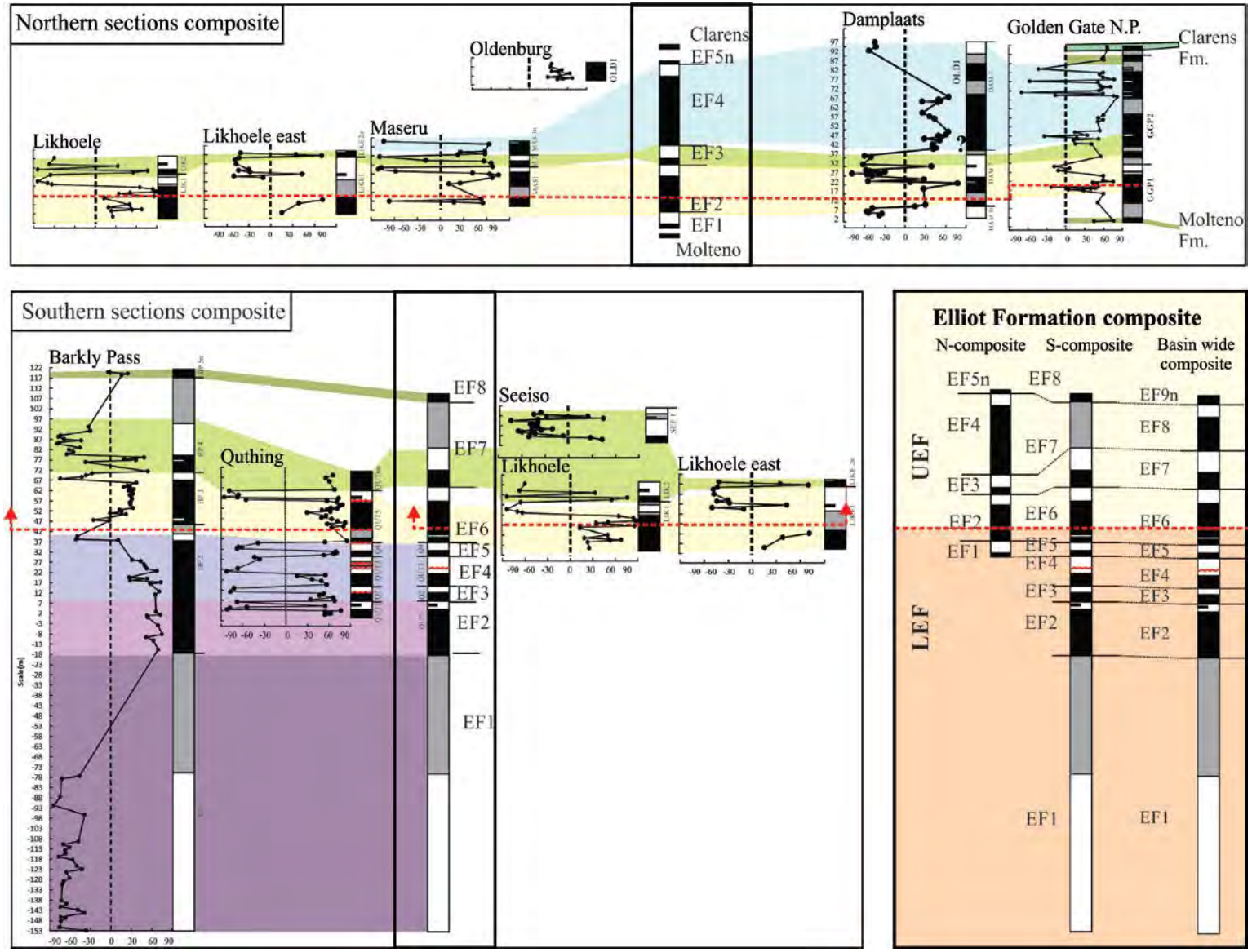

Figure 14.4. Magnetostratigraphic sections and their relative composites from the southern and northern part of the Basin as well the composite magnetostratigraphic section of the Elliot Formation.

At these three sites, the lowermost and middle parts of the LEF were sampled. BP, in particular, as a composite with the original sampling of de Kock (2003), represents an almost complete magnetic polarity zonation of the holostratotype (Figs. 14.5, 14.7).Barkly Pass and Quthing are the southernmost sites and therefore represent the regions where the LEF is thickest in the basin. Magnetic polarity patterns from these sites are likely to be more detailed than the northern, more condensed, sections. GGP is the northernmost section of this study and lies close to the northernmost limit of the Elliot Formation outcrop area. GGP captures the uppermost Molteno, LEF, UEF and lowermost Clarens Formations and also represents the thinnest LEF section sampled.

The LEF at Barkly Pass contains two polarity intervals. Firstly a ~75 m thick reverse polarity zone (BP1r) which was originally measured by de Kock (2003) (Figs. 14.6, 14.7). This is overlain by a poorly defined interval (60 m) in which samples, from the current study and those from de Kock (2003), did not yield stable end point vectors but poorly defined magnetization components inconsistent with expected results, and considered unsuitable for use. This interval also contains a large, ~1.5/2 m wide cross-cutting dolerite dyke. It is likely that the pervasive hydrothermal fluid flow from the dyke into the LEF country rock has led to the development of a Middle Jurassic overprint directly or that weathering, intensified by the presence of the dyke, and has allowed for the development of a present field chemical remanent magnetization. This sector in turn is overlain by an up to ~19 m thick, and well-defined, normal polarity zone (BP2n) and corresponding reverse polarity zone (BP2r). The BP2r reverse polarity zone straddles, with several samples bearing unknown polarity immediately over the transition of the sedimentological boundary between LEF and UEF.

Quthing is the second thickest section of LEF and represents sampling from approximately the lower part of the middle of the LEF into the UEF. Unlike the section at BP, the QUT section records 4 polarity pairs (QUT1 – 4) before the boundary of the LEF and UEF was intersected by the sampling (Fig. 14.5). The sedimentological boundary is in the 5th polarity pair (QUT5) within the normal polarity zone (QUT5n). Correlation between these two southernmost sites is difficult, because there is little biostratigraphic or other evidence to tie the lowermost Elliot Formation between them. The only reported fossil is the Brachyopoid temnospondyl from Ellenberger's (1972) zone A/7 at Quthing (Warren and Damiani, 1999) which lies below the LEF-UEF contact. Furthermore, the magnetic polarity zonation pattern is not similar and a large part of the middle of the LEF magnetic record is not constrained for the Barkly Pass (Figs. 14.4, 14.5) and is marked as a grey interval on figures. Correlation has been attempted purely on sedimentological grounds, i.e. using the position of the LEF-UEF contact relative to the nearest outcrops of the Molteno and Clarens Formations (Fig. 14.5).

Golden Gate National Park section is by far, for all sections sampled, the most condensed exposure of the Elliot Formation. This is to be expected as it is one of the northernmost sites. The LEF at GGP is dominated by normal primary magnetization directions. Two, single sample, reverse polarity zones occur below the LEF-UEF contact.

The remaining sites, Likhoele (LIK), Likhoele east (LIKE), Maseru (MAS), and Damplaats (DAM), all record a normal polarity zone, often overlain by poorly constrained intervals which transitions across the uppermost LEF and LEF-UEF contact. The lowermost extent of the LEF was very difficult to impossible to sample at these sites, and therefore comparison to the lowermost sections of BP, QUT and GGP sites is not possible. Unconstrained intervals are the result of either no sample collected or weathered samples with secondary present field overprint. The topography greatly contributes to this as these samples are usually over the LEF-UEF break which forms a geomorphological feature in the form of a weathered plateau and slope. The LEF at DAM is represented by a several thick channel bodies which record a reverse polarity (DAM1r). This has been correlated with QUT4r solely on the basis of the polarity and approximate position in the LEF (Fig. 14.5).

14.2.3 **Upper Elliot Formation**

The UEF is characterised by a pattern of 3 normal-reverse polarity intervals, capped by a single normal polarity zone, e.g. EF6, EF7, EF8 and EF9n (Fig. 14.5). The similarity in EF6-EF7 polarity pattern (N-R-N-R) in the UEF across the basin illustrates the palaeomagnetic stability of the Elliot Formation as also noted by de Kock (2003).

Figure 14.5. Correlations and composite magnetic stratigraphy of the Elliot Formation, from sections at Barkly Pass, Quthing, Likhoele and Likhoele east, Seeiso, Damplaats, Oldenburg and Golden Gate National Park (GGP and GGB). Dashed red line indicates the sedimentological contact between the LEF and UEF. Wavy red lines indicated on individual polarity logs are erosional surfaces identified in the field. Thickness variation of the Elliot Formation within the Karoo basin is indicated at the base of the figure with the schematic S-N cross-section. Idealised sedimentological log adapted from Bordy and Erikson (2015).

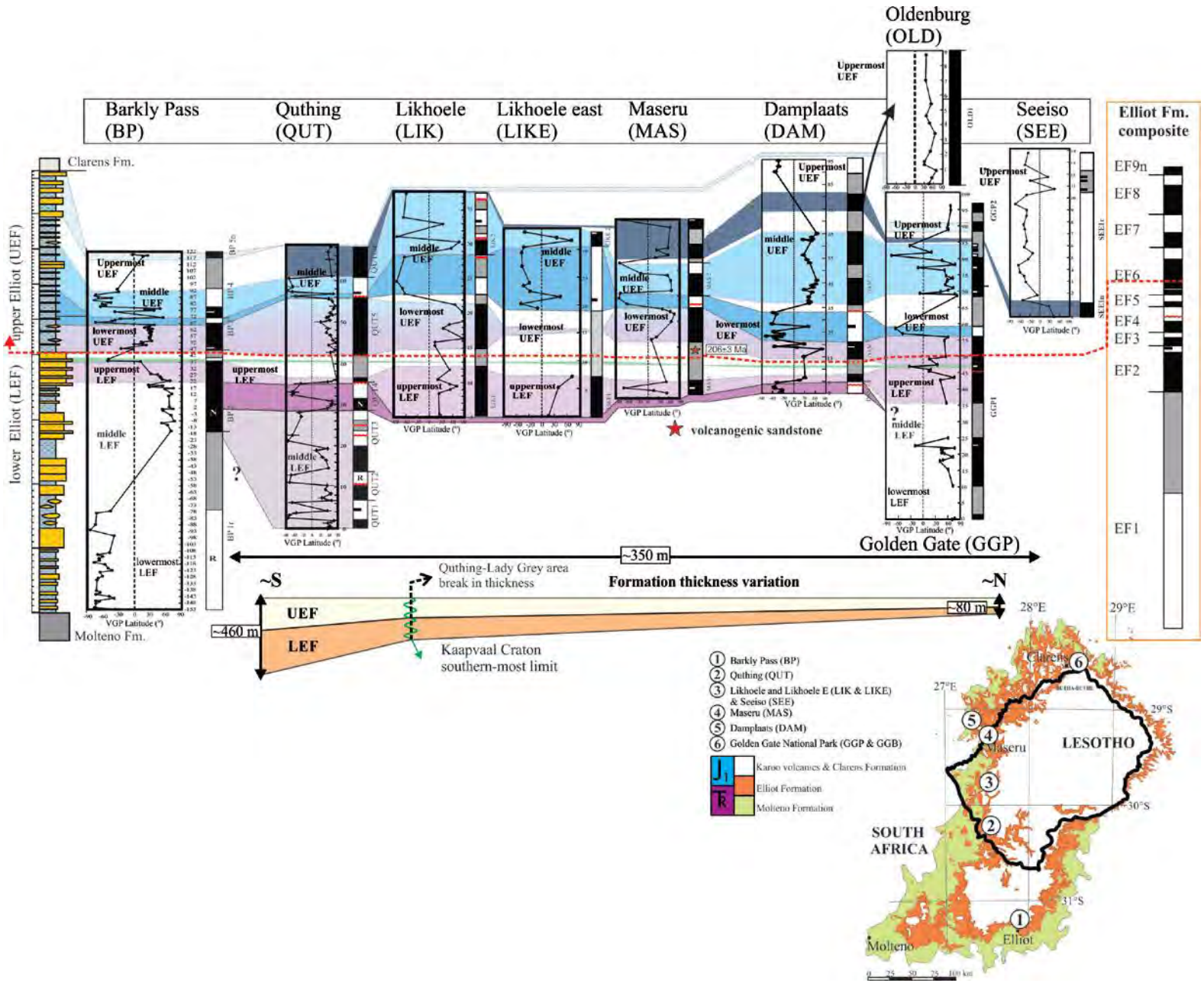
Barkly Pass (BP)
Quthing (QUT)
Likhoele (LIK)
Likhoele east (LIKE)
Maseru (MAS)
Damplaats (DAM)
Oldenburg (OLD)
Seeiso (SEE)
Golden Gate (GGP)
Elliot Fm. composite
EF9n
EF8
EF7
EF6
EF5
EF4
EF3
EF2
EF1
Clarens Fm.
Molteno Fm.
upper Elliot (UEF)
lower Elliot (LEF)
Uppermost UEF
middle UEF
lowermost UEF
uppermost LEF
middle LEF
lowermost LEF
VGP Latitude (°)
206±3 Ma
volcanogenic sandstone
~350 m
~80 m
~460 m
~S
~N
Quthing-Lady Grey area break in thickness
Formation thickness variation
UEF
LEF
Kaapvaal Craton southern-most limit
1 Barkly Pass (BP)
2 Quthing (QUT)
3 Likhoele and Likhoele E (LIK & LIKE) & Seeiso (SEE)
4 Maseru (MAS)
5 Damplaats (DAM)
6 Golden Gate National Park (GGP & GGB)
Karoo volcanics & Clarens Formation
Elliot Formation
Molteno Formation
LESOTHO
SOUTH AFRICA
Maseru
Clarens
Elliot
Molteno
27°E
28°E
29°E
29°S
30°S
31°S

Noteworthy and characteristic of the UEF are the multiple palaeosol horizons and the flash flood-type deposits which affect the time resolution as dictated by the unsteady rate of deposition. The fluctuations in sedimentation rate and the likelihood of stratigraphic gaps created by abrupt events is a limiting factor of the temporal resolution of the UEF magnetostratigraphy. The density of sampling was attempted to be adjusted over the UEF where feasible.

At Barkly Pass, the UEF is characterised by the transition from the reverse polarity zone that contains the LEF-UEF contact into two N-R polarity pairs (BP3 and BP4). At Quthing, the LEF-UEF boundary falls above a zone of unknown polarity and at the base of a normal-reverse polarity pair (QUT 5). At Likhoele, Likhoele east, Maseru and Damplaats, the LEF-UEF contact falls into a zone of unknown polarity followed by a lowermost UEF normal polarity zone (with exception of LIKE; Fig. 14.5).

The sections at LIK and LIKE contain a normal - long-reverse polarity pair within the middle UEF, which is present in BP, QUT and in the middle to uppermost UEF at Seeiso (SEE; Fig. 14.5). This is capped by a single normal polarity zone in sections BP (BP5n), QUT (QUT6n), LIKE (LIKE2n) and OLD (OLD1n). At GGP there is a single reverse sample within two samples of the LEF-UEF contact.

The OLD site samples the lower and upper palaeosol and TAZ and represents ~9 m thick normal polarity interval (OLD1n) which sits below the uppermost reverse polarity zone at DAM (DAM3r). This uppermost UEF reverse polarity interval is with ~10-15 m of the contact with the Clarens Formation at DAM (DAM3r) and SEE (See1r), and represents the last reverse polarity interval before the uppermost normal polarity zone which caps the Elliot Formation.

14.3 Composite Elliot Formation magnetostratigraphy

The composite magnetostratigraphic section of the Elliot Formation was constructed and scaled by correlating normal and reverse magnetozones defined by all study sites (Fig. 14.5, Figure 14.6, Figure 14.7). The resulting composite Elliot Formation section comprises 7 polarity pairs (EF2 – 8), and two single polarity intervals (the LEF EF1r and the UEF EF9n), encompassing an approximately ~270 m thick composite section. Composite magnetozones may be thinner/thicker at individual sections, given isopach changes

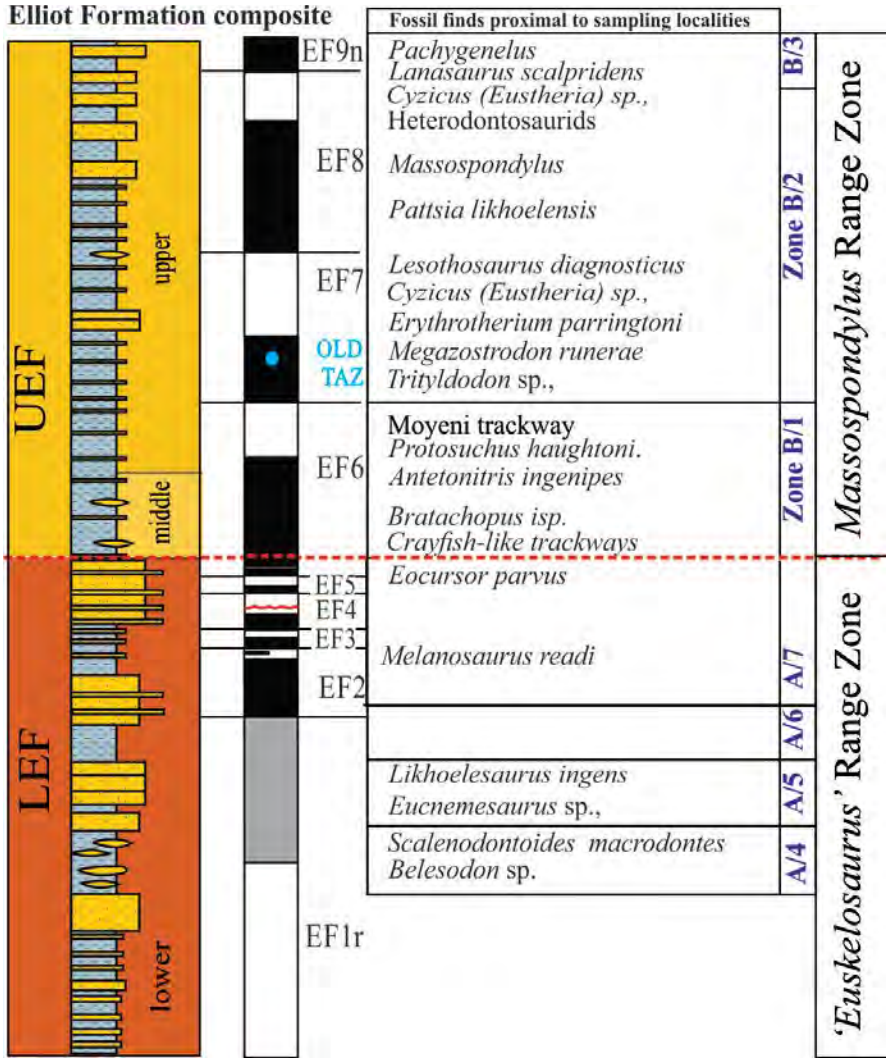

Figure 14.6. Composite magnetostratigraphy of the Elliot Formation with the polarity zones EF1r - 8n against the Bordy and Erikson (2015) stratigraphic section representative of the stratotype at Barkly Pass. The fossil occurrences roughly demarcated against the composite log are for the localities proximal to study sites. The dashed red line indicates the sedimentological contact between the LEF and UEF. The biozones A/4 – 7 and B/1 – 2 are as reported by Ellenberger (1970) and approximated for this composite.

due to local erosional events and variation in depositional conditions which are common within continental, especially fluvio-lacustrine environments (cf. Miall, 2014a, b; 2015). Thus, the polarity pairs in the composite section are idealized and the composite section should be used as a guide or norm for comparison and framework or baseline for future magnetostratigraphic work in the Elliot Formation. Representative fossils found at several sites are denoted against the composite section (Fig. 14.6). An

attempted correlation between the current composite magnetostratigraphic section of the Elliot Formation and that of de Kock's (2003) is presented in Figure 14.7.

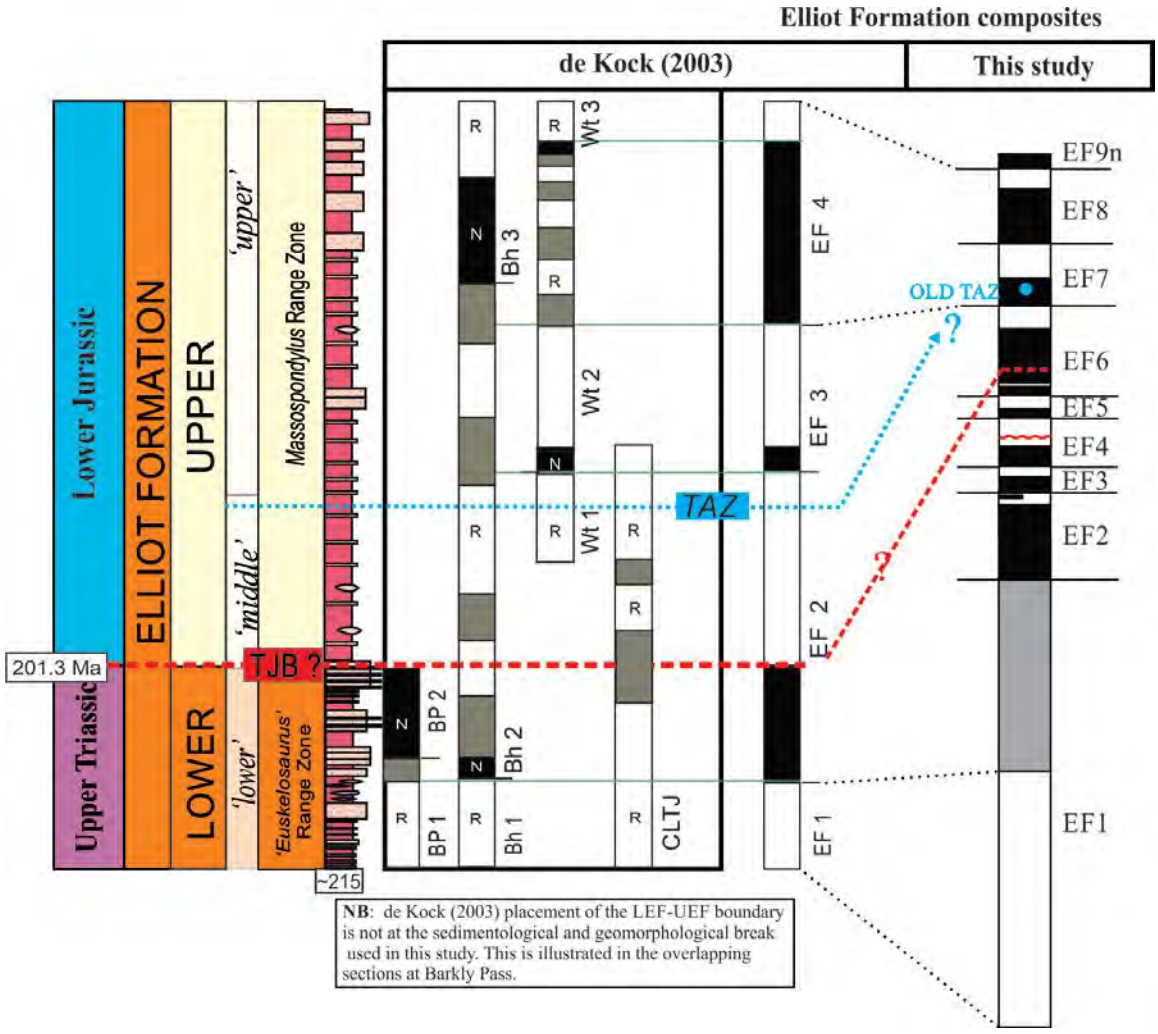

Figure 14.7. Correlation (dashed black lines) of the current composite magnetostratigraphic section of the Elliot Formation is correlated with that of de Kock's (2003). The sedimentological contact of the LEF-UEF falls within the normal magnetochron EF6n of the current study and at the top of EF2n of de Kock's (2003) as indicated with dashed red line. The *Tritylodon* Acme Zone (TAZ) marked in de Kock (2003) profile is within the EF6r magnetochron if correlated to the current section. However, the TAZ at Oldenburg Farm (OLD) lies in the normal magnetochron EF7n. This discrepancy may be explained with the diachronous nature of the TAZ zone.

As indicated in Figures 14.3, 14.4, 14.5, 14.6, and 14.7, the sedimentological boundary of the LEF-UEF falls within the normal magnetochron EF6n; which is directly above a short reversal that was only demonstrated in BP by two samples and a single sample at GGP.

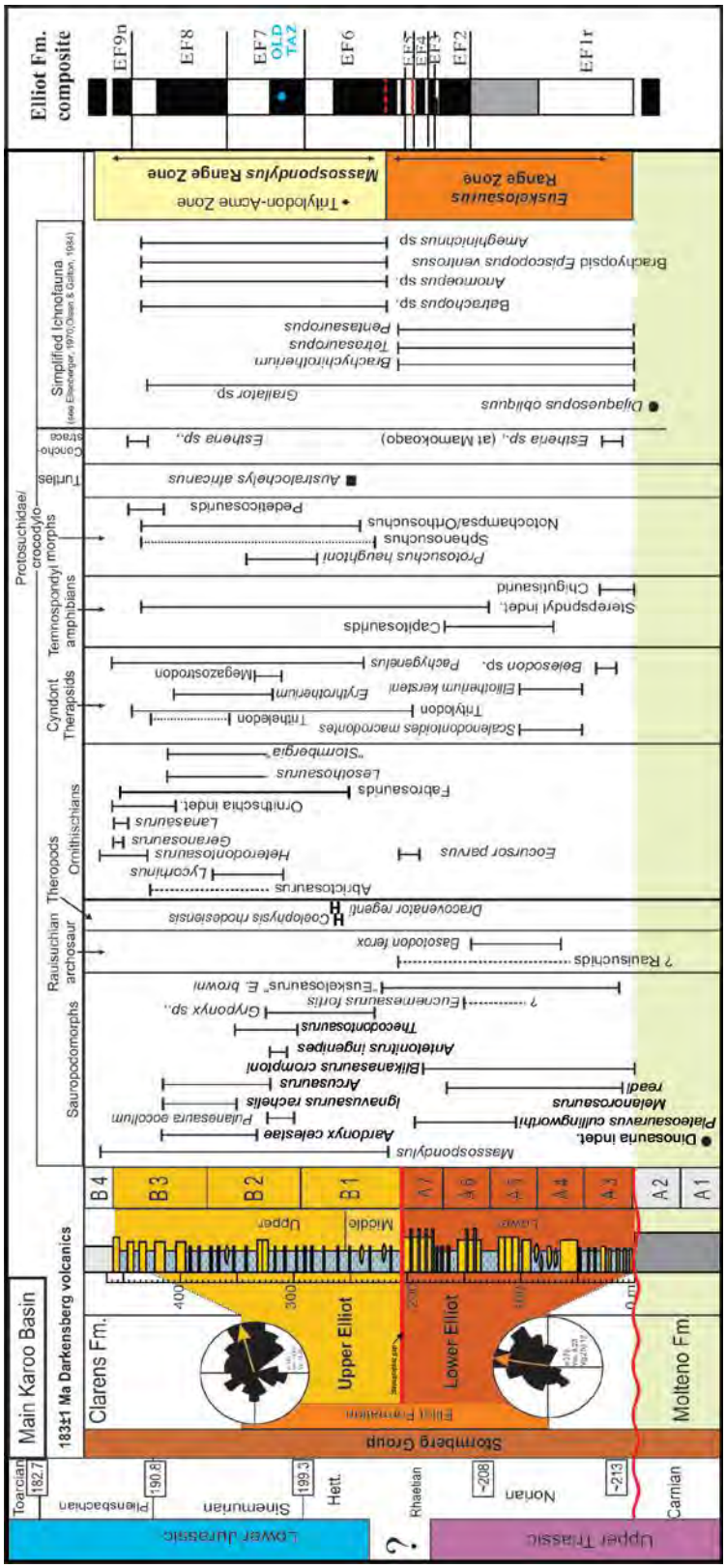

Figure 14.8. Biostratigraphy of the Elliot Formation presented in Section 3.1 (p.31) in relation to the current composite magnetostratigraphic section of the Elliot Formation.

Placement of the boundary within EF6n was on the basis of the LEF-UEF contact falling at the base of the normal polarity interval QUT5n and within the GGP1n. All other sites the LEF-UEF contact occurred over an unconstrained interval. This is due to the contact being developed along a geomorphological plateau, and as such many samples are poorly magnetised, most likely a result of recent weathering. For all other sites, the sedimentological contact of the LEF-UEF is directly below a normal polarity zone, with the exception of LIKE in which there is large break in samples due to their being poor recorders of magnetic polarity (Figure 14.5, 14.9).

The LEF-UEF transition which is coincident with the boundary between the '*Euskelosaurus'* and *Massopsondylus* Range Zones, has been long used as the marker for the faunal turnover between the Late Triassic and Early Jurassic, and thus has been speculated to coincide with the TJB in southern Africa (the TJB; Fig. 14.10.). This transition, a.k.a. the TJB, was originally noted (e.g., Kitching and Raath, 1984, Smith and Kitching, 1997) at the occurrence of a "large nodule horizon" in conjunction with the *Tritylodon* Acme Zone in the northern section. This approach was not utilised in this current study because (i) numerous, vertically reoccurring nodule horizons, with nodules of several sizes are developed within the UEF, and (ii) detailed sedimentological characterization of the diagnostic features of the "large nodule horizon" at the TJB are lacking.

14.4 Magnetostratigraphy summary

For all the sites presented here, it was found that the samples of normal polarity magnetization showed relatively dependable unblocking temperatures >350^{o}C, consistent remanence directions of north-western declination and moderately negative inclination. In correspondence, the samples which displayed reverse polarity magnetization demonstrated consistent remanence directions orientated south to south-easterly and with moderately steep positive inclination.

It is noted that there is also a secondary magnetization direction which overlaps with the normal and reverse polarity remanence directions, and that exhibits a northerly orientated declination and moderate negative inclination. This is considered to be a secondary incomplete overprint associated with Karoo volcanism in the Toarcian. It is hard to distinguish between this secondary overprint in the normal polarity samples owing to the fact the secondary overprint and the primary remanence are similar in declination and inclination. Barring the fact that the secondary magnetisation is often lost at low

unblocking temperatures, often falling below 350°C, it is suspected that the low temperature component may be held within maghemite and magnetite (as per de Kock, 2003); although the Curie temperature for maghemite has been reported as high as 615 °C to 645 °C (Özdemir and Banerjee, 1984; Gehring *et al*., 2009). The development of this secondary overprint is not localised to Elliot Formation samples only and has been reported in other older stratigraphic units within the Karoo Basin, e.g. Beaufort Group (de Kock, 2003; Ward *et al*., 2005; Lanci *et al*., 2013; Maré *et al*., 2014). The development of this secondary northerly steep remanent magnetization have been attributed to (i) recent weathering, and most likely (ii) partial overprint by Karoo volcanism (Ibid.).

14.5 Global correlations

Correlations of the Elliot Formation composite magnetostratigraphic section relies heavily on comparable fossil assemblages. The calculated palaeopoles, and the assessments thereof, aid in establishing global comparability and approximate age ranges. It is important to note that the Early Jurassic is globally known for its homogeneous tetrapod assemblages (Olsen and Galton, 1977; 1984; Attridge *et al*., 1985; Shubin *et al*., 1991; Irmis, 2005a). Recently, newly acquired but sporadic radiometric dates have been obtained for the lower, middle and upper Elliot Formation, but are currently under review and have yet to be published. They have not been used here in the attempt to correlate the sections globally.

Several global continental sections were used for correlation with the composite section of the Elliot Formation. These were included based on the following criteria:

i. Triassic/Jurassic continental deposits
ii. Gondwana/Laurasian
iii. Similarity of their fossil assemblages to that of the Elliot Formation
iv. Magnetostratigraphy
v. Reliable radiometric dates
vi. Useful correlation to marine sections

The Paris Basin, an epicontinental marine setting during the deposition of the Elliot Formation, provides a continuous and detailed record of the Early Jurassic polarity zones in the Northern Hemisphere (Tethys realm) (Yang *et al*., 1996) where one of high resolution is generally lacking.

Nonmarine and marine studies (i.e. Newark and Paris Basin for example) illustrate the dominance of normal-polarity in the Hettangian (Yang *et al*., 1996; Olsen *et al*., 2011). The long normal-polarity and low reversal frequency of the Hettangian Stage is considered to be a useful magnetostratigraphic signal for correlation (Yang *et al*., 1996). Late Hettangian-Early Sinemurian transition is not known from non-marine sections, but in marine sections it is considered to contain high reversal frequency (Yang *et al*., 1996).

14.5.1 **LEF correlations**

The main focus for LEF comparison thus fell onto the continental sections of the Argentinian Ischigualasto–Villa Union Basin, the North American Newark APTS as well as the Chinle Formation (which spans ~225.0 to 207.8Ma; Ramezani *et al*., 2014) and the Glen Canyon Group (specifically the Moenave Formation; Latest Triassic-Earliest Jurassic; Fig.14.2).

Lower Elliot fossil assemblages have been considered to be Norian in age (Knoll, 2004; Lucas and Hancox, 2001), and the sauropods, at least, are considered contemporaneous with those of middle Norian in Germany, the Norian Los Colorados Formation (Agua de la Peña Group, Ischigualasto–Villa Union Basin) and the uppermost Chinle Formation (Yates and Kitching, 2003; Yates, 2007a). Recent magnetostratigraphy and radiometric dates from these formations, and their tie to Newark-APTS 2010 has served as a useful comparison for LEF magnetozones.

14.5.2 **Subchron EF1r**

Three proponents for lowermost LEF, specifically the long reversal (EF1r), and its correlations with South and North America are ranked and explored here based on magnetostratigraphical comparisons:

(i) Firstly, the long reverse magnetozone EF1r as being representative of the Newark subchron E14r, Los Colorados LC7 and the uppermost reversal within the Black Forest Bed (Black Forest Bed dated to 209.926 Ma; Ramezani *et al*., 2011) of the Petrified Forest Member, Chinle Formation (Figs. 14.9, 14.10). This would place the lowermost LEF into the Norian at ~213 Ma.

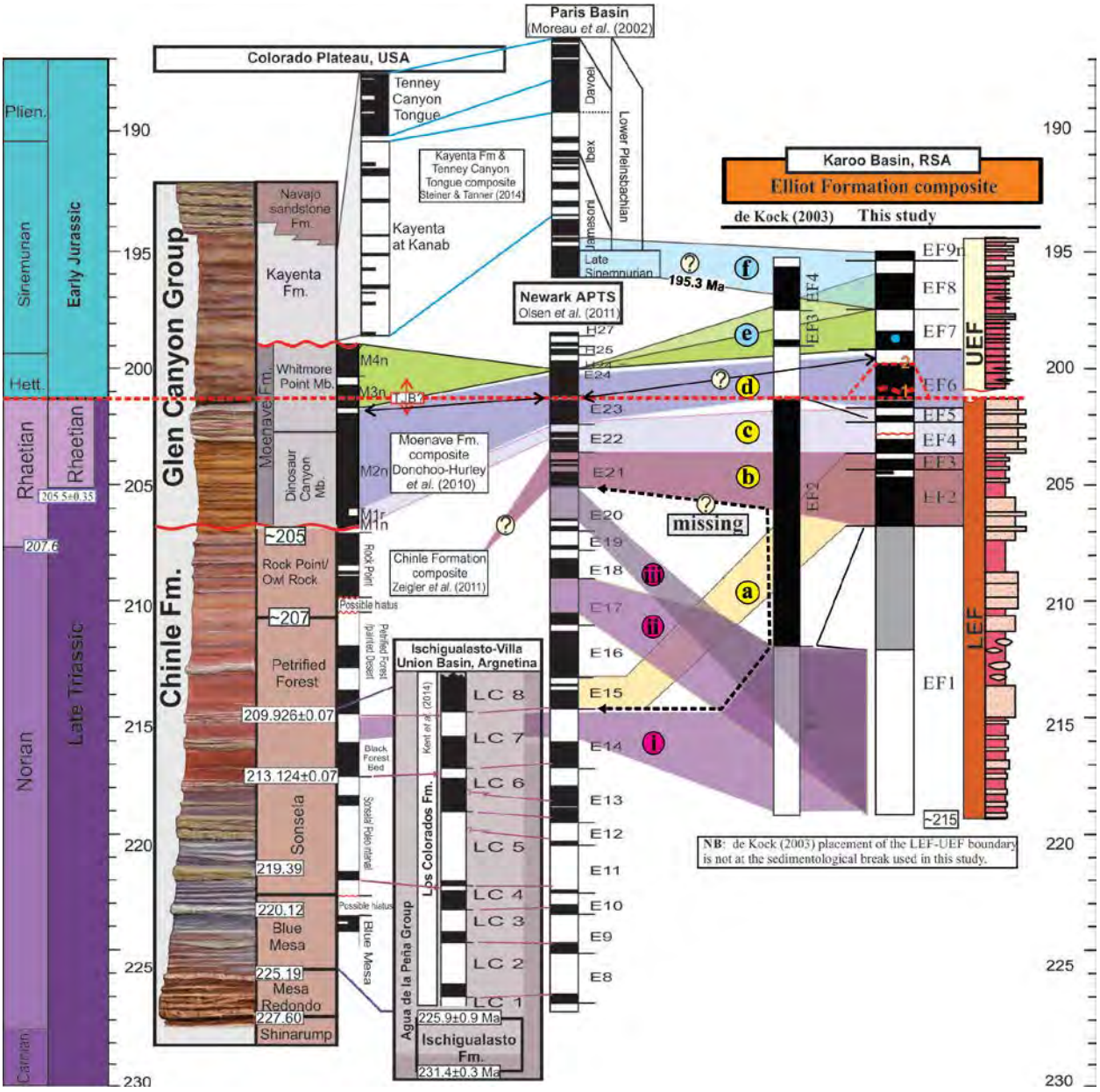

Figure 14.11.Comparison between Elliot Formation composite and the globally available continental sections, with the Paris Basin (marine) as a good proxy for the magnetostratigraphy of the Late Sinemurian/Early Pliensbachian. Block colours - correlation of the lower (LEF) Elliot Formation EF1r is given three options (i, ii, iii), and the correlation options (a) to (f) are discussed in text. Numbers 1 and 2 refer to the placement of the TJB with dashed wavy red line representing the sedimentological break noted in the field. The blue dot in EF7n chron is the location of the TAZ at the OLD site.

(ii) The second option places EF1r within the Newark E17r which broadly correlates with the uppermost Petrified Forest at an age between ~213 - ~209 Ma.

(iii) The third correlation option would place EF1r within the Newark E20.2r and is likely to be tied to the lowermost Rock Point/Owl Rock members of the Chinle Formation with an uppermost age range of ~ 209 – 205 Ma.

As there is no/little biostratigraphically support for correlation with the Newark magnetochrons, the tentative correlations of the EF1r with Newark Chron E17 (latest Norian) or Newark Chron E20.2r (Rhaetian) are purely based on magnetic polarity pattern (long reversal), and this comparison is not strong enough evidence to substantiate a correlation. Supporting evidence for the magnetostratigraphic correlation (i), listed above, as being the most likely scenario is explained in the following sections.

14.5.2.1 LEF sauropodomorphs

The LEF is considered by some (e.g. Yates, 2007b) as being the richest Late Triassic sauropodomorph fauna. It shares several affinities with Europe and South America (p.35). Parallels have been drawn with the Norian Los Colorados Formation which have led many to consider the two separate basins to be contemporary (Yates, 2007b; McPhee, 2013).

More specifically, *Eucnemesaurus fortis* is considered by Yates (2007b) as the sister taxon to the South America *Riojasaurus* and one of the two genera of the Riojasauridae (Yates, 2007b; McPhee *et al*., 2015a); while the Los Colorados Formation *Lessemsaurus* has been correlated with possible LEF sister-taxon *Antetonitrus* (Pol and Powell, 2007). Thus the shared derived presence of several characters between the South America and South African specimens has suggested a close biogeographic tie between the two continents (Bonaparte, 1971).

In light of the new age ranges for the Los Colorados Formation (~ 227 Ma to ~213 Ma by Kent *et al*., 2014), however, this connection is brought into question. It is more likely that this relationship is one along an evolutionary path with the LEF forms being more derived (less primitive, as per McPhee pers. comm.).

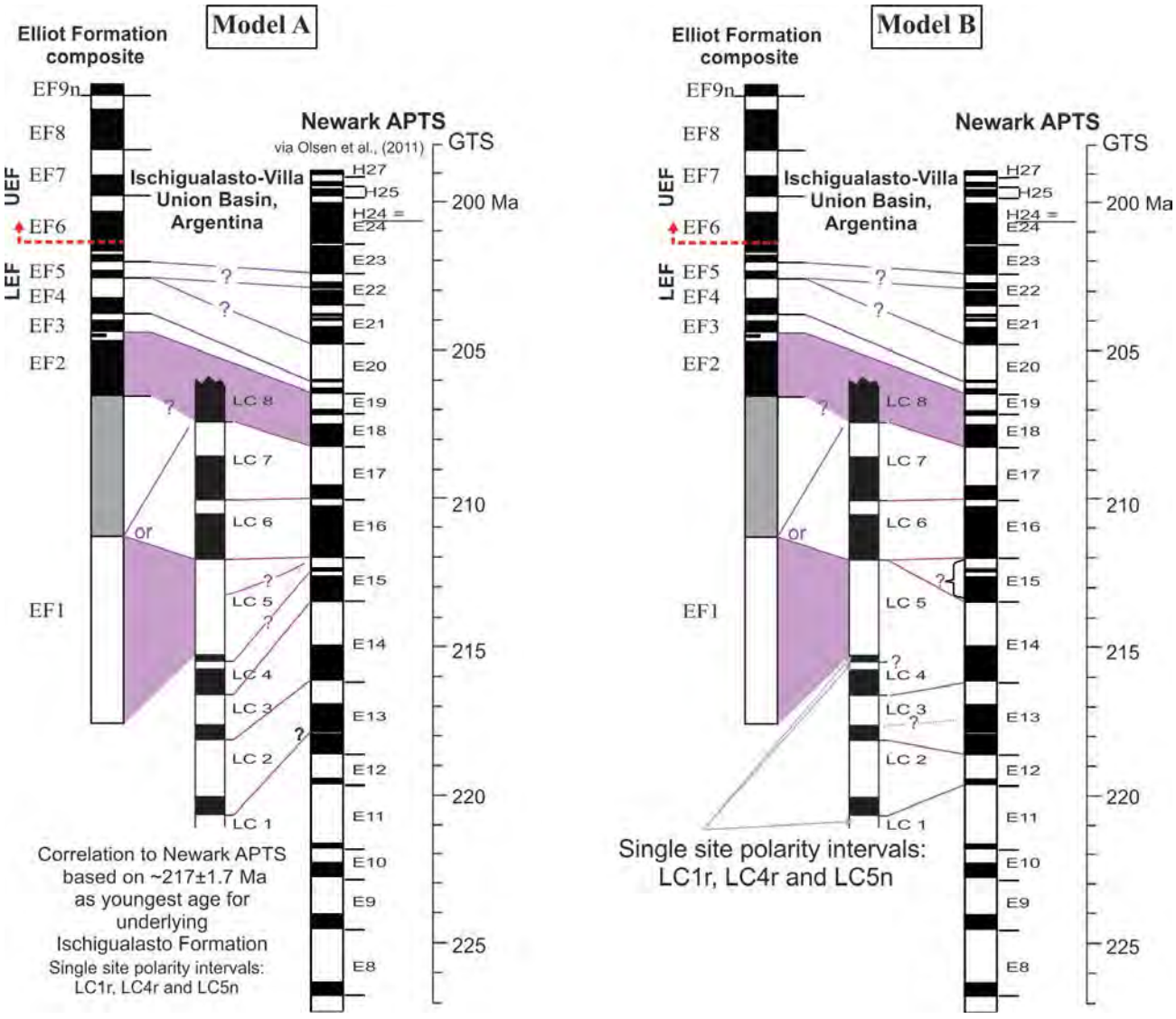

Figure 14.12. Correlation between the magnetostratigraphy of the Los Colorados Formation (Kent *et al*., 2014) and the lower Elliot Formation (LEF) of this study, mainly through the comparison of faunal similarities. Magnetostratigraphic correlation to the Newark APTS of Olsen *et al*. (2011). Solid correlations are discussed and utilised in text. The correlation of Kent *et al.* (2014) magnetostratigraphy utilises the erosive unconformity stated between the Ischigualasto and Los Colorados Formation, in conjunction with fossil occurrences between the LEF and Los Colorados as an indicator of a younger given age for the Los Colorados Formation. Model A corresponds to Newark E13.2r to E18.1r, whereas option B corresponds to Newark E11r to E18.1r. Model B considers the likelihood that LC4r and LC5n are unknown polarity intervals given then single sample polarity intervals.

Secondarily, it could mean that the placement and use of radiometric ages from the underlying Ischigualasto Formation causes biased magnetostratigraphic correlations, and that there may be a noteworthy lapse in time between the deposition of the Ischigualasto Formation and the overlying Los Colorados Formation. Arcucci *et al*. (2004) highlight the fact that the contact between the Los Colorados

and Ischigualasto Formations is an unconformity, although the nature of the unconformity is still debated. The radiometric age often used for correlation, 225.9 Ma, comes from the *Exaeretodon* Biozone which is still overlain by ~50 m of the sediments comprising the *Jachaleria* Biozone of the Ischigualasto Formation (Martinez *et al*., 2011, and their Figure 4 on p. 209).

An attempt to correlate the magnetostratigraphy of Kent *et al*. (2014) to the Elliot Formation, based on the shared fauna, cynodonts (cf. *Tritylodon*) and crocodilomorphs, and the Newark APTS is shown in Figure 14.10. Two correlation models are presented given that the correlation is based on polarity pattern and cannot be secondarily attributed to the Newark APTS based on fossils or radiometric ages. Model A shifts the age the Los Colorados Formation to between ~218 Ma (E13.1r) and ~208 Ma (E18n; Fig. 14.10) making it 9 myr younger than the range of Kent *et al*. (2014: ~227 Ma to ~213 Ma). The second option, model B, places the Los Colorados Formation between ~219/220 Ma (E11r) and ~208 Ma (E18n; Fig. 14.10). This model B considers that the single polarity intervals which constitute LC4r and LC5n are circumstantial and have been ignored. Furthermore, it makes the chron E15 difficult to place in the Los Colorados succession, making it possible that multiple hiatuses are a consideration through the LC4/ LC5 intervals (Fig.14.10).

Previous support for a younger age for the Los Colorados Formation on the basis of its fauna has been suggested (Lucas, 1998; Martinez, 2002; Arcucci *et al*., 2004). Lucas (1998) proposed it to be Apachean (Rhaetian-aged) based on the prosauropods, although acknowledging this as a fragile correlative. Furthermore the mix of Late Triassic and Early Jurassic forms in the Los Colorados Formation (see Arcucci *et al*., 2004) bears some consideration for the likely diachronous nature of the Formation between locations (i.e. La Sal and La Esquina sections) with many undetected paraconformities. If the correlation present here (model B: Fig. 14.10) is validated, it would mean that the Los Colorados Formation overlaps with the Sonsela and Petrified Forest Members of the Chinle Formation. It would also mean that the Adamanian–Revueltian faunal transition, documented by Ramezani *et al*. (2014) as occurring in the Chinle Formation, is present within the Los Colorados Formation.

The best fit scenario, given the above arguments, is that the lowermost LEF EF1r magnetozone ties (largely based on fossil assemblages) well with either the uppermost Los Colorados Formation's LC5r or the LC7r zone regardless of its correlation to the Newark APTS (Fig. 14.10). If Kent's *et al*. (2014) correlative to the Newark is considered, this would then tie to the chron E12r (? ~218/219 Ma) or E14r (~214 Ma; Fig. 14.9). If the current model A presented in Figure 14.10 is considered, this would be tentatively correlated to Newark chron E15r (~212 Ma) or Newark E17r (~209 Ma), respectively. The

magnetic correlation of LC5n and LC5r to the Newark E15.2n and .2r is uncertain given the duration of the LC5r interval. This could be reasoned as a factor of hiatuses, and variable and low sedimentation rates but as there is no field evidence to support or rebuke this hypothesis, it cannot be ascertained. If model B (Fig. 14.10) is considered the more likely a scenario, given the long reverse polarity interval, then the EF1r would tie equally well with the Los Colorados subchron LC5r and the Newark subchrons E14r (~214 Ma). The problem of imperfect correlation to the Newark APTS is likely a result of variable sedimentation rates, hiatus and erosion that is typical in non-stationary depositional environments.

Furthermore, it is difficult to narrow down which correlation is more accurate as the fossil assemblages do not establish more specificity to the ages. The uppermost (upper third; Kent *et al*., 2014) of the Los Colorados Formation is typified by the La Esquina local fauna which contains the prosauropod dinosaurs *Riojasaurus* and *Coloradisaurus* (Arcucci *et al*., 2004) giving credence to both ages suggested in models A and B (E15r at ~212 Ma and E14r at ~214 Ma, respectively) based on the stratigraphic occurrence of the LEF *Eucnemesaurus*. *Coloradisaurus* is the only known massospondylid from the Late Triassic but with uncertain phylogenetic affinities (Apaldetti *et al*., 2014).

If Kent *et al*. (2014) model (Fig. 14.9) is considered then this would set the base of the Elliot Formation to ~218/219 Ma. In light of the given, albeit contested age, of ~215 Ma for the onset of the LEF sedimentation (Hälbich *et al*., 1983; Catuneanu et al., 1998), the earlier age (E14r ; ~214 Ma of model B; Fig. 14.10) for the Lower LEF is more probable.

Magnetic correlation to the composite magnetostratigraphy of the Chinle Formation by Zeigler *et al.* (2011) is presented in Figure 14.9. The last reversal reported in the Black Forest Bed of the Petrified Forest Member (Zeigler *et al*., 2011) can be tentatively correlated, based purely on magnetic polarity, with LC7r. If the models of this study, presented in Figure 14.10 for the Los Colorados Formation correlation to the Newark APTS is considered, this would allow the LC7 to fall within the E17 at an age of ~208-209 Ma as previously suggested. Furthermore, this complements the new radiometric date for the Black Forest Bed at 209.926±0.072 Ma and the underlying uppermost Sonsela Member is 213.124±0.07 Ma (Ramezani *et al*., 2014). However, the composite Chinle Formation magnetostratigraphic section provided by Zeigler *et al*. (2011) makes interpretation of the chrons corresponding to the different members exceptionally difficult as they are unlabelled. Biostratigraphic information, reported by Parker and Martz (2010) indicate that common fossils within the Black Forest Bed are *Protosuchus*, the phytosaur *Pseudopalatus* and the aetosaur *Typothorax coccinarum* which have not been useful in substantiating the magnetostratigraphic link suggested above. Regardless, an acceptable lowermost age

range for the LEF is between ~ 213 - 209 Ma or latest Norian. This would fall within the already accepted biochronological range for the LEF.

Currently, the best high resolution U-Pb zircon chronostratigraphy for the continental Late Triassic comes from the Chinle Formation which closely and independently ties it to global Triassic marine beds and records the appearance of dinosaurs in North America at ~223 Ma (Irmis *et al*., 2011; Ramezani *et al*., 2011; Atchley *et al*., 2013; Ramezani *et al*., 2014).

Other possible correlations between the Formations could pivot on the preservation of more advanced theropods, such as *Coelophysis bauri*, which in the Chinle Formation co-occurs with basal saurischians and rauisuchids (Parker and Martz, 2010). This is contra that of the Los Colorados Formation where only a coelophysoid equivalent *Zupayasaurus rougieri* (Ezcurra and Novas, 2007) is reported. In South Africa and Lesotho, there are limited *Coelophysis* remains and mostly constrained to the UEF (some within the TAZ) as well as the overlying Clarens Formation. *Grallator* trackways referable to (coelophysid) theropods are found from LEF and into the UEF and Clarens Formation (Knoll, 2005).

Further contemporaneous Late Triassic European deposits, such as those of Germany (Keuper Group; Yates, 2003) and the Norwegian Lunde Formation have been shown to share *Plateosaurus* with the LEF. Although there are no radiometric dates associated with these finds, the *Plateosaurus* bone fragment from the Lunde Formation has been palynological constrained to the Rhaetian (~202/203 Ma; Hurum *et al*., 2006). In all likelihood it can be assumed that the range for this Late Triassic sauropodomorph extends close to the TJB.

14.5.3 **Magnetozones EF2 and EF3**

The position of magnetochron EF2 and EF3 may be placed at two intervals of disparate age within the Newark APTS. Firstly, biostratigraphically the EF2 and EF3 magnetochrons can be tied to the uppermost Los Colorados Formation. Based on an assessment of the model by Kent *et al*. (2014) (Fig. 14.9), the EF2n subchron can cautiously be establish within the LC8n (and the Newark magnetochron E15, ~213 Ma) given the correlation of EF1r within the LC7r interval shown in Figure 14.9. This would solely be based on polarity for the correlation to the Newark basin APTS, and secondarily on the biostratigraphy. A rapid rate of sedimentation over the unknown LEF interval would be consistent with this interpretation, but which cannot be sedimentologically supported at Barkly Pass.

A second option for correlation option (b), presented in Figure 14.9, tentatively correlates the EF2 and EF3 magnetochrons with Newark chron E21 (~203 – 205 Ma) based on polarity alone, and to the Rock

Point/ Owl Rock Member (Zeigler *et al*., 2011). The latter is considered to span in age approximately from ~207.2 Ma (Petrified Forest- Owl Rock contact) to 205 Ma (Ramezani *et al*., 2011, 2014). Thus, the EF2n may represent a lowermost age of ~207 Ma and the EF3r may represent an uppermost age of ~205 Ma. This would make the stratigraphic gap between the EF1r and EF2n a loss of ~2 – 6 million years. However, chronologically and biostratigraphically, it is difficult to link the Rock Point/Owl Rock Member with the LEF. Although conchostracans have been reported in LEF (e.g., *Estheria* sp., at Mamokoaqo; Ellenberger, 1970) and are present in the Late Norian Rock Point Member too (Lucas *et al*., 2011), these units have not been shown to be correlatives of those found in the Karoo Basin. The marine section at Pignola-Abriola places the Norian-Rhaetian boundary (MPA 5r magnetozone) at ca. 205.7 Ma (Maron *et al*., 2015) within the Newark APTS magnetozone E20r.2r directly below the proposed correlation here to Newark magnetochron E21. Biostratigraphic support for the correlation with the Rock Point/Owl Rock Member of the Chinle Formation is thin as the Revueltian-aged (early to mid-Norian) fossils (e.g. *Pseudopalatus*, *Typothorax*, *Trilophosaurus* and metoposaurs) from the Owl Rock Member have not proven fruitful for correlation (Parker and Martz, 2010); and furthermore, there are no sister taxon found within the Elliot Formation.

Conversely, the current models cited in Figure 14.10 would allow for the aforementioned correlation of EF1r to the Los Colorados Formation LC5 and thus polarity interval EF2 can, theoretically, fall between magnetochrons LC6 – LC8n because of imprecise biostratigraphy. That said the sampling gap between EF1r and EF2 must represent a significant amount of time given the width of the unknown polarity interval (~60 m). EF2 represents the lowermost middle section of the LEF and the, to date, last occurrences of *Melanorosaurus*, *Eucnemesaurus*, and the Capitosaurids (Fig. 14.8). It could convincingly tie with the LC8n of the Los Colorados Formation and be tentatively linked to the Newark E18 and E19 magnetochrons. This would characterize a time span between 207 – 206 Ma for EF2. It would, additionally, cautiously place EF3 into the overlying Newark chron E20, and likely denote the E20.1n and E20.1r (Fig. 14.10).

14.5.4 **Magnetozones EF4 and EF5**

It is difficult to place the magnetozones EF4 – 6 within the Newark APTS or within its potentially biostratigraphically tied Latest Triassic Dinosaur Canyon Member of the Moenave Formation (Glen Canyon Group). The incongruity in the magnetic correlation can be on the basis on the depositional hiatus/ paraconformities which lend to an incomplete stratigraphic sequence of the Elliot Formation; a

case in point is illustrated in Figure 14.10 where question marks denote the difficulty in tying magnetic chrons based on approximated biostratigraphic ranges and associated dates.

Figure 14.9 presents a correlation, option (c), which incorporates EF4 – EF5 into a single polarity unit which has been attempted to be correlated with Newark E22 magnetochron, and for which the uppermost reversal of both the Elliot composite (EF5r) and E22r corresponds to the Late Triassic Moenave Formation M1r (Donohoo-Hurley *et al*., 2010). Based on polarity pattern alone, the EF4 and EF5 magnetozones may be tentatively correlated to Newark E22 supplemented by the previous correlation of M1r within the Newark sequence (Figure 14.9). This magnetozone (M1r), as well as the overlying M2r (correlated to Newark E23r), have been tied with palynofloral shift (*Classopollis meyerianus* to *Classopollis torusus*) and the ichnogenus *Eubrontes* to the Newark APTS. Lucas *et al*. (2011) have proposed that the M1r is Late Norian in age based on the occurrence of Rhaetian conchostracan assemblage (the monospecific *Euestheria brodieana* assemblage) above the M2r interval, and thus that the M2r interval represents the TJB. This is based on the lithostratigraphic correlation of conchostracans from the Whitmore Point Member as the Dinosaur Canyon Member does not contain conchostracans (Kozur and Weems, 2010; Lucas *et al*., 2011).

Fossils which typify the fauna of the Dinosaur Canyon Member are coelophysoid theropods and a wealth of trackways with reported sauropodomorphs (*Eosauropus*), crurotarsans (*Brachychirotherium*), and theropods (*Grallator*) (Lucas *et al*., 2005; 2011).

14.5.5 **Straddling the LEF-UEF boundary: Magnetozone EF6**

The normal magnetozone EF6n occurs over the sedimentological divide between the LEF and UEF which traditionally and tentatively has been considered the TJB in the Elliot Formation (Figs. 14.4, 14.9). This boundary also reflects a shift in representative fauna within the Elliot Formation. The previous palaeomagnetic study of the Elliot Formation (de Kock 2003) illustrated the presence of one long normal polarity zone (EF2n) corresponding to the uppermost LEF and the transition into the UEF. The long normal polarity is approximately corresponding to the EF2 – EF6 of the current study (Fig. 14.9). The EF6.1n (av. ~5 - 15 m thick) is punctuated by a short reversal (2 samples at BP and one sample at GGP) just below the LEF-UEF divide (Figure 14.4). EF6.1r is approximately 3 -5 m thick.

Option (d) has been proposed for the correlation of the EF6 interval with the Newark APTS (E23 + E24) and the Moenave Formation (Fig. 14.9). Tentatively, the Rhaetian-aged (Kirkland *et al*., 2014) M2r has been linked to uppermost reversal EF6.2r. This link is lacking substantiating evidence and this correlation

is purely based on assumptions about the Late Triassic biostratigraphic age of the Elliot and Moenave Formations. This would place the E23r within the EF6.1r, and the TJB could be shifted upwards within EF6.2n which is a protracted normal polarity period typical of Earliest Jurassic or, less likely, within the EF7n (a thin normal magnetozone).

The Moenave Formation M2r has been considered to be correlated with Newark chron E23r, SA5n.2r or SA5n.3r of St Audrie's Bay, the H- from the section at Oyuklu, (Turkey) as well as BIT5n.1r (Italcementi Quarry, Italy; Donohoo-Hurley *et al*., 2010). In consideration with the Newark APTS, the Moenave (Molina-Garza *et al*., 2003; Donohoo-Hurley *et al*., 2010) and Elliot Formation magnetostratigraphy can tie in with E22/E23 magnetozones. Lucas *et al*. (2010) have questioned the position of the M2r interval within the E23r on the basis of the conchostracan biostratigraphy which places the M2r immediately below the Rhaetian-aged *Euestheria brodieana* Zone. Instead, these authors propose that a better correlation of E23r can be made with the poorly-defined lower Dinosaur Canyon member polarity magnetozone M1r. Contrastingly, Kirkland *et al*. (2014) have provided evidence for the ETE to occur over the M1 and M2 intervals with the TJB occurring over the M3 and M4 polarity intervals (an illustration to this effect is presented on p. 349, Fig. 20). This would tie in well with the magneto- and biostratigraphy of the Elliot Formation whereby the ETE would be more likely to occur over the LEF-UEF divide (Figs.14.9, 14.11)

The LEF-UEF divide is not only a sedimentological break with a change in fluvial style, palaeocurrent direction and provenance but also one which shows changes in isopach trends and fossil content (Bordy *et al*., 2004a, b, c). In consideration of a period of non-deposition and erosion over this sedimentological break and basin reorganization, one could assume that a loss of time could be reflected on and over the sedimentological divide between the LEF and UEF. The magnitude of this loss is undetermined to date, and the current biostratigraphic resolution does not allow predicting or measuring it. The need for a revised and more detailed biostratigraphy of the Elliot Formation and the fossil groups which straddle the transition is paramount, and so is the need for absolute dating (e.g., detrital zircon ages). Stratigraphic data on all collected fossil material from the Formation is in dire need of re-assessment.

14.5.6 **ETE and TJB within EF6 (?)**

The placement of the ETE within the UEF rests on its correlations with the Moenave Formation by Donohoo-Hurley *et al*. (2010) and the revisions by Kirkland *et al*. (2014) with respect to palaeontological

evidence. The first placement of the ETE is at the boundary at the base of the EF6.1n (sedimentological break labelled '1'), or at the boundary between EF6.2n and EF6.2r, the latter corresponding with E23 + E24n and the M2r (Fig. 14.9; labelled '2'). If this is the case for the placement of the ETE, then the likely placement of the TJB rests on the information given in Kirkland *et al*. (2014) whereby the TJB is likely within the M3n – M4n interval. This can be tied to either within the EF6.2n or higher in the sequence (Figure 14.11).

14.5.7 **UEF correlations**

The UEF has been considered to be Early Jurassic and more specifically Hettangian – Sinemurian in age (Kitching and Raath, 1984; Lucas and Hancox, 2001; Knoll, 2005). It has been largely compared with North and South America, because of the similarities between the ichnological records but also because of the faunal associations. The *Tritylodon* Acme Zone (TAZ) has been previously used as a marker horizon in the UEF, and has either considered to occur within the lowermost UEF (Kitching and Raath, 1984) or at the boundary between the '*Euskelosaurus*' and *Massospondylus* Range Zones (Smith *et al*., 2011). It was at one point considered to be a maker for the TJB (Olsen and Galton, 1984), although Kitching and Raath (1984) considered a palaeosol horizon of large pedogenic nodules occurring below TAZ to be the field marker for the TJB.

Based on the correlation of the magnetozone EF6 discussed above, it is likely that at least the lower part of the UEF, across the LEF-UEF divide, is latest Triassic in age. Thus, the first truly Jurassic-aged rocks may be those within the magnetochron EF7 and upwards.

14.5.8 **Magnetozone EF7**

A slightly prolonged normal polarity is represented in the EF7n chron which bears fossil remains of *Protosuchus, Pachygenelus, Megazostrodon, Erythrotherium* and *Lycorhinus,* in addition to trackways (e.g., the Moyeni site) of Early Jurassic age. It is also within the EF7n chron that the TAZ was found at the OLD site in this study (Figs.14.9; 14.11).

Based on the occurrence of similar body and ichnofossils (Ellenberger, 1970, 1972), for instance, a specimen of *Protosuchus,* conchostracans and the ichnotaxon *Eubrontes,* the Moenave Formation magnetochrons M3 and M4 (Donohoo-Hurley *et al*., 2010) of the Whitmore Point Member tie to the UEF EF7 (and potentially EF8; option e; Fig. 14.9) chron. *Grallator-Eubrontes* track zone and the *Anomoepus*-like trackways are considered representative of the Early Jurassic globally (Lockley, 1991; Knoll, 2005). Furthermore, *Protosuchus haughtoni* (Busby and Gow, 1984; Gow, 2000) is closely related to the

specimen (*Protosuchus richardsoni*) from the Dinosaur Canyon Member (Sues and Olsen, 2015). *Protosuchus haughtoni* readily occurs throughout the UEF and has been reported from the lower parts of the UEF, which would be coincident with the EF6/EF7 magnetochron (Fig. 14.9). Recently, Kirkland *et al*. (2014) proposed that, although traditionally considered earliest Hettangian in at the Dinosaur Canyon Member, this basal crocodylomorph is in latest Triassic strata in Nova Scotia. Conchostracans in the uppermost UEF have not been considered diagnostic and appear to exhibit provincialism (Tasch, 1984) despite being thoroughly used for North America- European correlations (Kozur and Weems, 2010).

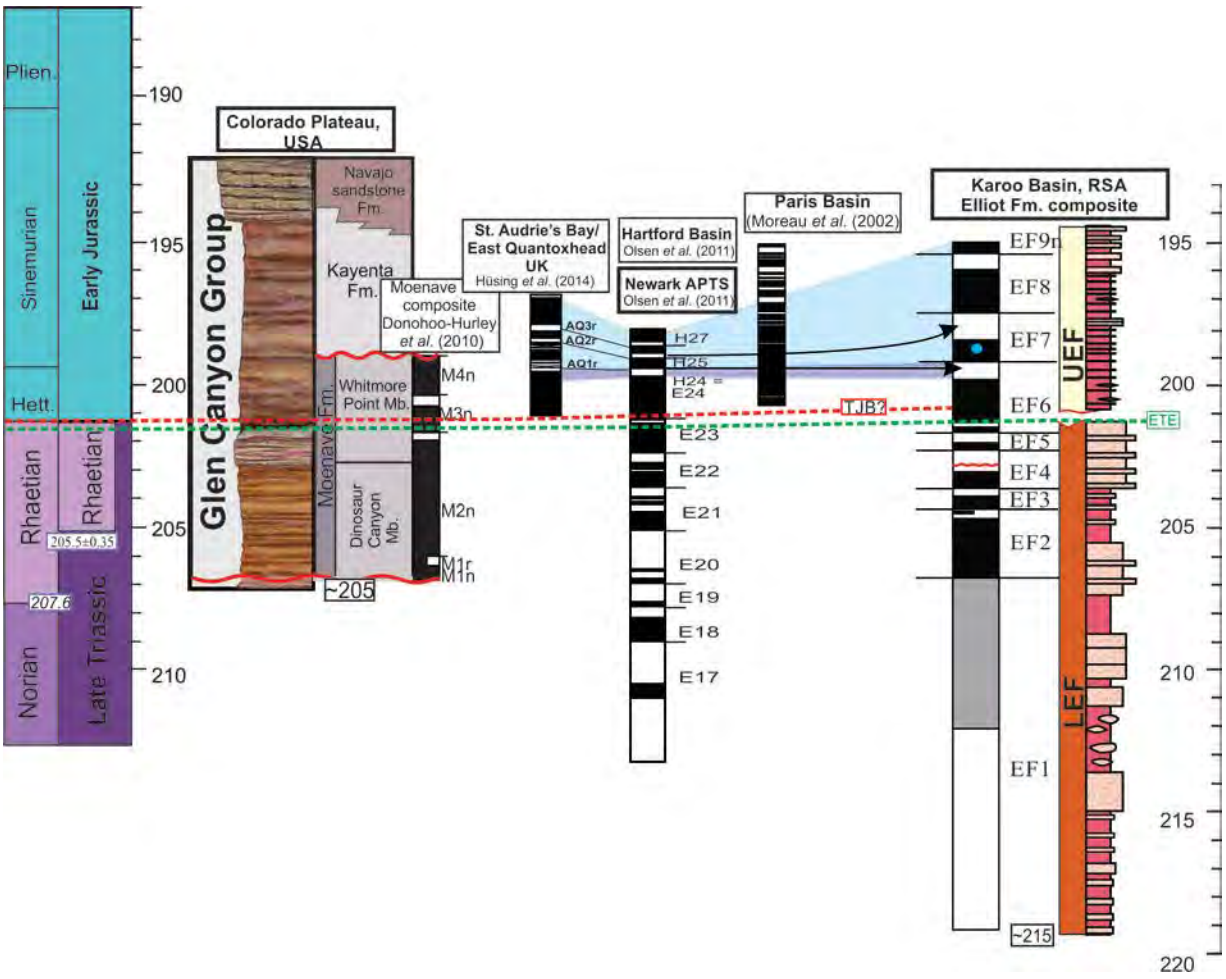

Figure 14.13 Comparison of Early Jurassic magnetostratigraphic sections from the St. Audrie's Bay/East Quantoxhead composite section (astronomically-calibrated magnetostratigraphic), Hartford Basin, Paris Basin and the Newark APTS. Placement of the End-Triassic mass extinction event (ETE) and the Triassic-Jurassic boundary within the Elliot Formation magnetozone EF6 is shown.

Donohoo-Hurley *et al*. (2010) used the above mentioned fossils (*Protosuchus*, *Eubrontes*, conchostracans) and their biostratigraphic position to provide relative ages that indicate an at least latest Triassic age for the Whitmore Point Member, and the likely occurrence of the TJB within its upper section. Thus, conservatively it is likely that the EF7 magnetochron, if correlated with Moenave M3 interval (option e; Fig. 14.9), could be Late Triassic-Early Jurassic in age, spanning the TJB if Kirkland *et al*. (2014) assertion for the placement of the boundary over the M3/M4 interval is uncritically accepted. Figure 14.9 indicates the Elliot Formation sedimentological break used as a TJB marker to be parallel to the marker in the Moenave Formation which falls within the E23r of the Newark APTS according to Donohoo-Hurley *et al*. (2010). They report a short reversal magnetozone from Moenave sections near the TJB this was not seen in the Elliot Formation sections, although a period of reverse polarity was noted within the BP section over the sedimentological divide. Furthermore, the Moenave M3r has not only been correlated with Newark polarity record, but has been said to be correlated to the St Audries SA5n.5r, and the Turkish reversal J-. Kirkland *et al*. (2014) are proponents of the M3r, or at least the M3/M4 transition, containing the TJB in the Moenave section, and that the ETE is represented over the interval suggested by Donohoo-Hurley *et al*. (2010) as being related to the TJB.

In contrast, Figure 14.11 utilised the recent work of Hüsing *et al*. (2014) which has established a reputable magnetostratigraphic composite for the Hettangian at St. Audrie's Bay/East Quantoxhead. This new composite repeats the terrestrial pattern of the Hartford Basin magnetostratigraphy (USA). Thus, the repeated corroboration of a. long normal period characteristic of the Early Jurassic which is interrupted by three short reverse polarity chrons is seen in more than one section in both the marine and continental sphere. If these sections are compared to the UEF it is likely that EF6 contains both the ETE at the break between the LEF and UEF and above this, within EF6.2n, or higher, the TJB falls. This would place the EF7 magnetozone into the earliest Jurassic. Figure 14.11 attempts to correlate the Elliot Formation EF6.2r – EF9n to Hartford Basin H24r – H27 and thereby AQ1r – AQ3r (of St. Audrie's Bay/East Quantoxhead composite; AQ). This correlation places the UEF EF6.2r – EF9n as Hettangian – Sinemurian in age.

14.5.9 **Magnetozones EF8 and EF9n**

Finally, magnetochrons EF8 and EF9n can then represent a much later time period (option f; Fig. 14.9) and can be correlated with the Hettangian Hartford Basin and St. Audrie's Bay/East Quantoxhead composite as well as the Late Sinemurian Paris Basin (Fig. 14.9; Hüsing et al., 2014). The Montcornet core reverse magnetozone at 1073.8 m, palynological equivalent to the magnetozone SA5r at St Audrie’s

Bay which lies a few metres above theoretical TJB (Hounslow and Muttoni, 2010). Support for this assertion is only likely if the occurrence of the tritheledontid *Pachygenelus monus* (Gow, 1980) is considered. The postcanine teeth of *Pachygenelus monus* are similar to *Pachygenelus* cf. *P. monus* from the McCoy Brook Formation which overlies the U-Pb dated North Mountain Basalts (201.566±0.031; Blackburn *et al*., 2013; Sues and Olsen, 2015). Many *Pachygenelus* specimens have been reported as occurring within ~3 m of the UEF-Clarens Formation contact (see Table 14.3; Sidor and Hancox, 2006) this could indicate an age of as young as ~201 Ma for the upper part of the UEF. Nevertheless, one has to consider the condensed nature of the Elliot Formation in the northern parts of the basin and their potential to record significant amounts of time over short depositional intervals. The first assumption may inaccurately bias support to the extension of the TJB to within the upper UEF and would mean that much of the LEF and lower UEF are Late Triassic in age. The weakness of this reasoning is evident as it is based on one fossil taxon, and although an intriguing possibility the occurrences with other contemporaneous fossil group and their biostratigraphic position, as well as correlation to global sites, is contrary to this hypothesis. Biostratigraphic evidence from South America (Caturrita Formation, Brazil and Los Colorados Formation, Argentina) of other tritheledontid taxa have been considered Norian in age (Sidor and Hancox, 2006), and thus do not lend support to the above assumption unless ideas of dispersal are considered.

The Glen Canyon Group (southwestern USA) shares *Tritylodontids* (Kayenta Formation contains the Pliensbachian tritylodontid cynodont *Oligokyphus* sp.; Sues and Olsen, 2015) Fabrosaurid ornithischians (*Scutellosaurus lawleri* and ?*Scelidosaurus* sp.; Tykoski, 2005), heterodontosaurids ornithischians (Sereno, 1997), prosauropods and protosuchian crocodiles on a familial level with the UEF. Lufeng Formation (Lower Jurassic; China) also shares on a familial level morganucodontid mammals, *Tritylodontids*, plateosaurid prosauropod dinosaurs, theropod dinosaur (*Megapnosaurus;* Irmis, 2004), fabrosaurid and heterodontosaurid ornithischians (Irmis and Knoll, 2008), protosuchian and sphenosuchid crocodiles (Olsen and Galton, 1984). Morganucodontid mammals are also shared with the English Fissure fills (Mendip Fissures, United Kingdom; Wall and Jenkyns, 2004), and these have been assigned (based originally on palynofloral correlations) to the Sinemurian. Morganucodontid mammals, in addition to the genus *Tritylodon*, are shared not only between North American, British and Chinese basins but also and famously within the “Rhaeto-Liassic” beds of Wurttemberg (Germany; Clemens, 1979, 1980*).* Thus many of the UEF mammals, *Erythrotherium* and *Megazostrodon*, originally considered Triassic in age (Jenkins and Parrington, 1976) could play a considerable role in aiding the magnetostratigraphic correlation of the Elliot Formation to other global sections because of their (comparatively) well-documented locations. At Likhoele field site in Lesotho, the occurrence of *Erythrotherium parringtoni* (Crompton, 1964, 1967) is

not far above the current LEF-UEF divide based on previously documented fossil location. Many of the other mammaliaformes appear to be Early Jurassic (Sinemurian) in age (e.g. Luo *et al*., 2001 *Hadrocodium* of the Lower Lufeng Formation).

Placement of the EF7 – 9n magnetochrons into the Early Jurassic seems plausible on sauropodomorph fossil evidence (Fig. 14.9) if comparison of the UEF sauropodomorphs to those in the Americas are considered; e.g. especially those been derived from the Early Jurassic Kayenta Formation (*Sarahsaurus*) and Navajo Sandstone (Rowe *et al*., 2010). *Sarahsaurus* is considered to be related to *Ignavusaurus* a plateosaurian from the UEF by Apaldetti *et al*. (2011), and both these taxa show similar ties to the Early Jurassic sauropodomorph, *Leyesaurus marayensis*, from the Quebrada del Barro Formation (Marayes-El Carrizal Basin, northwestern Argentina) which is the sister group (with *Adeopapposaurus*) of *Massopsondylus* (Apaldetti *et al*., 2011). McPhee *et al*. (2015a) suggest that a massospondylid position for *Sarahsaurus* is also plausible. Based on *Massopsondylus* and the relationship to its sister taxa, i.e. based on biostratigraphic correlations alone, it would place the *Massospondylus* Range Zone (UEF and lowermost Clarens Formation) into the Early Jurassic. This is somewhat circular reasoning because no plausible radiometric dates bind these sites over and above the biostratigraphy. The magnetostratigraphy of the Kayenta Formation by Steiner and Tanner (2014), however, shows that the formation is dominated by a long reverse polarity period which is punctuated by several short normal polarity intervals. This magnetic polarity stratigraphy matches the Early Pliensbachian (e-Pli R) polarity zone; and for which a range of ~187 – 190 Ma has been provided (Steiner and Tanner, 2014). The Jurassic, globally, is typified by constant inversion of the polarity intervals (McElhinny and McFadden, 2000), and these are not replicated in the Elliot Formation magnetostratigraphic composite section.

The UEF is typified by early ornithischians and their increasing abundance towards the contact with the Clarens Formation. Ornithischians are also common in the Lufeng Formation, Kayenta Formation and the Lower Lias of the United Kingdom (Irmis and Knoll, 2008). An intriguing and characteristic Elliot Formation early ornithischian dinosaur, *Eocursor parvus*, original stated as being discovered in the LEF, is said to have derived and basal traits similar to other ornithischians such as *Lesothosaurus*, *Scelidosaurus* and *Scutellosaurus* (Butler *et al*., 2007), the latter taxa being contemporaneous with *Sarahsaurus.* If *Eocursor parvus* is indeed a latest Triassic taxon, which would support a biostratigraphic Early Jurassic age for these fauna, however careful investigation of the type locality revealed that the *Eocursor parvus* was most probably excavated from beds well above the LEF-UEF boundary, and thus it is a UEF taxon.

Other globally comparable fauna are the theropod dinosaurs, such as *Coelophysis*. This ceratosaurian dinosaur taxon has been found in uppermost Karoo strata in Zimbabwe (Mana Pools area; Raath, 1969, 1977, 1990), but in South Africa the taxon is uncommon and is invariably associated with the *Tritylodon* Acme Zone (Early Jurassic; Raath, 1980; Kitching and Raath, 1984; Smith and Kitching, 1997; Munyikwa and Raath, 1999). This taxa is well-known from the Late Triassic of North America (e.g. Ghost Ranch *Coelophysis* quarry; Schwartz and Gillette, 1994), but the age range for the taxon is, however, not diagnostic enough to further refine this study.

Re-studied and revised UEF ichnofossils, such as those reported at the Moyeni tracksite (close to the QUT section of this study; see Smith *et al*., 2009; Wilson *et al*., 2009; Marsicano *et al*., 2014) and the ichnogenus *Batrachopus*, have been located in the current study (Maseru site, UEF). Incidentally, the Moyeni tracksite falls within the EF6r magnetochron. These and the revisions of Ellenberger's (1970) original identification (by Olsen and Galton, 1984; Rainforth, 2003; D'Orazi Porchetti and Nicosia, 2007) have been used in the current study. *Batrachopus* is a significant Early Jurassic ichnogenus which is found within several basins (e.g. McBrook Formation, Fundy Basin; Olsen and Padian, 1986; Sues and Olsen, 2015). It is documented within the Hartford Basin (East Berlin Formation), Glen Canyon Group (Moenave Formation) and in south-western France, 'lower Lias' of Veillon point (Lapparent and Montenant, 1967; Ellenberger, 1972; Olsen and Padian, 1986; Lockley *et al*., 2004). *Grallator* trackways are also known from these sites.

Otozoum ichnites are considered as a reliable biostratigraphic markers for the early Jurassic and are found to range from the Hettangian (Newark Supergroup) through to the earliest Pliensbachian (Navajo sandstone) (D'Orazi Porchetti *et al*., 2015). *Otozoum*, attributed to sauropodomorphs (Rainforth, 2003), is found within the McCoy Brook Formation, and the recent irrefutable *Otozoum moodii* tracks have been described from the Etjo Formation of Namibia (D'Orazi Porchetti *et al*., 2015). The Etjo Formation is considered to be the Clarens Formation equivalent in the Waterberg basin (Holzförster *et al*., 1999). The discovery of the *Otozoum* trackways from Etjo Formation, a Clarens Formation equivalent, provides secondary evidence for the placement of the TJB within the UEF. *Otozoum* trackways have been said to occur within the Elliot and Clarens Formation, in Lesotho, and similar tetradactyl ichnites are known (Ellenberger 1970, 1972), but lack formal description (D'Orazi Porchetti *et al*., 2015).

To date, the ichnofossils and ichnofossil assemblages of Ellenberger (1970) from the Elliot Formation need further revision and synonymy with validated ichnogenera (as per D'Orazi Porchetti and Nicosia, 2007) for more pertinent use in biostratigraphy. This is especially true in light of the advances in

ichnofossil identification methods and the revised lithostratigraphy of the Elliot Formation. Newly reconstructed ichno-zonations would ultimately aid advancing the chronostratigraphic framework of the Elliot Formation.

14.6 General Discussion

While highlighting the quality of the orbitally controlled magnetostratigraphy of the Newark Basin many consider correlation of this record with African continental counterparts very difficult (Marzoli *et al*., 2004; Whiteside *et al*., 2007; Deenen *et al*., 2010). Intra-basin correlations are therefore in desperate need of multi-proxy high-resolution chronological frameworks. The correlations attempted here attest to this statement and the tentative placement of many of the Elliot Formation chrons within the Newark APTS.

14.6.1 **Magnetic polarity stratigraphy**

Samples from all sites, with the exception of Oldenburg, show the unblocking of both normal and reverse polarity magnetization after the removal of a poorly-defined, low temperature (lost by 150 °C and infrequently remaining up to 350 °C) remanence with inconsistent declination and inclination. Normal polarity samples show a consistent isolation of a remanence with moderately negative, and steeper than the present field, inclination and north-north-westerly declination. Reverse magnetisation showed consistent remanence with a moderate positive inclination and a south-south easterly declination.

Given the present day field is very similar to that of the Early Jurassic, and that the Karoo magmatism is Early Jurassic in age, overprinting associated with Karoo magmatism cannot be dismissed (e.g. Beaufort Group rocks, Kirschvink and Ward, 1998). However, other studies in the main Karoo basin, such as that by Maré *et al*. (2014) show that the thermal effects are limited to rock close to intrusions, and Maré *et al*. (2014) provide evidence to suggest that sedimentary rock between sills experience temperatures only as high as 350 ^{o}C. Furthermore, chemical remanent magnetisation suggested by de Kock and Kirschvink (2004) provides low-temperature present field overprinting through the oxidation of magnetite to maghemite during weathering.

Given the (i) relatively well-defined, high temperature reverse polarity magnetization and, (ii) the relatively high (>350 ^{o}C) unblocking temperatures of normal polarity magnetization, it is likely that the results presented here are not expressly exaggerated by any Early Jurassic normal overprinting. This is

consistent with other works for the main Karoo basin (i.e. Lanci *et al*., 2013; Maré *et al*., 2014; Gastaldo *et al*., 2015) where primary (early acquired) normal polarity magnetisations were isolated at temperatures >450 ^{o}C.

Furthermore, sites which passed the reversals test for the LEF, UEF and combined Elliot Formation are more likely to indicate less bias of the younger overprint. Conversely, those that exhibited failures of the test, e.g. the UEF and combined Elliot Formation at Barkly Pass for instance, indicate that the normal polarity samples may be biased by a younger overprint of either the Jurassic normal polarity of the Karoo igneous event or of the present field. Due care has thus been taken in the interpretations carried forward into the magnetic polarity stratigraphy.

Attempting to distinguish and separate out the cause of the bias is not possible given the similarity of (and overlap between) the normal Early Jurassic polarity to that of the Pliensbachian KIP. Subsequently, all normal polarity magnetization presented here, given the above discussion, have been ruled out as being complete or near complete overprints of Early Jurassic Karoo magmatism.

14.6.2 **Geological hiatuses and abrupt events**

The correlation of magnetochrons between sections and sites which are separate geographically and, to a degree, transient through time is difficult. The position of abrupt depositional/erosive events of uncertain duration within the Elliot Formation is thus brought into question and highlights the imperfect nature of the stratigraphic record as an archive (Miall, 2014a, Kemp and Sexton, 2014).

From a magnetostratigraphic correlation viewpoint, Man (2011) argues that these stochastic processes can be approached using probabilities if they (i.e., deposition, compaction and erosion/depositional hiatus) are represented as normally distributed, independent events. This argument is largely based on several assumptions, such as a complete polarity column of roughly known age, geomagnetic reversals following Gaussian law and the thickness of the polarity zone remaining stationary (Man, 2011; Lallier *et al*., 2013). This method depends on the thickness of a magnetic polarity zone being a function of sediment accumulation rate and time, and Lallier *et al*. (2013) recognise the imperfect nature and uncertainty which correlations on this nature bear. Lallier *et al*. (2013) have proposed a second modelling method, Dynamic Time Warping, to tackle and manage the unrecorded chrons lost through depositional hiatus and/or erosional processes (or even poor sampling), and lends support to independent constrains from

biostratigraphy. Nevertheless, it seems that the sedimentation rates, and their uncertainty over time, are the main pitfalls in these correlation models (Lallier *et al*., 2013).

The magnetochrons within the Elliot Formation magnetic polarity composite column are distorted by the processes of vacillating accumulation rates, erosion and hiatuses From the sedimentological view point, the UEF is more likely to represent time slices of periods with low and continuous deposition (stationary periods), due to protracted periods of aridity, followed by flashy floods, rapid scouring and deposition (non-stationary). In essence, these are the abrupt events punctuating the succession and these vary greatly due to the nature of the depositional environment. Time resolution for the deposition of specific facies within the UEF has been touched upon by Smith and Kitching (1997). While that study uses modern case studies as a means for comparison for the formation of the palaeosols and *Tritylodon* Acme Zone within the UEF, it does not quantify the duration of the three events that led to the formation of TAZ and associated facies. In contrast, the LEF is likely to represent more continuous deposition (stationary) with few stratigraphic gaps relative to the UEF. However, this is no comparison for the deeper marine depositional units and the degree of stratigraphic completeness which they can preserve.

14.6.2.1 Preservational bias and palaeosols

Distortions of magnetochrons and the robustness of the magnetic polarity stratigraphy of a section can be further hindered by preservational bias. The UEF, in comparison to the LEF, records several palaeosol horizons, and the quantification of preservational bias in palaeosols is difficult (Marriott and Wright, 1993). A recent review by Marriott and Wright (2006) explores polygenetic palaeosols which can be the result of aggradational building of the profile followed by rapid scouring and erosional truncation. Repetitive cycling of this can reactivate different soil horizons and results in the displacement of carbonate nodules (see also Kraus, 1999) crucial in identification of the soil horizons.

The UEF is readily diffused with palaeosol horizons indicating periods of protracted preservation (non-erosional), and likely a stepwise accumulation rate between moderately long ‘stationary’ periods and rapid ‘non-stationary’ episodes. In contrast, the LEF has no extensive development of palaeosols, and when present are often truncated by an overlying sandstone channel. In general terms, the LEF mudstone/overbank deposits are often characterised by bioturbation (leaving structure-less mudstones) and grey/green mottling in purple mudstones, which is assumed to be pedogenic; however, diagenetic

processes associated with fluid flow cannot be ruled out. During the current study, one well-developed palaeosol was noted within the LEF at the Quthing section.

14.7 Magnetostratigraphic correlations are only as good as your biostratigraphy

Magnetostratigraphy is useful in supplementing the biostratigraphic dating of stratigraphic sections and for regional and global correlations of strata of similar age (Man, 2011). It is therefore confined, to an extent, by the precision of the biostratigraphic evidence or the other independent techniques used for correlation and dating.

This study provides novel information pertaining to the magnetostratigraphy of the Late Triassic to Early Jurassic Elliot Formation and its global correlations. The richly fossiliferous Elliot Formation has the potential to shed light onto the rise of the dinosaurs and early mammaliaformes in southern Africa as well as the Early Jurassic ecosystems after the end-Triassic mass extinction. This study should provide a foundation onto which further stratigraphy based investigations can be built, including, but not limited to the (a) study of faunal turnover within the Elliot and Clarens Formations; (b) assessment of the timing of dinosaur dispersal within southern Africa and its global contemporaries.

The magnetostratigraphic technique applied in this study, however, is troubled by several issues. These are inherent problems associated with magnetic polarity stratigraphy (e.g., unpredictability of sedimentary processes and accumulations rates, influence of dolerite intrusions), and its correlation to other polarity sections; as well as those pertaining to the biochronology. The latter may be rooted in poorly defined biostratigraphic range zones and other taxonomic issues of the fossil vertebrates of the Elliot Formation. This requires the revision and consolidation of the taxonomic status of various dinosaur forms (e.g. ‘*Euskelosaurus*’), and the improvement of precision in the stratigraphic placement of previously collected specimens in light of revised and formalized lithostratigraphy (Bordy and Eriksson, 2015). The latter could be achieved by the re-visitation of former excavation sites. Secondly, because the range zones themselves span relatively long durations in time, they require a refinement in order to be more manageable for regional and global correlations. These issues are likewise a fundamental problem with the ichnofossil taxonomy and the biozonation scheme of Ellenberger (1970, 1972).

The identification and institution of several index taxa which are (i) easily identifiable and abundantly found, and (ii) localised in stratigraphic occurrence would aid correlations. This problem has become more an issue in the LEF where revision of the sauropodomorph taxa is currently under way and where it is direly needed (McPhee *pers. comm*.). Conversely the UEF, having depositional environments favourable for fossil and ichnofossil preservation is less problematic for correlations; but it is marred by its cryptic, non-stationary preservation and accumulation rates for magnetostratigraphy. The internal subdivision of the UEF and the *Massopsondylus* Range zone could be more easily achieved with several taxa which could constitute internal range zones as already evidenced by *Tritylodon*, and the Heterodontosaurids. Thirdly, this problem is not a local/regional issue but extends globally as many the Late Triassic-Early Jurassic (specifically Early Jurassic) fauna and ichnofauna are very similar making the biostratigraphy, its correlation and relative age dating harder to refine.

Moreover, congeneric Late Triassic taxa with global distributions have been alluded to before by Lucas (1998). This is likely a result of the large continental landmass of Pangea having facilitated land-based pathways for biotic interchange which were only inhibited by the climatic gradients (McLoughlin, 2001; Preto *et al*., 2010), with the latter building the provincialism of Gondwanan biota (McLoughlin, 2001). However, an indication that parallel evolution of lineages from globally separated sites is problematic is illustrated in the attempt to correlate the Elliot Formation to other Gondwana basins of similar age. Frequently authors (e.g. Yates, 2007a) have used the LEF and the Los Colorados Formation as contemporaries resting on taxonomy with the fact that the fauna appear anatomically similar and therefore are likely to be sister taxon/lineages. Shared presence of supposed congeneric forms between geographically separated basins is an on-going means by which global correlations rest. This is further complicated by the point that global Late Triassic vertebrate biochronological correlations are difficult because they often rest on taxonomic assignments that are uncertain (Parker and Martz, 2010).

The position of key specimens in the stratigraphy is vital for the correct assignment of the (i) age of the specimen, (ii) age of the rocks it was found, as well as the (iii) evolutionary history its lineage could potential provide, not to mention a suite of (iv) palaeoecological and palaeoclimate conditions it could signify. A consideration not accounted for at the start of this study was that the literature pertaining to several fossil localities and the stratigraphic context of the fossils themselves could be erroneous under current rational. This limits not only the work in the palaeontological community (locally and globally) but also limits the reliability of taxa ranges for relative age dating. Ultimately it has several knock-on effects which degenerates the trustworthiness of correlation within southern Africa and abroad.

15 Conclusion

This project provides the first, detailed magnetostratigraphic composite log of the Triassic-Jurassic Elliot Formation. During sampling, particular focus was placed on targeting the sedimentological break between the LEF and the UEF as this boundary is traditionally considered to represent the TJB in southern Africa. Geochemical profiles of selected sites was also undertaken to assess chemical weathering and palaeoclimate across the same lithostratigraphic contact. Throughout this project, the emphasis for sections to be drilled has relied on three main features:

1. Previous work attempted at the site (palaeontological/sedimentology)

2. The absence of large dolerite intrusions

3. Easily accessible for palaeomagnetic drilling

These points were conceptualised and implemented rigorously during desktop studies with maps, Google earth and the literature to look for suitable sites. The first criteria, specifically pertaining to the palaeontological/sedimentology history of the sites, was implemented in order to tie the newly obtained magnetostratigraphic data to litho- and biostratigraphic results and thus achieve a more reliable correlation of the unit globally.

The driving force behind this magnetostratigraphic study was the need for the chronostratigraphic refinement of the Elliot Formation as the age of this globally important Triassic-Jurassic unit. Through this study it has become increasingly observable that the LEF-UEF boundary is likely to be close to or coincide with the ETE. Further refinement of this work would benefit from numeric ages from several newly discovered volcanogenic layers in addition to a thorough revision of the currently ‘raw’ biostratigraphic subdivision. On the composite magnetostratigraphic log of the Formation, a total of eight magnetochrons (EF1r – EF8n) can be identified and correlated to global magnetostratigraphically robust sections from South and North America. Preliminary geochemical studies of the Elliot Formation which have not previously been attempted, although useful in assessing source rock weathering and provenance, were conducted.

The UEF and combined Elliot Formation palaeomagnetic pole position, calculated from the average remanence directions, is in agreement with the palaeopole position from the Elliot Formation as computed by de Kock (2003). The LEF is less comparable with the palaeopole of de Kock (2003). It must be noted

that no inclination shallowing has been accounted for or corrected for here. The calculated palaeopoles presented for the Elliot Formation show considerable overlap with other African and South American Triassic-Jurassic poles (Fig. 14.2), and further confirm an overall Late Triassic age for the lower Elliot Formation and an Early Jurassic age for the upper Elliot Formation.

The magnetostratigraphic results of this study allowed the age range of the formation to be constrained to between ~213/209 Ma – ~ 195 - ~ 190 Ma. The LEF-UEF boundary falls at the base of a normal magnetic polarity chron EF6.2n and above the EF6.1r. The latter may be coincident with the ETE. The TJB is likely to be within the EF6.2n or within EF7n based on comparison with the works of Hüsing *et al*. (2014). Thus, the results show that the position of the TJB is likely to be within the UEF and not at the LEF-UEF boundary. If valid, this can account for the often considered traditional Triassic faunal forms found within the lower UEF, e.g. Moyeni tracksite chirotheroid-type trackways placement (Smith *et al*., 2009). Furthermore a Massospondylid sister taxon, *Mussaurus patagonicus,* traditionally considered Late Triassic has been more recently considered to represent an early Jurassic age, although Smith et al. (2014) provide an approximate age between 202/203 Ma for the occurrence of this Patagonian sauropodomorph and a large nest site.

The UEF is otherwise strongly correlated with Lower Jurassic magnetostratigraphy and fossil fauna of North America– placing it into the Hettangian and Early Sinemurian.

The geochemical study, presented in this dissertation (see Chapter 13, p. 185), is the first quantitative assessment of the palaeoclimatic conditions during the deposition of the Elliot Formation. Using palaeoenvironmental proxies (i.e. CIA, CIA_{molar} and ICV) it establishes that, in general, the Elliot Formation has index values typical of unweathered to slightly weathered detritus. In isolating samples from the UEF, however, regardless of grain size, they show the lowest degree of chemical weathering (low CIA, CIA_{molar} and high ICV values) as expected from palaeoclimatic inferences based on previous sedimentological observations (Bordy and Eriksson, 2015 and references therein). In general, the Formation showed depletion of major and trace elements relative to PAAS and UUC. Geochemical groupings within the LIK and LIKE sections did not show exact correspondence with the sedimentological LEF/UEF break.

The new radiometric age constraints (Ramezani et al., 2014) from South and North American sites, in conjunction with their magneto- and biostratigraphy, have aided the more accurate constraining of the LEF to the Norian and estimating the duration of the LEF (Figure 14.10). Furthermore, the results from what is considered the contemporaneous and biogeographically linked Los Colorados Formation. These

have been newly interpreted with the polarity column of Kent *et al*. (2014) and the Elliot Formation composite can be correlated using the occurrence of several sauropodomorph taxa (Fig. 14.8).

Magnetostratigraphy in sedimentary sections relies on sedimentary processes and accumulations rates where certain assumptions are made to facilitate correlation between regional sites and global timescales.

In this study, the difficulty in assessing changes in the ancient fluvio-lacustrine sediment accumulation rates and detecting significant erosional events or hiatuses have influenced the sampling technique used. This has meant that samples were taken at close (1 m or less) intervals where it was feasible; thus greatly adding to the number of samples needing processing and the efficiency of the analysis as a whole. Furthermore, the influence and characterisation of dolerite intrusions also inhibited interpretation of natural remanamet magnetism of the samples. Caution had to be taken in assessing demagnetization behaviour of individual samples. Lastly, the formation of the composite column from southern and northern sites relied heavily on the VGP distributions of each section as well as the lithostratigraphic subdivision of the Elliot Formation. This led to partly quantitative and qualitative interpretations for the correlation between sites from north and southern part of the basin. The global correlations of the Elliot Formation composite section relies heavily on subjective and qualitative interpretations relating to polarity pattern and biochronology.

Further multidisciplinary studies are needed for the refinement of several questions pertaining to the evolution of fauna and the continental response to the end-Triassic mass extinction event within the Eliot Formation. Evidence for faunal turnover is not readily apparent within the formation and the refinement of palaeoecological studies would contribute to further understanding the influence of the ETE on rates of evolution.

The magnetostratigraphic evidence presented here supports a Late Norian age for the LEF and Rhaetian to Sinemurian for UEF. However, the placement and nature of the TJB in the Elliot Formation is yet to be better resolved or understood. The data presented here supports the placement of the contact within the UEF, and not at the sedimentological and biostratigraphic divide between the LEF and UEF. This has important ramifications for biostratigraphic studies, and also for the climate and faunal changes associated with the end-Triassic extinction in southern Africa.

16 References

Abdala, F., Damiani, R., Yates, A., and Neveling, J. (2007). A non-mammaliaform cynodont from the Upper Triassic of South Africa: a therapsid Lazarus taxon? *Palaeontologia Africana, 42*: 17-23.

Akarish, A. I., & El-Gohary, A. M. (2011). Pre-Cenomanian Sandstones, East Sinai, Egypt. *Journal of Applied Sciences*, *11*(17): 3070-3088.

Ambrose, D. (1983). Lesotho's heritage in jeopardy. *Maseru: Protection and preservation commission*.

Ambrose, D. (1991). *A tentative history of Lesotho palaeontology*. NUL Journal of Research, National University of Lesotho, Lesotho. Pp. 38.

Ambrose, D. (2005). *Palaeontology*. House 9 Publications, National University of Lesotho.

Anderson, H.M., and Anderson, J.M. (1970). A preliminary review of the biostratigraphy of the uppermost Permian, Triassic and lowermost Jurassic of Gondwanaland. *Paleontologia Africana*, *13*: 1-22.

Anderson, J.M. (1974). A brief review of the flora of the Molteno Formation (Triassic), South Africa. *Palaeontologia africana, 17*: 1-10.

Anderson, J.M. and Anderson, H.M. (1983). Palaeoflora of southern Africa Molteno Formation (Triassic), A.A. Balkema, Rotterdam, The Netherlands, **2**, Pp. 227.

Anderson, J. M., & Anderson, H. M. (1984). The fossil content of the Upper Triassic Molteno Formation, South Africa. *Palaeontologia Africana, 25*: 39 – 59.

Anderson, J.M. and Anderson, H.M. (1995). The Molteno Formation: window onto Late Triassic floral diversity. In: D. D. Pant (Editor). *Proceedings of the International Conference on Global Environment and Diversification of Plants through Geological Time* (Birbal Sahni Centenary Volume). Society of Indian Plant Taxonomists, Allahabad, India, 27-40.

Anderson, J.M. and Anderson, H.M. (1998). In search of the world's richest flora: looking through the Late Triassic Molteno window. *Journal of African Earth Sciences, 27*(1A): 6-7.

Anderson, J. M., Anderson, H. M., and Cruickshank, A R. 1. (1998). Late Triassic ecosystems of the Molteno/Lower Elliot biome of southern Africa: *Palaeontology*, *41*: 387-421.

Anderson, J. M., Anderson, H. M., Archangelsky, S., Bamford, M., Chandra, S., Dettmann, M., Hill, R., Mcloughlin S., and Rosler, O. (1999). Patterns of Gondwana plant colonisation and diversification. *Journal of African Earth Sciences, 28*(1): 145 167.

Apaldetti, C., Martinez, R. N., Alcober, O. A., & Pol, D. (2011). A new basal sauropodomorph (Dinosauria: Saurischia) from Quebrada del Barro Formation (Marayes-El Carrizal Basin), northwestern Argentina. *PLoS One*, *6*(11), e26964-e26964.

Apaldetti, C., Pol, D., and Yates, A. M. (2013). The postcranial anatomy of *Coloradisaurus brevis* (Dinosauria: Sauropodomorpha) from the Late Triassic of Argentina and its phylogenetic implications. *Palaeontology*, *56*:277–301.

Apaldetti, C., Martinez, R. N., Pol, D., & Souter, T. (2014). Redescription of the Skull of Coloradisaurus brevis (Dinosauria, Sauropodomorpha) from the Late Triassic Los Colorados Formation of the Ischigualasto-Villa Union Basin, northwestern Argentina. *Journal of Vertebrate Paleontology*, *34*(5), 1113-1132.

Arcucci, A. B., Marsicano, C. A., & Caselli, A. T. (2004). Tetrapod association and palaeoenvironment of the Los Colorados Formation (Argentina): a significant sample from Western Gondwana at the end of the Triassic. *Geobios*, *37*(5): 557-568.

Armstrong-Altrin, J. S., Lee, Y. I., Verma, S. P., & Ramasamy, S. (2004). Geochemistry of sandstones from the upper Miocene Kudankulam Formation, southern India: Implications for provenance, weathering, and tectonic setting. *Journal of sedimentary Research*, *74*(2): 285-297.

Ash, S. R., & Creber, G. T. (2000). The Late Triassic Araucarioxylon arizonicum trees of the Petrified Forest National Park, Arizona, USA. *Palaeontology*, *43*(1): 15-28.

Atchley, S. C., Nordt, L. C., Dworkin, S. I., Ramezani, J., Parker, W. G., Ash, S. R., & Bowring, S. A. (2013). A linkage among Pangean tectonism, cyclic alluviation, climate change, and biologic turnover in the Late Triassic: The Record from the Chinle Formation, Southwestern United States. *Journal of Sedimentary Research*, *83*(12): 1147-1161.

Attridge, J., Crompton, A. W., & Jenkins Jr, F. A. (1985). The southern African Liassic prosauropod Massospondylus discovered in North America. *Journal of Vertebrate Paleontology*, *5*(2): 128-132.

Báez, A. M., and Marsicano, C. A. (2001). A heterodontosaurid ornithischian dinosaur from the Upper Triassic of Patagonia. *Ameghiniana*, *38*: 271–279.

Bahlburg, H., & Dobrzinski, N. (2011). A review of the Chemical Index of Alteration (CIA) and its application to the study of Neoproterozoic glacial deposits and climate transitions. *Geological Society, London, Memoirs*, *36*(1): 81-92.

Bamford, M. K. (2004). Diversity of the woody vegetation of Gondwanan southern Africa. *Gondwana Research*, *7*(1): 153-164.

Barbolini, N. (2014). *Palynostratigraphy of the South African Karoo Supergroup and correlations with coeval Gondwanan successions.* Unpublished PhD dissertation, University of the Witwatersrand, Johannesburg.

Barrett, P. M. (2000). Prosauropod dinosaurs and iguanas: speculations on the diets of extinct reptiles. In: Sues, H.-D. (Ed.). *Evolution of herbivory in terrestrial vertebrates: perspectives from the fossil record*. Pp. 42-78.

Barrett, P. M. (2004). Sauropodomorph dinosaur diversity in the upper Elliot Formation (Massospondylus range zone: Lower Jurassic) of South Africa: research letter. *South African Journal of Science*, *100*(9 & 10), p-501.

Barrett, P. M. (2009). A new basal sauropodomorph dinosaur from the upper Elliot Formation (Lower Jurassic) of South Africa. *Journal of Vertebrate Paleontology*, *29*(4): 1032-1045.

Barrett, P. M., McGowan, A. J., & Page, V. (2009). Dinosaur diversity and the rock record. *Proceedings of the Royal Society of London B: Biological Sciences*, rspb-2009.

Beerling, D.J. and Berner, R.A. (2002). Biogeochemical constraints on the Triassic-Jurassic boundary carbon cycle event. *Global Biogeochemical Cycles* 16.

Blackburn, T.J., Olsen, P.E., Bowring, S.A. , McLean, N.M., Kent, D.V., Puffer, J., McHone, G., Rasbury, E.T., & Et-Touhami, M. (2013). Zircon U-Pb geochronology links the end-Triassic extinction with the Central Atlantic Magmatic Province. *Science*, *340*(6135):941–945.

Bonaparte, J. F. (1971). Los tetrapodos del sector superior de la formacion los Colorados, La Rioja, Argentina (Triasico Superior). *Opera Lilloana, 22*, 1-183.

Bonis, N. R., Kürschner, W. M., & Krystyn, L. (2009). A detailed palynological study of the Triassic–Jurassic transition in key sections of the Eiberg Basin (Northern Calcareous Alps, Austria). *Review of Palaeobotany and Palynology*, *156*(3): 376-400.

Bonis, N. R. (2010). Palaeoenvironmental changes and vegetation history during the Triassic-Jurassic transition. PhD thesis. Utrecht University. LPP Contributions series No. 29.

Bordy, E. M., Hancox, P. J., Rubidge, B. S. (2004a). Fluvial style variations in the Late Triassic - Early Jurassic Elliot Formation, main Karoo Basin, South Africa. *Journal of African Earth Sciences*, *38:* 383–400.

Bordy, E. M., Hancox, P.J., Rubidge, B. S. (2004b). Basin development during the deposition of the Elliot Formation (Late Triassic - Early Jurassic), Karoo Supergroup, South Africa. *South African Journal of Geology*, *107*: 395-410.

Bordy, E. M., Hancox, P.J., & Rubidge, B.S. (2004c). Provenance Study of the Late Triassic – Early Jurassic Elliot Formation, main Karoo Basin, South Africa. *South African Journal of Geology, 107*: 587-602.

Bordy, E. M., Hancox, P. J., & Rubidge, B. S. (2005a). The contact of the Molteno and Elliot formations through the main Karoo Basin, South Africa: a second-order sequence boundary. *South African Journal of Geology*, *108*(3), 351-364.

Bordy, E. M., Hancox, P. J., & Rubidge, B. S. (2005b). A Reply Turner, BR and Thomson, K., Discussion on ‘Basin development during deposition of the Elliot Formation (Late Triassic–Early

Jurassic), Karoo Supergroup, South Africa' (South African Journal of Geology, 107, 397-412). *South African Journal of Geology*, *108*(3), 454-461.

Bordy, E.M., & Eriksson, P. (2015). Lithostratigraphy of the Elliot Formation (Karoo Supergroup), South Africa. *South African Journal of Geology, 118* (3): 311 -316.

Botha, B. J. V. (1968). The stratigraphy of the Red Beds Stage, Karroo System at Elliot, Cape Province. *Transactions of the Geological Society of South Africa, 71*:101-117.

Botha, B. J. V., & Theron, J. C. (1967). New evidence for the early commencement of Stormberg volcanism. *Tydskrif Natuurwet, 6*, 469-473.

Brack, P., Rieber, H., Nicora, A. & Mundil, R. (2005). The Global boundary Stratotype Section and Point (GSSP) of the Ladinian Stage (Middle Triassic) at Bagolino (Southern Alps, Northern Italy) and its implications for the Triassic time scale. *Episodes, 28* (4): 233–44.

Brink, A. S. (1959). A new small thecodont from the Red beds of the Stormberg series. *Palaeontologia Africana*, *6*: 109 - 115.

Broom, R. (1911). On the dinosaurs of the Stormberg, South Africa. *Annals of the South African Museum* 7(4): 291-308

Busbey III, A. B., & Gow, C. (1984). A new protosuchian crocodile from the Upper Triassic Elliot Formation of South Africa. *Palaeontologia Africana*, *25*: 127 -149.

Butler, R. F. (1992). *Paleomagnetism: magnetic domains to geologic terranes* (Vol. 319). Boston: Blackwell Scientific Publications.

Butler, R. J. (2005). The 'fabrosaurid' ornithischian dinosaurs of the upper Elliot Formation (Lower Jurassic) of South Africa and Lesotho. *Zoological Journal of the Linnean Society*, *145*(2): 175-218.

Butler, R. J. (2010). The anatomy of the basal ornithischian dinosaur Eocursor parvus from the lower Elliot Formation (Late Triassic) of South Africa. *Zoological Journal of the Linnean Society, 160*(4): 648-684.

Butler, R. J., Smith, R. M., & Norman, D. B. (2007). A primitive ornithischian dinosaur from the Late Triassic of South Africa, and the early evolution and diversification of Ornithischia. *Proceedings of the Royal Society of London B: Biological Sciences, 274*(1621): 2041-2046.

Catuneanu, O., Hancox, P. J., and Rubidge, B. S. (1998). Reciprocal flexural behaviour and contrasting stratigraphies: a new basin development model for the Karoo retroarc foreland system. *South Africa. Basin Research, 10*: 417-439.

Catuneanu, O., Wopfner, H., Eriksson, P. G., Cairncross, B., Rubidge, B. S., Smith, R. M. H., & Hancox, P. J. (2005). The Karoo basins of south-central Africa. *Journal of African Earth Sciences, 43*(1), 211-253.

Channell, J. E. T., Kozur, H. W., Sievers, T., Mock, R., Aubrecht, R., & Sykora, M. (2003). Carnian–Norian biomagnetostratigraphy at Silická Brezová (Slovakia): correlation to other Tethyan sections and to the Newark Basin. *Palaeogeography, Palaeoclimatology, Palaeoecology*, *191*(2): 65-109.

Clemens, W. A. (1979). A problem in morganucodontid taxonomy (Mammalia). *Zoological Journal of the Linnean Society*, *66*(1): 1-14.

Clemens, W. A. (1980). Rhaeto-Liassic mammals from Switzerland and West Germany. *Zitteliana*, *5*: 51-92.

Colbert, E. H. (1958). Tetrapod extinctions at the end of the Triassic Period. *Proceedings of the National Academy of Sciences of the United States of America*, *44*(9), 973.

Cole, D. I. (1992). Evolution and development of the Karoo Basin. In: De Wit, M. J. and Ransome, I. G. D. (Eds.). *Inversion Tectonics of the Cape Fold Belt, Karoo ad Cretaceous Basins of Southern Africa*. Balkema, Rotterdam. Pp. 87-99.

Cole, D. I. (2008). A Review of Uranium Deposits in the Karoo Supergroup of South Africa. *AAPG International Conference and Exhibition*, Cape Town, South Africa, October 26-29, 2008. Poster presentation.

Condie, K. C., Noll, P. D., & Conway, C. M. (1992). Geochemical and detrital mode evidence for two sources of Early Proterozoic sedimentary rocks from the Tonto Basin Supergroup, central Arizona. *Sedimentary Geology*, *77*(1): 51-76.

Cooper, M. R. (1981). The prosauropod dinosaur Massospondylus carinatus Owen from Zimbabwe: its biology, mode of life and phylogenetic significance. *Occasional papers of the National Museums and Monuments of Rhodesia*, *6*(10): 690-840.

Cornet, B. (1993). Applications and limitations of palynology in age, climatic, and paleoenvironmental analyses of Triassic sequences in North America. *Museum of Natural History Science Bulletin, 3:* 75-93.

Cox, R., Lowe, D. R., and Cullers, R. L. (1995). The influence of sediment recycling and basement composition of evolution of mudrock chemistry in the southwestern United States. *Geochim Cosmochim Acta, 59*: 2919–2940.

Crompton, A. W. (1964). A preliminary description of a new mammal from the Upper Triassic of South Africa. *Proceedings of the Zoological Society of London*, *142*(3): 441-452.

Crompton, A. (1967). The Late Triassic terrestrial fauna of Southern Africa. In: *Gondwana Stratigraphy" IUGS Symposium Buenos Aires, Abstract p. 33* (Vol. 1).

Crompton, A. W., & Ellenberger, F. (1957). On a new cynodont from the Molteno Beds and the origin of the tritylodontids. *Annals of the South African Museum*, *44*(1): 1-13.

Crompton, A. W., & Charig, A. J. (1962). A new ornithischian from the Upper Triassic of South Africa. *Nature, 196*: 1074-1077.

Crompton, A. W., & Jenkins, F. A. (1968). Molar occlusion in Late Triassic mammals. *Biological Reviews, 43*(4): 427-458.

Currie, B. S., Colombi, C. E., Tabor, N. J., Shipman, T. C., & Montañez, I. P. (2009). Stratigraphy and architecture of the Upper Triassic Ischigualasto Formation, Ischigualasto Provincial Park, San Juan, Argentina. *Journal of South American Earth Sciences*, *27*(1): 74-87.

De Kock, M. O. (2003). *Magnetostratigraphic studies in the main Karoo Basin (South Africa): implications for mass extinction events and the supercontinent of Pangea*. Unpublished M. Sc. Rand Afrikaans University. Johannesburg.

De Kock, M.O. and Kirschvink, J. L. (2004). Paleomagnetic constraints on the Permian-Triassic boundary in terrestrial strata of the Karoo Supergroup, South Africa: implications for causes of the end-Permian extinction event. *Gondwana Research, 7*(1), 175-183.

De Wit, M. J., & Ransome, I. G. (1992). Regional inversion tectonics along the southern margin of Gondwana. *Inversion Tectonics of the Cape Fold Belt, Karoo and Cretaceous Basins of Southern Africa. Balkema, Rotterdam*, 15-21.

Deenen, M. H., Ruhl, M., Bonis, N. R., Krijgsman, W., Kuerschner, W. M., Reitsma, M., & Van Bergen, M. J. (2010). A new chronology for the end-Triassic mass extinction. *Earth and Planetary Science Letters, 291*(1): 113-125.

d'Engelbronner, E. R. (1996). New palynological data from Karoo sediments, Mana Pools basin, northern Zimbabwe. *Journal of African Earth Sciences, 23*(1), 17-30.

Depetris, P. J., Pasquini, A. I., & Lecomte, K. L. (2014). Weathering: Intensity and Rate. In: *Weathering and the Riverine Denudation of Continents.* Springer Netherlands. Pp. 47-63.

Donohoo-Hurley, L. L., Geissman, J. W., & Lucas, S. G. (2010). Magnetostratigraphy of the uppermost Triassic and lowermost Jurassic Moenave Formation, western United States: Correlation with strata in the United Kingdom, Morocco, Turkey, Italy, and eastern United States. *Geological Society of America Bulletin, 122*(11-12): 2005-2019.

D'Orazi Porchetti, S., and Nicosia, U. (2007). Re-examination of some large early Mesozoic tetrapod footprints from the African collection of Paul Ellenberger. *Ichnos, 14*(3-4): 219-245.

D'Orazi Porchetti, S., Mocke, H.B., Latiano M. & Wagensommer A. (2015). First record of Otozoum from Namibia. *Lethaia, 48*: 72–82.

Doumani, G. A., & Tasch, P. (1963). Leaiid conchostracan zone in Antarctica and its Gondwana equivalents. *Science, 142*(3592): 591-592.

Du Toit, A. L. (1939). *The Geology of South Africa*. Oliver and Boyd. Edinburgh.

Du Toit, A. L. (1954). *The Geology of South Africa (3rd Ed.)*. Oliver and Boyd. Edinburgh.

Duncan, R. A., Hooper, P. R., Rehacek, J., Marsh, J. S., & Duncan, A. R. (1997). The timing and duration of the Karoo igneous event, southern Gondwana. *Journal of Geophysical Research: Solid Earth*, *102*(B8):18127-18138.

Dunn, E. J. (1898). Report on the Stormberg Coalfields. *Parl. Rep., Cape of Good Hope. Cape Town*. Pp. 267 – 302.

Dunning, G. R., & Hodych, J. P. (1990). U/Pb zircon and baddeleyite ages for the Palisades and Gettysburg sills of the northeastern United States: Implications for the age of the Triassic/Jurassic boundary. *Geology*, *18*(8): 795-798.

Dworkin, S. I., Nordt, L., & Atchley, S. (2005). Determining terrestrial paleotemperatures using the oxygen isotopic composition of pedogenic carbonate. *Earth and Planetary Science Letters*, *237*(1): 56-68.

Ellenberger, F. (1962). New Dinosaur tracks in Basutoland. *Basutoland news*, Maseru (Lesotho).

Ellenberger, P. (1970). Les niveaux paléontologiques de première apparition des mammifères primordiaux en Afrique du Sud et leur ichnologie. Establissement de zones stratigraphique détaillées dans le Stormberg du Lesotho (Afrique du Sud) (Trias superior a Jurassique). *Proceedings and Papers of the second Gondwana Symposium.* Pp.343–370.

Ellenberger, P. (1972). Contribution à la classification des Pistes de Vértebrés du Trias: les Stormberg d'Afrique du Sud (I). *Paleovertebrata, Memoire Extraordinaire* 1972, Montpellier. Pp. 152.

Ellenberger, P. (1974). Contribution a la classification des pistes de Vértebrés du Trias; les types du Stormberg d'Afrique du Sud, (2). *Palaeovertebrata*, Memoire Extraordinaire 1974, Montpellier. Pp. 170.

Ellenberger, F.; & Ellenberger, P (1956). Quelques precisions sur la Serie du Stormberg au Basutoland (Afrique du Sud). (Some details on the Stormberg Series in Basutoland, South Africa.). *Comptes Rendus des Seances de l 'Acadamie des Sciences (FR), 242*: 799-801.

Ellenberger, F., Ellenberger, P., Fabre, J., Ginsburg, L., & Mendrez, C. (1964). The Stormberg Series of Basutoland (South Africa). In *Report of 22nd session of the International Geological Congress*. Pp. 320-330.

Eriksson, P. G. (1983). A palaeoenvironmental study of the Molteno, Elliot and Clarens Formations in the Natal Drakensberg and North-eastern Orange Free State. Unpublished D.Phil. Thesis. University of Natal. Pietermaritzburg. Pp. 209.

Eriksson, P. G. (1984). A palaeoenvironmental analysis of the Molteno Formation in the Natal Drakensberg. *Transaction of the Geological Society of Southern Africa, 87*: 237-244.

Eriksson, P. G. (1985). The depositional palaeonvironment of the Elliot Formation in the Natal Drakensberg and north-eastern Orange Free State. *Transactions of the Geological Society South Africa*, *88*: 19-26.

Fairchild, J.M., and Hasiotis, S.T. (2011). Terrestrial and aquatic neoichnological laboratory experiments with the freshwater crayfish *Orconectes*: trackways on media of varying grain size, moisture, and inclination. *Palaios*, *26* (12): 790 – 804.

Fowell, S.J. and Olsen, P.E. (1995). Time calibration of Triassic/Jurassic microfloral turnover, eastern North America--Reply. *Tectonophysics, 245*: 96-99.

Fowell, S.J. and Traverse, A. (1995). Palynology and age of the upper Blomidon Formation, Fundy basin, Nova Scotia. *Review of Palaeobotany and Palynology, 86*: 211-233.

Fowell, S. J., Cornet, B., & Olsen, P. E. (1994). Geologically rapid Late Triassic extinctions: palynological evidence from the Newark Supergroup. *Geological Society of America Special Papers*, *288*: 197-206.

Gaffney, E. S., & Kitching, J. W. (1995). The morphology and relationships of Australochelys, an early Jurassic turtle from South Africa. *American Museum novitates*; no. 3130.

Gaffney, E. S., & Kitching J. W. (1994). The most ancient African turtle. *Nature*, *369*(6475): 55-58.

Gallet, Y., Krystyn, L., Besse, J., & Marcoux, J. (2003). Improving the Upper Triassic numerical time scale from cross-correlation between Tethyan marine sections and the continental Newark basin sequence. *Earth and Planetary Science Letters*, *212*(3): 255-261.

Gallet, Y., Krystyn, L., Marcoux, J., & Besse, J. (2007). New constraints on the end-Triassic (Upper Norian–Rhaetian) magnetostratigraphy. *Earth and Planetary Science Letters*, *255*(3): 458-470.

Galli, M. T., Jadoul, F., Bernasconi, S. M., & Weissert, H. (2005). Anomalies in global carbon cycling and extinction at the Triassic/Jurassic boundary: evidence from a marine C-isotope record. *Palaeogeography, Palaeoclimatology, Palaeoecology*, *216*(3): 203-214.

Galton, P. M. (1971). The Prosauropod Dinosaur Ammosaurus, the Crocodile Protosuchus, and Their Bearing on the Age of the Navajo Sandstone of Northeastern Arizona. *Journal of Palaeontology, 45*(5): 781-795.

Galton, P. M. & Van Heerden, J. (1985). Partial hind limb of *Blikanasaurus cromptoni* n. gen. and n. sp., representing a new family of prosauropod dinosaurs from the upper Triassic of South Africa. *Geobios, 18*: 509-516, doi:10.1016/s0016-6995(85)80003-6

Galton, P. M., & van Heerden, J. (1998). Anatomy of the prosauropod dinosaur *Blikanasaurus cromptoni* (Upper Triassic, South Africa), with notes on the other tetrapods from the lower Elliot Formation. *Paläontologische Zeitschrift, 72*(1-2): 163-177.

Gasith, A., & Resh, V. H. (1999). Streams in Mediterranean climate regions: abiotic influences and biotic responses to predictable seasonal events. *Annual review of ecology and systematics*, *30*: 51-81.

Gastaldo, R. A., Kamo, S. L., Neveling, J., Geissman, J. W., Bamford, M., & Looy, C. V. (2015). Is the vertebrate-defined Permian-Triassic boundary in the Karoo Basin, South Africa, the terrestrial expression of the end-Permian marine event?. *Geology*, *43*(10): 939-942.

Gehring, A. U., Fischer, H., Louvel, M., Kunze, K., and. Weidler, P. G. (2009). High temperature stability of natural maghemite: a magnetic and spectroscopic study. *Geophysical Journal International*, *179*: 1361–1371.

Ginsburg, L. (1964). Decouverte d'un Scelidosaurien (Dinosaure ornithischien) dans le Trias superieur du Basutoland. [Discovery of a Scelidosaurian (ornithischian dinosaur) in the Upper Triassic of Basutoland.] Comptes Rendus Hebdomadaires des Seances de l 'Academie des Sciences (FR), 258: 2366-2368.

Goldberg, K., & Humayun, M. (2010). The applicability of the Chemical Index of Alteration as a paleoclimatic indicator: An example from the Permian of the Paraná Basin, Brazil. *Palaeogeography, Palaeoclimatology, Palaeoecology*, *293*(1): 175-183.

Götz, A. E., Ruckwied, K., Pálfy, J., & Haas, J. (2009). Palynological evidence of synchronous changes within the terrestrial and marine realm at the Triassic/Jurassic boundary (Csővár section, Hungary). *Review of Palaeobotany and Palynology*, *156*(3): 401-409.

Gow, C. E. (1975). A new heterodontosaurid from the Redbeds of South Africa showing clear evidence of tooth replacement. *Zoological Journal of the Linnean Society*, *57*(4): 335-339.

Gow, C. E. (1980). The dentitions of the Tritheledontidae (Therapsida: Cynodontia). *Proceedings of the Royal Society of London B: Biological Sciences*, *208*(1173): 461-481.

Gow, C. E. (1986). A new skull of Megazastrodon (Mammalia, Triconodontia) from the Elliot Formation (Lower Jurassic) of southern Africa. *Palaeontologia Africana*, *26*:13-23.

Gow, C. E. (1990). A tooth-bearing maxilla referable to *Lycorhinus angustidens* Haughton, 1924 (Dinosauria, Ornithischia). *Annals of the South African Museum*, *99*: 567-580.

Gow, C.E. (2000). The skull of *Protosuchus haughtoni*, an early Jurassic crocodyliform from southern Africa. *Journal of Vertebrate Paleontology*, *20*(1): 49–56.

Gow, C. E., & Hancox, P. J. (1993). First complete skull of the Late Triassic Scalenodontoides (Reptilia, Cynodontia) from southern Africa. *The Nonmarine Triassic. New Mexico Museum of Natural History & Science Bulletin*, *3*: 161-168.

Gow, C.E., & Latimer, E.M. (1999). Preliminary report of dinosaur tracks in Qwa Qwa, South Africa. *Palaeontologia Africana, 35*: 41- 43.

Gradstein, F. M., Agterberg, F. P., Ogg, J. G., Hardenbol, J., Veen, P., Thierry, J., & Huang, Z. (1994). A Mesozoic time scale. *Journal of Geophysical Research: Solid Earth (1978–2012)*, *99*(B12): 24051-24074.

Gresse, P. G., Theron, J. N., Fitch F. J., & Miller, J. A. (1992). Tectonic inversion and radiometric resetting of the basement in the Cape Fold Belt. In: De Wit, M. J. and Ransome, I. G. D. (Eds.). *Inversion Tectonics of the Cape Fold Belt, Karoo and Cretaceous Basins of Southern Africa*. Balkema, Rotterdam. Pp. 217-228.

Groenevold, G. H. (1986). Geology of the Golden Gatee Highlands National Park. *Koedoe*, 29: 165 – 181.

Guex, J.,Schoene, B., Bartolini, A.,Spangenberg, J., Schaltegger, U., O'Dogherty, L., Taylor, D., Bucher, H., & Atudorei, V. (2012). Geochronological constraints on post-extinction recovery of the ammonoids and carbon cycle perturbations during the Early Jurassic. *Palaeogeography, Palaeoclimatology, Palaeoecology*, *346*: 1-11.

Hälbich, I. W. (1983). A geodynamic model for the Cape Fold Belt. In: *Geodynamics of the Cape Fold Belt*.Vol. 12. Geological Society South Africa Rotterdam. Pp. 77-184

Hallam, A. (1990). Correlation of the Triassic-Jurassic boundary in England and Austria. *Journal of the Geological Society*, *147*: 421-424.

Hallam, A. (2002). How catastrophic was the end-Triassic mass extinction? *Lethalia*, *35*: 147–157.

Hallam, A. & Wignall, P.B. (1999). Mass extinctions and sea-level changes. *Earth-Science Reviews*, *48*: 217–250.

Hames, W. E., Renne, P. R., & Ruppel, C. (2000). New evidence for geologically instantaneous emplacement of earliest Jurassic Central Atlantic magmatic province basalts on the North American margin. *Geology*, *28*(9):859-862.

Hancox, P. J. (2000). The continental Triassic of South Africa. *Zentralblatt für Geologie und Paläontologie Teil I, 1998*, 1285-1324.

Hansma, J., Tohver, E., Schrank, C., Jourdan, F., & Adams, D. (2015). The timing of the Cape Orogeny: New 40 Ar/39 Ar age constraints on deformation and cooling of the Cape Fold Belt, South Africa. *Gondwana Research. In press*. Available online 17 March 2015, ISSN 1342-937X, http://dx.doi.org/10.1016/j.gr.2015.02.005.

Hanson, E. K., Moore, J. M., Bordy, E. M., Marsh, J. S., Howarth, G., & Robey, J. V. A. (2009). Cretaceous erosion in central South Africa: Evidence from upper-crustal xenoliths in kimberlite diatremes. *South African Journal of Geology*, *112*(2), 125-140.

Hargraves, R. B., Rehacek, J., and Hooper, P.R. (1997). Palaeomagnetism of the Karoo igneous rocks in southern Africa. *South Africa Journal of Geology, 100*: 195-212.

Hasiotis, S. T. (1999). The origin and evolution of freshwater crayfish based on crayfish body and trace fossils. *Freshwater crayfish*, *12*: 49-70.

Hasiotis, S. T. (2002). Where is the fossil evidence for Gondwanan crayfish?. *Gondwana Research*, *5*(4): 872-878.

Haughton, S. H. (1924). The fauna and stratigraphy of the Stormberg Series. *Annals of the South African Museum*, *12*: 323- 495.

Haughton, S. H. (1969). *Geological history of southern Africa*. Geological Soc. of South Africa.

Haughton, S.H. & Brink, A., (1954). A bibliographical list of Reptilia from the Karroo beds of Africa. *Palaeontologia Africana, 2*: 1-187.

Hesselbo, S. P., Robinson, S. A., Surlyk, F., & Piasecki, S. (2002). Terrestrial and marine extinction at the Triassic-Jurassic boundary synchronized with major carbon-cycle perturbation: A link to initiation of massive volcanism? *Geology*, *30*(3): 251-254.

Hesselbo, S. P., Jenkyns, H. C., Duarte, L. V., & Oliveira, L. C. (2006). Carbon-isotope record of the Early Jurassic (Toarcian) Oceanic Anoxic Event from fossil wood and marine carbonate (Lusitanian Basin, Portugal). *Earth and Planetary Science Letters*, *253*(3): 455-470.

Hesselbo, S. P., McRoberts, C. A., & Pálfy, J. (2007). Triassic–Jurassic boundary events: problems, progress, possibilities. *Palaeogeography, Palaeoclimatology, Palaeoecology*, *244*(1): 1-10.

Hillebrandt, A., Krystyn, L., & Kuerschner, W. M. (2007). A candidate GSSP for the base of the Jurassic in the Northern Calcareous Alps (Kuhjoch section, Karwendel Mountains, Tyrol, Austria). *International Subcommission on Jurassic Stratigraphy Newsletter*, *34*(1): 2-20.

Hillebrandt, A.V. & Krystyn, L. (2009). On the oldest Jurassic ammonites of Europe (Northern Calcareous Alps, Austria) and their global significance: Neues Jahrbuch Geologie und Paläontologie Abh., v. 253/2-3, pp.163-195.

Hillebrandt, A. v., Krystyn, L., Kürschner, W. M., Bonis, N. R., Ruhl, M., Richoz, S., Schobben, M. A. N., Urlichs, M., Bown, P. R., Kment, K., McRoberts, C. A., Simms, M., and Tomãsových, A. (2013). The Global Stratotype Sections and Point (GSSP) for the base of the Jurassic System at Kuhjoch (Karwendel Mountains, Northern Calcareous Alps, Tyrol, Austria): *Episodes, 36*(3): 162-198.

Hitchcock, E. (1845). An attempt to name, classify, and describe the animals that made the fossil footmarks of New England. In: *Proceedings of the 6th Annual Meeting of the Association of American Geologists and Naturalists, New Haven, Connecticut*.Vol. 6. Pp. 23-25.

Holzförster, F., Stollhofen, H. & Stanistreet, I.G. (1999): Lithostratigraphy and depositional environments in the WaterbergErongo area, central Namibia, and correlation with the main Karoo Basin, South Africa. *Journal of African Earth Sciences*, *29*, 105–123.

Hopson, J. A. (1984). Late Triassic traversodont cynodonts from Nova Scotia and southern Africa. *Palaeontologia Africana*, *25*:181-201.

Hopson, J.A., and Kitching, J.W. (2001). A probainognathian cynodont from South Africa and the phylogeny of nonmammalian cynodonts. *Bulletin of the Museum of Comparative Zoology, 156 (1): 5–35*

Horn, G. F. J., and Strydom, J. H. (1998). Clay. *In*: Wilson, M. G. C., and Anhaeusser, C. R. (Eds.). The Mineral Resources of South Africa. Handbook, Council for Geoscience 16. Pp. 46-52.

Horn, B. L. D. , Melo, T.M., Schultz, C. L., Philipp, R. P., Kloss, H. P. Goldberg, K. (2014). A new third order sequence stratigraphic framework applied to the Triassic of the Paraná Basin, Rio Grande do Sul, Brazil, based on structural, stratigraphical and paleontological data. *Journal of South American Earth Sciences, 55*: 123–132. doi: 10.1016/j.jsames.2014.07.007.

Hounslow, M. W., & Muttoni, G. (2010). The geomagnetic polarity timescale for the Triassic: linkage to stage boundary definitions. *Geological Society, London, Special Publications*, *334*(1): 61-102.

Hounslow, M. W., Posen, P. E., & Warrington, G. (2004). Magnetostratigraphy and biostratigraphy of the Upper Triassic and lowermost Jurassic succession, St. Audrie's Bay, UK. *Palaeogeography, Palaeoclimatology, Palaeoecology*, *213*(3): 331-358.

Hurum, J.H., Bergan, M., Müller, R., Nystuen, J.P. & Klein, N. (2006). A Late Triassic dinosaur bone, offshore Norway. *Norwegian Journal of Geology*, *86*: 117-123.

Hüsing, S. K., Deenen, M. H., Koopmans, J. G., & Krijgsman, W. (2011). Magnetostratigraphic dating of the proposed Rhaetian GSSP at Steinbergkogel (Upper Triassic, Austria): Implications for the Late Triassic time scale. *Earth and Planetary Science Letters*, *302*(1): 203-216.

IAGA. (2005). Global Paleomagnetic Database, Version 4.6. Available at: http://www.ngu.no/geodynamics/gpmdb.

Iglesia Llanos, M. P. I., & Prezzi, C. B. (2013). The role of true polar wander on the Jurassic palaeoclimate. *International Journal of Earth Sciences*, *102*(3): 745-759.

Irmis, R. B. (2004). First report of Megapnosaurus (Theropoda: Coelophysoidea) from China. *PaleoBios*, *24*: 11-18.

Irmis, R. B. (2005a). The vertebrate fauna of the Upper Triassic Chinle Formation in northern Arizona. *Mesa Southwest Museum Bulletin*, *9*: 63-88.

Irmis, R.B. (2005b). A review of the vertebrate fauna of the lower Jurassic Navajo sandstone in Arizona. In: McCord, R.D. (Ed.). *Vertebrate Paleontolgy of Arizona*. Mesa Southwest Museum Bulletin Number 11. Pp. 55 – 71.

Irmis, R. B. (2010). Evaluating hypotheses for the early diversification of dinosaurs. *Earth and Environmental Science Transactions of the Royal Society of Edinburgh*, *101*(3-4), 397-426.

Irmis, R. B. & Knoll, F. (2008). New ornithischian dinosaur material from the Lower Jurassic Lufeng Formation of China. *Neues Jahrbuch für Geologie und Paläontologie., 247*: 117–128.

Irmis, R. B., Mundil, R., Martz, J. W., & Parker, W. G. (2011). High-resolution U–Pb ages from the Upper Triassic Chinle Formation (New Mexico, USA) support a diachronous rise of dinosaurs. *Earth and Planetary Science Letters*, *309*(3): 258-267.

Isbell, J.L., Cole, D.I., and Catuneanu, O. (2008). Carboniferous-Permian glaciation in the main Karoo Basin, South Africa: stratigraphy, depositional controls, and glacial dynamics, in Fielding, C.R., Frank, T.D., and Isbell, J.L., eds., Resolving the Late Paleozoic Ice Age in Time and Space: Boulder, CO, *Geological Society of America Special Paper 441*: 71-82.

Jenkins, F. A., & Parrington, F. R. (1976). The postcranial skeletons of the Triassic mammals Eozostrodon, Megazostrodon and Erythrotherium. *Philosophical Transactions of the Royal Society B: Biological Sciences*, *273*(926): 387-431.

Jin, Z., Li, F., Cao, J., Wang, S., & Yu, J. (2006). Geochemistry of Daihai Lake sediments, Inner Mongolia, north China: implications for provenance, sedimentary sorting, and catchment weathering. *Geomorphology*, *80*(3): 147-163.

Johnson, M.R. (1971). Provisional geological report on occurrences of bentonite in the Pronksberg (Mountain), Wodehouse District, Cape Province: Report, Geological Survey of South Africa, 1971-0012 (unpubl.).

Johnson, M.R. (1976). *Stratigraphy and sedimentology of the Cape and Karoo sequences in the Eastern Cape Province*. Unpublished Ph.D. Thesis. Rhodes University. Grahamstown.

Johnson, M. R. (1991). Sandstone petrography, provenance and plate tectonic setting in Gondwana context of the south-eastern Cape-Karoo basin. *South African Journal of Geology*, *94*: 137–154.

Johnson, M. R., Van Vuuren, C. J., Visser, J. N. J., Cole, D. I., Wickens, H. D. V., Christie, A. D. M., & Roberts, D. L. (1997). The foreland Karoo Basin, South Africa. *African basins. Sedimentary basins of the World*, *3*: 269-317.

Johnson, M. R., C. J. van Vuuren, J. N. J., Visser, D. I., Cole, H. d. V., Wickens, A. D. M., Christie, Roberts, D. L., & Brandl, G. (2006). Sedimentary rocks of the Karoo Supergroup. In: Johnson, M. R., Anhaeusser, C. R., and Thomas, R. J. (Eds.). *The Geology of South Africa*. Geological Society of South Africa and Council for Geoscience. Pp. 461-499.

Jones, C. H. (2002). User-driven integrated software lives:“Paleomag” paleomagnetics analysis on the Macintosh. *Computers & Geosciences*, 28(10): 1145-1151.

Jourdan, F., Féraud, G., Bertrand, H., Kampunzu, A.B., Tshoso, G., Watkeys, M.K.& Gall, B.L. (2005). The Karoo large igneous province: Brevity, origin, and relation with mass extinction questioned by new 40Ar/39Ar age data. *Geology, 33*: 745-748.

Jourdan, F., G. Bertrand, F. H., & Watkeys, M. K. (2007a). From flood basalts to the inception of oceanization: Example from the 40Ar/39Ar high-resolution picture of the Karoo large igneous province. *Geochemistry, Geophysics and Geosystems*, 8, *Q02002*, doi*:*10.1029/2006GC001392.

Jourdan, F., Féraud, G., Bertrand, H., Watkeys, M. K., & Renne, P. R. (2007b). Distinct brief major events in the Karoo large igneous province clarified by new ^{40} Ar/^{39} Ar ages on the Lesotho basalts. *Lithos*, *98*(1): 195-209.

Joyce, W. G. (2015). The origin of turtles: A paleontological perspective. *Journal of Experimental Zoology. Part B (Molecular and developmental evolution)*, *324B*:181–193.

Jubb, R.A. (1973). Brief synthesis of present information on the geographical and stratigraphical distribution of fossil fish within the Stormberg series, South Africa. *Palaeontologia Africana, 16*: 17–23.

Kadoma, K. P. (2012). *Paleomagnetism of Sedimentary Rocks: Process and Interpretation*. Wiley-Blackwell.

Kasanzu, C., Maboko, M. A., & Manya, S. (2008). Geochemistry of fine-grained clastic sedimentary rocks of the Neoproterozoic Ikorongo Group, NE Tanzania: Implications for provenance and source rock weathering. *Precambrian Research*, *164*(3): 201-213.

Kemp, D. B., & Sexton, P. F. (2014). Time-scale uncertainty of abrupt events in the geologic record arising from unsteady sedimentation. *Geology*, *42*(10): 891-894.

Kent, DV, and Olsen. RE., (1999). Astronomically tuned geomagnetic polarity time scale for the Late Triassic. *Journal of Geophysical Research, 104*: 12831-12841.

Kent, D. V., & Olsen, P. E. (2000). Magnetic polarity stratigraphy and paleolatitude of the Triassic–Jurassic Blomidon Formation in the Fundy basin (Canada): implications for early Mesozoic tropical climate gradients. *Earth and Planetary Science Letters*, *179*(2): 311-324.

Kent, D. V., & Tauxe, L. (2005). Corrected Late Triassic latitudes for continents adjacent to the North Atlantic. *Science*, *307*(5707): 240-244.

Kent, D. V., & Olsen, P. E. (2008). Early Jurassic magnetostratigraphy and paleolatitudes from the Hartford continental rift basin (eastern North America): Testing for polarity bias and abrupt polar wander in association with the central Atlantic magmatic province. *Journal of Geophysical Research: Solid Earth*, *113*(B6).

Kent, D. V., Witte, W. K., & Olsen, P.E. (1993). A complete magnetostratigraphy of the Late Triassic Newark Basin. In: Lucas, S.G. and M. Morales. (Eds.). *The Nonmarine Triassic*. New Mexico Museum of Natural History 8: Science Bulletin No. 3.

Kent, D. V., Olsen, P. E., & Witte, W. K. (1995). Late Triassic-earliest Jurassic geomagnetic polarity sequence and paleolatitudes from drill cores in the Newark rift basin, eastern North America. *Journal of Geophysical Research*, *100*(B8):14-965.

Kent, D. V., Malnis, P. S., Colombi, C. E., Alcober, O. A., & Martínez, R. N. (2014). Age constraints on the dispersal of dinosaurs in the Late Triassic from magnetochronology of the Los Colorados Formation (Argentina). *Proceedings of the National Academy of Sciences*, *111*(22): 7958-7963.

Kirkland, J.I., Milner, A. R.C., Olsen, P. E., and Hargrave, J.E. (2014). The Whitmore Point Member of the Moenave Formation in its type area in Northern Arizona and its age and correlation with the section in St. George, Utah: Evidence for two major lacustrine sequences. In: MacLean, J. S., Biek, R. F., & Huntoon, J. E. (Eds). *Geology of Utah's Far South*. Utah Geological Association Publication 43: 321–356.

Kirschvink, J. L. (1980). The least-squares line and plane and the analysis of palaeomagnetic data. *Geophysical Journal International*, *62*(3): 699-718.

Kirschvink, J. L. and Ward, P. D. (1998). Magnetostratigraphy of the Permian/Triassic boundary sediments in the Karoo of South Africa. *Journal of African Earth Sciences*, *27*(1A), Special Abstract Issue Gondwana 10, Events Stratigraphy of Gondwana. Pp. 124.

Kitching, J. W. (1979). Preliminary report on a clutch of six dinosaurian eggs from the Upper Triassic Elliot Formation, Northern Orange Free State. *Palaeontologia Africana, 22*: 41- 45.

Kitching, J. W. (1981). Preliminary report on a clutch of six dinosaurian eggs from the Upper Triassic Elliot Formation, Northern Orange Free State. *Palaeontologia Africana, 24*: 21.

Kitching, J. W., & Raath, M. A. (1984). Fossils from the Elliot and Clarens Formations (Karoo Sequence) of the northeastern Cape, Orange Free State and Lesotho, and a suggested biozonation based on tetrapods. *Palaeontologia Africana, 25*:111-125.

Klein, H. (2015). *Pers. comm*., at the First International conference of continental ichnology (ICCI 2015). El Jadida, Morocco.

Klein, H., & Lucas, S. G. (2010). Tetrapod footprints-their use in biostratigraphy and biochronology of the Triassic. *Geological Society, London, Special Publications*, *334*(1): 419-446.

Knoll, F. (2002). Nearly complete skull of Lesothosaurus (Dinosauria: Ornithischia) from the Upper Elliot Formation (Lower Jurassic: Hettangian) of Lesotho. *Journal of Vertebrate Paleontology, 22*: 238-243.

Knoll, F. (2004). Review of the tetrapod fauna of the “Lower Stormberg Group” of the main Karoo Basin (southern Africa): implication for the age of the Lower Elliot Formation. *Bulletin de la Societe géologique de France*, *175*(1): 73-83.

Knoll, F. (2005). The tetrapod fauna of the Upper Elliot and Clarens formations in the main Karoo Basin (South Africa and Lesotho). *Bulletin de la Société géologique de France*, *176*(1), 81-91.

Knoll, F. (2010). A primitive sauropodomorph from the upper Elliot Formation of Lesotho. *Geological Magazine*, *147*(06): 814-829.

Knoll, F. and Battail, B. (2001). New ornithischian remains from the Upper Elliot Formation (Lower Jurassic) of Lesotho and stratigraphical distribution of southern African fabrosaurids. *Géobios*, *34*: 415-421.

Knoll, F., Padian, K. & De Ricqlès, A. (2007). The growth trajectory and adult size of Lesothosaurus diagnosticus (Dinosauria: Ornithischia): taxonomic implications. *Journal of Vertebrate Paleontology*, *27* (3 Suppl.): 100A.

Knoll, F., Padian, K., & de Ricqlès, A. (2010). Ontogenetic change and adult body size of the early ornithischian dinosaur Lesothosaurus diagnosticus: Implications for basal ornithischian taxonomy. *Gondwana Research*, *17*(1): 171-179.

Kosterov, A. A. & Perrin, M. (1996), Paleomagnetism of the Lesotho basalt, southern Africa. *Earth and Planetary Science Letters*, *139*: 63-78.

Kozur, H. W., & Mock, R. (1993). The importance of conchostracans for the correlation of continental and marine beds. In: Lucas, S. G., & Morales, M. (Eds.). *The Nonmarine Triassic*. *New Mexico Museum of Natural History and Science, Bulletin*, (3): 261-266.

Kozur, H. W. & Weems, R. E. (2005). Conchostracan evidence for a late Rhaetian to early Hettangian age for the CAMP volcanic event in the Newark Supergroup, and a Sevatian (late Norian) age for the immediately underlying beds. *Hallesches Jahrbuch für Geowissenschaften*, *27*: 21-51.

Kozur, H. W., & Weems, R. E. (2010). The biostratigraphic importance of conchostracans in the continental Triassic of the northern hemisphere. *Geological Society, London, Special Publications*, *334*(1): 315-417.

Kraus, M. J. (1999). Paleosols in clastic sedimentary rocks: their geologic applications. *Earth-Science Reviews*, *47*(1): 41-70.

Krystyn, L., Gallet, Y., Besse, J., & Marcoux, J. (2002). Integrated Upper Carnian to Lower Norian biochronology and implications for the Upper Triassic magnetic polarity time scale. *Earth and Planetary Science Letters*, *203*(1): 343-351.

Krystyn, L., Böhm, F., Kürschner, W. and Delecat, S. (2005). The Triassic-Jurassic boundary in the Northern Calcareous Alps. In: Pálfy, J. and Ozsvárt, P. (Eds.), Program, Abstracts and Field Guide. 5th Field Workshop of IGCP Project 458. Pp. A1-A37.

Krystyn, L., Bouquerel, H., Kuerschner, W., Richoz, S., & Gallet, Y. (2007a). Proposal for a candidate GSSP for the base of the Rhaetian Stage. *The Global Triassic. New Mexico Museum of Natural History and Science Bulletin*, *41*, 189-199.

Krystyn, L., Richoz, S., Gallet, Y., Bouquerel, H., Kürschner, W. M., & Spötl, C. (2007b). Updated bio- and magnetostratigraphy from Steinbergkogel (Austria), candidate GSSP for the base of the Rhaetian stage. *Albertiana*, *36*, 164-172.

Kürschner, W. M., Bonis, N.R. & Krystyn, L. (2007). Carbon-isotope stratigraphy and palynostratigraphy of the Triassic-Jurassic transition in the Tiefengraben section - Northern Calcareous Alps (Austria). *Palaeogeography, Palaeoclimatology, Palaeoecology, 244*: 257-280.

Lallier, F., Antoine, C., Charreau, J., Caumon, G., & Ruiu, J. (2013). Management of ambiguities in magnetostratigraphic correlation. *Earth and Planetary Science Letters, 371*: 26-36.

Lanci, L., Tohver, E., Wilson, A., & Flint, S. (2013). Upper Permian magnetic stratigraphy of the lower Beaufort group, Karoo basin. *Earth and Planetary Science Letters, 175*: 123-134.

Lapparent, A. F., & de Montenant, C. (1967). Les empreintes des pas des reptiles **de** l'infralias du Veillon (Vendée) *Société Géologique de France, nouvelle série. Mémoire, 107*: 1–41.

Le Roux, J. P. (1990). Uranium mineralization in the Molteno and Elliot formations. *South African Journal of Geology, 93:* 738- 743.

Le Roux, J. P. (1995). Heartbeat of a mountain: diagnosing the age of depositional events in the Karoo (Gondwana) Basin from the pulse of the Cape Orogen. *Geologische Rundschau*, *84*(3): 626-635.

Le Roux, J. S., (1974). Palaeogeologiese en palaeogeografiese aspekte van die Etage Rooilae van die Sisteem Karoo. Ph.D. Thesis, University Orange Free State, Bloemfontein, Pp. 295.

Lee, Y. I. (2002). Provenance derived from the geochemistry of late Paleozoic–early Mesozoic mudrocks of the Pyeongan Supergroup, Korea. *Sedimentary Geology*, *149*(4): 219-235.

Lees, P. M., & Mills, R. (1983). A quasi-mammal from Lesotho. *Acta Palaeontologica Polonica*, 28(1): 171- 180.

Lehman, T., & Chatterjee, S. (2005). Depositional setting and vertebrate biostratigraphy of the Triassic Dockum Group of Texas. *Journal of Earth System Science*, *114*(3): 325-351.

Lindeque, A. S., De Wit, M. J. R., Weber, T., M., and Chevallier, L. (2011). Deep crustal profile across the Southern Karoo basin and Beattie magnetic anomaly, South Africa: An integrated interpretation with tectonic implications. *South African Journal of Geology, 114*: 265-292.

Lindström, S., van de Schootbrugge, B., Dybkjær, K., Pedersen, G. K., Fiebig, J., Nielsen, L. H., & Richoz, S. (2012). No causal link between terrestrial ecosystem change and methane release during the end-Triassic mass extinction. *Geology*, *40*(6): 531-534.

Litwin, R. J., Traverse, A., & Ash, S. R. (1991). Preliminary palynological zonation of the Chinle Formation, Southwestern U.S.A., and its correlation to the Newark Supergroup (eastern U.S.A.) *Review of Palaeobotany and Palynology, 68*:269–287.

Lockley, M. G. (1991). *Tracking dinosaurs: a new look at an ancient world*. . New York: Cambridge University Press. Pp. 243.

Lockley, M. G., Kirkland, J., & Milner, A. R. (2004). Probable relationships between the Lower Jurassic crocodilomorph trackways *Batrachopus* and *Selenichnus*: Evidence and implications based on new finds from the St. George Area southwestern Utah. *Ichnos*, *11*(1-2): 143-149.

Lockley, M. G., Lucas, S. G., Milàn, J., Harris, J. D., Avanzini, M., Foster, J. R., & Spielmann, J. A. (2010). The fossil record of crocodylian tracks and traces: an overview. In: Milàn, J., Lucas, S.G., Lockley, M.G. and Spielmann, J.A. (Eds.). Crocodyle tracks and traces. *New Mexico Museum of Natural History and Science Bulletin, 51*: 1-13.

Klein, H., & Lucas, S. G. (2010). Tetrapod footprints-their use in biostratigraphy and biochronology of the Triassic. *Geological Society, London, Special Publications*, *334*(1), 419-446.

Lucas, S. G. (1998). Global Triassic tetrapod biostratigraphy and biochronology. *Palaeogeography, Palaeoclimatology, Palaeoecology*, *143*(4): 347-384.

Lucas, S. G., & Hancox, P. J. (2001). Tetrapod-based correlation of the nonmarine Upper Triassic of southern Africa. *Albertiana*, *25*, 5-9.

Lucas, S. G., & Milner, A. R. C. (2006). Conchostraca from the Lower Jurassic Whitmore Point Member of the Moenave Formation, Johnson Farm, southwestern Utah. *New Mexico Museum of Natural History and Science Bulletin*, *37*: 421-423.

Lucas, S.G. & Tanner, L.H. (2007a). Tetrapod biostratigraphy and biochronology of the Triassic-Jurassic transition on the southern Colorado Plateau, USA. *Palaeogeography, Palaeoclimatology, Palaeoecology*, 244:242-256.

Lucas, S.G. & Tanner, L.H. (2007b). The nonmarine Triassic–Jurassic boundary in the Newark Supergroup of eastern North America. *Earth-Science Reviews, 84*: 1-20.

Lucas, S. G., & Tanner, L. H. (2008). Reexamination of the end-Triassic mass. In: Elewa, A. M. T. (Ed.). *Mass extinction.* Springer Berlin Heidelberg. Pp. 65-102.

Lucas, S. G., Heckert, A. B., & Tanner, L. H. (2005). Arizona's Jurassic fossil vertebrates and the age of the Glen Canyon Group. *Vertebrate Paleontology in Arizona: Bulletin 29, 29*, 94.

Lucas, S. G., Tanner, L. H., Donohoo-Hurley, L. L., Geissman, J. W., Kozur, H. W., Heckert, A. B., & Weems, R. E. (2011). Position of the Triassic–Jurassic boundary and timing of the end-Triassic extinctions on land: Data from the Moenave Formation on the southern Colorado Plateau, USA. *Palaeogeography, Palaeoclimatology, Palaeoecology*, *302*(3): 194-205.

Lucas, S. G., Tanner, L. H., Kozur, H. W., Weems, R. E., & Heckert, A. B. (2012). The Late Triassic timescale: age and correlation of the Carnian–Norian boundary. *Earth science reviews*, *114*(1): 1-18.

Luo, Z. X., Crompton, A. W., & Sun, A. L. (2001). A new mammaliaform from the early Jurassic and evolution of mammalian characteristics. Science, 292(5521): 1535-1540.

Man, O. (2011). The maximum likelihood dating of magnetostratigraphic sections. *Geophysical Journal International*, *185*(1): 133-143.

Maré, L. P., de Kock, M. O, Cairncross, B., & Mouri, H. (2014). Application of magnetic geothermometers in sedimentary basins: an example from the western Karoo Basin, South Africa. *South African Journal of Geology*, *117*: 1-14.

Maron, M., Rigo, M., Bertinelli, A., Katz, M. E., Godfrey, L., Zaffani, M., & Muttoni, G. (2015). Magnetostratigraphy, biostratigraphy, and chemostratigraphy of the Pignola-Abriola section: New constraints for the Norian-Rhaetian boundary. *Geological Society of America Bulletin*, B31106-1.

Marriott, S. B., & Wright, V. P. (1993). Palaeosols as indicators of geomorphic stability in two Old Red Sandstone alluvial suites, South Wales. *Journal of the Geological Society*, *150*(6): 1109-1120.

Marriott, S. B., & Wright, V. P. (2006). Investigating paleosol completeness and preservation in mid-Paleozoic alluvial paleosols: A case study in paleosol taphonomy from the Lower Old Red Sandstone. *Geological Society of America Special Papers*, *416*: 43-52.

Marsh, J. S., Hooper, P. R., Rehacek, J., Duncan, R. A., & Duncan, A. R. (1997). Stratigraphy and age of Karoo basalts of Lesotho and implications for correlations within the Karoo igneous province. In: Mahoney, J. J., and Coffin M. (Eds.). Large Igneous Provinces. *Geophysical Monograph-American Geophysical Union*, *100*: 247-272.

Marsicano, C. A., Wilson, J. A., & Smith, R. M. (2014). A Temnospondyl Trackway from the Early Mesozoic of Western Gondwana and Its Implications for Basal Tetrapod Locomotion. *PLoS ONE*, *9*(8): e103255.

Martin, A. J., Rich, T. H., Poore, G. C., Schultz, M. B., Austin, C. M., Kool, L., & Vickers-Rich, P. (2008). Fossil evidence in Australia for oldest known freshwater crayfish of Gondwana. *Gondwana Research*, *14*(3): 287-296.

Martinez, R. N., Sereno, P. C., Alcober, O. A., Colombi, C. E., Renne, P. R., Montañez, I. P., & Currie, B. S. (2011). A basal dinosaur from the dawn of the dinosaur era in southwestern Pangaea. *Science*, *331*(6014): 206-210.

Martínez, R.N., Apaldetti, C., Correa, G., Colombi, C. E., Fernández,E., Santi Malnis, P., Praderio, A., Abelín, D., Benegas, L.G., Aguilar-Cameo, A., & Alcober, O.A. (2015). A new Late Triassic vertebrate assemblage from northwestern Argentina. *Ameghiniana*, *52*: 379–390.

Marzoli, A., Renne, P. R., Piccirillo, E. M., Ernesto, M., Bellieni, G., & De Min, A. (1999). Extensive 200-million-year-old continental flood basalts of the Central Atlantic Magmatic Province. *Science, 284*(5414): 616-618.

Marzoli, A., Bertrand, H., Knight, K. B., Cirilli, S., Buratti, N., Vérati, C., & Bellieni, G. (2004). Synchrony of the Central Atlantic magmatic province and the Triassic-Jurassic boundary climatic and biotic crisis. *Geology, 32*(11): 973-976.

McElhinny, M.W. & McFadden, P.L. (2000). *Paleomagnetism: continents and oceans.* Academic Press. Pp.386.

McElwain, J. C., Beerling, D. J., & Woodward, F. I. (1999). Fossil plants and global warming at the Triassic-Jurassic boundary. *Science, 285*(5432):1386-1390.

McFadden, P. L., & McElhinny, M. W. (1990). Classification of the reversal test in palaeomagnetism. *Geophysical Journal International*, *103*(3): 725-729.

McKinley, J. M., Worden, R. H., Ruffell, A. H., & Morad, S. (2003). Smectite in sandstones: a review of the controls on occurrence and behaviour during diagenesis. In: Worden R.H, and Morad, S.(Eds). *Clay mineral cements in sandstones, International Association of Sedimentologists Special Publication, 34,* 109-128.

McLennan, S.M. (1989). Rare earth elements in sedimentary rocks: influence of provenance and sedimentary processes. *In*: Lipin, B.R., MacKay, G.A. (Eds.), Geochemistry and Mineralogy of Rare Earth Elements. *Mineral Society of America*. Pp. 169–200.

McLennan, S. M. (2001). Relationships between the trace element composition of sedimentary rocks and upper continental crust. *Geochemistry, Geophysics, Geosystems, 2*(4): 1525-2027. doi:*10.1029/2000GC000109*.

McLennan, S.M., Hemming, S., McDaniel, D.K., & Hanson, G.N. (1993). Geochemical approaches to sedimentation, provenance and tectonics. *Geological Society of America Special Paper 284*. Pp. 21–40.

McLoughlin, S. (2001). The breakup history of Gondwana and itsimpact on pre-Cenozoic floristic provincialism. *Australian Journal of Botany,47*: 271 – 300.

McPhee, B. W. (2013). The antanomy and phylogenetic relationships of Antetetonitrus ingenipes (Sauripodiformers, Dinosaruria): implications for the originas of Sauropoda. Unpublished MSc. Thesis. University of the Witswatersrand. Johannesburg.

McPhee, B. W., Yates, A. M., Choiniere, J. N., & Abdala, F. (2014). The complete anatomy and phylogenetic relationships of Antetonitrus ingenipes (Sauropodiformes, Dinosauria): implications for the origins of Sauropoda. *Zoological Journal of the Linnean Society*, *171*(1), 151-205.

McPhee, B. W., Choiniere, J. N., Yates, A. M., & Viglietti, P. A. (2015a). A second species of Eucnemesaurus Van Hoepen, 1920 (Dinosauria, Sauropodomorpha): new information on the diversity and evolution of the sauropodomorph fauna of South Africa's lower Elliot Formation (latest Triassic). *Journal of Vertebrate Paleontology*, *35*(5): e980504.

McPhee, B. W., Bonnan, M. F., Yates, A. M., Neveling, J., & Choiniere, J. N. (2015b). A new basal sauropod from the pre-Toarcian Jurassic of South Africa: evidence of niche-partitioning at the sauropodomorph–sauropod boundary? *Scientific reports*, *5*. doi:10.1038/srep13224

McPhee, B. W, Bordy E. M., Sciscio, L., & Choiniere, J. (in prep) Stratigraphic reassessment of historic fossils in the Elliot Formation, South Africa.

McRoberts, C. A., Furrer, H., & Jones, D. S. (1997). Palaeoenvironmental interpretation of a Triassic-Jurassic boundary section from Western Austria based on palaeoecological and geochemical data. *Palaeogeography, Palaeoclimatology, Palaeoecology*, *136*(1): 79-95.

McRoberts, C. A., Ward, P. D., & Hesselbo, S. (2007). A proposal for the base Hettangian Stage (= base Jurassic System) GSSP at New York Canyon (Nevada, USA) using carbon isotopes. *International Subcommission on Jurassic Stratigraphy Newsletter*, *34*(1): 43-49.

Miall, A. D. (2013). *Principles of sedimentary basin analysis*. Springer Science & Business Media. Pp. 668.

Miall, A. D. (2014a). Updating uniformitarianism: stratigraphy as just a set of “frozen accidents”. In: Smith, D. G., Bailey, R., J., Burgess, P., and Fraser, A. (Eds.). *Strata and time*. Geological Society, London, Special Publication 404 doi: 10.1144/SP404.4

Miall, A. D. (2014b). The emptiness of the stratigraphic record: a preliminary evaluation of missing time in the Mesaverde Group, Book Cliffs, Utah, USA. *Journal of Sedimentary Research, 84*(6): 457-469.

Miall, A. D. (2015). Modern chronostratigraphic data demonstrate that currently popular sequence models for fluvial systems don’t work. *GeoConvention 2015: New Horizons*. Conference Abstract. Calgary, Canada.

Molina-Garza, R. S., Geissman, J. W., Lucas, S. G., & Van der Voo, R. (1996). Palaeomagnetism and magnetostratigraphy of Triassic strata in the Sangre de Cristo Mountains and Tucumcari basin, New Mexico, USA. *Geophysical Journal International, 124*(3): 935-953.

Molina-Garza, R. S., Geissman, J. W., & Lucas, S. G. (2003). Paleomagnetism and magnetostratigraphy of the lower Glen Canyon and upper Chinle Groups, Jurassic-Triassic of northern Arizona and northeast Utah. *Journal of Geophysical Research: Solid Earth*, *108*(B4): 2181.

Moodley, A. (2015). The sedimentary petrology of carbonate nodules in the Elliot Formation, Karoo Supergroup, main Karoo Basin (South Africa). Unpublished MSc. University of Cape Town. Pp. 93.

Moreau, M-G., Boucher, H., Bodergat, A-M., & Guex, J. (2002). Pliensbachian magnetostratigraphy: new data from Paris Basin (France). *Earth and Planetary Science Letters, 203*: 755-767.

Morton, N. (2012). Inauguration of the GSSP for the Jurassic System. *Episodes, 35*(2): 328-332.

Morton, N., Warrington, G., & Bloos, G. (2008). Forward. *International Subcommission on Jurassic Stratigraphy, Newsletter 35*: 68–73.

Moulin, M., Fluteau, F., Courtillot, V., Marsh, J., Delpech, G., Quidelleur, X., Gérard, M., & Jay, A. E. (2011). An attempt to constrain the age, duration, and eruptive history of the Karoo flood basalt: Naude's Nek section (South Africa). *J. Geophys. Res., 116*: B07403, doi:10.1029/2011JB008210.

Moulin, M., Courtillot, V., Fluteau, F., & Valet J. P. (2012). The "van Zijl" Jurassic geomagnetic reversal revisited. *Geochemistry, Geophysics, Geosystems, 13*: Q03010, doi:10.1029/2011GC003910.

Moulin, M., Fluteau, F., Courtillot, V., Marsh, J., Delpech, G., Quidelleur, X., & Gérard, M. (in press). Further Constraints on the Age, Duration and Eruptive History of the Karoo Flood Basalt: the Oxbow-Moteng Pass Sections (Lesotho) and a Synthesis. *Preprint to be submitted to JGR, December 4, 2014.*

Müller, R., Nystuen, J. P., & Wright, V. P. (2004). Pedogenic mud aggregates and paleosol development in ancient dryland river systems: criteria for interpreting alluvial mudrock origin and floodplain dynamics. *Journal of Sedimentary Research, 74*(4): 537-551.

Mundil, R., Pálfy, J., Renne, P.R. & Brack, P. (2010). The Triassic time scale: A review of geochronological constraints. In: Lucas, S.G. (Ed.): *The Triassic Timescale*. Geological Society of London, Special Publication. 334: 41–60.

Munyikwa, D., & Raath, M.A. (1999). Further material of the ceratosaurian dinosaur *Syntarsus* from the Elliot Formation (Early Jurassic) of South Africa, *Palaeontologia Africana, 35*: 55-59.

Muttoni, G., Kent, D. V., & Channell, J. E. (1996). Evolution of Pangea: paleomagnetic constraints from the Southern Alps, Italy. *Earth and Planetary Science Letters, 140*(1): 97-112.

Muttoni, G., Kent, D. V., Olsen, P. E., Di Stefano, P., Lowrie, W., Bernasconi, S. M., & Hernández, F. M. (2004). Tethyan magnetostratigraphy from Pizzo Mondello (Sicily) and correlation to the Late Triassic Newark astrochronological polarity time scale. *Geological Society of America Bulletin, 116*(9-10): 1043-1058.

Muttoni, G., Kent, D. V., Jadoul, F., Olsen, P. E., Rigo, M., Galli, M. T., & Nicora, A. (2010). Rhaetian magneto-biostratigraphy from the Southern Alps (Italy): constraints on Triassic chronology. *Palaeogeography, Palaeoclimatology, Palaeoecology, 285*(1): 1-16.

Nadeau, P. H., Wilson, M. J., McHardy, W. J., and Tait, J. M. (1985). The conversion of smectite to illite during diagenesis: evidence from some illitic clays from bentonites and sandstones. *Mineralogical Magazine*, 49: 393 400.

Nash, D. S. (1975). The morphology and relationships of a crocodilian, *Orthosuchus stormbergi*, from the Upper Triassic of Lesotho. Annals of the South African Museum 67 (7):227-329.

Nesbitt, H. W., & Young, G. M. (1982). Early Proterozoic climates and plate motions inferred from major element chemistry of lutites. *Nature*, *299*(5885): 715-717.

Nesbitt, H. W., Fedo, C. M., & Young, G. M. (1997). Quartz and feldspar stability, steady and non-steady-state weathering, and petrogenesis of siliciclastic sands and muds. *The Journal of Geology*, *105*(2): 173-192.

Newell, N. D. (1963). Crises in the history of life. *Scientific American*, *208*: 76-93.

Newell, N.D. (1967). Revolutions in the history of life. *Special paper of the Geological society of America*, *89*: 63- 91.

Norman, D. B., Witmer, L. M. & Weishampel, D. B. (2004). Basal Ornithischia. In: Weishampel, D. B., Dodson, P. & Osmólska, H. (Eds.): *The Dinosauria*, 2nd edition. Berkeley. University of California Press.

Norman, D. B., Crompton, A. W., Butler, R. J., Porro, L. B., & Charig, A. J. (2011). The Lower Jurassic ornithischian dinosaur Heterodontosaurus tucki Crompton & Charig, 1962: cranial anatomy, functional morphology, taxonomy, and relationships. *Zoological Journal of the Linnean Society*, *163*(1): 182-276.

Novas, F. E., Ezcurra, M. D., Chatterjee, S., & Kutty, T. S. (2010). New dinosaur species from the Upper Triassic upper Maleri and lower Dharmaram formations of Central India. *Earth and Environmental Science Transactions of the Royal Society of Edinburgh*, *101*(3-4): 333-349.

Ogg, J.G., (2012). Triassic, in Gradstein, F.M, Ogg, J.G., Schmitz, M.D., and Ogg, G.M, eds., The Geologic Time Scale 2012: Oxford-Amsterdam-Waltham, Elsevier, p. 681-730.

Ogg, J. G., Agterberg, F. P., & Gradstein, F. M. (2004). A geologic time scale 2004. In: *Abstracts with Programs-Geological Society of America* , 36. P p. 74.

Ogg, J.G., and Hinnov, L.A. (2012). Jurassic. In: Gradstein, F.M., Ogg, J.G., Schmitz, M.D., and Ogg, G.M., (Eds.). *The Geologic Time Scale 2012*. Elsevier, Amsterdam, p. 731–791

Olsen, P. E. & Galton, P. M. (1977). Triassic-Jurassic tetrapod extinctions: are they real? *Science*, *197*: 983-986.

Olsen, P. E., & Galton, P. M. (1984). A review of the reptile and amphibian assemblages from the Stormberg of southern Africa, with special emphasis on the footprints and the age of the Stormberg. *Palaeontologia Africana*, *25*:87-110.

Olsen, RE., & Kent, D.V. (1996). Milankovitch climate forcing in the tropics of Pangea during the Late Triassic: *Palaeogeography, Palaeoclimatology, and Palaeoecology*, *122*: 1-26.

Olsen, RE., & Sues, H.-D. (1986). Correlation of the continental Late Triassic and Early Jurassic sediments, and patterns of the Triassic-Jurassic tetra-pod transition. In: Padian, K. (Ed.), *The beginning of the Age of Dinosaurs: Faunal change across the Triassic-Jurassic boundary*. New York, Cambridge University Press. Pp. 321-351.

Olsen, P. E., & Padian, K. (1986). Earliest records of Batrachopus from the southwestern United States, and a revision of some Early Mesozoic crocodylomorph ichnogenera. *The beginning of the age of dinosaurs: Cambridge University Press, Cambridge*. Pp. 259-273.

Olsen, P. E., & Rainforth, E. C. (2003). The Early Jurassic ornithischian dinosaurian ichnogenus Anomoepus. *The great rift valleys of Pangea in eastern North America*, *2*: 314-367.

Olsen, P. E., McCune, A. R. & Thomson, K. S. (1982). Correlation of the early Mesozoic Newark Supergroup by Vertebrates, principally fishes. *American Journal of Science, 282*: p. 1-44.

Olsen, P. E., Kent, D. V., & Whiteside, J. H. (2011). Implications of the Newark Supergroup-based astrochronology and geomagnetic polarity time scale (Newark-APTS) for the tempo and mode of the early diversification of the Dinosauria. *Earth and Environmental Science Transactions-Royal Society of Edinburgh*, *101*(3): 201.

Olsen, P.E., Kent, D.V., Et-Touhami, M., & Puffer, J. (2003). Cyclo-, magneto-, and bio- stratigraphic constraints on the duration of the CAMP event and its relationship to the Triassic–Jurassic boundary. *AGU, Geophysics Monographs*, 7–32.

Olsen, P.E., Kent, D.V., Sues, H.D., Koeberl, C., Huber, H., Montanari, A., Rainforth, E.C., Fowell, S.J., Szajna, M.J., & Hartline, B.W. (2002a). Ascent of dinosaurs linked to an iridium anomaly at the Triassic–Jurassic boundary. *Science, 296*: 1305–1307.

Olsen, P.E., Koeberl, C., Huber, H., Montanari, A., Fowell, S.J., Et-Touhami, M., & Kent, D.V. (2002b). Continental Triassic–Jurassic boundary in central Pangea: recent progress and discussion of an Ir anomaly. In: Koerberl, C., MacLeod, K.G. (Eds.). *Catastrophic Events and Mass Extinctions: Impacts and Beyond*. Boulder, Colorado, Volume 356, Geological Society of America Special Paper. Pp. 502–522.

Özdemir, Ö. & Banerjee, S. K. (1984), High temperature stability of maghemite (γ-Fe_2O_3). *Geophysical Research Letters, 11*: 161–164. doi:10.1029/GL011i003p00161.

Pálfy, J. (2003). The end-Triassic mass extinction. In: *Yearbook of Science and Technology*. McGraw Hill, New York.

Pálfy, J. (2008). The Triassic–Jurassic boundary. In: Pienkowski, G., Schudack, M. E. (Co-Ordinators), Bosák, P., Enay, R., Feldman-Olszewska, A., Golonka, J., Gutowski, J., Herngreen, G. F. W., Jordan, P.,

Krobicki, M., Lathuiliere, B., Leinfelder, R. R., Michalik, J., Mönnig, E., Noe-Nygaard, N., Pálfy, J., Pint, A., Rasser, M. W., Reisdorf, A. G., Schmid, D. U., Schweigert, G., Surlyk, F., Wetzel, A. and Wong, T. E.: Jurassic. In: McCann, T. (Ed.): *The Geology of Central Europe. Volume 2: Mesozoic and Cenozoic. Geological Society of London*. 826-827.

Pálfy, J., Mortensen, J. K., Carter, E. S., Smith, P. L., Friedman, R. M., & Tipper, H. W. (2000). Timing the end-Triassic mass extinction: First on land, then in the sea? *Geology, 28*(1): 39-42.

Pálfy, J., Demény, A., Haas, J., Hetényi, M., Orchardi, M.J., & Vetőj, I. (2001). Carbon isotope anomaly and other geochemical changes at the Triassic–Jurassic boundary from a marine section in Hungary. *Geology, 29*: 1047–1050.

Pálfy, J., Demény, A., Haas, J., Carter, E. S., Görög, Á., Halász, D., Oravecz-Schefferg, A., Hetényih, A., Mártonf, E., Orchardi, M. J., Ozsvárta, P., Vetőj, I., & Zajzon, N. (2007). Triassic–Jurassic boundary events inferred from integrated stratigraphy of the Csővár section, Hungary. *Palaeogeography, Palaeoclimatology, Palaeoecology*, 244(1-4):11–33.

Parker, W. G., & Martz, J. W. (2010). The Late Triassic (Norian) Adamanian–Revueltian tetrapod faunal transition in the Chinle Formation of Petrified Forest National Park, Arizona. *Earth and Environmental Science Transactions of the Royal Society of Edinburgh, 101*(3-4): 231-260.

Paton, D. A., Macdonald, D. I., & Underhill, J. R. (2006). Applicability of thin or thick skinned structural models in a region of multiple inversion episodes; southern South Africa. *Journal of structural geology, 28*(11), 1933-1947.

Pol, D. & Powell, J. E. (2007). New information on *Lessemsaurus sauropoides* (Dinosauria: Sauropodomorpha) from the Upper Triassic of Argentina. *Special Papers in Palaeontology, 77*: 223-243.

Porro, L. B., Butler, R. J., Barrett, P. M., Moore-Fay, S., & Abel, R. L. (2010). New heterodontosaurid specimens from the Lower Jurassic of southern Africa and the early ornithischian dinosaur radiation. *Earth and Environmental Science Transactions of the Royal Society of Edinburgh, 101*(3-4): 351-366.

Potter, P. E., Maynard, J. B., & Depetris, P. J. (2005). *Mud and Mudstones: Introduction and Overview*. Springer Berlin Heidelberg. Pp. 157-174.

Preto, N., Kustatscher, E., & Wignall, P.B. (2010). Triassic climates — State of the art and perspectives. *Palaeogeography, Palaeoclimatology, Palaeoecology, 290* : 1–10.

Prévot, M., Roberts, N., Thompson, J., Faynot, L., Perrin, M., and Camps, P. (2003). Revisiting the Jurassic geomagnetic reversal recorded in the Lesotho Basalt (Southern Africa). *Geophysical Journal International, 155*: 367-378.

Raath, M. A. (1969). A new coelurosaurian dinosaur from the Forest Sandstone of Rhodesia. *National Museums of Rhodesia*.

Raath, M. A. (1972). Fossil vertebrate studies in Rhodesia: a new dinosaur (Reptilia: Saurischia) from near the Triassic-Jurassic boundary. *Arnoldia, 5*(31):1-37.

Raath, M. A. (1977). The anatomy of the Triassic theropod *Syntarsus rhodesiensis* (Saurischia: Podokesauridae) and a consideration of its biology. Unpublished PhD Thesis, Rhodes University, Grahamstown.

Raath, M.A. (1980). The theropod dinosaur *Syntarsus* (Saurischia: Poclokesauridae) discovered in South Africa. *South African Journal of Science, 76*: 375-376.

Raath, M.A. (1996). Earliest evidence of dinosaurs from cenral Gondwana. *Memoirs of the Queensland Museum, 39*: 703 – 709.

Raath, M. A., Kitching, J. W., Shone, R. W., & Rossouw, G. J. (1990). Dinosaur tracks in Triassic Molteno sediments: the earliest evidence of dinosaurs in South Africa? *Paleontologia Africana, 27*: 89-95.

Raath, M., Oesterlen, P.M., & Kitching, J.W. (1992). The first record of Triassic Rhynchosauria (Reptilia: Diapsida) from the Lower Zambezi Valley, Zimbabwe. *Palaeontologia Africana, 29*: 1–10.

Rainforth, E.C. (2001). Late Triassic - Early Jurassic dinosaur ichnofaunas, eastern North America and southern Africa. *Journal of Vertebrate Paleontology 21* (3 Suppl.):91A.

Rainforth, E. C. (2003). Revision and re-evaluation of the Early Jurassic dinosaurian ichnogenus Otozoum. *Palaeontology, 46*(4): 803-838.

Rainforth, E. C. (2005). *Ichnotaxonomy of the fossil footprints of the Connecticut Valley (Early Jurassic, Newark Supergroup, Connecticut and Massachusetts)*. Unpublished PhD dissertation. Columbia University.

Rainforth, E. C., & Lockley, M. G. (1996). Tracking life in a Lower Jurassic desert: Vertebrate tracks and other traces from the Navajo Sandstone. *Museum of Northern Arizona Bulletin, 60*: 285-289.

Ramezani, J., Fastovsky, D. E., & Bowring, S. A. (2014). Revised chronostratigraphy of the Lower Chinle Formation strata in Arizona and New Mexico (USA): High-precision U-Pb geochronological constraints on the Late Triassic evolution of dinosaurs. *American Journal of Science, 314*(6): 981-1008.

Ramezani, J., Hoke, G. D., Fastovsky, D. E., Bowring, S. A., Therrien, F., Dworkin, S. I., Atchley, S. C., & Nordt, L. C. (2011). High-precision U-Pb zircon geochronology of the Late Triassic Chinle Formation, Petrified Forest National Park (Arizona, USA): Temporal constraints on the early evolution of dinosaurs. *Geological Society of America Bulletin, 123*(11-12): 2142-2159.

Raup, D. M. & Sepkoski, J. J. (1982). Mass Extinctions in the Marine Fossil Record. *Science, 215*:1501–1503.

Ray, S., & Chinsamy, A. (2002). A theropod tooth from the Late Triassic of southern Africa. *Journal of Biosciences*, *27*: 295–298.

Reed, J. J. (1976). Preliminary Report on Possible Quarry Sites for High-Grade Aggregate Rock in the Maseru District. UNDP, DEP, Special Report JR/I, DMG. Maseru.

Reisz, R. R., Scott, D. M., Sues, H.-D., Evans, D. C. and Raath, M. A.. (2005). Embryos of an Early Jurassic prosauropod dinosaur and their evolutionary significance. *Science*, *309*:761–764.

Reisz, R. R., Evans, D. C., Roberts, E. M., Sues, H. D., & Yates, A. M. (2012). Oldest known dinosaurian nesting site and reproductive biology of the Early Jurassic sauropodomorph Massospondylus. *Proceedings of the National Academy of Sciences*, *109*(7): 2428-2433.

Richoz, S., van de Schootbrugge, B., Pross, J., Püttmann, W., Quan, T. M., Lindström, S., Heunisch, C., Fiebig, J., Maquil, R., Schouten, S., Hauzenberger, C.A., & Wignall, P. B. (2012). Hydrogen sulphide poisoning of shallow seas following the end-Triassic extinction. *Nature Geoscience*, *5*(9): 662-667.

Rigo, M., Bertinelli, A., Concheri, G., Gattolin, G., Godfrey, L., Katz, M.E., Maron, M., Mietto, P., Muttoni, G., Sprovieri, M., Stellin, F. & Zaffani, M. (2015): The Pignola- Abriola section (southern Apennines, Italy): a new GSSP candidate for the base of the Rhaetian Stage. *Lethaia*, DOI: 10.1111/let.12145.

Romer, A. S. (1970). Tetrapod vertebrates and Gondwanaland. In: *Proceedings of the Second Gondwana Symposium*. CSIR Pretoria. Pp. 111-124.

Rooyani, F., & Schmitz, G. (1987). Lesotho: Geology, Geomorphology and Soils. *National University of Lesotho. Roma*. Pp. 204.

Roser, B. P., Cooper, R. A., Nathan, S., & Tulloch, A. J. (1996). Reconnaissance sandstone geochemistry, provenance, and tectonic setting of the lower Paleozoic terranes of the West Coast and Nelson, New Zealand. *New Zealand Journal of Geology and Geophysics*, *39*(1): 1-16.

Rowe, T. B., Sues, H. D., & Reisz, R. R. (2010). Dispersal and diversity in the earliest North American sauropodomorph dinosaurs, with a description of a new taxon. *Proceedings of the Royal Society of London B: Biological Sciences*, rspb20101867.

Rowland, S. M., & Mercadante, J. M. (2014). Trackways of a gregarious, dunefield-dwelling, Early Jurassic therapsid in the Aztec Sandstone of Southern Nevada. *Palaios*, *29*(10): 539-552.

Rubidge, B.S. (2005). Re-uniting lost continents – Fossil reptiles from the ancient Karoo and their wanderlust. *South African Journal of Geology*, *108* (3): 135-172.

Rudnick, R. L., & Gao, S. (2003). Composition of the continental crust. *Treatise on geochemistry*, *3*: 1-64.

Ruhl, M., Kürschner, W.M. and Krystyn, L. (2009). Triassic-Jurassic organic carbon isotope stratigraphy of key sections in the western Tethys realm (Austria). *Earth and Planetary Science Letters, 281*: 169-187.

Ruhl, M., Deenen, M. H. L., Abels, H. A., Bonis, N. R., Krijgsman, W., & Kürschner, W. M. (2010). Astronomical constraints on the duration of the early Jurassic Hettangian stage and recovery rates following the end-Triassic mass extinction (St Audrie's Bay/East Quantoxhead, UK). *Earth and Planetary Science Letters*, *295*(1): 262-276.

SACS (South African Committee for Stratigraphy) (1980). Stratigraphy of South Africa. Part 1. Lithostratigraphy of the Republic of South Africa, South West Africa/Namibia, and the Republics of Bophuthatswana, Transkei and Venda. Handbook of the Geological Survey of South Africa, 8. Pp. 690.

Santa Luca, A. P. (1980). *The postcranial skeleton of Heterodontosaurus tucki (Reptilia, Ornithischia) from the Stromberg of South Africa*. South Africa Museum.

Santi Malnis, P., Colombi, C. E., Kent, D. V., Alcober, O. A., & Martínez, R. N. (2011). Assessing the age of Los Colorados Formation, Ischigualasto-Villa Unión Basin, Argentina. *Temporal implications for Coloradian fauna. Resúmenes Ameghiniana*, *48*(4).

Savidge, R.A. (2007). Wood anatomy of Late Triassic trees in Petrified Forest National Park, Arizona, USA, in relation to *Araucarioxylon arizonicum* Knowlton, 1889. *Bulletin of Geosciences, 82*(4): 301–328.

Schaltegger, U., Guex, J., Bartolini, A., Schoene, B. and Ovtcharova, M. (2008). Precise U-Pb age constraints for end-Triassic mass extinction, its correlation to volcanism and Hettangian post-extinction recovery. *Earth and Planetary Science Letters, 267*: 266-275.

Scheffler, K., Buehmann, D., & Schwark, L. (2006). Analysis of late Palaeozoic glacial to postglacial sedimentary successions in South Africa by geochemical proxies–response to climate evolution and sedimentary environment. *Palaeogeography, Palaeoclimatology, Palaeoecology*, *240*(1): 184-203.

Scheiber-Enslin, S. E., Ebbing, J., & Webb, S. (2015). New depth maps of the Main Karoo Basin, used to explore the Cape Isostatic Anomaly, South Africa. *South African Journal of Geology*, *118*(3), 225-248.

Schmieder, M., Buchner, E., Schwarz, W. H., Trieloff, M., & Lambert, P. (2010). A Rhaetian $^{40}Ar/^{39}Ar$ age for the Rochechouart impact structure (France) and implications for the latest Triassic sedimentary record. *Meteoritics & Planetary Science*, *45*(8): 1225-1242.

Schoene, B., Guex, J., Bartolini, A., Schaltegger, U., & Blackburn, T. J. (2010). Correlating the end-Triassic mass extinction and flood basalt volcanism at the 100 ka level. *Geology*, *38*(5), 387-390.

Scholze, F., & Schneider, J. W. (2015). Improved methodology of ‘conchostracan’(Crustacea: Branchiopoda) classification for biostratigraphy. *Newsletters on Stratigraphy*, *48*(3): 287-298.

Schwartz, H. L., & Gillette, D. D. (1994). Geology and taphonomy of the Coelophysis quarry, Upper Triassic Chinle Formation, Ghost Ranch, New Mexico. *Journal of Paleontology*: 1118-1130.

Sciscio, L., & Bordy, E. M. (in prep). First fossil evidence suggesting cynodont burrowing in the Early Jurassic.

Sereno, P. C. (1991). Lesothosaurus,"fabrosaurids," and the early evolution of Ornithischia. *Journal of Vertebrate Paleontology, 11*(2):168-197.

Sereno, P. C. (1997). The origin and evolution of dinosaurs. *Annual Review of Earth and Planetary Sciences, 25*(1): 435-489.

Sha, J., Olsen, P.E., Pan, Y., Xu, D., Wang, Y., Zhang, X., Yao, X., & Vajda, V. (2015). Triassic–Jurassic climate in continental high-latitude Asia was dominated by obliquity-paced variations (Junggar Basin, Ürümqi, China). *Proceedings of the National Academy of Sciences, 112*: 3624-3629.

Sheldon, N. D., & Tabor, N. J. (2009). Quantitative paleoenvironmental and paleoclimatic reconstruction using paleosols. *Earth-Science Reviews, 95*(1): 1-52.

Shipman, T. C. (2004). Links between sediment accumulation rates and the development of alluvial architecture: Triassic Ischigualasto Formation, northwestern Argentina. Unpublished PhD thesis. University of Arizona, Tuscon, Arizona.

Shubin, N.H., Crompton, A.W., Sues, H.-D., & Olsen, P.E. (1991). New fossil evidence on the sister-group of mammals and early Mesozoic faunal distributions. *Science, 251*:1063-1065.

Sidor, C. A., & Hancox, P. J. (2006). Elliotherium kersteni, a new tritheledontid from the lower Elliot Formation (Upper Triassic) of South Africa. *Journal of Paleontology, 80*(2): 333-342.

Simms, M. J. (2003). Uniquely extensive seismite from the latest Triassic of the United Kingdom: Evidence for bolide impact? *Geology, 31*: 557-560.

Smith, N. D., & Pol, D. (2007). Anatomy of a basal sauropodomorph dinosaur from the Early Jurassic Hanson Formation of Antarctica. *Acta Palaeontologica Polonica, 52*(4): 657–674.

Smith, R. M., & Kitching, J. (1997). Sedimentology and vertebrate taphonomy of the Tritylodon acme zone: a reworked palaeosol in the Lower Jurassic Elliot Formation, Karoo Supergroup, South Africa. *Palaeogeography, Palaeoclimatology, Palaeoecology, 131*(1): 29-50.

Smith, R. M., Marsicano, C. A., & Wilson, J. A. (2009). Sedimentology and paleoecology of a diverse Early Jurassic tetrapod tracksite in Lesotho, southern Africa. *Palaios, 24*(10):672-684.

Smith R. M., Rubidge B. S., & Walt van der M. (2011). Therapsid biodiversity patterns and paleoenvironments of the Karoo Basin. In: Chinsamy-Turan, A. (ed.): *Forerunners of mammals*. Indiana University Press. Pp. 31-62.

Smith, R. M., Marsicano, C. A., Pol, D., & Mancuso, A. C. (2014). Ichnology of sauropodomorph nest from Patagonia indicates Early Jurassic origin for herd living and breeding site fidelity. 4th International Palaeontological Congress (IPC) (September/October 2014) Mendoza, Argnetina. P.a.

Steiner, M. B. (2014). New magnetostratigraphy and paleopole from the Whitmore Point Member of the Moenave Formation at Kanab, Utah. *Volumina Jurassica, 12*(2), 13-22.

Steiner, M. B., & Lucas, S. G. (2000). Paleomagnetism of the Late Triassic Petrified Forest Formation, Chinle Group, western United States: Further evidence of "large" rotation of the Colorado Plateau. *Journal of Geophysical Research, 105*(B11), 25-791.

Steiner, M. B., & Tanner, L. H. (2014). Magnetostratigraphy and paleopoles of the Kayenta Formation and the Tenney Canyon Tongue. *Volumina Jurassica, 12*(2): 31-38.

Sterli, J., de la Fuente, M. S., Guillermo, S. R., and Rougier, W. (2007). Anatomy and relationships of Palaeochersis talampayensis, a Late Triassic turtle from Argentina. *Palaeontogr A 281*:1–61.

Steyer, S, J., and Damiani, R. (2005). A giant brachyopoid temnopsondyl from the Upper Triassic or lower Jurassic of Lesotho. *Bulletin de la Societe Geologique de France, 176* (3): 243 – 248.

Stockley, G. M. (1947). *Report on the geology of Basutoland*. Basutoland.

Sues, H. D., & Olsen, P. E. (2015). Stratigraphic and temporal context and faunal diversity of Permian-Jurassic continental tetrapod assemblages from the Fundy rift basin, eastern Canada. *Atlantic Geology, 51*(1): 139-205.

Tankard, A., Welsink, H., Aukes, P., Newton, R., & Stettler, E. (2009). Tectonic evolution of the Cape and Karoo basins of South Africa. *Marine and Petroleum Geology, 26*(8), 1379-1412.

Tankard, A., Welsink, H., Aukes, P., Newton, R., and Stettler, E. (2012). Geodynamic interpretation of the Cape and the Karoo Basins, South Africa. Phanerozoic Passive Margins, Cratonic Basins and Global Tectonics Maps. USA and UK: Elsevier, 869-942.

Tanner, L. H., & Lucas, S. G. (2007). The Moenave Formation: Sedimentological and stratigraphic context of the Triassic–Jurassic boundary in the Four Corners area, southwestern USA. *Palaeogeography, Palaeoclimatology, Palaeoecology, 244*(1), 111-125.

Tanner, L. H., Lucas, S. G. & Chapman, M. G. (2004). Assessing the record and causes of Late Triassic extinctions. *Earth-Science Reviews, 65*(1-2): 103 – 139.

Tanner, L. H., Kyte, F. T. & Walker, A. E., (2008). Multiple Ir anomalies in uppermost Triassic to Jurassic-age strata of the Blomidon Formation, Fundy basin, eastern Canada. *Earth and Planetary Science Letters, 274*(1):103–111.

Tanner, L. H., Hubert, J. F., Coffey, B. P. & McInerney, D. P. (2001). Stability of atmospheric CO_2 levels across the Triassic/Jurassic boundary. *Nature, 411*: 675-677.

Tasch, P. (1979). Crustacean Branchiopod distribution and speciation in Mesozoic lakes of the Southern continents. *American Geophysical Union Antarctic Research Series, 30*:p.65-74.

Tasch, P. (1980). Conchostracan genus *Cornia* in the Cave Sandstone (Thabaneng, Mafeteng District). In: Abstractrs with progress, South Central Geological Society of America. Wichita, Kansas, p. 17.

Tasch, P. (1984). Biostratigraphy and palaeontology of some conchostracan-bearing beds in Southern Africa. *Palaeontologia africana*, *25*: 61–85.

Tasch, P. (1987). Fossil Conchostraca of the Southern Hemisphere and continental drift. *Geological Society of America Memoirs, 165*, xi-282.

Taylor, S. R., & McLennan, S. M. (1985). The continental crust: its composition and evolution. Blackwell Scientific Publications, Palo Alto. P.p. 328.

Thulborn, R. A. (1970). The skull of Fabrosaurus australis, a Triassic ornithischian dinosaur. *Palaeontology*, *13*(3): 414-432.

Thulborn, R. A. (1971). Tooth wear and jaw action in the Triassic ornithischian dinosaur Fabrosaurus. *Journal of Zoology*, *164*: 165-179.

Thulborn, R. A. (1972). The post-cranial skeleton of the Triassic ornithischian dinosaur Fabrosaurus australis. *Palaeontology*, *15*(1): 29-60.

Torsvik, T. H., Van der Voo, R., Preeden, U., Mac Niocaill, C., Steinberger, B., Doubrovine, P. V., van Hinsbergen, D.J.J., Domeier, M., Gaina, C., Tohver, E., Meert, J.G., McCausland, P.J.A., & Cocks, L. R. M. (2012). Phanerozoic polar wander, palaeogeography and dynamics. *Earth-Science Reviews, 114*(3): 325-368.

Turner B. R. (1972). Revision of the stratigraphic position of cynodonts from the upper part of the Karroo (Gondwana) System in Lesotho. *Geological Magazine*, *109*: 349-360.

Turner, B. R. (1978). Trace Fossils from the Upper Triassic Fluviatile Molteno Formation of the Karoo (Gondwana) Supergroup, Lesotho. J*ournal of Palaeontology, 52*: 959-963.

Tykoski, R. S. (2005). Vertebrate paleontology in the Arizona Jurassic. *Mesa Southwest Museum Bulletin*, *11*: 72-93.

Van Zijl, J. S. V., Graham, K. W. T., & Hales, A. L. (1962a). The palaeomagnetism of the Stormberg lavas of South Africa 1: Evidence for a genuine reversal of the Earth's field in Triassic-Jurassic times. *Geophysical Journal of the Royal Astronomy Society*, *7*: 23–39.

Van Zijl, J. S. V., Graham, K. W. T., & Hales, A. L. (1962b). The palaeomagnetism of the Stormberg lavas of South Africa 2: The behaviour of the magnetic field during a reversal. *Geophysical Journal of the Royal Astronomy Society*, *7*: 169–182.

Verati, C., Rapaille, C., Féraud, G., Marzoli, A., Bertrand, H., & Youbi, N. (2007). ^{40} Ar/^{39} Ar ages and duration of the Central Atlantic Magmatic Province volcanism in Morocco and Portugal and its relation to the Triassic–Jurassic boundary. *Palaeogeography, Palaeoclimatology, Palaeoecology*, *244*(1): 308-325.

Visser, J. (1984). A review of the Stormberg Group and Drakensberg volcanics in southern Africa. *Palaeontologia africana, 25*: 5–27.

Visser, J.N.J. & Botha, B.J.V. (1980). Meander channel, point bar, crevasse splay and aeolian deposits from the Elliot Formation in Barkly Pass, North-Eastern Cape. *Transactions of the Geological Society of South Africa, 83*: 55 – 62.

Wall, G. R., & Jenkyns, H. C. (2004). The age, origin and tectonic significance of Mesozoic sediment-filled fissures in the Mendip Hills (SW England): implications for extension models and Jurassic sea-level curves. *Geological Magazine*, *141*(04): 471-504.

Ward, P. D., Haggart, J. W., Carter, E. S., Wilbur, D., Tipper, H. W. & Evans, T. (2001). Sudden productivity collapse associated with the Triassic-Jurassic boundary mass extinction. *Science, 292*: 1148-1151.

Ward, P. D., Garrison, G. H., Haggart, J. W., Kring, D. A. & Beattie, M. J. (2004). Isotopic evidence bearing on Late Triassic extinction events, Queen Charlotte Islands, British Columbia, and implications for the duration and cause of the Triassic/Jurassic mass extinction. *Earth and Planetary Science Letters*, *224*: 589-600.

Ward, P. D., Botha, J., Buick, R., Dekock, M. O., Erwin, D. H., Garrison, G., Kirschvink, J., and Smith, R. H. M. (2005). Abrupt and gradual extinction among Late Permian land vertebrates in the Karoo Basin, South Africa: *Science, 307*: 709–714.

Ward, P.D., Garrison, G.H., Williford, K.H., Kring, D.A., Goodwin, D., Beattie, M.J. & McRoberts, C.A., (2007). The organic carbon isotopic and paleontological record across the Triassic-Jurassic boundary at the Candidate GSSP section at Ferguson Hill, Muller Canyon, Nevada, USA. *Palaeogeography, Palaeoclimatology, Palaeoecology, 244*: 281-289.

Warren, A., & Damiani, R. (1999). Stereospondyl amphibians from the Elliot Formation of South Africa. *Palaeontologia Africana, 35*: 45-54.

Wedepohl, K. H. (1995). The composition of the continental crust. *Geochimica et cosmochimica Acta*, *59*(7): 1217-1232.

Welman, J. (1998). Euskelosaurus and the origin of dinosaurs. *Journal of African Earth Sciences*, *27*(1): 209.

Welman, J. (2000). Cool brained Euskelosaurus and the origin of dinosaurs. *Culna, 55*: 24-26.

Weltje, G. J., & von Eynatten, H. (2004). Quantitative provenance analysis of sediments: review and outlook. *Sedimentary Geology*, *171*(1): 1-11.

Whiteside, J. H., Olsen, P. E., & Sambrotto, R. N. (2003). Negative δ13C carbon isotopic anomaly in continental strata at the Triassic–Jurassic boundary in eastern North America (Newark Basin, Pennsylvania, USA). *Geological Society of America, Abstracts with Programs, 34* (7)*:* 160.

Whiteside, J. H., Olsen, P. E., Kent, D.V., Fowell, S. J., & Et-Touhami, M. (2007). Synchrony between the CAMP and the Triassic–Jurassic mass-extinction event? *Palaeogeography, Palaeoclimatology, Palaeoecology, 244*: 345–367.

Whiteside, J. H., Olsen, P. E., Eglinton, T., Brookfield, M. E., & Sambrotto, R. N. (2010). Compound-specific carbon isotopes from Earth's largest flood basalt eruptions directly linked to the end-Triassic mass extinction. *Proceedings of the National Academy of Sciences, 107*: 6721–6725.

Whiteside, J. H., Lindström, S., Irmis, R. B., Glasspool, I. J., Schaller, M. F., Dunlavey, M., Nesbitt, S. J., Smith, N. D., & Turner, A. H. (2015). Extreme ecosystem instability suppressed tropical dinosaur dominance for 30 million years. *Proceedings of the National Academy of Sciences, 112* (26): 7909-7913.

Wignall, P. B. (2001). Large igneous provinces and mass extinctions. *Earth-Science Reviews, 53*: 1-33.

Wignall, P. B. (2005). The link between large igneous province eruptions and mass extinctions. *Elements, 1*: 293-297.

Wilson, J. A., Marsicano, C. A., & Smith, R. M. (2009). Dynamic locomotor capabilities revealed by early dinosaur trackmakers from Southern Africa. *PLoS One, 4*(E7331): 1-10.

Wotzlaw, J. F., Guex, J., Bartolini, A., Gallet, Y., Krystyn, L., McRoberts, C. A., Taylor, D., Schoene, B., & Schaltegger, U. (2014). Towards accurate numerical calibration of the Late Triassic: High-precision U-Pb geochronology constraints on the duration of the Rhaetian. *Geology, 42* (7): 571-574.

Yang, Z., Moreau, M-G., Bucher, H., Dommergues, J.-L., & Trouiller, A. (1996). Hettangian and Sinemurian magnetostratigraphy from Paris basin. *Journal of Geophysical Research, 101*(B4), 8025-8042.

Yates, A. M. (2005a). The skull of the Triassic sauropodomorph, *Melanorosaurus readi*, from South Africa and the definition of Sauropoda. *Journal of Vertebrate Paleontology, 25* (3): 132A-132A.

Yates, A. M. (2005b). A new theropod dinosaur from the Early Jurassic of South Africa and its implications for the early evolution of theropods. *Palaeontologia Africana, 41*: 105-122.

Yates, A. M. (2007a).The first complete skull of the Triassic dinosaur *Melanorosaurus* Haughton (Sauropodomorpha: Anchisauria). *Special Papers in Paleontology 77*, 9-55

Yates A.M. (2007b) Solving a dinosaurian puzzle: the identity of *Aliwalia rex* Galton, Historical Biology. *An International Journal of Paleobiology, 19*:1, 93-123.

Yates A.M. and Kitching J.W. (2003). The earliest known sauropod dinosaur and the first steps towards sauropod locomotion. *Proceedings of the Royal Society of London: Biological Sciences Series B, 270*: 1753-1758.

Yates, A. M., & Barrett, P. M. (2010). Massospondylus carinatus Owen 1854 (Dinosauria: Sauropodomorpha) from the Lower Jurassic of South Africa: Proposed conservation of the usage by designation of a neotype.

Yates, A. M., Hancox, P. J., & Rubidge, B. S. (2004). First record of a sauropod dinosaur from the upper Elliot Formation (Early Jurassic) of South Africa: research letter. *South African Journal of Science*, *100*(9 & 10): 504 – 506.

Yates, A. M., Bonnan, M. F., & Neveling, J. (2011). A new basal sauropodomorph dinosaur from the Early Jurassic of South Africa. *Journal of Vertebrate Paleontology*, *31*(3): 610-625.

Yates, A. M., Bonnan, M. F., Neveling, J., Chinsamy, A. & Blackbeard, M. G. (2010). A new transitional sauropodomorph dinosaur from the Early Jurassic of South Africa and the evolution of sauropod feeding and quadrupedalism. *Proceedings of the Royal Society of London: Biological Sciences Series B, 277*: 787-794, doi:10.1098/rspb.2009.1440.

Zeigler, K. E., & Geissman, J. W. (2008). Magnetostratigraphy of the Upper Triassic Chinle Group and Implications for the Age and Correlation of Upper Triassic Strata in North America. Geological Society of America Abstracts with programs (online). http://a-c-s.confex.com/crops/2008am/webprogram/Paper47897.html -

Zeigler, K. E. & Geissman, J. W. (2011). Magnetostratigraphy of the Upper Triassic Chinle Group of New Mexico: Implications for regional and global correlations among Upper Triassic sequences. *Geosphere*, *7*(3): 802–829.

Zhang, Y., Pe-Piper, G. & Piper, D. J. (2014). Sediment geochemistry as a provenance indicator: Unravelling the cryptic signatures of polycyclic sources, climate change, tectonism and volcanism. *Sedimentology, 61*(2): pp.383–410.

Appendices

Raw palaeomagnetic data, from all sampling localities, is available upon request from the author or the supervisors of this thesis.

Appendices **Likhoele (LIK) samples**

Table A1. Whole rock geochemistry, showing major elements (wt %), weathering indices (CIA, CIA molar and ICV) and geochemical ratios for Likhoele. Facies codes explained in text.

				Major elements														Weathering indices			Ratios							
	Sample#	Strat.ht. (m)	Facies	SiO_2	TiO_2	Al_2O_3	Fe_2O_3	MnO	MgO	CaO	Na_2O	K_2O	P_2O5	SO_3	Cr_2O_3	NiO	LOI	Total	CIA	CIAmolar	ICV	SiO_2/Al_2O_3	Fe_2O_3/Al_2O_3	K_2O/Al_2O_3	Al_2O_3/TiO_2	MgO/Al_2O_3	CaO/Al_2O_3	Na_2O/Al_2O_3	K_2O/Na_2O	
LEF	LIK-001	5.5	Sm (?)	77.96	0.63	10.12	2.23	0.03	1.08	0.41	1.86	2.25	0.03	0.01	0.02	0.01	2.37	99.74	61.90	1.62	0.84	7.71	0.22	0.22	16.04	0.11	0.04	0.18	1.21	
	LIK-002	7.25	Fm	74.46	0.68	11.30	2.77	0.03	1.20	0.40	1.79	2.65	0.02	0.01	0.02	0.01	2.70	99.11	63.37	1.73	0.84	6.59	0.25	0.23	16.70	0.11	0.04	0.16	1.48	
	LIK-004	9.2	Fm	69.89	0.58	12.46	3.55	0.05	1.40	0.79	1.98	3.39	0.05	0.01	0.01	0.01	3.41	99.56	59.86	1.49	0.94	5.61	0.29	0.27	21.47	0.11	0.06	0.16	1.72	
	LIK-005	9.8	Fm	70.49	0.58	12.24	3.26	0.05	1.42	0.77	1.99	3.30	0.06	0.00	0.01	0.01	3.17	99.28	59.76	1.49	0.93	5.76	0.27	0.27	21.14	0.12	0.06	0.16	1.66	
	LIK-006	10.5	Fm	74.40	0.49	9.54	2.21	0.07	1.13	2.55	2.44	2.13	0.02	0.02	0.02	0.01	3.27	99.72	46.54	0.87	1.16	7.80	0.23	0.22	19.41	0.12	0.27	0.26	0.88	
	LIK-007A	9.5	Sm	66.95	0.42	8.22	1.59	0.17	0.86	9.11	1.77	1.86	0.02	0.01	0.01	0.00	7.92	99.75	27.68	0.38	1.92	8.14	0.19	0.23	19.70	0.10	1.11	0.22	1.05	
	LIK_007B	10.9	Fm	72.18	0.57	10.91	2.63	0.06	1.16	1.71	2.56	2.59	0.07	0.02	0.01	0.00	4.13		51.86	1.08	1.03	6.61	0.24	0.24	19.15	0.11	0.16	0.23	1.01	
	LIK-008	12	Fm	73.16	0.61	11.37	2.81	0.05	1.20	0.80	2.57	2.87	0.05	0.00	0.01	0.01	2.95	99.70	56.40	1.29	0.96	6.43	0.25	0.25	18.78	0.11	0.07	0.23	1.12	
	LIK-009	13.8	Fm	70.33	0.55	11.75	3.11	0.06	1.53	1.25	2.43	3.06	0.03	0.01	0.02	0.01	3.64	99.41	55.06	1.23	1.02	5.99	0.26	0.26	21.47	0.13	0.11	0.21	1.26	
	LIK-010A	14.9	P2	64.39	0.50	9.79	2.33	0.15	1.15	7.85	2.15	2.48	0.03	0.02	0.01	0.01	7.93	99.97	32.32	0.48	1.70	6.58	0.24	0.25	19.50	0.12	0.80	0.22	1.15	
UEF	LIK-010B	15.45	Fm	68.33	0.52	11.58	2.98	0.06	1.42	2.37	2.47	2.91	0.03	0.01	0.01	0.01	4.49	99.13	50.11	1.00	1.10	5.90	0.26	0.25	22.25	0.12	0.20	0.21	1.18	
	LIK-011	15.95	Fm	70.89	0.55	11.86	2.98	0.05	1.35	1.01	2.47	3.05	0.03	0.00	0.01	0.01	3.25	99.29	56.28	1.29	0.97	5.98	0.25	0.26	21.63	0.11	0.09	0.21	1.23	
	LIK-012	16.45	Fm	70.97	0.45	9.85	1.91	0.20	1.07	3.86	2.80	2.28	0.06	0.03	0.01	0.00	4.73	99.21	41.17	0.70	1.27	7.21	0.19	0.23	22.00	0.11	0.39	0.28	0.81	
	LIK-013	16.95	Fm	70.01	0.51	11.64	3.03	0.07	1.39	2.05	2.23	2.93	0.04	0.01	0.02	0.01	4.19	99.77	52.40	1.10	1.05	6.02	0.26	0.25	22.76	0.12	0.18	0.19	1.31	Geochem unit 1 (?)
	LIK-014	17.45	P3	70.90	0.51	11.46	2.96	0.06	1.36	1.25	2.32	2.86	0.03	0.01	0.01	0.00	3.58	99.27	55.47	1.25	0.99	6.19	0.26	0.25	22.56	0.12	0.11	0.20	1.23	
	LIK-016	18.45	Fm	67.92	0.46	10.33	2.43	0.05	1.25	5.24	2.42	2.46	0.02	0.01	0.01	0.00	5.87	99.80	39.00	0.64	1.38	6.57	0.24	0.24	22.61	0.12	0.51	0.23	1.01	
	LIK-017-018	18.95	Gmm	72.97	0.38	8.30	1.16	0.30	0.83	5.17	2.61	1.85	0.01	0.00	0.01	0.00	5.16	99.52	34.57	0.53	1.48	8.79	0.14	0.22	21.58	0.10	0.62	0.32	0.71	
	LIK-025	20.4	Sc	75.50	0.45	10.48	2.16	0.03	1.15	0.92	2.53	2.58	0.02	0.01	0.01	0.01	2.86	100.08	54.89	1.22	0.94	7.20	0.21	0.25	23.20	0.11	0.09	0.24	1.02	
	LIK-026	21.4	P4	75.99	0.43	10.06	2.05	0.05	1.03	1.29	2.51	2.41	0.01	0.02	0.01	0.01	2.92	100.09	52.56	1.11	0.97	7.55	0.20	0.24	23.32	0.10	0.13	0.25	0.96	
	LIK-027	21.9	Sc	73.38	0.46	9.93	2.10	0.06	1.13	2.69	2.49	2.37	0.05	0.01	0.01	0.00	3.71	99.42	46.22	0.86	1.14	7.39	0.21	0.24	21.77	0.11	0.27	0.25	0.95	
	LIK-028	23	Sh/Sl	73.17	0.37	8.59	1.40	0.21	0.92	5.25	2.40	1.99	0.01	0.01	0.01	0.01	4.19	99.29	35.42	0.55	1.46	8.52	0.16	0.23	23.25	0.11	0.61	0.28	0.83	
	LIK-029	23.75	Sc	76.58	0.40	8.99	1.66	0.07	0.99	2.06	2.19	2.17	0.01	0.03	0.01	0.00	3.06	99.19	48.12	0.93	1.06	8.52	0.18	0.24	22.53	0.11	0.23	0.24	0.99	
	LIK-030	24.75	Sm	76.73	0.60	8.94	1.53	0.08	0.96	2.49	2.28	2.11	0.02	0.03	0.01	0.00	3.13	99.81	45.84	0.85	1.12	8.58	0.17	0.24	14.99	0.11	0.28	0.25	0.92	
	LIK-031	27	P5	76.44	0.48	9.88	2.54	0.05	1.22	0.68	2.01	2.76	0.04	0.01	0.01	0.00	2.66	100.02	56.75	1.31	0.98	7.73	0.26	0.28	20.80	0.12	0.07	0.20	1.37	
	LIK-032	28.25	Sm	77.24	0.45	9.19	2.20	0.05	1.11	0.99	1.94	2.50	0.04	0.02	0.01	0.00	2.57	99.39	54.44	1.20	1.00	8.40	0.24	0.27	20.33	0.12	0.11	0.21	1.29	
	LIK-033	29.5	Sh/Sl	71.58	0.39	7.29	1.31	0.21	0.88	7.22	1.88	1.82	0.01	0.02	0.01	0.00	6.64	99.91	28.63	0.40	1.88	9.82	0.18	0.25	18.84	0.12	0.99	0.26	0.97	
	LIK-034	30.5	Fm	72.53	0.53	9.59	2.45	0.06	1.14	3.12	2.08	2.48	0.01	0.01	0.01	0.00	4.27	99.23	44.89	0.81	1.23	7.56	0.25	0.26	18.15	0.12	0.33	0.22	1.19	
	LIK-035	31.2	Fm	72.61	0.56	10.65	3.17	0.06	1.36	1.44	1.90	2.94	0.04	0.01	0.02	0.01	3.71	99.30	54.40	1.19	1.07	6.82	0.30	0.28	18.98	0.13	0.13	0.18	1.55	
	LIK-036	33.05	P6	77.55	0.46	7.72	1.75	0.05	0.99	2.79	1.68	2.12	0.03	0.02	0.01	0.01	3.70	99.65	43.28	0.76	1.27	10.04	0.23	0.27	16.69	0.13	0.36	0.22	1.26	
	LIK-037	34	Sm	77.87	0.48	8.20	1.87	0.07	0.98	2.15	1.90	2.21	0.08	0.02	0.01	0.01	3.23	99.87	46.52	0.87	1.18	9.49	0.23	0.27	17.10	0.12	0.26	0.23	1.16	
	LIK-038	34.9	Sm	77.92	0.48	8.64	1.92	0.04	1.01	1.21	1.95	2.25	0.03	0.01	0.01	0.00	2.83	99.14	52.43	1.10	1.03	9.02	0.22	0.26	17.85	0.12	0.14	0.23	1.16	
	LIK-039	35.65	Fm	75.52	0.55	9.68	2.44	0.05	1.15	1.28	2.30	2.44	0.06	0.03	0.02	0.00	3.16	99.61	52.49	1.10	1.05	7.80	0.25	0.25	17.75	0.12	0.13	0.24	1.06	
	LIK-040	36.05	Fm	74.25	0.55	10.35	2.66	0.04	1.26	1.02	2.26	2.58	0.04	0.02	0.02	0.01	3.07	99.12	55.32	1.24	1.00	7.17	0.26	0.25	18.65	0.12	0.10	0.22	1.14	
	LIK-041	37.5	Fm	73.79	0.60	10.89	2.97	0.05	1.35	0.74	2.52	2.70	0.06	0.04	0.01	0.01	2.76	99.74	56.39	1.29	1.00	6.77	0.27	0.25	18.06	0.12	0.07	0.23	1.07	
	LIK-042	38.55	Fm	63.40	0.63	12.04	3.87	0.13	1.66	4.73	2.58	2.92	0.07	0.03	0.02	0.01	6.42	99.87	42.92	0.75	1.37	5.27	0.32	0.24	19.09	0.14	0.39	0.21	1.13	Geochem unit 2 (?)
	Elliot		Mean	72.81	0.51	10.11	2.40	0.08	1.17	2.53	2.24	2.52	0.04	0.02	0.01	0.00	3.93	99.56	49.01	1.02	1.15	7.36	0.23	0.25	20.00	0.12	0.27	0.22	1.14	
	n=35		Stdev.	3.74	0.08	1.37	0.66	0.06	0.20	2.22	0.30	0.41	0.02	0.01	0.00	0.00	1.44	0.31	9.26	0.34	0.27	1.24	0.04	0.02	2.29	0.01	0.27	0.03	0.23	
	LEF		Mean	71.42	0.56	10.77	2.65	0.07	1.21	2.56	2.15	2.66	0.04	0.01	0.01	0.01	4.150	99.582	51.48	1.17	1.13	6.722	0.243	0.245	19.338	0.112	0.271	0.202	1.253	
	n = 10		Stdev.	3.92	0.07	1.33	0.58	0.05	0.19	3.20	0.32	0.50	0.02	0.01	0.00	0.00	2.05	0.27	12.40	0.46	0.37	0.88	0.03	0.02	1.85	0.01	0.37	0.03	0.28	
	UEF		Mean	73.36	0.49	9.85	2.30	0.09	1.16	2.52	2.27	2.47	0.03	0.02	0.01	0.00	3.846	99.548	48.02	0.96	1.16	7.613	0.230	0.251	20.272	0.117	0.271	0.233	1.101	
	n=25		Stdev.	3.59	0.07	1.32	0.67	0.07	0.20	1.77	0.29	0.36	0.02	0.01	0.00	0.00	1.16	0.33	7.77	0.27	0.22	1.28	0.04	0.02	2.43	0.01	0.22	0.03	0.19	
			variance σ	15.38	0.01	1.78	0.34	0.00	0.04	10.23	0.10	0.25	0.00	0.00	0.00	0.00			153.74	0.22	0.14	0.78	0.00	0.00	3.41	0.00	0.14	0.00		
			variance σ	12.91	0.00	1.73	0.45	0.00	0.04	3.13	0.08	0.13	0.00	0.00	0.00	0.00			60.36	0.07	0.05	1.65	0.00	0.00	5.91	0.00	0.05	0.00		

Correlation coeffiecient between Al and Si	-0.43	Al and Fe	0.92
Correlation coeffiecient between Al and Ca	-0.44	Al and K	0.92
correlation coefficient between Al and Ti	0.67		
Al and Mg	0.90		
Al and Na	0.33		

Table A2. Coarse-grained (Sm - Gmm) and fine-grained (Fm) samples, from Likhoele, and associated major element (wt %), weathering indices and ratios.

Sm- Gmm ' coarse-grained' rocks

Sample	Strat.ht. (m)	Facies code	SiO_2	TiO_2	Al_2O_3	Fe_2O_3	MnO	MgO	CaO	Na_2O	K_2O	P_2O5	SO_3	Cr_2O_3	NiO	LOI	Total	CIA	CIAmolar	ICV	SiO_2/Al_2O_3	Fe_2O_3/Al_2O_3	K_2O/Al_2O_3	Al_2O_3/TiO_2	MgO/Al_2O_3	CaO/Al_2O_3	Na_2O/Al_2O_3	K_2O/Na_2O
LIK-001	5.5 Sm (*)		77.96	0.63	10.12	2.23	0.03	1.08	0.41	1.86	2.25	0.03	0.01	0.02	0.01	2.37	99.74	62	2	0.8	7.71	0.22	0.22	16.04	0.11	0.04	0.18	1.21
LIK-007A	9.5 Sm		66.95	0.42	8.22	1.59	0.17	0.86	9.11	1.77	1.86	0.02	0.01	0.01	0.00	7.92	99.75	28	0.4	1.9	8.14	0.19	0.23	19.70	0.10	1.11	0.22	1.05
LIK-017-018	18.95 Gmm		72.97	0.38	8.30	1.16	0.30	0.83	5.17	2.61	1.85	0.01	0.00	0.01	0.00	5.16	99.52	35	1	1.5	8.79	0.14	0.22	21.58	0.10	0.62	0.32	0.71
LIK-025	20.4 Sc		75.50	0.45	10.48	2.16	0.03	1.15	0.92	2.53	2.58	0.02	0.01	0.01	0.01	2.86	100.08	55	1	0.9	7.20	0.21	0.25	23.20	0.11	0.09	0.24	1.02
LIK-027	21.9 Sc		73.38	0.46	9.93	2.10	0.06	1.13	2.69	2.49	2.37	0.05	0.01	0.01	0.00	3.71	99.42	46	1	1.1	7.39	0.21	0.24	21.77	0.11	0.27	0.25	0.95
LIK-028	23 Sh/Sl		73.17	0.37	8.59	1.40	0.21	0.92	5.25	2.40	1.99	0.01	0.01	0.01	0.01	4.19	99.29	35	1	1.5	8.52	0.16	0.23	23.25	0.11	0.61	0.28	0.83
LIK-029	23.75 Sc		76.58	0.40	8.99	1.66	0.07	0.99	2.06	2.19	2.17	0.01	0.03	0.01	0.00	3.06	99.19	48	1	1.1	8.52	0.18	0.24	22.53	0.11	0.23	0.24	0.99
LIK-030	24.75 Sm		76.73	0.60	8.94	1.53	0.08	0.96	2.49	2.28	2.11	0.02	0.03	0.01	0.00	3.13	99.81	46	1	1.1	8.58	0.17	0.24	14.99	0.11	0.28	0.25	0.92
LIK-032	28.25 Sm		77.24	0.45	9.19	2.20	0.05	1.11	0.99	1.94	2.50	0.04	0.02	0.01	0.00	2.57	99.39	54	1	1.0	8.40	0.24	0.27	20.33	0.12	0.11	0.21	1.29
LIK-033	29.5 Sh/Sl		71.58	0.39	7.29	1.31	0.21	0.88	7.22	1.88	1.82	0.01	0.02	0.01	0.00	6.64	99.91	29	0.4	1.9	9.82	0.18	0.25	18.84	0.12	0.99	0.26	0.97
LIK-037	34 Sm		77.87	0.48	8.20	1.87	0.07	0.98	2.15	1.90	2.21	0.08	0.02	0.01	0.01	3.23	99.87	47	1	1.2	9.49	0.23	0.27	17.10	0.12	0.26	0.23	1.16
LIK-038	34.9 Sm		77.92	0.48	8.64	1.92	0.04	1.01	1.21	1.95	2.25	0.03	0.01	0.01	0.00	2.83	99.14	52	1	1.0	9.02	0.22	0.26	17.85	0.12	0.14	0.23	1.16
Mean			74.82	0.46	8.91	1.76	0.11	0.99	3.30	2.15	2.16	0.03	0.02	0.01	0.00	3.97	99.59	44.723	0.875	1.254	8.465	0.197	0.243	19.767	0.112	0.396	0.242	1.022
Std dev.			3.34	0.08	0.91	0.37	0.09	0.11	2.76	0.30	0.25	0.02	0.01	0.00	0.00	1.74	0.31	10.91	0.37	0.36	0.78	0.03	0.02	2.82	0.01	0.36	0.03	0.17

Fm 'fine grained' rocks

Sample	Strat.height (m)	Facies code	SiO_2	TiO_2	Al_2O_3	Fe_2O_3	MnO	MgO	CaO	Na_2O	K_2O	P_2O5	SO_3	Cr_2O_3	NiO	LOI	Total	CIA	CIAmolar	ICV	SiO_2/Al_2O_3	Fe_2O_3/Al_2O_3	K_2O/Al_2O_3	Al_2O_3/TiO_2	MgO/Al_2O_3	CaO/Al_2O_3	Na_2O/Al_2O_3	K_2O/Na_2O
LIK-002	7.25 Fm		74.46	0.68	11.30	2.77	0.03	1.20	0.40	1.79	2.65	0.02	0.01	0.02	0.01	2.70	99.11	63	2	0.8	6.59	0.25	0.23	16.70	0.11	0.04	0.16	1.48
LIK-004	9.2 Fm		69.89	0.58	12.46	3.55	0.05	1.40	0.79	1.98	3.39	0.05	0.01	0.01	0.01	3.41	99.56	60	1	0.9	5.61	0.29	0.27	21.47	0.11	0.06	0.16	1.72
LIK-005	9.8 Fm		70.49	0.58	12.24	3.26	0.05	1.42	0.77	1.99	3.30	0.06	0.00	0.01	0.01	3.17	99.28	60	1	0.9	5.76	0.27	0.27	21.14	0.12	0.06	0.16	1.66
LIK-006	10.5 Fm		74.40	0.49	9.54	2.21	0.07	1.13	2.55	2.44	2.13	0.02	0.02	0.02	0.01	3.27	99.72	57	1	1.2	7.80	0.23	0.22	19.41	0.12	0.27	0.26	0.88
LIK_007B	10.9 Fm		72.18	0.57	10.91	2.63	0.06	1.16	1.71	2.56	2.59	0.07	0.02	0.01	0.00	4.13		52	1	1.0	6.61	0.24	0.24	19.15	0.11	0.16	0.23	1.01
LIK-008	12 Fm		73.16	0.61	11.37	2.81	0.05	1.20	0.80	2.57	2.87	0.05	0.00	0.01	0.01	2.95	99.70	56	1	1.0	6.43	0.25	0.25	18.78	0.11	0.07	0.23	1.12
LIK-009	13.8 Fm		70.33	0.55	11.75	3.11	0.06	1.53	1.25	2.43	3.06	0.03	0.01	0.02	0.01	3.64	99.41	55	1	1.0	5.99	0.26	0.26	21.47	0.13	0.11	0.21	1.26
LIK-010A	14.9 P2		64.39	0.50	9.79	2.33	0.15	1.15	7.85	2.15	2.48	0.03	0.02	0.01	0.01	7.93	99.97	32	0.5	1.7	6.58	0.24	0.25	19.50	0.12	0.80	0.22	1.15
LIK-010B	15.45 Fm		68.33	0.52	11.58	2.98	0.06	1.42	2.37	2.47	2.91	0.03	0.01	0.01	0.01	4.49	99.13	50	1	1.1	5.90	0.26	0.25	22.25	0.12	0.20	0.21	1.18
LIK-011	15.95 Fm		70.89	0.55	11.86	2.98	0.05	1.35	1.01	2.47	3.05	0.03	0.00	0.01	0.01	3.25	99.29	56	1	1.0	5.98	0.25	0.26	21.63	0.11	0.09	0.21	1.23
LIK-012	16.45 Fm		70.97	0.45	9.85	1.91	0.20	1.07	3.86	2.80	2.28	0.06	0.03	0.01	0.00	4.73	99.21	41	1	1.3	7.21	0.19	0.23	22.00	0.11	0.39	0.28	0.81
LIK-013	16.95 Fm		76.01	0.51	11.64	3.03	0.07	1.39	2.05	2.23	2.93	0.04	0.01	0.02	0.01	4.19	99.77	52	1	1.1	6.02	0.26	0.25	22.76	0.12	0.18	0.19	1.31
LIK-014	17.45 P3		70.90	0.51	11.46	2.96	0.06	1.36	1.25	2.32	2.86	0.03	0.01	0.01	0.00	3.58	99.27	55	1	1.0	6.19	0.26	0.25	22.56	0.12	0.11	0.20	1.23
LIK-016	18.45 Fm		67.92	0.46	10.33	2.43	0.05	1.25	5.24	2.42	2.46	0.02	0.01	0.01	0.00	5.87	99.80	39	1	1.4	6.57	0.24	0.24	22.61	0.12	0.51	0.23	1.01
LIK-026	21.4 P4		75.99	0.43	10.06	2.05	0.05	1.03	1.29	2.51	2.41	0.01	0.02	0.01	0.01	2.92	100.09	53	1	1.0	7.55	0.20	0.24	23.32	0.10	0.13	0.25	0.96
LIK-031	27 P5		76.44	0.48	9.88	2.54	0.05	1.22	0.68	2.01	2.76	0.04	0.01	0.01	0.00	2.66	100.02	57	1	1.0	7.73	0.26	0.28	20.80	0.12	0.07	0.20	1.37
LIK-034	30.5 Fm		72.53	0.53	9.59	2.45	0.06	1.14	3.12	2.08	2.48	0.01	0.01	0.01	0.00	4.27	99.23	45	1	1.2	7.56	0.25	0.26	18.15	0.12	0.33	0.22	1.19
LIK-035	31.2 Fm		72.61	0.56	10.65	3.17	0.06	1.36	1.44	1.90	2.94	0.04	0.01	0.02	0.01	3.71	99.30	54	1	1.1	6.82	0.30	0.28	18.98	0.13	0.13	0.18	1.55
LIK-036	33.05 P6		77.55	0.46	7.72	1.75	0.05	0.99	2.79	1.68	2.12	0.03	0.02	0.01	0.01	3.70	99.65	43	1	1.3	10.04	0.23	0.27	16.69	0.13	0.36	0.22	1.26
LIK-039	35.65 Fm		75.52	0.55	9.68	2.44	0.05	1.15	1.28	2.30	2.44	0.06	0.03	0.02	0.00	3.16	99.61	52	1	1.1	7.80	0.25	0.25	17.75	0.12	0.13	0.24	1.00
LIK-040	36.05 Fm		74.25	0.55	10.35	2.66	0.04	1.26	1.02	2.26	2.58	0.04	0.02	0.02	0.01	3.07	99.12	55	1	1.0	7.17	0.26	0.25	18.65	0.12	0.10	0.22	1.14
LIK-041	37.5 Fm		73.79	0.60	10.89	2.97	0.05	1.35	0.74	2.52	2.70	0.06	0.04	0.01	0.01	2.76	99.74	56	1	1.0	6.77	0.27	0.25	18.06	0.12	0.07	0.23	1.07
LIK-042	38.55 Fm		63.40	0.63	12.04	3.87	0.13	1.66	4.73	2.58	2.92	0.07	0.03	0.02	0.01	6.42	99.87	43	1	1.4	5.27	0.32	0.24	19.09	0.14	0.39	0.21	1.13
Mean			71.76	0.54	10.74	2.73	0.07	1.27	2.13	2.28	2.71	0.04	0.01	0.01	0.01	3.91	99.54	51.244	1.096	1.100	6.781	0.253	0.252	20.129	0.118	0.206	0.214	1.209
Std dev.			3.56	0.06	1.13	0.51	0.04	0.16	1.81	0.29	0.34	0.02	0.01	0.00	0.00	1.30	0.31	7.61	0.31	0.19	1.03	0.03	0.02	2.02	0.01	0.18	0.03	0.23

		SiO_2	TiO_2	Al_2O_3	Fe_2O_3	MnO	MgO	CaO	Na_2O	K_2O	P_2O5	SO_3	Cr_2O_3	NiO
Mean	coarse-grained saples	74.82	0.46	8.91	1.76	0.11	0.99	3.30	2.15	2.16	0.03	0.02	0.01	0.00
Mean	fine-grained samples	71.76	0.54	10.74	2.73	0.07	1.27	2.13	2.28	2.71	0.04	0.01	0.01	0.01
PAAS		62.400	0.990	18.780	7.180		2.190	1.290	1.190	3.680	0.160			

Al_2O_3 F-Test Two-Sample for Variances t-Test: Two-Sample Assuming Equal Variances

	Coarse	Fines
Mean	8.9083227	10.736933
Variance	0.8348408	1.2792712
Observations	12	23
df	11	22
F	0.6525909	
P(F<=f) one-tail	0.2342615	
F Critical one-tail	0.3807889	

	Variable 1	Variable 2
Mean	8.9083227	10.736933
Variance	0.8348408	1.2792712
Observations	12	23
Pooled Variance	1.1277	
Hypothesized Mean Difference		
df	33	
t Stat	-4.8282069	
P(T<=t) one-tail	1.529E-05	
t Critical one-tail	1.6923603	
P(T<=t) two-tail	3.058E-05	
t Critical two-tail	2.0345153	

CaO F-Test Two-Sample for Variances

	Coarse	Fines
Mean	3.3049527	2.1292248
Variance	7.6434331	3.2860551
Observations	12	23
df	11	22
F	2.326021	
P(F<=f) one-tail	0.0442542	
F Critical one-tail	2.2585184	

Table A3. Rare earth elements (ppm) and provenance ratios for Likhoele.

| | | REE (ppm) | | | | | | | | | | | | | | LREEs | | | | HREEs | | | | | | | | | | | | | |

Table A4. Lower Eliot (LEF) and upper Elliot (UEF) Formation REEs and REE ratio comparisons, in addition to LIK REE coarse-grained and fine-grained sample comparisons.

REE (ppm)

LEF		Sc	V	Cr	Co	Ni	Cu	Zn	Ga	Rb	Sr	Y	Zr	Nb	Cs	Ba	La	Ce	Nd	Sm	Eu	Gd	Yb	Lu	Hf	Ta	Pb	Th	U	La/Sc	Sc/Th	Co/Th	Th/Cr	Cr/Th	Th/U	La/Y	U/Th	V/Cr
LIK001	Sm (?)	5.77	60.3	44.0	9.64	17.5	15.3	55.1	14.0	84.1	86.4	37.6	215	11.4	4.28	473	37.2	85.7	36.5	7.19	1.23	6.10	3.73	0.59	6.00	0.88	22.1	13.3	2.71	6.45	0.43	0.72	0.30	3.30	4.93	1.35	0.20	1.37
LIK002	Fm	6.76	76.4	43.8	8.53	20.4	16.7	71.8	23.7	101	89.9	29.0	222	12.4	6.37	418	35.9	74.1	32.2	6.02	1.05	5.08	2.91	0.42	6.11	0.92	14.7	12.2	2.30	5.31	0.56	0.70	0.28	3.60	5.28	1.24	0.19	1.74
LIK004	Fm	6.90	48.4	40.7	7.12	15.4	48.2	61.7	27.6	131	140	26.8	191	12.1	8.82	488	35.1	73.0	32.0	6.21	1.11	5.52	2.66	0.38	5.15	0.89	21.3	13.5	2.03	5.08	0.52	0.54	0.33	3.05	6.56	1.31	0.15	1.19
LIK005	Fm	6.42	44.0	34.9	6.79	14.9	16.3	66.3	26.5	119	146	25.5	193	11.9	8.60	465	32.4	67.6	30.3	5.89	1.06	5.17	2.51	0.37	5.20	0.85	18.8	12.5	2.02	5.05	0.53	0.56	0.35	2.86	6.04	1.27	0.17	1.26
LIK006	Fm	3.67	48.9	26.3	2.92	5.74	12.0	31.2	29.2	72.9	172	21.9	199	9.22	4.44	729	29.3	60.6	26.9	5.08	0.89	4.25	2.36	0.35	5.47	0.67	14.3	9.89	2.03	8.46	0.35	0.30	0.35	2.87	4.87	1.34	0.21	1.73
LIK007a	Sm	3.39	28.6	23.0	<d.l.	<d.l.	15.3	27.6	17.4	68.3	216	23.1	191	7.88	3.96	535	27.1	56.5	27.8	5.67	1.04	5.05	2.20	0.32	5.14	0.56	19.1	10.2	1.54	8.00	0.33		0.44	2.25	6.65	1.17	0.15	1.23
LIK007b	Fm	5.20	46.5	32.8	5.51	10.3	14.3	46.6	23.7	98.7	138	25.2	207	11.7	8.61	413	33.1	68.7	30.5	5.87	0.99	5.30	2.52	0.36	5.84	0.82	18.4	12.6	2.42	6.36	0.41	0.44	0.39	2.60	5.23	1.31	0.19	1.42
LIK008	Fm	5.05	44.1	30.2	5.97	12.2	13.4	46.6	23.8	98.4	116	24.7	204	11.9	8.30	443	32.8	71.2	31.0	6.09	1.01	5.01	2.60	0.38	5.91	1.12	17.7	12.5	2.29	6.50	0.40	0.48	0.41	2.42	5.45	1.33	0.18	1.46
LIK009	Fm	5.80	41.8	28.6	6.45	12.6	15.3	51.0	25.8	111	138	24.5	190	11.8	7.93	468	36.3	77.4	33.3	6.38	1.04	5.08	2.54	0.36	5.37	0.90	17.4	12.9	2.00	6.26	0.45	0.56	0.45	2.22	6.42	1.48	0.16	1.46
LIK010a	P2	4.53	33.5	24.8	1.23		18.1	38.5	21.1	87.6	228	24.0	219	9.72	5.54	397	30.1	60.9	27.2	5.32	0.90	4.55	2.56	0.37	6.06	0.71	16.5	10.1	2.10	7.10	0.42	0.12	0.41	2.44	4.84	1.25	0.21	1.35
Mean		5.30	47.23	33.11	6.02	13.65	15.47	49.64	24.28	98.06	147.13	25.22	202.97	10.99	6.62	459.83	32.94	69.57	30.77	5.97	1.03	5.14	2.56	0.37	5.63	0.85	18.02	11.92	2.14	6.46	0.44	0.48	0.37	2.70	5.63	1.31	0.18	1.42
Stdev		1.28	13.42	7.58	2.60	4.51	1.96	14.58	3.33	19.37	47.09	2.11	12.27	1.51	1.94	104.90	3.22	8.73	2.96	0.58	0.10	0.53	0.19	0.03	0.40	0.16	2.51	1.33	0.31	1.16	0.07	0.19	0.06	0.46	0.72	0.08	0.02	0.19

UEF		Sc	V	Cr	Co	Ni	Cu	Zn	Ga	Rb	Sr	Y	Zr	Nb	Cs	Ba	La	Ce	Nd	Sm	Eu	Gd	Yb	Lu	Hf	Ta	Pb	Th	U	La/Sc	Sc/Th	Co/Th	Th/Cr	Cr/Th	Th/U	La/Y	U/Th	V/Cr
LIK010b	Fm	4.78	33.9	26.7	4.42	8.79	12.9	34.3	21.5	86.4	127	17.3	153	9.36	5.68	379	29.3	70.6	28.2	5.34	0.90	4.23	1.84	0.26	4.37	0.69	14.3	10.4	1.54	6.12	0.46	0.42	0.39	2.56	4.95	1.09	0.18	1.27
LIK011	Fm	5.14	40.8	28.1	6.24	12.6	13.8	76.6	24.4	102	131	17.9	164	11.2	6.89	406	28.7	59.9	26.2	4.93	0.83	3.81	2.04	0.30	4.73	0.81	15.4	10.7	1.59	5.58	0.48	0.58	0.58	2.61	6.77	1.60	0.15	1.45
LIK012	Fm	3.68	39.5	23.7	2.63	3.24	13.0	29.4	18.6	79.5	205	21.5	180	8.92	4.81	1884	25.0	56.8	24.6	4.87	0.84	4.40	1.99	0.27	4.01	0.63	16.5	9.38	1.36	6.80	0.39	0.28	0.40	2.53	6.90	1.08	0.14	1.87
LIK013	Fm	5.04	40.3	26.8	5.60	11.5	17.9	43.4	33.6	109	158	21.3	196	10.6	6.67	752	30.3	61.2	28.2	5.57	0.96	4.67	2.14	0.31	5.47	0.76	18.5	12.0	1.82	6.06	0.42	0.47	0.45	2.23	6.61	1.42	0.15	1.51
LIK014	P3	4.29	39.4	27.2	5.95	12.9	16.0	42.5	23.9	91.2	117	18.8	189	10.5	5.78	390	27.4	54.4	28.2	5.54	0.95	4.34	2.20	0.32	5.31	0.74	16.7	11.2	1.61	6.06	0.38	0.53	0.40	2.42	6.99	1.46	0.14	1.45
LIK016	Fm	5.89	34.9	23.1	2.42	2.56	10.5	38.0	23.2	86.7	202	22.3	196	9.84	5.21	414	27.9	62.0	25.2	5.00	0.89	4.25	2.50	0.37	5.33	0.69	16.2	10.0	1.94	7.16	0.39	0.24	0.45	2.21	5.16	1.24	0.19	1.58
LIK017	Gmm	2.95	33.9	24.4	2.63	8.90	10.4	32.1	22.8	84.6	133	16.7	160	8.74	4.58	435	32.8	55.1	27.7	4.82	0.84	3.58	1.90	0.29	4.40	0.76	14.9	10.4	1.36	11.11	0.28	0.35	0.43	2.35	7.66	1.90	0.13	1.39
LIK025	Sc	3.63	34.73	25.15	3.82	9.02	10.64	29.97	24.72	89.20	150.50	16.43	157.10	8.67	4.81	465.00	33.49	58.92	28.27	4.93	0.88	3.69	1.86	0.28	4.21	0.72	15.54	10.29	1.41	9.22	0.35	0.37	0.41	2.44	7.32	2.04	0.14	1.38
LIK027	Sc	3.37	33.27	23.05	3.05	5.72	13.45	31.25	26.89	82.43	175.80	15.82	156.20	8.59	4.47	588.60	31.50	43.43	18.49	3.47	0.63	2.86	1.85	0.28	4.18	0.67	15.63	7.77	1.64	6.40	0.43	0.39	0.34	2.97	4.73	1.56	0.21	1.44
LIK028	Sh/Sl	2.71	25.69	17.73	0.76	<d.l.	10.98	20.93	22.06	64.23	210.70	12.82	120.60	6.87	3.00	481.80	19.66	31.84	17.13	3.10	0.66	2.48	1.34	0.19	3.23	0.57	12.53	4.16	1.07	7.24	0.65	0.18	0.23	4.27	3.90	1.53	0.26	1.45
LIK029	Sc	2.51	27.11	19.24	2.45	5.18	11.26	22.56	29.91	69.85	151.60	15.22	163.80	7.09	3.21	741.50	23.71	39.88	21.14	3.88	0.72	3.14	1.70	0.25	4.50	0.62	12.97	6.07	1.32	9.44	0.41	0.40	0.32	3.17	4.58	1.56	0.22	1.41
LIK030	Sm	1.48	35.16	22.82	2.37	27.06	21.01	22.59	26.02	66.67	160.30	18.73	291.90	9.88	3.15	616.50	31.85	66.35	29.16	5.48	0.85	4.20	2.17	0.34	8.50	0.75	12.21	9.55	2.41	21.53	0.16	0.25	0.42	2.40	3.95	1.70	0.25	1.54
LIK032	Sm	3.61	32.77	28.50	4.39	24.27	13.00	70.55	28.30	82.71	132.10	16.60	158.50	8.59	3.94	623.60	27.04	49.12	25.14	4.91	0.92	4.17	1.73	0.26	4.53	0.69	13.42	8.63	1.48	7.49	0.42	0.51	0.30	3.50	5.83	1.63	0.17	1.15
LIK033	Sh/Sl	1.97	23.72	18.78	<d.l.	2.66	10.88	16.36	16.93	58.96	268.10	15.55	142.90	6.63	2.46	338.30	23.02	37.48	22.05	4.37	0.87	3.61	1.43	0.21	3.96	0.52	12.64	5.16	1.10	11.68	0.38		0.27	3.64	4.71	1.48	0.21	1.26
LIK037	Sm	2.34	37.15	18.96	3.26	6.58	13.51	33.80	29.79	70.35	137.60	16.21	219.10	8.49	3.16	733.90	26.71	53.04	25.14	4.82	0.81	3.98	2.01	0.30	6.26	0.65	13.23	8.71	1.71	11.41	0.27	0.37	0.46	2.18	5.08	1.47	0.20	1.96
LIK038	Sm	3.11	55.40	23.28	3.71	7.64	13.57	28.71	19.76	75.05	118.80	13.84	177.30	9.25	3.45	373.30	30.34	54.59	26.72	4.89	0.71	3.53	1.61	0.24	5.09	0.67	14.52	10.16	2.03	9.75	0.31	0.37	0.43	2.39	4.99	2.19	0.20	2.38
Mean		3.07	35.63	24.08	3.71	11.49	13.32	32.63	24.08	74.69	161.75	17.55	179.39	8.56	3.71	517.16	27.88	52.66	25.44	4.79	0.85	3.87	1.88	0.28	5.00	0.67	14.90	8.70	1.65	9.98	0.37	0.39	0.36	2.88	5.36	1.62	0.20	1.50
Stdev		1.08	11.22	7.01	2.32	8.44	2.99	15.37	4.42	9.68	49.41	4.09	45.27	1.28	0.74	142.13	5.36	14.36	5.26	1.07	0.17	0.99	0.38	0.05	1.29	0.10	2.97	2.57	0.59	4.08	0.12	0.15	0.08	0.66	1.24	0.30	0.04	0.34

COARSE-GRAINED ROCKS

		Sc	V	Cr	Co	Ni	Cu	Zn	Ga	Rb	Sr	Y	Zr	Nb	Cs	Ba	La	Ce	Nd	Sm	Eu	Gd	Yb	Lu	Hf	Ta	Pb	Th	U	La/Sc	Sc/Th	Co/Th	Th/Cr	Cr/Th	Th/U	La/Y	U/Th	V/Cr
LIK001	Sm (?)	5.77	60.27	44.00	9.64	17.52	15.25	55.14	24.00	84.11	86.35	27.57	215.10	11.40	4.28	473.40	37.24	85.70	36.50	7.19	1.23	6.19	2.73	0.39	6.00	0.88	22.09	13.34	2.71	6.45	0.43	0.72	0.30	3.30	4.93	1.35	0.20	1.37
LIK007a	Sm	3.39	28.35	23.01	<d.l.	<d.l.	15.33	27.59	17.43	68.25	215.80	23.08	190.70	7.88	3.96	535.10	27.11	56.51	27.81	5.67	1.04	5.05	2.20	0.32	5.14	0.56	19.11	10.22	1.54	8.00	0.33		0.44	2.25	6.65	1.17	0.15	1.23
LIK017	Gmm	2.95	33.90	24.42	3.63	8.90	10.38	32.06	22.81	84.60	133.40	16.74	159.30	8.74	4.58	434.60	32.79	55.08	27.71	4.82	0.84	3.58	1.90	0.29	4.40	0.76	14.86	10.40	1.36	11.11	0.28	0.35	0.43	2.35	7.66	1.90	0.13	1.39
LIK025	Sc	3.63	34.73	25.15	3.82	9.02	10.64	29.97	24.72	89.20	150.50	16.43	157.10	8.67	4.81	465.00	33.49	58.92	28.27	4.93	0.88	3.69	1.86	0.28	4.21	0.72	15.54	10.29	1.41	9.22	0.35	0.37	0.41	2.44	7.32	2.04	0.14	1.38
LIK027	Sc	3.37	33.27	23.05	3.05	5.72	13.45	31.25	26.89	82.43	175.80	15.82	156.20	8.59	4.47	588.60	31.50	43.43	18.49	3.47	0.63	2.86	1.85	0.28	4.18	0.67	15.63	7.77	1.64	6.40	0.43	0.39	0.34	2.97	4.73	1.56	0.21	1.44
LIK028	Sh/Sl	2.71	25.69	17.73	0.76	<d.l.	10.98	20.93	22.06	64.23	210.70	12.82	120.60	6.87	3.00	481.80	19.66	31.84	17.13	3.10	0.66	2.48	1.34	0.19	3.23	0.57	12.53	4.16	1.07	7.24	0.65	0.18	0.23	4.27	3.90	1.53	0.26	1.45
LIK029	Sc	2.51	27.11	19.24	2.45	5.18	11.26	22.56	29.91	69.85	151.60	15.22	163.80	7.09	3.21	741.50	23.71	39.88	21.14	3.88	0.72	3.14	1.70	0.25	4.50	0.62	12.97	6.07	1.32	9.44	0.41	0.40	0.32	3.17	4.58	1.56	0.22	1.41
LIK030	Sm	1.48	35.16	22.82	2.37	27.06	21.01	22.59	26.02	66.67	160.30	18.73	291.90	9.88	3.15	616.50	31.85	66.35	29.16	5.48	0.85	4.20	2.17	0.34	8.50	0.75	12.21	9.55	2.41	21.53	0.16	0.25	0.42	2.40	3.95	1.70	0.25	1.54
LIK032	Sm	3.61	32.77	28.50	4.39	24.27	13.00	70.55	28.30	82.71	132.10	16.60	158.50	8.59	3.94	623.60	27.04	49.12	25.14	4.91	0.92	4.17	1.73	0.26	4.53	0.69	13.42	8.63	1.48	7.49	0.42	0.51	0.30	3.50	5.83	1.63	0.17	1.15
LIK033	Sh/Sl	1.97	23.72	18.78	<d.l.	2.66	10.88	16.36	16.93	58.96	268.10	15.55	142.90	6.63	2.46	338.30	23.02	37.48	22.05	4.37	0.87	3.61	1.43	0.21	3.96	0.52	12.64	5.16	1.10	11.68	0.38		0.27	3.64	4.71	1.48	0.21	1.26
LIK037	Sm	2.34	37.15	18.96	3.26	6.58	13.51	33.80	29.79	70.35	137.60	16.21	219.10	8.49	3.16	733.90	26.71	53.04	25.14	4.82	0.81	3.98	2.01	0.30	6.26	0.65	13.23	8.71	1.71	11.41	0.27	0.37	0.46	2.18	5.08	1.47	0.20	1.96
LIK038	Sm	3.11	55.40	23.28	3.71	7.64	13.57	28.71	19.76	75.05	118.80	13.84	177.30	9.25	3.45	373.30	30.34	54.59	26.72	4.89	0.71	3.53	1.61	0.24	5.09	0.67	14.52	10.16	2.03	9.75	0.31	0.37	0.43	2.39	4.99	2.19	0.20	2.38
Mean		3.07	35.63	24.08	3.71	11.49	13.32	32.63	24.08	74.69	161.75	17.55	179.39	8.56	3.71	517.16	27.88	52.66	25.44	4.79	0.85	3.87	1.88	0.28	5.00	0.67	14.90	8.70	1.65	9.98	0.37	0.39	0.36	2.88	5.36	1.62	0.20	1.50
Stdev		1.08	11.22	7.01	2.32	8.44	2.99	15.37	4.42	9.68	49.41	4.09	45.27	1.28	0.74	142.13	5.36	14.36	5.26	1.07	0.17	0.99	0.38	0.05	1.29	0.10	2.97	2.57	0.59	4.08	0.12	0.15	0.08	0.66	1.24	0.30	0.04	0.34

FINE-GRAINED ROCKS

		Sc	V	Cr	Co	Ni	Cu	Zn	Ga	Rb	Sr	Y	Zr	Nb	Cs	Ba	La	Ce	Nd	Sm	Eu	Gd	Yb	Lu	Hf	Ta	Pb	Th	U	La/Sc	Sc/Th	Co/Th	Th/Cr	Cr/Th	Th/U	La/Y	U/Th	V/Cr
LIK002	Fm	6.259	76.4	43.8	8.527	20.42	16.66	71.78	23.7	101.3	89.85	28.96	221.6	12.38	6.372	417.5	35.93	74.13	32.16	6.015	1.032	5.479	2.914	0.422	6.106	0.923	14.69	12.17	2.303	5.315875	0.6	0.7	0.277854	3.599014	5.284412	1.240677	0.188236	1.744292
LIK004	Fm	6.90	48.40	40.65	7.12	15.41	18.20	61.71	27.63	131.30	140.10	26.81	191.10	12.09	8.82	488.10	35.07	72.98	32.01	6.21	1.11	5.52	2.66	0.38	5.15	0.89	21.28	13.51	2.03	5.08	0.52	0.54	0.33	3.05	6.56	1.31	0.15	1.19
LIK005	Fm	6.42	44.00	34.92	6.79	14.85	16.31	66.32	26.49	118.80	146.30	25.47	193.30	11.88	8.60	465.20	32.41	67.64	30.31	5.89	1.06	5.17	2.51	0.37	5.20	0.85	18.78	12.20	2.02	5.05	0.51	0.56	0.35	2.86	6.04	1.27	0.17	1.26
LIK006	Fm	3.67	48.94	28.34	2.92	5.74	11.99	31.22	29.16	77.93	172.20	21.90	198.60	9.22	4.44	728.50	29.34	60.62	26.93	5.08	0.89	4.25	2.36	0.35	5.47	0.67	14.33	9.89	2.03	8.46	0.35	0.30	0.35	2.87	4.87	1.34	0.21	1.73
LIK007b	Fm	5.20	46.48	32.82	5.51	10.30	14.26	46.59	23.71	99.72	138.30	25.22	206.60	11.65	8.61	412.50	33.07	68.09	30.50	5.87	0.99	5.30	2.52	0.36	5.84	0.82	18.36	12.64	2.42	6.36	0.41	0.44	0.39	2.60	5.23	1.31	0.19	1.42
LIK008	Fm	5.05	44.10	30.22	5.97	12.18	13.40	46.64	23.77	98.36	116.20	24.68	203.90	11.93	8.30	412.80	32.82	71.17	30.97	6.09	1.01	5.01	2.60	0.38	5.91	1.12	17.66	12.48	2.29	6.50	0.40	0.48	0.41	2.42	5.45	1.33	0.18	1.46
LIK009	Fm	5.80	41.78	28.56	6.45	12.64	15.25	50.99	25.75	113.20	138.30	24.48	189.60	11.79	7.93	468.40	36.32	77.35	33.25	6.38	1.04	5.08	2.54	0.36	5.37	0.90	17.42	12.65	2.00	6.26	0.45	0.56	0.45	2.22	6.42	1.48	0.16	1.46
LIK010a	P2	4.23	33.53	24.75	1.23		18.09	38.46	21.11	87.60	227.60	24.01	219.20	9.72	5.51	396.80	30.06	60.92	27.22	5.32	0.90	4.55	2.56	0.37	6.06	0.71	16.51	10.14	2.10	7.10	0.42	0.12	0.41	2.44	4.84	1.25	0.21	1.35
LIK010b	Fm	4.78	33.90	26.66	4.42	8.79	12.90	34.28	21.47	86.38	126.90	17.34	152.80	9.36	5.68	379.10	29.27	70.55	28.16	5.34	0.90	4.23	1.84	0.26	4.37	0.69	14.28	10.40	1.54	6.12	0.46	0.42	0.39	2.56	4.95	1.09	0.18	1.27
LIK011	Fm	5.14	40.81	28.06	6.24	12.63	13.76	76.58	24.39	102.10	131.40	17.93	164.20	11.18	6.89	405.70	28.66	59.92	26.21	4.93	0.83	3.81	2.04	0.30	4.73	0.81	15.42	10.74	1.59	5.58	0.48	0.58	0.58	2.61	6.77	1.60	0.15	1.45
LIK012	Fm	3.68	39.48	23.71	2.63	3.24	12.97	29.44	18.60	79.53	204.90	21.54	179.50	8.92	4.81	1884.00	25.00	56.77	24.56	4.87	0.84	4.40	1.99	0.27	4.01	0.63	16.49	9.38	1.36	6.80	0.39	0.28	0.40	2.53	6.92	1.16	0.14	1.67
LIK013	Fm	5.04	40.34	26.78	5.60	11.51	17.92	43.41	33.63	109.20	158.30	21.30	196.10	10.58	6.67	751.90	30.25	61.15	28.22	5.57	0.96	4.67	2.14	0.31	5.47	0.76	18.48	12.03	1.82	6.00	0.42	0.47	0.45	2.23	6.61	1.42	0.15	1.51
LIK014	P3	4.29	39.42	27.19	5.95	12.89	15.99	42.88	23.86	91.19	117.00	18.76	188.40	10.51	5.78	390.00	27.43	54.38	28.19	5.54	0.95	4.34	2.20	0.32	5.31	0.74	16.67	11.24	1.61	6.40	0.38	0.53	0.41	2.42	6.99	1.46	0.14	1.45
LIK016	Fm	5.89	34.93	22.09	2.42	2.56	10.52	37.99	23.17	86.69	201.80	22.50	196.00	9.84	5.21	434.10	27.88	62.00	25.20	5.00	0.89	4.25	2.50	0.37	5.33	0.69	16.15	10.01	1.94	7.16	0.39	0.24	0.45	2.21	5.16	1.24	0.19	1.58
LIK026	P4	3.15	33.06	24.48	3.41	7.26	11.03	28.17	25.06	84.84	152.70	11.62	147.20	8.87	4.75	497.90	22.19	42.36	19.05	3.37	0.62	2.44	1.34	0.19	3.98	0.71	14.63	6.52	1.28	7.04	0.48	0.52	0.27	3.76	5.09	1.91	0.20	1.35
LIK031	P5	4.28	35.34	29.76	5.06	11.34	14.33	34.60	23.81	94.10	111.00	17.14	150.70	8.75	4.82	493.90	30.95	55.91	27.29	5.17	0.93	4.04	1.79	0.27	4.33	0.78	14.91	9.31	1.49	7.23	0.46	0.54	0.31	3.20	6.20	1.81	0.16	1.19
LIK034	Fm	3.98	36.35	26.64	3.85	6.34	14.36	35.34	24.16	85.28	166.40	19.52	183.80	9.64	4.26	468.30	24.07	43.00	21.80	4.15	0.82	3.56	2.14	0.32	5.24	0.74	16.31	6.83	1.64	6.06	0.58	0.56	0.26	3.90	4.17	1.23	0.24	1.36
LIK035	Fm	5.04	55.22	34.92	6.64	14.87	23.10	46.89	26.89	108.20	163.40	17.61	153.70	10.66	6.67	492.60	28.48	53.48	25.18	4.69	0.85	3.69	2.06	0.30	4.58	0.79	17.18	8.54	1.69	5.65	0.66	0.78	0.24	4.09	5.03	1.62	0.20	1.58
LIK036	Pb	2.31	34.42	21.12	2.65	6.20	12.69	30.29	26.84	99.05	134.00	14.30	212.80	8.29	3.02	610.50	25.28	40.64	23.12	4.22	0.74	3.32	1.64	0.26	5.89	0.61	11.66	6.88	1.64	10.92	0.34	0.39	0.33	3.07	4.20	1.77	0.24	1.63
LIK039	Fm	3.72	46.43	26.14	5.06	10.36	19.01	31.95	22.02	80.44	130.40	17.39	183.80	9.89	4.21	406.00	27.61	47.56	23.78	4.48	0.80	3.59	1.91	0.29	5.23	0.75	17.54	8.30	1.69	7.43	0.45	0.61	0.32	3.15	4.92	1.59	0.20	1.78
Mean		4.69	42.68	29.08

Table A5. F- test and t-Test for variances between the Al_2O_3 and CaO content in the coarse-grained and fine-grained (fines) LIK samples

Al_2O_3	F-Test Two-Sample for Variances		t-Test: Two-Sample Assuming Equal Variances		
	Coarse	*Fines*		*Variable 1*	*Variable 2*
Mean	8.90832272	10.7369331	Mean	8.90832272	10.7369331
Variance	0.83484076	1.27927123	Variance	0.83484076	1.27927123
Observations	12	23	Observations	12	23
df	11	22	Pooled Variance	1.13112774	
F	0.6525909		Hypothesized Mean Difference	0	
P(F<=f) one-tail	0.23426146		df	33	
F Critical one-tail	0.3807889		t Stat	-4.82820687	
			P(T<=t) one-tail	1.5288E-05	
			t Critical one-tail	1.69236031	
			P(T<=t) two-tail	3.0576E-05	
			t Critical two-tail	2.0345153	

CaO	F-Test Two-Sample for Variances	
	Coarse	*Fines*
Mean	3.30495274	2.12922479
Variance	7.64343311	3.28605506
Observations	12	23
df	11	22
F	2.32602101	
P(F<=f) one-tail	0.04425416	
F Critical one-tail	2.25851836	

Appendices **Likhoele (LIK) cont.**

Figure A1. Likhoele (LIK) samples LIK15 and LIK 35 clay separate diffractometers.

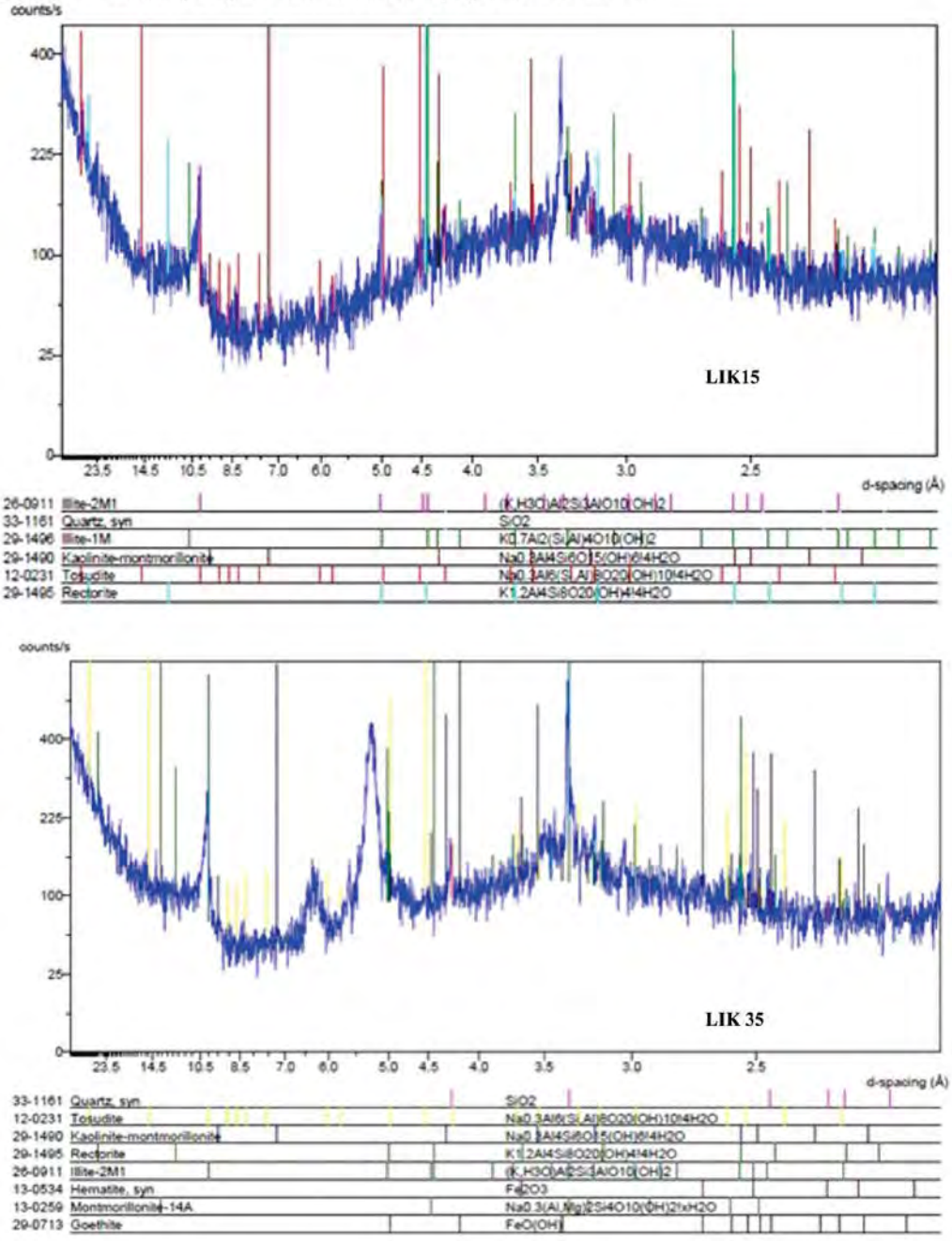

Table A6. Bulk rock geochemistry and associated weathering and major element ratios for Likhoele East (LIKE).

				Major elements													Weathering indices			Ratios						
	Sample #	Strat ht.	Facies code	SiO_2	TiO_2	Al_2O_3	Fe_2O_3	MnO	MgO	CaO	Na_2O	K_2O	P_2O5	SO_3	Cr_2O_3	NiO	LOI	Total	CIA	CIAmolar	ICV	SiO_2/Al_2O_3	Fe_2O_3/Al_2O_3	K_2O/Al_2O_3	Al_2O_3/TiO_2	MgO/Al_2O_3	CaO/Al_2O_3	Na_2O/Al_2O_3	K_2O/Na_2O
Lower Elliot (LEF)	LIKE01	0.0	Fm	72.3	0.6	13.2	3.9	0.0	1.0	0.660	1.466	2.980	0.039	0.004	0.004	0.007	3.101	99.344	66	1.9	0.7	5.5	0.3	0.23	20.8	0.08	0.1	0.1	2.0
	LIKE02	1.9	Fm	72.9	0.6	13.4	3.6	0.0	1.0	0.781	1.647	2.931	0.039	0.009	0.006	0.010	3.101	100.086	65	1.8	0.7	5.3	0.3	0.22	20.7	0.07	0.1	0.1	1.8
	LIKE03	3.1	Fm	71.9	0.7	13.6	3.9	0.0	1.1	0.767	1.618	2.995	0.032	0.009	0.006	0.008	3.198	99.772	65	1.9	0.7	5.4	0.3	0.22	20.4	0.08	0.1	0.1	1.9
	LIKE04	3.6	Fm	71.9	0.7	13.2	3.6	0.0	1.1	1.133	1.600	2.965	0.033	0.010	0.006	0.008	3.482	99.692	63	1.7	0.8	5.2	0.3	0.22	20.3	0.08	0.1	0.1	1.9
	LIKE05	5.1	Sm	71.3	0.7	13.8	3.8	0.1	1.2	0.732	1.584	3.111	0.042	0.002	0.005	0.007	3.345	99.529	65	1.9	0.7	5.2	0.3	0.23	20.8	0.08	0.1	0.1	2.0
	LIKE06	6.1	Sh	68.7	0.6	13.3	3.6	0.1	1.1	2.461	1.474	3.027	0.038	0.016	0.005	0.010	4.744	99.187	57	1.3	0.8	4.9	0.3	0.23	20.9	0.08	0.2	0.1	2.1
	LIKE07	7.1	Sh	70.4	0.7	14.5	3.9	0.0	1.1	0.656	1.520	3.319	0.035	0.001	0.005	0.007	3.466	99.647	67	2.0	0.7	7.5	0.3	0.23	21.4	0.08	0.0	0.1	2.2
	LIKE08	8.4	Sh	78.0	0.5	10.3	2.9	0.0	0.7	0.598	1.226	2.208	0.034	0.067	0.004	0.007	2.580	99.149	65	1.9	0.7	5.1	0.3	0.21	20.0	0.06	0.1	0.1	1.8
	LIKE09	8.9	Sm	71.9	0.7	14.2	3.8	0.0	0.9	0.505	1.368	2.958	0.038	0.001	0.007	0.016	3.321	99.650	69	2.2	0.7	5.7	0.3	0.21	20.0	0.06	0.0	0.1	2.2
	LIKE10	9.9	Fm	73.6	0.7	13.0	3.6	0.0	0.8	0.403	1.419	2.808	0.033	0.002	0.003	0.008	3.071	99.486	67	2.1	0.7	6.5	0.3	0.22	19.9	0.06	0.0	0.1	2.0
	LIKE11	10.9	Psol	76.1	0.6	11.7	2.7	0.0	0.7	0.290	1.580	2.434	0.050	0.037	0.004	0.007	2.910	99.720	64	1.8	0.7	5.3	0.2	0.21	18.0	0.06	0.1	0.1	1.5
	LIKE12	12.4	Psol	72.2	0.7	13.6	3.8	0.0	0.8	0.527	1.413	2.944	0.036	0.001	0.004	0.011	3.284	99.376	68	2.1	0.7	5.5	0.3	0.22	20.2	0.06	0.0	0.1	2.1
	LIKE13	13.4	Fm	73.6	0.7	13.5	3.5	0.0	0.8	0.552	1.639	2.881	0.031	0.004	0.005	0.009	3.004	100.07	66	2.0	0.7	5.5	0.2	0.21	19.9	0.06	0.0	0.1	1.8
	LIKE14	14.4	Fm	72.8	0.6	13.2	3.8	0.0	0.9	0.561	1.421	2.873	0.043	0.017	0.003	0.008	3.173	99.473	67	2.0	0.7	5.1	0.3	0.22	21.1	0.07	0.0	0.1	2.0
	LIKE15	14.9	Sh	71.4	0.6	13.9	4.0	0.0	1.0	0.626	1.469	3.072	0.045	0.018	0.005	0.007	3.476	99.733	67	2.0	0.7	5.8	0.3	0.22	21.4	0.07	0.0	0.1	2.1
	LIKE16	15.9	Fm	74.2	0.7	12.8	2.9	0.0	0.8	0.712	1.419	2.726	0.087	0.009	0.006	0.012	3.166	99.551	66	1.9	0.7	5.3	0.2	0.21	18.4	0.06	0.1	0.1	1.9
	LIKE17	17.4	Fm	69.4	0.6	13.0	3.4	0.1	1.1	2.652	1.500	2.966	0.054	0.004	0.005	0.008	4.841	99.592	55	1.2	0.9	5.3	0.3	0.23	20.7	0.08	0.2	0.1	2.0
	LIKE18	18.4	Fm	71.8	0.7	14.1	3.4	0.0	0.9	0.600	1.416	3.070	0.042	0.018	0.005	0.010	3.479	99.543	68	2.1	0.7	4.9	0.2	0.22	21.3	0.07	0.0	0.1	2.2
	LIKE19	18.9	Fm	70.8	0.7	14.4	3.9	0.0	1.0	0.628	1.425	3.220	0.039	0.046	0.005	0.010	3.603	99.805	67	2.1	0.7	5.3	0.3	0.22	21.0	0.07	0.0	0.1	2.3
Upper Elliot (UEF)	LIKE20	19.4	Fm	72.2	0.7	13.6	3.5	0.0	0.8	0.590	1.590	2.816	0.030	0.001	0.007	0.008	3.270	99.056	67	2.0	0.7	8.9	0.3	0.21	20.1	0.06	0.0	0.1	1.8
	LIKE21	20.2	Sm	81.5	0.5	9.2	2.4	0.0	0.6	0.434	1.028	1.883	0.022	0.004	0.001	0.009	2.173	99.677	67	2.0	0.7	10.7	0.3	0.21	20.1	0.07	0.0	0.1	1.8
	LIKE22	21.4	Sm	83.7	0.5	7.8	1.6	0.1	0.5	0.827	1.130	1.534	0.022	0.014	0.003	0.007	2.272	99.931	61	1.6	0.7	6.3	0.2	0.20	17.1	0.06	0.1	0.1	1.4
	LIKE23	22.4	Fm/Fl	75.7	0.6	11.9	3.4	0.0	0.7	0.461	1.252	2.594	0.041	0.004	0.036	0.088	2.655	99.453	68	2.1	0.7	5.5	0.3	0.22	21.0	0.06	0.0	0.1	2.1
	LIKE24	23.4	Fm/Fl	72.8	0.6	13.3	3.8	0.0	0.8	0.596	1.352	2.962	0.030	0.008	0.006	0.008	3.032	99.414	67	2.0	0.7	5.6	0.3	0.22	21.8	0.06	0.0	0.1	2.2
	LIKE25	23.9	Fm/Fl	73.0	0.6	13.1	3.5	0.0	0.9	0.624	1.391	2.963	0.035	0.001	0.006	0.009	2.970	99.371	66	2.0	0.7	7.0	0.3	0.23	22.1	0.07	0.0	0.1	2.1
	LIKE26	24.9	Fm/Fl	72.6	0.5	10.4	2.5	0.2	0.7	3.575	1.432	2.225	0.058	0.245	0.004	0.007	4.650	99.133	48	0.9	1.0	8.9	0.2	0.21	19.5	0.06	0.3	0.1	1.6
	LIKE27	25.9	Fl	67.3	0.5	7.5	1.4	0.3	0.4	10.301	1.318	1.565	0.030	0.055	0.004	0.012	9.202	99.794	25	0.3	2.0	4.8	0.2	0.21	16.2	0.05	1.4	0.2	1.2
	LIKE28	26.9	Sm	70.1	0.6	14.7	4.7	0.0	1.1	0.631	1.298	3.421	0.055	-0.001	0.007	0.008	3.251	99.910	68	2.1	0.7	8.9	0.3	0.23	24.2	0.08	0.0	0.1	2.6
	LIKE29	28.1	Sm	80.1	0.5	9.0	1.7	0.1	0.6	1.550	1.202	2.007	0.023	0.002	0.019	0.048	2.729	99.499	56	1.3	0.8	9.9	0.2	0.22	25.8	0.06	0.2	0.1	1.7
	LIKE30	29.4	Sm	80.9	0.5	8.2	2.4	0.1	0.6	1.378	1.006	1.722	0.052	0.027	0.003	0.008	2.673	99.575	58	1.4	0.9	9.8	0.3	0.21	15.4	0.08	0.2	0.1	1.7
	LIKE31	30.4	Sm	81.5	0.5	8.4	2.5	0.1	0.7	0.792	1.003	1.782	0.069	0.034	0.004	0.008	2.135	99.482	62	1.7	0.8	8.3	0.3	0.21	15.8	0.08	0.1	0.1	1.8
	LIKE32	31.6	Fm biotur	80.5	0.5	9.7	2.2	0.0	0.5	0.324	1.541	1.922	0.040	0.001	0.002	0.010	1.811	99.100	65	1.9	0.7	8.1	0.2	0.20	19.2	0.05	0.0	0.2	1.2
	LIKE33	32.1	Sr	80.3	0.5	9.9	1.9	0.0	0.5	0.735	1.856	1.902	0.047	0.049	0.003	0.007	1.956	99.733	60	1.5	0.7	6.1	0.2	0.19	18.3	0.05	0.1	0.2	1.0
	Mean			74.172	0.600	12.098	3.190	0.054	0.828	1.189	1.412	2.630	0.041	0.022	0.006	0.012	3.307	99.562	62.888	1.778	0.769	6.450	0.260	0.216	20.124	0.068	0.117	0.119	1.868
	Stdev			4.26	0.09	2.20	0.83	0.05	0.21	1.78	0.19	0.55	0.01	0.04	0.01	0.02	1.27	0.26	8.23	0.40	0.24	1.72	0.03	0.01	2.12	0.01	0.23	0.02	0.33
	LEF	Mean		72.38	0.65	13.29	3.57	0.04	0.94	0.86	1.48	2.92	0.04	0.01	0.00	0.01	3.39	99.60	65.03	1.89	0.72	5.48	0.27	0.22	20.39	0.07	0.07	0.11	
		Stdev		2.16	0.04	0.96	0.38	0.02	0.15	0.61	0.11	0.25	0.01	0.02	0.00	0.00	0.55	0.25	3.54	0.25	0.05	0.62	0.02	0.01	0.91	0.01	0.05	0.01	
	UEF	Mean		76.60	0.53	10.48	2.68	0.07	0.67	1.63	1.31	2.24	0.04	0.03	0.01	0.02	3.20	99.51	59.92	1.63	0.84	7.76	0.25	0.21	19.76	0.06	0.19	0.13	
		Stdev		5.21	0.08	2.40	1.00	0.07	0.18	2.63	0.24	0.60	0.01	0.06	0.01	0.02	1.87	0.28	11.52	0.52	0.35	1.88	0.05	0.01	3.10	0.01	0.35	0.03	

Geochem unit 1 (?)

Geochem unit 2 (?)

Table A7. Coarse- and fine-grained LIKE samples bulk rock geochemistry and associated weathering and major element ratios.

Coarse-grained samples "Sm- Gmm"																												
#	Facies code	Strat ht. (m)	SiO_2	TiO_2	Al_2O_3	Fe_2O_3	MnO	MgO	CaO	Na_2O	K_2O	P_2O5	SO_3	Cr_2O_3	NiO	LOI	Total	CIA	CIAmolar	ICV	SiO_2/Al_2O_3	Fe_2O_3/Al_2O_3	K_2O/Al_2O_3	Al_2O_3/TiO_2	MgO/Al_2O_3	CaO/Al_2O_3	Na_2O/Al_2O_3	K_2O/Na_2O
LIKE05	Sm	5.12	71.25	0.66	13.76	3.80	0.06	1.17	0.73	1.58	3.11	0.04	0.00	0.005	0.01	3.34	100	65	1.88	0.72	5.17	0.28	0.23	20.81	0.08	0.05	0.12	0.23
LIKE06	Sh	6.12	68.73	0.63	13.29	3.56	0.08	1.12	2.46	1.47	3.03	0.04	0.02	0.005	0.01	4.74	99	57	1.31	0.85	4.86	0.27	0.23	20.95	0.08	0.19	0.11	0.23
LIKE07	Sh	7.12	70.42	0.68	14.49	3.85	0.04	1.15	0.66	1.52	3.32	0.04	0.00	0.005	0.01	3.47	100	67	1.99	0.69	7.54	0.27	0.23	21.40	0.08	0.05	0.10	0.23
LIKE08	Sh	8.37	78.01	0.52	10.34	2.86	0.03	0.67	0.60	1.23	2.21	0.03	0.07	0.004	0.01	2.58	99	65	1.88	0.72	5.07	0.28	0.21	20.01	0.06	0.06	0.12	0.21
LIKE09	Sm	8.87	71.91	0.71	14.18	3.75	0.02	0.86	0.50	1.37	2.96	0.04	0.00	0.007	0.02	3.32	100	69	2.23	0.66	5.68	0.26	0.21	20.00	0.06	0.04	0.10	0.21
LIKE15	Sh	14.87	71.45	0.65	13.92	4.01	0.03	0.95	0.63	1.47	3.07	0.04	0.02	0.005	0.01	3.48	100	67	2.02	0.71	5.80	0.29	0.22	21.44	0.07	0.04	0.11	0.22
LIKE21	Sm	20.17	81.51	0.46	9.16	2.38	0.02	0.60	0.43	1.03	1.88	0.02	0.00	0.001	0.01	2.17	100	67	2.03	0.68	10.69	0.26	0.21	20.12	0.07	0.05	0.11	0.21
LIKE22	Sm	21.42	83.73	0.46	7.83	1.56	0.05	0.48	0.83	1.13	1.53	0.02	0.01	0.003	0.01	2.27	100	61	1.56	0.71	6.34	0.20	0.20	17.05	0.06	0.11	0.14	0.20
LIKE28	Sm	26.92	70.07	0.61	14.68	4.74	0.04	1.10	0.63	1.30	3.42	0.06	0.00	0.007	0.01	3.25	100	68	2.10	0.73	8.89	0.32	0.23	24.18	0.08	0.04	0.09	0.23
LIKE29	Sm	28.12	80.13	0.35	9.01	1.71	0.14	0.58	1.55	1.20	2.01	0.02	0.00	0.019	0.05	2.73	99	56	1.29	0.77	9.86	0.19	0.22	25.85	0.06	0.17	0.13	0.22
LIKE30	Sm	29.37	80.9	0.5	8.2	2.4	0.1	0.6	1.4	1.0	1.7	0.1	0.0	0.003	0.01	2.7	100	57.7	1.4	0.9	9.8	0.3	0.2	15.4	0.1	0.2	0.1	0.2
LIKE31	Sm	30.37	81.5	0.5	8.4	2.5	0.1	0.7	0.8	1.0	1.8	0.1	0.0	0.004	0.01	2.1	99	62.5	1.7	0.8	8.3	0.3	0.2	15.8	0.1	0.1	0.1	0.2
LIKE33	Sr	32.07	80.32	0.54	9.88	1.86	0.04	0.54	0.73	1.86	1.90	0.05	0.05	0.003	0.01	1.96	100	60	1.53	0.70	6.13	0.19	0.19	18.27	0.05	0.07	0.19	0.19
Mean			76.2	0.6	11.3	3.0	0.1	0.8	0.9	1.3	2.5	0.0	0.0	0.005	0.01	2.9	99.6	63.3	1.8	0.7	7.2	0.3	0.2	20.1	0.1	0.1	0.1	0.2
stdev.			5.5	0.1	2.7	1.0	0.0	0.3	0.6	0.3	0.7	0.0	0.0	0.004	0.01	0.8	0.2	4.4	0.3	0.1	2.0	0.0	0.0	3.0	0.0	0.1	0.0	0.0
Fine-grained samples "Fm"																												
#	Facies code	Strat ht.	SiO_2	TiO_2	Al_2O_3	Fe_2O_3	MnO	MgO	CaO	Na_2O	K_2O	P_2O5	SO_3	Cr_2O_3	NiO	LOI	Total	CIA	CIAmolar	ICV	SiO_2/Al_2O_3	Fe_2O_3/Al_2O_3	K_2O/Al_2O_3	Al_2O_3/TiO_2	MgO/Al_2O_3	CaO/Al_2O_3	Na_2O/Al_2O_3	K_2O/Na_2O
LIKE01	Fm	0	72.28	0.63	13.19	3.94	0.03	1.01	0.66	1.47	2.98	0.04	0.00	0.00	0.01	3.10	99	66	1.93	0.74	5.48	0.30	0.23	20.80	0.08	0.05	0.11	0.23
LIKE02	Fm	1.87	72.92	0.64	13.36	3.65	0.04	0.96	0.78	1.65	2.93	0.04	0.01	0.01	0.01	3.10	100	65	1.83	0.73	5.30	0.27	0.22	20.74	0.07	0.06	0.12	0.22
LIKE03	Fm	3.12	71.92	0.66	13.57	3.86	0.05	1.08	0.77	1.62	2.99	0.03	0.01	0.01	0.01	3.20	100	65	1.86	0.73	5.44	0.28	0.22	20.42	0.08	0.06	0.12	0.22
LIKE04	Fm	3.62	71.90	0.65	13.22	3.58	0.04	1.06	1.13	1.60	2.97	0.03	0.01	0.01	0.01	3.48	100	63	1.67	0.75	5.18	0.27	0.22	20.31	0.08	0.09	0.12	0.22
LIKE10	Fm	9.87	73.58	0.65	12.96	3.60	0.02	0.84	0.49	1.42	2.81	0.03	0.00	0.00	0.01	3.07	99	67	2.07	0.69	6.50	0.28	0.22	19.93	0.06	0.04	0.11	0.22
LIKE11	Psol	10.87	76.09	0.65	11.71	2.71	0.05	0.69	0.79	1.58	2.43	0.05	0.04	0.00	0.01	2.91	100	64	1.76	0.70	5.32	0.23	0.21	18.04	0.06	0.07	0.13	0.21
LIKE12	Psol	12.37	72.23	0.67	13.58	3.80	0.03	0.85	0.53	1.41	2.94	0.04	0.00	0.00	0.01	3.28	99	68	2.10	0.69	5.46	0.28	0.22	20.23	0.06	0.04	0.10	0.22
LIKE13	Fm	13.37	73.58	0.68	13.47	3.34	0.03	0.85	0.55	1.64	2.88	0.03	0.00	0.00	0.01	3.00	100	66	1.98	0.68	5.52	0.25	0.21	19.89	0.06	0.04	0.12	0.21
LIKE14	Fm	14.37	72.82	0.63	13.20	3.82	0.03	0.88	0.56	1.42	2.87	0.04	0.02	0.00	0.01	3.17	99	67	2.04	0.71	5.13	0.29	0.22	21.11	0.07	0.04	0.11	0.22
LIKE16	Fm	15.87	74.23	0.70	12.79	2.88	0.03	0.79	0.71	1.42	2.73	0.09	0.01	0.01	0.01	3.17	100	66	1.94	0.66	5.31	0.23	0.21	18.39	0.06	0.06	0.11	0.21
LIKE17	Fm	17.37	69.36	0.63	13.05	3.37	0.08	1.08	2.65	1.50	2.97	0.05	0.00	0.00	0.01	4.84	100	55	1.24	0.86	5.11	0.26	0.23	20.68	0.08	0.20	0.11	0.23
LIKE18	Fm	18.37	71.83	0.66	14.05	3.42	0.03	0.92	0.60	1.42	3.07	0.04	0.02	0.00	0.01	3.48	100	68	2.08	0.65	4.93	0.24	0.22	21.31	0.07	0.04	0.10	0.22
LIKE19	Fm	18.87	70.80	0.68	14.36	3.94	0.03	1.02	0.63	1.43	3.22	0.04	0.05	0.00	0.01	3.60	100	67	2.06	0.69	5.33	0.27	0.22	21.00	0.07	0.04	0.10	0.22
LIKE20	Fm	19.37	72.23	0.67	13.56	3.46	0.03	0.79	0.59	1.59	2.82	0.03	0.00	0.01	0.01	3.27	99	67	2.01	0.68	8.90	0.26	0.21	20.12	0.06	0.04	0.12	0.21
LIKE23	Fm/Fl	22.42	75.70	0.57	11.94	3.35	0.03	0.74	0.46	1.25	2.59	0.04	0.00	0.04	0.09	2.66	99	68	2.09	0.69	5.46	0.28	0.22	20.98	0.06	0.04	0.10	0.22
LIKE24	Fm/Fl	23.42	72.81	0.61	13.35	3.80	0.03	0.82	0.60	1.35	2.96	0.03	0.01	0.01	0.01	3.03	99	67	2.05	0.70	5.55	0.28	0.22	21.78	0.06	0.04	0.10	0.22
LIKE25	Fm/Fl	23.92	72.96	0.59	13.14	3.78	0.03	0.87	0.62	1.39	2.96	0.03	0.00	0.01	0.01	2.97	99	66	1.98	0.71	6.96	0.29	0.23	22.12	0.07	0.05	0.11	0.23
LIKE26	Fm/Fl	24.92	72.65	0.54	10.45	2.47	0.17	0.67	3.57	1.43	2.23	0.06	0.24	0.00	0.01	4.65	99	48	0.93	1.00	8.94	0.24	0.21	19.52	0.06	0.34	0.14	0.21
LIKE27	Fl	25.92	67.28	0.46	7.53	1.37	0.26	0.41	10.30	1.32	1.56	0.03	0.06	0.00	0.01	9.20	100	25	0.33	2.03	4.77	0.18	0.21	16.21	0.05	1.37	0.18	0.21
LIKE32	Fm bioturbated	31.57	80.53	0.50	9.66	2.21	0.02	0.52	0.32	1.54	1.92	0.04	0.00	0.00	0.01	1.81	99	65	1.85	0.68	8.13	0.23	0.20	19.24	0.05	0.03	0.16	0.20
Mean			72.9	0.6	12.6	3.3	0.1	0.8	1.4	1.5	2.7	0.0	0.0	0.01	0.01	3.6	99.5	62.6	1.8	0.8	5.9	0.3	0.2	20.1	0.1	0.1	0.1	0.2
stdev.			2.6	0.1	1.7	0.7	0.1	0.2	2.2	0.1	0.4	0.0	0.1	0.01	0.02	1.5	0.3	10.1	0.5	0.3	1.3	0.0	0.0	1.4	0.0	0.3	0.0	0.0

Table A8. Proposed geochemical break up of the LIKE samples via bulk rock major element ratios.

	Sample #	Facies code	Strat ht	SiO_2/Al_2O_3	Al_2O_3/TiO_2	MgO/Al_2O_3	Fe_2O_3/Al_2O_3	K_2O/Al_2O_3
LIKE 1- 20	LIKE01	Fm	0.0	5.48	20.80	0.08	0.30	0.23
	LIKE02	Fm	1.9	5.30	20.74	0.07	0.27	0.22
	LIKE03	Fm	3.1	5.44	20.42	0.08	0.28	0.22
	LIKE04	Fm	3.6	5.18	20.31	0.08	0.27	0.22
	LIKE05	Sm	5.1	5.17	20.81	0.08	0.28	0.23
	LIKE06	Sh	6.1	4.86	20.95	0.08	0.27	0.23
	LIKE07	Sh	7.1	7.54	21.40	0.08	0.27	0.23
	LIKE08	Sh	8.4	5.07	20.01	0.06	0.28	0.21
	LIKE09	Sm	8.9	5.68	20.00	0.06	0.26	0.21
	LIKE10	Fm	9.9	6.50	19.93	0.06	0.28	0.22
	LIKE11	Psol	10.9	5.32	18.04	0.06	0.23	0.21
	LIKE12	Psol	12.4	5.46	20.23	0.06	0.28	0.22
	LIKE13	Fm	13.4	5.52	19.89	0.06	0.25	0.21
	LIKE14	Fm	14.4	5.13	21.11	0.07	0.29	0.22
	LIKE15	Sh	14.9	5.80	21.44	0.07	0.29	0.22
	LIKE16	Fm	15.9	5.31	18.39	0.06	0.23	0.21
	LIKE17	Fm	17.4	5.11	20.68	0.08	0.26	0.23
	LIKE18	Fm	18.4	4.93	21.31	0.07	0.24	0.22
	LIKE19	Fm	18.9	5.33	21.00	0.07	0.27	0.22
	LIKE20	Fm	19.4	8.90	20.12	0.06	0.26	0.21
	Mean			5.65	20.38	0.07	0.27	0.22
	Stdev			0.97	0.89	0.01	0.02	0.01
LIKE21-33	LIKE21	Sm	20.2	10.69	20.12	0.07	0.26	0.21
	LIKE22	Sm	21.4	6.34	17.05	0.06	0.20	0.20
	LIKE23	Fm/Fl	22.4	5.46	20.98	0.06	0.28	0.22
	LIKE24	Fm/Fl	23.4	5.55	21.78	0.06	0.28	0.22
	LIKE25	Fm/Fl	23.9	6.96	22.12	0.07	0.29	0.23
	LIKE26	Fm/Fl	24.9	8.94	19.52	0.06	0.24	0.21
	LIKE27	Fl	25.9	4.77	16.21	0.05	0.18	0.21
	LIKE28	Sm	26.9	8.89	24.18	0.08	0.32	0.23
	LIKE29	Sm	28.1	9.86	25.85	0.06	0.19	0.22
	LIKE30	Sm	29.4	9.75	15.42	0.08	0.29	0.21
	LIKE31	Sm	30.4	8.34	15.77	0.08	0.30	0.21
	LIKE32	Fm biotur.	31.6	8.13	19.24	0.05	0.23	0.20
	LIKE33	Sr	32.1	6.13	18.27	0.05	0.19	0.19
	Mean			7.68	19.73	0.06	0.25	0.2
	Stdev			1.92	3.23	0.01	0.05	0.012

Table A9. Damplaats (DAM) bulk rock major elements, weathering indices and major element ratios.

			MAJORS	Major elements														Weathering indices			Ratios						
	Sample	Strat. Ht	Facies Code	SiO_2	TiO_2	Al_2O_3	Fe_2O_3	MnO	MgO	CaO	Na_2O	K_2O	P_2O5	SO_3	Cr_2O_3	NiO	LOI	Total	CIA	CIAmolar	ICV	SiO_2/Al_2O_3	Fe_2O_3/Al_2O_3	K_2O/Al_2O_3	Al_2O_3/TiO_2	MgO/Al_2O_3	CaO/Al_2O_3	Na_2O/Al_2O_3
LEF	DAM-1	0	Fl	73.70	0.82	12.79	3.66	0.04	0.75	0.81	1.88	2.66	0.04	0.00	0.01	0.02	2.82	100.00	63.19	1.72	0.77	5.76	0.29	0.21	15.65	0.06	0.06	0.15
	DAM-2	0.5	Sr	82.85	0.50	8.88	1.32	0.08	0.40	0.36	2.13	1.58	0.03	0.00	0.01	0.02	1.49	99.65	60.19	1.51	0.67	9.33	0.29	0.18	17.69	0.05	0.04	0.24
	DAM-3	1.5	Sr	84.43	0.47	7.81	1.02	0.15	0.23	0.27	2.18	1.28	0.03	0.00	0.00	0.01	1.23	99.10	58.86	1.43	0.69	10.81	0.15	0.16	16.79	0.03	0.04	0.28
	DAM-4	2.1	Sm/Sl	83.62	0.55	8.36	1.05	0.04	0.25	0.44	2.10	1.42	0.03	0.00	0.00	0.01	1.49	99.36	59.03	1.44	0.67	10.00	0.13	0.17	15.18	0.03	0.05	0.25
	DAM-5	2.6	Fm	49.47	0.42	8.01	1.90	0.12	0.59	19.09	1.09	1.64	0.03	0.02	0.00	0.02	17.02	99.42	17.31	0.21	3.03	6.17	0.13	0.20	18.97	0.07	2.38	0.14
	DAM-6	4.4	Gcm	74.14	0.59	11.77	3.29	0.07	0.70	1.31	1.65	2.54	0.19	0.01	0.00	0.01	3.20	99.50	59.96	1.50	0.80	6.30	0.24	0.22	19.79	0.06	0.11	0.14
	DAM-7	5.4	Sm	81.89	0.44	8.77	1.78	0.04	0.52	0.78	1.30	1.85	0.04	0.00	0.00	0.01	2.47	99.89	61.22	1.58	0.71	9.34	0.28	0.21	19.77	0.06	0.09	0.15
	DAM-8	6.4	Sr	82.66	0.59	8.25	2.06	0.03	0.46	0.39	1.24	1.55	0.04	0.00	0.00	0.01	2.17	99.47	65.08	1.86	0.71	10.02	0.20	0.19	13.88	0.06	0.05	0.15
	DAM-9	8.4	Sm	84.07	0.34	7.73	1.93	0.03	0.39	0.31	1.55	1.21	0.04	0.00	0.00	0.01	2.18	99.80	63.56	1.74	0.69	10.88	0.25	0.16	22.76	0.05	0.04	0.20
UEF	DAM-10	15	Fm	73.14	0.51	11.99	2.90	0.06	0.82	1.96	1.89	2.58	0.08	0.03	0.01	0.01	3.78	99.75	55.91	1.27	0.83	6.10	0.25	0.22	23.62	0.07	0.16	0.16
	DAM-11	16	Sm	78.47	0.49	9.92	2.09	0.06	0.63	1.46	1.67	1.95	0.07	0.02	0.00	0.01	2.99	99.82	56.87	1.32	0.78	7.91	0.24	0.20	20.37	0.06	0.15	0.17
	DAM-12	16.4	Sm	79.57	0.43	8.44	1.38	0.09	0.46	2.65	1.90	1.44	0.04	0.02	0.00	0.01	3.53	99.96	47.04	0.89	0.93	9.43	0.21	0.17	19.68	0.05	0.31	0.23
	DAM-13	17.6	Fm	66.04	0.63	14.09	4.20	0.08	1.13	3.14	1.38	3.25	0.11	0.01	0.01	0.01	5.81	99.88	55.06	1.23	0.90	4.69	0.16	0.23	22.35	0.08	0.22	0.10
	DAM-14	18	Fm	69.15	0.60	13.55	3.71	0.06	1.03	1.86	1.62	3.12	0.13	0.01	0.00	0.01	4.38	99.24	58.99	1.44	0.81	5.10	0.30	0.23	22.43	0.08	0.14	0.12
	DAM-15	18.7	Fm	68.39	0.58	12.05	2.98	0.09	0.90	4.42	1.63	2.70	0.30	0.01	0.00	0.01	5.76	99.84	46.88	0.88	1.03	5.68	0.27	0.22	20.72	0.07	0.37	0.14
	DAM-16	19.1	Fm	67.60	0.57	13.10	3.47	0.09	1.01	3.17	1.57	2.96	0.10	0.01	0.01	0.01	5.38	99.06	53.14	1.13	0.90	5.16	0.25	0.23	22.85	0.08	0.24	0.12
	DAM-17	20.1	Sm	65.64	0.54	12.09	3.15	0.07	0.88	5.83	1.61	2.76	0.05	0.02	0.00	0.01	7.12	99.77	42.70	0.75	1.15	5.43	0.26	0.23	22.34	0.07	0.48	0.13
	DAM-18	21.9	Sm	68.02	0.59	13.67	3.65	0.05	1.11	2.29	1.56	3.15	0.08	0.01	0.01	0.01	4.93	99.13	57.42	1.35	0.83	4.98	0.26	0.23	23.10	0.08	0.17	0.11
	DAM-19	22.7	Sr	69.63	0.41	9.00	1.60	0.18	0.53	6.96	1.72	1.86	0.07	0.06	0.00	0.01	7.14	99.18	33.97	0.51	1.41	7.74	0.27	0.21	21.91	0.06	0.77	0.19
	DAM-20	23	Sr	75.36	0.43	9.43	1.59	0.13	0.55	3.45	1.92	1.79	0.04	0.07	0.00	0.03	4.40	99.20	45.33	0.83	0.99	8.00	0.18	0.19	21.72	0.06	0.37	0.20
	DAM-21	23.3	Sr	72.49	0.55	9.73	1.47	0.12	0.61	5.36	1.80	1.97	0.05	0.01	0.00	0.01	5.19	99.38	39.59	0.66	1.16	7.45	0.17	0.20	17.59	0.06	0.55	0.18
	DAM-22	23.55	Sr	75.22	0.40	9.78	1.68	0.11	0.61	3.26	1.87	1.91	0.03	0.02	0.00	0.01	4.25	99.14	46.90	0.88	0.94	7.69	0.15	0.20	24.54	0.06	0.33	0.19
	DAM-23	24.05	Sr	74.42	0.50	10.00	1.76	0.13	0.63	3.54	1.92	1.96	0.04	0.04	0.00	0.01	4.49	99.43	46.04	0.85	0.98	7.44	0.17	0.20	20.02	0.06	0.35	0.19
	DAM-24	24.65	Fm	68.66	0.58	12.50	3.09	0.06	0.99	3.68	1.79	2.88	0.09	0.01	0.00	0.01	5.55	99.90	49.47	0.98	0.97	5.49	0.18	0.23	21.39	0.08	0.29	0.14
	DAM-25	25.15	Fm	68.65	0.57	13.17	3.38	0.06	1.16	2.52	1.68	3.03	0.09	0.03	0.00	0.01	4.91	99.25	55.34	1.24	0.85	5.21	0.25	0.23	23.17	0.09	0.19	0.13
	DAM-26	25.75	Fm	70.94	0.53	12.51	3.05	0.05	1.07	1.96	1.79	2.89	0.06	0.01	0.00	0.01	4.32	99.19	56.48	1.30	0.82	5.67	0.26	0.23	23.58	0.09	0.16	0.14
	DAM-27	26.75	Fm	69.76	0.55	12.55	3.04	0.07	1.04	2.53	1.79	2.91	0.05	0.02	0.00	0.01	5.60	99.93	53.98	1.17	0.87	5.56	0.24	0.23	22.74	0.08	0.20	0.14
	DAM-32	28.25	Sp	89.65	0.29	5.13	0.91	0.04	0.29	0.18	1.04	0.99	0.02	0.00	0.00	0.01	1.34	99.89	62.16	1.64	0.67	17.48	0.24	0.19	17.84	0.06	0.04	0.20
	DAM-33	29.25	Sp	89.85	0.25	4.44	0.89	0.02	0.32	0.22	0.73	0.67	0.02	0.00	0.00	0.02	1.77	99.21	65.60	1.91	0.63	20.23	0.18	0.15	17.43	0.07	0.05	0.16
	DAM-34	33.25	Fm	79.16	0.44	9.70	2.21	0.03	0.69	0.68	1.65	2.05	0.03	0.00	0.00	0.01	2.63	99.29	61.12	1.57	0.73	8.16	0.20	0.21	21.94	0.07	0.07	0.17
	DAM-35	33.85	Fm	74.15	0.56	12.13	3.17	0.04	0.87	0.74	2.01	2.70	0.05	0.00	0.00	0.02	3.12	99.57	61.57	1.60	0.76	6.11	0.23	0.22	21.64	0.07	0.06	0.17
	DAM-36	34.45	Sr	82.73	0.74	7.57	1.19	0.05	0.46	1.08	1.49	1.60	0.03	0.01	0.00	0.01	2.34	99.32	55.15	1.23	0.81	10.92	0.26	0.21	10.30	0.06	0.14	0.20
	DAM-37	35.45	Sm	80.60	0.41	8.16	1.43	0.06	0.55	1.76	1.52	1.77	0.02	0.01	0.00	0.01	3.09	99.37	51.74	1.07	0.85	9.88	0.16	0.22	20.00	0.07	0.22	0.19
	DAM-38	36.45	Fm	70.52	0.55	14.21	3.63	0.03	1.07	0.87	1.85	3.41	0.09	0.00	0.01	0.02	3.62	99.87	63.11	1.71	0.73	4.96	0.18	0.24	25.91	0.08	0.06	0.13
	DAM-39	37.65	Fm	75.37	0.42	11.98	2.29	0.02	0.82	0.92	2.12	2.57	0.03	0.00	0.00	0.01	2.98	99.53	60.15	1.51	0.70	6.29	0.26	0.21	28.35	0.07	0.08	0.18
	DAM-40	38.15	Sm	87.02	0.22	6.49	0.74	0.09	0.26	0.47	1.57	1.47	0.02	0.00	0.04	0.07	1.37	99.83	56.35	1.29	0.70	13.40	0.19	0.23	30.04	0.04	0.07	0.24
	DAM-41	38.65	Sm	87.99	0.23	6.07	0.61	0.04	0.23	0.31	1.54	1.36	0.02	0.00	0.00	0.01	1.47	99.87	57.08	1.33	0.67	14.50	0.11	0.22	26.92	0.04	0.05	0.25
	DAM-42	40.15	Fm	78.54	0.37	9.61	1.92	0.03	0.66	1.02	2.12	2.04	0.05	0.00	0.00	0.01	2.72	99.08	56.01	1.27	0.78	8.17	0.10	0.21	26.02	0.07	0.11	0.22
	DAM-43	42.15	Fm	79.29	0.39	9.76	1.93	0.03	0.70	0.66	2.03	2.15	0.02	0.01	0.00	0.01	2.43	99.41	58.69	1.42	0.74	8.12	0.20	0.22	24.96	0.07	0.07	0.21
	DAM-44	44.15	Sm	77.64	0.45	7.51	1.39	0.09	0.49	3.87	1.65	1.72	0.02	0.00	0.00	0.01	4.60	99.44	39.26	0.65	1.22	10.34	0.20	0.23	16.59	0.07	0.52	0.22
	DAM-45	44.45	Fm	66.66	0.35	6.82	1.70	0.07	0.54	10.68	1.37	1.65	0.15	0.01	0.00	0.01	9.67	99.67	22.52	0.29	2.32	9.78	0.19	0.24	19.34	0.08	1.57	0.20
	DAM-46	44.85	Gp	37.47	0.36	5.29	1.03	0.16	0.62	28.40	0.88	1.21	0.22	0.04	0.00	0.01	23.36	99.06	8.86	0.10	6.06	7.09	0.25	0.23	14.61	0.12	5.37	0.17
	DAM-48	46.95	Sr	80.77	0.42	8.01	1.23	0.03	0.44	2.40	2.16	1.42	0.03	0.02	0.00	0.01	2.92	99.86	45.89	0.85	0.96	10.08	0.20	0.18	19.12	0.05	0.30	0.27
	DAM-50	54.3	Sm	80.34	0.42	8.48	1.41	0.04	0.58	1.64	1.96	1.71	0.05	0.01	0.00	0.01	2.62	99.25	51.34	1.05	0.85	9.48	0.15	0.20	20.40	0.07	0.19	0.23
	DAM-51	55.3	Sm	69.38	0.55	7.40	1.54	0.09	0.54	8.63	1.77	1.44	0.05	0.01	0.00	0.01	8.15	99.56	26.86	0.37	1.89	9.38	0.17	0.19	13.39	0.07	1.17	0.24
	DAM-52	56.2	Fm/Fl	73.88	0.33	6.75	1.21	0.11	0.47	6.72	1.37	1.74	0.03	0.01	0.00	0.01	7.40	100.02	29.22	0.41	1.70	10.94	0.21	0.26	20.60	0.07	1.00	0.20
	DAM-53	57.2	Fm/Fl	67.32	0.35	7.64	1.55	0.07	0.64	9.30	1.40	1.95	0.09	0.01	0.00	0.02	8.91	99.23	26.37	0.36	1.91	8.81	0.18	0.25	21.71	0.08	1.22	0.18
	DAM-55	62.5	Fm/Fl	75.97	0.39	8.64	2.00	0.05	0.70	2.99	1.58	2.33	0.05	0.01	0.00	0.02	5.26	99.99	44.99	0.82	1.08	8.80	0.20	0.27	22.10	0.08	0.35	0.18
	DAM-56	62.7	Gcm	37.48	0.33	5.31	1.15	0.21	0.64	28.76	0.92	1.27	0.21	0.04	0.00	0.01	23.44	99.76	8.77	0.10	6.15	7.06	0.23	0.24	16.24	0.12	5.42	0.17
	DAM-60	89.2	Sp	70.66	0.42	7.08	1.41	0.15	0.48	8.56	1.53	1.58	0.06	0.01	0.00	0.02	8.07	100.02	26.35	0.36	1.93	9.98	0.22	0.22	16.91	0.07	1.21	0.22
	DAM-61	89.6	Gcm	34.50	0.31	5.87	1.71	0.14	0.93	29.38	0.84	1.22	0.71	0.04	0.00	0.01	23.69	99.35	9.47	0.10	5.73	5.88	0.20	0.21	18.63	0.16	5.01	0.14
	DAM-62	90	Sp	80.46	0.49	9.10	1.50	0.05	0.56	0.80	2.27	1.73	0.04	0.01	0.00	0.02	2.38	99.41	56.28	1.29	0.75	8.84	0.29	0.19	18.47	0.06	0.09	0.25
	DAM-63	91	Fm	65.58	0.67	15.39	4.82	0.04	1.56	1.11	1.57	3.67	0.12	0.00	0.01	0.02	4.75	99.30	64.26	1.80	0.77	4.26	0.16	0.24	23.06	0.10	0.07	0.10
	DAM-64	91.6	Fm	63.99	0.45	10.35	2.29	0.09	0.89	8.58	1.80	2.46	0.09	0.00	0.00	0.02	8.65	99.66	32.78	0.49	1.51	6.18	0.31	0.24	22.85	0.09	0.83	0.17
	DAM-65	92.2	Fm	69.20	0.33	9.07	1.56	0.12	0.62	7.23	2.04	2.09	0.05	0.01	0.00	0.01	7.00	99.33	32.59	0.48	1.47	7.63	0.22	0.23	27.82	0.07	0.80	0.23
	DAM-66	92.6	Fm	58.03	0.72	18.35	7.00	0.08	2.11	1.55	1.21	4.20	0.59	0.01	0.01	0.01	6.08	99.95	66.23	1.96	0.80	3.16	0.17	0.23	25.44	0.12	0.08	0.07
	DAM-67	94.6	Fm	58.36	0.71	18.06	6.74	0.09	2.10	1.58	1.30	4.18	0.59	0.01	0.01	0.01	6.19	99.92	65.49	1.90	0.81	3.23	0.38	0.23	25.51	0.12	0.09	0.07
	DAM-68	96.6	Fm	70.32	0.60	12.72	3.74	0.06	1.28	1.67	1.93	3.13	0.14	0.00	0.01	0.02	4.12	99.73	57.02	1.33	0.87	5.53	0.37	0.25	21.25	0.10	0.13	0.15
		Elliot	Mean	72.26	0.48	9.88	2.28	0.08	0.73	4.42	1.64	2.14	0.10	0.01	0.00	0.01	5.51	99.55	48.84	1.10	1.27	8.07	0.22	0.21	20.86	0.07	0.60	0.18
			Stdev.	11.59	0.13	3.07	1.32	0.04	0.38	6.67	0.36	0.79	0.14	0.01	0.01	0.01	5.01	0.31	15.37	0.52	1.20	3.15	0.06	0.02	3.89	0.02	1.19	0.05
		LEF	Mean	77.42	0.53	9.15	2.00	0.07	0.48	2.64	1.68	1.75	0.05	0.01	0.00	0.01	3.79	99.58	56.49	1.44	0.97	8.73	0.22	0.19	17.83	0.05	0.32	0.19
		n = 9	Stdev.	10.62	0.13	1.73	0.87	0.04	0.17	5.82	0.39	0.49	0.05	0.01	0.00	0.01	4.72	0.27	14.00	0.46	0.73	1.95	0.06	0.02	2.62	0.01	0.73	0.05
		UEF	Mean	71.31	0.47	10.01	2.33	0.08	0.78	4.75	1.64	2.22	0.11	0.01	0.00	0.01	5.83	99.55	47.44	1.04	1.32	7.95	0.22	0.22	21.42	0.08	0.65	0.17
		n=49	Stdev.	11.39	0.13	3.21	1.37	0.04	0.39	6.70	0.35	0.80	0.15	0.02	0.01	0.01	4.95	0.31	15.04	0.50	1.25	3.28	0.06	0.02	3.79	0.02	1.23	0.05

Table A10. Damplaats (DAM) coarse- and fine-grained sample comparison via bulk rock major elements, weathering indices and major element ratios.

Coarse-grained samples (Sm - Gcm)

Sample	Strat. ht (m)	Facies	SiO_2	TiO_2	Al_2O_3	Fe_2O_3	MnO	MgO	CaO	Na_2O	K_2O	P_2O5	SO_3	Cr_2O_3	NiO	LOI	Total	CIA	CIAmolar	ICV	SiO_2/Al_2O_3	Fe_2O_3/Al_2O_3	K_2O/Al_2O_3	Al_2O_3/TiO_2	MgO/Al_2O_3	CaO/Al_2O_3	Na_2O/Al_2O_3
DAM-2	0.5	Sr	82.85	0.50	8.88	1.32	0.08	0.40	0.36	2.13	1.58	0.03	0.00	0.01	0.02	1.49	99.65	60.19	1.51	0.67	9.33	0.29	0.18	17.69	0.05	0.04	0.24
DAM-3	1.5	Sr	84.43	0.47	7.81	1.02	0.15	0.23	0.27	2.18	1.28	0.03	0.00	0.00	0.01	1.23	99.10	58.86	1.43	0.69	10.81	0.15	0.16	16.79	0.03	0.04	0.28
DAM-4	2.1	Sm/Sl	83.62	0.55	8.36	1.05	0.04	0.25	0.44	2.10	1.42	0.03	0.00	0.00	0.01	1.49	99.36	59.03	1.44	0.67	10.00	0.13	0.17	15.18	0.03	0.05	0.25
DAM-6	4.4	Gcm	74.14	0.59	11.77	3.29	0.07	0.70	1.31	1.65	2.54	0.19	0.01	0.00	0.01	3.20	99.50	59.96	1.50	0.80	6.30	0.24	0.22	19.79	0.06	0.11	0.14
DAM-7	5.4	Sm	81.89	0.44	8.77	1.78	0.04	0.52	0.78	1.30	1.85	0.04	0.00	0.00	0.01	2.47	99.89	61.22	1.58	0.71	9.34	0.28	0.21	19.77	0.06	0.09	0.15
DAM-8	6.4	Sr	82.66	0.59	8.25	2.06	0.03	0.46	0.39	1.24	1.55	0.04	0.00	0.00	0.01	2.17	99.47	65.08	1.86	0.71	10.02	0.20	0.19	13.88	0.06	0.05	0.15
DAM-9	8.4	Sm	84.07	0.34	7.73	1.93	0.03	0.39	0.31	1.55	1.21	0.04	0.00	0.00	0.01	2.18	99.80	63.56	1.74	0.69	10.88	0.25	0.16	22.76	0.05	0.04	0.20
DAM-11	16	Sm	78.47	0.49	9.92	2.09	0.06	0.63	1.46	1.67	1.95	0.07	0.02	0.00	0.01	2.99	99.82	56.87	1.32	0.78	7.91	0.24	0.20	20.37	0.06	0.15	0.17
DAM-12	16.4	Sm	79.57	0.43	8.44	1.38	0.09	0.46	2.65	1.90	1.44	0.04	0.02	0.00	0.01	3.53	99.96	47.04	0.89	0.93	9.43	0.21	0.17	19.68	0.05	0.31	0.23
DAM-17	20.1	Sm	65.64	0.54	12.09	3.15	0.07	0.88	5.83	1.61	2.76	0.05	0.02	0.00	0.01	7.12	99.77	42.70	0.75	1.15	5.43	0.26	0.23	22.34	0.07	0.48	0.13
DAM-18	21.9	Sm	68.02	0.59	13.67	3.65	0.05	1.11	2.29	1.56	3.15	0.08	0.01	0.01	0.01	4.93	99.13	57.42	1.35	0.83	4.98	0.26	0.23	23.10	0.08	0.17	0.11
DAM-19	22.7	Sr	69.63	0.41	9.00	1.60	0.18	0.53	6.96	1.72	1.86	0.07	0.06	0.00	0.01	7.14	99.18	33.97	0.51	1.41	7.74	0.27	0.21	21.91	0.06	0.77	0.19
DAM-20	23	Sr	75.26	0.43	9.43	1.59	0.13	0.55	3.45	1.92	1.79	0.04	0.07	0.00	0.03	4.40	99.20	45.33	0.83	0.99	8.00	0.18	0.19	21.72	0.06	0.37	0.20
DAM-21	23.3	Sr	72.49	0.55	9.73	1.47	0.12	0.61	5.36	1.80	1.97	0.05	0.01	0.00	0.01	5.19	99.38	39.59	0.66	1.16	7.45	0.17	0.20	17.59	0.06	0.55	0.18
DAM-22	23.55	Sr	75.22	0.40	9.78	1.68	0.11	0.61	3.26	1.87	1.91	0.03	0.02	0.00	0.01	4.25	99.14	46.90	0.88	0.94	7.69	0.15	0.20	24.54	0.06	0.33	0.19
DAM-23	34.05	Sr	74.42	0.50	10.00	1.76	0.13	0.63	3.54	1.92	1.96	0.04	0.04	0.00	0.01	4.49	99.43	46.04	0.85	0.98	7.44	0.17	0.20	20.02	0.06	0.35	0.19
DAM-32	28.25	Sp	89.65	0.29	5.13	0.91	0.04	0.29	0.18	1.04	0.99	0.02	0.00	0.00	0.01	1.34	99.89	62.16	1.64	0.67	17.48	0.24	0.19	17.84	0.06	0.04	0.20
DAM-33	29.25	Sp	89.85	0.25	4.44	0.89	0.02	0.32	0.22	0.73	0.67	0.02	0.00	0.00	0.02	1.77	99.21	65.60	1.91	0.63	20.23	0.18	0.15	17.43	0.07	0.05	0.16
DAM-36	34.45	Sr	82.73	0.74	7.57	1.19	0.05	0.46	1.08	1.49	1.60	0.03	0.01	0.00	0.01	2.34	99.32	55.15	1.23	0.81	10.92	0.26	0.21	10.30	0.06	0.14	0.20
DAM-37	35.45	Sm	80.80	0.41	8.16	1.43	0.06	0.55	1.76	1.52	1.77	0.02	0.01	0.00	0.01	3.09	99.37	51.74	1.07	0.85	9.88	0.16	0.22	20.00	0.07	0.22	0.19
DAM-40	38.15	Sm	87.02	0.22	6.49	0.74	0.09	0.26	0.47	1.57	1.47	0.02	0.09	0.04	0.07	1.37	99.83	56.35	1.29	0.70	13.40	0.19	0.23	30.04	0.04	0.07	0.24
DAM-41	38.65	Sm	87.99	0.23	6.07	0.61	0.04	0.23	0.31	1.54	1.36	0.02	0.00	0.00	0.01	1.47	99.87	57.08	1.33	0.67	14.50	0.11	0.22	26.92	0.04	0.05	0.25
DAM-44	44.15	Sm	77.64	0.45	7.51	1.39	0.09	0.49	3.87	1.65	1.72	0.02	0.00	0.00	0.01	4.60	99.44	39.26	0.65	1.22	10.34	0.20	0.23	16.59	0.07	0.52	0.22
DAM-48	46.95	Sr	80.77	0.42	8.01	1.23	0.03	0.44	2.40	2.16	1.42	0.03	0.02	0.00	0.01	2.92	99.86	45.89	0.85	0.96	10.08	0.20	0.18	19.12	0.05	0.30	0.27
DAM-50	54.3	Sm	80.34	0.42	8.48	1.41	0.04	0.58	1.64	1.96	1.71	0.05	0.01	0.00	0.01	2.62	99.25	51.34	1.05	0.85	9.48	0.15	0.20	20.40	0.07	0.19	0.23
DAM-51	55.3	Sm	69.38	0.35	7.40	1.54	0.09	0.54	8.63	1.77	1.44	0.05	0.01	0.00	0.01	8.15	99.56	26.86	0.37	1.89	9.38	0.17	0.19	13.39	0.07	1.17	0.24
DAM-60	89.2	Sp	70.66	0.42	7.08	1.41	0.15	0.48	8.56	1.53	1.58	0.06	0.01	0.00	0.02	8.07	100.02	26.35	0.36	1.93	9.98	0.22	0.22	16.91	0.07	1.21	0.22
DAM-62	90	Sp	80.46	0.49	9.10	1.50	0.05	0.56	0.80	2.27	1.73	0.04	0.01	0.00	0.02	2.38	99.41	56.28	1.29	0.75	8.84	0.29	0.19	18.47	0.06	0.09	0.25
	Mean		78.51	0.45	8.54	1.61	0.08	0.51	2.45	1.69	1.70	0.05	0.01	0.00	0.01	3.51	99.53	51.35	1.15	0.93	9.90	0.21	0.20	19.45	0.06	0.28	0.20
	std Dev	(n = 28)	6.61	0.12	1.96	0.72	0.04	0.19	2.52	0.35	0.50	0.03	0.02	0.01	0.01	2.07	0.29	10.89	0.44	0.34	3.27	0.05	0.02	4.06	0.01	0.32	0.04

Conglomerate samples

Sample	Strat. Ht. (m)	Facies	SiO_2	TiO_2	Al_2O_3	Fe_2O_3	MnO	MgO	CaO	Na_2O	K_2O	P_2O5	SO_3	Cr_2O_3	NiO	LOI	Total	CIA	CIAmolar	ICV	SiO_2/Al_2O_3	Fe_2O_3/Al_2O_3	K_2O/Al_2O_3	Al_2O_3/TiO_2	MgO/Al_2O_3	CaO/Al_2O_3	Na_2O/Al_2O_3
DAM-46	44.85	Gp	37.47	0.36	5.29	1.03	0.16	0.62	28.40	0.88	1.21	0.22	0.04	0.00	0.01	23.36	99.06	8.86	0.10	6.06	7.09	0.25	0.23	14.61	0.12	5.37	0.17
DAM-56	62.7	Gcm	37.48	0.33	5.31	1.15	0.21	0.64	28.76	0.92	1.27	0.21	0.04	0.00	0.01	23.44	99.76	8.77	0.10	6.15	7.06	0.23	0.24	16.24	0.12	5.42	0.17
DAM-61	89.6	Gcm	34.50	0.31	5.87	1.71	0.14	0.93	29.38	0.84	1.22	0.71	0.04	0.00	0.01	23.69	99.35	9.47	0.10	5.73	5.88	0.29	0.21	18.63	0.16	5.01	0.14
	Mean		36.48	0.33	5.49	1.30	0.17	0.73	28.85	0.88	1.23	0.38	0.04	0.00	0.01	23.50	99.39	9.03	0.10	5.98	6.68	0.23	0.23	16.49	0.13	5.27	0.16
	stdev	(n = 3)	1.72	0.02	0.33	0.36	0.04	0.18	0.49	0.04	0.03	0.29	0.00	0.00	0.00	0.17	0.36	0.38	0.00	0.22	0.69	0.03	0.02	2.02	0.02	0.23	0.02

Fine-grained samples (Fm)

Sample	Strat. ht. (m)	Facies	SiO_2	TiO_2	Al_2O_3	Fe_2O_3	MnO	MgO	CaO	Na_2O	K_2O	P_2O5	SO_3	Cr_2O_3	NiO	LOI	Total	CIA	CIAmolar	ICV	SiO_2/Al_2O_3	Fe_2O_3/Al_2O_3	K_2O/Al_2O_3	Al_2O_3/TiO_2	MgO/Al_2O_3	CaO/Al_2O_3	Na_2O/Al_2O_3
DAM-1	0	Fl	73.70	0.82	12.79	3.66	0.04	0.75	0.81	1.88	2.66	0.04	0.00	0.01	0.02	2.82	100.00	63.19	1.72	0.77	5.76	0.29	0.21	15.65	0.06	0.06	0.15
DAM-5	2.6	Fm	69.47	0.42	8.01	1.90	0.12	0.59	10.09	1.09	1.64	0.03	0.02	0.09	0.02	17.02	99.42	17.31	0.21	3.03	8.17	0.13	0.20	18.97	0.07	2.38	0.14
DAM-10	15	Fm	73.14	0.51	11.99	2.90	0.06	0.82	1.96	1.89	2.58	0.08	0.03	0.01	0.01	3.78	99.75	55.91	1.27	0.83	6.10	0.25	0.22	23.62	0.07	0.16	0.16
DAM-13	17.6	Fm	66.04	0.63	14.09	4.20	0.08	1.13	3.14	1.38	3.25	0.11	0.01	0.01	0.01	5.81	99.88	55.06	1.23	0.90	4.69	0.16	0.23	22.35	0.08	0.22	0.10
DAM-14	18	Fm	69.15	0.60	13.55	3.71	0.06	1.03	1.86	1.62	3.12	0.13	0.01	0.00	0.01	4.38	99.24	58.99	1.44	0.81	5.10	0.30	0.23	22.43	0.08	0.14	0.12
DAM-15	18.7	Fm	68.39	0.58	12.05	2.98	0.09	0.90	4.42	1.63	2.70	0.30	0.01	0.00	0.01	5.76	99.84	46.88	0.88	1.03	5.68	0.27	0.22	20.72	0.07	0.37	0.14
DAM-16	19.1	Fm	67.60	0.57	13.10	3.47	0.09	1.01	3.17	1.57	2.96	0.10	0.01	0.01	0.01	5.38	99.06	53.14	1.13	0.90	5.16	0.25	0.23	22.85	0.08	0.24	0.12
DAM-24	24.65	Fm	68.66	0.58	12.50	3.09	0.06	0.99	3.68	1.79	2.88	0.09	0.01	0.00	0.01	5.55	99.90	49.47	0.98	0.97	5.49	0.18	0.23	21.39	0.08	0.29	0.14
DAM-25	25.15	Fm	68.65	0.57	13.17	3.38	0.06	1.16	2.52	1.68	3.03	0.09	0.03	0.00	0.01	4.91	99.25	55.34	1.24	0.85	5.21	0.25	0.23	23.17	0.09	0.19	0.13
DAM-26	25.75	Fm	70.94	0.53	12.51	3.05	0.05	1.07	1.96	1.79	2.89	0.06	0.01	0.00	0.01	4.32	99.19	56.48	1.30	0.82	5.67	0.26	0.23	23.58	0.09	0.16	0.14
DAM-27	26.75	Fm	69.76	0.55	12.55	3.04	0.07	1.04	2.53	1.79	2.91	0.05	0.02	0.00	0.01	5.60	99.93	53.98	1.17	0.87	5.56	0.24	0.23	22.74	0.08	0.20	0.14
DAM-34	33.25	Fm	79.16	0.44	9.70	2.21	0.03	0.69	0.68	1.65	2.05	0.03	0.00	0.00	0.01	2.63	99.29	61.12	1.57	0.73	8.16	0.20	0.21	21.94	0.07	0.07	0.17
DAM-35	33.85	Fm	74.15	0.56	12.13	3.17	0.04	0.87	0.74	2.01	2.70	0.05	0.00	0.00	0.02	3.12	99.57	61.57	1.60	0.76	6.11	0.23	0.22	21.64	0.07	0.06	0.17
DAM-38	36.45	Fm	70.52	0.55	14.21	3.63	0.03	1.07	0.87	1.85	3.41	0.09	0.00	0.01	0.02	3.62	99.87	63.11	1.71	0.73	4.96	0.18	0.24	25.91	0.08	0.06	0.13
DAM-39	37.65	Fm	75.37	0.42	11.98	2.29	0.02	0.82	0.92	2.12	2.57	0.03	0.00	0.00	0.01	2.98	99.53	60.15	1.51	0.70	6.29	0.26	0.21	28.35	0.07	0.08	0.18
DAM-42	40.15	Fm	78.54	0.37	9.61	1.92	0.03	0.66	1.02	2.12	2.04	0.05	0.00	0.00	0.01	2.72	99.08	56.01	1.27	0.78	8.17	0.20	0.21	26.02	0.07	0.11	0.22
DAM-43	42.15	Fm	79.29	0.39	9.76	1.93	0.03	0.70	0.66	2.03	2.15	0.02	0.01	0.00	0.01	2.43	99.41	58.69	1.42	0.74	8.12	0.20	0.22	24.96	0.07	0.07	0.21
DAM-45	44.45	Fm	66.66	0.35	6.82	1.70	0.07	0.54	10.68	1.37	1.65	0.15	0.01	0.00	0.01	9.67	99.67	32.52	0.29	2.32	9.78	0.19	0.24	19.34	0.08	1.57	0.20
DAM-52	56.2	Fm/Fl	73.88	0.33	6.75	1.21	0.11	0.47	6.72	1.37	1.74	0.03	0.01	0.00	0.01	7.40	100.02	29.22	0.41	1.70	10.94	0.21	0.26	20.60	0.07	1.00	0.20
DAM-53	57.2	Fm/Fl	67.32	0.35	7.64	1.55	0.07	0.64	9.30	1.40	1.95	0.09	0.01	0.00	0.02	8.91	99.23	26.37	0.36	1.91	8.81	0.18	0.25	21.71	0.08	1.22	0.18
DAM-55	62.5	Fm/Fl	75.97	0.39	8.64	2.00	0.05	0.70	2.99	1.58	2.33	0.05	0.01	0.00	0.02	5.26	99.99	44.99	0.82	1.08	8.80	0.20	0.27	22.10	0.08	0.35	0.18
DAM-63	91	Fm	65.58	0.67	15.39	4.82	0.04	1.56	1.11	1.57	3.67	0.12	0.00	0.01	0.02	4.75	99.30	64.26	1.80	0.77	4.26	0.16	0.24	23.06	0.10	0.07	0.10
DAM-64	91.6	Fm	63.99	0.45	10.35	2.29	0.09	0.89	8.58	1.80	2.46	0.09	0.00	0.00	0.02	8.65	99.66	32.78	0.49	1.51	6.18	0.31	0.24	22.85	0.09	0.83	0.17
DAM-65	92.2	Fm	69.20	0.33	9.07	1.56	0.12	0.62	7.23	2.04	2.09	0.05	0.01	0.00	0.01	7.80	99.33	32.59	0.48	1.47	7.63	0.22	0.23	27.82	0.07	0.80	0.23
DAM-66	92.6	Fm	58.03	0.72	18.35	7.00	0.08	2.11	1.55	1.21	4.20	0.59	0.01	0.01	0.01	6.08	99.95	66.23	1.96	0.80	3.16	0.17	0.23	25.44	0.12	0.08	0.07
DAM-67	94.6	Fm	58.36	0.71	18.06	6.74	0.09	2.10	1.58	1.30	4.18	0.59	0.01	0.01	0.01	6.19	99.92	65.49	1.90	0.81	3.23	0.38	0.23	25.51	0.12	0.09	0.07
DAM-68	96.6	Fm	70.32	0.60	12.72	3.74	0.06	1.28	1.67	1.93	3.13	0.14	0.00	0.01	0.02	4.12	99.73	57.02	1.33	0.87	5.53	0.37	0.25	21.25	0.10	0.13	0.15
Mean			72.26	0.48	9.88	2.28	0.08	0.73	4.42	1.64	2.14	0.10	0.01	0.00	0.01	5.51	99.55	48.84	1.10	1.27	8.07	0.22	0.21	20.86	0.07	0.60	0.18
Stdev.	n = 27		11.49	0.13	3.05	1.31	0.04	0.38	6.61	0.35	0.78	0.14	0.01	0.00	0.01	4.97	0.30	15.24	0.51	1.19	3.12	0.06	0.02	3.86	0.02	1.17	0.05